The Development of Unorthodox Amine–Acid Coupling Reactions and Their Applications Towards Complex Molecules for a Systems Approach to Chemistry

by

Andrew McGrath

A dissertation submitted in partial fulfillment
of the requirements for the degree of
Doctor of Philosophy
(Medicinal Chemistry)
in the University of Michigan
2024

Doctoral Committee:

Assistant Professor Timothy Cernak, Chair
Professor Pavel Nagorny
Assistant Professor Jonny Z. Sexton
Associate Professor Peter Toogood

Andrew T. McGrath

amcgrat@umich.edu

ORCID iD: 0000-0001-9275-0017

Dedication

I would like to dedicate this thesis to my wonderful family. I am forever grateful for all you have done to get me to where I am.

Acknowledgements

First and foremost, I would like to thank my advisor, Dr. Tim Cernak, for giving me a plethora of opportunities. I have learned an enormous amount from him and have grown not only as a scientist, but as a person. I have seen more of the world than ever before during my PhD, and I have him to thank for that.

I would like to thank all of the members of the Cernak lab past and present. I have learned something from everyone I've interacted with, and they are generally a great group of people to work with. I especially would like to thank Dr. Bo Mahjour, Andrew Outlaw, Dr. Sam Zhang, Dr. Chris Audu, Dr. Yuning Shen, Dr. Haiyan Huang, Dr. Sandip Das, Dr. Yingfu Lin, Dr. James Douthwaite, Yu-ting Kao, and Di Wang. You have all been wonderful friends and colleagues during my time here and in one way or another I could not have completed my PhD without each of you.

I would like to thank my committee members Dr. Pavel Nagorny, Dr. Jonny Sexton, and Dr. Peter Toogood for their helpful discussions and feedback as well as their flexibility with scheduling and rescheduling. I would also like to thank my former committee member Dr. Heather Carlson, whom I also learned a lot from.

I am grateful to Janssen Pharmaceuticals, the College of Pharmacy, and the NIH for providing funding for my PhD. From Janssen I am glad to have worked with Dr.'s Christine Gelin and J.F. Brazeau. They have been excellent collaborators.

I thank Dr. Larissa Yeomans for her help with NMRs, but also for being a wonderful person and friend. I thank all of the friends I made outside of the lab. Ryan and Luis from my cohort; we've been on so many adventures and I hope many more. Jessee, I will always remember our times at Heidelberg. To my roommates, the 903 S. Main boys Austin Ventura, Jake Hitchens, Justin Balog, Tim Emmel, and Dr.'s Troy Halseth and Garrett Dow, it was a joy to live with you all. Let's continue the trend of living on the same coast.

To my undergraduate friends Jose, Justin, Sarah, Shebastian, and Wille, I am so glad we have had the opportunity to get together during my PhD. They have been bright spots for sure. To Dr. Z. who subconsciously instilled Michigan into my mind and to Dr. Allen Schoffstall who opened my mind to the idea of graduate school, thank you.

To my parents, who did everything possible to make sure I ended up here, I am grateful. Your support makes all the difference.

Finally, to my partner Dr. Anzu Giri, who has supported me through every step of this journey and has been with me through the best and worst times. I am so glad you are in my life, and I look forward to our future together.

Table of Contents

List of Tables

List of Figures

List of Schemes

List of Spectra

Abstract

A molecule's properties are intimately linked to its medicinal function, yet there is a gap in our understanding of the interaction between properties and chemical synthesis. The most popular reaction in medicinal chemistry, the amide coupling, is an ideal arena to explore the relationship of reactions to properties, and ultimately function. Amines and carboxylic acids are among the most abundant materials available for organic synthesis. They are traditionally coupled together using the amide coupling. This is due to the robustness of the reaction as well as challenges associated with generating reactive species from these stable functionalities. Theoretically there are many unique ways in which these two plentiful materials can be combined with each of them generating products with diverse properties. Indeed, there has been a heavy focus recently on developing methodologies to use these pervasive molecules as partners for cross coupling reactions. Our lab is interested in further exploring and developing unique reactivities of amines and acids to complement the amide coupling and using them to explore the complex interplay between physicochemical properties and biological function. By activating the amine as its pyridinium salt and using robotics and high throughput experimentation (HTE), we have developed a selective, deaminative esterification that generates a molecule geometrically identical to the amide but contains one fewer hydrogen bond donor. Mechanistic investigations revealed this reaction proceeds through an alkyl halide intermediate that can be isolated in a one pot manner from the free amine. We have capitalized on this intermediate to synthesize halides and phenolic ethers from amines. To achieve the corresponding amine–acid etherification, we

have leveraged HTE to develop an *in-situ* reduction extension to our esterification protocol. These reactions and several others have been applied to an amine–acid pair to synthesize a series of proteolysis targeting chimeras (PROTACs) as well as fluorescent dyes. These series span a wide range of partition coefficient, charge, and polar surface area while maintaining bulk similarity (and molecular weight) to the "traditional" molecule one would synthesize from amine and acid. We confirm that these subtle structural changes realized by subjecting the same building blocks to varying reaction conditions have a profound effect on the biological activity of the newly synthesized molecules. This dissertation will explore the interplay between these effects through the lens of amine–acid coupling reactions as well as discuss the teaching of new techniques that will enable this understanding.

Chapter 1 A Systems Level Approach to Chemistry

1.1 An Introduction to Systems Chemistry

Systems are interconnected and interdependent. Changes in one part of a system can influence a seemingly distal part of the system, or the system in its entirety. For this reason, systems theory favors holism over reductionism, looking at the entire system at once and considering the interconnections and dependencies of individual parts.[1] From these holistic studies comes the ability to build predictive models, to reveal unexpected patterns in the data, to design towards targeted objectives, and to reveal system components that remain poorly understood. As synthetic chemistry becomes more intimately partnered with data science, a systems approach could help stitch together seemingly disparate chemistry datasets. While systems theory is engrained in biology, as in systems biology,[2] and "systems chemistry" has been used to describe studies in self-assembly,[3–6] and the origins of life,[7–10] the systems approach has not been applied in synthetic chemistry. We propose an extension of systems chemistry that focuses on chemical synthesis. Our view of systems chemistry borrows from the architecture of modern systems biology, the *de facto* workflow of the pharmaceutical industry, which uses multi-omics experimental tools to illuminate drug targets from patient populations. This systems chemistry for synthesis would tie chemical reactions to molecular function with an aim to invent new functional molecular products, reactions, catalysts, and predictive models in industrial and academic settings. Viewed through the lens of drug discovery, one could use systems chemistry to link synthetic reaction conditions to a complex phenotypic function such as selective distribution of a small molecule medicine to the brain, and subsequent binding to a target protein

in that tissue. This medicinal phenotype would correlate with parameters such as physicochemical properties, chemical structure, reaction conditions, conceivable transformations and available chemical building blocks used to make the product (Fig. 1). While a systems biology approach may link available biological data, often multi-omics data, to a specific biological target localized within a specific target tissue and patient population, a systems chemistry approach could tie together the requisite data to invent a molecule – a medicine for instance – that inhibits the biological target. In medicinal chemistry, the notion of a design-make-test cycle of invention is an established tactic.[11] Systems chemistry layers the appropriate packages of data onto the design-make-test cycle, which is applicable to functional molecules beyond medicines like agrochemicals and materials. The holism offered by systems chemistry will become increasingly necessary to tie together the complex data packages that have become popular within contemporary partnerships of synthetic chemistry with machine learning, for instance that systematically document the synthesis of molecules[12] and the functional outcomes of those molecules.[13]

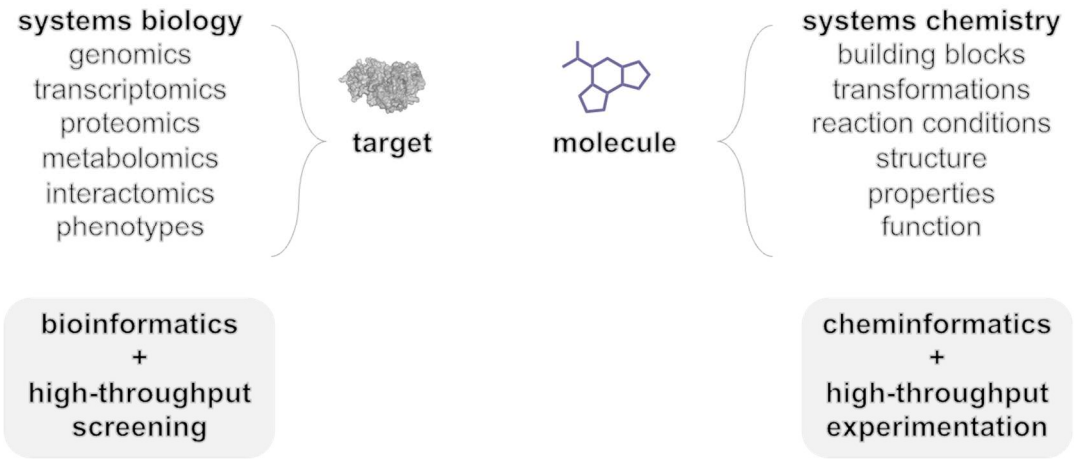

Figure 1.1 Systems chemistry unites big data packages to link available chemical building blocks to function. The output would be a functional molecule, and the data can be generated with high-throughput experimentation, if not already available, and studied with chemoinformatics. The complementary field of systems biology would generally propose a therapeutic target. We define a reaction as comprising both a transformation – to map the changing of atoms and bonds – and reaction conditions to experimentally realize the transformation.

Molecules are designed to satisfy functional objectives such as shrinking a tumor using a once daily pill or inhibiting fungal growth on a food crop using a water-soluble agrichemical. A molecule's function is dependent on its physicochemical properties, which are defined by molecular structure. A simple example would be the distribution of a lipophilic compound into adipose tissue because the compound has many hydrocarbon bonds. Recognizing that, for a novel molecule, the structural arrangement of atoms and bonds arises from a synthetic sequence of transformations that only succeeds experimentally if winning reaction conditions are selected. Meanwhile, modern chemistry allows a single pair of building blocks to be converted into diverse products, depending on the catalyst chosen.[14,15] So, in the example above one can propose that reaction conditions are linked to tissue distribution. While seemingly distal, these parameters are interconnected and interdependent and highlight how the "above-the-arrow" recipe used to make a molecule can directly influence the functional outcome of the product. This interactive web of parameters can be viewed as a system linking synthesis to function, and with the advent of artificial intelligence (AI) could lead to better medicines, agrochemicals, and materials of the future. A thread connecting chemical building blocks, transformations, reaction conditions, molecular structure, physicochemical properties to macroscopic function thus serves as a framework for systems chemistry (Fig. 2A). In analogy to systems biology, the computational and mathematical modeling of complex chemical systems, enabled by the accessibility of large amounts of data could steer models towards meaningful outcomes. The goal of systems biology is to tie genes, proteins, metabolites, and interaction pathways to disease phenotypes (Fig. 1), generally arriving at a therapeutic disease target, such as a specific protein. The complementary goal of systems chemistry is to tie transformations, conditions, structure, and properties to function with a goal of producing a molecule to bind the target identified by

systems biology or other means. A systems approach to chemistry is timely given the increasing role that AI is playing in chemistry, and the current state of the art of multi-omics tools. Both systems biology and systems chemistry rely on high volumes of data to tease out patterns and trends, and from there to build predictive models. Whereas the advent of high-throughput screening (HTS) genomic, proteomic, metabolomic, and bioinformatic techniques ushered in the field of systems biology, modern high-throughput chemical methods are the foundation upon which systems chemistry can be built. The rapid advancement of high-throughput experimentation (HTE)[16–22]for chemical synthesis in the past decade, as well as the evolution of chemoinformatics in support of structure-bioactivity predictions,[23] and more recently structure-reactivity predictions[24] opens the door to systems level thinking in chemical synthesis.

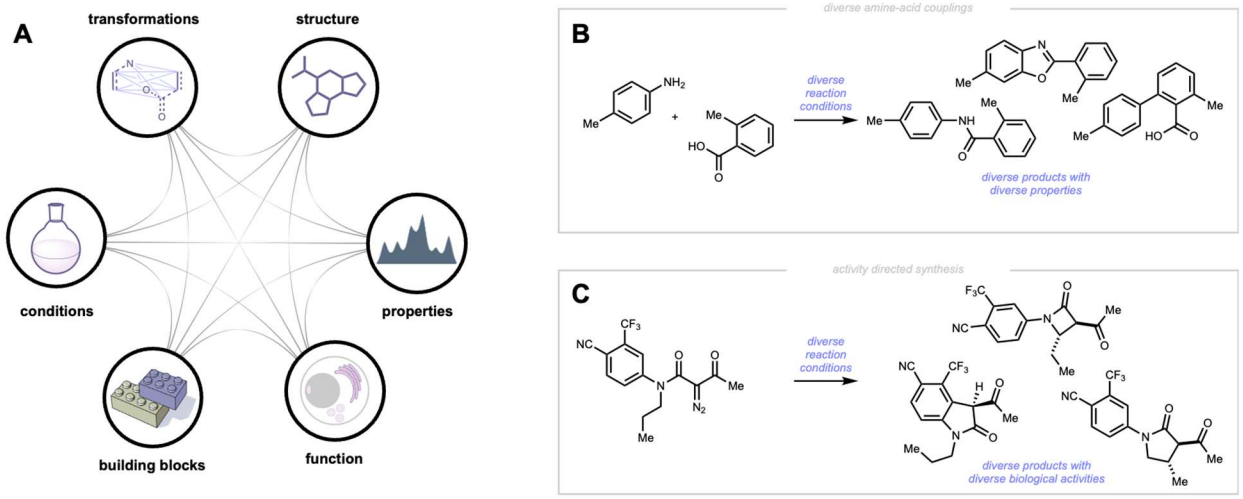

Figure 1.2 A. The interplay of available data packages can suggest the invention of new chemical transformations. B. This interplay has been exploited with diverse amine-acid coupling reactions to modulate physicochemical properties via reaction conditions, and C. in activity-directed synthesis to modulate bioactivity via choice of catalyst.

We anticipate that a systems chemistry lens will help realize the power of AI in chemistry, at least in the invention of drugs, materials, agrichemicals, and other products that arise from chemical synthesis. The practice of organic chemistry favors the pattern recognition of

reactions, often named after the chemists associated with the earliest reports of the reaction. Today, however, new chemical reaction methods are published at such a pace that it is no longer possible for a human to keep up with all of the modern reaction literature. Additionally, human selection of reaction methods is biased by familiarity with existing methods or the reputation of certain methods in a chemist's peer group. In the future, computational searches will increasingly remove these human biases and select reaction methods that arrive at desired product functions based on available building blocks. While often discussed as a single entity, a reaction method can be broken down into two main components for computational or logical exercises. The first component of a reaction method is the transformation, which describes the mapping of atom-bond positions from the starting building blocks into products. This transformation maps where the bonds and atoms go throughout the reaction and is required to study reactions computationally, but agnostic of the experimental conditions required to execute the reaction in the real world. The second critical component of a reaction method is the "above-the-arrow" reaction conditions, comprising combinations of catalysts, ligands, reagent additives, solvents, temperature, and other operational parameters required to experimentally execute the transformation in the lab. Systems chemistry connects transformations and reaction conditions to structure and properties, or, by zooming out one more layer, building blocks to function.

Today, only a handful of studies link building blocks to properties or function, but the field of organic chemistry is increasingly tying threads through large amounts of data defined by parameters in Figure 1. In one recent study, it was shown that the selection of a catalyst can lead alter the lipophilic partition coefficient by up to two orders of magnitude, with a diversity of catalysts converting the same two amine and carboxylic acid building blocks into a diversity of

products with a diversity of properties (Fig. 2B).[14] In a separate study (Fig. 2C), catalysts were surveyed to lead to distinct products tested directly in a bioassay. Here the catalysts that generated the most bioactive compounds, based on a diversity of accessible chemical structures, were selected for future rounds of activity-directed synthesis.[25] These strategies build from diversity-oriented synthesis,[26] but incorporate deeper exploration on the reaction condition axis.

This interplay of reaction conditions, transformations, structure, properties, function and building blocks ties together multiple threads of data-rich contemporary medicinal, materials, and agrichemistry research under the umbrella of systems chemistry. Just as systems biology leads to the identification of viable biological targets to therapeutic intervention, systems chemistry navigates large data inputs and combinatorial and vast experimental spaces, ultimately leading to the molecules that will modulate those biological targets. The systems chemistry concept here is applied to highlight the interconnections of datasets that go into the design-make-test cycle of medicinal or agrichemical invention, in part because of the direct correlation to the established field of systems biology. Of course, such interconnections can as easily be applied to systems level studies of materials or batteries and have been already applied to describe origins of life. As artificial intelligence and data science play an increasingly significant role in synthetic chemistry towards academic and industrial objectives, codifying the links between virtual, commercial, experimental, and calculated data packages can accelerate the invention of the molecules of tomorrow.

1.2 An Introduction to Amine–Acid Coupling Reactions.

The amide coupling, the fundamental building block of protein backbones is also the most popular reaction in drug discovery.[27] This reaction, used to forge bonds between amines

and carboxylic acids, has seen nearly over 140 years of development beginning with activation of the carboxylic acid as its azide[28] or acid chloride,[29,30] followed by the development of the carbodiimide reagents[31], benzotriazoles,[32] and uranyl reagents such as Hexafluorophosphate Azabenzotriazole Tetramethyl Uronium (HATU).[33] Today there exist well over 100 amide coupling reagents.[34,35] Due to this development, the amide coupling is an incredibly robust reaction, a likely reason for its popularity. Additionally, amines and acids are ubiquitous in nature, so a plethora of them are commercially available and pharmaceutical building block libraries are well stocked with them.

While the amide coupling is by far the most popular way to unite amines and carboxylic acids, it is not the only one. Theoretically, there exist on the order of hundreds[14] to millions[36] of ways that a simple amine and simple acid can come together. Each of these new transformations would be responsible for imparting a physicochemical footprint on the new product. This allows for a fine tuning of these properties through single atom control of the molecule. In this way, one can understand the interplay between selected reaction conditions and final physicochemical properties of the molecule. This is exemplified by work from the Cernak group in figure 1.3 where amine **1.1** and acid **1.2** are coupled together via the amide reaction and five others. Each of these products has a unique molecular weight, $\log_{10}$ lipophilic partition coefficient (LogP, and polar surface area and span a large range of each.[14] This method is an alternative to the building block centric approach of diversifying molecules.

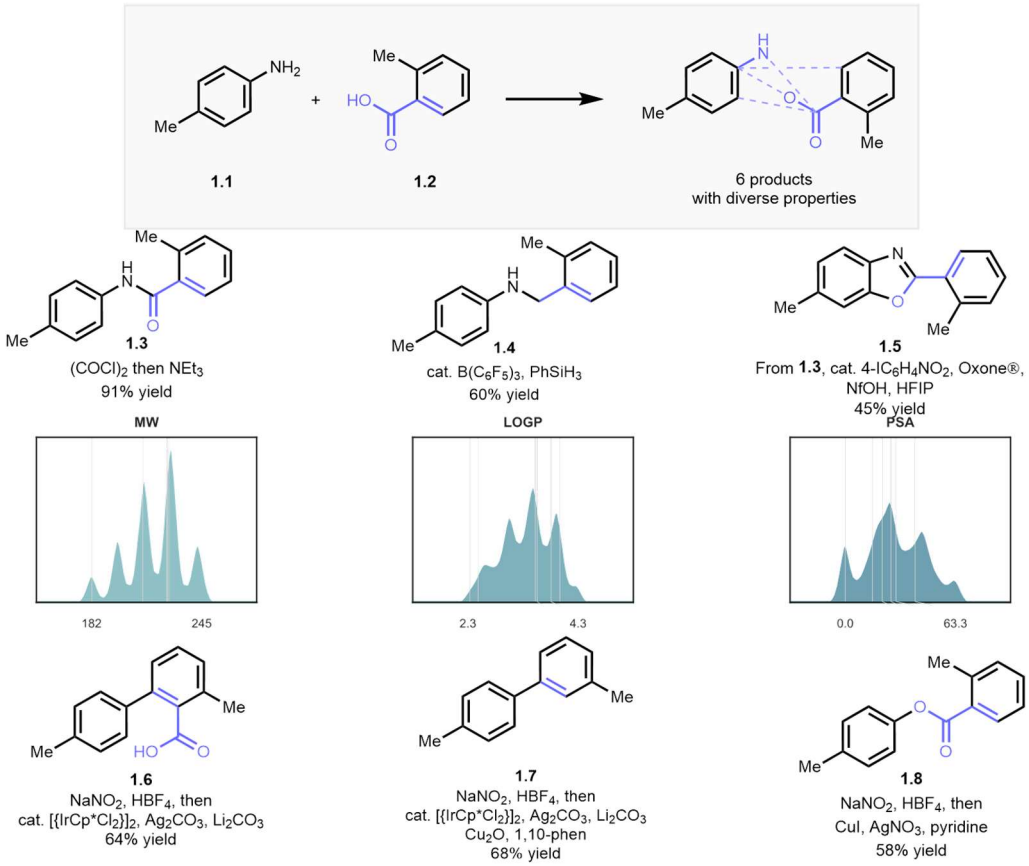

Figure 1.3 Six unique ways to couple amines and acids. Each molecule has a unique property footprint imparted by the transformation. Each vertical line in the Kernel Density Estimate plots represents one of the six molecules.

Several methods have been developed to unite amines and acids beyond the amide coupling. These include a reductive amination type reaction,[37,38] arylation via a diazonium,[39] deaminative esterification,[40–42] deaminative ketonylation,[43] decarboxylative-deaminative alkylation,[44–46] and decarboxylative sulfonamidation.[47] Current state of the art synthesis generally relies on activation groups to facilitate decarboxylation or deamination to generate reactive intermediates that can couple to each other. These are discussed below.

1.2.1 Amine Activation Methods

Given the free lone pair and basicity of amines, they are classically used as nucleophiles in chemical reactions. When presented with electrophiles such as alkyl halides, carbonyls, or

activated carboxylic acids, amines will react to produce alkylated products or amides. These reactions take advantage of the inherent properties of amines and as such are incredibly robust and hold an important place in modern drug discovery.[27,48] However, as described above there is immense interest and value in generating umpolung reactivity of amines. This involves converting amines into good leaving groups and is usually achieved through converting the nitrogen into a cation or via oxidation.

In principle, the simplest activating group for a basic amine would be a proton. The amine becomes positively charged and could leave as an ammonia derivative. However, since nearly all nucleophiles are basic and ammonium salts readily dissociate in solvent, this idea has not been implemented. Along similar lines, one of the first reported methods for activating amines was to exhaustively methylate them to form persistent ammonium cations. This was first reported by Hofmann where quaternary ammonium hydroxides were heated to generate alkenes from amines.[49] The Wenkert group first reported that aryl trimethylammonium salts could participate in metal catalyzed cross couplings. Trimethylammonium Salt **1.13** was reacted with phenylmagnesium bromide in a nickel catalyzed Kumada coupling to furnish **1.14** in 31% yield (Scheme 1.1, A).[50] The MacMillan group expanded the utility by demonstrating trimethylammonium salts could be coupled with aryl boronic acids with the use of a nickel 0 catalyst combined with a N-heterocyclic carbene ligand.[51] Using this method, biaryl **1.17** was synthesized from p-toluyl boronic acid and **1.16** in 83% yield (Scheme 1.1, C). Since then, the reactivities have been expanded to include coupling with amines[52], electrophiles[53], organozincs[54], and hydrogen[52]. By taking advantage of other metals such as palladium and copper, the scope of trimethylammonium salts has been expanded to include benzylic[52,55,56] and propargylic[57] substrates, but still excludes most aliphatic amines.

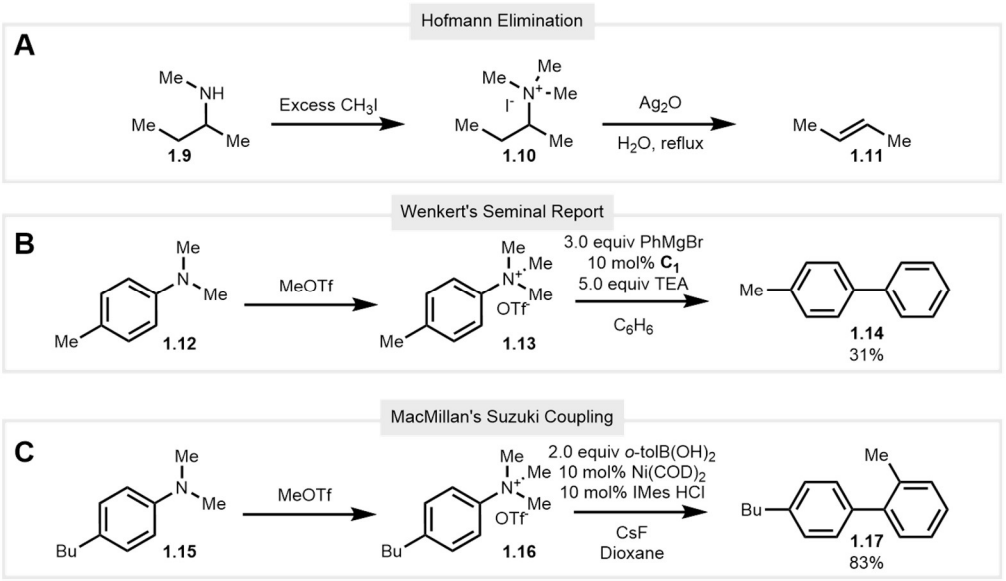

Scheme 1.1 Key Discoveries in the activation of amines as quaternary ammonium salts. A) The Hofmann Elimination. B) Wenkert's Seminal Report using them as substrates in the Kumada coupling demonstrates they can participate in transition metal reactions. C) MacMillan's use of them in a Suzuki coupling was the first demonstration of their utility.

Pyridiniums are another leaving group which amines can be converted to. By reacting a primary amine with a 1,5-dicarbonyl or equivalent, one can generate a stable pyridinium salt that can leave as a neutral aromatic ring. The most well-known examples of these are the triphenyl pyridinium salts reported by the Katritzky group in the late 1970s.[58] Easily prepared from a primary amine and 2,4,6-triphenylpyrylium tetrafluoroborate, Katritzky's group demonstrated these salts as well as more decorated versions could react with various nucleophiles such as azides,[59] halogens,[60,61] esters,[42] thioethers,[58] carbanions,[62] or amines[63] via an S_{N1}, S_{N2}, or radical mechanism depending on the nucleophile used (Scheme 1.2, A). Reported conditions often included pyrolysis of the substrate under vacuum which limited the utility and scope of these reactions. There was a massive resurgence in their popularity in 2017 when the Watson group demonstrated they could participate as electrophiles in nickel catalyzed cross couplings by coupling Katritzky salt **1.21** with *p*-chlorophenylboronic acid in 52% yield (Scheme 1.2, B).[64] This marked the first general solution to an alkyl amine deaminative cross coupling. Since then,

pyridinium salts have been used to cross couple amines and halides,[65–67] acyl fluorides,[43] alkyl zinc reagents,[68] aldehydes,[69] aromatics,[70] and alkenes.[71] All current mechanistic evidence points to a single electron reduction of the pyridinium salt to generate an alkyl radical which can then participate in transition metal couplings. These triphenyl pyridinium salts can also be reduced to an alkyl radical via photoredox catalysis.[72–77] The Cornella group has employed an unsubstituted pyrylium salt for the conversion of heteroaryl amines to amines, ethers, sulfones, thioethers[78], and chlorides[79] though this is believed to proceed through an S_{NAr} type mechanism. A limitation of this amine activation mode is the amine must be bound to a primary or secondary carbon. To accommodate tertiary carbons, the Rovis group has employed the use of trimethoxybenzaldehydes with photoredox catalysis.[80] With this strategy, they are able to couple 3° amine **1.23** with an electron deficient aryl bromide to give **1.25** (Scheme 1.2, C).

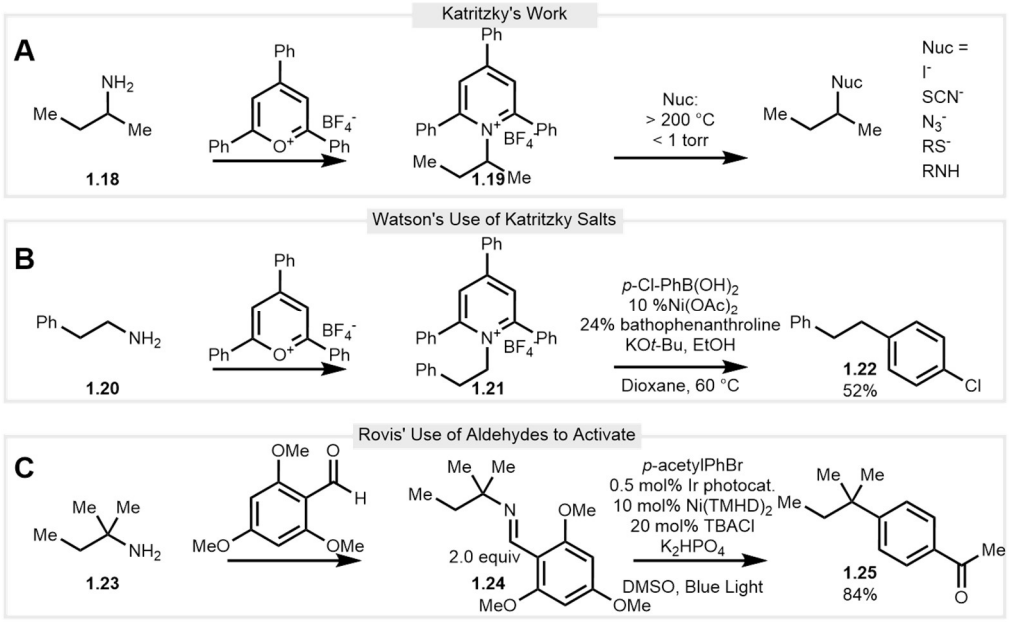

Scheme 1.2 Key discoveries in the activation of alkyl amines. A) Katritzky's pioneering work in the use of pyridiniums as activating groups. B) Watson's discovery they could participate in transition metal cross couplings. C) Rovis' Approach to activate sterically hindered alkyl amines. Ir photocat = $Ir(dF\text{-}CF_3\text{-}ppy)_2(dtbbpy)PF_6$, TMHD = 2,2,6,6-Tetramethyl-3,5-heptanedione, TBACl = tetrabutyl ammonium chloride

Another important strategy to activate amines is to oxidize them. The classic method to accomplish this for anilines is to form diazonium salts. Diazonium salts can be used to synthesize esters[40], biaryls[39], and via the Sandmeyer Reaction[81]: halides, nitriles, phenols, thioethers, and deaminated products. The corresponding alkyl diazoniums have seen fewer applications owing to their instability. Diazomethane is a well-known reagent for methylation of carboxylic acids but is also highly toxic and explosive. Larger alkyl diazo compounds that are not stabilized have few reported uses. In an analogous reaction to the Hofmann elimination, the Cope elimination relies on oxidation of a tertiary amine to its N-oxide followed by heating to form an alkene (Scheme 1.3, A). A similar concept is used to generate aminium cations which are useful intermediates for the formation of C–N bonds[82–84] or C–C bonds via an iminium.[85–87] The Cernak group has reported this strategy to achieve a one-pot synthesis of bromhexine (**1.29**) from **1.27** and **1.28** in a 41% yield. A recent major development in the field of oxidative deamination came from the Levin group. By using anomeric N,N-dialkoxyamides to generate isodiazene species *in-situ*, they were able to "delete" the nitrogen from amine **1.30** and replace it with a carbon–carbon bond.[88] The anomeric amides have also been used to replace amines in molecules with hydrogen, bromides, sulfides, phosphinates, and alcohols.[89] Notably, this activation mode seems quite general and can be used for alpha- primary and secondary amines as well as anilines and heteroaryl amines. The Lambert group has also reported a method to generate isodiazene species *in-situ* using *O*-nosylhydroxyamines (ONHA) and blue light. This strategy generates a less reactive intermediate, and they are able to achieve diastereoselectivity using amine **1.32** and ONHA **1.33** to synthesize **1.34** in 63% yield and >98:2 dr (Scheme 1.3, D).[90]

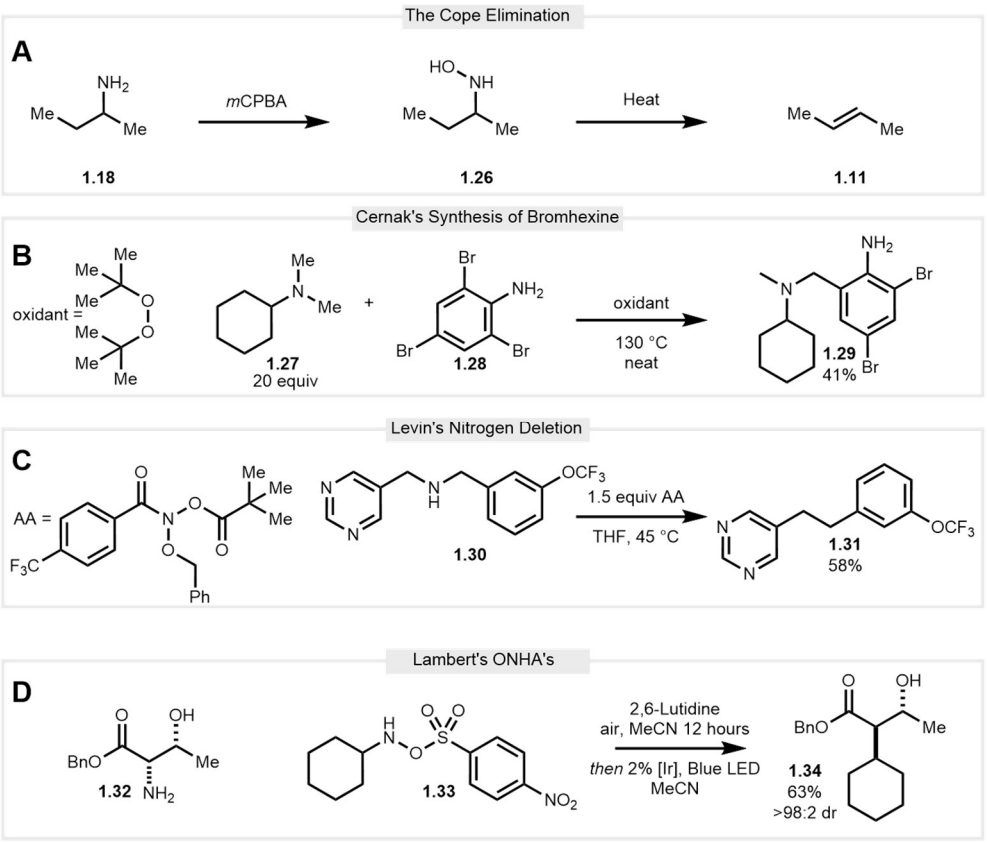

Scheme 1.3 Representative methods of amine activation by oxidation. A) The Cope elimination. B) a one-step synthesis of bromhexine via alpha oxidation to an iminium ion. C) deamination via *in-situ* formation of an isodiazene. D) The Lambert group's approach to isodiazene formation. [Ir] = $Ir(dCF_3ppy)_2dtbpyPF_6$

1.2.2 Carboxylic Acid Activation Methods

There have been several activation modes beyond the methods described above to activate carboxylic acids. While uronium and imide-based agents activate acids towards nucleophilic attack, taking advantage of altering modes of reactivity requires other activation modes. Some of the most powerful of these are decarboxylative cross couplings. These methodologies have emerged as robust ways to form carbon–carbon[91] and carbon–hetero atom bond formation.[92] The use of sp^3 acids has focused on activation methods that involve generating alkyl radicals which can participate in coupling reactions.[91] The corresponding aryl radical however forms at a much slower rate than hydrogen atom transfer (HAT),[93] and as such aryl

carboxylic acids until recently,[94,95] were generally decarboxylated via two electron methods.[96] Given the differences in approach to decarboxylation these two will be treated separately.

1.2.2.1 Aliphatic Decarboxylation

A major strategy to generate alkyl radicals from carboxylic acids is the use of redox active esters. The use of these, specifically thiohydroxamidate esters, were pioneered by the Barton group.[97] This group reported activating carboxylic acids via the acid chloride and sodium salt of N-hydroxypyridine-2-thione which was subsequently treated with tributyl tin hydride to reductively decarboxylate. Key to the success of this reaction is the homolysis of the N–O bond which generates a carboxy radical that readily leaves as CO_2 to generate an alkyl radical.[97] In the seminal report, it was demonstrated that abietic acid was readily decarboxylated in 52% yield to give the corresponding hydrodecarboxy derivative **1.37** (Scheme 1.4, A). Soon after, the Barton group also reported that by replacing tributyl tin hydride with carbon tetrachloride or bromotrichloromethane as a solvent, one could exchange hydrodecarboxylation with halodecarboxylation.[98] These alkyl radicals can also participate in Giese type reactions.[99] In 2016, the Baran group reported that Barton esters could readily be reduced by nickel (II) complexes to generate the same alkyl radical that could be intercepted by the nickel complex and coupled to an aryl zinc species. Subsequent optimization revealed N-hydroxyphthalimide (NHPI), which had previously only been reported to reduce with photocatalysts[100,101] to be the optimal redox active ester in their coupling. This led them to decarboxylatively couple **1.38** to phenylzinc chloride to give **1.39** in 92% yield (Scheme 1.4, B). Concomitantly the Weix group reported NHPI esters could be reductively coupled to aryl iodides using a similar nickel catalyst and zinc powder as the terminal reductant.[102] They demonstrated acid **1.40** coupling to iodobenzene in 87% yield (Scheme 1.4, C). Since this initial report, NHPI esters have been used

to forge C–C bonds with alkyl zincs,[103] aryl boronic acids,[104] vinyl halides,[105] alkenes,[106] pyridinium salts[46] and others as well as carbon heteroatom bonds.[107]

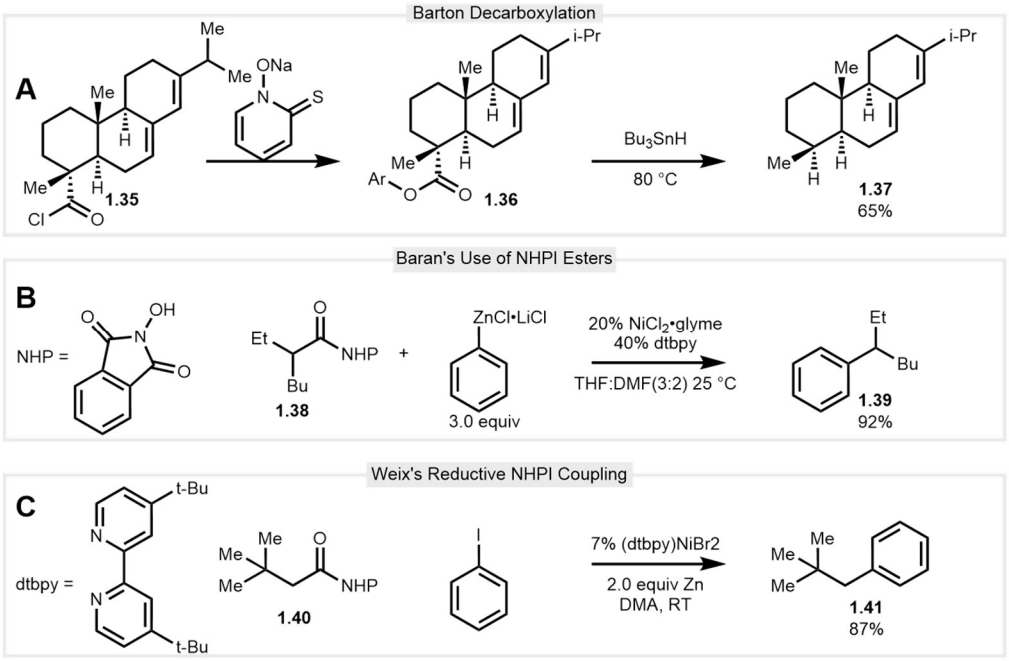

Scheme 1.4 Representative methods of carboxylic acid activation with redox active esters. A) The Barton Decarboxylation. B) The Baran group's use of NHPI esters in nickel catalyzed redox neutral cross couplings with aryl zincs. C) The Weix group's use of NHPI esters in nickel catalyzed reductive couplings.

While effective, pre-activation of carboxylic coupling partners adds synthetic steps and is often laborious if purification is required. As such, it would be ideal to have methods to decarboxylate carboxylic acids that do not rely on isolated activating groups. Minisci pioneered using an alkyl radical generated from a carboxylic acid in a seminal report in 1971.[108] By combining silver nitrate and ammonium persulfate, pivalic acid was oxidatively decarboxylated to form a tert-butyl radical that added into a protonated pyridine, giving a mixture of 2 & 4 alkylated products in 52% yield. Developments have been made in this area, but fundamentally there is still a regioselectivity issue. Another major development in activation free decarboxylative coupling came out of the MacMillan and Doyle groups when they demonstrated alkyl radicals generated photo-catalytically could be trapped by nickel catalysts and coupled to

aryl halides. Alpha heteroatom containing acids such as boc proline (**1.45**) were coupled to aryl halides to give benzylic amines and ethers. In one example, **1.45** was coupled to *p*-iodotoluene to give **1.46** in 78% yield using an iridium photocatalyst, a nickel II salt, and a bipyridine ligand (Scheme 1.5, B). This strategy has been used extensively to generate varying bond types.[109]

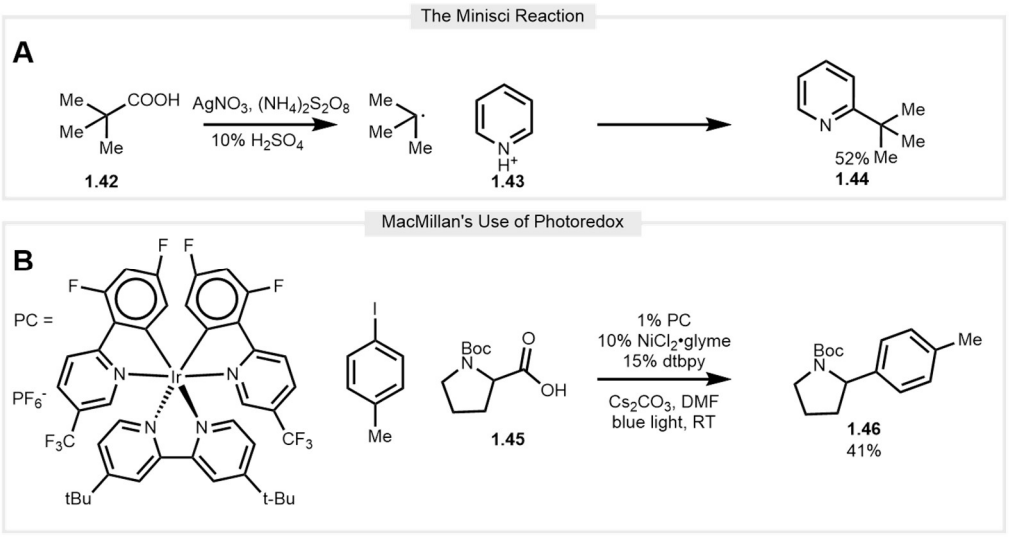

Scheme 1.5 Representative methods of decarboxylative cross coupling without activating groups. A) The Minisci Reaction. B) The MacMillan group's merging of photocatalysis and nickel catalysis for decarboxylative cross coupling.

1.2.2.2 Aromatic Decarboxylation

The first practical aryl carboxylic acid coupling was reported by the Gooßen group, wherein aryl carboxylic acids were decarboxylated using a copper catalyst and trapped with a palladium catalyst to couple with aryl bromides.[110] Acid **1.47** was coupled to 4-chlorobromobenzene at 160 °C in 99% yield. This temperature can be lowered to 130 °C by using a silver salt instead of a copper salt to facilitate the decarboxylation.[111] The Gooßen group demonstrated acid **1.47** could also be coupled to an aryl triflate to give product **1.48** in 87% yield using this strategy (Scheme 1.6, A). A key limitation to this methodology is the so called "ortho effect" where the aryl acids must have a highly electron donating or withdrawing group, or heteroatom ortho to the acid. The scope of this style of reaction was greatly expanded by the

Sanford group by activating the carboxylic acid as its acyl fluoride. Probenecid (**1.49**) was activated as its acyl fluoride *in-situ* and coupled with p-fluorophenylboronic acid in the presence of a ligated nickel (0) catalyst to give **1.50** in 82% yield (Scheme 1.6, B). Other strategies used to facilitate the decarboxylation for cross coupling include the use of twisted amides[45,112], pyridyl esters[44], and aryl esters[113], though all of these methods require elevated temperatures. A breakthrough wherein aryl carboxylic acids could generally be decarboxylated at room temperature came independently from the Ritter[95] and MacMillan[94] groups. They took advantage of ligand to metal charge transfer (LMCT) between a copper salt and the carboxylate to generate a carboxy radical that when decarboxylated can either react with atom transfer reagents[47,94] or be trapped by copper to form an metalated intermediate that can participate in coupling reactions.[94,95,114] To overcome HAT with the solvent, they use acetonitrile which mitigates the protodecarboxylation pathway. In their initial report, the Ritter group uses copper sacrificially to synthesize aryl fluoride **1.52** in 70% yield from the corresponding acid **1.51**. The use of superstoichiometric copper is due to the copper (I) species no longer being able to participate in LMCT after reductive elimination. To overcome this, the MacMillan group uses an N-fluoro collodinium salt as an oxidant to regenerate the active copper to species. Using this strategy, they generate aryl chloride **1.53** from **1.51** in 52% yield (Scheme 1.6, C).

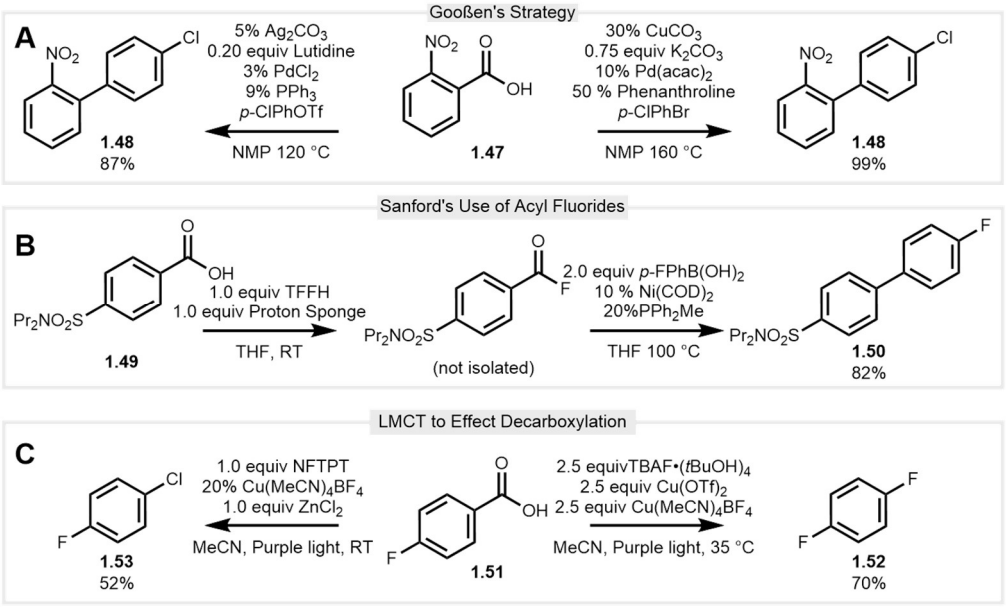

Scheme 1.6 Representative methods of amine activation by oxidation. A) The Cope elimination. B) a one-step synthesis of bromhexine via alpha oxidation to an iminium ion. C) deamination via *in-situ* formation of an isodiazene.

1.3 Applications in Drug Discovery

While a building block centered approach is a tried-and-true strategy in drug discovery,[115,116] it necessarily optimizes the molecule by altering its periphery. This is convenient at an early stage when trying to understand structure-activity relationships (SAR). However, as binding of a pharmacophore becomes optimized and focus shifts toward optimization of physicochemical properties, large changes in the periphery of a molecule become less tolerated. At this stage, edits to the core of the molecule are often explored, but generally require multistep resynthesis to access.[117] By simply shifting the transformations used to unite the building blocks, a chemist can access a variety of derivatives from late stage (often precious) intermediates. Each of these derivatives will have a unique set of properties which will affect the final function of the molecule. Figure 1.4 is a representation of this as a cartoon.

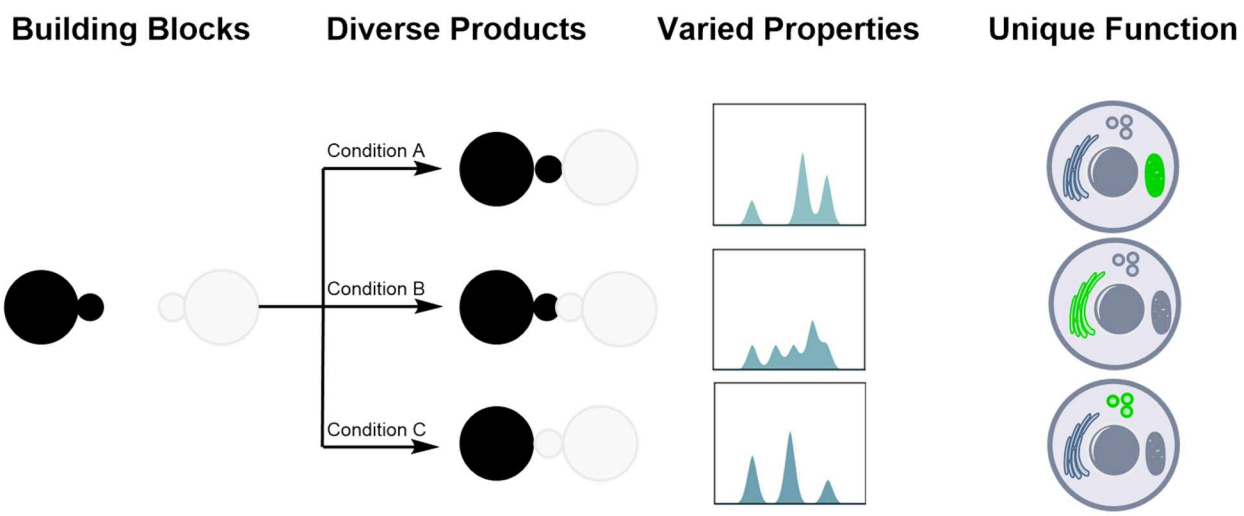

Figure 1.4 Cartoon representation of a transformations-based approach. The large black and grey balls represent building blocks and the small balls functional handles. When the two building blocks are subjected to different reaction conditions, unique products are generated that each have a unique property profile. This profile imparts varied functions of the molecule, in this case it is cellular distribution.

This is further exemplified in work from the Ciulli group where it was shown that in Proteolysis Targeting Chimeras (PROTACs), exchanging an amide bond for an ester increased the permeability of the overall molecule through the removal of a hydrogen bond donor.[118] However this required resynthesis of the intermediate material. It was shown that PROTAC **1.54** gained a 10-fold increase in a parallel artificial membrane permeability assay (PAMPA), and a 1.5 fold increase in degradation potency when the amide bond uniting the protein binder and the linker was replaced with an ester (scheme 1.7). This strategy has also been employed in cyclic peptides.[119] Again, a large boost in permeability was seen, but the synthesis required the use of alpha hydroxy derivatives of amino acids which required several steps to synthesize.

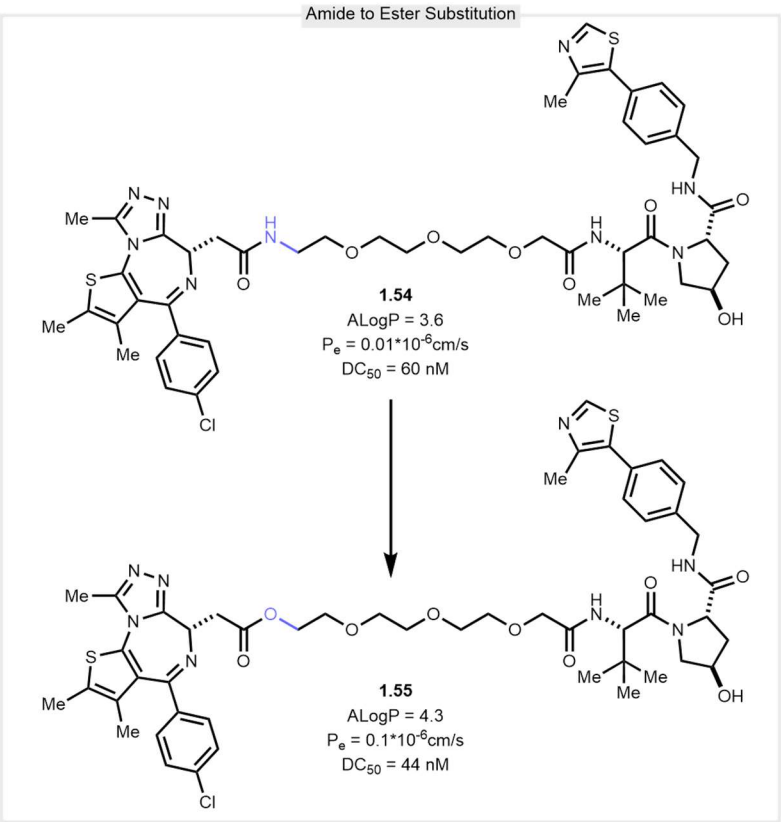

Scheme 1.7 Amide to ester substitution increases both permeability and DC50. Presumably this effect is through an increase in permeability from removing the hydrogen bond donor.

The strategy of coupling common building blocks in unique ways has also been applied at earlier stages in the drug discovery process. The Nelson group has relied on this strategy in what has been dubbed "activity directed synthesis" to develop novel androgen receptor agonists.[25] Diazo compound **1.56** was subjected to various rhodium catalysts and they were able to generate a large variety of products. By screening the activity of each crude mixture, they found that the solvent and catalyst choice varied the ratio of active to inactive products (Scheme 1.8, A). When Rhodium salts containing a non-carboxylate counterion were screened, all activity was lost, suggesting the active compound was not formed (Scheme 1.8, B). Through several rounds of screening and scaleup, they determined that the most active compound in the mixture

was **1.58** with an EC_{50} of 340 nM (Scheme 1.8, C). This close interplay between choice of catalyst and functional outcome of the molecule warrants further study.

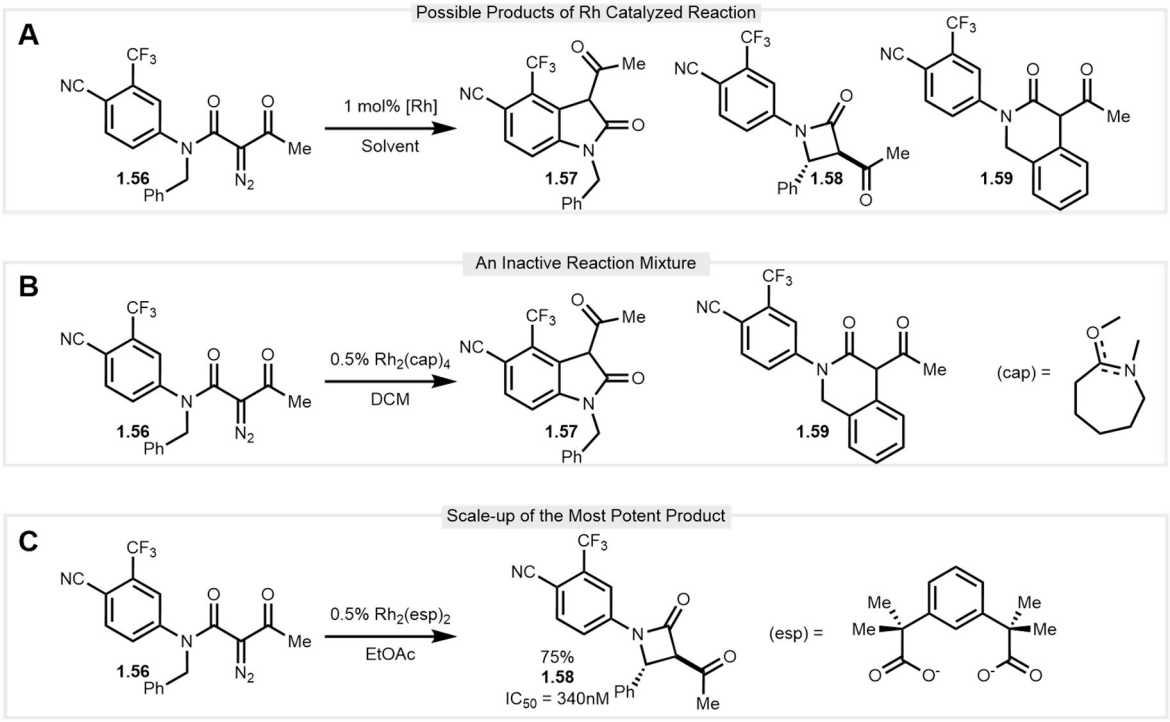

Scheme 1.8 The Nelson group's use of activity directed synthesis to discover novel androgen receptor agonists. A) An array of rhodium catalysts and solvents was executed to generate a diverse array of products with potential biological activity. Not all possible products are listed. B) By changing the catalyst to a non-carboxylate anion, the bioactive compound was no longer formed in appreciable yields. C) The highest yielding conditions for **1.58** were used to scale up and isolate it in 75% yield. Cap = caprolactam, esp = α,α,α′,α′-Tetramethyl-1,3-benzenedipropionic acid.

1.4 High-Throughput Experimentation (HTE) and the Importance of Training Future Scientists.

Using AI and machine learning will lead to a more holistic understanding of chemistry as a system and will require the generation of vast amounts of data. Whereas a chemist would traditionally run reactions in flasks or vials in a serial manner, High-Throughput Experimentation (HTE) is a technique that allows for the parallelization of chemical synthesis. This is accomplished by setting up arrays of small glass shell vials in metal heating blocks (typically 24 or 96 wells) or using microtiter plates (typically 384 or 1536 wells). The chemist is

then able to design a grid to explore the interplay of combinations of reagents either for the sake of optimizing reaction conditions[21] or to generate large libraries of molecules[18]. The process of setting up these large numbers of reactions is greatly enhanced by the preparation of stock solutions. This allows for a single weighing operation per reagent that can be dosed into many reactions as opposed to a single weighing operation per reagent per reaction. In addition to saving time, HTE also saves precious material with a single well containing on the order of micrograms to a few milligrams of material. This practice allows dozens to thousands of data points to be generated with the amount of material used to generate a single data point in a traditional round bottom flask reaction.[20]

While High-Throughput Screening in biology has been in practice since at least the early 1980's[120], currently consistently have workflows run in 3456 plates and is common practice throughout academic labs across the world, HTE in chemistry has lagged behind. This may be due to the engineering challenges associated with running chemistry in a high-throughput format. While biological experiments are typically homogenous solutions in water/DMSO mixtures conducted at or near room temperature in air, the heterogeneity in conditions for chemical reactions complicates matters. For example, reactions are run in a variety of solvents; the glass shell vials used in 24 and 96 well plates are generally resilient to solvent. However, the polypropylene used in 384 and 1536 well plates is incompatible with many solvents, especially at elevated temperature. Further, many reactions require an inert atmosphere to perform and are run at cryogenic temperatures while others are run well above boiling. The small volume of solvent used coupled with the volatility of many organic solvents can lead to evaporation issues. As well, the broad diversity of reagents used in synthesis means homogenous solutions are not

always possible. Taken together, careful consideration must be put into the types of chemical reactions that are compatible with HTE, or engineering solutions must be implemented.

1.4.1 Hardware implementation in HTE

To address the challenges associated with running chemistry in a miniaturized format, several solutions have been implemented with different strategies for 24 and 96 wells compared to 384 and 1536 wells. 24 and 96 well aluminum heat blocks that hold glass vials are commercially available (Figure 2). These shell vials are chemically resistant and the 24 well blocks fit on a hot plate which allows for heating, cooling, and stirring. 96 well plates, which are standard SBS dimensions, do not evenly stir on a hot plate and as such commercial tumble stirrers with optional heating attachments have been developed. 384 and 1536 plates are available in glass but are prohibitively expensive. Cyclic olefin copolymer (COC) plates present alternative chemical stability to traditional polypropylene and are more heat resistant.

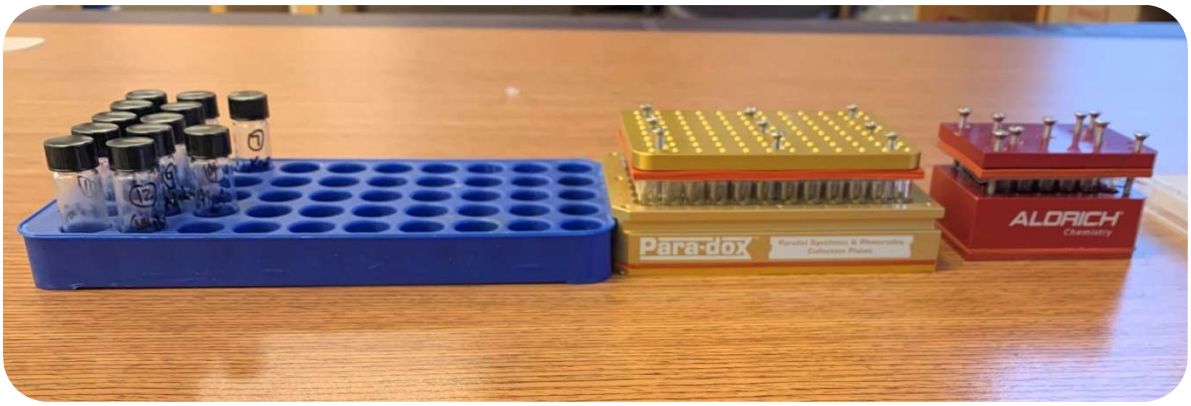

Figure 1.5 An example of 24 and 96 well aluminum heating blocks containing glass shell vials. The stock solutions are prepared in one-dram vials and dosed into the corresponding wells.

Transfer of reagents from stock solutions in a consistent manner also requires tools. Perhaps the most accessible of these is the implementation of single and multichannel micropipettes. They are affordable, common in most labs, and facilitate the dosing of stock solutions into the desired wells. Liquid handling robots such as the TTP Mosquito, Waters Andrew Alliance, Beckman

Coulter Echo, Opentrons OT2, and Unchained Labs Junior have been implemented to reduce the strain imparted by excessive pipetting, as well as provide consistent dosing in larger 384 or 1536 well formats. Many of these robots are unable to handle heterogeneous solutions. To overcome this, stir plates and wide bore tips have been used to slurry load, or solid handling robots have been deployed. Each of these platforms can be assembled in an inert atmosphere glovebox to overcome air and water sensitivities.

Solutions have been developed to address unique reaction conditions explored within chemistry. These include plates with space for light,[121,122] the use of flow,[123] or the use of microfluidics[123] to perform photoredox in HTE, parallelized electrodes for electrochemistry,[124,125] pressurized reactors for hydrogenations[126,127] or carbonylations.[128] Analytical challenges are also apparent beyond reaction setup. While it is practical to run NMR to characterize the products of a single reaction, analyzing each product of a 24 well screen would take weeks. Even crude NMR analysis of reaction mixtures becomes unmanageable beyond 96 experiments. The most commonly employed and arguably the most information rich technique employed is ultra performance liquid chromatography mass spectrometry (UPLC-MS). With modern instruments it is possible to gather data on product formation as well as side products and gain insight into the reaction in as little as 30 seconds per well.[21] By bypassing the autosampler in favor of microfluidic droplet injections and using a shorter column, this can be reduced to ~1 second per sample.[129] For 24 and 96 well plates, gas-chromatography-mass spectrometry (GC-MS) instruments have also been used and are typically more accessible for academic labs. An even more accessible method is to analyze by thin layer chromatography.[130] Desorption electrospray ionization (DESI) mass spectrometry[131,132] and matrix-assisted LASER Desorption Ionization (MALDI) coupled to time of flight (TOF) MS[133] have been used due to

their rapid throughput of less than one second per sample, but they do not provide as much quantitative information as other methods. While tremendous progress has been made in recent years, there is still room for improvement to speed up throughput while maintaining information density in plate analysis.

1.4.2 Software Implementation in HTE

Design of experiment is a critical step in effective data collection. Single experiments can easily be planned and recorded using a laboratory notebook, but experimental arrays require some form of tabulation to manage the design and record keeping. Microsoft Excel is capable of performing these functions, particularly in 24 and 96 well format, but requires macros that potentially need to be rewritten for every screen depending on the needs of the chemist. Further, when trying to design 384 and 1536 well screens, Excel quickly becomes unmanageable. As such, several commercial software packages have been developed including ACD Labs Katalyst and Unchained Labs LEA. To process the data, commercial software such as Virscidian, MNova MSChroms, and Katalyst have been implemented as well as freeware such as MZMine and several python packages.[134–136]

Our lab has developed a software called Phactor™ which functions to design experiments as well as process and store data.[137] Phactor™ is integrated into each step of a HTE experiment, including array design, script generation for robot assisted dosing, data visualization, and data storage. A typical workflow begins with the chemist deciding the type of reaction they would like to run and deciding on the variables or "phactors" they would like to screen. For example, a 96 well array could be composed of 4 phactors: 4 catalysts, 6 ligands, 2 additives, and 2 solvents. The chemist would then load each of these variables into Phactor. Array design speed is increased by full incorporation of our in-house inventory which is searchable by name or CAS

number. Phactor is then able to design the array and output a recipe for the screen. The chemist then runs the screen either manually or with the assistance of robotics, analyzes the reaction output via UPLC-MS, processes it with Virscidian, and loads the processed data back into Phactor for data visualization. This workflow is used extensively throughout this body of work.

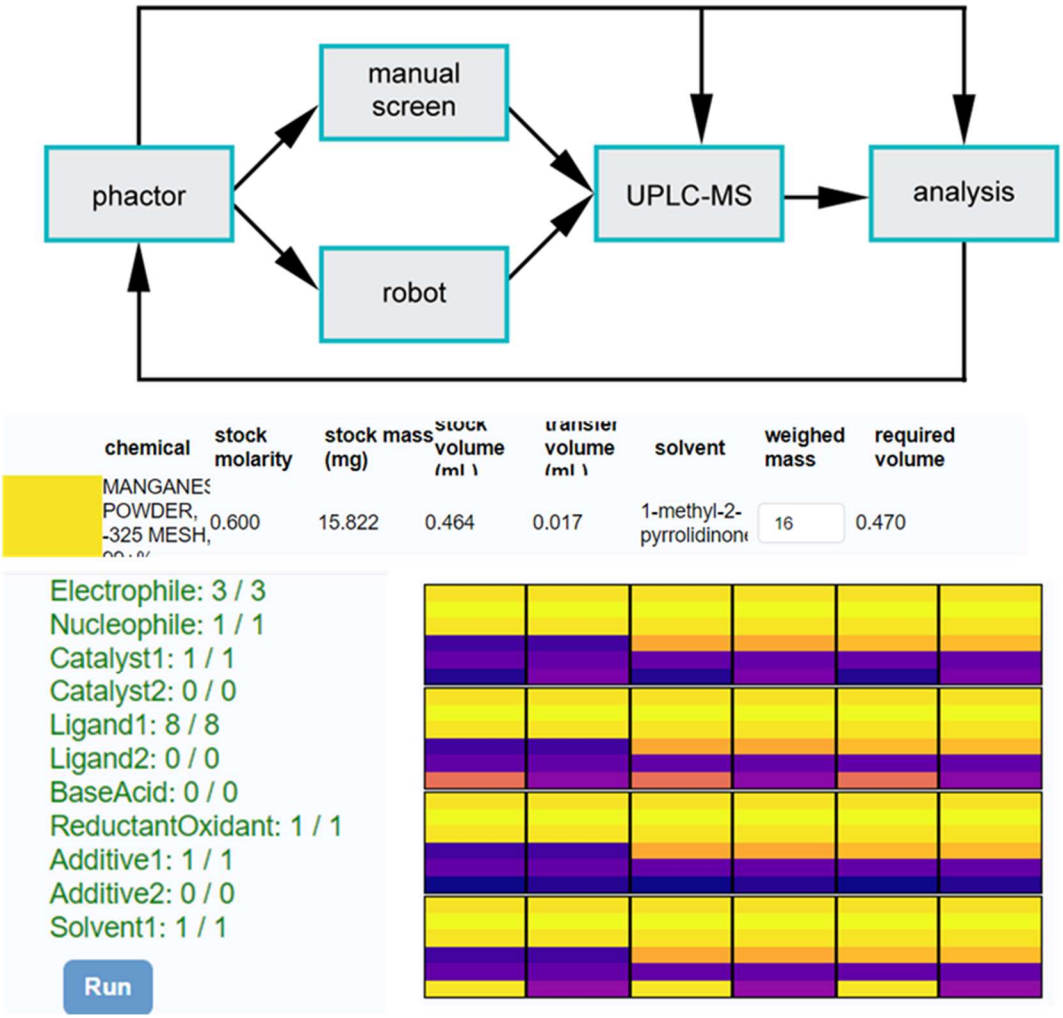

Figure 1.6 The general HTE workflow in our lab. Phactor is incorporated into every step of the process. Once the "phactors" of the screen are planned out, Phactor is able to generate an appropriate array as well as a recipe to perform it.

1.4.3 Training the Next Generation of Chemists

While HTE has become standard practice in industry, its uptake has been much slower in academic labs.[138] While some of this may be due to a cost barrier to entry, certainly another

piece is a lack of training. Traditional training in chemistry does not include a foundation in coding or data management. As such, adopting HTE practices that necessarily generate large amounts of data can be a daunting task for a PhD student, especially when there is an absence of senior members to look to for assistance. As big data becomes increasingly involved in the chemical sciences, there will be an ever-increasing need for the next generation of scientists to incorporate coding and data management skills into their training.[12,139]

There has been some incorporation of this idea in recent years. The University of Washington has added a data science option to its chemistry PhD program. Several other universities have also begun to implement data science education initiatives into their undergraduate curriculum.[140–144] Perhaps the most comprehensive approach comes from Imperial College of London where an entire PhD program has been created centered around automation in synthesis. The training incorporates the use of Unchained Labs technology to solve synthetic problems.[145] Programs of this type will likely become increasingly common in the future as well as a more robust incorporation of automation and coding training in the undergraduate curriculum.

1.5 References

(1) Gerald M. Weinberg. *An Introduction to General Systems Thinking*; Dorset House, 2001.

(2) Tavassoly, I.; Goldfarb, J.; Iyengar, R. Systems Biology Primer: The Basic Methods and Approaches. *Essays Biochem.* **2018**, *62* (4), 487–500. https://doi.org/10.1042/EBC20180003.

(3) Whitesides, G. M.; Grzybowski, B. Self-Assembly at All Scales. *Science* **2002**, *295* (5564), 2418–2421. https://doi.org/10.1126/science.1070821.

(4) Li, J.; Nowak, P.; Otto, S. Dynamic Combinatorial Libraries: From Exploring Molecular Recognition to Systems Chemistry. *J. Am. Chem. Soc.* **2013**, *135* (25), 9222–9239. https://doi.org/10.1021/ja402586c.

(5) Verma, A.; Rotello, V. M. Surface Recognition of Biomacromolecules Using Nanoparticle Receptors. *Chem. Commun.* **2005**, No. 3, 303–312. https://doi.org/10.1039/B410889B.

(6) Gentili, P. L. The Fuzziness in Molecular, Supramolecular, and Systems Chemistry. *Molecules* **2020**, *25* (16). https://doi.org/10.3390/molecules25163634.

(7) Ashkenasy, G.; Hermans, T. M.; Otto, S.; Taylor, A. F. Systems Chemistry. *Chem. Soc. Rev.* **2017**, *46* (9), 2543–2554. https://doi.org/10.1039/C7CS00117G.

(8) Stankiewicz, J.; Eckardt, L. H. Chembiogenesis 2005 and Systems Chemistry Workshop. *Angew. Chem. Int. Ed.* **2006**, *45* (3), 342–344. https://doi.org/10.1002/anie.200504139.

(9) Kindermann, M.; Stahl, I.; Reimold, M.; Pankau, W. M.; von Kiedrowski, G. Systems Chemistry: Kinetic and Computational Analysis of a Nearly Exponential Organic Replicator. *Angew. Chem. Int. Ed.* **2005**, *44* (41), 6750–6755. https://doi.org/10.1002/anie.200501527.

(10) Ludlow, R. F.; Otto, S. Systems Chemistry. *Chem. Soc. Rev.* **2008**, *37* (1), 101–108. https://doi.org/10.1039/B611921M.

(11) Cernak, T. Synthesis in the Chemical Space Age. *Chem* **2016**, *1* (1), 6–9. https://doi.org/10.1016/j.chempr.2016.06.002.

(12) Kearnes, S. M.; Maser, M. R.; Wleklinski, M.; Kast, A.; Doyle, A. G.; Dreher, S. D.; Hawkins, J. M.; Jensen, K. F.; Coley, C. W. The Open Reaction Database. *J. Am. Chem. Soc.* **2021**, *143* (45), 18820–18826. https://doi.org/10.1021/jacs.1c09820.

(13) Gaulton, A.; Hersey, A.; Nowotka, M.; Bento, A. P.; Chambers, J.; Mendez, D.; Mutowo, P.; Atkinson, F.; Bellis, L. J.; Cibrián-Uhalte, E.; Davies, M.; Dedman, N.; Karlsson, A.; Magariños, M. P.; Overington, J. P.; Papadatos, G.; Smit, I.; Leach, A. R. The ChEMBL Database in 2017. *Nucleic Acids Res.* **2017**, *45* (D1), D945–D954. https://doi.org/10.1093/nar/gkw1074.

(14) Mahjour, B.; Shen, Y.; Liu, W.; Cernak, T. A Map of the Amine–Carboxylic Acid Coupling System. *Nature* **2020**, *580* (7801), 71–75. https://doi.org/10.1038/s41586-020-2142-y.

(15) He, J.; Hamann, L. G.; Davies, H. M. L.; Beckwith, R. E. J. Late-Stage C–H Functionalization of Complex Alkaloids and Drug Molecules via Intermolecular Rhodium-Carbenoid Insertion. *Nat. Commun.* **2015**, *6* (1), 5943. https://doi.org/10.1038/ncomms6943.

(16) Cernak, T.; Gesmundo, N. J.; Dykstra, K.; Yu, Y.; Wu, Z.; Shi, Z.-C.; Vachal, P.; Sperbeck, D.; He, S.; Murphy, B. A.; Sonatore, L.; Williams, S.; Madeira, M.; Verras, A.; Reiter, M.; Lee, C. H.; Cuff, J.; Sherer, E. C.; Kuethe, J.; Goble, S.; Perrotto, N.; Pinto, S.; Shen, D.-M.; Nargund, R.; Balkovec, J.; DeVita, R. J.; Dreher, S. D. Microscale High-Throughput Experimentation as an Enabling Technology in Drug Discovery: Application in the Discovery of

(Piperidinyl)Pyridinyl-1H-Benzimidazole Diacylglycerol Acyltransferase 1 Inhibitors. *J. Med. Chem.* **2017**, *60* (9), 3594–3605. https://doi.org/10.1021/acs.jmedchem.6b01543.

(17) Krska, S. W.; DiRocco, D. A.; Dreher, S. D.; Shevlin, M. The Evolution of Chemical High-Throughput Experimentation To Address Challenging Problems in Pharmaceutical Synthesis. *Acc. Chem. Res.* **2017**, *50* (12), 2976–2985. https://doi.org/10.1021/acs.accounts.7b00428.

(18) Shevlin, M. Practical High-Throughput Experimentation for Chemists. *ACS Med. Chem. Lett.* **2017**, *8* (6), 601–607. https://doi.org/10.1021/acsmedchemlett.7b00165.

(19) Schmink, J. R.; Bellomo, A.; Berritt, S. Scientist-Led High-Throughput Experimentation (HTE) and Its Utility in Academia and Industry. *Aldrichimica Acta* **2013**, *46*, 71–80.

(20) Wong, H.; Cernak, T. Reaction Miniaturization in Eco-Friendly Solvents. *Pharm. Green Process. Technol.* **2018**, *11*, 91–98. https://doi.org/10.1016/j.cogsc.2018.06.001.

(21) Mennen, S. M.; Alhambra, C.; Allen, C. L.; Barberis, M.; Berritt, S.; Brandt, T. A.; Campbell, A. D.; Castañón, J.; Cherney, A. H.; Christensen, M.; Damon, D. B.; Eugenio de Diego, J.; García-Cerrada, S.; García-Losada, P.; Haro, R.; Janey, J.; Leitch, D. C.; Li, L.; Liu, F.; Lobben, P. C.; MacMillan, D. W. C.; Magano, J.; McInturff, E.; Monfette, S.; Post, R. J.; Schultz, D.; Sitter, B. J.; Stevens, J. M.; Strambeanu, I. I.; Twilton, J.; Wang, K.; Zajac, M. A. The Evolution of High-Throughput Experimentation in Pharmaceutical Development and Perspectives on the Future. *Org. Process Res. Dev.* **2019**, *23* (6), 1213–1242. https://doi.org/10.1021/acs.oprd.9b00140.

(22) Allen, C. L.; Leitch, D. C.; Anson, M. S.; Zajac, M. A. The Power and Accessibility of High-Throughput Methods for Catalysis Research. *Nat. Catal.* **2019**, *2* (1), 2–4. https://doi.org/10.1038/s41929-018-0220-4.

(23) Muratov, E. N.; Bajorath, J.; Sheridan, R. P.; Tetko, I. V.; Filimonov, D.; Poroikov, V.; Oprea, T. I.; Baskin, I. I.; Varnek, A.; Roitberg, A.; Isayev, O.; Curtalolo, S.; Fourches, D.; Cohen, Y.; Aspuru-Guzik, A.; Winkler, D. A.; Agrafiotis, D.; Cherkasov, A.; Tropsha, A. QSAR without Borders. *Chem. Soc. Rev.* **2020**, *49* (11), 3525–3564. https://doi.org/10.1039/D0CS00098A.

(24) Taylor, C. J.; Pomberger, A.; Felton, K. C.; Grainger, R.; Barecka, M.; Chamberlain, T. W.; Bourne, R. A.; Johnson, C. N.; Lapkin, A. A. A Brief Introduction to Chemical Reaction Optimization. *Chem. Rev.* **2023**, *123* (6), 3089–3126. https://doi.org/10.1021/acs.chemrev.2c00798.

(25) Karageorgis, G.; Warriner, S.; Nelson, A. Efficient Discovery of Bioactive Scaffolds by Activity-Directed Synthesis. *Nat. Chem.* **2014**, *6* (10), 872–876. https://doi.org/10.1038/nchem.2034.

(26) Burke, M. D.; Schreiber, S. L. A Planning Strategy for Diversity-Oriented Synthesis. *Angew. Chem. Int. Ed.* **2004**, *43* (1), 46–58. https://doi.org/10.1002/anie.200300626.

(27) Boström, J.; Brown, D. G.; Young, R. J.; Keserü, G. M. Expanding the Medicinal Chemistry Synthetic Toolbox. *Nat. Rev. Drug Discov.* **2018**, *17* (10), 709–727. https://doi.org/10.1038/nrd.2018.116.

(28) Curtius, Th. Ueber Die Einwirkung von Chlorbenzoyl Auf Glycocollsilber. *J. Für Prakt. Chem.* **1881**, *24* (1), 239–240. https://doi.org/10.1002/prac.18810240120.

(29) Baumann, E. Ueber Eine Einfache Methode Der Darstellung von Benzoësäureäthern. *Berichte Dtsch. Chem. Ges.* **1886**, *19* (2), 3218–3222. https://doi.org/10.1002/cber.188601902348.

(30) Schotten, C. Ueber Die Oxydation Des Piperidins. *Berichte Dtsch. Chem. Ges.* **1884**, *17* (2), 2544–2547. https://doi.org/10.1002/cber.188401702178.

(31) Sheehan, J. C.; Hess, G. P. A New Method of Forming Peptide Bonds. *J. Am. Chem. Soc.* **1955**, *77* (4), 1067–1068. https://doi.org/10.1021/ja01609a099.

(32) König, W.; Geiger, R. Eine Neue Methode Zur Synthese von Peptiden: Aktivierung Der Carboxylgruppe Mit Dicyclohexylcarbodiimid Unter Zusatz von 1-Hydroxy-Benzotriazolen. *Chem. Ber.* **1970**, *103* (3), 788–798. https://doi.org/10.1002/cber.19701030319.

(33) Carpino, L. A. 1-Hydroxy-7-Azabenzotriazole. An Efficient Peptide Coupling Additive. *J. Am. Chem. Soc.* **1993**, *115* (10), 4397–4398. https://doi.org/10.1021/ja00063a082.

(34) Joullie, M. M.; Lassen, K. M. Evolution of Amide Bond Formation. *ARKIVOC* **2010**, *2010* (8), 189–250. https://doi.org/10.3998/ark.5550190.0011.816.

(35) Valeur, E.; Bradley, M. Amide Bond Formation: Beyond the Myth of Coupling Reagents. *Chem. Soc. Rev.* **2009**, *38* (2), 606–631. https://doi.org/10.1039/B701677H.

(36) Zhang, R.; Mahjour, B.; Cernak, T. Exploring the Combinatorial Explosion of Amine–Acid Reaction Space via Graph Editing. *ChemRxiv* **2022**. https://doi.org/10.26434/chemrxiv-2022-917k5.

(37) Fu, M.-C.; Shang, R.; Cheng, W.-M.; Fu, Y. Boron-Catalyzed N-Alkylation of Amines Using Carboxylic Acids. *Angew. Chem. Int. Ed.* **2015**, *54* (31), 9042–9046. https://doi.org/10.1002/anie.201503879.

(38) Sorribes, I.; Junge, K.; Beller, M. Direct Catalytic N-Alkylation of Amines with Carboxylic Acids. *J. Am. Chem. Soc.* **2014**, *136* (40), 14314–14319. https://doi.org/10.1021/ja5093612.

(39) Huang, L.; Hackenberger, D.; Gooßen, L. J. Iridium-Catalyzed Ortho-Arylation of Benzoic Acids with Arenediazonium Salts. *Angew. Chem. Int. Ed.* **2015**, *54* (43), 12607–12611. https://doi.org/10.1002/anie.201505769.

(40) Shen, Y.; Mahjour, B.; Cernak, T. Development of Copper-Catalyzed Deaminative Esterification Using High-Throughput Experimentation. *Commun. Chem.* **2022**, *5* (1), 83. https://doi.org/10.1038/s42004-022-00698-0.

(41) McGrath, A.; Zhang, R.; Shafiq, K.; Cernak, T. Repurposing Amine and Carboxylic Acid Building Blocks with an Automatable Esterification Reaction. *Chem. Commun.* **2023**, *59* (8), 1026–1029. https://doi.org/10.1039/D2CC05670D.

(42) Gruntz, U.; Katritzky, A. R.; Kenny, D. H.; Rezende, M. C.; Sheikh, H. Pyridines as Leaving Groups in Synthetic Transformations: Conversion of Amines into Esters. *J. Chem. Soc. Chem. Commun.* **1977**, No. 20, 701–701. https://doi.org/10.1039/C39770000701.

(43) Wang, J.; Hoerrner, M. E.; Watson, M. P.; Weix, D. J. Nickel-Catalyzed Synthesis of Dialkyl Ketones from the Coupling of N-Alkyl Pyridinium Salts with Activated Carboxylic Acids. *Angew. Chem. Int. Ed.* **2020**, *59*, 13484. https://doi.org/10.1002/anie.202002271.

(44) Wang, J.; Ehehalt, L. E.; Huang, Z.; Beleh, O. M.; Guzei, I. A.; Weix, D. J. Formation of C(Sp2)–C(Sp3) Bonds Instead of Amide C–N Bonds from Carboxylic Acid and Amine Substrate Pools by Decarbonylative Cross-Electrophile Coupling. *J. Am. Chem. Soc.* **2023**. https://doi.org/10.1021/jacs.2c11552.

(45) Douthwaite, J. L.; Zhao, R.; Shim, E.; Mahjour, B.; Zimmerman, P. M.; Cernak, T. Formal Cross-Coupling of Amines and Carboxylic Acids to Form Sp3–Sp2 Carbon–Carbon Bonds. *J. Am. Chem. Soc.* **2023**, *145* (20), 10930–10937. https://doi.org/10.1021/jacs.2c11563.

(46) Zhang, Z.; Cernak, T. The Formal Cross-Coupling of Amines and Carboxylic Acids to Form Sp3–Sp3 Carbon–Carbon Bonds. *Angew. Chem. Int. Ed.* **2021**, *60* (52), 27293–27298. https://doi.org/10.1002/anie.202112454.

(47) Pedersen, P. S.; Blakemore, D. C.; Chinigo, G. M.; Knauber, T.; MacMillan, D. W. C. One-Pot Synthesis of Sulfonamides from Unactivated Acids and Amines via Aromatic Decarboxylative Halosulfonylation. *J. Am. Chem. Soc.* **2023**, *145* (39), 21189–21196. https://doi.org/10.1021/jacs.3c08218.

(48) Brown, D. G.; Boström, J. Analysis of Past and Present Synthetic Methodologies on Medicinal Chemistry: Where Have All the New Reactions Gone? *J. Med. Chem.* **2016**, *59* (10), 4443–4458. https://doi.org/10.1021/acs.jmedchem.5b01409.

(49) Hofmann, A. W. V.; Clark, J. XIV. Researches into the Molecular Constitution of the Organic Bases. *Philos. Trans. R. Soc. Lond.* **1851**, *141*, 357–398. https://doi.org/10.1098/rstl.1851.0017.

(50) Wenkert, E.; Han, A.-L.; Jenny, C.-J. Nickel-Induced Conversion of Carbon–Nitrogen into Carbon–Carbon Bonds. One-Step Transformations of Aryl, Quaternary Ammonium Salts into Alkylarenes and Biaryls. *J. Chem. Soc. Chem. Commun.* **1988**, No. 14, 975–976. https://doi.org/10.1039/C39880000975.

(51) Blakey, S. B.; MacMillan, D. W. C. The First Suzuki Cross-Couplings of Aryltrimethylammonium Salts. *J. Am. Chem. Soc.* **2003**, *125* (20), 6046–6047. https://doi.org/10.1021/ja034908b.

(52) Yi, Y.-Q.-Q.; Yang, W.-C.; Zhai, D.-D.; Zhang, X.-Y.; Li, S.-Q.; Guan, B.-T. Nickel-Catalyzed C–N Bond Reduction of Aromatic and Benzylic Quaternary Ammonium Triflates. *Chem. Commun.* **2016**, *52* (72), 10894–10897. https://doi.org/10.1039/C6CC04531F.

(53) He, R.-D.; Li, C.-L.; Pan, Q.-Q.; Guo, P.; Liu, X.-Y.; Shu, X.-Z. Reductive Coupling between C–N and C–O Electrophiles. *J. Am. Chem. Soc.* **2019**, *141* (32), 12481–12486. https://doi.org/10.1021/jacs.9b05224.

(54) Xie, L.-G.; Wang, Z.-X. Nickel-Catalyzed Cross-Coupling of Aryltrimethylammonium Iodides with Organozinc Reagents. *Angew. Chem. Int. Ed.* **2011**, *50* (21), 4901–4904. https://doi.org/10.1002/anie.201100683.

(55) Pound, S. M.; Watson, M. P. Asymmetric Synthesis via Stereospecific C–N and C–O Bond Activation of Alkyl Amine and Alcohol Derivatives. *Chem. Commun.* **2018**, *54* (87), 12286–12301. https://doi.org/10.1039/C8CC07093H.

(56) Maity, P.; Shacklady-McAtee, D. M.; Yap, G. P. A.; Sirianni, E. R.; Watson, M. P. Nickel-Catalyzed Cross Couplings of Benzylic Ammonium Salts and Boronic Acids: Stereospecific Formation of Diarylethanes via C–N Bond Activation. *J. Am. Chem. Soc.* **2013**, *135* (1), 280–285. https://doi.org/10.1021/ja3089422.

(57) Guisán-Ceinos, M.; Martín-Heras, V.; Tortosa, M. Regio- and Stereospecific Copper-Catalyzed Substitution Reaction of Propargylic Ammonium Salts with Aryl Grignard Reagents. *J. Am. Chem. Soc.* **2017**, *139* (25), 8448–8451. https://doi.org/10.1021/jacs.7b05273.

(58) Bapat, J. B.; Blade, R. J.; Boulton, A. J.; Epsztajn, J.; Katritzky, A. R.; Lewis, J.; Molina-Buendia, P.; Nie, P.-L.; Ramsden, C. A. Pyridines as Leaving Groups in Synthetic Transformations: Nucleophilic Displacements of Amino Groups, and Novel Preparations of Nitriles and Isocyanates. *Tetrahedron Lett.* **1976**, *17* (31), 2691–2694. https://doi.org/10.1016/S0040-4039(00)77797-5.

(59) Katritzky, A. R.; Liso, G.; Lunt, E.; Patel, R. C.; Thind, S. S.; Zia, A. Heterocycles in Organic Synthesis. Part 42. Preparation of Azides, Phthalimides, and Sulphonamides from Primary Amines. *J. Chem. Soc. Perkin 1* **1980**, No. 0, 849–851. https://doi.org/10.1039/P19800000849.

(60) EWEISS, N. F. K., Alan R; NIE, Pai-Lin; RAMSDEN, Christopher A. The Conversion of Amines into Iodides. *Synthesis* **2002**, *1977* (09), 634–635. https://doi.org/10.1055/s-1977-24510.

(61) Katritzky, A. R.; Gruntz, U.; Ikizler, A. A.; Kenny, D. H.; Leddy, B. P. Heterocycles in Organic Synthesis. Part 17. Conversion of Primary Amines into Bromides and Chlorides. *J. Chem. Soc. Perkin 1* **1979**, No. 0, 436–441. https://doi.org/10.1039/P19790000436.

(62) Katritzky, A. R.; De Ville, G.; Patel, R. C. Carbon-Alkylation of Simple Nitronate Anions by N-Substituted Pyridiniums. *Tetrahedron* **1981**, *37*, 25–30. https://doi.org/10.1016/0040-4020(81)85037-5.

(63) Katritzky, A. R.; Abdel-Megeed, M. F.; Lhommet, G.; Ramsden, C. A. Heterocycles in Organic Synthesis. Part 7. Synthesis of Furfuryl Derivatives via 2,4,6-Trisubstituted Pyridinium Salts. *J. Chem. Soc. Perkin 1* **1979**, No. 0, 426–429. https://doi.org/10.1039/P19790000426.

(64) Basch, C. H.; Liao, J.; Xu, J.; Piane, J. J.; Watson, M. P. Harnessing Alkyl Amines as Electrophiles for Nickel-Catalyzed Cross Couplings via C–N Bond Activation. *J. Am. Chem. Soc.* **2017**, *139* (15), 5313–5316. https://doi.org/10.1021/jacs.7b02389.

(65) Ni, S.; Li, C.-X.; Mao, Y.; Han, J.; Wang, Y.; Yan, H.; Pan, Y. Ni-Catalyzed Deaminative Cross-Electrophile Coupling of Katritzky Salts with Halides via C─N Bond Activation. *Sci. Adv.* **2019**, *5* (6), eaaw9516–eaaw9516. https://doi.org/10.1126/sciadv.aaw9516.

(66) Liao, J.; Basch, C. H.; Hoerrner, M. E.; Talley, M. R.; Boscoe, B. P.; Tucker, J. W.; Garnsey, M. R.; Watson, M. P. Deaminative Reductive Cross-Electrophile Couplings of Alkylpyridinium Salts and Aryl Bromides. *Org. Lett.* **2019**, *21* (8), 2941–2946. https://doi.org/10.1021/acs.orglett.9b01014.

(67) Yi, J.; Badir, S. O.; Kammer, L. M.; Ribagorda, M.; Molander, G. A. Deaminative Reductive Arylation Enabled by Nickel/Photoredox Dual Catalysis. *Org. Lett.* **2019**, *21* (9), 3346–3351. https://doi.org/10.1021/acs.orglett.9b01097.

(68) Plunkett, S.; Basch, C. H.; Santana, S. O.; Watson, M. P. Harnessing Alkylpyridinium Salts as Electrophiles in Deaminative Alkyl–Alkyl Cross-Couplings. *J. Am. Chem. Soc.* **2019**, *141* (6), 2257–2262. https://doi.org/10.1021/jacs.9b00111.

(69) Kim, I.; Im, H.; Lee, H.; Hong, S. N-Heterocyclic Carbene-Catalyzed Deaminative Cross-Coupling of Aldehydes with Katritzky Pyridinium Salts. *Chem. Sci.* **2020**, *11* (12), 3192–3197. https://doi.org/10.1039/D0SC00225A.

(70) Wei, W.; Yu, H.; Zangarelli, A.; Ackermann, L. Deaminative Meta-C–H Alkylation by Ruthenium(Ii) Catalysis. *Chem. Sci.* **2021**, *12* (23), 8073–8078. https://doi.org/10.1039/D1SC00986A.

(71) Sun, S.-Z.; Cai, Y.-M.; Zhang, D.-L.; Wang, J.-B.; Yao, H.-Q.; Rui, X.-Y.; Martin, R.; Shang, M. Enantioselective Deaminative Alkylation of Amino Acid Derivatives with Unactivated Olefins. *J. Am. Chem. Soc.* **2022**, *144* (3), 1130–1137. https://doi.org/10.1021/jacs.1c12350.

(72) Klauck, F. J. R.; James, M. J.; Glorius, F. Deaminative Strategy for the Visible-Light-Mediated Generation of Alkyl Radicals. *Angew. Chem. Int. Ed.* **2017**, *56* (40), 12336–12339. https://doi.org/10.1002/anie.201706896.

(73) Klauck, F. J. R.; Yoon, H.; James, M. J.; Lautens, M.; Glorius, F. Visible-Light-Mediated Deaminative Three-Component Dicarbofunctionalization of Styrenes with Benzylic Radicals. *ACS Catal.* **2019**, *9* (1), 236–241. https://doi.org/10.1021/acscatal.8b04191.

(74) Yang, M.; Cao, T.; Xu, T.; Liao, S. Visible-Light-Induced Deaminative Thioesterification of Amino Acid Derived Katritzky Salts via Electron Donor–Acceptor Complex Formation. *Org. Lett.* **2019**, *21* (21), 8673–8678. https://doi.org/10.1021/acs.orglett.9b03284.

(75) Wu, J.; He, L.; Noble, A.; Aggarwal, V. K. Photoinduced Deaminative Borylation of Alkylamines. *J. Am. Chem. Soc.* **2018**, *140* (34), 10700–10704. https://doi.org/10.1021/jacs.8b07103.

(76) Yue, H.; Zhu, C.; Shen, L.; Geng, Q.; Hock, K. J.; Yuan, T.; Cavallo, L.; Rueping, M. Nickel-Catalyzed C–N Bond Activation: Activated Primary Amines as Alkylating Reagents in Reductive Cross-Coupling. *Chem. Sci.* **2019**, *10* (16), 4430–4435. https://doi.org/10.1039/C9SC00783K.

(77) Ociepa, M.; Turkowska, J.; Gryko, D. Redox-Activated Amines in C(Sp3)–C(Sp) and C(Sp3)–C(Sp2) Bond Formation Enabled by Metal-Free Photoredox Catalysis. *ACS Catal.* **2018**, *8* (12), 11362–11367. https://doi.org/10.1021/acscatal.8b03437.

(78) Moser, D.; Duan, Y.; Wang, F.; Ma, Y.; O'Neill, M. J.; Cornella, J. Selective Functionalization of Aminoheterocycles by a Pyrylium Salt. *Angew. Chem. Int. Ed.* **2018**, *57* (34), 11035–11039. https://doi.org/10.1002/anie.201806271.

(79) Ghiazza, C.; Faber, T.; Gómez-Palomino, A.; Cornella, J. Deaminative Chlorination of Aminoheterocycles. *Nat. Chem.* **2022**, *14* (1), 78–84. https://doi.org/10.1038/s41557-021-00812-0.

(80) Ashley, M. A.; Rovis, T. Photoredox-Catalyzed Deaminative Alkylation via C–N Bond Activation of Primary Amines. *J. Am. Chem. Soc.* **2020**, *142* (43), 18310–18316. https://doi.org/10.1021/jacs.0c08595.

(81) Sandmeyer, T. Ueber Die Ersetzung Der Amidgruppe Durch Chlor in Den Aromatischen Substanzen. *Berichte Dtsch. Chem. Ges.* **1884**, *17* (2), 1633–1635. https://doi.org/10.1002/cber.18840170219.

(82) Ganley, J. M.; Murray, P. R. D.; Knowles, R. R. Photocatalytic Generation of Aminium Radical Cations for C–N Bond Formation. *ACS Catal.* **2020**, *10* (20), 11712–11738. https://doi.org/10.1021/acscatal.0c03567.

(83) Geunes, E. P.; Meinhardt, J. M.; Wu, E. J.; Knowles, R. R. Photocatalytic Anti-Markovnikov Hydroamination of Alkenes with Primary Heteroaryl Amines. *J. Am. Chem. Soc.* **2023**, *145* (40), 21738–21744. https://doi.org/10.1021/jacs.3c08428.

(84) Feng, G.; Ku, C. K.; Zhao, J.; Wang, Q. Copper-Catalyzed Three-Component Aminofluorination of Alkenes and 1,3-Dienes: Direct Entry to Diverse β-Fluoroalkylamines. *J. Am. Chem. Soc.* **2022**, *144* (44), 20463–20471. https://doi.org/10.1021/jacs.2c09118.

(85) Chen, M.; Ventura, A. M.; Das, S.; Ibrahim, A. F.; Zimmerman, P. M.; Montgomery, J. Oxidative Cross Dehydrogenative Coupling of N-Heterocycles with Aldehydes through C(Sp3)–H Functionalization. *J. Am. Chem. Soc.* **2023**, *145* (37), 20176–20181. https://doi.org/10.1021/jacs.3c06532.

(86) Yatabe, T.; Yamaguchi, K. Regiospecific α-Methylene Functionalisation of Tertiary Amines with Alkynes via Au-Catalysed Concerted One-Proton/Two-Electron Transfer to O2. *Nat. Commun.* **2022**, *13* (1), 6505. https://doi.org/10.1038/s41467-022-34176-x.

(87) Lin, Y.; Zhang, Z.; Mahjour, B.; Wang, D.; Zhang, R.; Shim, E.; McGrath, A.; Shen, Y.; Brugger, N.; Turnbull, R.; Trice, S.; Jasty, S.; Cernak, T. Reinforcing the Supply Chain of Umifenovir and Other Antiviral Drugs with Retrosynthetic Software. *Nat. Commun.* **2021**, *12* (1), 7327. https://doi.org/10.1038/s41467-021-27547-3.

(88) Kennedy, S. H.; Dherange, B. D.; Berger, K. J.; Levin, M. D. Skeletal Editing through Direct Nitrogen Deletion of Secondary Amines. *Nature* **2021**, *593* (7858), 223–227. https://doi.org/10.1038/s41586-021-03448-9.

(89) Dherange, B. D.; Yuan, M.; Kelly, C. B.; Reiher, C. A.; Grosanu, C.; Berger, K. J.; Gutierrez, O.; Levin, M. D. Direct Deaminative Functionalization. *J. Am. Chem. Soc.* **2023**, *145* (1), 17–24. https://doi.org/10.1021/jacs.2c11453.

(90) Steiniger, K. A.; Lamb, M. C.; Lambert, T. H. Cross-Coupling of Amines via Photocatalytic Denitrogenation of In Situ Generated Diazenes. *J. Am. Chem. Soc.* **2023**, *145* (21), 11524–11529. https://doi.org/10.1021/jacs.3c03634.

(91) Laudadio, G.; Palkowitz, M. D.; El-Hayek Ewing, T.; Baran, P. S. Decarboxylative Cross-Coupling: A Radical Tool in Medicinal Chemistry. *ACS Med. Chem. Lett.* **2022**, *13* (9), 1413–1420. https://doi.org/10.1021/acsmedchemlett.2c00286.

(92) Arshadi, S.; Ebrahimiasl, S.; Hosseinian, A.; Monfared, A.; Vessally, E. Recent Developments in Decarboxylative Cross-Coupling Reactions between Carboxylic Acids and N–H Compounds. *RSC Adv.* **2019**, *9* (16), 8964–8976. https://doi.org/10.1039/C9RA00929A.

(93) Candish, L.; Freitag, M.; Gensch, T.; Glorius, F. Mild, Visible Light-Mediated Decarboxylation of Aryl Carboxylic Acids to Access Aryl Radicals. *Chem. Sci.* **2017**, *8* (5), 3618–3622. https://doi.org/10.1039/C6SC05533H.

(94) Chen, T. Q.; Pedersen, P. S.; Dow, N. W.; Fayad, R.; Hauke, C. E.; Rosko, M. C.; Danilov, E. O.; Blakemore, D. C.; Dechert-Schmitt, A.-M.; Knauber, T.; Castellano, F. N.; MacMillan, D. W. C. A Unified Approach to Decarboxylative Halogenation of (Hetero)Aryl Carboxylic Acids. *J. Am. Chem. Soc.* **2022**, *144* (18), 8296–8305. https://doi.org/10.1021/jacs.2c02392.

(95) Xu, P.; López-Rojas, P.; Ritter, T. Radical Decarboxylative Carbometalation of Benzoic Acids: A Solution to Aromatic Decarboxylative Fluorination. *J. Am. Chem. Soc.* **2021**, *143* (14), 5349–5354. https://doi.org/10.1021/jacs.1c02490.

(96) Rodríguez, N.; Goossen, L. J. Decarboxylative Coupling Reactions: A Modern Strategy for C–C-Bond Formation. *Chem. Soc. Rev.* **2011**, *40* (10), 5030–5048. https://doi.org/10.1039/C1CS15093F.

(97) Barton, D. H. R.; Crich, D.; Motherwell, W. B. New and Improved Methods for the Radical Decarboxylation of Acids. *J. Chem. Soc. Chem. Commun.* **1983**, No. 17, 939–941. https://doi.org/10.1039/C39830000939.

(98) Barton, D. H. R.; Crich, D.; Motherwell, W. B. A Practical Alternative to the Hunsdiecker Reaction. *Tetrahedron Lett.* **1983**, *24* (45), 4979–4982. https://doi.org/10.1016/S0040-4039(01)99826-0.

(99) Barton, D. H. R.; De Almeida, M. V.; Liu, W.; Shinada, T.; Jaszberenyi, J. C.; Dos Santos, H. F.; Le Hyaric, M. Radical Homologation of D-Gluconic Acid: Highly Diastereoselective Synthesis of d-Gluco-KDO Derivatives. *Tetrahedron* **2001**, *57* (42), 8767–8771. https://doi.org/10.1016/S0040-4020(01)00865-1.

(100) Okada, K.; Okubo, K.; Morita, N.; Oda, M. Reductive Decarboxylation of N-(Acyloxy)Phthalimides via Redox-Initiated Radical Chain Mechanism. *Int. J. Rapid Publ. Prelim.* **1992**, *33* (48), 7377–7380. https://doi.org/10.1016/S0040-4039(00)60192-2.

(101) Pratsch, G.; Lackner, G. L.; Overman, L. E. Constructing Quaternary Carbons from N-(Acyloxy)Phthalimide Precursors of Tertiary Radicals Using Visible-Light Photocatalysis. *J. Org. Chem.* **2015**, *80* (12), 6025–6036. https://doi.org/10.1021/acs.joc.5b00795.

(102) Huihui, K. M. M.; Caputo, J. A.; Melchor, Z.; Olivares, A. M.; Spiewak, A. M.; Johnson, K. A.; DiBenedetto, T. A.; Kim, S.; Ackerman, L. K. G.; Weix, D. J. Decarboxylative Cross-Electrophile Coupling of N-Hydroxyphthalimide Esters with Aryl Iodides. *J. Am. Chem. Soc.* **2016**, *138* (15), 5016–5019. https://doi.org/10.1021/jacs.6b01533.

(103) Qin, T.; Cornella, J.; Li, C.; Malins, L. R.; Edwards, J. T.; Kawamura, S.; Maxwell, B. D.; Eastgate, M. D.; Baran, P. S. A General Alkyl-Alkyl Cross-Coupling Enabled by Redox-

Active Esters and Alkylzinc Reagents. *Science* **2016**, *352* (6287), 801–805. https://doi.org/10.1126/science.aaf6123.

(104) Wang, J.; Qin, T.; Chen, T.-G.; Wimmer, L.; Edwards, J. T.; Cornella, J.; Vokits, B.; Shaw, S. A.; Baran, P. S. Nickel-Catalyzed Cross-Coupling of Redox-Active Esters with Boronic Acids. *Angew. Chem. Int. Ed.* **2016**, *55* (33), 9676–9679. https://doi.org/10.1002/anie.201605463.

(105) Suzuki, N.; Hofstra, J. L.; Poremba, K. E.; Reisman, S. E. Nickel-Catalyzed Enantioselective Cross-Coupling of N-Hydroxyphthalimide Esters with Vinyl Bromides. *Org. Lett.* **2017**, *19* (8), 2150–2153. https://doi.org/10.1021/acs.orglett.7b00793.

(106) Lu, X.; Xiao, B.; Liu, L.; Fu, Y. Formation of C(Sp3)–C(Sp3) Bonds through Nickel-Catalyzed Decarboxylative Olefin Hydroalkylation Reactions. *Chem. – Eur. J.* **2016**, *22* (32), 11161–11164. https://doi.org/10.1002/chem.201602486.

(107) Murarka, S. N-(Acyloxy)Phthalimides as Redox-Active Esters in Cross-Coupling Reactions. *Adv. Synth. Catal.* **2018**, *360* (9), 1735–1753. https://doi.org/10.1002/adsc.201701615.

(108) Minisci, F.; Bernardi, R.; Bertini, F.; Galli, R.; Perchinummo, M. Nucleophilic Character of Alkyl Radicals—VI: A New Convenient Selective Alkylation of Heteroaromatic Bases. *Tetrahedron* **1971**, *27* (15), 3575–3579. https://doi.org/10.1016/S0040-4020(01)97768-3.

(109) Beil, S. B.; Chen, T. Q.; Intermaggio, N. E.; MacMillan, D. W. C. Carboxylic Acids as Adaptive Functional Groups in Metallaphotoredox Catalysis. *Acc. Chem. Res.* **2022**, *55* (23), 3481–3494. https://doi.org/10.1021/acs.accounts.2c00607.

(110) Gooßen, L. J.; Deng, G.; Levy, L. M. Synthesis of Biaryls via Catalytic Decarboxylative Coupling. *Science* **2006**, *313* (5787), 662. https://doi.org/10.1126/science.1128684.

(111) Gooßen, L. J.; Lange, P. P.; Rodríguez, N.; Linder, C. Low-Temperature Ag/Pd-Catalyzed Decarboxylative Cross-Coupling of Aryl Triflates with Aromatic Carboxylate Salts. *Chem. – Eur. J.* **2010**, *16* (13), 3906–3909. https://doi.org/10.1002/chem.200903319.

(112) Shi, S.; Szostak, M. Decarbonylative Borylation of Amides by Palladium Catalysis. *ACS Omega* **2019**, *4* (3), 4901–4907. https://doi.org/10.1021/acsomega.9b00081.

(113) Malapit, C. A.; Borrell, M.; Milbauer, M. W.; Brigham, C. E.; Sanford, M. S. Nickel-Catalyzed Decarbonylative Amination of Carboxylic Acid Esters. *J. Am. Chem. Soc.* **2020**, *142* (13), 5918–5923. https://doi.org/10.1021/jacs.9b13531.

(114) Su, W.; Xu, P.; Ritter, T. Decarboxylative Hydroxylation of Benzoic Acids. *Angew. Chem. Int. Ed.* **2021**, *60* (45), 24012–24017. https://doi.org/10.1002/anie.202108971.

(115) Goldberg, F. W.; Kettle, J. G.; Kogej, T.; Perry, M. W. D.; Tomkinson, N. P. Designing Novel Building Blocks Is an Overlooked Strategy to Improve Compound Quality. *Drug Discov. Today* **2015**, *20* (1), 11–17. https://doi.org/10.1016/j.drudis.2014.09.023.

(116) Wang, Y.; Haight, I.; Gupta, R.; Vasudevan, A. What Is in Our Kit? An Analysis of Building Blocks Used in Medicinal Chemistry Parallel Libraries. *J. Med. Chem.* **2021**, *64* (23), 17115–17122. https://doi.org/10.1021/acs.jmedchem.1c01139.

(117) Peplow, M. "Almost Magical": Chemists Can Now Move Single Atoms in and out of a Molecule's Core. *Nature* **2023**, *618* (7963), 21–24. https://doi.org/10.1038/d41586-023-01735-1.

(118) Klein, V. G.; Bond, A. G.; Craigon, C.; Lokey, R. S.; Ciulli, A. Amide-to-Ester Substitution as a Strategy for Optimizing PROTAC Permeability and Cellular Activity. *J. Med. Chem.* **2021**, *64* (24), 18082–18101. https://doi.org/10.1021/acs.jmedchem.1c01496.

(119) Hosono, Y.; Uchida, S.; Shinkai, M.; Townsend, C. E.; Kelly, C. N.; Naylor, M. R.; Lee, H.-W.; Kanamitsu, K.; Ishii, M.; Ueki, R.; Ueda, T.; Takeuchi, K.; Sugita, M.; Akiyama, Y.; Lokey, S. R.; Morimoto, J.; Sando, S. Amide-to-Ester Substitution as a Stable Alternative to N-Methylation for Increasing Membrane Permeability in Cyclic Peptides. *Nat. Commun.* **2023**, *14* (1), 1416. https://doi.org/10.1038/s41467-023-36978-z.

(120) Pereira, D. A.; Williams, J. A. Origin and Evolution of High Throughput Screening. *Br. J. Pharmacol.* **2007**, *152* (1), 53–61. https://doi.org/10.1038/sj.bjp.0707373.

(121) González-Esguevillas, M.; Fernández, D. F.; Rincón, J. A.; Barberis, M.; de Frutos, O.; Mateos, C.; García-Cerrada, S.; Agejas, J.; MacMillan, D. W. C. Rapid Optimization of Photoredox Reactions for Continuous-Flow Systems Using Microscale Batch Technology. *ACS Cent. Sci.* **2021**, *7* (7), 1126–1134. https://doi.org/10.1021/acscentsci.1c00303.

(122) Qi, N.; Wismer, M. K.; Conway, D. V.; Krska, S. W.; Dreher, S. D.; Lin, S. Development of a High Intensity Parallel Photoreactor for High Throughput Screening. *React. Chem. Eng.* **2022**, *7* (2), 354–360. https://doi.org/10.1039/D1RE00317H.

(123) Sun, A. C.; Stephenson, C. R. J.; Kennedy, R. T. High-Throughput Photochemistry Using Droplet Microfluidics. In *The Power of High-Throughput Experimentation: General Topics and Enabling Technologies for Synthesis and Catalysis (Volume 1)*; ACS Symposium Series; American Chemical Society, 2022; Vol. 1419, pp 131–143. https://doi.org/10.1021/bk-2022-1419.ch008.

(124) Rein, J.; Annand, J. R.; Wismer, M. K.; Fu, J.; Siu, J. C.; Klapars, A.; Strotman, N. A.; Kalyani, D.; Lehnherr, D.; Lin, S. Unlocking the Potential of High-Throughput Experimentation for Electrochemistry with a Standardized Microscale Reactor. *ACS Cent. Sci.* **2021**, *7* (8), 1347–1355. https://doi.org/10.1021/acscentsci.1c00328.

(125) Palkowitz, M. D.; Laudadio, G.; Kolb, S.; Choi, J.; Oderinde, M. S.; Ewing, T. E.-H.; Bolduc, P. N.; Chen, T.; Zhang, H.; Cheng, P. T. W.; Zhang, B.; Mandler, M. D.; Blasczak, V.

D.; Richter, J. M.; Collins, M. R.; Schioldager, R. L.; Bravo, M.; Dhar, T. G. M.; Vokits, B.; Zhu, Y.; Echeverria, P.-G.; Poss, M. A.; Shaw, S. A.; Clementson, S.; Petersen, N. N.; Mykhailiuk, P. K.; Baran, P. S. Overcoming Limitations in Decarboxylative Arylation via Ag–Ni Electrocatalysis. *J. Am. Chem. Soc.* **2022**, *144* (38), 17709–17720. https://doi.org/10.1021/jacs.2c08006.

(126) Shevlin, M. High-Throughput Experimentation-Enabled Asymmetric Hydrogenation. In *The Power of High-Throughput Experimentation: General Topics and Enabling Technologies for Synthesis and Catalysis (Volume 1)*; ACS Symposium Series; American Chemical Society, 2022; Vol. 1419, pp 107–130. https://doi.org/10.1021/bk-2022-1419.ch007.

(127) Shultz, C. S.; Krska, S. W. Unlocking the Potential of Asymmetric Hydrogenation at Merck. *Acc. Chem. Res.* **2007**, *40* (12), 1320–1326. https://doi.org/10.1021/ar700141v.

(128) Felten, S.; He, C. Q.; Weisel, M.; Shevlin, M.; Emmert, M. H. Accessing Diverse Azole Carboxylic Acid Building Blocks via Mild C–H Carboxylation: Parallel, One-Pot Amide Couplings and Machine-Learning-Guided Substrate Scope Design. *J. Am. Chem. Soc.* **2022**, *144* (50), 23115–23126. https://doi.org/10.1021/jacs.2c10557.

(129) Makey, D. M.; Diehl, R. C.; Xin, Y.; Murray, B. E.; Stoll, D. R.; Ruotolo, B. T.; Grinias, J. P.; Narayan, A. R. H.; Lopez-Carillo, V.; Stark, M.; Johnen, P.; Kennedy, R. T. High-Throughput Liquid Chromatographic Analysis Using a Segmented Flow Injector with a 1 s Cycle Time. *Anal. Chem.* **2023**, *95* (46), 17028–17036. https://doi.org/10.1021/acs.analchem.3c03719.

(130) Cabrera, J.; Padilla, R.; Dehn, R.; Deuerlein, S.; Gułajski, Ł.; Chomiszczak, E.; Teles, J. H.; Limbach, M.; Grela, K. Olefin Metathesis on a TLC Plate as a Tool for a High-Throughput Screening of Catalyst-Substrate Sets. *Adv. Synth. Catal.* **2012**, *354* (6), 1043–1051. https://doi.org/10.1002/adsc.201100863.

(131) Jaman, Z.; Logsdon, D. L.; Szilágyi, B.; Sobreira, T. J. P.; Aremu, D.; Avramova, L.; Cooks, R. G.; Thompson, D. H. High-Throughput Experimentation and Continuous Flow Evaluation of Nucleophilic Aromatic Substitution Reactions. *ACS Comb. Sci.* **2020**, *22* (4), 184–196. https://doi.org/10.1021/acscombsci.9b00212.

(132) Huang, K.-H.; Morato, N. M.; Feng, Y.; Cooks, R. G. High-Throughput Diversification of Complex Bioactive Molecules by Accelerated Synthesis in Microdroplets. *Angew. Chem. Int. Ed.* **2023**, *62* (22), e202300956. https://doi.org/10.1002/anie.202300956.

(133) Lin, S.; Dikler, S.; Blincoe, W. D.; Ferguson, R. D.; Sheridan, R. P.; Peng, Z.; Conway, D. V.; Zawatzky, K.; Wang, H.; Cernak, T.; Davies, I. W.; DiRocco, D. A.; Sheng, H.; Welch, C. J.; Dreher, S. D. Mapping the Dark Space of Chemical Reactions with Extended Nanomole Synthesis and MALDI-TOF MS. *Science* **2018**, *361* (6402), eaar6236. https://doi.org/10.1126/science.aar6236.

(134) Mason, J.; Wilders, H.; Fallon, D. J.; Thomas, R. P.; Bush, J. T.; Tomkinson, N. C. O.; Rianjongdee, F. Automated LC-MS Analysis and Data Extraction for High-Throughput Chemistry. *Digit. Discov.* **2023**, *2* (6), 1894–1899. https://doi.org/10.1039/D3DD00167A.

(135) Haas, C. P.; Lübbesmeyer, M.; Jin, E. H.; McDonald, M. A.; Koscher, B. A.; Guimond, N.; Di Rocco, L.; Kayser, H.; Leweke, S.; Niedenführ, S.; Nicholls, R.; Greeves, E.; Barber, D. M.; Hillenbrand, J.; Volpin, G.; Jensen, K. F. Open-Source Chromatographic Data Analysis for Reaction Optimization and Screening. *ACS Cent. Sci.* **2023**, *9* (2), 307–317. https://doi.org/10.1021/acscentsci.2c01042.

(136) Jansen, B. C.; Hafkenscheid, L.; Bondt, A.; Gardner, R. A.; Hendel, J. L.; Wuhrer, M.; Spencer, D. I. R. HappyTools: A Software for High-Throughput HPLC Data Processing and Quantitation. *PLOS ONE* **2018**, *13* (7), e0200280. https://doi.org/10.1371/journal.pone.0200280.

(137) Mahjour, B.; Zhang, R.; Shen, Y.; McGrath, A.; Zhao, R.; Mohamed, O. G.; Lin, Y.; Zhang, Z.; Douthwaite, J. L.; Tripathi, A.; Cernak, T. Rapid Planning and Analysis of High-Throughput Experiment Arrays for Reaction Discovery. *Nat. Commun.* **2023**, *14* (1), 3924. https://doi.org/10.1038/s41467-023-39531-0.

(138) Caldentey, X.; Romero, E. High-Throughput Experimentation as an Accessible Technology for Academic Organic Chemists in Europe and Beyond**. *Chemistry–Methods* **2023**, *3* (5), e202200059. https://doi.org/10.1002/cmtd.202200059.

(139) National Academies of Sciences, E., and Medicine. *Data Science: Opportunities to Transform Chemical Sciences and Engineering: Proceedings of a Workshop—in Brief*; Linda Casola, Ellen Mantus, Series Eds.; The National Academies Press: Washington, DC, 2018. https://doi.org/10.17226/25191.

(140) Brunk, R.; Shulka, K.; Wang, Y.; Verber, M.; Gutierrez For, C.; Dennis, W.; Mehta, A.; Hogan, B.; Swetnam, T.; Brunk, E. Data Science for Chemists: Integrating and Evaluating the Use of Interactive Digital Python Notebooks in a Large Enrollment Undergraduate Biochemistry Course. *ChemRxiv* **2023**. https://doi.org/10.26434/chemrxiv-2023-qqcs9.

(141) Renu, N.; Sunil, K. Integrating Computational Data Science in University Curriculum for the New Generation of Scientists. *High. Educ. Future* **2023**, *10* (2), 183–195. https://doi.org/10.1177/23476311231183204.

(142) Bravenec, A. D.; Ward, K. D. Interactive Python Notebooks for Physical Chemistry. *J. Chem. Educ.* **2023**, *100* (2), 933–940. https://doi.org/10.1021/acs.jchemed.2c00665.

(143) Mahjour, B.; McGrath, A.; Outlaw, A.; Zhao, R.; Zhang, C.; Cernak, T. Interactive Python Notebook Modules for Chemoinformatics in Medicinal Chemistry. *J. Chem. Educ.* **2023**, *100* (12), 4895–4902. https://doi.org/10.1021/acs.jchemed.3c00357.

(144) Tan, S. W. B.; Naraharisetti, P. K.; Chin, S. K.; Lee, L. Y. Simple Visual-Aided Automated Titration Using the Python Programming Language. *J. Chem. Educ.* **2020**, *97* (3), 850–854. https://doi.org/10.1021/acs.jchemed.9b00802.

(145) Peplow, M. Automation for the People: Training a New Generation of Chemists in Data-Driven Synthesis. *Chemical & Engineering News*. October 27, 2019. https://cen.acs.org/synthesis/Automation-people-Training-new-generation/97/i42.

Chapter 2 Educating the Next Generation of Chemists[1]

This work is an adaptation of a series of labs we implemented in MedChem 410 that provides an educational component to some of the ideas discussed in chapter one. Students in one exercise begin to relate structure to the function of a molecule by analyzing solubility as it relates to logP and aromatic rings (Figure 2.5). Further they are provided with a foundation in how to visualize large data sets in a meaningful way. This is exemplified in their use of PCA to cluster a large dataset of molecules based on their properties. They are then instructed to filter this dataset to exclude only molecules that pass the Lipinski rules.

The second portion of this chapter is also being prepared for publication in the Journal of Chemical Education in combination with a computational exercise developed by Drs Irina Pogozheva and Andrei Lomize. It provides are more experimental basis to the foundations laid in chapter one. Students are encouraged to think about how the structure of a molecule relates to its function of permeability by running a parallel artificial membrane permeability assay (PAMPA) on two different brightly colored drugs. The lab also includes an exposure to automation where students are instructed to write code to control an Opentrons robot to transfer the drugs from one well plate to a plate reader plate.

The third portion of this chapter is targeted toward a much younger audience. It involves a children's toy where children are given plant-based dyes, a well plate, and plastic pipettes, and

[1] The first portion of this chapter is published in the Journal of Chemical Education: **Interactive Python Notebook Modules for Chemoinformatics in Medicinal Chemistry** Babak Mahjour, Andrew McGrath, Andrew Outlaw, Ruheng Zhao, Charles Zhang, and Tim Cernak *Journal of Chemical Education* **2023** *100* (12), 4895-4902 DOI: 10.1021/acs.jchemed.3c00357

subsequently encouraged to mix the dyes in the well plates to observe color changes. On the surface it may not seem to reinforce the concept, but students are taught very basically that the color (function) of each of the dyes is related to the molecules (structure) that are contained within it.

2.1 Interactive Python Notebook Modules for Chemoinformatics in Medicinal Chemistry[2]

2.1.1 Introduction

Chemoinformatics is the use of computational informatics techniques to solve problems in chemistry. These *in silico* methods can be used to transform data into information and aid in drug discovery. Recently, a rise in computational power and increased availability of software tools have made chemoinformatics an invaluable tool for research. Meanwhile, there has been recent interest in teaching young scientists how to work at the interface of physical science and data science.[2–7] In previous works, lesson plans have been developed incorporating programming into physical chemistry,[2,4] general chemistry,[5] analytical chemistry,[6,8] bioinformatics,[7] and other topics.[9–17] This paper extends the previous works through a lesson plan that introduces students to the basics of chemoinformatics in medicinal chemistry with the most popular scripting language, Python. Specifically, the exercises included in this activity are based on traditional techniques used by medicinal chemists to visualize and analyze chemical space.

2.1.2 Objectives.

[2] Bo developed the foundational exercise to teach the basics of Python. Bo and I then worked together to develop the chemoinformatics portion of the lab which was bolstered by the release of Diamond XChem's COVID Moonshot project[1] dataset, which during the pandemic gave relevant data for the students to interact with. This lab has been taught for several years with generally positive feedback from students.

The purpose of this experiment is to introduce fundamental chemoinformatics using Python through medicinal chemistry-based exercises. The modules teach:

- how to load compiled medicinal chemistry datasets that are suitable for sharing and analysis
- how to visualize chemical space in a multitude of ways
- how to filter chemical datasets based on drug-like properties
- how to validate medicinal chemistry principles using data visualization
- how to simplify multidimensional physicochemical properties of drugs using principal component analyses (PCA)

2.1.3 Structure and Context

In this text, "lesson plan" refers to the entirety of the work and consists of two "class sessions". Each "class session" consists of a brief lecture, to be administered at the beginning of the class session, a Python notebook consisting of several "modules" to be completed by students, and a lab report to be completed and submitted for a grade. As mentioned, this lesson plan is executed over two separate three-hour class sessions, supervised by one or two graduate student teaching assistants with some familiarity with Python. Students participating in this activity are expected to have familiarity with basic concepts of medicinal chemistry, such as how structures impact druglike properties. Classes typically comprised 20–40 students. Each class session consists of a brief slide deck and lecture introducing the very basics of Python and its capabilities, presented to the students, followed by an interactive Python notebook, composed of multiple modules. Additionally, there is a preliminary 90-minute lecture given introducing chemoinformatic and drug design concepts such as chemical space, partition coefficient (LogP), Lipinski rules, molecular fingerprints, diversity, and qualitative structure activity relationships. In this lecture

students learn how drugs are classified by the "Lipinski rule of five" and how commercial drugs may (Figure 2.1, **2.1** and **2.2**) or may not (Figure 2.1, **2.3** and **2.4**) meet these guidelines. Alongside this preliminary lecture are two recitation exercises, where students review and summarize papers from the literature describing the quantitative estimate of drug-likeness (QED) score[18] and the central nervous system multiparameter optimization (CNS-MPO) tool[19] – chemoinformatic concepts that are applied in the subsequent labs.

These notebooks are written in Google Colaboratory (Colab)[20], an easily accessible online Python environment that executes code on the cloud for free, based on the popular Jupyter software.[21] Colab has several important data science packages preinstalled, including Pandas,[22] Numpy,[23] Scipy,[24] and Matplotlib[25] – Python add-ons that simplify the manipulation and visualization of data. Its primary advantages here are allowing a fast and simple way for new students to get started coding, as it is agnostic of computer, operating system and requires no technical setup. Code is separated into blocks called 'cells', which execute independently of each other. The two Colab notebooks are organized by modules, each with specific objectives and corresponding questions in the notebook's respective lab report and walk the students through various exercises to meet the teaching objectives. Each notebook is to be completed alongside provided lab report templates consisting of module-specific questions and discussion items. Graduate student teaching assistants provide guidance and feedback to students during the class.

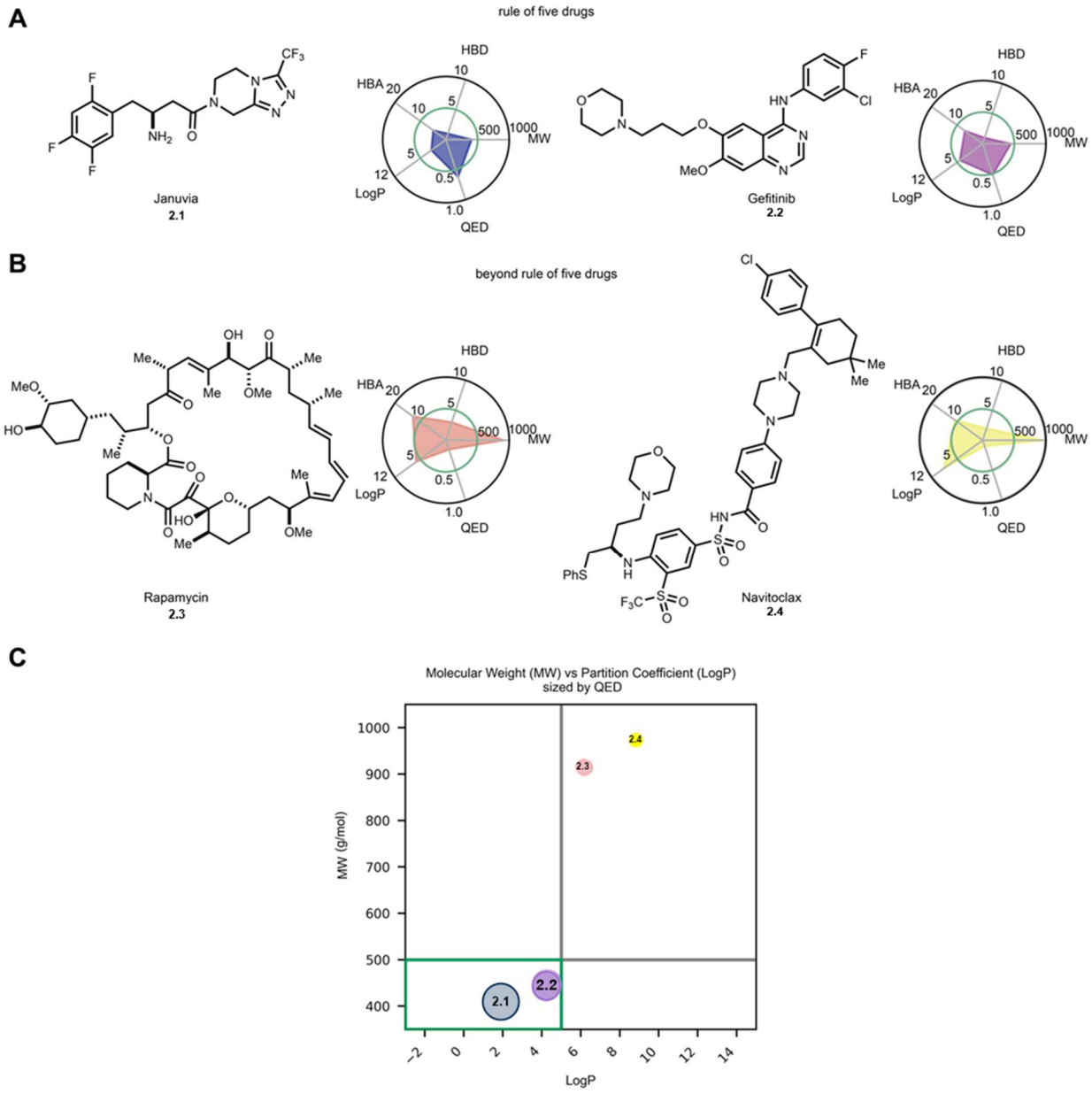

Figure 2.1 Medicinal chemistry concepts taught in a preliminary lecture before the lab. **(A)** Examples of drugs passing the Lipinski rules. Radar plots display physicochemical properties of the adjacent molecule. Values within the green concentric circle are within the rule of five threshold (except for QED score). **(B)** Examples of drugs failing the Lipinski rules. Some properties break through the rule of five threshold shown in the radar plots. **(C)** A scatter plot of molecular weight (MW) versus partition coefficient (LogP, a dimensionless quantity representing a molecule's distribution between hydrophobic and aqueous environments) for the drugs shown, where each point is sized by QED. The green boundary demarcates the "Lipinski rule of five". HBA = Hydrogen bond acceptor, HBD = Hydrogen bond donor.

2.1.4 Class Session 1: Introduction to Colab, Python, and Chemoinformatics.

In the first class session, an initial slide deck is presented by the graduate student teaching assistants to the class explaining the increasing popularity of scripting languages and their use in industry and academia. Several examples of data visualizations generated by Python are shared with the students (Figure 2.8). Python as a scripting language is then formally introduced, as well as Colab. Students are shown how to execute *print("hello world")* and are encouraged to log into Colab from their computer and run a line of code. Lists and dictionaries are introduced as two basic data structures. *If* statements and *for* loops are introduced through an example of their use in filtering a list of dictionaries. Finally, it is shown how the Python package Pandas[22] can be used to load tabulated datasets from comma-separated value (CSV) or JavaScript Object Notation (JSON) files. Students then complete the first Python notebook and its corresponding lab report template after the brief (~15 minute) lecture in the remaining class time with graduate student supervision.

The notebook given in the initial class session introduces students to Google Colab, plotting in Python, and basic chemoinformatic concepts. The objectives of this notebook are to learn basic python coding and to quickly load and plot chemoinformatic data from spreadsheets or other data formats. The module also exemplifies how to customize plots generated in Python.

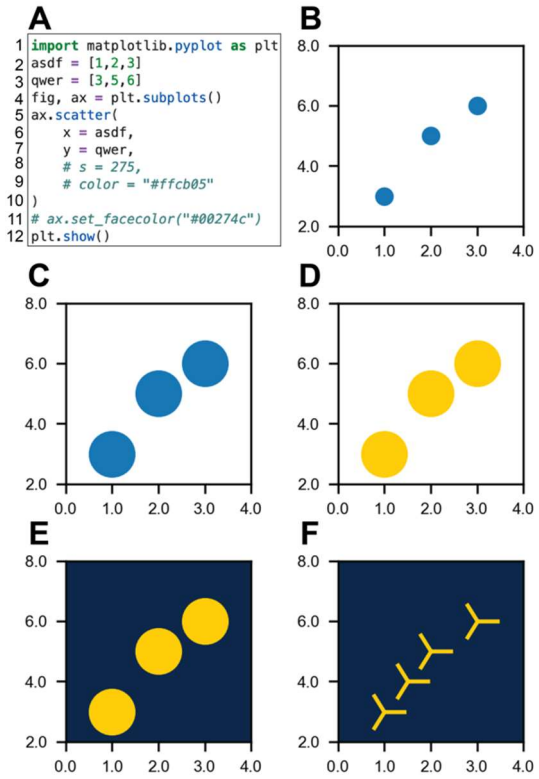

Figure 2.2 **(A)** A self-contained code template generates several plots and is provided to students. Several lines are deactivated, as indicated by green text. Lines of code can be reactivated by removing the leading "#", resulting the code to produce a different visual output when executed. 'asdf' and 'qwer' represent the dataset for the following plots. **(B)** The plot generated by the code in **A** when run as is. The three plotted points are defined in the code template, connecting the code to its visual output. Later in the lesson plan, code is introduced to include axis labels. **(C)** The plot generated when line 8 of **A** is activated, resulting in larger points. **(D)** The plot generated when line 9 is also activated, resulting in different point colors. **(E)** The plot generated when line 11 is activated, creating the same scatter plot with a blue background. **(F)** A potential plot generated after students are instructed to include an additional parameter to the scatter function. In this case, the shapes of the points are changed.

The first module walks through basic plotting in Python. The students receive a code template (Figure 2.2, A, Figure 2.9), which generates a plot when executed in the notebook. Several lines have been "commented out", and thus deactivated, as indicated by lines containing green text and beginning with a #. Students are instructed to run the script, note what happens, then reactivate a line of code (by deleting the # symbol) and run the script again. This approach is intended to build familiarity with Colab and to exemplify how certain lines of code affect the script's output.

As with the code template, most Python scripts begin with a list of package imports, lines of code that allow prewritten code to be used succinctly in the current script and always contain the keyword *import*. For instance, to avoid writing the code to render plots from scratch, Python is instructed to import the Pyplot module from the package Matplotlib, a well maintained and versatile graphing software. As seen in the first line of the code template, a package is imported through specific syntax: *import* <*package_name*> or *import* <*package_name*> *as* <*alias*>. In the first syntax, future references to the package must use the exact package name written in the import statement. In the second syntax, the *as* keyword instructs Python to allow the coder to refer to the package as *plt*, a commonly used short-hand alias for the Pyplot module of Matplotlib that represents the package in code. At this point onward in the code, functions (reusable blocks of code that perform a specific task or set of tasks when executed) provided by the imported package can be utilized by "calling" them, which is done by appending parenthesis () to the function name – for example, *plt.subplots()*, where the period between *plt* and *subplots* indicates that *subplots* is a function defined in the module *plt* (the short-hand alias given for the Pyplot module of Matplotlib). Variables are pointers to objects (data stored in computer memory) that are named by the user and can reference data or the results of previously written code in other files or installed packages. Variables are subsequently referred to in code by their given name.

In the following two lines, two lists are instantiated. Lists are Python objects that store data in a fixed order, similar to a row in a spreadsheet, and can be referred to by variables. The first list is referred to by a variable named *asdf*, and stores the integers 1,2, and 3, in that order. The second list is named *qwer* and stores the integers 3,5, and 6 in this order. In the following line of code, the variables *fig* and *ax* are instantiated and assigned to the output of the function *plt.subplots()*.

The response of this function when called is captured in the variables *fig* and *ax*, as named by the user, and are later referred to in the code to draw and save a plot. The portion of the response that is stored in *fig* is described as "the top-level container for all the plot elements" in its documentation.[26] In essence, the variable *fig* now represents the digital data structure, stored in the computers random access memory, that will eventually render into a visual image. Similarly, *ax* represents an abstract object that is used in code to draw plots. The *scatter()* function, found in the object represented by the variable *ax*, can be provided data to generate a scatter plot. As with before, the function is called by appending parenthesis to the name of the function, *ax.scatter().* Data is "passed" to the function as input through what is written between the parenthesis of the function call, otherwise known as the "parameters" of the function. In the case of the code template, 4 lines of code are written in-between the parentheses, each representing a parameter to the scatter function. Syntactically, parameters must be separated by commas, and new lines between parameters are optional but encouraged for legibility. The first parameter is passed in line six, where it is specified to the function that the x axis data is equal to the list of data that is represented by the variable *asdf*. In the following line, the y data is set to *qwer*. The final two lines of parameters are commented out. The scatter function requires both x axis data and y axis data to be provided. The remaining parameters are optional. The final line of code is *plt.show(),* which instructs the notebook to render the plot. Thus, running the code as given generates the scatter plot shown in Figure 2.2, B. By uncommenting the line *# s = 275*, students reactivate the size parameter of the scatter plot function. Rerunning the code now generates the plot shown in Figure 2.2, C. Reactivating the color parameter creates the plot in Figure 2.2, D, which changes the color of the markers in the plot. Students then change the background color of the plot by using the *set_facecolor()* function provided by *ax*. By uncommenting the line of code,

a hexadecimal color code is passed as a parameter to the function, and the plot of Figure 2.2, E is produced. In the module, students are provided the documentation to the scatter function,[27] and are asked to add an additional parameter to change the shape of the points, generating a plot such as Figure 2.2, F. This simple plotting exercise is designed to give students at a minimum a new skill of plotting: while few students in the class are likely to go on to a career in data science, nearly all of them will need to plot data in many diverse settings, and this learning module complements what they would generally perform in the Microsoft Excel software.

To expand on module one, the second module guides the students through creating a plot of a large dataset. The data file is a json file and contains a list of dictionaries (similar to a list, but in Python dictionaries, data is stored via key:value pairs, where the value is retrieved by passing the key to the Python dictionary). Each Python dictionary in the list contains information regarding a drug in DrugBank,[28] containing its SMILES string ("Simplified Molecular Input Line Entry System", a text encoding of molecules readable by the machine commonly used to store chemicals in a dataset)[29] as well as pre-calculated physicochemical properties. Students are instructed to upload their data file into Colab. (Figure 2.9) With provided code, students are then instructed to import the data contained in the given file using the json package and to convert the data into a DataFrame, a data structure representation provided by the Pandas package, allowing for spreadsheet like manipulation of the dataset (Figure 2.10). Using a *for* loop, ten dictionaries from the json file are added to a list, and the *pd.DataFrame()* function is used to store the data as a DataFrame. Students then print the contents of the DataFrame and inspect the contents of the json file. (Figure 2.3, Figure 2.11) Finally, another graphing template is provided, and the students must execute it to plot the drugs by their properties in an x-y scatter plot. In this template, a *for* loop is used to iterate through the DataFrame, and store the LogP, polar surface

area (PSA), and QED of each drug into respective initialized lists. Then, the scatter function is used to plot the drugs on a graph with LogP on the x-axis and PSA on the y-axis represents (Figure 2.12

). Each point is then colored by QED using the color parameter (c). This exercise helps to visualize the Lipinski properties and concepts of drug-likeness, while visualizing a large chemical space.

OUTPUT

	SMILES
0	CC[C@H](C)[C@H](NC(=O)[C@H](CCC(O)=O)NC(=O)[C@...
1	CC(C)C[C@H](NC(=O)[C@@H](COC(C)(C)C)NC(=O)[C@H...

	LOGP	HBD	HBA	PSA	ROTB	AROM	FSP3	FC
-8.11643	28	29	901.57	66	3	0.540816	0	
-3.10570	17	16	495.89	31	4	0.508475	0	

Figure 2.3 Students are provided with the code to import any tabular JSON file. The utility of the package Pandas is used in reading tables programmatically. The “alldrugsprops.json” file is provided to students, and provided with a template to import the data into Python, as seen in the input block. Students then inspect the contents of the file with Python, revealing a data file of over 9,000 drugs and their properties downloaded from DrugBank.

In the third module, the student uses the code provided in module 2 to generate another plot that visualizes the uploaded DrugBank data but with a different color than before. In this module, additional physicochemical properties are introduced. Common parameters of druglikeness are included in the dataset such as LogP, PSA, number of aromatic rings, hydrogen bond donors (HBD) and hydrogen bond acceptors (HBA). The full list of included properties is listed in the Supporting Information. Concepts such as variables (user specified names that represent values stored in the computer’s memory) and f-strings (a feature in Python that allows values to be embedded in text) are explicitly introduced here. The user can set the color variable to a column header from the DataFrame. Through a function parameter, the color of the plot is automatically updated, and the title of the output figure is modified through a separate function.

In the final module, students are asked to swap the data represented by the axes of the plots, which can be easily performed by switching the DataFrame header referred to in the code. The student also has the option to investigate a third dimension by modifying the color of the

plotted points. In the accumulation of this notebook, students are now comparing trends of physicochemical properties by modifying the x-axis, y-axis, and color attributes. Several plots generated by students are showcased in Figure 2.4.

This notebook is concluded with the following questions, which the students answer in their lab report:

1. What are the Lipinski rules?
2. Write code for filtering to drugs that pass all the Lipinski rules
3. Suggest a research question that you could ask of the DrugBank dataset

These discussion questions evaluate student understanding of medicinal chemistry concepts and their ability to manipulate datasets using basic Python code. Given the importance of the online Python community, it is expected and encouraged that students will utilize internet searches to assist in the writing of filter code to answer the second question. This emphasizes the importance of independent problem solving when encountering unfamiliar bugs or errors when coding. Filters can be written manually with if statements and for loops, as explained in the preliminary presentation, or using a function included in the Pandas package.

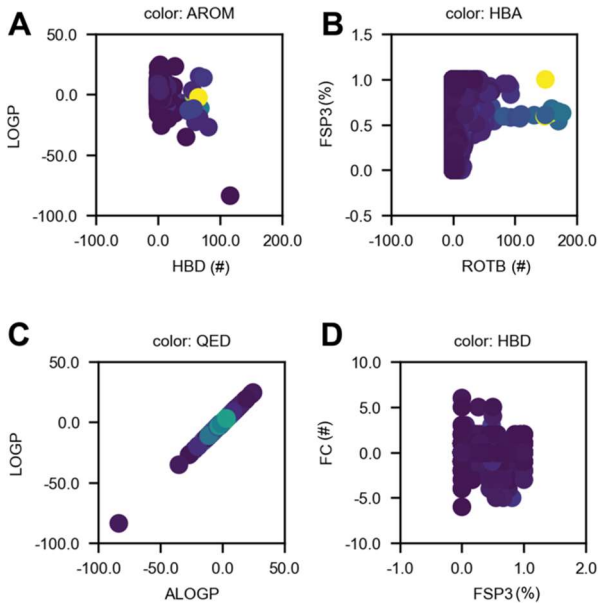

Figure 2.4 Four chemoinformatic experiments run by students during the first session. In each graph, over 9,000 drugs are graphed onto scatter plots using calculated properties of the drug. Students learn to change the axes and colors of the plot, exposing them to a strategy to rapidly investigate chemical space and generate reports in Python. **(A)** A plot of LogP (a dimensionless quantity representing a molecule's distribution between hydrophobic and aqueous environments) against the number of hydrogen bond donors (HBD), colored by number of aromatic bonds (AROM). **(B)** A plot of fraction sp^3 (FSP3, the ratio of sp^3 hybridized atoms to all atoms) against the number of rotatable bonds (ROTB), colored by the number of hydrogen bond acceptors (HBA). **(C)** A plot of LogP against aLogP (a similar quantity to LogP representing a molecule's lipophilic nature but calculated differently with a focus on the molecules constituent atoms), colored by quantitated estimate of druglikedness (QED). **(D)** A plot of formal charge (FC) against FSP3, colored by hydrogen bond donors.

2.1.5 Class Session 2: Principal Component Analysis

The second class session begins with another short lecture. In this lecture, the concept of machine-readable molecular representations is introduced through SMILES. Box plots are shown as a way to visualize molecular datasets via distributions of Lipinski[30] and other relevant medicinal chemistry properties. Finally, histograms and principal component analyses (PCA) are introduced. The second notebook and its lab report are then completed after the lecture.

The notebook provided with this class session utilizes a dataset from Diamond XChem's COVID Moonshot project.[1] Inhibition data against the SARS-COV-2 main protease (MPro) alongside precalculated physicochemical properties and SMILES for various inhibitors are included in a provided CSV file. The learning objectives of this notebook are to filter out

unusable data, use data visualization to validate medicinal chemistry principles, perform basic statistical analyses, and simplify multidimensional data using PCA.

In the first module, students are provided with the Moonshot CSV and are instructed to load and inspect the CSV using the Pandas package (Figure 2.14, 2.15). Some lines are missing data, and the concept of cleaning datasets is introduced. Using Pandas, entries without IC_{50} values are then filtered, and students are asked to record the number of remaining molecules in their report.

In the second module, the students are asked to validate GlaxoSmithKline's (GSK) Solubility Forecast Index (SFI),[31] which predicts aqueous solubility based on a compound's polarity (logP or logD) and number of aromatic rings (AROM), using the filtered dataset from the previous module (Figure 2.16). The students are directed to use the template, plotting code to show how solubility is affected by the number of aromatic rings and LogP (Figure 2.5). In this case, the template script is missing lines of code, requiring students to fill in the missing portions themselves (Figure 2.17). This requires students to correctly plot certain properties from the dataset, which is possible given an understanding of the components in the index and the script template, directly building on the concepts of the first lab exercise. By this point, students should be comfortable loading datasets into Python and creating and styling plots based on column headers and have growing familiarity with visualizing and exploring chemical space via relevant properties.

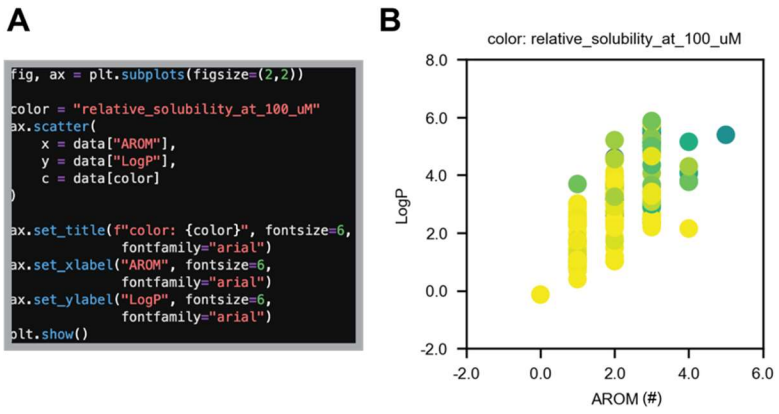

Figure 2.5 **(A)** The template plotting code is incrementally improved until it can be used effectively to make manuscript-ready graphics. This code creates a scatter plot of the Moonshot compounds provided in the CSV, where the x-axis is the number of aromatic rings (AROM), and the y-axis is LogP. **(B)** By coloring the points by the compound's reported experimental solubility, a trend is revealed where compounds with fewer aromatic rings and lower LogP are more soluble. Validating GSK's Solubility Forecast Index is a simple experiment to allow students to build confidence in their ability to manipulate and analyze datasets.

Also in this module, students are instructed to make box plots of various properties encoded in the data file, providing an alternative visualization of the dataset. The code template is provided, and students are asked to analyze and modify the code to reshape the grid of boxplots. Students are encouraged to improve the plots aesthetically and to practice modifying the data that is plotted by changing the variables. Here the ability to plot multiple distributions into the same figure using Matplotlib's *subplots* function is explicitly introduced. As molecules can have many descriptors, multiplexed figures are powerful in evaluating medicinal chemistry datasets.

In the third module, the multidimensional scaling PCA is performed on the dataset. The utility of a PCA is explained to the students within the lecture slides as a method to combine multiple features of a datapoint into fewer features, while the math is omitted as it is beyond the scope of this medicinal chemistry course. Students are instructed to create a matrix containing the Lipinski physicochemical properties for each entry in the dataset, resulting in a DataFrame with five columns and a row for each compound. Using the provided template code (Figure 2.18), the students feed their matrix into scikit-learn's PCA decomposition algorithm, where the

matrix is reduced to two dimensions. The resultant data is then plotted and colored by a property. Students are subsequently instructed to filter out non-Lipinski compliant molecules, rerun the reduction and compare the final graphs (Figure 2.6). To complete this objective, students must use what they have learned in the previous modules or in the lecture notes to write a *for* loop and use *if* statements to collect datapoints that comply with the Lipinski rules. Alternatively, students are encouraged to search for Pandas documentation and to perform the data filtration using a Pandas function. In this module students begin to familiarize with dimensionality reduction and the identification of features that lead to dataset variance.

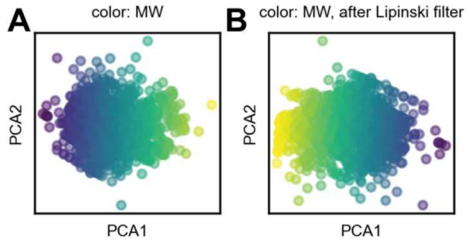

Figure 2.6 By the end of the modules, students have implemented a data filter and a principal component analysis on a dataset of SARS-COV-2 Main Protease inhibitors. **(A)** the PCA before the data filter is applied. Points represent DrugBank compounds and are colored by their molecular weight. By changing the color of the points, the correlation of the reduced features can be mapped to specific features of the dataset. In this instance, molecular weight tracks with the first principal component, increasing as the x value increases. **(B)** The PCA plot after the Lipinski filter is applied. Outliers are removed by the filter, and the distribution of molecular weights in the first principal component becomes wider. The direction of the color gradient has changed as the sign of the principal components are arbitrarily assigned.

In the final module, students use the filtered dataset and are introduced to a new package that allows for the creation of interactive plots. Using the template code, students use the package plotly to generate an interactive PCA that displays SMILES and other information for each plotted entry. Plotly works similarly to the Matplotlib package, but instead produces an interactive scatter plot, where datapoints can be hovered over with the cursor to inspect additional information. Students are asked to engage with the interactive scatter plot, record several of molecules from different clusters, and answer a question about sampled molecules from various clusters (Figure 2.19).

2.1.6 Participants

The participants in this lesson plan were students enrolled in a senior level undergraduate medicinal chemistry course. Through informal in-class surveys, it was found that nearly all participants had little to no previous coding experience, and these modules were their first introduction to a hands-on coding activity. This lesson plan was developed and conducted over five years of students; in an in-person and remote format. In the first two years, only the first module was taught. Over 100 students have participated in the class.

2.1.7 Implementation

This lesson plan was given to undergraduate classes of pharmaceutical science majors in mid-semester of their senior year, after several units introducing basic medicinal chemistry concepts are completed. In this case, each class consisted of around 30 students and were supervised by two graduate student teaching assistants. As mentioned, the lesson plan is split into two three- hour class sessions. At the beginning of each class session, graduate student teaching assistants present a lecture and slide deck with basic coding and Python concepts before the students begin working on the notebook corresponding to the class session (notebook 1 for the first class, notebook 2 for the second class). The initial implementation of this activity was done without Colab, with tutorials provided to install Python on each student's personal computers. The diverse operating systems and security settings of each individual student required some installation guidance for a handful of students each year. With the introduction of Colab to the academic community, the onboarding process for the activity was greatly simplified as it became guaranteed any student could complete the activities on their own computer agnostic of hardware or software. During the class sessions, graduate student teaching assistants are available for troubleshooting and questions. In this implementation, the most common problem students

encountered were syntax issues in their code. While the templates and instructions provided were meant to minimize syntax errors, it was beneficial for the graduate student teaching assistants to have familiarity with common Python error messages to quickly identify the source of the bug and to direct the students to correct the invalid syntax. Students are permitted to work in groups to complete the exercises, and most students were able to independently complete all exercises without supervision or additional guidance from an instructor.

2.1.8 Assessment of effectiveness

As of 2023, nearly all senior undergraduates who have enrolled in the class have reported having little to no experience in coding or programming prior to taking this lab exercise. Throughout the lesson plan, students submitted plots they have generated to the graduate student teaching assistants alongside their code to be graded for accuracy. By the end of the two classes, each student was able to successfully use the code to generate various plots of chemical space that were correctly labeled. Grades for submitted lab reports were consistently above 90%, with competent students able to produce plots from text prompts and no provided template. Furthermore, after the lab sessions, students from the last two years' lab were asked to complete the following five-question survey:

1. This exercise improved my understanding of chemistry
2. This exercise improved my understanding of Python
3. This exercise improved my understanding of chemical space
4. This exercise improved my data science
5. I enjoyed this exercise

Based on the responses received and the high marks earned by the students on their lab reports, it is concluded that the current state of the module is effective in improving the

understanding of basic data science and informatics in medicinal chemistry for most students (Figure 2.7).

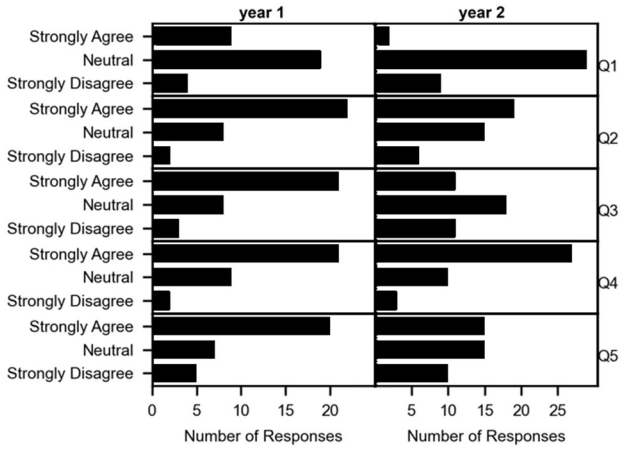

Figure 2.7 Bar charts showing student feedback to the lesson plan collected after the lab. Questions were intended to gauge the student's perspective on their learning experience. In the first year, students felt strongly that their understanding of Python, chemical space, and data science were improved. In the second year, students felt strongly that their understanding of data science improved but were neutral on other learning objectives. The difference between the two years may be accounted for by the level of involvement the graduate student teaching assistance had in developing the course. In the first year, the class was taught by the writer of the lesson plan; the second year was taught by assistants who were given the lesson plan to teach.

2.1.9 Summary

A lesson plan to teach undergraduates the basics of data science in medicinal chemistry was developed and validated over several semesters. Over the course of two lab sessions, students are introduced to Python, Google Colaboratory, and several Python packages. Students learn these tools through guided, interactive modules that begin at learning how to function Colab and ends with developing a program that reads abstractable datasets and generates user-interactive data analytics through Python. An assessment reveals the lesson plan seems to be effective in improving student's familiarity with modern chemoinformatic tools and concepts. It is postulated that the lesson plan may be effective for younger students and can be completed by anyone with a computer and internet access.

2.2 Lab Protocol and Report Template for Interactive Python Notebook Modules for Chemoinformatics in Medicinal Chemistry

2.2.1 Lab 1 Protocol: Chemoinformatics and Python

Chemoinformatics is the use of computational techniques to solve problems in chemistry. These *in silico* methods can be used to transform data into information and aid in the process of drug discovery. Recently, a rise in computational power and increased availability of developed tools have turned chemoinformatics into an invaluable tool for research.

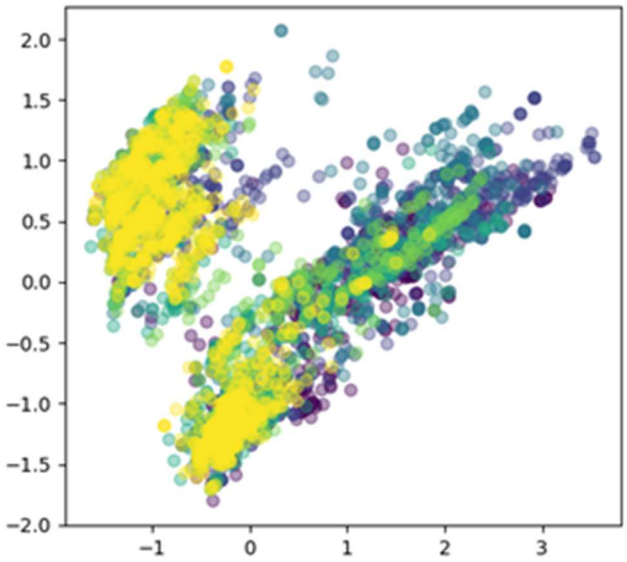

Figure 2.8 An example of a plot that can be generated using the code provided in this module. The module walks students through the provided code template, building familiarity with plotting datasets using Python.

The purpose of this experiment is to introduce you to chemoinformatics using Python. By the end of this module you will have the ability to use Python to quickly compile and plot data. During this lab, you will:

- Learn about data structures in Python
- Load compiled data that is suitable for sharing and later use
- Effectively parse through compiled data

- Perform mathematical operation on compiled data
- Plot data in a multitude of ways

2.2.1.1 Google Colab

This tutorial will be complemented by Google Colaboratory (Colab), which is an online python environment with preinstalled packages and executes code on the cloud provided for free by Google. Its primary advantages here are allowing a fast and simple way for new students to get started coding instantly, as it is agnostic of computer and operating system and requires no setup. In the first requirement of this tutorial, you will have to download 'lab1_notebook.ipynb' from Canvas and upload it to your Google Drive. Open your file in the 'colab app'. As explained in the video, code is separated into blocks called 'cells', which execute independently of each other. Hit control or command-enter to execute the code in a cell. In the following sections, you will be executing code cell-by-cell and editing code as outlined in the colab file. Also, ensure that you have downloaded the alldrugprops.json file from canvas.

Before starting this module ensure that:

1. You have downloaded lab1_notebook.ipynb and added it to your drive.
2. You have downloaded 'alldrugprops.json' from Canvas.

2.2.1.2 Module 1: Simple plotting using MatplotLib

1A) Type in the text below, then Run (ctrl+enter) (CMND+Return on Mac). Alternatively, you can press the play button. If you get a syntax error, you likely have a missing comma or bracket somewhere – proofread your code to identify any typos. In this script, we have defined two lists, their names are "asdf" and "qwer".

```
import matplotlib
import matplotlib.pyplot as plt

asdf = [1,2,3]
qwer = [3,5,6]

fig, ax = plt.subplots()

ax.scatter(
    x = asdf,
    y = qwer,
    #s = 275,
    #color = '#ffcb05'
)

#ax.set_facecolor('#00274c')
plt.show()
```

Figure 2.9 Basic template script provided to the students that can be modified through activation and deactivation of lines of code.

lines of code.

1B) The plt.show() command from the matplotlib package opens your plot in a new window. Later we will save our plots as a .png, but for now we will see how things change in the plt.show() window. **Take a screen shot of your plot for your lab report.**

1C) Delete the first hashtag to activate the line: s = 275. Rerun your code (CTRL+S then ctrl+enter). What happened? Play with different values for s (size) until you are happy with the result. **Take a screen shot of your plot for your lab report.**

1D) Remove the next hashtag. This should change the color. #ffcb05 is a hex code, which is one of several ways to describe a color. **Take a screen shot of your plot for your lab report.**

1E) Remove the next two hashtags. Run the code. **Take a screen shot of your plot for your lab report.**

1F) Add in a fourth point at x = 1.5, y = 4. **Take a screen shot of your plot for your lab report.**

2.2.1.3 Module 2: Plotting data from a file.

In module 1, we worked from two lists named “asdf” and “qwer”. In reality, you would more often read in lists from a larger data set, which we will do here. The file alldrugsprops.json contains information for all of the 9,279 drugs in the DrugBank database, with appended chemoinformatics data which was calculated in RDKit (a free python package specifically for chemoinformatics) or Pipeline Pilot (a powerful chemoinformatics software which is not free). [TIP: The DrugBank database is an important source of free data for chemoinformatics. CHEMBL is another important free database for drug discovery which includes thousands of chemical structures (as their SMILES strings) and associated biochemical, *in vivo*, and pharmacokinetic data collected from patents and the scientific literature.]

2A) To start, you must have downloaded the alldrugprops.json file. To allow colab to read the file, open the file directory by clicking on the folder icon to the left. Drag the alldrugprops.json file into the opened side bar to upload the file.

1. Click folder icon to open sidebar 2. Drag and drop 'alldrugprops.json' in the sidebar

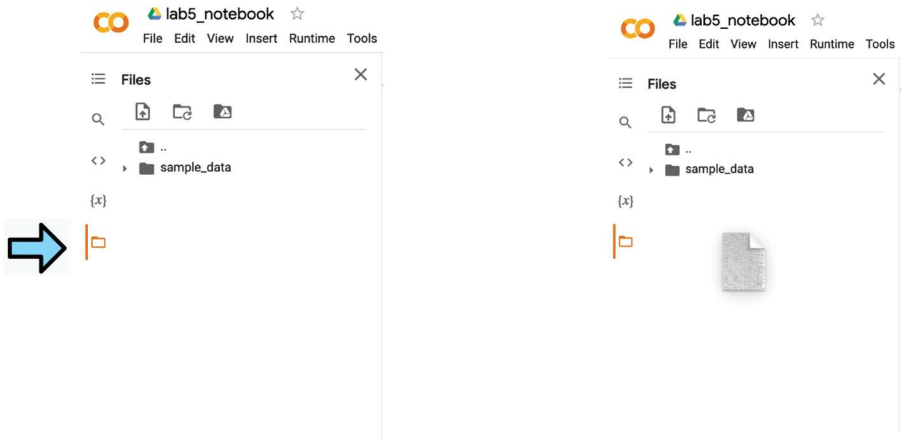

If it worked, you should see the file in the sidebar:

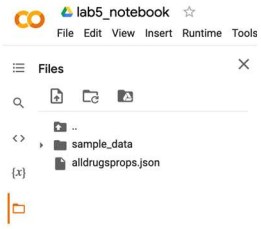

Figure 2.10 The workflow describing uploading data to Colab. With the provided datafile, students are expected to follow the visual instructions and drop in the file. Once the file is visible in the file browser, Python can be used to read its data.

2C) Run the next block of code to get a sense of what the data looks like

```
import json
import pandas as pd

with open('alldrugsprops.json') as f:
  drugProps = json.load(f)

data = []
for prop in drugProps[0:10]:
  data.append(prop)

df = pd.DataFrame(data=data)
print(df.to_string())
```

Figure 2.11 A code template provided that reads the data uploaded to Colab, and uses a "for loop" to add ten data points to a list. The list of 10 datapoints is converted into a DataFrame, which is then visualized in tabular format.

	SMILES	MR	LOGP	HBD	HBA	PSA	ROTB	AROM	FSP3	FC	QED	ALOGP
0	...O)C(=O)N[C@@H](CC1=CC=C(O)C=C1)C(=O)N[C@@H](CC(C)C)C(O)=O	539.8094	-8.11643	28	29	901.57	66	3	0.540816	0	0.014176	-8.11643
1	...)N1)C(=O)N[C@@H](CCCN=C(N)N)C(=O)N1CCC[C@H]1C(=O)NNC(N)=O	328.5382	-3.10570	17	16	495.89	31	4	0.508475	0	0.010267	-3.10570
2	...O)N[C@H](CC(C)C)C(=O)N[C@@H](CC1=CNC2=C1C=CC=C2)C(=O)NCCO	500.1181	4.86760	20	16	519.89	51	8	0.510417	0	0.022619	4.86760
3	...1=O)C(=O)N1CCC[C@H]1C(=O)N[C@@H](CCCNC(N)=N)C(=O)NCC(N)=O	271.4037	-4.13203	14	15	435.41	19	2	0.478261	0	0.027501	-4.13203
4	...O)N[C@@H](CCCNC(N)=N)C(=O)N1CCC[C@H]1C(=O)N[C@H](C)C(N)=O	377.7252	-0.50613	17	16	495.67	38	5	0.428571	0	0.013447	-0.50613
5	...@H](CC(O)=O)NC(=O)[C@H](CCCN)NC(=O)CNC1=O)[C@H](C)CC(O)=O	400.2605	-5.62180	22	24	702.02	35	3	0.527778	0	0.011297	-5.62180
6	...C)C(=O)[C@@H](NC(=O)[C@H](CC(C)C)N(C)C(=O)CN(C)C1=O)C(C)C	328.4446	3.26900	5	12	278.80	15	0	0.790323	0	0.147925	3.26900
7	...C@@H](CCC(N)=O)C(=O)N[C@@H](CC(N)=O)C(=O)N1)C(=O)NCC(N)=O	266.8519	-4.03470	12	15	405.32	19	2	0.500000	0	0.047101	-4.03470
8	...I[C@H](CO)[C@@H](C)O)NC(=O)[C@H](N)CC1=CC=CC=C1)[C@@H](C)O	272.0538	-0.80540	13	14	332.22	17	4	0.448980	0	0.045518	-0.80540
9	...O)N[C@@H](CCCCNC(C)C)C(=O)N1CCC[C@H]1C(=O)N[C@H](C)C(N)=O	377.1827	1.16800	13	16	424.98	38	5	0.458333	0	0.024675	1.16800

Figure 2.12 The table generated by printing the DataFrame containing the 10 datapoints. Students can scroll while their mouse cursor hovers over the output table to inspect all data columns.

2D) Now that you have a sense of what the data structure in the .json file looks like, let's make a plot. Copy the following code in colab and run it to produce the plot. Recall that hashtag inactivates a line of code. The text with hashtags below is just instruction and does not need to be entered. If you get a syntax error, check for missing parentheses or commas or other typos. **Take a screenshot of your plot for your lab report.**

```
logp, psa, qed = [], [], [] # initialize lists
for prop in drugProps: #iterate through each item in drugProps
  logp.append(prop["LOGP"])
  psa.append(prop["PSA"]) #append valeus into respective lists
  qed.append(prop["QED"])

fig, ax = plt.subplots()
ax.scatter(
    x = logp,
    y = psa,
    c = qed
)
ax.set_xlabel("logp")
ax.set_ylabel("psa")
plt.show()
```

Figure 2.13 The graphing template provided to the students to plot the data from the given datafile. A for loops is used to select specific columns of data, which is then fed into the scatter function to plot the DrugBank drugs via their properties. The code template is very similar to the template provided in the first module, showing how incremental changes in the code can lead to more complex visualizations.

2.2.1.4 Module 3.

Create the same plot as in module 2, but color by a different quantity.

Keys you can use from the JSON:

- MR

- LOGP
- HBD
- HBA
- PSA
- ROTB
- AROM
- FSP3
- QED
- ALOGP

Be sure to label/write down the quantity you chose. Use ax.set_title("title") to add a title to your plot.

2.2.1.5 Module 4

Create the same plot as in module 3, but use different quantities for the x and y axis. Do not use logp and psa again. Change your x and y labels accordingly.

Use Google to find an answer in the python user community. Search "How do I _____ in matplotlib". You can change the shape of the points, add in a plot title, switch the axes to a log scale, turn up the transparency on your plots for example. A big part of using python is learning how to extract information from the very large user community. There are many sophisticated things you can do once you've got some comfort in python. You could run a principal component analysis on several of the properties in the .json file. You could write a FOR loop to plot three different plots on the same page with different y-axes. Give your plot a personal touch.

Take a screenshot of your plot for your lab report

For the laboratory report:

Save all plots you made. Ensure that they are all labelled and titled accordingly. Answer the discussion questions.

2.2.2 Lab Report for Lab 1: Chemoinformatics.

Name: _____

Date: _____

Objective:

2.2.2.1 Data and Results

1. First five simple plots (Steps **1B - 1F**)
2. Plot of LogP vs PSA colored by QED **(2D)**
3. Plot of LogP vs PSA colored by _____ **(Module 3)**
4. Plot of ____ vs _____ colored by ____ **(Module 4)**

2.2.2.2 Discussion

1. What are the Lipinski rules?
2. Write code for filtering by drugs that pass all of the Lipinski rules (Hint: this can be done with an if statement and a for loop. See slide 14)
3. Now that you've done some basic coding, suggest a research question that you could ask of the DrugBank dataset. You do not need to write the code, but what hypothesis could you formulate, and then test within the data, using python?

2.2.3 Lab 2 Protocol: Chemoinformatics and Python

Chemoinformatics is the use of computational techniques to solve problems in chemistry. These *in silico* methods can be used to transform data into information and aid in the process of drug

discovery. Recently, a rise in computational power and increased availability of developed tools have turned chemoinformatics into an invaluable tool for research.

In this lab we will expand on what we learned in the previous lab. Specifically, we will

- filter out unusable data
- use data visualization to validate medicinal chemistry principles
- perform basic statistical analysis
- Simplify multidimensional data using Principal Component Analysis

Notes:

Before starting this module ensure that:

1. Ensure that you have downloaded the activity_data_with_props.csv and lab2_notebook.ipynb file from canvas.

2.2.3.1 Module 1: Importing and Filtering Data in Pandas.

This csv is taken from diamond Xchem's COVID moonshot project (https://covid.postera.ai/covid/activity_data) and is inhibition data against the SARS-COV2 main protease. The physical properties were calculated based on the SMILES strings using RDKit (a free python package specifically for chemoinformatics).

1A) We will begin by importing the packages that we need as well as uploading the data file into colab, just like in lab 1. Add lab2_notebook.ipynb to your google drive, open in colab, and add "activity_data_with_props.csv" to the file system as shown below.

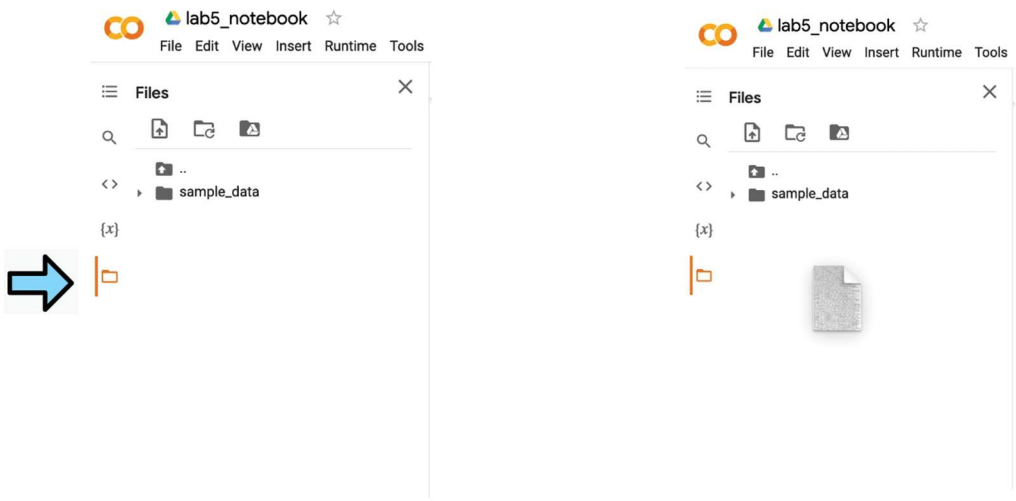

Figure 2.14 Another visual example of uploading a given datafile to Colab via dragging and dropping the file onto the file manager.

1B) We are opening the activity_data_with_props csv and calling it "data". We will also use the "len" function to see we have 1699 data points

```
data.head()
```

	Unnamed: 0	SMILES	CID	Unnamed: 2	f_inhibition_at_50_uM	f_avg_IC50	f_avg_pIC50	relative_solubility_at_20_uM	relative_solubility_at
0	0	O=C(Cn1ccnc1)NCC1(C(=O)Nc2cncc3ccccc23)CCOc2cc...	EDG-MED-70ae9412-1	NaN	NaN	2.879609	5.540667	NaN	
1	1	CN(C)CC(=O)NCC1(C(=O)Nc2cncc3ccccc23)CCOc2ccc(...	EDG-MED-70ae9412-2	NaN	NaN	5.004724	5.300620	NaN	
2	2	O=C(Nc1cncc2ccccc12)[C@@]1(O)CCOc2ccc(Cl)cc21	MAT-POS-9db1e783-1	NaN	NaN	NaN	NaN	NaN	

```
len(data)
```

```
1699
```

Figure 2.15 Inspection of the data from the provided datafile in tabular format using Pandas. The number of points in the datafile is revealed by using the len() function.

1C) You will notice entry 2 does not have an IC50 value. We will want to remove any molecules without inhibition data. Run the next block of code to accomplish that.

1D) Now use the len function again to see how many data points are left. **Record this value for your lab report**

2.2.3.2 Module 2: Plotting data from a file.

In Module 1, we opened a large set of data and filtered out incomplete entries. Now we are going to perform analysis on our data.

2A) To start, we will create shortcuts for each property in this dataset. Run the first block of code.

```
LOGP = data_cleaned['LogP'] # Log Partition Coefficient
PSA = data_cleaned['PSA'] # Polar Surface Area
MW = data_cleaned['MW'] # Molecular Weight
QED = data_cleaned['QED'] # Quantitative Estimate of Druglikeness
HBD = data_cleaned['HBD'] # Hydrogen Bond Donors
HBA = data_cleaned['HBA'] # Hydrogen Bond Acceptors
ROTB = data_cleaned['ROTB'] # Rotatable Bonds
AROM = data_cleaned['AROM'] # Num Aromatic Rings
FSP3 = data_cleaned['FSP3'] # Fraction sp3
Solubility = data_cleaned['relative_solubility_at_100_uM']
IC50 = data_cleaned['f_avg_IC50'] # IC50 of Molecule
```

Figure 2.16 Provided code showing how columns of data can be extracted from the DataFrame into variables. These variables are referred to later in the code to simplify plotting.

2B) Now we are going to validate GSK's Solubility Forecast Index[31]. Create a scatter plot that shows how solubility is affected by number of aromatic rings and LogP. You will need to type your own code into the empty cell and fill in the appropriate words:

```
fig, ax = plt.subplots()
ax.scatter(
    x = ,
    y = ,
    c =
)
ax.set_xlabel("")
ax.set_ylabel("")
plt.show()
```

Figure 2.17 Empty template code to plot physicochemical properties of the dataset. At this point, students are expected to understand the parameters of the scatter function, as well as other functions provided by the Axes object generated from matplotlib.

If you get a syntax error, you likely have a missing comma or bracket somewhere – proofread your code to identify any typos. **Take a screenshot of this plot for your lab report**

2C) Now we are going to do some basic statistics on our data. Box plots are a common way to visualize large sets of data. Run the block of code and discuss with your group what it is doing. **Take a screenshot of the plot for your report.**

2D) Instead of a 5x2 grid, make a 10x1 grid of box plots. **Take a screenshot for your lab report**

2.2.3.3 Module 3.

3A) Now we are going to be doing our principal component analysis. To do this we are going to define features and create a list of lists containing values for the features. Run the next block of code.

```
from sklearn.decomposition import PCA
import matplotlib.pyplot as plt

features = ["MW", "LogP", "HBA", "HBD","PSA"]
input_data = data[features]
print(input_data)

X = PCA(n_components=2).fit_transform(input_data)
plt.scatter(X[:,0],X[:,1],c=data['LogP'])
plt.show()
```

```
            MW     LogP  HBA  HBD    PSA
0      475.936  3.56010    6    2  98.14
1      452.942  3.22500    5    2  83.56
2      354.793  3.49700    4    2  71.45
3      368.820  3.53950    4    2  71.45
4      450.878  4.04330    6    0  85.80
...        ...      ...  ...  ...    ...
1694   248.673  2.77400    3    2  66.91
1695   238.250  1.52948    4    1  78.67
1696   287.322  3.28768    3    1  65.78
1697   262.312  3.41600    2    1  41.99
1698   280.305  1.47150    5    1  89.27

[1699 rows x 5 columns]
```

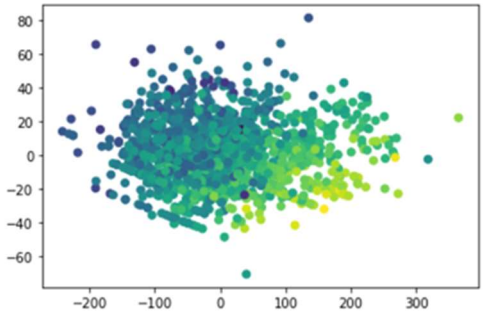

Figure 2.18 Template code provided to the student to execute and visualize a principal component analysis performed on the given dataset. The resultant chemical space is colored by a specific property, revealing a coorelation between the resultant axes of the PCA and drug properties.

Take a screen shot of the plot for your lab report. Now color by another feature and screenshot. Finally color by a property from module 2 that was not included in the features. Screen shot this for your lab report as well.

3B) Now we are going to filter our molecules according to the Lipinski rules. You will notice that the code that worked for filtering a json does not work for a csv. This is because data in a CSV is structured differently than in a JSON file. To figure out how to address this Google the

phrase “filter pandas dataframe by multiple conditions”. Now run and plot a PCA on your Lipinski filtered set. **Take a screenshot of both your code and the plot for your lab report**

2.2.3.4 Module 4.

This block of code will generate an interactive graph that can be used to see values of individual data points. **Copy down the SMILES string and IC_{50} values of 3 molecules that clustered near each other into your lab report. It may be easier to write these by hand and type them into the word document after.**

2.2.4 Lab Report for Lab 2: Chemoinformatics II

Name: _____

Date: _____

Objective:

2.2.4.1 Data and results:

1. How many Molecules were there with IC_{50} data?
2. Plot of from module **2A** validating Solubility forecast index.
3. Box Plots arranged 5x2
4. Box plots arranged 10x1
5. 3 plots from module **3A**
6. Screenshot of your code for your Lipinski filter and your PCA.
7. List of 3 smiles strings and IC_{50}’s from module 4.

2.2.4.2 Discussion

1. What is a principal component analysis?

2. Convert your SMILES you wrote down into a chemical structure. This can be done by pasting into ChemDraw or by typing it in at the following link: https://pubchem.ncbi.nlm.nih.gov//edit3/index.html
3. The following three molecules clustered very near each other on the PCA yet have vastly different IC_{50} values. What structural feature(s) do you think account for this and why?

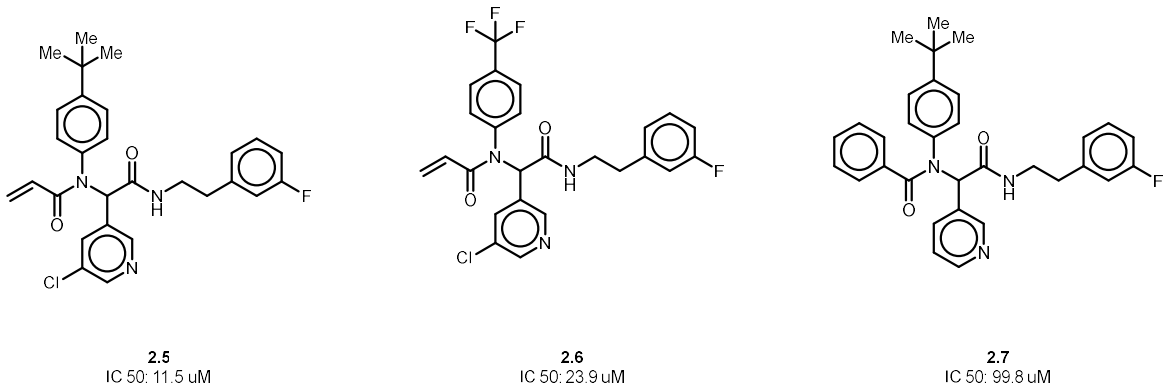

Figure 2.19 Example molecules used to test student understanding of dimensionality reduction algorithms in a molecular context.

2.3 An Automated and Colorful PAMPA Assay to Investigate Drug Permeability

2.3.1 Introduction

New medicines are developed by a careful balancing of a variety of physicochemical properties. One such property that drives efficacy by ensuring the medicine reaches its target is permeability. For an orally active drug, a molecule must permeate across cell walls in the intestine to reach the blood stream, and again when it reaches the target tissue. Further permeation through the blood brain barrier (BBB) is required if the target is in the brain. Therefore, an understanding of a permeability is essential for a career in developing drugs.

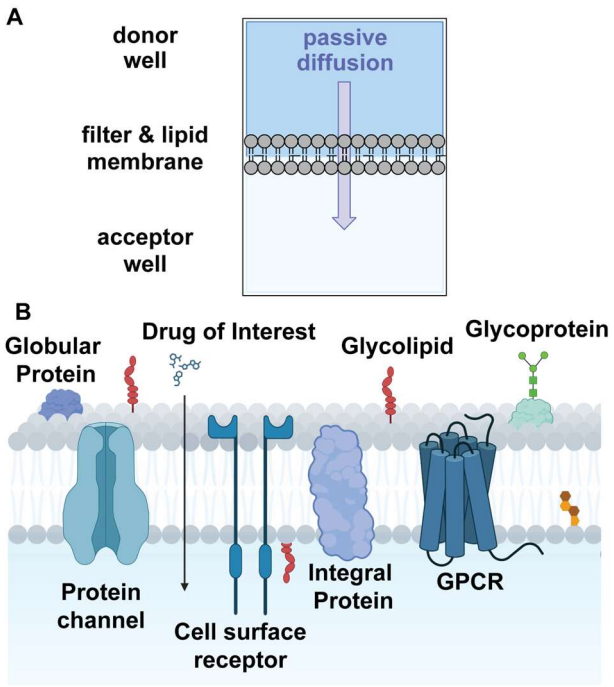

Figure 2.20 A) A representative cartoon of how PAMPA works. B) A cartoon of drug molecules passively permeating through the cell membrane.

Nearly all synthesized small molecules in the pharmaceutical industry are run in a permeability assay.[32] Several of the high-throughput permeability assays that are routinely used in drug discovery include the human colonic adenocarcinoma cell (Caco-2) assay,[33] the Madin–Darby canine kidney cell line (MDCK) permeability assay,[34] and the parallel artificial membrane permeability assay (PAMPA).[35] Among these, the PAMPA is the most accessible. This is due to its low cost, high throughput, and lack of cell culture requirements. These qualities also make it an ideal teaching instrument for undergraduates learning medicinal chemistry principles. PAMPA works by creating an artificial membrane in the base of each well of a donor plate. Each well is then loaded with compound and the donor plate placed in an acceptor plate. After an incubation time, the donor plate is removed and the concentration of compound in the acceptor plate is calculated (Figure 2.20, A). This is then used to calculate the effective permeability of the compound as given in equation one.[36]

Equation 1 V_D is the volume of the donor well, V_A is the volume of the acceptor well, time in seconds, $[drug]_{equilibrium} = ([drug]_{donor} \times V_D + [drug]_{acceptor} \times V_A)/(V_D + V_A)$

$$P_e = C \times \left\{ -\ln\left(1 - \frac{[drug]_{acceptor}}{[drug]_{equilibrium}}\right)\right\} where\ C = \left(\frac{V_D \times V_A}{(V_D + V_A) \times Area \times time}\right)$$

This lab consists of two sections. The first section is a one-hour lecture in which students are introduced to the concept of oral bioavailability which leads into a discussion of permeability and factors that affect it. This begins with a discussion on the Lipinski[30] and Veber[37] rules that expands to discuss how pKa and charge affect permeability.[38] There is an explanation of passive permeability (Figure 2.20, B), active transport, and efflux, and how these can affect permeability assay choice as well as in-vivo properties.[39] The advantages and disadvantages of caco-2, MDCK, and PAMPA are elaborated upon. The lecture concludes by covering drug permeability through the blood brain barrier and introducing the central nervous system multi parameter optimization (CNS-MPO) tool.[19]

To give the students hands on experience, they spend a three-hour lab period using PAMPA to determine the permeability of two brightly colored drug molecules, phenazopyridine (**2.8**) and methylene blue (**2.9**) (Figure 2.21). 1 is a dark orange molecule used to relieve pain associated with a urinary tract infection and is uncharged a physiological pH. 2 is a dark blue compound used to treat methemoglobinemia and exists as a persistent cation. Due to the difference in charge at physiological pH, 1 will permeate the artificial membrane whereas 2 will not. The bright color associated with each dye allows for both qualitative determination of permeability visually and quantitative determination of permeability spectrophotometrically.

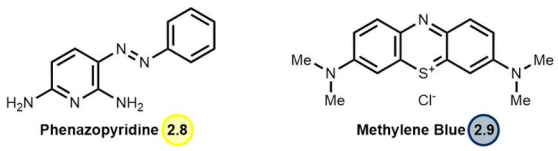

Figure 2.21 Structures of phenazopyridine and methylene blue.

As the assay primarily consists of dilutions and transferring of stock solutions from a vial into a well plate or one well plate into another, it is an excellent candidate for automation using a liquid handling robot. As automation is becoming increasingly prevalent in the pharmaceutical industry, this represents an opportunity to introduce students to the concept and give them applied knowledge. The Opentrons OT2 robot is an inexpensive liquid handling robot that can be controlled using simple python code or a protocol generation software developed by Opentrons.[40–42] This robot is increasingly being adopted to automate chemical tasks.

The goal of this lab is to use PAMPA to determine the permeability of two drug molecules. In doing so, they learn how the structure of a molecule and passive permeability are related, as well as develop pipetting skills, an understanding of calibration curves, and exposure to several techniques/instruments used in the pharmaceutical industry. Additionally, there is an optional introduction to automation of repetitive tasks using robotics.[43]

2.3.2 Participants

Each three-hour lab section consisted of approximately 20 fourth year undergraduate students in a pharmaceutical sciences program. They had previously performed a lab where they were taught coding principles as they relate to cheminformatics. Prior to the lab, students had attended the one-hour lecture and previously completed an exercise in basic python.[2] PAMPA was covered briefly and conceptually explained as was its relevance. Upon entering lab, students were broken into groups of four or five.

2.3.3 Experimental setup.

Each group was assigned 12 wells in a 96 well plate to dose either **2.8**, **2.9**, or a 1:1 mixture of **2.8** and **2.9**. The students were given 5 mM stock solutions of each drug in DMSO and instructed

to generate 250 μM solutions of each compound and 125 μM solution of the mixture by diluting with phosphate buffer solution (PBS). Students were then instructed to create the membrane by dosing 5 μL of a 1% lecithin in dodecane solution into their assigned wells. They were instructed to do so carefully to avoid puncturing the membrane and invalidating their experiment. Following this each student pipetted 150 μL of each solution into 3 of their assigned wells. Further, they dosed 5% DMSO in PBS into their assigned wells in the acceptor plate so there would be contact between the donor and acceptor plates. When all students had finished pipetting into their assigned wells. The donor plate was placed into the acceptor plate and allowed to incubate for one hour (Figure 2.22).

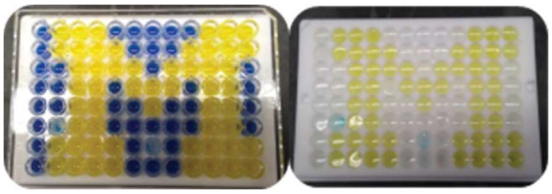

Figure 2.22 A PAMPA plate donor plate (left) and the acceptor plate (right) after a one-hour incubation. Note only phenazopyridine is permeable.

During the incubation period, students worked on an additional computational exercise. Additionally, one group of students at a time was brought to the Opentrons where they used the liquid handling robot to create calibration curve samples for **4.8** and **4.9** (Figure 2.23). The students were shown how to calibrate the pipetting arm and then instructed to change values in a Python script to build their curves in the correct wells. The protocol was loaded onto the robot, and if any errors were discovered such that the protocol would not run, the students were guided toward the error. After fixing the error if present the students executed the protocol. After completion the labeled plate was placed on the lab bench until completion of the assay.

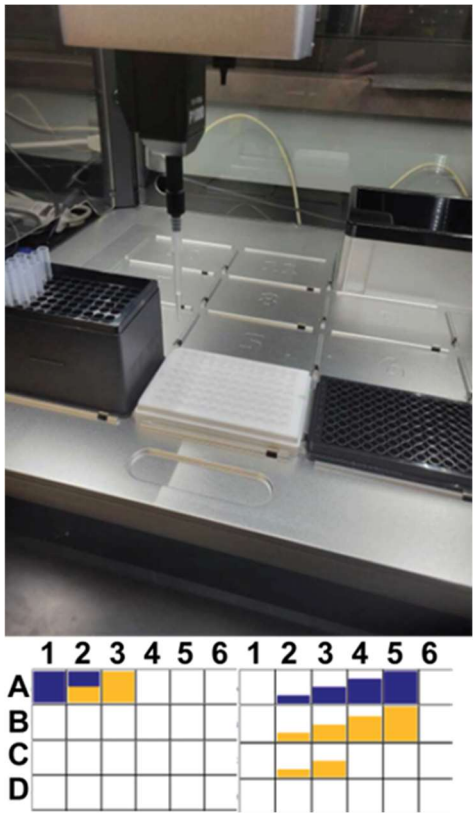

Figure 2.23 **Top**) Opentrons transferring from PAMPA plate to plate reader plate. **Bottom left**) Representation of PAMPA acceptor plate (white) Blue represents methylene blue and yellow represents phenazopyridine. The height of the color represents relative concentration. **Bottom right**) Representation of plate reader (black, destination) plate for Opentrons Dosing. Row A is the methylene blue calibration curve, Row B is the phenazopyridine calibration curve, and row C is what permeated through the donor plate.

After one hour, the donor plate was removed, and each group of students inspected their wells and recorded the color they observed. Additionally, they transferred their assigned wells from the acceptor plate into their plate containing the standard curve samples. The plate was then loaded into a plate reader and absorbance recorded at 413 and 609 nm. The CSV readout of absorbance values was distributed to each group. Students were given one week to process the data, select the correct color for determination of concentration, and complete the accompanying lab report.

2.3.4 Hazards

Students are required to wear appropriate lab attire including safety googles, a lab coat, and gloves during the lab. All chemicals should be handled as indicated by the SDS. Phenazopyridine is acutely toxic and a suspected carcinogen. Both phenazopyridine and methylene blue will stain skin.

2.3.5 Learning outcomes and results

For their report, students were required to summarize the objective of the experiment, describe potential safety hazards, generate calibration curves, and calculate the concentration of each compound in the acceptor wells, and answer discussion questions. Discussion questions were as follows:

(1) Draw the structure of phenazopyridine and methylene blue.

(2) At pH 7.4 why do you think phenazopyridine was permeable and methylene blue was not?

(3) If we reran this experiment at pH 3, what do you think the results would be?

Based on the lab report results (Table 2.1), students were able to effectively (>85%) summarize objectives, identify hazards associated with the experiment, translate the structures of molecules into ChemDraw, and understand how pH affects structure, and therefore logD and permeability. Students struggled to correctly develop calibration curves. The primary issue encountered was in accounting for the detector response at 0 concentration. The lowest % correct question was discussion question 3. The primary reason this question was answered incorrectly stemmed from a misunderstanding of pKa as opposed to not understanding the learning outcomes. Students often assumed that when the pH was below the pKa of **2.9**, it would lose its positive charge and thus become more permeable. This demonstrates an understanding of learning outcomes two and three, even if there is a misunderstanding in pKa. Since students ran their code on the Opentrons

and errors were corrected over the course of the lab, they were not formally evaluated on their code. However, no fundamental issues in the programming were observed. The major issues, if any, were present were syntax errors that were easily remedied.

Table 2.1 Distribution of students correctly answering each part of the lab report. N=75

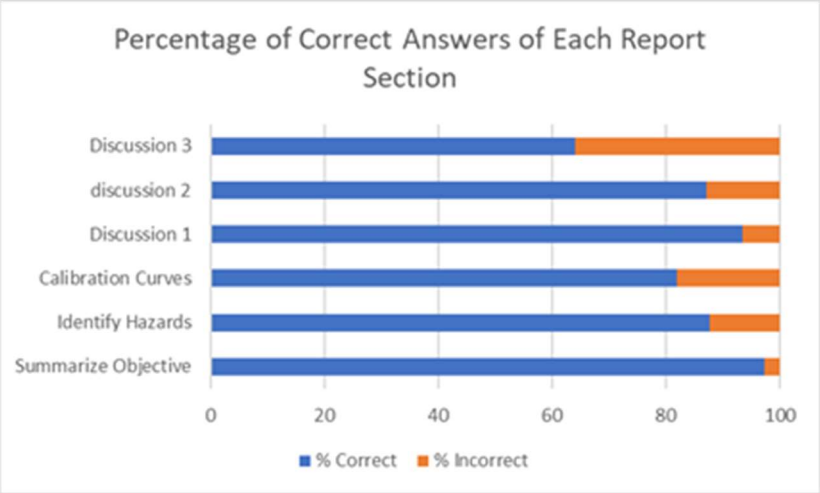

2.3.6 Conclusions

A PAMPA lab was developed and implemented to introduce students to the concepts of permeability and how structural components of a molecule affect them. This was accomplished using brightly colored drug molecules which allowed students to gain exposure to several techniques and instrumentation. In general students were able to effectively summarize the goals of the experiment as well as understand how structure relates to function. The proper way to generate a calibration curve was less well understood and as such students may benefit from a formal lecture on the basics of this subject. As well students struggled to understand the changes that occur in molecules after a change in pH. A review of these concepts may also be beneficial for future student improvement.

2.4 Protocol and Lab Report Template for An Automated and Colorful PAMPA Assay to Investigate Drug Permeability[3]

2.4.1 Lab Protocol

The Parallel Artificial Membrane Permeability Assay (PAMPA) is a biochemical method used to determine passive diffusion of compounds across a membrane. An artificial membrane is created in a donor plate which has wells with a teflon membrane at the bottom. This plate is then filled with solutions of the test compounds and placed upon an acceptor plate containing enough buffer to ensure contact with the membrane. After a set incubation time, the amount of compound in the acceptor plate is measured to determine how well each compound passed through the membrane.

This lab is designed to qualitatively and quantitatively compare the membrane permeability of two brightly colored compounds, methylene blue and phenazopyridine. Methylene blue is a strong dye, which is also used as a medication for methemoglobinemia, a condition caused by elevated levels of methemoglobin in the blood which decreases the ability of red blood cells to release oxygen to tissues. Phenazopyridine is a dark orange/red compound (yellow in dilute solution) which is used to treat pain associated with urinary tract infections. Since these compounds are brightly colored, the concentration of each in the acceptor plate can be determined by measuring the absorbance at a visible wavelength and comparing to a standard calibration curve.

Note:

[3] Dr. Deanna Montgomery developed the initial protocol and found the drugs used in the assay. I developed the opentrons portion as well as expanded the protocol.

1. Work in groups of 4 or 5.
2. The compounds used in this experiment are strong dyes, which may stain your skin or clothes. Be sure to wear proper PPE, including eyewear, lab coat, and gloves.

Part 1: Preparing solutions of test compounds

- Obtain three 1.5 mL eppendorf tubes
- Prepare 900 µL of a 250 µM solution of each test compound in PBS in one of the eppendorf tubes. For each test compound, a 5 mM stock solution in DMSO will be provided. You will need to calculate how much of the stock solution and how much PBS to use.

_____ µL PBS

_____ µL 5 mM test compound in DMSO

- Prepare a 1:1 mixture of methylene blue and phenazopyridine by taking out 300 µL of each diluted solutions from last step and acquire the 125 µM mixture solution.

Part 2: Preparing the membrane

- Obtain 9 assigned wells from the GSI

Wells: _____

- The bottom of each well in the donor plate contains a filter which will be coated with a solution of 1% lecithin in dodecane to create an artificial membrane.
- With assistance from the GSI, add 5 µL of the lecithin solution to each of your assigned wells. Avoid touching the bottom of the well with the pipette tip.

Part 3: Adding test solutions to the donor plate

- Pipette 150 µL of your methylene blue solution into three of your assigned wells.

- Pipette 150 µL of your phenazopyridine solution into three of your assigned wells.
- Pipette 150 µL of your mixture solution into three of your assigned wells.
- For your report, make note of the color of each of your wells in the donor plate in the table below.

Well	**Test compound**	**Color in donor plate**

Part 4: Preparing the acceptor plate

- Pipette 300 uL of 5% DMSO in PBS into each of your assigned wells in the acceptor plate.
- Once everyone has completed this step, the GSI will place the donor plate into the acceptor plate and begin the assay.

Part 5: Prepare the standard curve dilutions

- Your GSI will assist you in using the Opentrons to develop a calibration curve. You will be called one group at a time to run a plate containing 0, 5, 25, 125, and 250 µM of each compound in the plate reader. This data will be given to you to generate a calibration curve.

Part 6: Data collection

- After one hour incubation at room temperature, the donor plate will be removed from the acceptor plate. For your report, make note of the color of each of your wells in the acceptor plate in the table below.

Well	**Test compound**	**Color in acceptor plate**

- The Opentrons will be used to transfer 200 µL from each well of the acceptor plate into a plate reader plate.
- The plate will be read at 413 nm and 609 nm. Data will be provided.

For the laboratory report:

Use the template for Experiment 6.

1. State the objective of the experiment.
2. Describe potential safety and hazards issues.
3. Enter qualitative and quantitative data collected during the experiment. You may include pictures if you wish, but this is not required.
4. Generate the calibration curves to determine the concentration of test compound in each acceptor well and the average concentration for each test compound. You only need to show ONE sample calculation complete with derivation and units. Be sure to include the correct units when reporting these values.

5. Answer the discussion questions.

2.4.2 Lab Report Template for PAMPA

Name:

Group:

Date:

Objective:

2.4.2.1 Data and Results

1. **Qualitative results**

In the table below, report the color of each wells before and after the assay.

Well	**Test compound**	**Color in donor plate before assay**	**Color in acceptor plate after assay**

2. **Quantitative results**

Report the measured absorbance at 413 nm and 609 nm for each of your wells below.

3. **Determining concentrations of test compound**

Report the measured absorbance at 413 nm and 609 nm for wells of each standard curve; plot your standard curve (y: Abs; x: Conc). Remember to label the axes, add a linear trend line, **show the equation and the R^2.**

Choose the appropriate calibration curve to determine the concentration of test compound in the acceptor plate for each of your wells. Show your calculations for one of the wells in each group (methylene blue, phenazopryidine, and the mixture).

2.4.2.2 Discussion

1) Draw the structure of phenazopyridine and methylene blue. If you do not have chemdraw, you may use the following link: https://pubchem.ncbi.nlm.nih.gov//edit3/index.html.
2) At pH 7.4 why do you think phenazopyridine was permeable and methylene blue was not? (Hint: think about logD.)
3) If we reran this experiment at pH 3, what do you think the results would be?
4) Please list any safety hazards.

2.4.3 Sample Opentrons file

```python
from opentrons import protocol_api

metadata = {'apiLevel': '2.0',
            'protocolName': 'MC 410 Mixing',
            'author': 'Tim Cernak',
            'description': 'Making green from yellow and blue'}

def run(protocol: protocol_api.ProtocolContext):
#Load tiprack
    tiprack1 = protocol.load_labware('opentrons_96_tiprack_1000ul', 1)
    #tiprack1 = protocol.load_labware('opentrons_96_tiprack_300ul', 1)
    #Load pipette
    pipette = protocol.load_instrument('p1000_single', 'left', tip_racks=[tiprack1])
    #pipette = protocol.load_instrument('p300_single', 'left', tip_racks=[tiprack1])
    #Load plate
    plate = protocol.load_labware('nest_96_wellplate_200ul_flat', '2')
    #Load test tube holder
    #source = protocol.load_labware('opentrons_10_tuberack_falcon_4x50ml_6x15ml_conical','3')
    source = protocol.load_labware('opentrons_6_tuberack_falcon_50ml_conical','3')
    #Define Blue and Yellow stocks
    blue = source['A1']
    yellow = source['A2']
    diluent = source['A3']
```

Figure 2.24 The setup script for running the Opentrons. This portion would be written by the GSI.

```python
    # Start of protocol
    #Person 1 A1, A2, A3, A4, A5
    pipette.transfer(100, diluent, [plate.wells_by_name()[well_name].top() for well_name in ['A2','A3','A4','A5']])
    pipette.transfer(200, blue, [plate.wells_by_name()[well_name].top() for well_name in ['A1']])
    pipette.transfer(100, [plate.wells_by_name()[well_name].top() for well_name in ['A1']], [plate.wells_by_name()[well_name].top() for well_name in ['A2']])
    pipette.transfer(25, [plate.wells_by_name()[well_name].top() for well_name in ['A2']], [plate.wells_by_name()[well_name].top() for well_name in ['A3']])
    pipette.transfer(25, [plate.wells_by_name()[well_name].top() for well_name in ['A3']], [plate.wells_by_name()[well_name].top() for well_name in ['A4']])
    #Person 2 B1, B2, B3, B4, B5
    pipette.transfer(100, diluent, [plate.wells_by_name()[well_name].top() for well_name in ['XX','XX','XX','XX']])
    pipette.transfer(200, yellow, [plate.wells_by_name()[well_name].top() for well_name in ['A1']])
    pipette.transfer(100, [plate.wells_by_name()[well_name].top() for well_name in ['XX']], [plate.wells_by_name()[well_name].top() for well_name in ['XX']])
    pipette.transfer(25, [plate.wells_by_name()[well_name].top() for well_name in ['XX']], [plate.wells_by_name()[well_name].top() for well_name in ['XX']])
    pipette.transfer(25, [plate.wells_by_name()[well_name].top() for well_name in ['XX']], [plate.wells_by_name()[well_name].top() for well_name in ['XX']])
    #Person 3 A6, A7, A8, A9, A10
    pipette.transfer(100, diluent, [plate.wells_by_name()[well_name].top() for well_name in ['XX','XX','XX','XX']])
    pipette.transfer(200, blue, [plate.wells_by_name()[well_name].top() for well_name in ['A1']])
    pipette.transfer(100, [plate.wells_by_name()[well_name].top() for well_name in ['XX']], [plate.wells_by_name()[well_name].top() for well_name in ['XX']])
    pipette.transfer(25, [plate.wells_by_name()[well_name].top() for well_name in ['XX']], [plate.wells_by_name()[well_name].top() for well_name in ['XX']])
    pipette.transfer(25, [plate.wells_by_name()[well_name].top() for well_name in ['XX']], [plate.wells_by_name()[well_name].top() for well_name in ['XX']])
    #Person 4 B6, B7, B8, B9, B10
```

Figure 2.25 The protocol script. Wells are filled in for person 1 as an example. The students would fill in their assigned wells in the script to generate a functioning protocol.

2.5 A Wellplate Based Children's Toy to Encourage Scientific Exploration from a Young Age.[4]

To train the next generation of scientists, early exposure to science is key.[44] Children tend to be naturally inquisitive and fostering that quality from a young age is an important in determinant in inspiring children to pursue a career in science, technology, engineering, or math (STEM). Though not a substitute for having a mentor or role model that looks like them,[45] early exposure to STEM is an important factor in increasing participation in STEM from

[4] This idea was conceived by Dr. Tim Cernak and his daughter during the COVID pandemic and developed with collaboration between us.

underrepresented groups.[46,47] By making it fun and accessible, STEM seems a more viable career option.

With this in mind we sought to develop a product that would gamify scientific principles while also exposing children to the types of equipment used in modern laboratories. Specifically, we believed children would enjoy mixing and matching different colored dyes and using pipettes to deliver them into various wells in well plates. The dyes would have to be non-toxic and ideally non-staining. To accomplish this we sourced plant based, water soluble dyes. This provides the added educational advantage of relating color to molecules in a medium children can relate to. The color of the plants and dyes come from the molecules present within it. After extensive searching and experimentation, we chose four dyes. For a blue dye, we turned to blue butterfly pea which owes its color to an anthocyanin known as ternatin A (**4.11**)[48]. Our red dye is sourced from beetroot powder and is colored due to the presence of betanin (**4.10**).[49] When searching for a yellow plant-based dye, our initial hopes of using curcumin from turmeric, but quickly discovered it is not water soluble and readily stains clothing. Instead, we used vitamin B2, riboflavin (**4.12**). To incorporate further educational component, cabbage was sourced as a fourth dye as the anthocyanins present in it are a natural pH indicator. Therefore, when dissolved, it will turn purple, but when mixed with vinegar it will turn red.

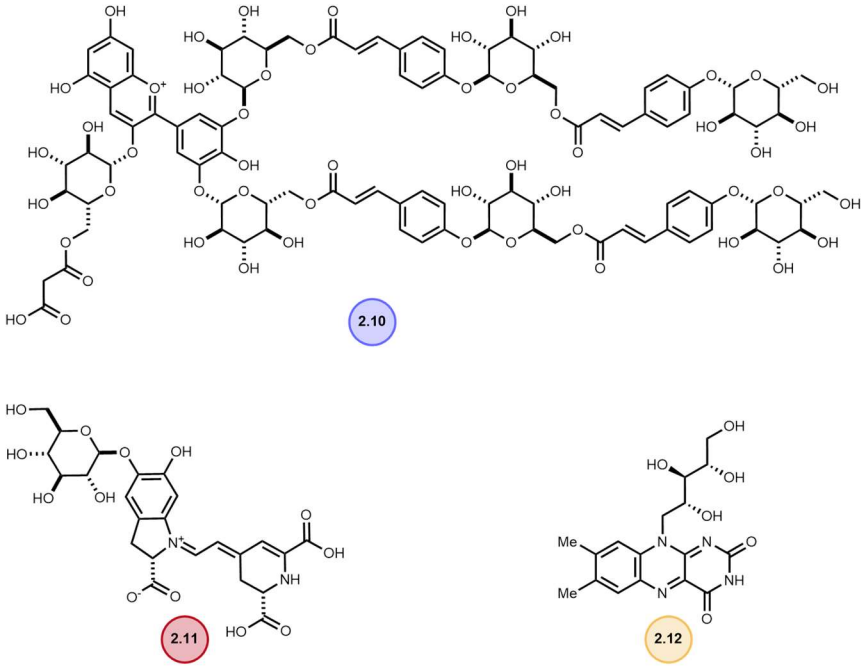

Figure 2.26 Structures of ternatin A (**2.10**, blue), betanin (**2.11**, red), and riboflavin (**2.12**, yellow).

The dyes were subsequently packaged in a wellpaint™ box and brought for demonstration to a first-grade class. Generally, the children seemed to enjoy playing with it and gained exposure to molecules as they relate to function.

Figure 2.27 wellpaint logo.

Figure 2.28 A wellplate after use in wellpaint.

2.5.1 Incorporating wellpaint into phactor software.

To further increase the educational value of wellpaint, incorporation into the open-source version of Phactor may be an option. In essence this would be a web app with well plate grids that would allow for adding various colors into each well to make designs. By doing this, children are able to be creative as well as gain exposure to thinking in arrays that are useful for designing HTE experiments.

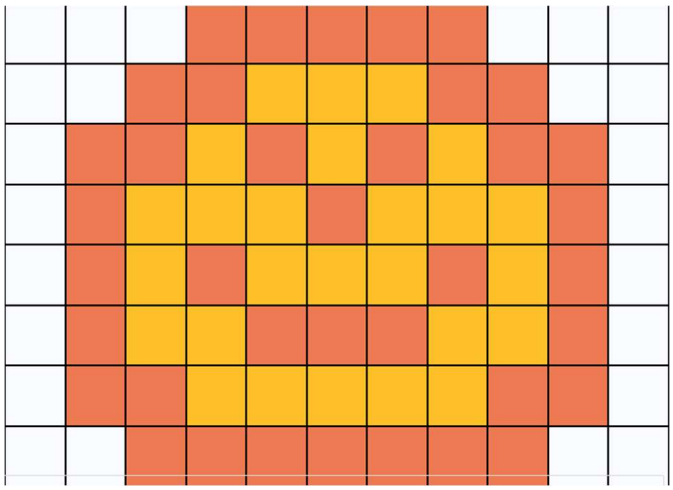

Figure 2.29 A pixelated smiley face designed in phactor that could then be reproduced using wellpaint.

2.6 References

(1) Boby, M. L.; Fearon, D.; Ferla, M.; Filep, M.; Koekemoer, L.; Robinson, M. C.; The COVID Moonshot Consortium‡; Chodera, J. D.; Lee, A. A.; London, N.; von Delft, A.; von Delft, F.; Achdout, H.; Aimon, A.; Alonzi, D. S.; Arbon, R.; Aschenbrenner, J. C.; Balcomb, B. H.; Bar-David, E.; Barr, H.; Ben-Shmuel, A.; Bennett, J.; Bilenko, V. A.; Borden, B.; Boulet, P.; Bowman, G. R.; Brewitz, L.; Brun, J.; BVNBS, S.; Calmiano, M.; Carbery, A.; Carney, D. W.; Cattermole, E.; Chang, E.; Chernyshenko, E.; Clyde, A.; Coffland, J. E.; Cohen, G.; Cole, J. C.; Contini, A.; Cox, L.; Croll, T. I.; Cvitkovic, M.; De Jonghe, S.; Dias, A.; Donckers, K.; Dotson, D. L.; Douangamath, A.; Duberstein, S.; Dudgeon, T.; Dunnett, L. E.; Eastman, P.; Erez, N.; Eyermann, C. J.; Fairhead, M.; Fate, G.; Fedorov, O.; Fernandes, R. S.; Ferrins, L.; Foster, R.; Foster, H.; Fraisse, L.; Gabizon, R.; García-Sastre, A.; Gawriljuk, V. O.; Gehrtz, P.; Gileadi, C.; Giroud, C.; Glass, W. G.; Glen, R. C.; Glinert, I.; Godoy, A. S.; Gorichko, M.; Gorrie-Stone, T.; Griffen, E. J.; Haneef, A.; Hassell Hart, S.; Heer, J.; Henry, M.; Hill, M.; Horrell, S.; Huang, Q. Y. J.; Huliak, V. D.; Hurley, M. F. D.; Israely, T.; Jajack, A.; Jansen, J.; Jnoff, E.; Jochmans, D.; John, T.; Kaminow, B.; Kang, L.; Kantsadi, A. L.; Kenny, P. W.; Kiappes, J. L.; Kinakh, S. O.; Kovar, B.; Krojer, T.; La, V. N. T.; Laghnimi-Hahn, S.; Lefker, B. A.; Levy, H.; Lithgo, R. M.; Logvinenko, I. G.; Lukacik, P.; Macdonald, H. B.; MacLean, E. M.; Makower, L. L.; Malla, T. R.; Marples, P. G.; Matviiuk, T.; McCorkindale, W.; McGovern, B. L.; Melamed, S.; Melnykov, K. P.; Michurin, O.; Miesen, P.; Mikolajek, H.; Milne, B. F.; Minh, D.; Morris, A.; Morris, G. M.; Morwitzer, M. J.; Moustakas, D.; Mowbray, C. E.; Nakamura, A. M.; Neto, J. B.; Neyts, J.; Nguyen, L.; Noske, G. D.; Oleinikovas, V.; Oliva, G.; Overheul, G. J.; Owen, C. D.; Pai, R.; Pan, J.; Paran, N.; Payne, A. M.; Perry, B.; Pingle, M.; Pinjari, J.; Politi, B.; Powell, A.; Pšenák, V.; Pulido, I.; Puni, R.; Rangel, V. L.; Reddi, R. N.; Rees, P.; Reid, S. P.; Reid, L.; Resnick, E.; Ripka, E. G.; Robinson, R. P.; Rodriguez-Guerra, J.; Rosales, R.; Rufa, D. A.; Saar, K.; Saikatendu, K. S.; Salah, E.; Schaller, D.; Scheen, J.; Schiffer, C. A.; Schofield, C. J.; Shafeev, M.; Shaikh, A.; Shaqra, A. M.; Shi, J.; Shurrush, K.; Singh, S.; Sittner, A.; Sjö, P.; Skyner, R.; Smalley, A.; Smeets, B.; Smilova, M. D.; Solmesky, L. J.; Spencer, J.; Strain-Damerell, C.; Swamy, V.; Tamir, H.; Taylor, J. C.; Tennant, R. E.; Thompson, W.; Thompson, A.; Tomásio, S.; Tomlinson, C. W. E.; Tsurupa, I. S.; Tumber, A.; Vakonakis, I.; van Rij, R. P.; Vangeel, L.; Varghese, F. S.; Vaschetto, M.; Vitner, E. B.; Voelz, V.; Volkamer, A.; Walsh, M. A.; Ward, W.; Weatherall, C.; Weiss, S.; White, K. M.; Wild, C. F.; Witt, K. D.; Wittmann, M.; Wright, N.; Yahalom-Ronen, Y.; Yilmaz, N. K.; Zaidmann, D.; Zhang, I.; Zidane, H.; Zitzmann, N.; Zvornicanin, S. N. Open Science Discovery of Potent Noncovalent SARS-CoV-2 Main Protease Inhibitors. *Science 382* (6671), eabo7201. https://doi.org/10.1126/science.abo7201.

(2) Bravenec, A. D.; Ward, K. D. Interactive Python Notebooks for Physical Chemistry. *J. Chem. Educ.* **2023**, *100* (2), 933–940. https://doi.org/10.1021/acs.jchemed.2c00665.

(3) Lafuente, D.; Cohen, B.; Fiorini, G.; García, A. A.; Bringas, M.; Morzan, E.; Onna, D. A Gentle Introduction to Machine Learning for Chemists: An Undergraduate Workshop Using Python Notebooks for Visualization, Data Processing, Analysis, and Modeling. *J. Chem. Educ.* **2021**, *98* (9), 2892–2898. https://doi.org/10.1021/acs.jchemed.1c00142.

(4) van Staveren, M. Integrating Python into a Physical Chemistry Lab. *J. Chem. Educ.* **2022**, *99* (7), 2604–2609. https://doi.org/10.1021/acs.jchemed.2c00193.

(5) Weiss, C. J. A Creative Commons Textbook for Teaching Scientific Computing to Chemistry Students with Python and Jupyter Notebooks. *J. Chem. Educ.* **2021**, *98* (2), 489–494. https://doi.org/10.1021/acs.jchemed.0c01071.

(6) Menke, E. J. Series of Jupyter Notebooks Using Python for an Analytical Chemistry Course. *J. Chem. Educ.* **2020**, *97* (10), 3899–3903. https://doi.org/10.1021/acs.jchemed.9b01131.

(7) Gupta, Y. M.; Kirana, S. N.; Homchan, S.; Tanasarnpaiboon, S. Teaching Python Programming for Bioinformatics with Jupyter Notebook in the Post-COVID-19 Era. *Biochemistry and Molecular Biology Education* **2023**, *51* (5), 537–539. https://doi.org/10.1002/bmb.21746.

(8) De Haan, D. O.; Schafer, J. A.; Gillette, E. I. Using a Modular Approach to Introduce Python Coding to Support Existing Course Learning Outcomes in a Lower Division Analytical Chemistry Course. *J. Chem. Educ.* **2021**, *98* (10), 3245–3250. https://doi.org/10.1021/acs.jchemed.1c00456.

(9) Dickson-Karn, N. M.; Orosz, S. Implementation of a Python Program to Simulate Sampling. *J. Chem. Educ.* **2021**, *98* (10), 3251–3257. https://doi.org/10.1021/acs.jchemed.1c00597.

(10) Green, M.; Chen, X. Data Functionalization for Gas Chromatography in Python. *J. Chem. Educ.* **2020**, *97* (4), 1172–1175. https://doi.org/10.1021/acs.jchemed.9b00818.

(11) Srnec, M. N.; Upadhyay, S.; Madura, J. D. A Python Program for Solving Schrödinger's Equation in Undergraduate Physical Chemistry. *J. Chem. Educ.* **2017**, *94* (6), 813–815. https://doi.org/10.1021/acs.jchemed.7b00003.

(12) Wallum, A.; Liu, Z.; Lee, J.; Chatterjee, S.; Tauzin, L.; Barr, C. D.; Browne, A.; Landes, C. F.; Nicely, A. L.; Gruebele, M. An Instrument Assembly and Data Science Lab for Early Undergraduate Education. *J. Chem. Educ.* **2023**, *100* (5), 1866–1876. https://doi.org/10.1021/acs.jchemed.2c01072.

(13) Weiss, C. J. Scientific Computing for Chemists: An Undergraduate Course in Simulations, Data Processing, and Visualization. *J. Chem. Educ.* **2017**, *94* (5), 592–597. https://doi.org/10.1021/acs.jchemed.7b00078.

(14) Chen, E.; Asta, M. Using Jupyter Tools to Design an Interactive Textbook to Guide Undergraduate Research in Materials Informatics. *J. Chem. Educ.* **2022**, *99* (10), 3601–3606. https://doi.org/10.1021/acs.jchemed.2c00640.

(15) Thrall, E. S.; Lee, S. E.; Schrier, J.; Zhao, Y. Machine Learning for Functional Group Identification in Vibrational Spectroscopy: A Pedagogical Lab for Undergraduate Chemistry Students. *J. Chem. Educ.* **2021**, *98* (10), 3269–3276. https://doi.org/10.1021/acs.jchemed.1c00693.

(16) Konkol, J. A.; Tsilomelekis, G. Porchlight: An Accessible and Interactive Aid in Preprocessing of Spectral Data. *J. Chem. Educ.* **2023**, *100* (3), 1326–1332. https://doi.org/10.1021/acs.jchemed.2c00812.

(17) Engelberger, F.; Galaz-Davison, P.; Bravo, G.; Rivera, M.; Ramírez-Sarmiento, C. A. Developing and Implementing Cloud-Based Tutorials That Combine Bioinformatics Software, Interactive Coding, and Visualization Exercises for Distance Learning on Structural Bioinformatics. *J. Chem. Educ.* **2021**, *98* (5), 1801–1807. https://doi.org/10.1021/acs.jchemed.1c00022.

(18) Bickerton, G. R.; Paolini, G. V.; Besnard, J.; Muresan, S.; Hopkins, A. L. Quantifying the Chemical Beauty of Drugs. *Nature Chemistry* **2012**, *4* (2), 90–98. https://doi.org/10.1038/nchem.1243.

(19) Wager, T. T.; Hou, X.; Verhoest, P. R.; Villalobos, A. Central Nervous System Multiparameter Optimization Desirability: Application in Drug Discovery. *ACS Chem. Neurosci.* **2016**, *7* (6), 767–775. https://doi.org/10.1021/acschemneuro.6b00029.

(20) Bisong, E. *Building Machine Learning and Deep Learning Models on Google Cloud Platform*; 2019.

(21) Kluyver, T.; Ragan-Kelley, B.; Pérez, F.; Granger, B.; Bussonnier, M.; Frederic, J.; Kelley, K.; Hamrick, J.; Grout, J.; Corlay, S.; Ivanov, P.; Avila, D.; Abdalla, S.; Willing, C.; Jupyter Development Team. Jupyter Notebooks—a Publishing Format for Reproducible Computational Workflows. In *IOS Press*; 2016; pp 87–90. https://doi.org/10.3233/978-1-61499-649-1-87.

(22) McKinney, W. Data Structures for Statistical Computing in Python. In *Proceedings of the 9th Python in Science Conference*; Walt, S. van der, Millman, J., Eds.; 2010; pp 56–61. https://doi.org/10.25080/Majora-92bf1922-00a.

(23) Harris, C. R.; Millman, K. J.; van der Walt, S. J.; Gommers, R.; Virtanen, P.; Cournapeau, D.; Wieser, E.; Taylor, J.; Berg, S.; Smith, N. J.; Kern, R.; Picus, M.; Hoyer, S.; van Kerkwijk, M. H.; Brett, M.; Haldane, A.; del Río, J. F.; Wiebe, M.; Peterson, P.; Gérard-Marchant, P.; Sheppard, K.; Reddy, T.; Weckesser, W.; Abbasi, H.; Gohlke, C.; Oliphant, T. E. Array Programming with NumPy. *Nature* **2020**, *585* (7825), 357–362. https://doi.org/10.1038/s41586-020-2649-2.

(24) Virtanen, P.; Gommers, R.; Oliphant, T. E.; Haberland, M.; Reddy, T.; Cournapeau, D.; Burovski, E.; Peterson, P.; Weckesser, W.; Bright, J.; van der Walt, S. J.; Brett, M.; Wilson, J.; Millman, K. J.; Mayorov, N.; Nelson, A. R. J.; Jones, E.; Kern, R.; Larson, E.; Carey, C. J.; Polat, İ.; Feng, Y.; Moore, E. W.; VanderPlas, J.; Laxalde, D.; Perktold, J.; Cimrman, R.; Henriksen, I.; Quintero, E. A.; Harris, C. R.; Archibald, A. M.; Ribeiro, A. H.; Pedregosa, F.; van Mulbregt, P.; Vijaykumar, A.; Bardelli, A. P.; Rothberg, A.; Hilboll, A.; Kloeckner, A.; Scopatz, A.; Lee, A.; Rokem, A.; Woods, C. N.; Fulton, C.; Masson, C.; Häggström, C.; Fitzgerald, C.;

Nicholson, D. A.; Hagen, D. R.; Pasechnik, D. V.; Olivetti, E.; Martin, E.; Wieser, E.; Silva, F.; Lenders, F.; Wilhelm, F.; Young, G.; Price, G. A.; Ingold, G.-L.; Allen, G. E.; Lee, G. R.; Audren, H.; Probst, I.; Dietrich, J. P.; Silterra, J.; Webber, J. T.; Slavič, J.; Nothman, J.; Buchner, J.; Kulick, J.; Schönberger, J. L.; de Miranda Cardoso, J. V.; Reimer, J.; Harrington, J.; Rodríguez, J. L. C.; Nunez-Iglesias, J.; Kuczynski, J.; Tritz, K.; Thoma, M.; Newville, M.; Kümmerer, M.; Bolingbroke, M.; Tartre, M.; Pak, M.; Smith, N. J.; Nowaczyk, N.; Shebanov, N.; Pavlyk, O.; Brodtkorb, P. A.; Lee, P.; McGibbon, R. T.; Feldbauer, R.; Lewis, S.; Tygier, S.; Sievert, S.; Vigna, S.; Peterson, S.; More, S.; Pudlik, T.; Oshima, T.; Pingel, T. J.; Robitaille, T. P.; Spura, T.; Jones, T. R.; Cera, T.; Leslie, T.; Zito, T.; Krauss, T.; Upadhyay, U.; Halchenko, Y. O.; Vázquez-Baeza, Y.; SciPy 1.0 Contributors. SciPy 1.0: Fundamental Algorithms for Scientific Computing in Python. *Nature Methods* **2020**, *17* (3), 261–272. https://doi.org/10.1038/s41592-019-0686-2.

(25) J. D. Hunter. Matplotlib: A 2D Graphics Environment. *Computing in Science & Engineering* **2007**, *9* (03), 90–95. https://doi.org/10.1109/MCSE.2007.55.

(26) Matplotlib. https://matplotlib.org/stable/api/figure_api.html#matplotlib.figure.Figure.

(27) Matplotlib. https://matplotlib.org/stable/api/_as_gen/matplotlib.pyplot.scatter.html.

(28) Wishart, D. S.; Knox, C.; Guo, A. C.; Shrivastava, S.; Hassanali, M.; Stothard, P.; Chang, Z.; Woolsey, J. DrugBank: A Comprehensive Resource for in Silico Drug Discovery and Exploration. *Nucleic Acids Research* **2006**, *34* (suppl_1), D668–D672. https://doi.org/10.1093/nar/gkj067.

(29) Weininger, D. SMILES, a Chemical Language and Information System. 1. Introduction to Methodology and Encoding Rules. *J. Chem. Inf. Comput. Sci.* **1988**, *28* (1), 31–36. https://doi.org/10.1021/ci00057a005.

(30) Lipinski, C. A.; Lombardo, F.; Dominy, B. W.; Feeney, P. J. Experimental and Computational Approaches to Estimate Solubility and Permeability in Drug Discovery and Development Settings. *Advanced Drug Delivery Reviews* **1997**, *23* (1), 3–25. https://doi.org/10.1016/S0169-409X(96)00423-1.

(31) Hill, A. P.; Young, R. J. Getting Physical in Drug Discovery: A Contemporary Perspective on Solubility and Hydrophobicity. *Drug Discovery Today* **2010**, *15* (15), 648–655. https://doi.org/10.1016/j.drudis.2010.05.016.

(32) Di, L.; Whitney-Pickett, C.; Umland, J. P.; Zhang, H.; Zhang, X.; Gebhard, D. F.; Lai, Y.; Federico, J. J.; Davidson, R. E.; Smith, R.; Reyner, E. L.; Lee, C.; Feng, B.; Rotter, C.; Varma, M. V.; Kempshall, S.; Fenner, K.; El-kattan, A. F.; Liston, T. E.; Troutman, M. D. Development of a New Permeability Assay Using Low-efflux MDCKII Cells. *Journal of Pharmaceutical Sciences* **2011**, *100* (11), 4974–4985. https://doi.org/10.1002/jps.22674.

(33) van Breemen, R. B.; Li, Y. Caco-2 Cell Permeability Assays to Measure Drug Absorption. *Expert Opinion on Drug Metabolism & Toxicology* **2005**, *1* (2), 175–185. https://doi.org/10.1517/17425255.1.2.175.

(34) Irvine, J. D.; Takahashi, L.; Lockhart, K.; Cheong, J.; Tolan, J. W.; Selick, H. E.; Grove, J. R. MDCK (Madin-Darby Canine Kidney) Cells: A Tool for Membrane Permeability Screening. *Journal of Pharmaceutical Sciences* **1999**, *88* (1), 28–33. https://doi.org/10.1021/js9803205.

(35) Kansy, M.; Senner, F.; Gubernator, K. Physicochemical High Throughput Screening: Parallel Artificial Membrane Permeation Assay in the Description of Passive Absorption Processes. *J. Med. Chem.* **1998**, *41* (7), 1007–1010. https://doi.org/10.1021/jm970530e.

(36) Wohnsland, F.; Faller, B. High-Throughput Permeability pH Profile and High-Throughput Alkane/Water Log P with Artificial Membranes. *J. Med. Chem.* **2001**, *44* (6), 923–930. https://doi.org/10.1021/jm001020e.

(37) Veber, D. F.; Johnson, S. R.; Cheng, H.-Y.; Smith, B. R.; Ward, K. W.; Kopple, K. D. Molecular Properties That Influence the Oral Bioavailability of Drug Candidates. *J. Med. Chem.* **2002**, *45* (12), 2615–2623. https://doi.org/10.1021/jm020017n.

(38) Ruell, J. A.; Tsinman, K. L.; Avdeef, A. PAMPA—a Drug Absorption in Vitro Model: 5. Unstirred Water Layer in Iso-pH Mapping Assays and pKaflux—Optimized Design (pOD-PAMPA). *European Journal of Pharmaceutical Sciences* **2003**, *20* (4), 393–402. https://doi.org/10.1016/j.ejps.2003.08.006.

(39) Kell, D. B.; Oliver, S. G. How Drugs Get into Cells: Tested and Testable Predictions to Help Discriminate between Transporter-Mediated Uptake and Lipoidal Bilayer Diffusion. *Frontiers in Pharmacology* **2014**, *5*.

(40) Politi, M.; Baum, F.; Vaddi, K.; Antonio, E.; Vasquez, J.; Bishop, B. P.; Peek, N.; Holmberg, V. C.; Pozzo, L. D. A High-Throughput Workflow for the Synthesis of CdSe Nanocrystals Using a Sonochemical Materials Acceleration Platform. *Digital Discovery* **2023**, *2* (4), 1042–1057. https://doi.org/10.1039/D3DD00033H.

(41) McGrath, A.; Zhang, R.; Shafiq, K.; Cernak, T. Repurposing Amine and Carboxylic Acid Building Blocks with an Automatable Esterification Reaction. *Chem. Commun.* **2023**, *59* (8), 1026–1029. https://doi.org/10.1039/D2CC05670D.

(42) Rodriguez, J.; Politi, M.; Adler, S.; Beck, D.; Pozzo, L. High-Throughput and Data Driven Strategies for the Design of Deep-Eutectic Solvent Electrolytes. *Mol. Syst. Des. Eng.* **2022**, *7* (8), 933–949. https://doi.org/10.1039/D2ME00050D.

(43) Norquist, A. J.; Jones-Thomson, G.; He, K.; Egg, T.; Schrier, J. A Modern Twist on an Old Measurement: Using Laboratory Automation and Data Science to Determine the Solubility Product of Lead Iodide. *J. Chem. Educ.* **2023**, *100* (9), 3445–3453. https://doi.org/10.1021/acs.jchemed.3c00445.

(44) Hattar, M. *The Benefits of Early STEM Education*. Keysight. https://www.keysight.com/blogs/en/keys/exec/2023/12/the-benefits-of-early-stem-education#:~:text=Exposure%20to%20the%20STEM%20fields,in%20the%20world%20around%20them.

(45) Kricorian, K.; Seu, M.; Lopez, D.; Ureta, E.; Equils, O. Factors Influencing Participation of Underrepresented Students in STEM Fields: Matched Mentors and Mindsets. *International Journal of STEM Education* **2020**, *7* (1), 16. https://doi.org/10.1186/s40594-020-00219-2.

(46) Stuart, R. T.; Downey, M. A Black College President on Importance of STEM: 'I Never Heard of Engineering until College.' *The Atlanta Journal-Constitution*. September 2021. https://www.ajc.com/education/get-schooled-blog/a-black-college-president-on-importance-of-stem-i-never-heard-of-engineering-until-college/TYKY4KYPWRCSVP5PWLCYRAXDLM/.

(47) Mugisha, A. *How to encourage girls to choose STEM careers: Three ideas that work*. Worldbank.org. https://blogs.worldbank.org/youth-transforming-africa/how-encourage-girls-choose-stem-careers-three-ideas-work.

(48) Vidana Gamage, G. C.; Lim, Y. Y.; Choo, W. S. Anthocyanins From Clitoria Ternatea Flower: Biosynthesis, Extraction, Stability, Antioxidant Activity, and Applications. *Front Plant Sci* **2021**, *12*, 792303. https://doi.org/10.3389/fpls.2021.792303.

(49) Vieira Teixeira da Silva, D.; dos Santos Baião, D.; de Oliveira Silva, F.; Alves, G.; Perrone, D.; Mere Del Aguila, E.; M. Flosi Paschoalin, V. Betanin, a Natural Food Additive: Stability, Bioavailability, Antioxidant and Preservative Ability Assessments. *Molecules* **2019**, *24* (3). https://doi.org/10.3390/molecules24030458.

Chapter 3 Amine–Acid C–N to C–O Coupling Reactions[5]

This work describes a deaminative esterification reaction that proceeds via activation of the amine as its Katritzky salt. The optimization and scope of this reaction are discussed before moving into an automated platform for library synthesis that was developed to synthesize 96 amlodipine derivatives. We discovered the reaction proceeds through a halide intermediate and could be run from the free amine by generating the pyridinium salt *in-situ*.

The second half of this chapter details a deaminative etherification reaction that builds upon the esterification reaction. By using the free amine esterification reaction, we generate an ester which we reduce *in-situ*. We observe we can use this method to selectively reduce esters in the presence of amides and can incorporate deuterium instead of hydrogen. We performed several mechanistic studies to understand the nature of the selectivity and finished by exploring the scope of the halogenation and subsequent phenol-based etherification.

3.1 Repurposing amine and carboxylic acid building blocks with an automatable esterification reaction[6]

3.1.1 Introduction of Esterification Reaction

[5] The first half of this chapter was published in: McGrath, A.; Zhang, R.; Shafiq, K.; Cernak, T. ***Chem. Commun.***, 2023,**59**, 1026-1029 DOI: https://doi.org/10.1039/D2CC05670D

[6] Dr. Sam Zhang and I worked together to initially configure the Opentrons to run chemical reactions. Sam then took the lead on interfacing the robot with Phactor as well as implementing the game controller so the user could stand at the glovebox to calibrate the robot. Khadija worked with me as an REU student over a summer to help optimize the reaction.

The exploration of chemical space is fuelled by diverse building blocks.[1–3] Traditionally, these building blocks are coupled together through known, robust reactions to generate combinatorial libraries.[4] We hypothesize that the chemical space accessible of a building block collection can be expanded by repurposing them using unconventional reactions that forge moieties not traditionally associated with the functional groups involved. We have been exploring the repurposing of amine and carboxylic acid building blocks using new amine–acid transformations that complement the popular amide coupling.[5] A variety of amine activation strategies currently exist to enable use of C–N bonds[6–9] as a handle for synthesis. While significant progress has recently been made in the field of C–N to C–C bond conversion, comparatively little work has been reported in C–N to C–O bond conversion, leading us to consider utilizing amines as substrates for esterification reactions with acids (Figure 3.1, A). Esters are among the most prevalent functional groups in natural products, pharmaceuticals, plastics, fragrances, and agrochemicals (Figure 3.2, B). In medicine, the ester functionality is widely used in prodrug strategies and as a metabolically stable functionality with unique properties. For instance, esters typically exhibit improved membrane permeability over analogous amides.[10] While the venerable coupling of alcohols and acids via the Fischer esterification provides a simple access to esters,[11] there are many instances where alcohol building blocks are unavailable, or where regiochemical esterification is challenged by the presence of other unprotected alcohol functionalities on the substrate. In contrast, a wide diversity of amines is available from natural and synthetic sources, so an amine–acid esterification would be a valuable complement to the classic alcohol–acid esterification. We have recently developed a protocol for esterification from arylamine-derived diazonium salts and

carboxylic acids.[12] Here we report a complementary esterification from alkylamine-derived pyridinium salts (Figure 3.3, C).

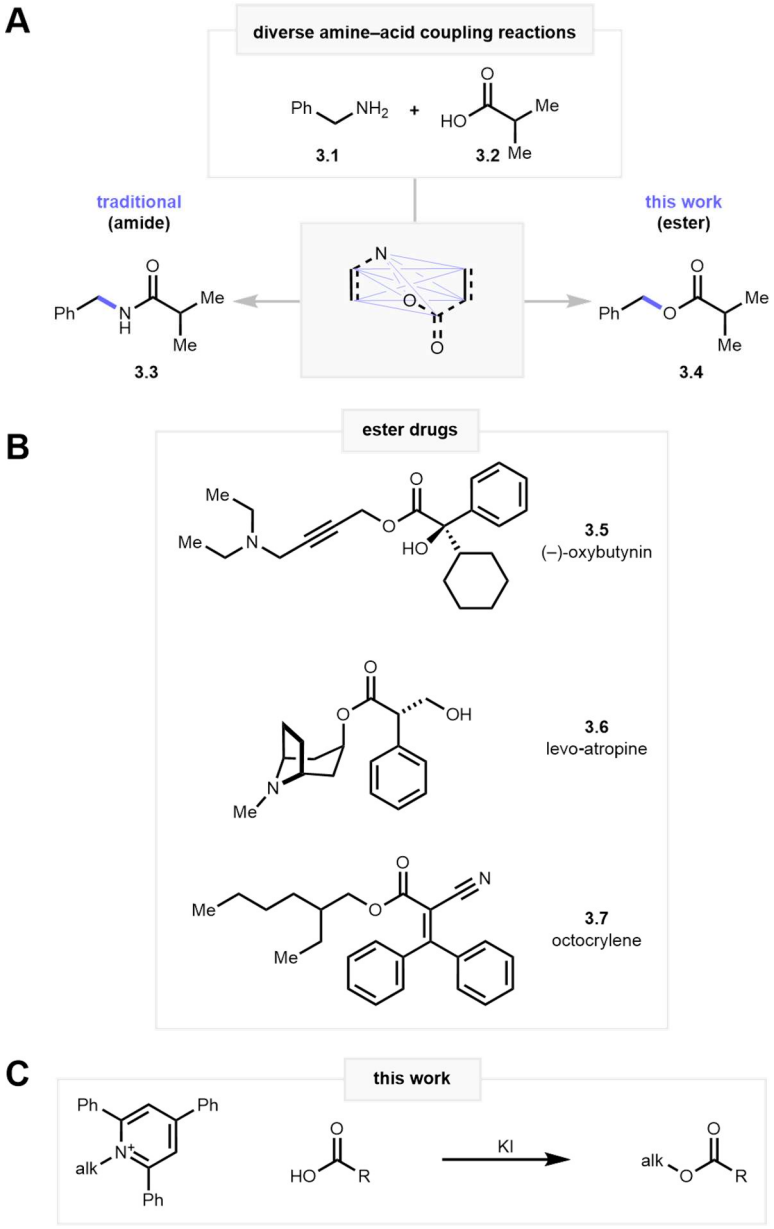

Figure 3.1. A) Diverse amine–acid coupling reactions complement the amide coupling. B) Selected examples of esters in pharmaceuticals. C) This work: A carboxylic acid–Katritzky salt deaminative esterification.

Alkyl pyridinium salts have seen recent development for C–C bond formation,[6,13–18] but considerably less for carbon–heteroatom bond formation.[19–22] Available methods for carbon–heteroatom bond formation typically use specialized substrates or extreme reaction

conditions, such as heating above 175 °C with molten Katritzky salt as the reaction medium. As part of our effort in identifying new C–O bond formation tactics, we sought to discover reaction conditions for C–N to C–O bond conversion using Katritzky salts, targeting conditions mild enough to enable automation, and with broad substrate scope for effective amine–acid building block repurposing in medicinal chemistry.

3.1.2 Optimization and Substrate Scope Evaluation of a Deaminative Esterification Reaction

We began our investigation by coupling **3.8** with **3.9** to form **3.10** (Table 3.1) and identified malonate **3.11** as a capable promoter at 20 mol% loading. We used the potassium salt of **3.9**, producing **3.10** in 73% NMR yield (entry 1), and subsequently found that free acid substrates could be used with one equivalent of potassium *tert*-butoxide for *in situ* deprotonation (entry 2). Use of triethylamine as a base led to lower yields (entry 3), however diisopropylethylamine (DIPEA) was a viable base (entry 6). Only trace product was observed in the absence of **3.11** (entry 4). Further studies revealed that when dioxane was used as the solvent, potassium iodide was an excellent promoter of the reaction (entry 5 and 6) and greatly simplified product isolation since most reaction by-products could be removed with an aqueous workup. Based on these studies, we moved forward with dioxane as the solvent (0.3 M), using 1.0 equivalent each of KI, DIPEA, and free acid relative to the Katritzky salt as our preferred conditions.

Table 3.1 Reaction optimization table. All reactions were performed at 0.2 mmol scale under an atmosphere of N_2. KI = potassium iodide, DMF = N,N'-dimethylformamide, KOtBu = potassium tert-butoxide, Et_3N = triethylamine. Yields determined by 1H NMR using 1,3,5-trimethoxybenzene as an internal standard, values in parentheses are isolated yields.

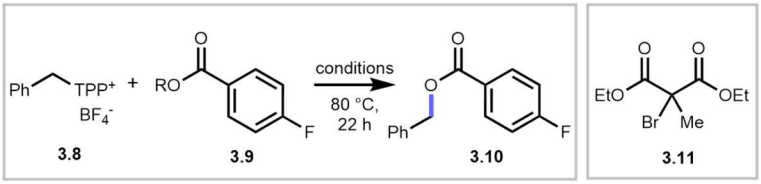

3.8 3.9 3.10 3.11

entry	9 (eq.)	R	base	additive	solvent	% yield (isolated)
1	1.2	K^+	–	0.2 eq **11**	DMF	73
2	1.2	H	1.2 eq KO^tBu	0.2 eq **11**	DMF	76 (76)
3	1.2	H	1.2 eq Et_3N	0.2 eq **11**	DMF	27
4	1.2	H	1.2 eq KO^tBu	–	DMF	trace
5	1	H	1 eq KO^tBu	1 eq KI	DMF	41
6	1	H	1 eq DIPEA	1 eq KI	dioxane	75 (73)

With optimized conditions in hand, we began exploring the generality of the reaction of **3.8** with various acids (Figure 3.2). The reaction is tolerant of aliphatic (**3.12**, **3.14**, **3.18**, **3.19**) as well as aromatic (**3.10**, **3.13**, **3.15**, **3.16**, **3.17**) acids, giving yields ranging from 61–91%. For example, the herbicide 2,4,5-T delivered ester **3.14** in 76% yield. Electron-poor (**3.10**, **3.13**, **3.17**), electron-rich (3.**16**), and heterocyclic (**3.15**, **3.18**, **3.19**) acids with various substitution patterns also performed well. Notably, densely functionalized acids such as probenecid (**3.17**), etodolac (**3.18**) and theophylline-7-acetic acid (**3.19**) are smoothly esterified. Selectivity for esterification over aniline alkylation is also achievable using this method (**3.16**).

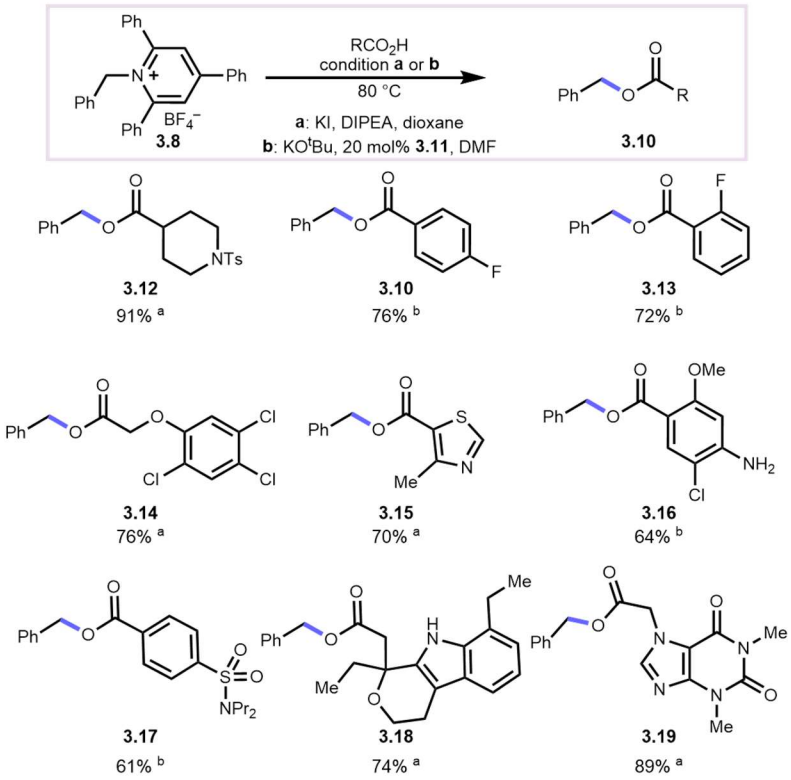

Figure 3.2 Acid substrate scope. Reactions were run with pyridinium salt 0.2 mmol (1 eq). For condition a, reactions were run with one equivalent each of carboxylic acid, KI, DIPEA, pyridinium salt in anhydrous dioxane at 0.3 M. For condition b, reactions were run with carboxylic acid (1.2 eq) and **3.11** (0.2 eq) in anhydrous DMF at 0.1 M.

Our scope studies were expanded to include Katritzky salts derived from primary aliphatic amines (**3.22**, **3.24**, **3.26**–**27**, **3.30**–**33**, **3.36**), as well as electron-poor or heterocyclic benzylic amines (**3.23**, **3.28**, **3.37**), although these substrates required heating to 110 °C (Figure 3.3). The method is quite general, tolerating basic amines (**3.32**–**33**, **3.36**), amides (**3.25**), esters (**3.26**–**27**, **3.30**), Michael acceptors (**3.37**), acetals (**3.26**–**27**), protecting groups including Boc and tosyl (**3.22**–**23**, **3.26, 3.29**–**30**), and oxime ethers (**3.31**) as well as polyfunctionalities seen in drug molecules such as levofloxacin (**3.35**), Boc-lysine methyl ester (**3.30**) enoxolone (**3.37**), and fluvoxamine (**3.31**). **3.32** and **3.33** are matched molecular pairs of moclobemide and metoclopramide, respectively, wherein the nitrogen atom has been replaced by an oxygen. In addition to anilines, selective esterification was achieved in the presence of other alcohols (**3.24**

and **3.37**). These latter results showcase the ability to regioselectively esterify without the need for alcohol protecting groups, in contrast to the classic alcohol–acid esterification.

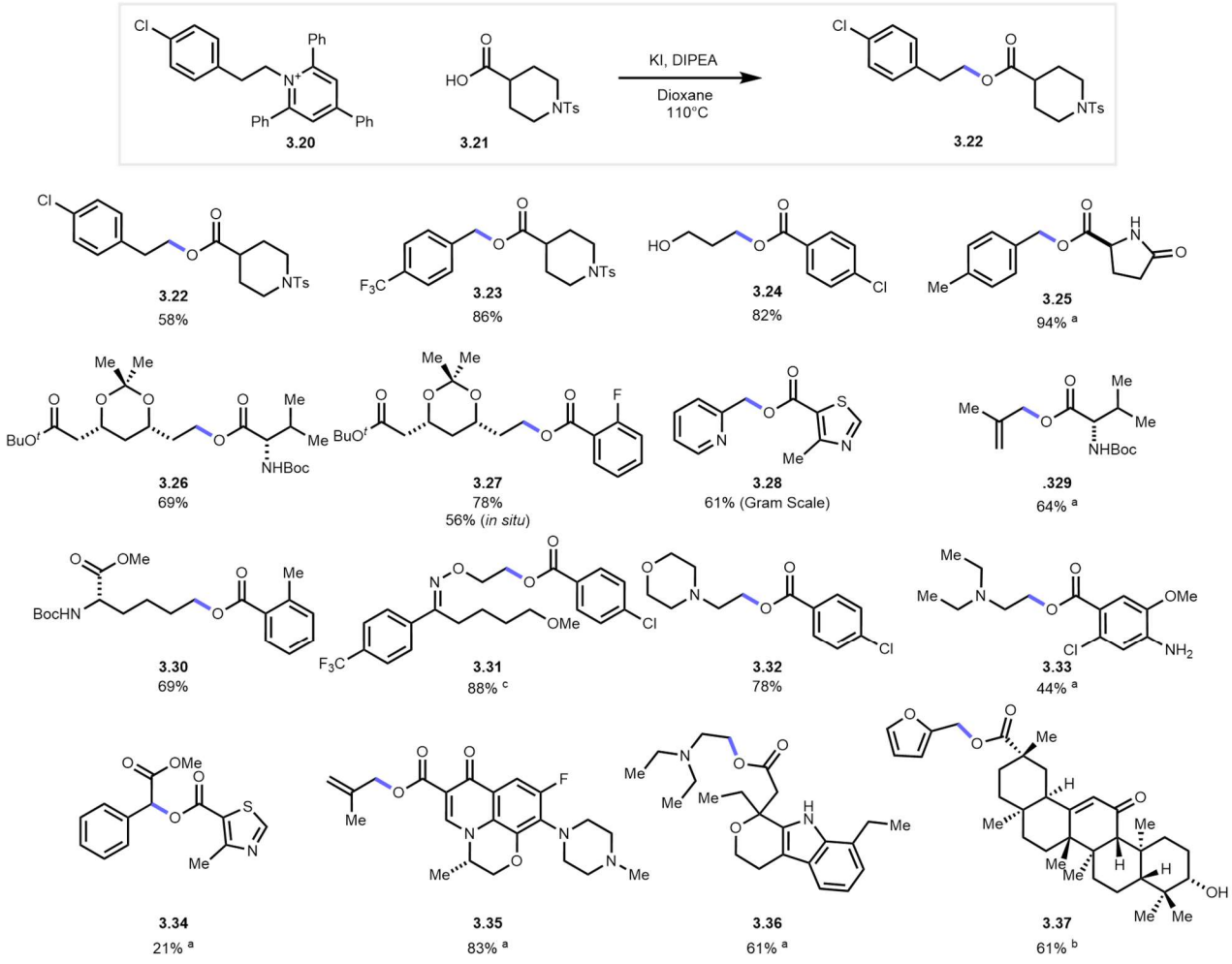

Figure 3.3 Substrate scope. Reactions were run with one equivalent each of carboxylic acid, KI, DIPEA, and pyridinium salt in anhydrous dioxane at 0.3 M. A) 80 °C instead of 110 °C. B) 60 °C instead of 110 °C. C) 2 equiv of KI.

To fully realize the scope of this method and highlight its utility in late-stage diversification, we sought to develop a platform for concise library synthesis (Fig. 3.5A–C). We envisioned that the Opentrons OT2 liquid handling robot could be used for library generation by speeding up dosing and stock solution preparation. Amlodipine (cf. **3.38**) was chosen as a substrate for the library synthesis campaign. 96 acids were weighed into a source plate which was brought into a nitrogen filled glovebox (Fig. 5E), along with solvent and stock solutions of

Katritzky salt **3.38** and finely ground potassium iodide. To vastly simplify the preparation of stock solutions, acids were weighed quickly into glass shell vials – targeting 0.300 mL of 0.30 M stock solution – with a tolerance of ± 10 mg. The weight was accurately recorded in a spreadsheet, and the appropriate solvent volume for each well computed and written into an OT2 script, which could then automatically direct the autopipetter to dose the correct volume of solvent to produce a 0.30 M stock solution. This protocol greatly simplifies the preparation of stock solutions from diverse substrates with the robotic dilution obviating the need to accurately weigh each substrate to the 0.1 mg accuracy typically associated with library preparation. The roughly weighed but accurately documented acid samples were placed on the robot deck as shown in Figure 3.5E. To improve dosing reliability, stock solutions were stirred vigorously on a tumble stirrer to generate well-behaved slurries (Figure 3.5C), which were subsequently dosed with wide-bored pipette tips. The source plate of 96 acids was filled with solvent to generate 0.30 M solutions (Figure 3.5D), with the OT2 adjusting solvent volume "on-the-fly". Of the 96 acids tested, most delivered the ester product (Figure 3.5B) as observed by UPLC-MS. Select reactions from this microscale library were repeated on a larger scale, with the ester products isolated by column chromatography (see **3.46**–**49**, Figure 3.5F and Experimental). The yields were good to excellent. The results lead us to interrogate the mechanism. By leaving out the carboxylic acid and reacting **3.38** with potassium iodide, we were able to isolate the corresponding iodide (see section3.3.6).

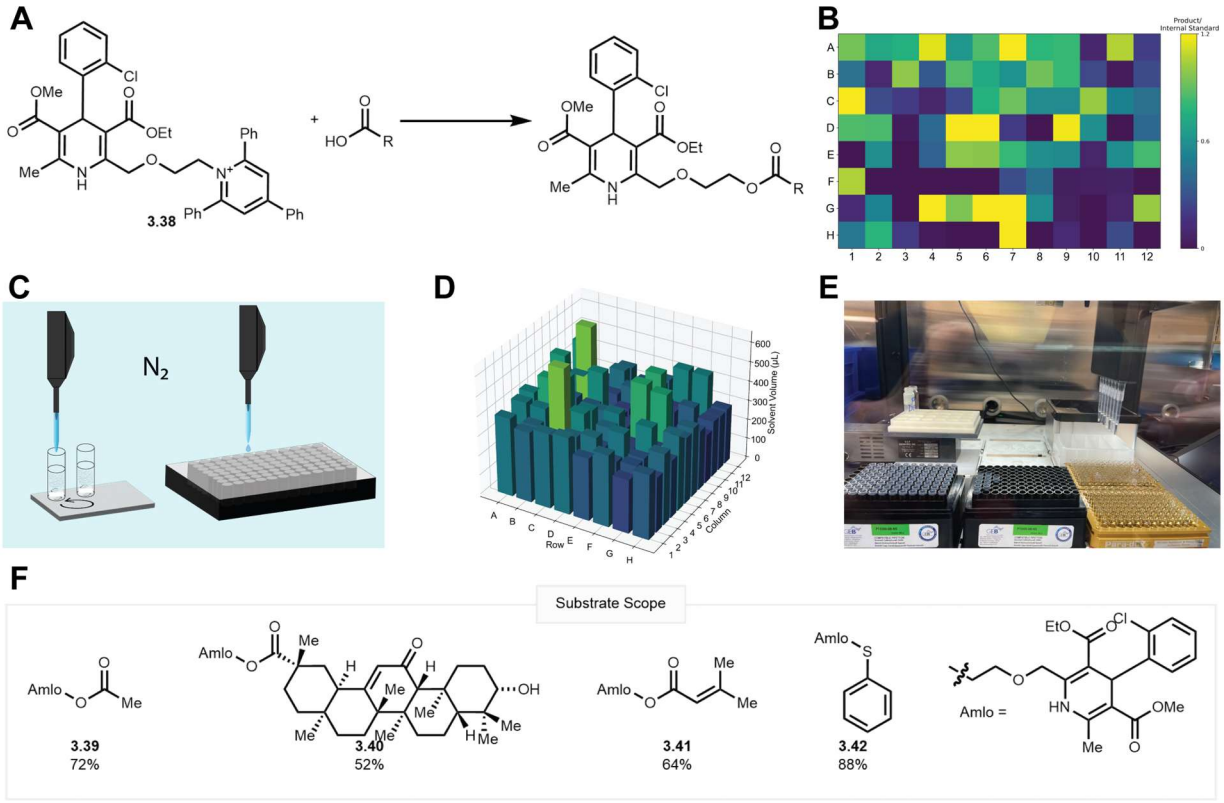

Figure 3.4 A) General reaction scheme. B) Heatmap of products. Yields are represented as product UV area over internal standard. Acids are aligned such that rows A and B contain mono- and poly-substituted (hetero)aryl acids, row C contains acetic acids, row D contains aliphatic acids with varying functionality, row E contains amino acids with various protecting groups, row F contains non-carboxylic acidic molecules, row G contains drugs with carboxylic acid moieties, and row H contains carboxylate salts with varying counterions. C) A cartoon depicting slurry loading taking place inside an inert atmosphere glovebox. D) A heatmap depicting the volume of solvent added to each of the 96 acids. Rather than try to weigh a specific amount, the amount is simply recorded, and the correct amount of solvent added. E) A photograph of the Opentrons transferring eight acids using its multichannel pipette head. F) Scale up of wells D2, G1, D5, and F8.

3.2 Experimental for the esterification reaction.

3.2.1 General Methods Summary

All reactions were conducted in oven- or flame-dried glassware under an atmosphere of nitrogen unless stated otherwise. Reactions were set up in an MBraun LABmaster Pro Glove Box (H_2O level <0.1 ppm, O_2 level <0.1 ppm), or using standard Schlenk technique with a glass vacuum manifold connected to an inlet of dry nitrogen gas. Acetonitrile (MeCN) was purified using an MBraun SPS solvent purification system by purging with nitrogen, and then passing the

solvent through a column of activated alumina. 1,4-dioxane, *N,N*-dimethylformamide (DMF), and dimethyl sulfoxide (DMSO) were purchased as anhydrous solvents and used as received. Reagents were purchased from Sigma Aldrich, Alfa Aesar, Oakwood Chemical, or TCI Chemical. Liquid primary amines were passed through a plug of basic alumina prior to use in making Katritzky salts. Potassium iodide was ground with a mortar and pestle prior to use. All other chemicals were used as received. Glass 1 dram (Fisher Scientific #03-339-21B) or 2-dram vials (Fisher Scientific #03-339-21D) were used as reaction vessels, fitted with a screw cap and Teflon-coated silicone septa (ChemGlass #CG-4910-02), and magnetic stir bars (Fisher Scientific #14-513-93 or #14-513-65).

Proton nuclear magnetic resonance (^{1}H NMR) spectra were recorded on a Varian MR-500 MHz, or Varian MR-400 MHz spectrometer and chemical shifts are reported in parts per million (ppm) using the solvent residual peak as an internal standard ($CDCl_3$ at 7.26 ppm, DMSO-d_6 at 2.50 ppm, D_2O at 4.80). Data are reported using the abbreviations: app = apparent, s = singlet, d = doublet, t = triplet, q = quartet, m = multiplet, comp = complex, br = broad. Coupling constant(s) are reported in Hz. Proton-decoupled carbon nuclear magnetic resonance spectra (^{13}C NMR) spectra were recorded on a Varian MR-500 MHz or Varian MR-400 MHz spectrometer and chemical shifts are reported in ppm using the solvent as an internal standard ($CDCl_3$ at 77.16 ppm, DMSO-d_6 at 39.52 ppm). High resolution mass spectrometry data (HRMS) was obtained on a Micromass AutoSpec Ultima Magnetic Sector instrument. Reaction analysis was typically performed by thin-layer chromatography (TLC) on silica gel 60 F_{254} glass plates (Fisher Scientific #S07876) and visualized using ultraviolet light (254 nm), ninhydrin stain, or potassium permanganate ($KMnO_4$) stain; or using a Waters I-class ACQUITY UPLC-MS (Waters Corporation, Milford, MA, USA) equipped with in-line photodiode array detector (PDA) and

QDa mass detector (ESI positive ionization mode). 0.1 µL sample injections were taken from acetonitrile solutions of reaction mixtures or products (~1 mg/mL). A partial loop injection mode was used with the needle placement at 1.0 mm from bottom of the wells and a 0.2 µL air gap at pre-aspiration and post-aspiration. Column used: Waters Cortecs UPLC C18+ column, 2.1mm · 50 mm with (Waters #186007114) with Waters Cortecs UPLC C18+ VanGuard Pre-column 2.1mm · 5 mm (Waters #186007125), Mobile Phase A: 0.1 % formic acid in Optima LC/MS-grade water, Mobile Phase B: 0.1% formic acid in Optima LC/MS-grade MeCN. Flow rate: 0.8 mL/min. Column temperature: 45 °C. The PDA sampling rate was 20 points/sec. The QDa detector monitored m/z 150-750 with a scan time of 0.06 seconds and a cone voltage of 30 V. The PDA detector range was between 210 nm – 400 nm with a resolution of 1.2 nm. 1-minute and 2-minute methods were used. The method gradients are as follows: 0 min: 0.8 mL/ min, 95% 0.1% formic acid in water/ 5% 0.1% formic acid in acetonitrile; 1.5 min: 0.8 mL/ min, 0.1% 0.1% formic acid in water/ 99.9% 0.1% formic acid in acetonitrile; 1.91 min: 0.8 mL/min, 95% 0.1% formic acid in water/ 5% 0.1% formic acid in acetonitrile. Flash chromatography was performed on silica gel (230 – 400 Mesh, Grade 60) under a positive pressure of air.

3.2.2 Data Visualization

Analytical Studio Pro from Virscidian (version 10.8) was used to process the UPLC data files in total wavelength chromatogram (TWC), and to generate machine-readable reports in .csv files. Code for chemoinformatics and visualization was written in Python (version 3.9.7). All Python dependencies were installed using Conda version 4.10.3, via Miniforge's arm64 distribution. Matplotlib (version 3.4.3) and Seaborn (version 0.11.2) were both used to create plots and graphs. Pandas (1.3.4) was used to parse excel files and other data formats.

3.2.3 General Procedures for the Esterification Reaction

3.2.3.1 General Optimization Procedure for Benzylic Katritzky Salts

In an inert atmosphere glovebox, either potassium carboxylate salt (0.12 mmol, 1.2 equiv) or free carboxylic acid (0.12 mmol, 1.2 equiv) and associated base (0.12 mmol, 1.2 equiv) were weighed into a dry 2-dram vial. 1 mL of solvent was added, and the mixture stirred for 5 minutes. Following this, Katritzky salt (0.1 mmol, 1 equiv) and additive (1 equiv or 0.2 equiv) were added. The vial was capped, removed from the glovebox, and heated at 80 °C with stirring for 22 hours. Upon completion, 1.00 mL of a 0.033 M trimethoxybenzene solution in ethyl acetate (EtOAc) was added to the reaction mixture. This was further diluted with 3 mL of EtOAc and partitioned between 10 mL of EtOAc and 10 mL of saturated sodium sulfate. Additional EtOAc (10 mL/0.1 mmol acid) and saturated aqueous sodium sulfate (10 mL / 0.1 mmol acid) was added. The aqueous layer was extracted twice more with EtOAc (10 mL / 0.1mmol). The organic layers were combined, dried over sodium sulfate and the solvent removed *in vacuo*. The crude material was then redissolved in chloroform-d and the NMR yield calculated.

Table 3.2 Extended benzylic ester optimization table.

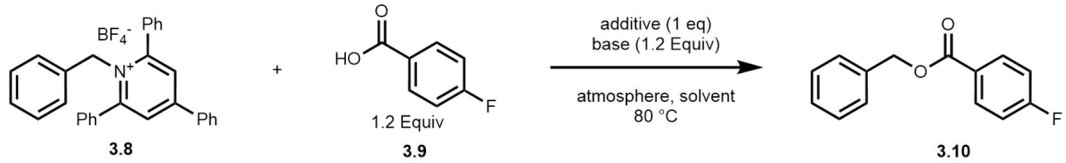

entry	base	additive	solvent	% NMR yield
1	R-CO_2K	BMDM	DMF	74
2	KO^{t}Bu	BMDM	DMF	74
3[a]	KO^{t}Bu	BMDM	MeCN	72
4[a]	KO^{t}Bu	BMDM	DMSO	66
5[a]	KO^{t}Bu	BMDM	Cyrene	61
6	R-CO_2K	TBAI	DMF	72
7[b]	KO^{t}Bu	BMDM	DMF	55
8[a,c]	KO^{t}Bu	BMDM	DMF	72

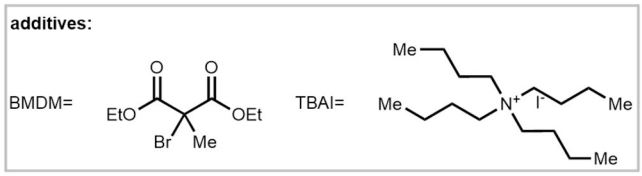

a = 0.2 eq additive
b = under air
c= in the dark

3.2.3.2 General Optimization Procedure for non-benzylic Katritzky Salts

In an inert atmosphere glovebox, carboxylic acid (1.2 mmol, 10 equiv) and Katritzky salt (1.2 mmol, 10 equiv) were weighed into a dry 2-dram vial. 3.78 mL of dioxane and 210 µL (1.2 mmol, 10 equiv) of diisopropylethylamine was added, and the mixture stirred for 5 minutes. 270 µL (1 equiv) of this solution was added to a vial containing 30 µL dioxane, 16 mg (0.1 mmol, 1 equiv) KI, and an additive if present. The reaction was heated for the designated time for 22 hours and cooled to room temperature. After this, internal standard (4.1 µL of benzotrifluoride 0.033 mmol, 0.33 equiv) was added to reach reaction and stirred for 5 minutes, and a 30 µL aliquot dissolved in 570 µL of $CDCl_3$. ^{19}F NMR was performed and the yield calculated.

For the reaction in the dark, the vial was wrapped in tin foil. For the reaction in light, a CFL bulb was shined onto the reaction from six inches away. For the 0.25 M reaction, 130 µL of dioxane

was in the vial instead of 30. For the 0.4M reaction the dioxane was not added. For the reaction under air, a needle was poked in the septum.[23]

Table 3.3 Extended optimization table for primary amine derived esters.

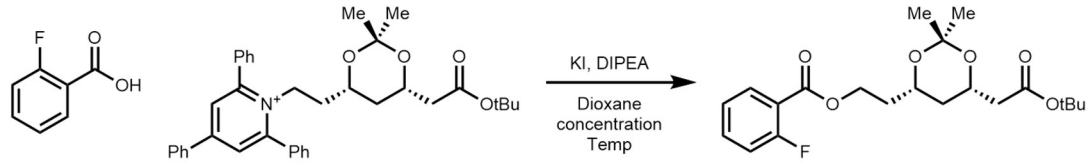

Entry	Concentration	Temperature	Additive	% NMR Yield (isolated)
1	0.3M	110 °C	none	82% (78%)
2	0.3M	110 °C	Light	80%
3	0.3M	110 °C	Dark	77%
4	0.3M	120 °C	none	77%
5	0.3M	95 °C	none	82%
6	0.3M	110 °C	Air	69%
7	0.3M	110 °C	H_2O 2 eq	65%
8	0.4 M	110 °C	none	70%
9	0.25 M	110 °C	none	67%
10	0.3M	110 °C	2 equiv KI	81%
11	0.3M	110 °C	0.5 equiv KI	45%

3.2.3.3 General Procedure 3.1: Preparation of esters in dioxane

Carboxylic acid (1 equiv), Katritzky salt (1 equiv), and potassium iodide (1 equiv) were added to an oven dried vial containing a stir bar. The vial was then capped, evacuated, and refilled with N_2 three times. Dioxane (0.3 mL/0.1 mmol acid) was added through the septum to produce a 0.33 M solution. To this solution diisopropylethylamine (DIPEA) (1 equiv, 17.4 µL/ 0.1 mmol acid) was added via syringe, the cap wrapped with parafilm, and heated to the indicated temperature for 22 hours. Following this, the reaction was diluted with EtOAc (2.5 mL/0.1 mmol acid) and partitioned between additional EtOAc (10 mL/0.1 mmol acid) and saturated aqueous sodium sulfate (10 mL/ 0.1 mmol acid). The aqueous layer was extracted twice more with EtOAc (10

mL / 0.1 mmol). The organic layers were combined, dried over sodium sulfate and the solvent removed *in vacuo*. Purification was achieved as described.

3.2.3.4 General Procedure 3.2: Preparation of esters in DMF

Carboxylic acid (1.2 equiv) and potassium *tert*-butoxide (KO^tBu) (1.2 equiv) were added to a dried vial and dissolved in 1 mL of dimethylformamide (DMF). This was stirred at room temperature for five minutes followed by the addition of Katritzky salt (1.0 equiv) and 2-bromo-2-methyl diethylmalonate (BMDM) (0.2 equiv, 3.8 μL/0.1 mmol) via syringe. The vial was degassed with N_2 and heated to 80 °C for 22 hours. Following this, the reaction was diluted with EtOAc (2.5 mL/0.1mmol acid) and partitioned between additional EtOAc (10 mL/0.1 mmol acid) and saturated aqueous sodium sulfate (10 mL/ 0.1mmol acid). The aqueous layer was extracted twice more with EtOAc (10 mL / 0.1mmol). The organic layers were combined, dried over sodium sulfate and the solvent removed *in vacuo*. Purification was achieved as described.

3.2.3.5 General Procedure 3.3: Preparation of esters from free amine

To an oven-dried vial was added 0.2 mmol of amine, followed by 0.2 mmol of carboxylic acid and 0.2 mmol (32 mg) of potassium iodide. The vial was then capped, evacuated, and refilled with N_2 three times. Dioxane (0.6 mL) was added through the septum via syringe to produce a 0.33 M solution followed by 35 μL of DIPEA. This solution was stirred at room temperature for 5 minutes followed by addition of 0.2 mmol (79 mg) of triphenylpyrylium tetrafluoroborate under a positive pressure of nitrogen. The cap was replaced, wrapped with parafilm, and heated to 110 °C for 22 hours. Following this, the reaction was diluted with EtOAc (5 mL) partitioned between additional EtOAc (20 mL) and saturated aqueous sodium sulfate (20 mL). The aqueous layer was extracted twice more with EtOAc (20 mL). The organic layers were combined, dried over sodium sulfate and the solvent removed *in vacuo*. Purification was achieved as described.

3.2.4 Procedure for Automated Library Synthesis

Katritzky salt **3.38** (790 mg) and potassium iodide (239 mg) were weighed into oven-dried glass vials (ChemGlass #CG-4912-02). 4.8 mL and 3.33 mL of diglyme were added to the Katritzky salt and potassium iodide respectively to make two 0.3 M solutions. Acids were weighed out into individual glass shell vials (Analytical Sales & Services #84001) and loaded onto an empty 96-well tray (Analytical Sales & Services #884001). The weighed masses were submitted to Phactor™, our HTE web application, where the appropriate solvent volumes to generate a 0.3 M stock solution was calculated for each microvial, and then imported into the setup script substrate_screen_solvent_katsalt_KI.py. One parylene-coated stir dowel (Analytical Sales & Services # 13258) was added to each well, and the setup was brought into the glovebox along with the solutions of Katritzky salt and potassium iodide, a 96-well aluminum microvial plate (Analytical Sales & Services # 96973) loaded with empty glass shell vials, diglyme, DIPEA and a deep well reservoir (Analytical Sales & Services # 962144). The Katritzky salt and potassium iodide solutions were placed on a 24-well stirring block (Analytical Sales & Services #24125) mounted on a tumble stirrer (V&P Scientific Inc. 710D3) fitted with a SLAS footprint adaptor (V&P Scientific Inc. 710D3-2), and deck adapter (V&P Scientific Inc. 581B). The glovebox circulation was turned off, and the setup script was loaded into the Opentrons app. The two microvial plates, deep well reservoir and tumble stirrer were mounted on the Opentrons deck as directed by the protocol. 40 mL of a 0.3 M solution of DIPEA in diglyme (prepared by mixing 3.66 mL DIPEA in 66.34 mL diglyme) was prepared and added to the deep well reservoir. The setup script was subsequently executed, which directs the OT-2 robot to dose appropriate amounts of solvent to each microvial using a single-channel 300 μL pipette (Opentrons P300 Gen 1 Single) fitted with the recommended pipette tips (Opentrons PT0300-9B-NS). The

protocol was paused, the tumble stirrer activated to suspend the potassium iodide and Katritzky salt in solution, then the protocol resumed to dose 33 µL of each solution to the blank microvial plate. The Katritzky salt was dosed with Opentrons pipette tips, while potassium iodide was dosed with large orifice tips (USA Scientific 1011-8000). Next, the script substrate_screen_acids.py was executed to transfer each acid solution into the corresponding microwell on the plate containing Katritzky salt and potassium iodide, using an 8-channel pipette (Opentrons P300 Gen 1 Multi) with wide orifice tips. The robot was programmed to pre-mix each solution with 3 repetitions of 100 µL each. The microvial plate was sealed with two layers of rubber mat (Analytical Sales & Services # 96965) and one layer of PFA film (Analytical Sales & Services # 96979), removed from the glovebox, and heated using a heating block (V&P Scientific Inc. 741GA) at 110 °C for 22 hours stirring at 500 RPM (V&P Scientific Inc. 710E5X).

After the reaction time has elapsed, the microvial plate was returned to the robot deck along with a polypropylene 96-well deep well plate (Analytical Sales & Services # 17P687Z) and a fresh deep well reservoir containing 0.1 M caffeine solution in acetonitrile in one well, and Optima grade acetonitrile in the other. Protocol substrate_screen_quench.py was then executed using the 8-channel pipette to first transfer 100 µL of the caffeine "quench" solution into the microvial plate, then transfer 40 µL of the quenched reaction to the polypropylene deep well plate, with premixing of 3 repetitions of 100 µL each. Next, 560 µL of acetonitrile was added to each well of the polypropylene deep well plate. Lastly, the plate was sealed with a polypropylene cap mat (Analytical Sales & Services # 96057) and analyzed with UPLC-MS.

In order for users to calibrate the robot while maintaining eye contact with the robot deck containing pipette tips and labware, a video game controller (PDP 049-005-NA) was connected

to the computer on which the Opentrons App was installed, and button presses mapped to the required keyboard inputs for calibration (Figure S2) using Antimicro[24] (version 2.23).

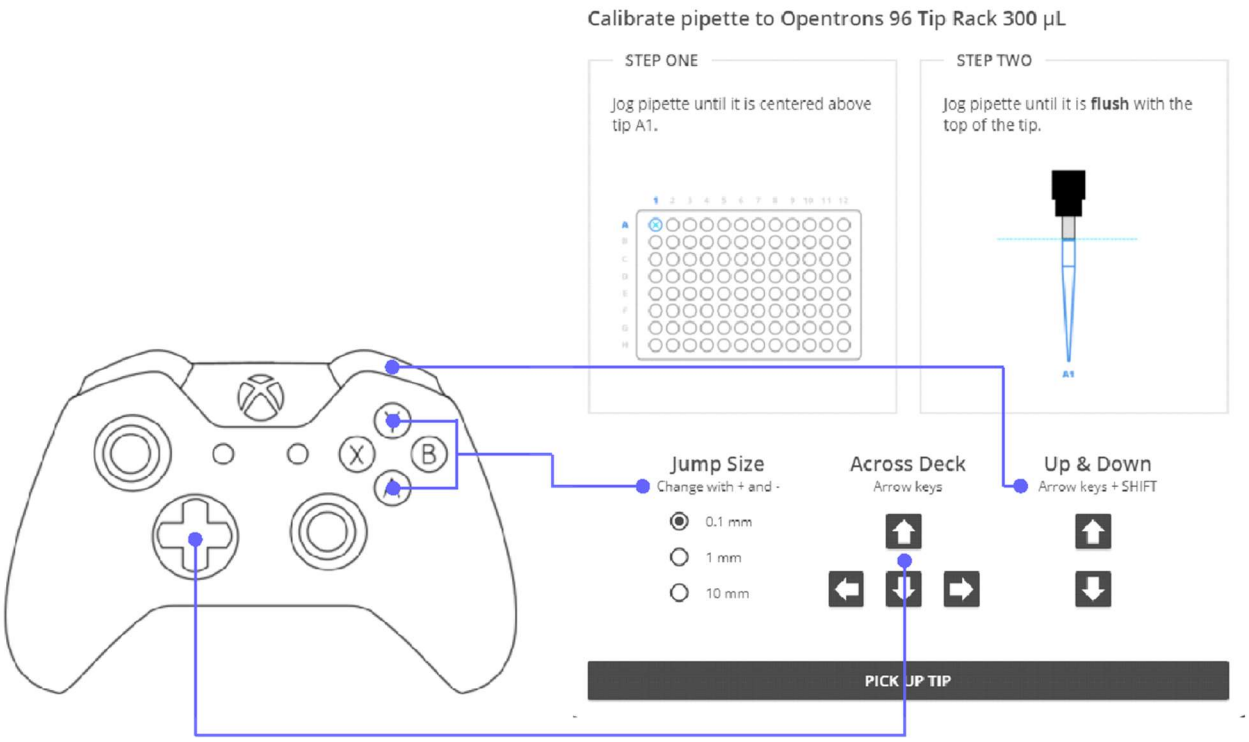

Figure 3.5 Input mappings for OT-2 robot calibration using a video game controller.[25] The Xbox® controller is pictured, but those of other consoles can also be used as long as they can interface with the driving computer.

3.2.4.1 List Of Carboxylic Acids Used in the Screen

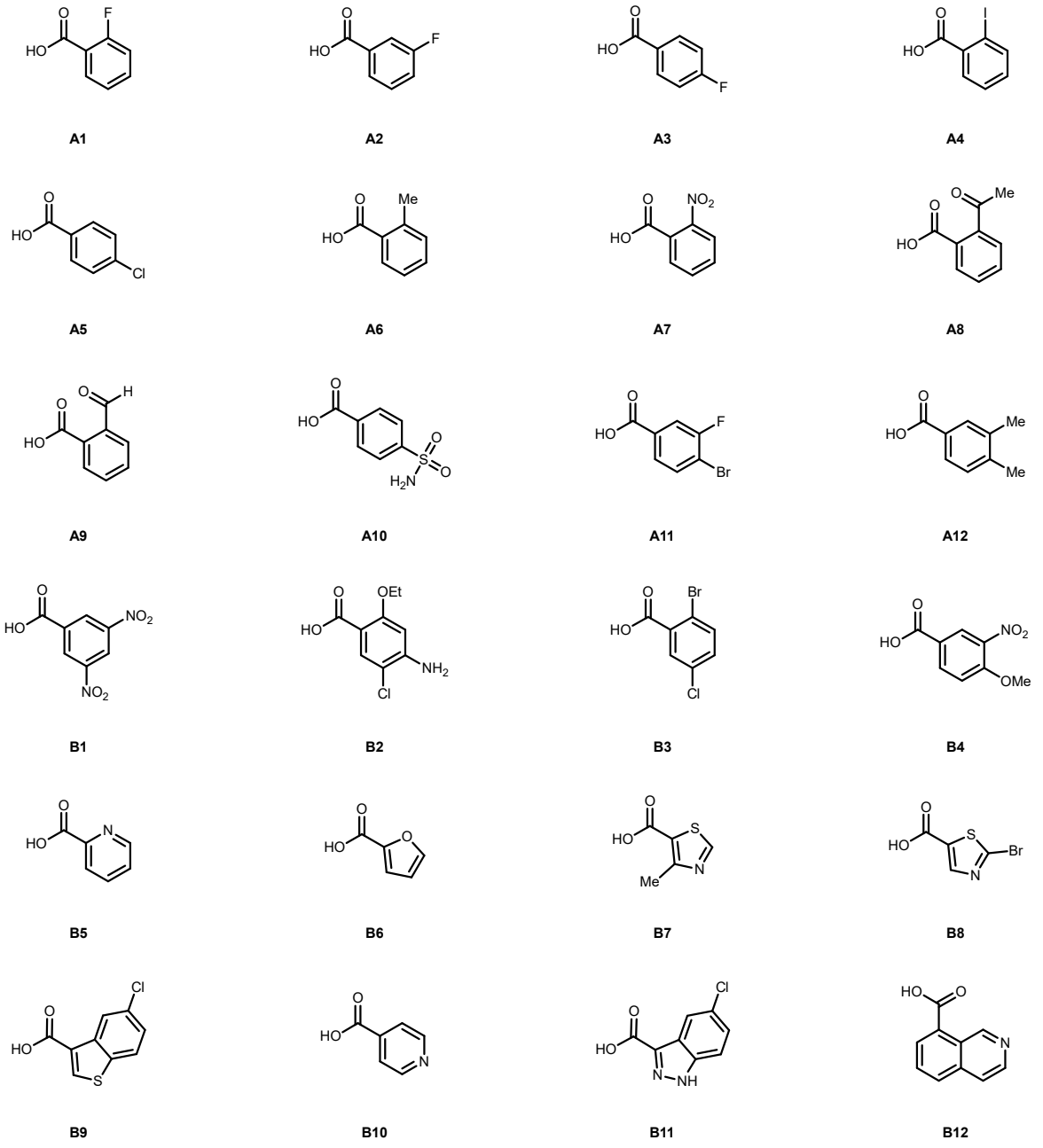

Figure 3.6. List of Carboxylic Acids used in wells A1–B12. Note the label corresponds to which well the acid was used in.

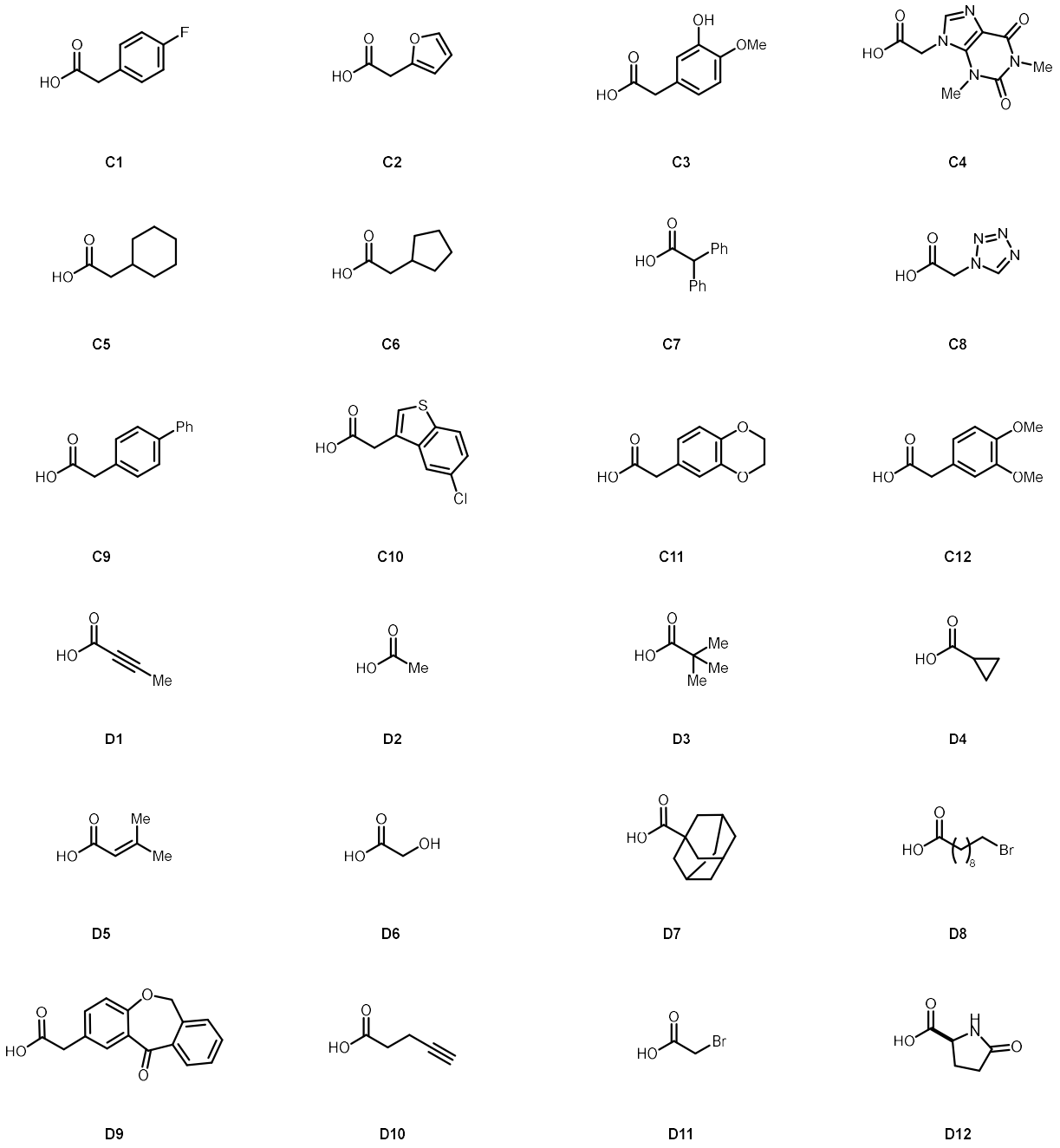

Figure 3.7 List of Carboxylic Acids used in wells C1–D12. Note the label corresponds to which well the acid was used in.

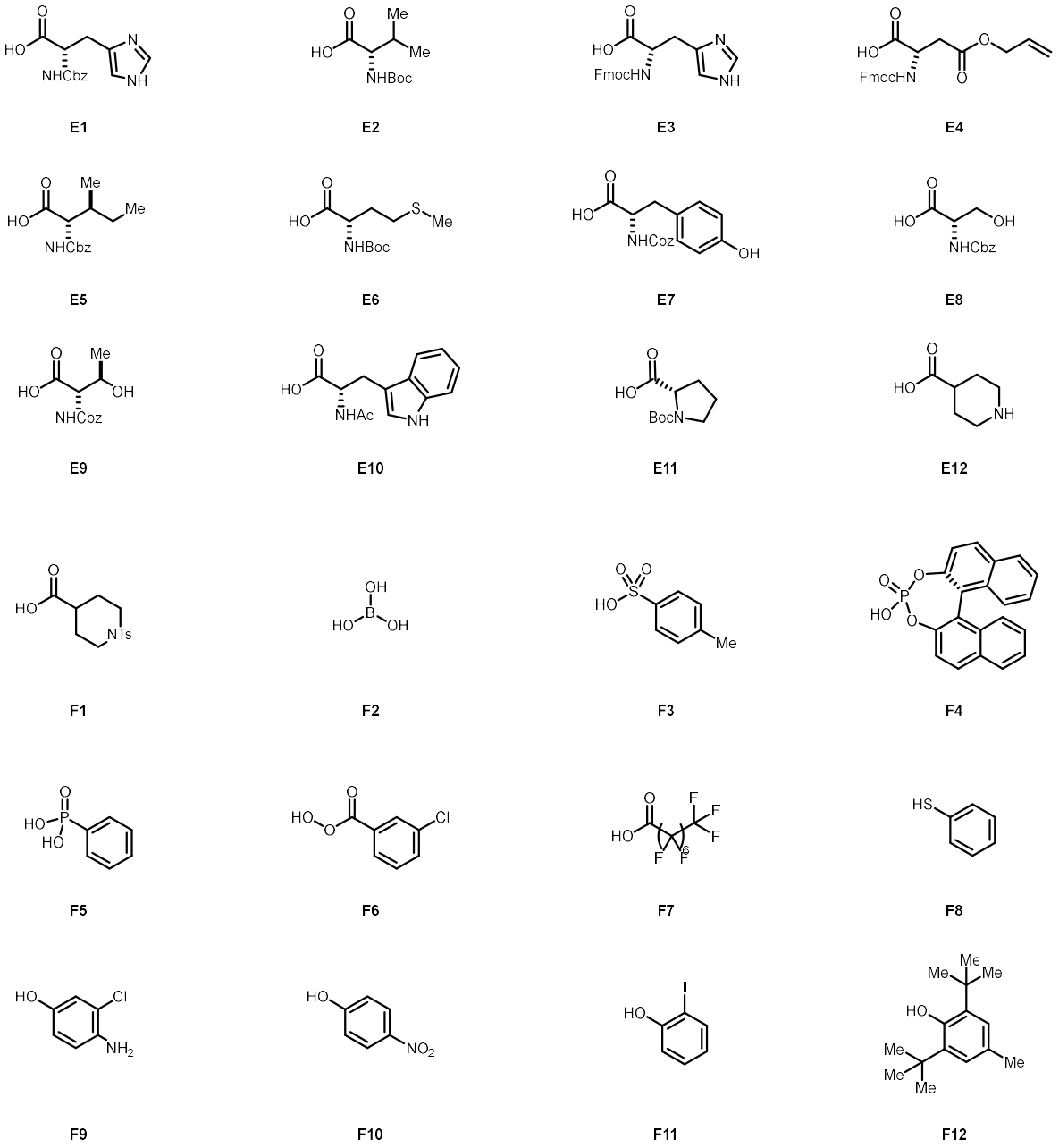

Figure 3.8 List of Carboxylic Acids used in wells E1–F12. Note the label corresponds to which well the acid was used in.

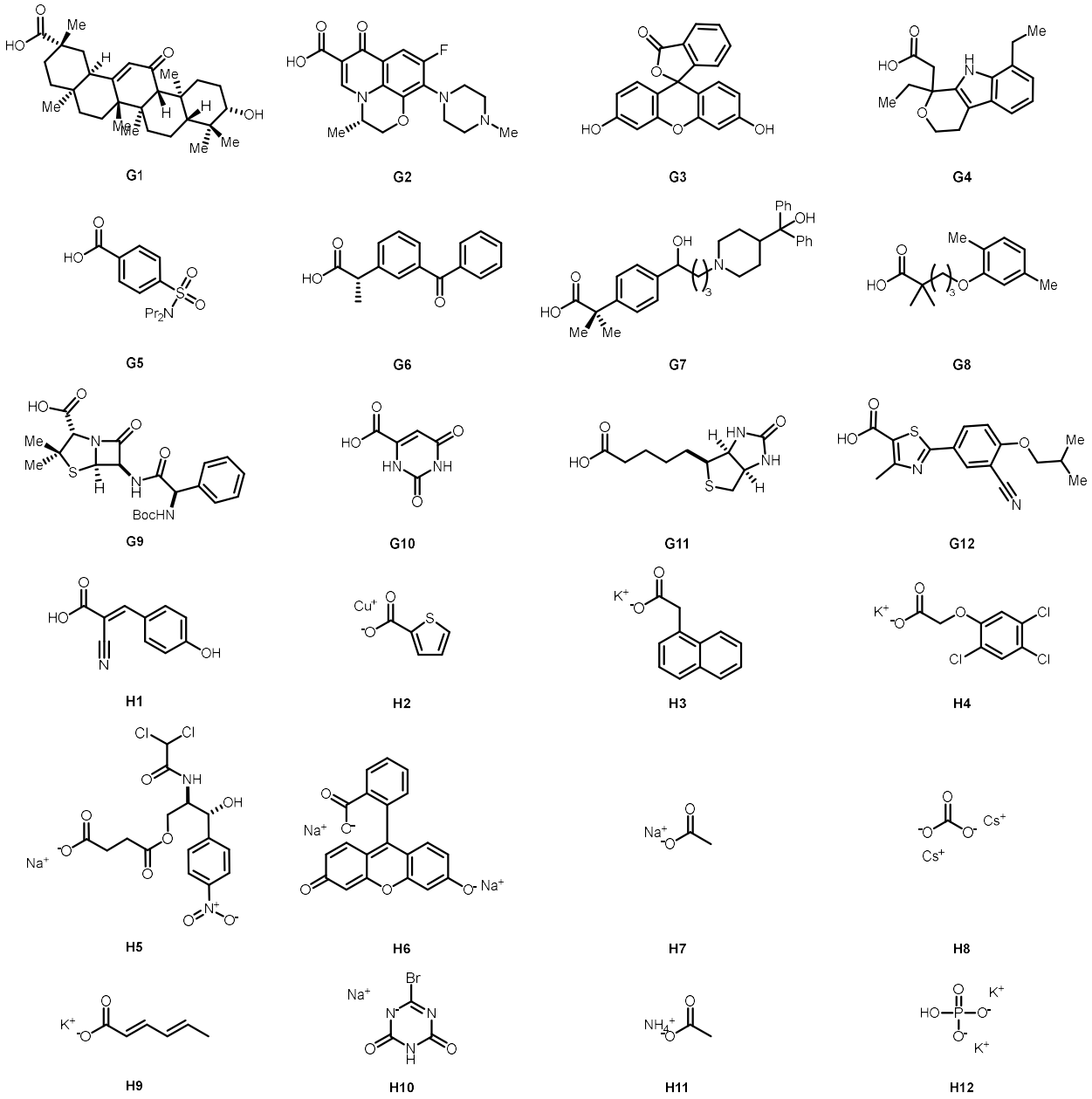

Figure 3.9 List of Carboxylic Acids used in wells G1–H12. Note the label corresponds to which well the acid was used in.

3.2.5 Preparation of Starting Materials for the Esterification Reaction

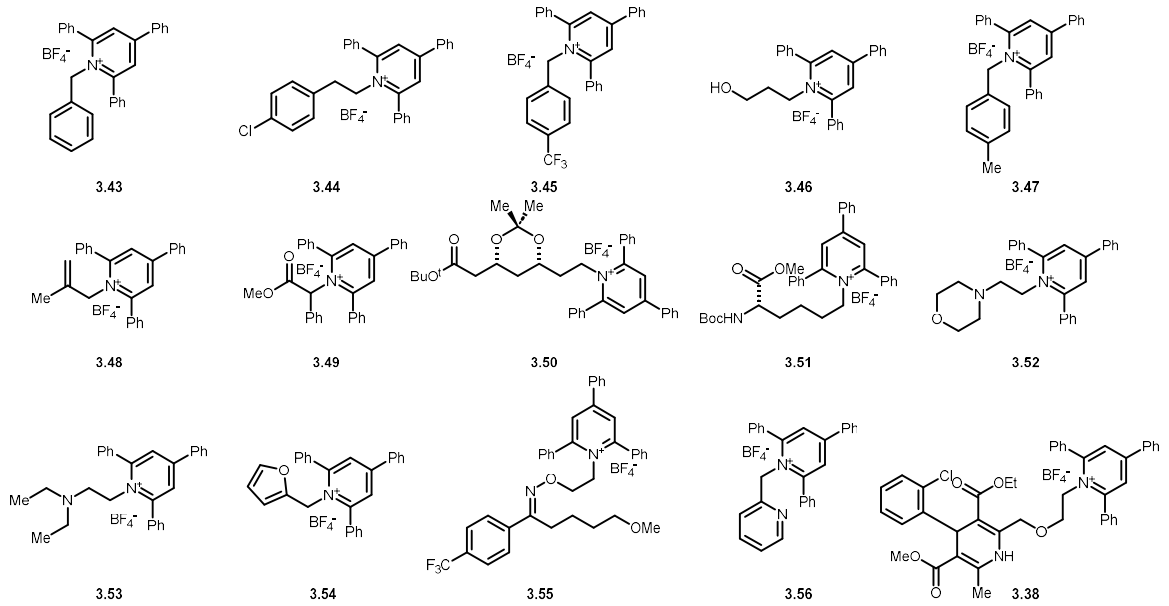

Figure 3.10 All Pyridinium salts used in the esterification reaction.

3.43,[13] **3.44**,[26] **3.45**,[13] **3.46**,[27] **3.47**,[13] **3.48,**[28] **3.49,**[29] **3.50,**[6] **3.53**,[30] **3.54**,[31] **3.56**,[31] and **3.38**[27] were prepared as previously reported. **3.51**, **3.52**, and **3.55** were prepared as described below.

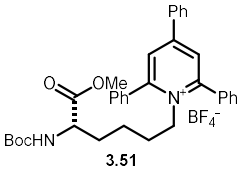

(S)-1-(5-((tert-Butoxycarbonyl)amino)-6-methoxy-6-oxohexyl)-2,4,6-triphenylpyridin-1-ium tetrafluoroborate (3.51)

Boc-L-lysine methyl ester HCl salt (540 mg, 1.8 mmol, 1.2 equiv) was suspended in ethanol (1.5 mL) followed by the addition of triethylamine (253 µL, 1.8 mmol, 1.2 equiv). This was stirred for 20 minutes followed by the addition of triphenylpyrylium tetrafluoroborate (600 mg, 1.5 mmol, 1.0 equiv). The reaction mixture was heated at 80 °C for four hours. After cooling to room temperature, the reaction mixture was poured into a separatory funnel containing 15 mL of dichloromethane (DCM) and washed with 10 mL of 1 M HCl. The organic layer was collected, dried over sodium sulfate, concentrated *in vacuo,* and purified via column chromatography

(0→30% acetone in DCM) to give 700 mg (72%) of an off-white solid. Characterization data matches those of the reported compound.[19]

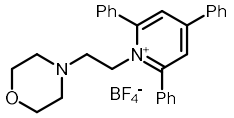

3.52

1-(2-Morpholinoethyl)-2,4,6-triphenylpyridin-1-ium tetrafluoroborate (3.52)

2-morpholinoethan-1-amine (156 mg, 1.2 mmol, 1.2 equiv) was dissolved in 1.0 mL of ethanol followed by the addition of triphenylpyrylium tetrafluoroborate (396 mg, 1.0 mmol, 1.0 equiv). This solution was heated at 80 °C for four hours. Upon cooling to room temperature, the product precipitated and was then filtered, washed with 3×2 mL portions of ethanol, 3×2 mL portions of ether and dried under vacuum overnight to give 340 mg (69%) of product.

^{1}H NMR (499 MHz, $CDCl_3$) δ 7.84 (d, *J* = 4.6 Hz, 6H), 7.76 – 7.71 (m, 2H), 7.62 – 7.57 (m, 6H), 7.56 – 7.46 (m, 3H), 4.66 (t, *J* = 7.4 Hz, 2H), 3.37 (t, *J* = 4.5 Hz, 4H), 2.36 (s, 2H), 1.83 (s, 4H).

^{13}C NMR (126 MHz, $CDCl_3$) δ 157.0, 156.1, 134.0, 132.9, 132.3, 131.3, 129.8, 129.5, 129.5, 128.3, 126.8, 66.6, 56.9, 53.0, 51.6.

^{19}F NMR (470 MHz, $CDCl_3$) δ −153.0.

HRMS (ESI) Calculated $C_{29}H_{29}N_2O^+$ $[M\text{-}BF_4]^+$: 421.2274, Found 421.2270.

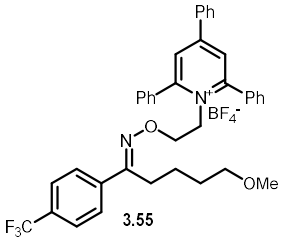

3.55

(E)-1-(2-(((5-Methoxy-1-(4-(trifluoromethyl)phenyl)pentylidene)amino)oxy)ethyl)-2,4,6-triphenylpyridin-1-ium (3.55)

Fluvoxamine maleate (1060 mg, 2.40 mmol, 1.2 equiv) was suspended in 2 mL of ethanol followed by the addition of triethylamine (486 mg, 669 µL, 4.8 mmol, 2.4 equiv). This was stirred for 30 min until homogenous, and followed by the addition of triphenylpyrylium tetrafluoroborate (792 mg, 2.0 mmol, 1.0 equiv). The solution was heated to 80 °C for four hours. Upon cooling to room temperature, the product precipitated and was filtered, washed with 2×2 mL of cold water, 2×2 mL of cold ethanol, and 2×2 mL of diethyl ether. The collected powder was dried under high vacuum to give 1200 mg (86%) of a white solid.

^{1}H NMR (499 MHz, $CDCl_3$) δ 7.85 – 7.78 (m, 6H), 7.67 – 7.61 (m, 2H), 7.61 – 7.54 (m, 6H), 7.54 – 7.44 (m, 5H), 7.37 (d, *J* = 8.2 Hz, 2H), 5.05 (t, *J* = 5.8 Hz, 2H), 4.01 (t, *J* = 5.8 Hz, 2H), 3.24 (d, *J* = 6.5 Hz, 5H), 2.55 (t, *J* = 7.9 Hz, 2H), 1.45 (dt, *J* = 12.0, 6.1 Hz, 2H), 1.37 (ddd, *J* = 15.9, 9.4, 6.1 Hz, 2H).

^{13}C NMR (126 MHz, $CDCl_3$) δ 158.8, 157.8, 156.2, 138.0, 133.7, 133.1, 132.5, 131.5 (q, J = 32.5 Hz), 131.3, 129.9, 129.6, 129.6, 128.1, 126.6, 126.5, 125.5 (q, J = 3.8 Hz), 125.0 (q, J = 272.9 Hz), 72.1, 70.4, 58.7, 54.6, 29.6, 26.0, 23.2.

^{19}F NMR (470 MHz, $CDCl_3$) δ −62.81, −152.95, −153.01.

HRMS (ESI) Calculated $C_{38}H_{36}F_3N_2O_2^+$ $[M\text{-}BF_4]^+$: 609.2723, Found 609.2714.

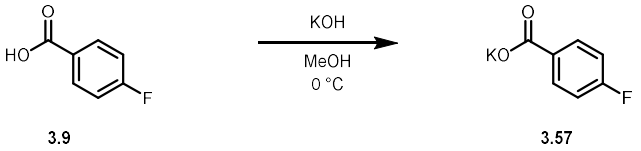

3.9 3.57

Scheme 3.1 Preparation of the potassium salt of 3.9.

Potassium 4-fluorobenzoate (3.57)

3.57 was prepared by dissolving 2.544 g (18.2 mmol, 1 equiv) of 4-fluorobenzoic acid in 5 mL of methanol within a 25 mL round bottom flask. This solution was cooled in an ice bath with stirring followed by the dropwise addition of a 4 M solution of methanolic KOH (4.50 mL, 18

mmol). The slurry was stirred at 0 °C for one hour, filtered, and vacuum dried overnight to give 2.879 g (89%) of the desired salt.

3.2.6 Characterization of Ester Products

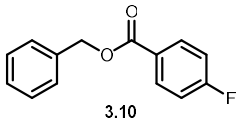

3.10

Benzyl 4-fluorobenzoate (3.10)

Ester **3.10** was prepared on a 0.2 mmol scale from 4-fluorobenzoic acid and **3.43** at 80 °C via General Procedure 3.2 to give 36 mg (76%) of a clear oil after purification with EtOAc/hexanes. Note: Product has an identical R_f to triphenylpyridine in all attempted solvent systems. To remedy this, before loading onto the column, the crude material was taken up in 0.3 mL of EtOAc 30 µL of TFA was added. The product was then eluted with 15% EtOAc in hexanes.

R_f 0.60 in 7:93 EtOAc:hexanes.

^{1}H NMR (499 MHz, $CDCl_3$) δ 8.13 – 8.06 (m, 2H), 7.47 – 7.42 (m, 2H), 7.42 – 7.32 (m, 3H), 7.11 (t, J = 8.6 Hz, 2H), 5.36 (s, 2H).

^{13}C NMR (126 MHz, $CDCl_3$) δ 166.1 (d, J = 172.0 Hz), 165.0, 136.1, 132.3 (d, J = 9.2 Hz), 128.8, 128.5, 128.4, 126.6, 115.5 (d, J = 22.0 Hz), 67.0.

^{19}F NMR (470 MHz, $CDCl_3$) δ −105.6 (tt, J = 8.4, 5.1 Hz).

HRMS (ESI) Calculated $C_{14}H_{12}FO_2^+$ $[M+H]^+$: 231.0816, Found 231.0742.

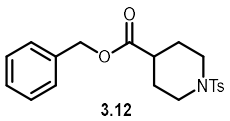

3.12

Benzyl 1-tosylpiperidine-4-carboxylate (3.12)

Ester **3.12** was prepared on a 0.2 mmol scale from N-tosylisonipecotic acid[32] and **3.43** at 80 °C via General Procedure 3.1 to give 68 mg (91%) of a white solid after purification with EtOAc/hexanes.

R_f: 0.40 in 20:80 EtOAc:hexanes

^{1}H NMR (499 MHz, $CDCl_3$) δ 7.65 – 7.59 (m, 2H), 7.38 – 7.26 (m, 7H), 5.09 (s, 2H), 3.61 (dt, *J* = 11.5, 4.1 Hz, 2H), 2.50 – 2.41 (m, 5H), 2.30 (tt, *J* = 10.6, 4.0 Hz, 1H), 2.02 – 1.95 (m, 2H), 1.83 (dtd, *J* = 14.4, 10.8, 4.0 Hz, 2H).

^{13}C NMR (126 MHz, $CDCl_3$) δ 173.7, 143.7, 135.8, 133.2, 129.8, 128.7, 128.4, 128.1, 127.8, 66.5, 45.5, 40.2, 27.5, 21.6.

HRMS (ESI) Calculated $C_{20}H_{24}NO_4S^+$ $[M+H]^+$: 374.1421, Found 374.1414.

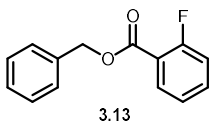

3.13

Benzyl 2-fluorobenzoate (3.13)

Ester **3.13** was prepared on a 0.2 mmol scale from 2-fluorobenzoic acid and **3.43** at 80 °C via General Procedure 3.2 to give 33 mg (72%) of a clear oil after purification with diethyl ether/hexanes.

R_f 0.70 in 7:93 Et_2O:hexanes.

^{1}H NMR (499 MHz, $CDCl_3$) δ 8.01 – 7.94 (m, 1H), 7.55 – 7.50 (m, 1H), 7.50 – 7.44 (m, 2H), 7.44 – 7.40 (m, 1H), 7.40 – 7.33 (m, 2H), 7.21 (ddt, *J* = 8.9, 6.4, 1.2 Hz, 1H), 7.15 (ddd, *J* = 10.9, 8.3, 1.4 Hz, 1H), 5.40 (d, *J* = 2.1 Hz, 2H).

^{13}C NMR (126 MHz, $CDCl_3$) δ 164.2 (d, *J* = 3.7 Hz), 162.1 (d, *J* = 260.4 Hz), 135.9, 134.6 (d, *J* = 9.1 Hz), 132.3, 128.7, 128.4, 128.2, 124.0 (d, *J* = 3.9 Hz), 118.7 (d, *J* = 9.5 Hz), 117.0 (d, *J* = 22.4 Hz), 67.0.

^{19}F NMR (470 MHz, $CDCl_3$) δ −108.9– −109.2 (m).

HRMS (ESI) Calculated $C_{14}H_{12}FO_2^+$ $[M+H]^+$: 231.0816, Found 231.0764.

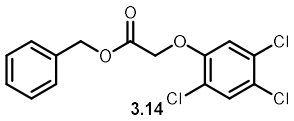

3.14

Benzyl 2-(2,4,5-trichlorophenoxy)acetate (3.14)

Ester **3.14** was prepared on a 0.2 mmol scale from commercially available potassium 2,4,5-trichlorophenoxyacetate and **3.43** at 80 °C via a modified procedure A where base was excluded to give 53 mg (76%) of a white solid after purification with EtOAc/hexanes.

R_f = 0.54 in 15:85 EtOAc:hexanes

^{1}H NMR (499 MHz, $CDCl_3$) δ 7.47 (d, *J* = 0.8 Hz, 1H), 7.41 – 7.31 (m, 5H), 6.89 (s, 1H), 5.25 (s, 2H), 4.72 (s, 2H).

^{13}C NMR (126 MHz, $CDCl_3$) δ 167.6, 152.7, 135.0, 131.4, 131.3, 128.8, 128.6, 125.7, 122.8, 115.7, 67.5, 66.6.

HRMS (ESI) Calculated $C_{15}H_{12}Cl_3O_3^+$ $[M+H]^+$: 344.9847, Found 344.9832.

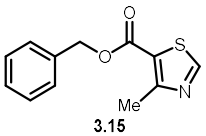

3.15

Benzyl 4-methylthiazole-5-carboxylate (3.15)

Ester **3.15** was prepared on a 0.2 mmol scale from 4-methylthiazole-5-carboxylic acid and **3.43** at 80 °C via General Procedure 3.1 to give 33 mg (70%) of a white solid after purification with EtOAc/hexanes.

R_f = 0.26 in 15:85 EtOAc:hexanes

^{1}H NMR (499 MHz, $CDCl_3$) δ 8.78 (s, 1H), 7.45 – 7.33 (m, 5H), 5.33 (s, 2H), 2.78 (s, 3H).

^{13}C NMR (126 MHz, $CDCl_3$) δ 161.9, 161.1, 155.4, 135.5, 128.7, 128.4, 128.2, 128.2, 67.0, 17.4.

HRMS (ESI) Calculated $C_{12}H_{12}NO_2S^+$ $[M+H]^+$: 234.0583, Found 234.0587.

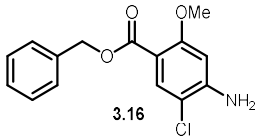

Benzyl 4-amino-5-chloro-2-methoxybenzoate (3.16)

Ester **3.16** was prepared on a 0.1 mmol scale from 4-amino-5-chloro-2-methoxy benzoic acid and **3.43** at 80 °C via General Procedure 3.2 to give 19 mg (64%) of a white solid after purification with EtOAc/hexanes.

R_f = 0.45 in 50:50 EtOAc:hexanes

^{1}H NMR (499 MHz, $CDCl_3$) δ 7.86 (s, 1H), 7.46 – 7.41 (m, 2H), 7.41 – 7.30 (m, 3H), 6.30 (s, 1H), 5.29 (s, 2H), 3.84 (s, 3H).

^{13}C NMR (126 MHz, $CDCl_3$) δ 164.5, 160.6, 147.9, 136.6, 133.5, 128.6, 128.2, 128.1, 110.2, 109.8, 98.5, 66.2, 56.2.

HRMS (ESI) Calculated $C_{15}H_{15}ClNO_3^+$ $[M+H]^+$: 292.0735, Found 292.0729.

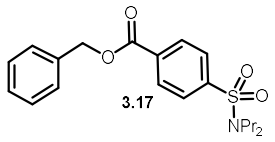

3.17

Benzyl 4-(N,N-dipropylsulfamoyl)benzoate (3.17)

Ester **3.17** was prepared on a 0.1 mmol scale from probenecid and **3.43** at 80 °C via General Procedure 3.2 to give 24 mg (64%) of a white solid after purification with EtOAc/hexanes.

R_f = 0.41 in 15:85 EtOAc:hexanes

^{1}H NMR (499 MHz, $CDCl_3$) δ 8.18 (d, *J* = 8.5 Hz, 2H), 7.87 (d, *J* = 8.5 Hz, 2H), 7.48 – 7.33 (m, 4H), 5.39 (s, 2H), 3.09 (t, *J* = 7.5 Hz, 4H), 1.54 (h, *J* = 7.4 Hz, 4H), 0.86 (t, *J* = 7.4 Hz, 6H).

^{13}C NMR (126 MHz, $CDCl_3$) δ 165.1, 144.4, 135.5, 133.4, 130.3, 128.7, 128.5, 128.4, 127.0, 67.3, 49.9, 21.9, 11.1.

HRMS (ESI) Calculated $C_{20}H_{26}NO_4S^+$ $[M+H]^+$: 376.1577, Found 376.1570.

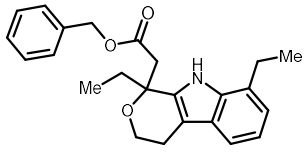

3.18

Benzyl 2-(1,8-diethyl-1,3,4,9-tetrahydropyrano[3,4-b]indol-1-yl)acetate (3.18)

Ester **3.18** was prepared on a 0.2 mmol scale from etodolac and **3.43** at 80 °C via General Procedure 3.1 to give 55 mg (74%) of a white solid after purification with EtOAc/hexanes.

R_f = 0.46 in 15:85 EtOAc:hexanes

^{1}H NMR (499 MHz, $CDCl_3$) δ 8.99 (s, 1H), 7.36 (d, *J* = 7.7 Hz, 1H), 7.36 – 7.29 (m, 4H), 7.10 – 7.03 (m, 1H), 7.01 (dt, *J* = 7.2, 1.0 Hz, 1H), 5.21 – 5.10 (m, 2H), 4.08 – 4.00 (m, 1H), 3.98 – 3.89 (m, 1H), 3.07 (d, *J* = 16.5 Hz, 1H), 2.97 (d, *J* = 16.6 Hz, 1H), 2.90 – 2.82 (m, 2H), 2.84 –

2.78 (m, 1H), 2.74 (dt, *J* = 15.2, 4.5 Hz, 1H), 2.16 (dq, *J* = 14.8, 7.4 Hz, 1H), 2.01 (dq, *J* = 14.0, 7.3, 6.8 Hz, 1H), 1.55 (s, 1H), 1.36 (td, *J* = 7.6, 0.9 Hz, 3H), 0.83 (td, *J* = 7.4, 0.9 Hz, 3H).

^{13}C NMR (126 MHz, $CDCl_3$) δ 172.6, 135.9, 135.4, 128.6, 128.4, 128.2, 126.6, 126.2, 120.4, 119.6, 115.9, 108.5, 74.6, 66.8, 60.6, 43.1, 30.7, 24.2, 22.4, 13.7, 7.6.

HRMS (ESI) Calculated $C_{24}H_{28}NO_3^+$ $[M+H]^+$: 378.2064, Found 378.2067.

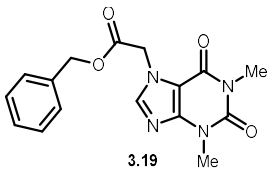

3.19

Benzyl 2-(1,3-dimethyl-2,6-dioxo-1,2,3,6-tetrahydro-7H-purin-7-yl)acetate (3.19)

Ester **3.19** was prepared on a 0.35 mmol scale from theophylline-7-acetic acid and **3.43** at 80 °C via General Procedure 3.1 to give 102 mg (89%) of a white solid after purification with EtOAc/hexanes.

R_f = 0.38 in 100% EtOAc

^{1}H NMR (499 MHz, $CDCl_3$) δ 7.60 (s, 1H), 7.36 (dd, *J* = 3.1, 1.1 Hz, 5H), 5.24 (s, 2H), 5.13 (s, 2H), 3.60 (s, 3H), 3.38 (s, 3H).

^{13}C NMR (126 MHz, $CDCl_3$) δ 167.0, 155.4, 151.8, 148.6, 141.9, 134.8, 128.9, 128.8, 128.7, 107.3, 68.2, 47.5, 30.0, 28.1.

HRMS (ESI) Calculated $C_{16}H_{17}N_4O_4^+$ $[M+H]^+$: 329.1244, Found 329.1235.

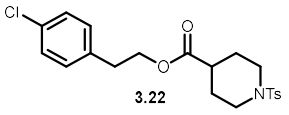

3.22

4-Chlorophenethyl 1-tosylpiperidine-4-carboxylate (3.22)

Ester **3.22** was prepared on a 0.2 mmol scale from N-tosylisonipecotic acid and **3.44** at 110 °C via General Procedure 3.1 to give 49 mg (58%) of a white solid after purification with EtOAc/hexanes.

R_f = 0.28 in 25:75 EtOAc:hexanes

^{1}H NMR (499 MHz, $CDCl_3$) δ 7.65 – 7.59 (m, 2H), 7.31 (d, *J* = 8.0 Hz, 2H), 7.25 (dd, *J* = 8.6, 2.3 Hz, 2H), 7.13 – 7.06 (m, 2H), 4.24 (t, *J* = 6.8 Hz, 2H), 3.58 (dt, *J* = 12.1, 4.1 Hz, 2H), 2.86 (t, *J* = 6.8 Hz, 2H), 2.43 (dd, *J* = 22.8, 3.0 Hz, 2H), 2.43 (s, 3H), 2.20 (tt, *J* = 10.6, 4.0 Hz, 1H), 1.95 – 1.85 (m, 2H), 1.75 (dtd, *J* = 14.3, 10.7, 3.9 Hz, 2H).

^{13}C NMR (126 MHz, $CDCl_3$) δ 173.8, 143.7, 136.2, 133.2, 132.6, 130.3, 129.8, 128.7, 127.8, 64.8, 45.5, 40.1, 34.5, 27.5, 21.6.

HRMS (ESI) Calculated $C_{21}H_{25}ClNO_4S^+$ $[M+H]^+$: 422.1187, Found 422.1181.

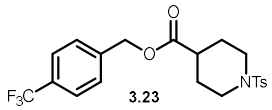

3.23

4-(Trifluoromethyl)benzyl 1-tosylpiperidine-4-carboxylate (3.23)

Ester **3.23** was prepared on a 0.2 mmol scale from N-tosylisonipecotic acid and **3.45** at 110 °C via General Procedure 3.1 to give 76 mg (86%) of a white solid after purification with EtOAc/hexanes.

R_f = 0.31 in 20:80 EtOAc:Hexanes

^{1}H NMR (400 MHz, $CDCl_3$) δ 7.66 – 7.57 (m, 4H), 7.40 (d, *J* = 8.0 Hz, 2H), 7.32 (d, *J* = 8.0 Hz, 2H), 5.14 (s, 2H), 3.64 (dt, *J* = 12.3, 4.0 Hz, 2H), 2.51 – 2.40 (m, 5H), 2.32 (tt, *J* = 10.7, 4.0 Hz, 1H), 2.00 (dd, *J* = 13.7, 3.8 Hz, 2H), 1.84 (dtd, *J* = 14.4, 10.8, 4.0 Hz, 2H).

^{13}C NMR (126 MHz, $CDCl_3$) δ 173.6, 143.8, 139.9, 133.3, 130.6(q, *J* = 32.6 Hz), 129.8, 128.2, 127.8, 125.7(q, *J* = 3.8 Hz), 123.0(q, *J* = 268.4 Hz), 65.6, 45.5, 40.2, 27.6, 21.7.

^{19}F NMR (376 MHz, $CDCl_3$) δ −62.67.

HRMS (ESI) Calculated $C_{21}H_{23}F_3NO_4S^+$ $[M+H]^+$: 442.1294, Found 442.1290.

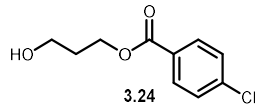

3.24

3-Hydroxypropyl 4-chlorobenzoate (3.24)

Ester **3.24** was prepared on a 0.1 mmol scale from p-chlorobenzoic acid and **3.46** at 110 °C via General Procedure 3.1 to give 18 mg (82%) of a yellow oil after purification with EtOAc/hexanes.

R_f = 0.16 in 25:75 EtOAc:hexanes

^{1}H NMR (499 MHz, $CDCl_3$) δ 7.96 (dd, *J* = 8.7, 2.0 Hz, 2H), 7.40 (dt, *J* = 9.1, 2.2 Hz, 2H), 4.47 (td, *J* = 6.2, 1.8 Hz, 2H), 3.76 (td, *J* = 6.1, 1.4 Hz, 2H), 2.12 (s, 1H), 2.00 (pd, *J* = 6.1, 1.3 Hz, 2H).

^{13}C NMR (126 MHz, $CDCl_3$) δ 166.2, 139.6, 131.1, 128.9, 128.7, 62.2, 59.2, 32.0.

HRMS (ESI) Calculated $C_{10}H_{12}ClO_3^+$ $[M+H]^+$: 215.0469, Found 215.0448.

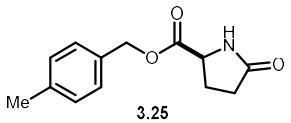

3.25

4-Methylbenzyl (*S*)-5-oxopyrrolidine-2-carboxylate (3.25)

Ester **3.25** was prepared on a 0.2 mmol scale from pyroglutamic acid and **3.47** at 80 °C via General Procedure 3.1 to give 44 mg (94%) of a white solid after purification with EtOAc/hexanes.

R_f: 0.34 in 100% EtOAc

^{1}H NMR (499 MHz, CDCl3) δ 7.23 (d, J = 8.2 Hz, 2H), 7.16 (d, J = 8.2 Hz, 2H), 6.89 (s, 1H), 5.13 (s, 2H), 4.24 (dd, J = 8.5, 4.9 Hz, 1H), 2.45 – 2.24 (m, 6H), 2.22 – 2.12 (m, 1H).

^{13}C NMR (126 MHz, $CDCl_3$) δ 178.2, 172.0, 138.5, 132.2, 129.4, 128.6, 67.3, 55.6, 29.3, 24.8, 21.2.

HRMS (ESI) Calculated $C_{13}H_{16}NO_3^+$ $[M+H]^+$: 234.1125, Found 234.1126.

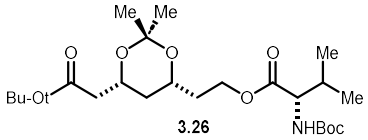

2-((4*R*,6*R*)-6-(2-(tert-Butoxy)-2-oxoethyl)-2,2-dimethyl-1,3-dioxan-4-yl)ethyl (*tert*-butoxycarbonyl)-*L*-valinate (3.26)

Ester **3.26** was prepared on a 0.2 mmol scale from N-Boc-*L*-valine and **3.50** at 110 °C via General Procedure 3.1 to give 65 mg (69%) of a clear oil after purification with EtOAc/hexanes.

R_f = 0.33 in 15:85 EtOAc:Hexanes

^{1}H NMR (499 MHz, $CDCl_3$) δ 5.02 (d, *J* = 9.1 Hz, 1H), 4.29 – 4.16 (m, 4H), 3.97 (dtd, *J* = 11.7, 6.3, 5.6, 2.4 Hz, 1H), 2.42 (dd, *J* = 15.2, 7.1 Hz, 1H), 2.29 (dd, *J* = 15.1, 6.1 Hz, 1H), 2.11 (dq, *J* = 13.1, 6.8 Hz, 1H), 1.81 – 1.74 (m, 2H), 1.56 (dt, *J* = 12.7, 2.4 Hz, 1H), 1.44 (d, *J* = 1.3 Hz, 18H), 1.41 (s, 3H), 1.34 (s, 3H), 1.28 – 1.15 (m, 1H), 0.95 (d, *J* = 6.8 Hz, 3H), 0.88 (d, *J* = 6.8 Hz, 3H).

^{13}C NMR (126 MHz, $CDCl_3$) δ 165.8, 158.2, 139.7, 139.0, 131.2, 131.0, 128.9, 128.8, 128.7, 126.7, 125.6, 125.5, 125.5, 125.5, 72.4, 72.1, 63.8, 58.7, 29.7, 26.4, 23.2.

HRMS (ESI) Calculated $C_{24}H_{43}NNaO_8^+$ $[M+Na]^+$: 496.2881, Found 496.2932.

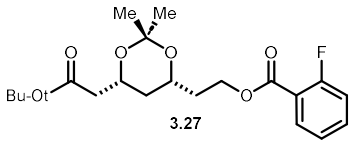

3.27

2-((4*R*,6*R*)-6-(2-(*tert*-Butoxy)-2-oxoethyl)-2,2-dimethyl-1,3-dioxan-4-yl)ethyl 2-fluorobenzoate (3.27)

Ester **3.27** was prepared on a 0.2 mmol scale from 2-fluorobenzoic acid and **3.50** at 110 °C via General Procedure 3.1 to give 61 mg (78%) of a clear oil after purification with EtOAc/hexanes.

Ester **3.27** was also prepared on a 0.2 mmol scale from 2-fluorobenzoic acid and tert-butyl 2-((4R,6R)-6-(2-aminoethyl)-2,2-dimethyl-1,3-dioxan-4-yl)acetate *in situ* via General Procedure 3.3 to give 44 mg (56%) of a clear oil after purification.

R_f = 0.44 in 15:85 EtOAc:hexanes

^{1}H NMR (499 MHz, $CDCl_3$) δ 7.89 (td, *J* = 7.6, 1.9 Hz, 1H), 7.48 (dddd, *J* = 8.6, 6.9, 4.7, 1.8 Hz, 1H), 7.18 (t, 1H), 7.10 (dd, *J* = 10.8, 8.3 Hz, 1H), 4.41 (td, *J* = 6.4, 2.5 Hz, 2H), 4.25 (dtd, *J* = 11.6, 6.5, 2.4 Hz, 1H), 4.07 (qd, *J* = 7.5, 2.4 Hz, 1H), 2.41 (dd, *J* = 15.1, 7.0 Hz, 1H), 2.28 (dd, *J* = 15.1, 6.1 Hz, 1H), 1.86 (q, *J* = 6.3 Hz, 2H), 1.59 (dt, *J* = 12.7, 2.5 Hz, 1H), 1.41 (d, *J* = 2.8 Hz, 12H), 1.33 (s, 3H), 1.23 (q, *J* = 11.9 Hz, 1H).

^{13}C NMR (126 MHz, $CDCl_3$) δ 170.4, 164.6 (d, J = 3.8 Hz), 162.1 (d, J = 259.8 Hz), 134.5 (d, J = 9.0 Hz), 132.2, 124.1 (d, J = 4.1 Hz), 119.1 (d, J = 10.0 Hz), 117.1 (d, J = 22.4 Hz), 99.0, 80.7, 66.4, 65.9, 61.7, 42.8, 36.7, 35.5, 30.2, 28.2, 19.8.

^{19}F NMR (470 MHz, $CDCl_3$) δ −109.4 (tt, *J* = 10.3, 4.9 Hz).

HRMS (ESI) Calculated $C_{21}H_{29}FNaO_6^+$ $[M+Na]^+$: 419.1846, Found 419.1828.

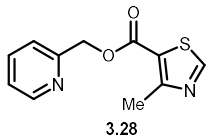

3.28

Pyridin-2-ylmethyl 4-methylthiazole-5-carboxylate (3.28)

Ester **3.28** was prepared on a 5.00 mmol scale from 4-methyl-5-thiazole carboxylic acid and **3.56** at 110 °C via a modified General Procedure 3.1 where a 50 mL round bottom flask equipped a reflux condenser and a septum was used in place of a vial and workup was accomplished with 75 mL of aqueous sodium sulfate and 3×100 mL of EtOAc. 670 mg (61%) of a tan solid was obtained after purification with EtOAc/hexanes.

R_f: 0.50 in 100% EtOAc

^{1}H NMR (499 MHz, $CDCl_3$) δ 8.79 (s, 1H), 8.60 (ddd, *J* = 4.8, 1.8, 1.0 Hz, 1H), 7.72 (td, *J* = 7.7, 1.6 Hz, 1H), 7.40 (dt, *J* = 7.8, 0.9 Hz, 1H), 7.24 (ddd, *J* = 7.6, 4.9, 1.2 Hz, 1H), 5.44 (s, 2H), 2.79 (d, *J* = 1.0 Hz, 3H).

^{13}C NMR (126 MHz, $CDCl_3$) δ 161.8, 161.5, 155.7, 155.5, 149.6, 137.0, 123.1, 121.8, 121.7, 67.5, 17.5.

HRMS (ESI) Calculated $C_{11}H_{11}N_2O_2S^+$ $[M+H]^+$: 235.0536, Found 235.0544.

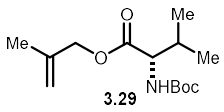

3.29

2-Methylallyl (*tert*-butoxycarbonyl)-*L*-valinate (3.29)

Ester **3.29** was prepared on a 0.2 mmol scale from N-Boc-*L*-valine and **3.48** at 80 °C via General Procedure 3.1 to give 35 mg (64%) of a clear oil after purification with EtOAc/hexanes.

R_f: 0.50 in 15:85 EtOAc:Hexanes

^{1}H NMR (499 MHz, $CDCl_3$) δ 5.05 – 4.98 (m, 2H), 4.97 – 4.93 (m, 1H), 4.61 – 4.49 (m, 2H), 4.26 (dd, *J* = 9.2, 4.7 Hz, 1H), 2.16 (ddd, *J* = 14.3, 9.9, 6.4 Hz, 1H), 1.76 (d, *J* = 1.4 Hz, 3H), 1.44 (s, 9H), 0.98 (d, *J* = 6.8 Hz, 3H), 0.90 (d, *J* = 6.9 Hz, 3H).

^{13}C NMR (126 MHz, $CDCl_3$) δ 172.3, 155.8, 139.6, 113.8, 79.9, 68.5, 58.7, 31.4, 28.4, 19.7, 19.2, 17.6.

HRMS (ESI) Calculated $C_{14}H_{25}NNaO_4^+$ $[M+Na]^+$: 294.1681, Found 294.1672.

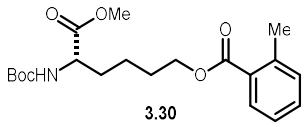

3.30

(*S*)-5-((*tert*-Butoxycarbonyl)amino)-6-methoxy-6-oxohexyl 2-methylbenzoate (3.30)

Ester **3.30** was prepared on a 0.117 mmol scale from o-toluic acid and **3.51** at 110 °C via General Procedure 3.1 to give 26 mg (69%) of a white solid after purification with EtOAc/hexanes.

R_f = 0.40 in 25:75 EtOAc:hexanes

^{1}H NMR (499 MHz, $CDCl_3$) δ 7.88 (dd, *J* = 8.1, 1.5 Hz, 1H), 7.38 (td, *J* = 7.5, 1.5 Hz, 1H), 7.28 – 7.20 (m, 2H), 5.07 – 5.02 (m, 1H), 4.34 – 4.24 (m, 3H), 3.72 (s, 3H), 2.58 (s, 3H), 1.87 (ddt, *J* = 15.3, 9.9, 6.3 Hz, 1H), 1.83 – 1.73 (m, 2H), 1.73 – 1.63 (m, 1H), 1.57 – 1.44 (m, 2H), 1.43 (s, 9H).

^{13}C NMR (126 MHz, $CDCl_3$) δ 173.3, 167.8, 155.5, 140.2, 132.0, 131.8, 130.6, 129.9, 125.8, 80.0, 64.4, 53.4, 52.4, 32.6, 28.4, 28.4, 22.1, 21.9.

HRMS (ESI) Calculated $C_{20}H_{29}NNaO_6^+$ $[M+Na]^+$: 402.1893, Found 402.1882.

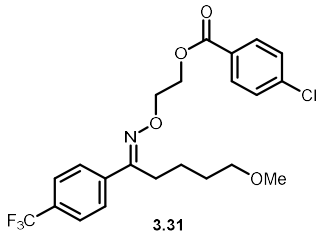

3.31

(*E*)-2-(((5-Methoxy-1-(4-(trifluoromethyl)phenyl)pentylidene)amino)oxy)ethyl 4-chlorobenzoate (3.31)

Ester **3.31** was prepared on a 0.1 mmol scale from p-chloro benzoic acid and **3.55** at 110 °C via a modified General Procedure 3.1 where the solvent was 90/10 v/v dioxane/DMF and two equivalents of potassium iodide (32 mg) were used to give 40 mg (88%) of a white solid after purification with EtOAc/hexanes.

R_f: 0.38 in 15:85 EtOAc:hexanes

^{1}H NMR (499 MHz, $CDCl_3$) δ 8.01 – 7.96 (m, 2H), 7.72 (d, *J* = 8.2 Hz, 2H), 7.60 (d, *J* = 8.2 Hz, 2H), 7.42 – 7.36 (m, 2H), 4.65 – 4.59 (m, 2H), 4.54 – 4.48 (m, 2H), 3.27 (d, *J* = 10.2 Hz, 5H), 2.81 – 2.74 (m, 2H), 1.58 (t, *J* = 3.4 Hz, 4H).

^{13}C NMR (126 MHz, $CDCl_3$) δ 165.8, 158.2, 139.7, 139.0, 131.2, 131.0, 128.8, 128.7, 126.7, 125.5 (q, *J* = 3.9 Hz), 125.2 (q, *J* = 270.7 Hz), 72.4, 72.1, 63.8, 58.7, 29.7, 26.4, 23.2.

^{19}F NMR (470 MHz, $CDCl_3$) δ −62.8.

HRMS (ESI) Calculated $C_{22}H_{24}ClF_3NO_4^+$ $[M+H]^+$: 458.1340, Found 458.1371.

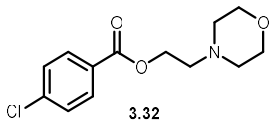

3.32

2-Morpholinoethyl 4-chlorobenzoate (3.32)

Ester **3.32** was prepared on a 0.15 mmol scale from p-chlorobenzoic acid and **3.52** at 110 °C via a modified General Procedure 3.1 where there was no aqueous work up. Instead, the reaction mixture was concentrated and loaded directly onto a silica gel column to give 31 mg (78%) of a yellow oil after purification with DCM, methanol, and triethylamine.

R_f = 0.38 in 94:5:1 DCM:MeOH:TEA

^{1}H NMR (499 MHz, $CDCl_3$) δ 7.96 (d, *J*=8.5 Hz, 2H), 7.42 (d, *J*=8.5 Hz, 2H), 4.46 (t, *J* = 5.8 Hz, 2H), 3.75 (t, *J*=4.6 Hz, 4H), 2.78 (t, *J* = 5.9 Hz, 2H), 2.58 (t, *J* = 4.7 Hz, 4H).

^{13}C NMR (126 MHz, $CDCl_3$) δ 165.7, 139.8, 131.2, 129.0, 128.6, 66.6, 62.2, 57.1, 53.8.

HRMS (ESI) Calculated $C_{13}H_{17}ClNO_3^+$ $[M+H]^+$: 270.0891, Found 270.0891.

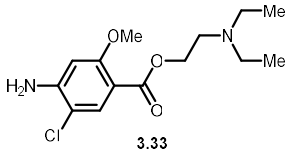

3.33

2-(Diethylamino)ethyl 4-amino-5-chloro-2-methoxybenzoate (3.33)

Ester **3.33** was prepared on 0.2 mmol scale from 4-amino-5-chloro-2-methoxy benzoic acid and **3.53** at 80 °C via a modified General Procedure 3.1 where there was no aqueous work up. Instead the reaction mixture was concentrated and loaded directly onto a silica gel column to give 26 mg (44%) of a yellow oil after purification with chloroform/methanol/triethylamine.

R_f: 0.33 in 94:5:1 $CHCl_3$:MeOH:TEA

^{1}H NMR (499 MHz, dmso) δ 7.59 (s, 1H), 6.44 (s, 1H), 6.13 (s, 2H), 4.14 (t, *J* = 5.9 Hz, 2H), 3.71 (s, 3H), 2.71 (s, 2H), 2.55 (s, 4H), 0.97 (t, *J* = 7.1 Hz, 6H).

^{13}C NMR (126 MHz, dmso) δ 163.6, 159.8, 149.9, 132.4, 107.8, 97.7, 67.0, 55.5, 50.7, 47.0, 45.7, 25.1.

HRMS (ESI) Calculated $C_{14}H_{22}ClN_2O_3^+$ $[M+H]^+$: 301.1313, Found 301.1304.

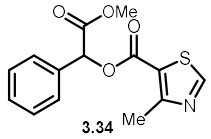

3.34

2-Methoxy-2-oxo-1-phenylethyl 4-methylthiazole-5-carboxylate (3.34)

Ester **3.34** was prepared on a 0.2 mmol scale from 4-methyl-thiazole-5-carboxylic acid and **3.49** at 80 °C via General Procedure 3.1 to give 12 mg (21) % of a white solid after purification with EtOAc/ hexanes.

Rf: 0.13 in 15:85 EtOAc:hexanes

^{1}H NMR (499 MHz, $CDCl_3$) δ 8.82 (s, 1H), 7.56 – 7.50 (m, 2H), 7.45 – 7.40 (m, 3H), 6.13 (s, 1H), 3.76 (s, 3H), 2.81 (s, 3H).

^{13}C NMR (126 MHz, $CDCl_3$) δ 169.1, 162.0, 161.4, 156.1, 133.6, 129.6, 129.1, 127.8, 121.4, 75.2, 53.0, 17.7.

HRMS (ESI) Calculated $C_{14}H_{14}NO_4S^+$ $[M+H]^+$: 292.0638, Found 292.0590.

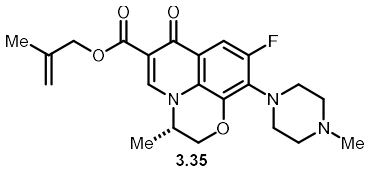

3.35

2-Methylallyl(*S*)-9-fluoro-3-methyl-10-(4-methylpiperazin-1-yl)-7-oxo-2,3-dihydro-7H-[1,4]oxazino[2,3,4-ij]quinoline-6-carboxylate (3.35)

Ester **3.35** was prepared on a 90 μmol scale from levofloxacin and **3.48** at 80 °C via a modified General Procedure 3.1. After completion of the reaction, one equivalent of KO^{t}Bu (10 mg) was added to the reaction mixture, and all solvent completely removed. The crude mixture was

partitioned between 1 mL of EtOAc and 1 mL of water. The aqueous layer was collected and purified by PrepLC on a Teledyne ISCO CombiFlash® EZ Prep (RediSep Prep C18, 100 Å, 5 μm, 150 mm × 20 mm (part no. 692203810), eluent: gradient from 10% MeCN/H_2O to 100% MeCN/H_2O (0 to 2.5 min 10% MeCN. 2.5 to 10 min ramp to 25% hold 5 min. Ramp to 100 % over 7 min. Hold for 3 min. Product came off at 7 min)). Solvent acetonitrile was removed *in vacuo* by a rotary evaporator and water was removed *in vacuo* through lyophilization to give 28 mg (76%) of desired ester.

^{1}H NMR (499 MHz, D_2O) δ 8.36 (s, 1H), 7.42 (d, *J* = 12.6 Hz, 1H), 5.69 – 5.65 (m, 1H), 5.49 – 5.46 (m, 1H), 4.66 – 4.61 (m, 1H), 4.57 – 4.51 (m, 1H), 4.44 (d, *J* = 11.5 Hz, 1H), 4.11 (s, 2H), 3.73 (t, *J* = 12.2 Hz, 4H), 3.59 (d, *J* = 9.7 Hz, 4H), 3.25 (s, 3H), 2.06 (s, 3H), 1.51 (d, *J* = 6.7 Hz, 3H).

^{13}C NMR (126 MHz, D_2O) δ 174.9, 172.3, 160.3, 156.5, 154.6, 144.1, 140.8 (d, *J* = 6.6 Hz), 132.6, 128.4 (d, *J* = 15.6 Hz), 127.7, 124.6, 123.8, 117.3, 103.4 (d, *J* = 23.8 Hz), 70.8, 68.4, 60.6, 54.6, 46.28, 44.0 (t, *J* = 3.5 Hz), 23.2, 17.1.

^{19}F NMR (470 MHz, D_2O) δ −122.9 (d, *J* = 12.5 Hz).

HRMS (ESI) Calculated $C_{22}H_{27}FN_3O_4^+$ $[M+H]^+$: 416.1980, Found 416.1974.

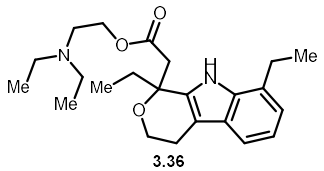

3.36

2-(Diethylamino)ethyl 2-(1,8-diethyl-1,3,4,9-tetrahydropyrano[3,4-b]indol-1-yl)acetate (3.36)

Ester **3.36** was prepared on a 0.1 mmol scale from etodolac and **3.53** at 80 °C via General Procedure 3.1 to give 24 mg (61%) of a white solid after purification with DCM/Methanol/triethylamine.

R_f = 0.30 in 5:94:1 MeOH:DCM:TEA

^{1}H NMR (499 MHz, $CDCl_3$) δ 9.09 (s, 1H), 7.36 (d, *J* = 7.7 Hz, 1H), 7.09 – 7.03 (m, 1H), 7.01 (d, *J* = 7.0 Hz, 1H), 4.26 – 4.12 (m, 2H), 4.09 – 4.01 (m, 1H), 3.94 (ddd, *J* = 11.1, 7.3, 4.1 Hz, 1H), 3.03 (d, *J* = 16.6 Hz, 1H), 2.95 (s, 1H), 2.89 (dt, *J* = 15.0, 6.9 Hz, 2H), 2.85 (d, *J* = 0.9 Hz, 1H), 2.79 – 2.72 (m, 1H), 2.68 (t, *J* = 6.7 Hz, 2H), 2.57 (q, *J* = 8.1, 7.7 Hz, 4H), 2.18 (dq, *J* = 14.8, 7.4 Hz, 1H), 2.02 (dq, *J* = 14.0, 7.3, 6.7 Hz, 1H), 1.37 (t, *J* = 8.1 Hz, 3H), 1.02 (t, *J* = 6.6 Hz, 6H), 0.88 – 0.81 (m, 3H).

^{13}C NMR (126 MHz, $CDCl_3$) δ 172.9, 136.1, 134.6, 126.8, 126.3, 120.5, 119.7, 116.1, 108.5, 74.8, 63.3, 60.8, 51.1, 47.8, 43.2, 30.8, 24.4, 22.6, 13.9, 12.0, 7.7.

HRMS (ESI) Calculated $C_{23}H_{35}N_2O_5^+$ $[M+H]^+$: 387.2642, Found 387.2652.

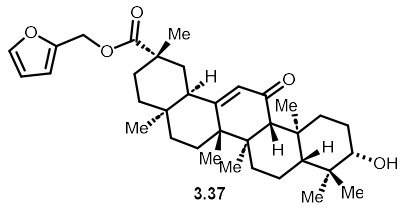

3.37

Furan-2-ylmethyl (2*S*,4a*S*,6a*S*,6b*R*,8a*R*,10*S*,12a*S*,12b*R*,14b*R*)-10-hydroxy-2,4a,6a,6b,9,9,12a-heptamethyl-13-oxo-1,2,3,4,4a,5,6,6a,6b,7,8,8a,9,10,11,12,12a,12b,13,14b-icosahydropicene-2-carboxylate (3.37)

Ester **3.37** was prepared on a 0.1 mmol scale from18β-Glycyrrhetinic acid and **3.54** at 60 °C via General Procedure 3.1 to give 32 mg (61%) of a white solid after purification with EtOAc/hexanes.

R_f = 0.25 in 25:75 EtOAc:hexanes

^{1}H NMR (499 MHz, $CDCl_3$) δ 7.44 (dd, J = 1.9, 0.8 Hz, 1H), 6.39 (dd, J = 3.3, 0.7 Hz, 1H), 6.35 (dd, J = 3.2, 1.9 Hz, 1H), 5.55 (s, 1H), 5.18 (d, J = 13.0 Hz, 1H), 4.99 (d, J = 13.0 Hz, 1H), 3.21 (dd, J = 11.1, 5.2 Hz, 1H), 2.77 (dt, J = 13.5, 3.6 Hz, 1H), 2.31 (s, 1H), 1.98 (ddd, J = 12.7, 4.3, 1.7 Hz, 3H), 1.89 (ddd, J = 13.6, 4.3, 2.7 Hz, 1H), 1.80 (td, J = 13.6, 4.7 Hz, 1H), 1.68 – 1.56 (m, 6H), 1.48 – 1.29 (m, 3H), 1.33 (s, 3H), 1.29 (d, J = 3.4 Hz, 1H), 1.29 – 1.21 (m, 2H), 1.20 – 1.14 (m, 1H), 1.13 (d, J = 2.2 Hz, 6H), 1.10 (s, 3H), 0.99 (s, 3H), 1.02 – 0.94 (m, 1H), 0.79 (s, 3H), 0.73 (s, 3H), 0.68 (dd, J = 11.8, 1.8 Hz, 1H).

^{13}C NMR (126 MHz, $CDCl_3$) δ 200.4, 176.1, 169.2, 149.8, 143.4, 128.6, 110.7, 110.6, 78.9, 61.9, 58.0, 55.1, 48.4, 45.5, 44.2, 43.3, 41.2, 39.3, 39.3, 37.7, 37.2, 32.9, 31.9, 31.7, 31.3, 28.6, 28.2, 28.2, 27.4, 26.6, 26.5, 23.4, 18.8, 17.6, 16.5, 15.7.

HRMS (ESI) Calculated $C_{35}H_{51}O_5^+$ $[M+H]^+$: 551.3731, Found 551.3723.

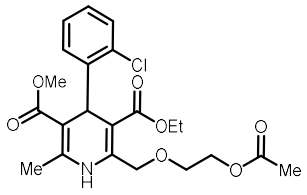

3.39

3-Ethyl-5-methyl 2-((2-acetoxyethoxy)methyl)-4-(2-chlorophenyl)-6-methyl-1,4-dihydropyridine-3,5-dicarboxylate (39)

Ester **3.39** was prepared on a 0.1 mmol scale from acetic acid and **3.38** at 110 °C via a modified General Procedure 3.1 where two equivalents of acid (12 mg, 11 μL) and two equivalents of base (26 mg, 35 μL) to give 32 mg (72 %) of a yellow oil after purification with EtOAc/hexanes.

R_f: 0.41 in 40:60 EtOAc:hexanes

^{1}H NMR (400 MHz, $CDCl_3$) δ 7.36 (dd, *J* = 7.8, 1.7 Hz, 1H), 7.22 (dd, *J* = 7.9, 1.4 Hz, 1H), 7.12 (ddd, *J* = 7.6, 6.5, 1.4 Hz, 2H), 7.03 (ddd, *J* = 7.9, 7.3, 1.7 Hz, 1H), 5.40 (s, 1H), 4.78 (dd, *J* = 16.1, 0.7 Hz, 1H), 4.74 – 4.66 (m, 1H), 4.34 (ddd, *J* = 12.2, 5.7, 3.5 Hz, 1H), 4.27 (ddd, *J* = 12.3, 5.3, 3.5 Hz, 1H), 4.05 (dd, *J* = 7.1, 3.0 Hz, 1H), 4.02 (dd, *J* = 7.1, 2.9 Hz, 1H), 3.82 – 3.72 (m, 2H), 3.60 (s, 3H), 2.35 (s, 3H), 2.11 (s, 3H), 1.17 (t, *J* = 7.1 Hz, 3H).

^{13}C NMR (101 MHz, $CDCl_3$) δ 171.1, 168.1, 167.2, 145.8, 145.1, 144.1, 132.4, 131.6, 129.3, 127.5, 127.0, 104.1, 101.6, 69.6, 68.2, 63.3, 59.9, 50.9, 37.2, 21.1, 19.6, 14.4.

HRMS (ESI) Calculated $C_{22}H_{27}ClNO_7^+$ $[M+H]^+$: 452.1471, Found 452.1418.

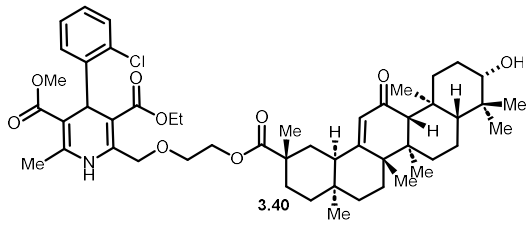

3-Ethyl-5-methyl 4-(2-chlorophenyl)-2-((2-(((2*S*,4a*S*,6a*S*,6b*R*,8a*R*,10*S*,12a*S*,12b*R*,14b*R*)-10-hydroxy-2,4a,6a,6b,9,9,12a-heptamethyl-13-oxo-1,2,3,4,4a,5,6,6a,6b,7,8,8a,9,10,11,12,12a,12b,13,14b-icosahydropicene-2-carbonyl)oxy)ethoxy)methyl)-6-methyl-1,4-dihydropyridine-3,5-dicarboxylate (3.40)

Ester **3.40** was prepared on a 0.1 mmol scale from 18β-Glycyrrhetinic acid and **3.38** at 110 °C via General Procedure 3.1 to give 46 mg (52 %) of a yellow oil after purification with EtOAc/hexanes.

R_f: 0.25 in 40:60 EtOAc:hexanes

^{1}H NMR (499 MHz, $CDCl_3$) δ 7.35 (ddd, *J* = 7.6, 5.7, 1.7 Hz, 1H), 7.21 (d, *J* = 7.8 Hz, 1H), 7.16 (d, *J* = 10.3 Hz, 1H), 7.10 (qd, *J* = 7.5, 1.4 Hz, 1H), 7.03 (tt, *J* = 7.5, 2.1 Hz, 1H), 5.66 (d, *J* = 5.0 Hz, 1H), 5.39 (d, *J* = 2.0 Hz, 1H), 4.77 (dd, *J* = 15.7, 2.1 Hz, 1H), 4.68 (dd, *J* = 15.7, 1.8 Hz, 1H), 4.48 – 4.39 (m, 1H), 4.32 (ddd, *J* = 12.1, 5.4, 3.1 Hz, 1H), 4.04 (ddtt, *J* = 8.7, 7.2, 4.9, 2.3 Hz, 2H), 3.78 (dtdd, *J* = 19.9, 11.1, 6.3, 3.3 Hz, 2H), 3.60 (s, 3H), 3.22 (dd, *J* = 11.0, 5.2 Hz, 1H), 2.79 (dd, *J* = 13.3, 2.2 Hz, 1H), 2.34 (d, *J* = 2.9 Hz, 4H), 2.11 (dd, *J* = 13.5, 4.1 Hz, 1H), 2.02 (ddt, *J* = 13.3, 7.2, 3.5 Hz, 2H), 1.94 (ddd, *J* = 13.6, 4.4, 2.2 Hz, 1H), 1.83 (td, *J* = 13.7, 4.6 Hz, 1H), 1.63 (qd, *J* = 16.2, 14.9, 7.8 Hz, 5H), 1.50 – 1.28 (m, 8H), 1.20 (d, *J* = 12.1 Hz, 1H), 1.20 – 1.14 (m, 6H), 1.17 – 1.11 (m, 7H), 1.07 – 1.00 (m, 1H), 1.00 (s, 3H), 0.96 (dd, *J* = 12.9, 4.4 Hz, 1H), 0.84 – 0.78 (m, 6H), 0.73 – 0.67 (d, *J* = 10.8 Hz, 1H).

^{13}C NMR (126 MHz, $CDCl_3$) δ 200.3, 176.7, 176.7, 169.3, 169.2, 168.2, 167.2, 145.9, 145.9, 144.9, 144.9, 144.3, 144.2, 132.5, 131.6, 129.4, 128.7, 127.5, 127.4, 127.0, 127.0, 104.0, 104.0, 101.8, 101.8, 78.9, 72.1, 70.7, 69.9, 69.8, 68.2, 68.2, 62.9, 62.8, 62.0, 59.9, 59.2, 55.1, 50.9, 48.6, 48.6, 45.5, 44.3, 43.4, 41.3, 39.3, 37.9, 37.3, 37.3, 37.3, 32.9, 32.0, 32.0, 31.4, 28.8, 28.7, 28.7, 28.5, 28.4, 28.2, 27.5, 26.6, 26.6, 26.6, 23.6, 19.6, 19.6, 18.8, 17.6, 16.5, 15.7, 14.4.

HRMS (ESI) Calculated $C_{50}H_{69}ClNO_9^+$ $[M+H]^+$: 862.4655, Found 862.4556.

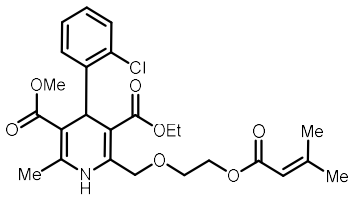

3.41

3-Ethyl-5-methyl 4-(2-chlorophenyl)-6-methyl-2-((2-((3-methylbut-2-enoyl)oxy)ethoxy)methyl)-1,4-dihydropyridine-3,5-dicarboxylate (41)

Ester **3.41** was prepared on a 0.15 mmol scale from 3-methylcrotonic acid and **3.38** at 110 °C via General Procedure 3.1 to give 48 mg (64 %) of a clear oil after purification with EtOAc/hexanes.

R_f: 0.62 in 40:60 EtOAc:hexanes

^{1}H NMR (499 MHz, $CDCl_3$) δ 7.38 (dd, *J* = 7.8, 1.7 Hz, 1H), 7.24 (dd, *J* = 8.0, 1.4 Hz, 1H), 7.18 (s, 1H), 7.14 (td, *J* = 7.5, 1.4 Hz, 1H), 7.05 (td, *J* = 7.6, 1.7 Hz, 1H), 5.74 (p, *J* = 1.4 Hz, 1H), 5.41 (s, 1H), 4.79 (d, *J* = 16.1 Hz, 1H), 4.72 (d, *J* = 16.2 Hz, 1H), 4.36 (dd, *J* = 5.8, 3.5 Hz, 1H), 4.33 (dd, *J* = 5.5, 3.4 Hz, 1H), 4.05 (tq, *J* = 7.1, 3.7 Hz, 2H), 3.79 (ddd, *J* = 5.8, 3.4, 2.3 Hz, 2H), 3.62 (s, 3H), 2.35 (s, 3H), 2.20 (d, *J* = 1.3 Hz, 3H), 1.93 (s, 3H), 1.19 (t, *J* = 7.1 Hz, 3H).

^{13}C NMR (126 MHz, $CDCl_3$) δ 168.2, 167.3, 166.6, 158.2, 145.9, 145.3, 144.2, 132.5, 131.6, 129.4, 127.5, 127.0, 115.6, 104.1, 101.6, 70.0, 68.3, 62.3, 59.9, 50.9, 37.3, 27.6, 20.4, 19.5, 14.4.

HRMS (ESI) Calculated $C_{25}H_{31}ClNO_7^+$ $[M+H]^+$: 492.1784, Found 492.1714.

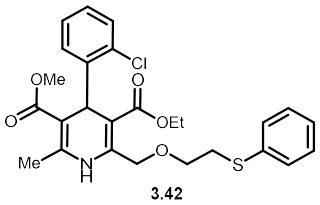

3.42

3-Ethyl-5-methyl 4-(2-chlorophenyl)-6-methyl-2-((2-(phenylthio)ethoxy)methyl)-1,4-dihydropyridine-3,5-dicarboxylate (3.42)

Compound **42** was prepared from thiophenol and **38** on a 0.15 mmol scale at 110 °C via General Procedure 3.1 to give 66 mg (88 %) of a clear oil after purification with EtOAc/hexanes.

^{1}H NMR (499 MHz, $CDCl_3$) δ 7.43 – 7.38 (m, 2H), 7.37 – 7.29 (m, 4H), 7.29 – 7.22 (m, 2H), 7.11 (td, *J* = 7.5, 1.4 Hz, 1H), 7.05 (dd, *J* = 7.7, 1.8 Hz, 1H), 5.41 (s, 1H), 4.78 (d, *J* = 16.2 Hz, 1H), 4.72 (d, *J* = 16.3 Hz, 1H), 4.09 – 4.01 (m, 2H), 3.78 (t, *J* = 5.9 Hz, 2H), 3.62 (s, 3H), 3.21 (td, *J* = 5.9, 2.0 Hz, 2H), 2.32 (s, 3H), 1.19 (t, *J* = 7.1 Hz, 3H).

^{13}C NMR (126 MHz, $CDCl_3$) δ 168.1, 167.3, 145.9, 145.4, 144.2, 135.6, 132.5, 131.6, 129.7, 129.4, 129.3, 127.4, 127.0, 126.8, 104.0, 101.6, 70.0, 68.0, 59.9, 50.9, 37.4, 34.2, 19.7, 19.5, 14.4.

HRMS (ESI) Calculated $C_{26}H_{29}ClNO_5S^+$ $[M+H]^+$: 502.1449, Found 502.1386.

3.3 An amine–acid reductive etherification reaction.[7]

3.3.1 Introduction

Carbon–oxygen bonds are among the most ubiquitous bonds in organic chemistry and provide a natural retrosynthetic disconnection strategy.[33] Ethers are a representative class of compounds with these bonds that stand out due to their stability. They are well represented in pharmaceuticals,[34,35] fuels,[36] and materials (Figure 3.11, B).[37] Classical methods to synthesize ethers, such as the Williamson ether synthesis,[38] are powerful, but the strongly basic conditions and poor availability of the requisite alkyl halides limit their use in complex settings. Acid catalyzed hydroalkoxylation of alkenes overcomes some of these challenges but depends on harsh acidic conditions. As a result, several other methods for preparing ethers have been proposed to address these shortcomings. These include reductive etherification from alcohols and ketones or aldehydes,[39,40] as well as the reduction of esters to their corresponding ethers using metal/reductant combinations[37,41–45]. Sakai *et al*. have reported a powerful extension of this transformation that allows for a one-pot ether synthesis from alcohols and carboxylic acids.[46,47] By coupling two building blocks together the chemical space accessible from this transformation vastly increases. Deaminative etherification reactions have been reported, but rely on activated

[7] DFT calculations in this study were performed by Eunjae Shim. Dr. Sandip Das performed most of the substrate scope, and as such the bulk of the scope is not included here. This manuscript is currently being prepared for publication.

amines and require isolation of the activated substrate as its pyridinium or trimethylammonium salt.[21,30,48]

Our lab is interested in repurposing amine and carboxylic acid building blocks to provide alternatives to the venerable amide coupling.[5] We recently disclosed an automatable deaminative esterification reaction. This strategy allows for an orthogonal functionalization handle, access to a complementary set of building blocks as compared to the fisher esterification, and can proceed without isolation of the intermediate pyridinium salt required for amine activation.[49] We believed this method could be extended via an *in-situ* reduction of the intermediate ester to synthesize ethers from amine and acid building blocks (Figure 3.11, A). This method would have to be capable of performing in the presence of stoichiometric Lewis basic triphenylpyridine that is generated in the reaction. Previous studies in our lab using a remote access automation platform (Figure 3.12) had discovered this reaction could be promoted by platinum, but we were unable to optimize these conditions (see Experimental).

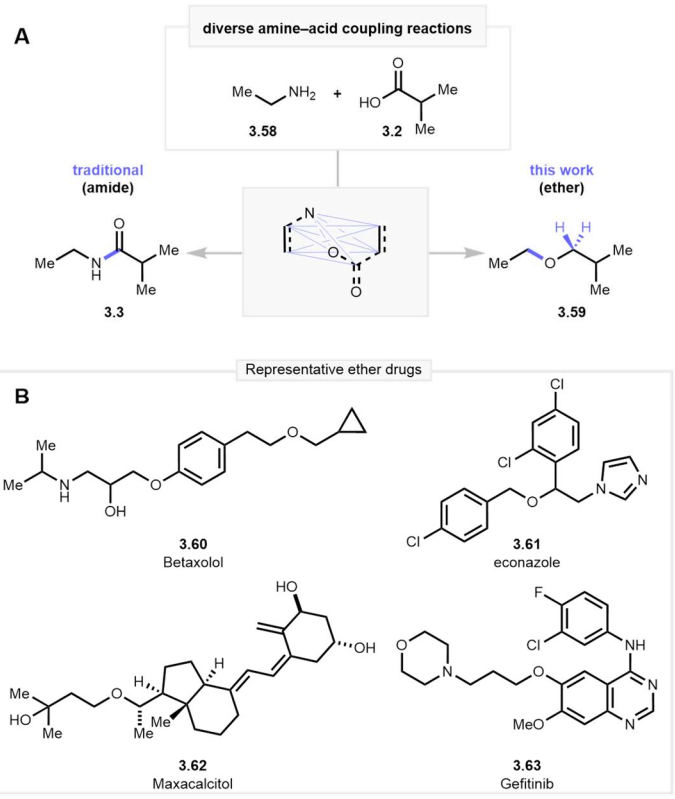

Figure 3.11 A) A deaminative etherification reaction as an alternative to the amide coupling. B) Alkyl ether containing drugs.

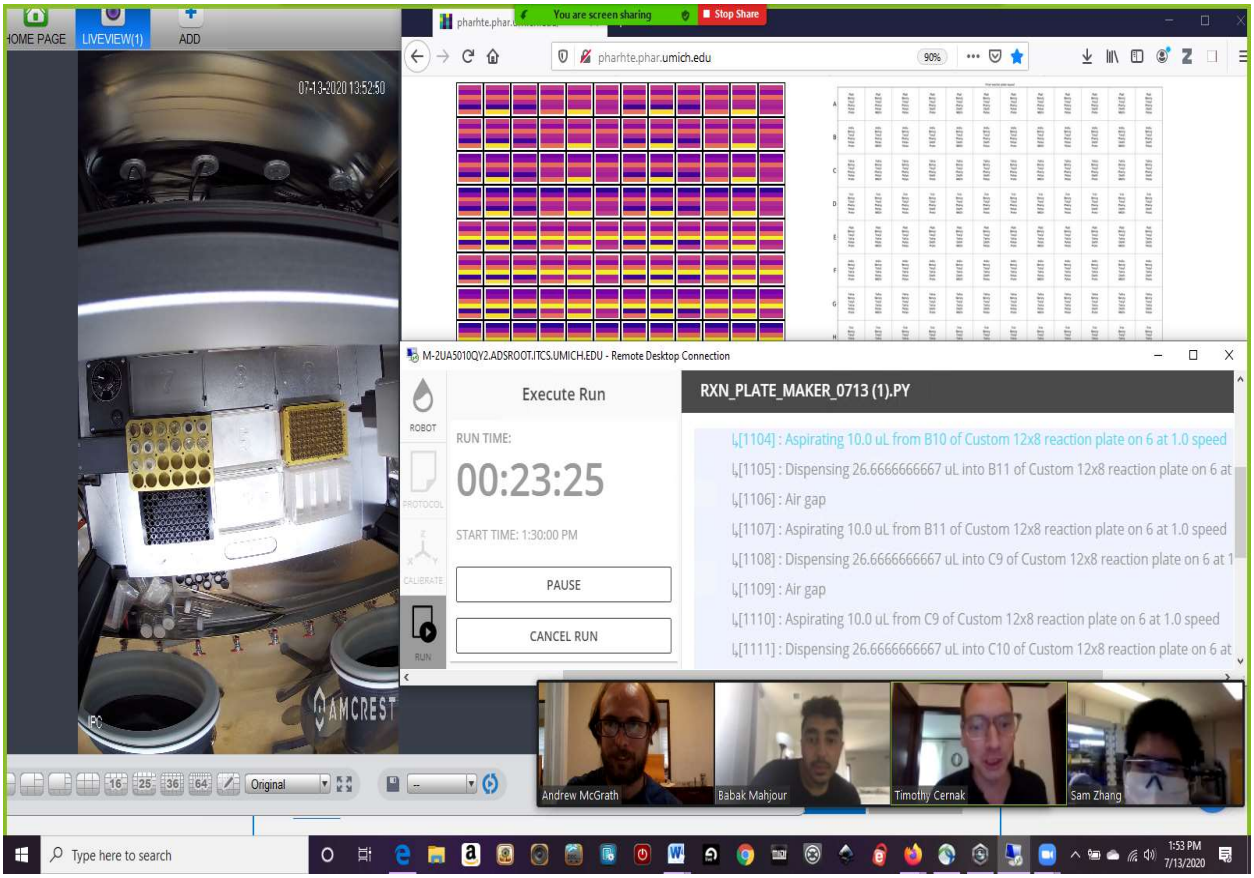

Figure 3.12 Remote access platform on the Opentrons robot for reaction optimization.

3.3.2 Reductive etherification reaction optimization

To accomplish this goal, we embarked on a high throughput experimentation (HTE) optimization campaign. We selected acid **3.64** and amine **3.65** as our model system. Experimentally, the crude ester reaction from could serve as a stock solution to dose into a mixture of the other reagents to give a two-step, one pot protocol. We began our investigation with a 6 by 4 reaction array using oxophilic metals such as gallium[37], iron,[42] indium,[50] or aluminum, either alone or in combination with boron-based Lewis acids such as trispentafluorophenyl borane (**3.68**), or triphenylborane (Ph_3B), and using either **3.69**, or 1,1,3,3-tetramethyldisiloxane (TMDS), as a terminal reductant (Figure 3.13, B, Entry 1). An initial reaction array using 0.5 equivalents of each metal did not produce desired ether **3.67**, in any well

and instead yielded unreacted ester **3.70**, presumably due to poisoning of the Lewis acids by triphenylpyridine. The same array was repeated using 3 equivalents of each metal, which yielded desired ether in 7 of 24 wells. $GaBr_3$ with or without the use of a cocatalyst consistently delivered desired product. Additionally, $AlCl_3$ was able to deliver **3.67**, but only using **3.68** as a cocatalyst. In our hands, neither $InBr_3$ nor $Fe_3(CO)_{12}$ furnished the desired product and instead yielded mostly unreacted ester. We used these results to plan our next 12 by 8 reaction array. We investigated the chloride, bromide, and iodide salt of both Ga and Al, as well as three boron Lewis acids and a blank, and four silane reductants. From this array, the combination of GaI_3, Ph_3B, and **3.69** emerged as the highest yielding conditions, furnishing **3.67** in 36% assay yield (Figure 3.13, B, Entry 2). Further exploration of other boranes, Gallium sources, and solvents failed to provide a significant increase in yield (See Experimental). We then turned our attention towards additives which have been shown to have a beneficial effect in ester reductions.[51,52] We investigated the use of Lewis and Bronsted acidic additives as well as borate salts[53] in order to improve yield and reduce the equivalents of Gallium. An array of six additives, two boranes, and two equivalencies of Gallium (0.5 or 3) revealed trimethylsilyl chloride as a key additive to increase yield (Figure 3.13, B, Entry 3), though it was unable to reduce the required amount of gallium. Gallium is known to interact with trimethylsilyl chloride to generate a silylium cation to activate carbonyls.[54] With this new data one final six by four array was performed examining various silyl halides and their interplay with borane Lewis acid additives (Figure 3.13, B, Entry 4). This array revealed **3.72** to be the highest yielding silyl halide, with optimal performance when used with either **3.68** or **3.671**, furnishing **3.67** in 71% assay yield (63% isolated). Further studies revealed diphenylsilane produced a difficult to remove byproduct and was sensitive to peroxides present in the solvent (see Experimental). Switching to phenylsilane resolved these

issues while maintaining yield. As such we moved forward with GaI_3, **3.68**, **3.72**, and phenylsilane as our optimized conditions.

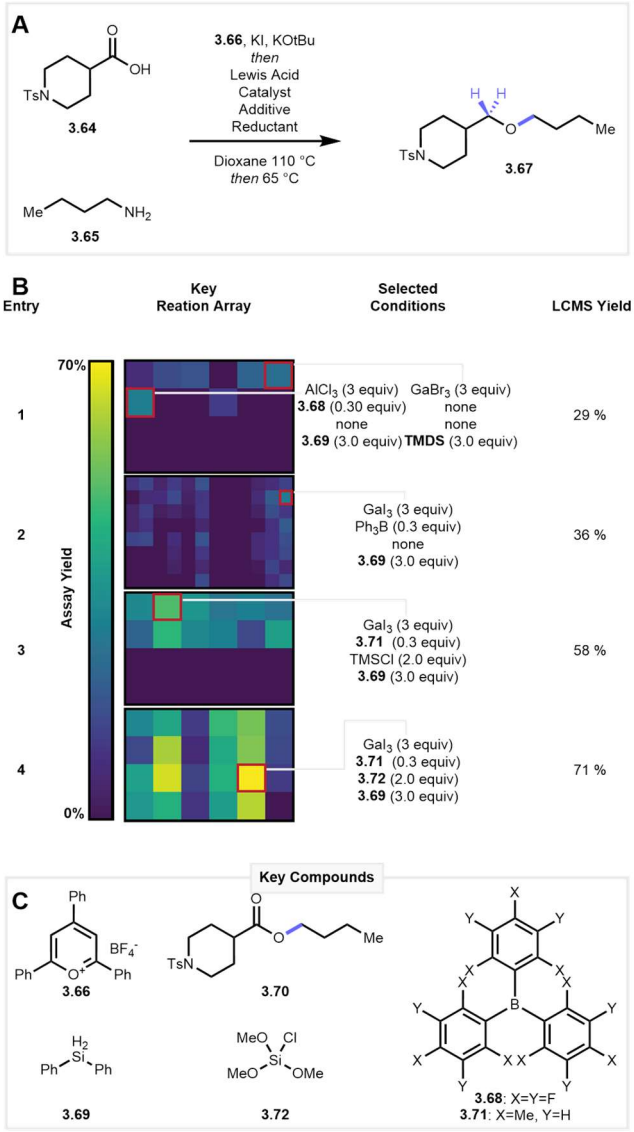

Figure 3.13 A HTE campaign for etherification optimization. A) The model substrates chosen to optimize with. B) results of key HTE arrays for reaction optimization. C) Key compounds used in optimization.

3.3.3 Substrate scope exploration of the reductive etherification reaction

With our optimized conditions in hand, we began exploring the scope of the reaction. Other amines participated in the reaction (**3.73**–**82**). The reaction proceeds in the presence of basic amines (**3.77**), tolerates aryl halides (**3.74**) and heterocycles (**3.74**), can be applied on

secondary amines (**3.79**), and works intramolecularly (**3.78**). When using purified ester, the Gallium loading can be lowered to 0.50 equivalents, suggesting that components of the esterification reaction do poison the catalyst. Notably selective reduction over amides can be achieved using this method (**3.80**, **3.81**) but it requires purification of the intermediate ester. Given the prevalence of deuterium in pharmaceuticals,[55] we pondered whether we could incorporate deuterium into the metabolically labile alpha hetero C–H bond by changing the reductant to $PhSiD_3$. This strategy successfully produced deuterated ether **3.82** 55% yield with full deuterium incorporation by NMR.

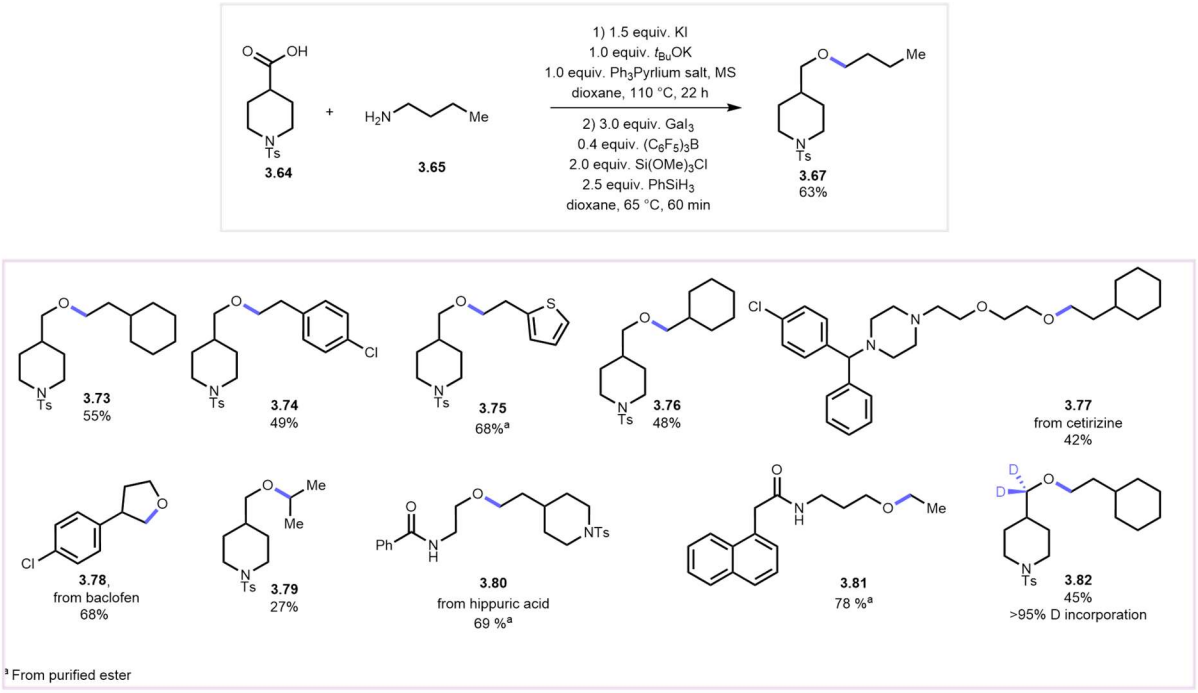

Figure 3.14 Partial Status of the Substrate Scope.

3.3.4 Mechanistic investigations of the reductive etherification

Intrigued by the unprecedented reduction selectivity of esters over amides as observed in **3.80** and **3.81**, we investigated the role of each reagent and order of addition from purified ester

3.83. We confirmed that gallium, **3.68**, and **3.72** were all essential to achieve the desired selectivity and reactivity. When **3.72** was excluded, there was a significant loss in selectivity suggesting that it is involved in ester activation (Table 3.4, Entry 2). When GaI_3 was excluded, selectivity was retained, but conversion dropped sharply, indicating that it helps to mediate the reduction (Entry 3). In contrast, when **3.68** was excluded, there was a reversal in selectivity and a drop in conversion (Entry 4). This suggests **3.68** acts synergistically with gallium to mediate the reduction, but also plays a role in selectivity. This is further exemplified by entries 5 and 6 that demonstrate neither gallium nor **3.68** are able to meaningfully mediate the reduction on their own. Entry 7 confirms **3.72** is inert in the reaction without an activator. Intriguingly two additional equivalents of gallium can replace **3.72** while retaining selectivity (Entry 8), suggesting gallium may play a dual role once a certain threshold is reached.

Table 3.4 Order of addition and reagent necessity studies for the selective reduction of esters in the presence of amides. P/IS = Product/Internal standard values determined by UPLC-MS using caffeine as an internal standard.

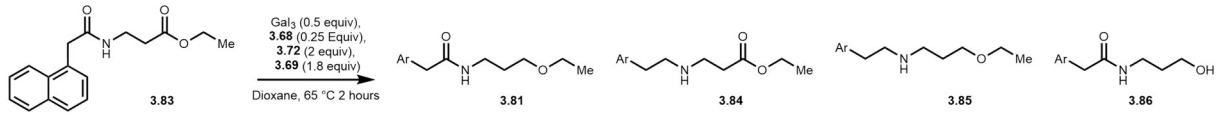

Entry	Order of addition	Reagent Excluded	Additional Additive	P/IS **3.81**	P/IS **3.84**	**3.85**	**3.86**	RSM
1	Ga,**3.68**,**3.72** then **3.69**	None		1.89	0	0.38	0.18	0
2	Ga,**3.68** then **3.69**	**3.72**		1.21	0.91	0.29	1.18	0.10
3	**3.68**, **3.72** then **3.69**	GaI_3		0.48	0.0	0.0	0.34	1.31
4	Ga, **3.72** then **3.69**	**3.68**		0	0.78	0.0	0.0	2.99
5	Ga,then **3.69**	**3.68**, **3.72**		trace	trace	0	0	2.95
6	**3.68** then **3.69**	GaI_3, **3.72**		trace	0.0	0.0	0	2.93
7	**3.72** then **3.69**	GaI_3, **3.68**		0	0.00	0.0	0.0	2.99
8	Ga, **3.72** then **3.69**	**3.72**	$GaCl_3$ (2 equiv)	1.82	0	0	0.04	0
9	Fe, **3.68**, **3.72** then **3.69**	GaI_3	$FeCl_3$ (0.5 equiv)	0.65	0.15	0.08	0.04	1.50

3.68 = $B(C_6F_5)_3$ **3.69 =** Ph_2SiH_2 **3.72 =** $Si(OMe)_3Cl$

Further evidence for each reagent role was provided by NMR studies. Carbon NMR revealed that Gallium shifts both carbonyl carbons downfield (Spectrum 3.71). **3.68** interacted with the amide carbonyl when alone with the substrate (spectrum 3.72), and silyl chloride **3.72**

did not interact with either carbonyl alone (see Experimental). When GaI_3, **3.68**, and **3.72** were mixed there was a dramatic shift of the ester carbonyl and a shift in the amide carbonyl suggesting the ester carbonyl is activated to a greater extent (Spectrum 3.73). **3.68** is also no longer bound to any Lewis basic site (see Experimental).

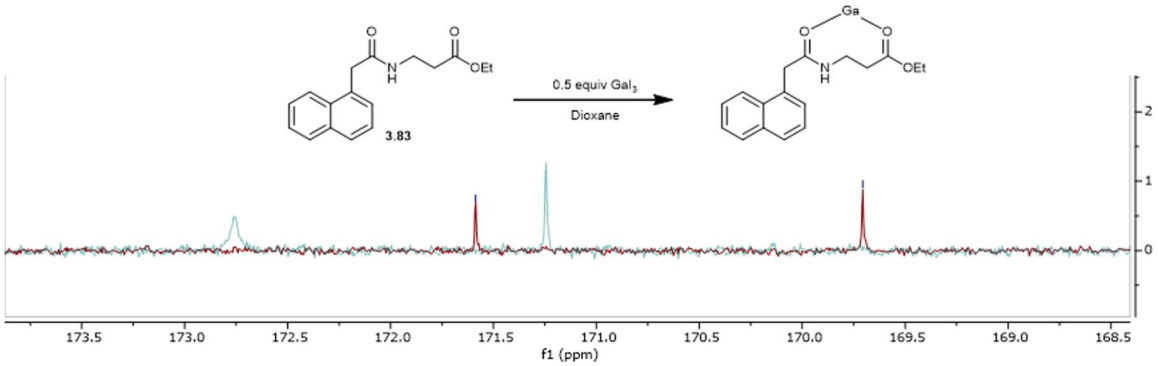

Spectrum 3.1 ^{13}C NMR of carbonyl region of **3.83** (dark/red) and **3.83** plus 0.5 equivalents of GaI_3(light/blue) in dioxane. Note both carbonyls shift. The more downfield carbon is the ester carbon (See Experimental)

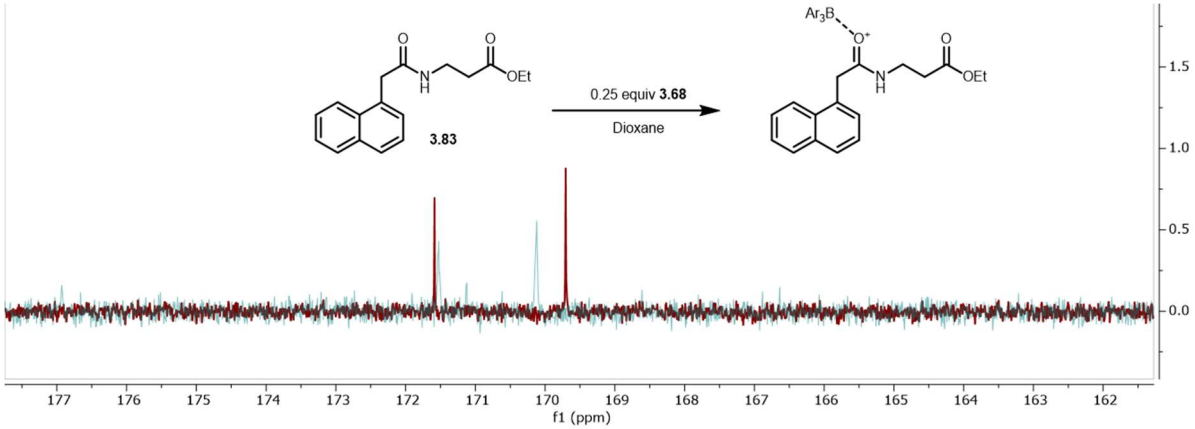

Spectrum 3.2 ^{13}C NMR of carbonyl region of **3.83** (dark/red) and **3.83** plus 0.5 equivalents of GaI_3(light/blue) in dioxane. Note the amide carbonyl shift. The more downfield carbon is the ester carbon (See Experimental)

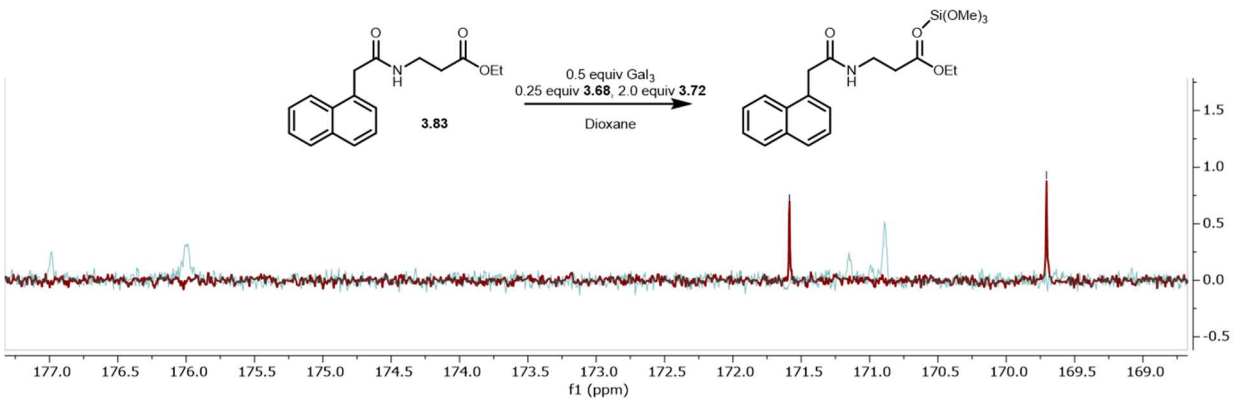

Spectrum 3.3 ^{13}C NMR of carbonyl region of **3.83** (dark/red) and **3.83** plus 0.5 equivalents of GaI_3(light/blue) in dioxane. Note the shift of both carbonyls, but the ester shifts 4.5 ppm compared to 1.5 ppm for the amide. The more downfield carbon is the ester carbon (See Experimental)

A GC-MS analysis of the reaction headspace revealed both iodomethane and chloromethane were present. Presumably these are derived **3.72**, suggesting it is involved in Gallium turnover. Based upon previous reports[54,56] we hypothesized gallium is abstracting the chloride from **3.72** to generate silylium cation **3.87** which binds to and activates both carbonyls. **3.68** then abstracts a hydride from **3.69** and can deliver a hydride to the activated ester carbonyl. This generates a silyl acetal intermediate which is further activated by gallium to lose a siloxane and generate an oxocarbenium intermediate which is once again reduced by **3.68** hydride (Scheme 3.2). To provide evidence for this mechanism, we investigated the use of $FeCl_3$ instead of GaI_3 which is also known to abstract halides from silyl chlorides. Albeit reduced, we did observe similar selectivity and reactivity to our gallium catalyzed reaction (Table 3.4, Entry 9). DFT calculations provide further evidence for this mechanism and show that any combination of silane activation and hydride delivery favors ester reduction over amide reduction with activation by **3.87** being barrierless. Among Lewis acids, gallium seems privileged in its selective activation as demonstrated by examination of 16 Lewis acids only giving gallium as a selective activator, though platinum can reduce esters if not amides are present (see Experimental).

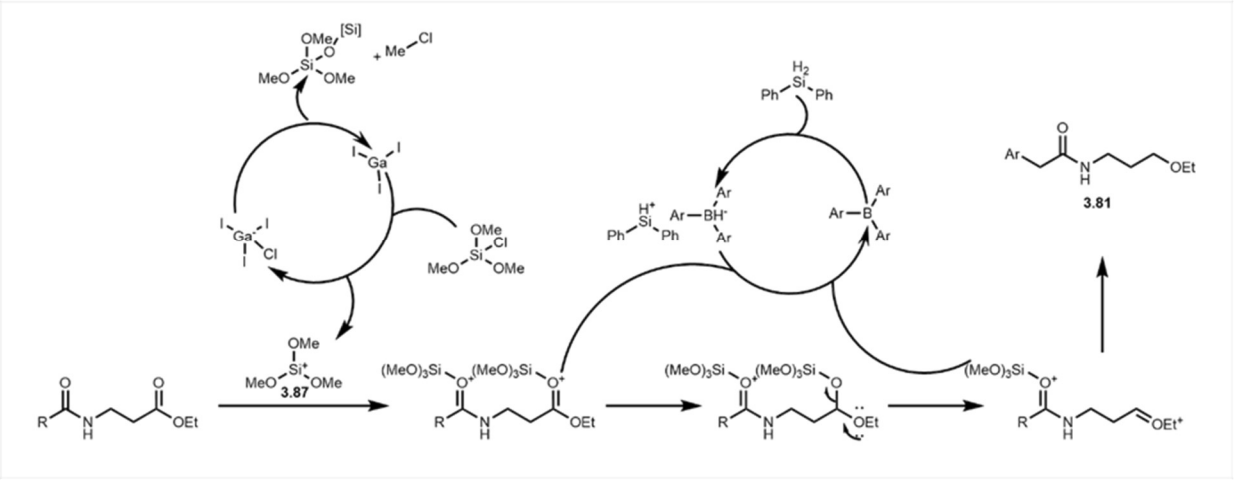

Scheme 3.2. Proposed mechanism for the selective ester reduction.

3.3.5 An amine–phenol etherification

To expand on the initial scope of the reaction reported by Katritzky,[21,30] we became interested in developing a sp^2–sp^3 etherification using phenols instead of carboxylic acids. We investigated using phenol **3.88** in combination with Lipitor intermediate **3.89** and found through modification of the esterification protocol (see Experimental), we could isolate ether **3.90** in 62% yield in a two-step one pot protocol. This method was used to alkylate ivacaftor to give **3.91** in 40% yield. We also used it to forge a bond between lysine and tyrosine (**3.92**) that is an alternative to the classic peptide bond. Finally, we applied our method to an amine targeting the E3 ligase Von-Hippel Lindau (VHL)[57] and estradiol to highlight the utility of this strategy in synthesizing proteolysis targeting chimeras (PROTACs) to give **3.93** in 25% yield.

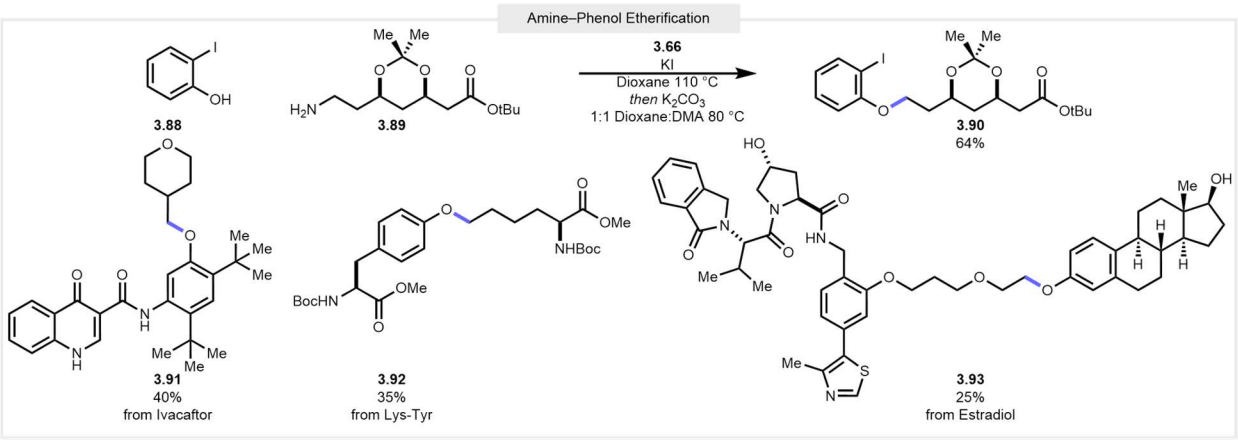

Figure 3.15 The scope of the amine–phenol deaminative etherification.

3.3.6 A deaminative halogenation reaction

We next investigated the mechanism by which the ester is formed. Based on other reports on pyridinium salts we hypothesized it may be a radical mechanism, however experiments involving the use of TEMPO failed to inhibit product formation (see Experimental). Next, we left the carboxylic acid out of the reaction, and were able to isolate the alkyl iodide of **3.88**. By switching the halide salt, we were able to isolate the corresponding bromide and chloride of **3.88**. We applied this method to four other amines and isolated various halogens of each of them. This provides an alternative method for synthesizing alkyl halides from amines.[58]

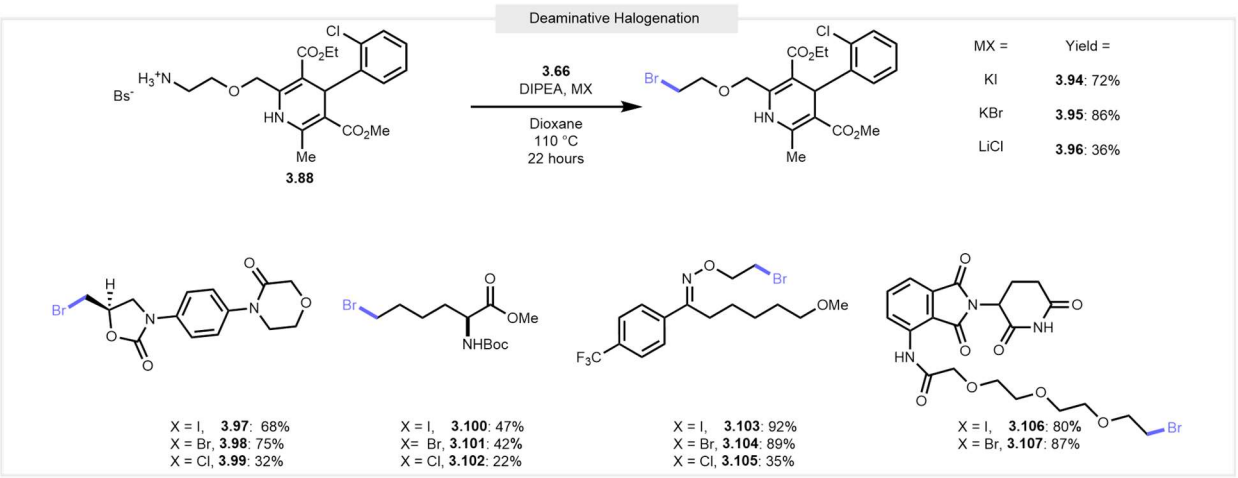

Figure 3.16 The scope of the deaminative halogenation. The bromide is shown for clarity. When KI is used, the iodide is obtained, when KBr is used, the bromide is obtained, and when LiCl is used the chloride is obtained.

3.3.7 Conclusions

In summary we have developed a methodology to synthesize ethers directly from amines and acids. The reaction is selective for esters in the presence of amides and appears to proceed via gallium catalyzed activation of a silyl chloride and a boron mediated hydride reduction. The deamination strategy can be applied to other nucleophiles in order to synthesize phenolic ethers as well as various halogen products.

3.4 Experimental section for the reductive etherification reaction

See Sections 3.2.1 and 3.2.2 for a general methods summary. For the esterification procedure see section 3.3.

3.4.1 General Procedures

3.4.1.1 General Procedure 3.4: amine–acid reductive etherification

In a nitrogen filled glovebox, a dry two-dram vial (vial **1**) equipped with a stir bar was charged with potassium iodide (1.5 equiv), triphenylpyrylium tetrafluoro borate (**3.66**) (1.0 equiv), powdered 4 Å mol sieves (500 mg/ mmol amine), potassium *tert*-butoxide (1.0 equiv, 2.0

equiv for amine salts), the carboxylic acid (if solid) and the amine (if solid) (1.0 equiv). 1,4-dioxane (3.33 mL/ mmol amine) was added. If either the amine or the acid was a liquid, they were added to the reaction after the addition of solvent. After all reagents were added, the vial was capped, removed from the glovebox, and stirred at 500 rpm at 110 °C for 22 hours for amines on a primary carbon (80 °C for amines on a secondary carbon). Upon completion, the reaction vial was cooled to room temperature and returned to the glovebox along with two additional flame dried vials. Dioxane was added (1.67 mL/mmol amine) to vial **1**. Gallium (III) iodide (GaI_3) (3.0 equiv) was weighed into a second vial (vial **2**) and dioxane (2.50 mL/mmol amine) added. Tris-(pentafluorophenyl)borane (BCF, **3.68**) (0.40 equiv) was weighed into a third vial (vial **3**) and dioxane (2.50 mL/mmol amine) added. Vials **2** and **3** were capped and vortexed until each reagent had fully dissolved. Vial **2** was added to vial **1** without stirring followed by vial **3**. Trimethoxychlorosilane (**3.72**) (2.0 equiv) was added to vial **1** followed by phenylsilane (2.5 equiv) (**Caution: this will generate a lot of heat and effervescence of hydrogen and methylchloride which are flammable. We encountered no issues up to a 0.35 mmol scale, but there may be hazards at larger scales**). Upon addition of the silane, the vial was capped, and removed from the glovebox. The reaction was stirred at 500 rpm at 65 °C for 90 minutes. Upon cooling to room temperature, the vial was uncapped (**Caution: pressure may have built up in the vial which can cause solvent to overflow**), diluted with (EtOAc) (25 mL/mmol) partitioned between additional EtOAc (100 mL/mmol) and saturated aqueous sodium bicarbonate (100 mL/mmol). The aqueous layer was extracted twice more with EtOAc (100 mL/mmol). The organic layers were combined, dried over sodium sulfate and the solvent removed *in vacuo*. Purification was achieved as described.

3.4.1.2 General Procedure 3.5: Reduction of purified esters to ethers

Three dried two-dram vials were brought into the glovebox. Vial **1** was equipped with a stir bar and had ester (1.0 equiv) added. Dioxane was added (3.33 mL/mmol ester) to vial **1**. GaI_3 (0.5 equiv) was weighed into a second vial (vial **2**) and dioxane (3.33 mL/mmol ester) added. Tris-(pentafluorophenyl)borane or trimesityl borane (0.25 equiv) was weighed into a third vial (vial **3**) and dioxane (3.33 mL/mmol ester) added. Vials **2** and **3** were capped and vortexed until each reagent had fully dissolved. Vial **2** was added to vial **1** without stirring followed by vial **3**. Trimethoxychlorosilane (2.0 equiv) was added to vial **1** followed by diphenylsilane (1.5 equiv) (**Caution: this will generate heat and effervescence of hydrogen and methylchloride which are flammable.**). Upon addition of the silane, the vial was capped, and removed from the glovebox. The reaction was stirred at 500 rpm at 65 °C for 90 minutes. Upon cooling to room temperature, the vial was uncapped (**Caution: pressure may have built up in the vial which can cause solvent to overflow**), diluted with (EtOAc) (25 mL/mmol) partitioned between additional EtOAc (100 mL/mmol) and saturated aqueous sodium bicarbonate (100 mL/mmol). The aqueous layer was extracted twice more with EtOAc (100 mL/mmol). The organic layers were combined, dried over sodium sulfate and the solvent removed *in vacuo*. Purification was achieved as described.

3.4.1.3 General Procedure 3.6: Platinum catalyzed ether synthesis from pyridinium salts and carboxylic acids

An oven dried two-dram vial was equipped with a stir bar and had pyridinium salt (1.0 equiv) added. KI (1.0 equiv) was then added followed by the carboxylic acid (1.0 equiv), and proton sponge (1.0 equiv) The vial was then capped with a septa cap and evacuated/backfilled with nitrogen 3 times. Chlorobenzene (3.33 mL/ mmol acid) was added via syringe followed by

phenylsilane (3.0 equiv). The vial was transferred to a hotplate, stirred at 500 rpm at 80 °C for benzylic pyridiniums or 110 °C for primary pyridiniums for 22 hours. Upon cooling to room temperature, the vial was brought into the glovebox and platinum (II) chloride (2.5 mol%) was added followed by phenylsilane (3.0 equiv). The vial was removed from the glovebox and stirred at 500 rpm at 80 °C for two hours. Upon completion the reaction was diluted with (EtOAc) (25 mL/mmol) partitioned between additional EtOAc (100 mL/mmol) and saturated aqueous sodium bicarbonate (100 mL/mmol). The aqueous layer was extracted twice more with EtOAc (100 mL/mmol). The organic layers were combined, dried over sodium sulfate and the solvent removed *in vacuo*. Purification was achieved as described.

3.4.1.4 General Procedure 3.7: Preparation of ethers from phenols and amines

An oven dried two-dram vial was equipped with a stir bar and had **3.66** (1.0 equiv) added. KI (1.5 equiv) was then added followed by the amine (1.0 equiv) if it was solid and potassium *tert*-butoxide (1.0 equiv) if the amine was a salt. The vial was then capped with a septa cap and evacuated/backfilled with nitrogen 3 times. Dioxane (3.33 mL/ mmol amine) was added via syringe. If the amine was a liquid, it was also added via syringe at this point. The vial was transferred to a hotplate, stirred at 500 rpm at 110 °C for 22 hours. The reaction was cooled to room temperature and transferred via syringe to a vial containing the desired phenol (1.0 equiv), potassium carbonate (3.0 equiv), and DMA (3.33 mL/mmol amine). This was stirred at 500 rpm at 80 °C for 4 hours. upon completion, the reaction was diluted with ethyl acetate (EtOAc) (25 mL/mmol) partitioned between additional EtOAc (100 mL/mmol) and saturated aqueous sulfate (100 mL/mmol). The aqueous layer was extracted twice more with EtOAc (100

mL/mmol). The organic layers were combined, dried over sodium sulfate and the solvent removed *in vacuo.* Purification was achieved as described.

3.4.1.5 General Procedure 3.8: Preparation of alkyl halides from amines

An oven dried two-dram vial was equipped with a stir bar and had **3.66** (1.0 equiv) added. The appropriate metal halide salt (KI, potassium bromide, or lithium chloride) (3.0 equiv) was then added followed by the amine (1.0 equiv) if it was solid and potassium *tert*-butoxide (1.0 equiv) if the amine was a salt. The vial was then capped with a septa cap and evacuated/backfilled with nitrogen 3 times. Dioxane (3.33 mL/ mmol amine) or DMA (10.0 mL/mmol amine) was added via syringe. If the amine was a liquid, it was also added via syringe at this point. The vial was transferred to a hotplate, stirred at 500 rpm at 110 °C for 22 hours. For reactions in dioxane upon completion, the reaction was diluted with ethyl acetate (EtOAc) (25 mL/mmol) and filtered through a pad of celite. The solvent was removed *in vacuo*. For reactions in DMA, upon completion, the reaction was diluted with ethyl acetate (EtOAc) (25 mL/mmol) partitioned between additional EtOAc (100 mL/mmol) and saturated aqueous sulfate (100 mL/mmol). The aqueous layer was extracted twice more with EtOAc (100 mL/mmol). The organic layers were combined, dried over sodium sulfate and the solvent removed *in vacuo.* Purification was achieved as described.

3.4.1.6 General Procedure 3.9: Procedure for HTE reaction optimization

Stock solutions, or suspensions, were prepared as shown in the heatmap preparation table. Apart from the ester stock solution, which was prepared according to General Procedure **3.3** (no work-up), in an inert atmosphere glovebox, all were weighed and dissolved or suspended in anhydrous solvent to achieve their listed concentrations in table. Stock solutions of reagents were stirred until either a clear solution or a uniform slurry was achieved. A 24 or 96-well

aluminum microvial (Analytical Sales & Services cat. no. 25243) was equipped with oven-dried shell vials (Analytical Sales & Services cat. no. 884001). A parylene-coated stir dowel (Analytical Sales & Services cat. no. 13258) was then added to each vial, and the apparatus moved into the glovebox. Stock solutions were dosed to the appropriate shell vials according to the plate map shown in table using single channel micropipetters. The microvial plate was sealed, removed from the glove box, and stirred on a hot plate with heating at the indicated temperature for planned reaction time. The reactions were quenched by opening the reaction block and adding 400 μL of a 7 mg/mL caffeine in methanol solution as an internal standard. Reactions were then stirred for 5 minutes at room temperature and 1000 rpm. Using six channels of an eight channel micropipetter, from each reaction, a 50 μL aliquot of the quenched reaction mixture was added into a 96-well polypropylene collection plate (Analytical Sales & Services cat. no. 17P687). The solvent was evaporated by blowing nitrogen down on the analytical plate. Acetonitrile (600 μL) was added and mixed by pipetting up and down. The reactions were then analyzed by UPLCMS. The Product/Internal Standard value was produced by measuring the UV absorbance of desired product relative to the caffeine internal standard.

3.4.2 Preparation of starting materials

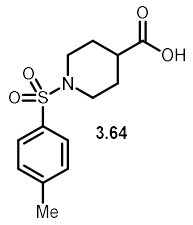

3.64

1-tosylpiperidine-4-carboxylic acid (**3.64**)

Following a previously reported procedure,[32] a dry 250 mL round bottom flask equipped with a stir bar was charged with piperidine-4-carboxylic acid (6.45 g, 50.0 mmol, 1.0 equiv) and NaOH

(4.00 g, 100 mmol, 2.0 equiv). 100 mL of a 1:1 mixture of Et_2O and H_2O were added followed by tosyl chloride (9.55 g, 50.0 mmol, 1.0 equiv). The clear mixture was vigorously stirred at rt for 18 h. A white cloudy precipitate was formed, and in a separatory funnel, the mixture was diluted with 100 mL of Et_2O and H_2O added until the precipitate was completely dissolved. The two layers were separated, and the pH of the aqueous layer was adjusted to 3 by addition of 3 M HCl. The precipitate was filtered and reconstituted in EtOAc. solvent removed *in vacuo* to give **3.64** (8.6 g, 60%) as a white solid.

The NMR spectra match those reported in the literature.

LRMS (UPLC) Calculated $C_{13}H_{18}NO_4S^+$ $[M+H]^+$: 284, Found 284

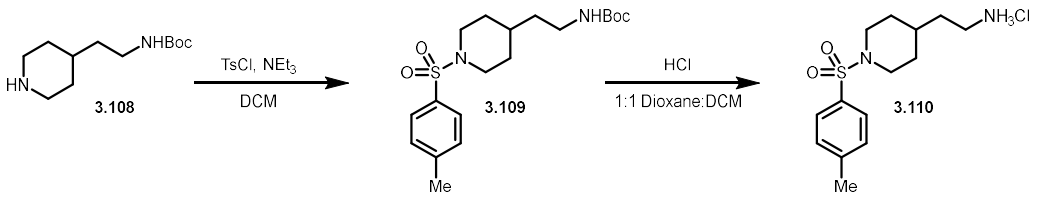

Scheme 3.3: Preparation of amine 3.110

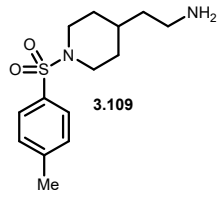

tert-butyl (2-(1-tosylpiperidin-4-yl)ethyl)carbamate (**3.109**)

Following a literature procedure[59], a dry two-dram vial equipped with a stir bar was charged with tert-butyl (2-(piperidin-4-yl)ethyl)carbamate (1.00 g, 4.38 mmol, 1.0 equiv). The vial was evacuated and refilled with nitrogen 3x. 2.75 mL of dichloromethane (DCM) was added followed by triethylamine (1.22 mL, 886 mg, 8.76 mmol, 2.0 equiv). This was stirred until all solids dissolved followed by a dropwise addition of tosyl chloride (835 mg, 4.38 mmol, 1.0 equiv) in 1.75 mL of DCM containing 10 µL of TEA. This mixture was stirred for 14 hours at

room temperature. Upon completion, the reaction was diluted with (DCM) (5.0 mL) partitioned between additional DCM (75 mL) and 1M aqueous hydrochloric acid (HCl) (30 mL). The layers were separated, and the organic layer washed with aqueous sodium bicarbonate (30 mL). The organic layer was separated, dried over sodium sulfate and the solvent removed *in vacuo* to give **3.109** (1.59 g, 95%) as a white solid. This product was used without further purification.

LRMS (UPLC) Calculated $C_{14}H_{22}N_2O_2S^+$ $[M\text{-}Boc]^+$: 282, Found 282

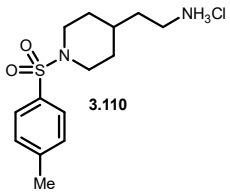

3.110

2-(1-tosylpiperidin-4-yl)ethan-1-amine (**3.110**)

A dry 50 mL round bottom flask equipped with a stir bar was charged with **3.109** (1.59 g, 4.16 mmol, 1.0 equiv). Under air, 10 mL of DCM was added, and the solution stirred until it completely dissolved. 4M HCl in dioxane (10.4 mL, 1.52 g, 41.6 mmol, 10.0 equiv) was added dropwise to the solution. This was stirred for 2 hours. The cloudy white solution was diluted with 30 mL of Et_2O and filtered. The filtrate was washed with another 25 mL of ether and dried under high-vacuum overnight to give **3.110** (1273 mg, 96%) as a white solid.

^{1}H NMR (499 MHz, DMSO) δ 7.90 (s, 2H), 7.61 (d, *J* = 8.2 Hz, 2H), 7.45 (d, *J* = 8.0 Hz, 2H), 3.59 (dt, *J* = 11.6, 3.5 Hz, 2H), 2.73 (h, *J* = 5.8 Hz, 2H), 2.41 (s, 3H), 2.13 (td, *J* = 11.9, 2.5 Hz, 2H), 1.69 (d, *J* = 10.2 Hz, 2H), 1.44 (q, *J* = 7.3 Hz, 2H), 1.29 (dtq, *J* = 14.3, 7.1, 3.5 Hz, 1H), 1.14 (qd, *J* = 12.1, 4.0 Hz, 2H).

^{13}C NMR (126 MHz, dmso) δ 143.47, 132.37, 129.78, 127.49, 45.93, 36.30, 32.92, 31.40, 30.49, 20.99.

LRMS (UPLC) Calculated $C_{14}H_{23}N_2O_2S^+$ $[M\text{-}Cl]^+$: 283, Found 283

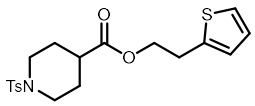

3.111

2-(thiophen-2-yl)ethyl 1-tosylpiperidine-4-carboxylate (**3.111**)

Compound **3.111** was prepared on a 0.2 mmol scale from **3.64** and 2-(2-thiophenyl)-ethylamine according to a modified general procedure **3.3** where **3.66** was replaced with 2,4,6-tris(4-(trifluoromethyl)phenyl)pyrylium tetrafluoroborate to give 20.0 mg (26%) of a yellow oil after purification with ethyl acetate & hexanes.

R_f = 0.24 in 20% EA in hexanes

^{1}H NMR (400 MHz, $CDCl_3$) δ 7.63 (d, *J* = 8.2 Hz, 2H), 7.32 (d, *J* = 8.0 Hz, 2H), 7.14 (dd, *J* = 5.1, 1.2 Hz, 1H), 6.92 (dd, *J* = 5.1, 3.4 Hz, 1H), 6.81 (dd, *J* = 3.4, 1.2 Hz, 1H), 4.27 (t, *J* = 6.5 Hz, 2H), 3.59 (dt, *J* = 12.2, 4.1 Hz, 2H), 3.11 (t, *J* = 6.5 Hz, 2H), 2.49 – 2.38 (m, 5H), 2.25 (tt, *J* = 10.6, 4.0 Hz, 1H), 1.94 (dt, *J* = 12.0, 3.9 Hz, 2H), 1.79 (dtd, *J* = 14.3, 10.7, 4.0 Hz, 2H).

^{13}C NMR (101 MHz, $CDCl_3$) δ 173.8, 143.7, 139.9, 133.1, 129.8, 127.8, 127.0, 125.7, 124.2, 64.9, 45.5, 40.1, 29.3, 27.5, 21.7, 21.6.

LRMS (UPLC) Calculated $C_{19}H_{24}NO_4S_2^+$ $[M+H]^+$: 394, Found 394

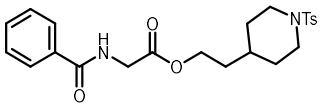

3.112

2-(1-tosylpiperidin-4-yl)ethyl benzoylglycinate (**3.112**)

Compound **3.112** was prepared from on a 0.2 mmol scale hippuric acid and **3.110** via a modified general procedure 3.3 where 2 equivalents of base were used to give 64.8 mg (73%) of a white solid after purification with ethyl acetate.

R_f = 100% EA: 0.25

^{1}H NMR (400 MHz, $CDCl_3$) δ 7.82 – 7.75 (m, 2H), 7.67 – 7.59 (m, 2H), 7.56 – 7.47 (m, 1H), 7.48 – 7.39 (m, 2H), 7.32 (d, *J* = 7.7 Hz, 2H), 6.61 (s, 1H), 4.20 (dd, *J* = 7.5, 5.8 Hz, 4H), 3.76 (d, *J* = 11.4 Hz, 2H), 2.43 (s, 3H), 2.25 – 2.15 (m, 2H), 1.74 (d, *J* = 9.8 Hz, 2H), 1.60 (q, *J* = 6.2 Hz, 2H), 1.33 (s, 2H).

Carbon NMR not performed.

LRMS (UPLC) Calculated $C_{23}H_{29}N_2O_5S^+$ $[M+H]^+$: 445, Found 445

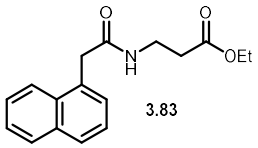

3.83

ethyl 3-(2-(naphthalen-1-yl)acetamido)propanoate (**3.83**)

To an oven dried 50 mL round bottom flask equipped with a stir bar was added potassium 2-(naphthalen-1-yl)acetate (1.00 g, 4.50 mmol, 1.0 equiv) followed by 15 mL of DCM and 1.00 mL of dimethylformamide. Thionyl chloride (363 μL, 595 mg, 5.00 mmol, 1.1 equiv was added) followed by stirring at 35 °C for one hour. During this time a 2-dram vial was charged with beta alanine ethyl ester hydrochloride salt (830 mg, 5.4 mmol, 1.20 equiv). This was suspended in 5.0 mL of DCM and DIPEA (1342 mg, 1.80 mL, 10.8 mmol, 2.40 equiv). After one hour, the beta alanine solution was transferred to the acid chloride solution via syringe. This was allowed to stir for 20 additional minutes at 35 °C. Upon completion, the reaction was cooled to room temperature, diluted with an additional 30 mL of DCM, and washed with 50 mL of aqueous 1M HCl followed by 50 mL of saturated sodium carbonated. The organic layer was dried over sodium sulfate and concentrated *in vacuo*. The resulting residue was purified via column chromatography with ethyl acetate and hexanes to give 1064 mg (83%) of **3.83** as a white solid.

^{1}H NMR (499 MHz, dioxane) δ 8.03 (d, *J* = 8.3 Hz, 1H), 7.88 (dd, *J* = 7.6, 1.8 Hz, 1H), 7.80 (d, *J* = 8.0 Hz, 1H), 7.50 (pd, *J* = 6.8, 1.5 Hz, 2H), 7.42 (dt, *J* = 15.2, 7.1 Hz, 2H), 6.55 (t, *J* = 6.2 Hz, 1H), 3.96 (q, *J* = 7.1 Hz, 2H), 3.90 (s, 2H), 3.33 (q, *J* = 6.3 Hz, 2H), 2.40 (t, *J* = 6.3 Hz, 2H), 1.13 (t, *J* = 7.1 Hz, 3H).

^{13}C NMR (126 MHz, dioxane) δ 171.62, 169.76, 133.94, 132.48, 132.37, 128.42, 127.63, 127.51, 126.08, 125.63, 125.39, 124.11, 59.76, 40.75, 35.01, 33.64, 13.57.

LRMS (UPLC) Calculated $C_{17}H_{20}NO_3^+$ $[M+H]^+$: 286, Found 286

3.4.3 Troubleshooting tips

In several instances of running these reactions when a pyridinium salt is dissolved in dioxane, after stirring with a halide salt, a precipitate forms. It is often a fine yellow or white powder that is presumed to be the pyridinium halide salt that is no longer soluble. When this precipitate forms, the reaction will no longer proceed in dioxane and only starting pyridinium salt is observed. This issue occurred most often with phenethylamines but happens in other cases with no apparent trend. There are two ways to remedy this. If not performing the reductive etherification, adding 10 volume percent dimethylacetamide (DMA) will make the reaction proceed, but will shut down the reductive etherification, requiring purification of the intermediate ester. The other option is to start a new reaction but instead of using **3.66**, use 2,4,6-tris(4-(trifluoromethyl)phenyl)pyrylium tetrafluoroborate which is prepared in a single step from the requisite starting materials.[60]

The other issue we encountered was around peroxide content in dioxane bottles. We found that when using diphenylsilane as a reductant dioxane that tested positive for 0.5 mg/mL of peroxide using MQuant® peroxide testing strips (Sigma-Aldrich 1100110002), the desired

reductive etherification would not take place. When using phenylsilane as the reductant we found up to 5.0 mg/mL was tolerated.

The following flow chart describes what conditions to use when reducing a purified ester. This is helpful in preparing deuterated derivatives if deuterated phenylsilane is not available as deuterated diphenylsilane is commercially available, or if for any other reason the intermediate ester must be purified. For selective reduction in the presence of amides it is ***highly recommended*** to purify the intermediate ester as any excess silane will begin to reduce the amide carbonyl. We have found if a reaction does not go to completion, adding another equivalent of Gallium and silane will generally accomplish this.

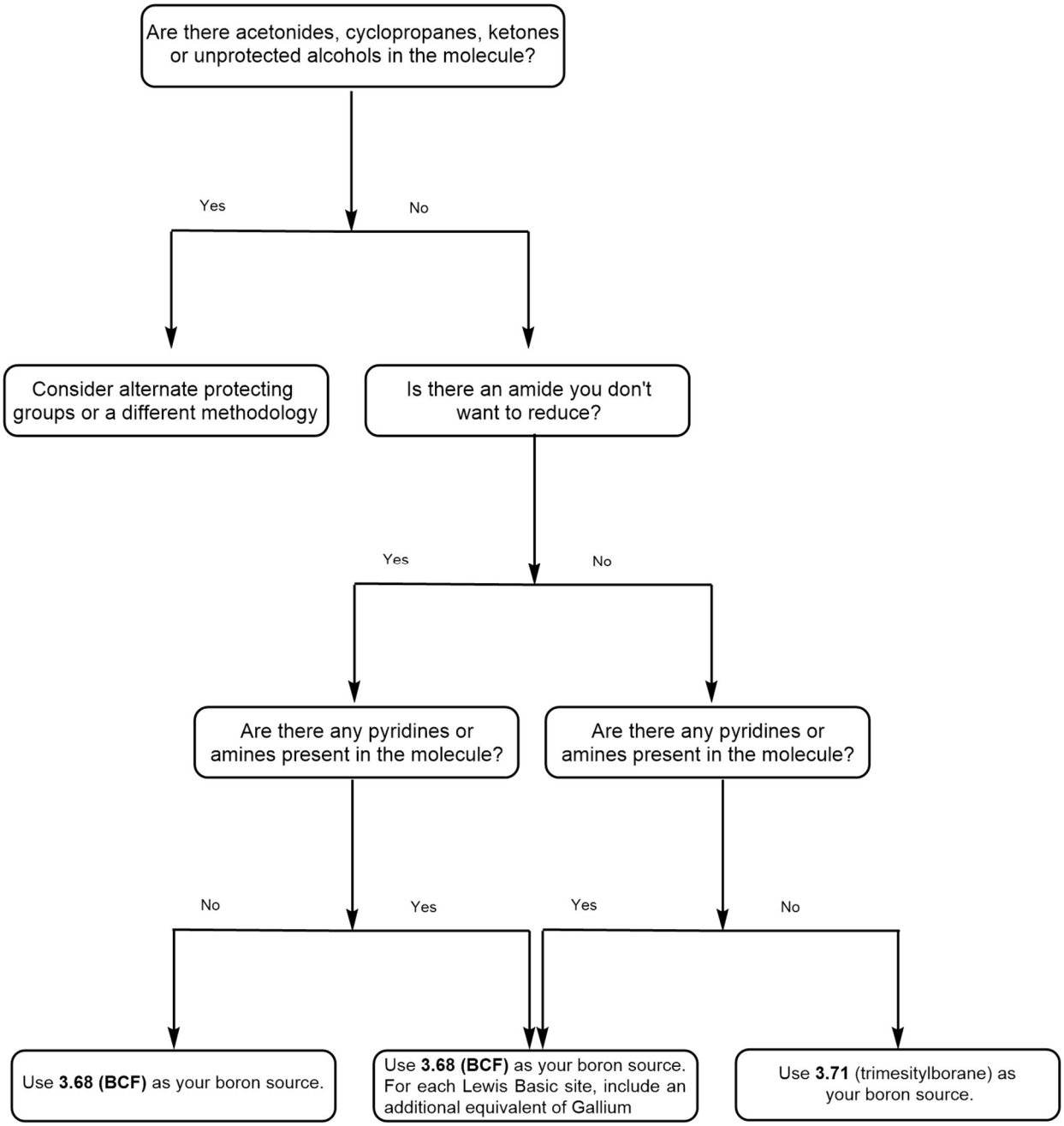

Scheme 3.4 Flowchart depicting conditions to use based on the substrate being reduced.

3.4.4 HTE Optimization of deaminative reductive etherification.

3.4.4.1 Screen examining 3 Lewis acids (0.3 equiv), 2 boranes, and 2 silanes.

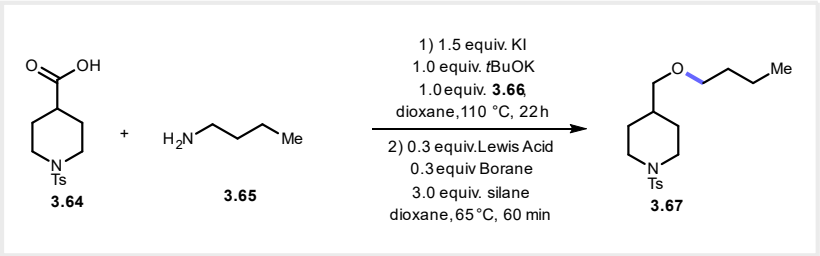

Scheme 3.5 A screen examining four Lewis acids, +/- **3.68**, and two silanes.

Table 3.5 A table showing color coding of reagents as well as their molarity in the phactor screen design.

name	molarity	color
Gallium Bromide	0.1	#48039f
Aluminum Chloride	0.1	#fdb130
Indium (III) Bromide	0.1	#44039e
DODECACARBONYLTRIIRON	0.03	#280592
TRIS(PENTAFLUOROPHENYL)BORANE	0.03	#b02991
triphenylborane	0.03	#e87059
Catalyst 2 blank	0.03	#ce4b75
diphenylsilane	0.3	#7801a8
tetramethyldisiloxane	0.3	#e26660
Ester SM	0.1	#fada24

Reagents	Solvent	C_{stock} (M)	V_{dose} (µL)	Wells	Order Added
Gallium (III) Bromide	Dioxane	0.12	25	A, 1-6	1
Aluminium Chloride	Dioxane	0.12	25	B, 1-6	1
Indium (III) Bromide	Dioxane	0.12	25	C, 1-6	1
Dodecacarbonyltriiron	Dioxane	0.12	25	D, 1-6	1
3.68	Dioxane	0.12	25	A,B,C,D, 1,4	2
triphenylborane	Dioxane	0.12	25	A,B,C,D, 2,5	2
Borane blank	Dioxane	0.12	25	A,B,C,D, 3,6	2
3.70 ester solution	Dioxane	0.3	25	All	3
diphenylsilane	Dioxane	0.9	25	A,B,C,D, 1-3	4
tetramethyldisiloxane	Dioxane	0.9	25	A,B,C,D, 4-6	4

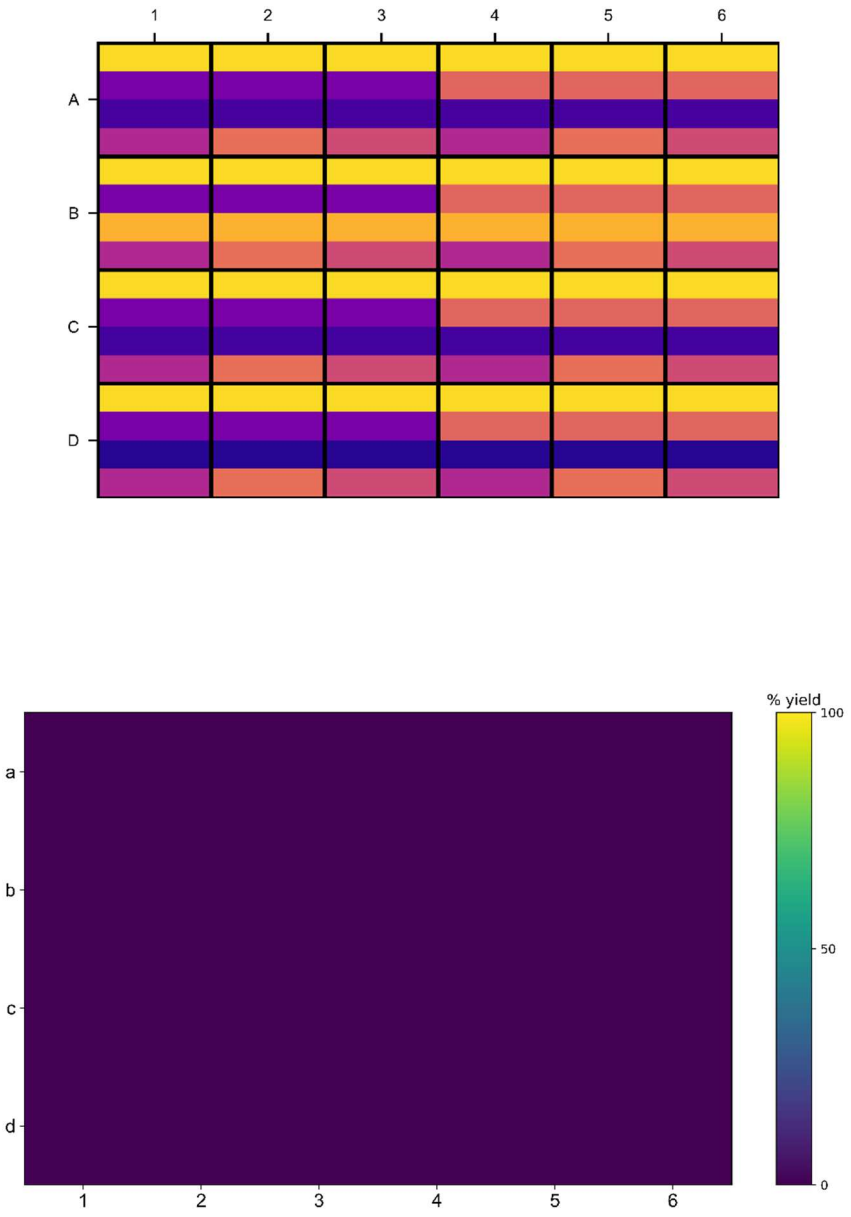

Figure 3.17 Results of screen examining 3 Lewis acids (0.3 equiv), 2 boranes, and 2 silanes.

3.4.4.2 Screen examining 3 Lewis acids (3.0 equiv), 2 boranes, and 2 silanes.

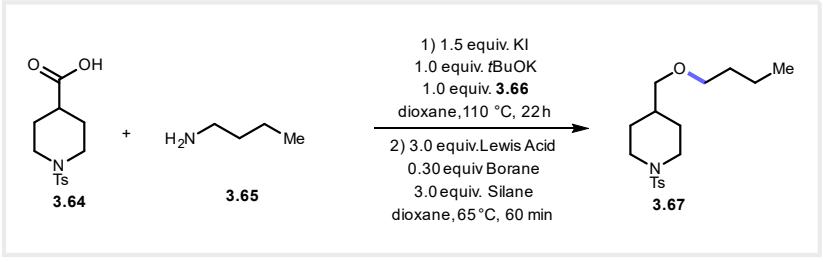

Table 3.6 Color coordinated table of reagents and concentrations.

name	molarity	color
Gallium Bromide	0.3	#48039f
Aluminum Chloride	0.3	#fdb130
Indium (III) Bromide	0.3	#44039e
DODECACARBONYLTRIIRON	0.1	#280592
TRIS(PENTAFLUOROPHENYL)BORANE	0.03	#b02991
triphenylborane	0.03	#e87059
Catalyst 2 blank	0.03	#ce4b75
diphenylsilane	0.3	#7801a8
tetramethyldisiloxane	0.3	#e26660
Ester SM	0.1	#fada24

Reagents	Solvent	C_{stock} (M)	V_{dose} (µL)	Wells	Order Added
Gallium (III) Bromide	Dioxane	0.9	25	A, 1-6	1
Aluminium Chloride	Dioxane	0.9	25	B, 1-6	1
Indium (III) Bromide	Dioxane	0.9	25	C, 1-6	1
Dodecacarbonyltriiron	Dioxane	0.9	25	D, 1-6	1
3.68	Dioxane	0.12	25	A,B,C,D, 1,4	2
triphenylborane	Dioxane	0.12	25	A,B,C,D, 2,5	2
Borane blank	Dioxane	0.12	25	A,B,C,D, 3,6	2
3.70 ester solution	Dioxane	0.3	25	All	3
diphenylsilane	Dioxane	0.9	25	A,B,C,D, 1-3	4
tetramethyldisiloxane	Dioxane	0.9	25	A,B,C,D, 4-6	4

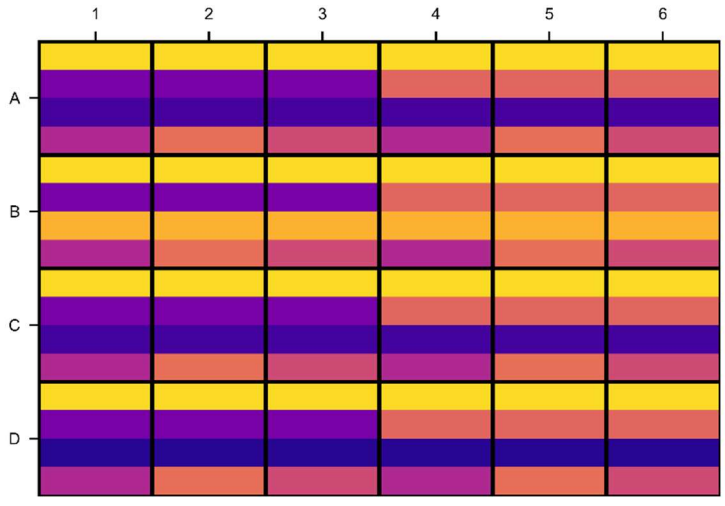

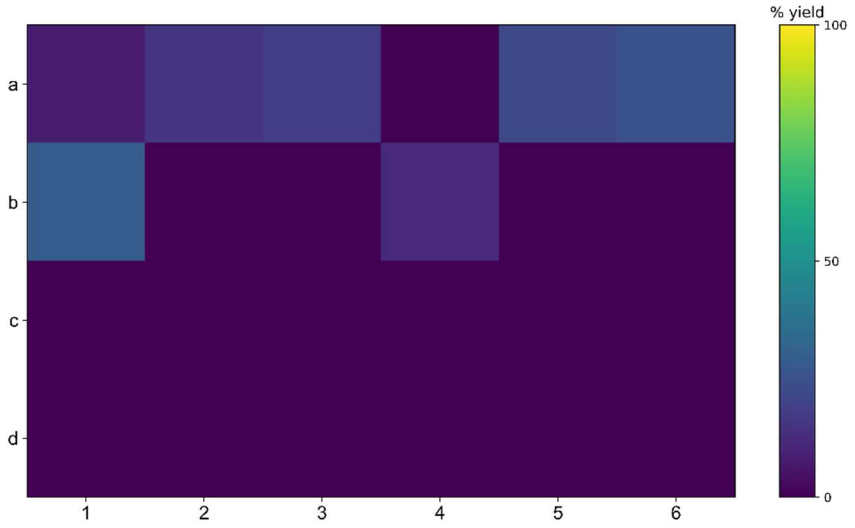

Figure 3.18 Results of screen examining 3 Lewis acids (3.0 equiv), 2 boranes, and 2 silanes.

3.4.4.3 96 well screen examining 6 Lewis acids, 4 boranes, and 4 silanes.

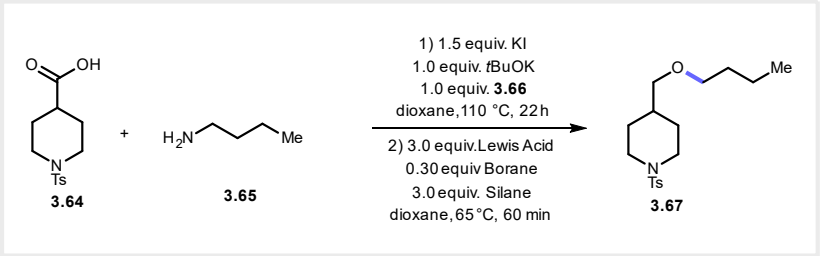

Table 3.7 Color coordinated table of reagents and concentrations.

name	molarity	color
Aluminum Chloride	0.3	#febe2a
Aluminum bromide	0.3	#f79342
Aluminum iodide	0.3	#cc4977
Gallium(III) chloride	0.3	#46039f
Gallium(III) bromide	0.3	#48039f
Gallium(III) Iodide	0.3	#4903a0
Diphenylsilane	0.3	#e26660
Phenylsilane	0.3	#f99a3e
1,1,3,3-Tetramethyldisiloxane	0.3	#f3f027
Triethylsilane	0.3	#da5b69
TRIS(PENTAFLUOROPHENYL)BORANE	0.03	#fbd724
Triphenylborane	0.03	#9e199d
Catalyst blank	0.1	#cb4679
Boron trifluoride etherate, ca. 48% BF3	0.06	#ee7b51
Ester SM	0.1	#a72197

Reagents	Solvent	C_{stock} (M)	V_{dose} (µL)	Wells	Order Added
Aluminum Chloride	Dioxane	0.9	25	A-H, 1,7	1
Aluminum Bromide	Dioxane	0.9	25	A-H, 2,8	1
Aluminum Iodide	Dioxane	0.9	25	A-H, 3,9	1
Gallium (III) Chloride	Dioxane	0.9	25	A-H, 4,10	1
Gallium (III) Bromide	Dioxane	0.9	25	A-H, 5,11	1
Gallium (III) Iodide	Dioxane	0.9	25	A-H, 6,12	1
3.68	Dioxane	0.12	25	A-D, 1-6	2
triphenylborane	Dioxane	0.12	25	A-D, 7-12	2
Borane blank	Dioxane	0.12	25	E-H, 1-6	2
BF3 etherate	Dioxane	0.12	25	E-H, 7-12	2
3.70 ester solution	Dioxane	0.3	25	All	3
phenylsilane	Dioxane	0.9	25	A,E 1-12	4
diphenylsilane	Dioxane	0.9	25	B, F 1-12	4
tetramethyldisiloxane	Dioxane	0.9	25	C,G 1-12	4
triethylsilane	Dioxane	0.9	25	D,H 1-12	4

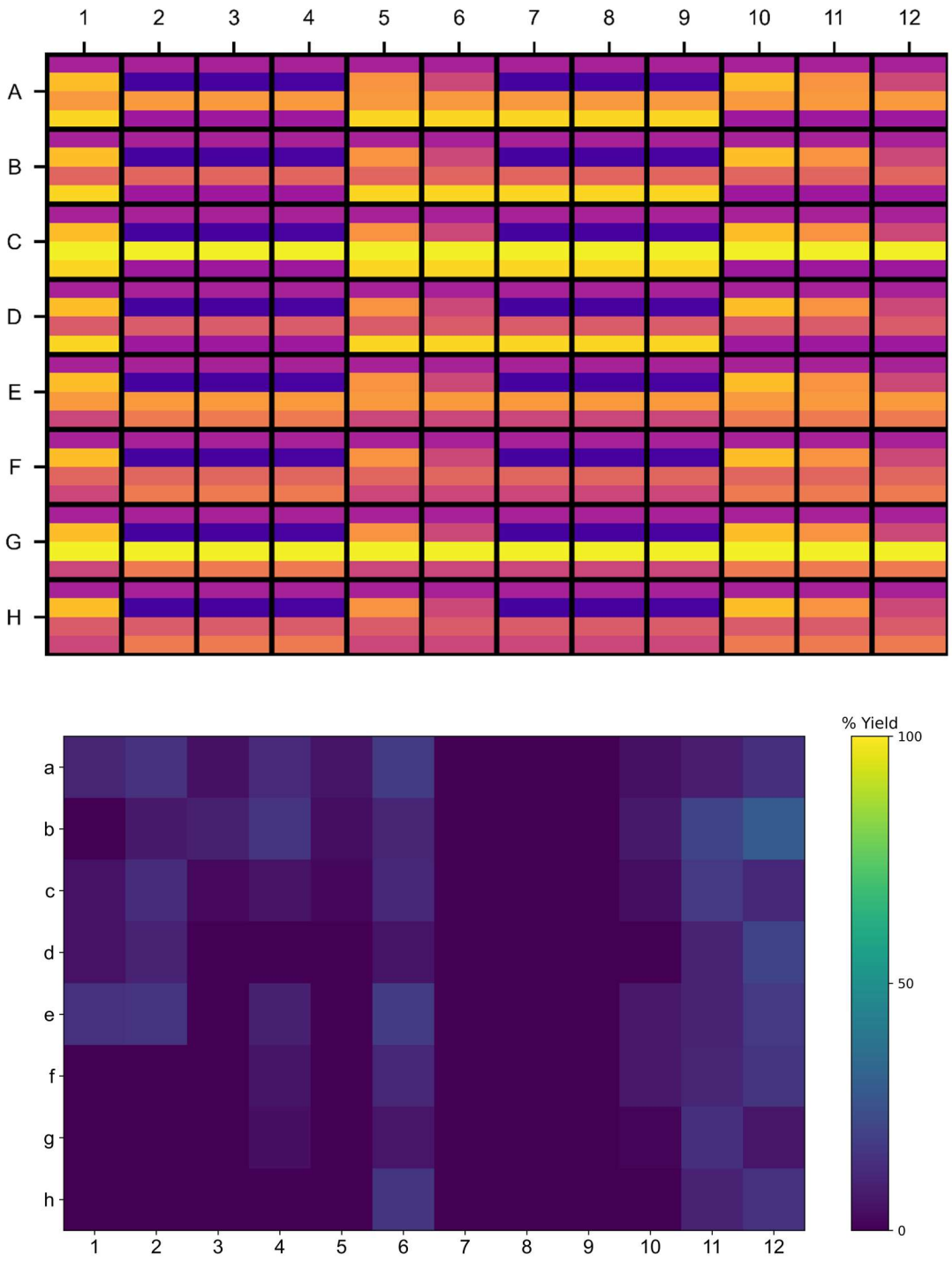

Figure 3.19 Results of 96 well screen examining 6 Lewis acids, 4 boranes, and 4 silanes.

3.4.4.4 Screen examining 6 additives, 2 boranes, and 2 gallium loadings.

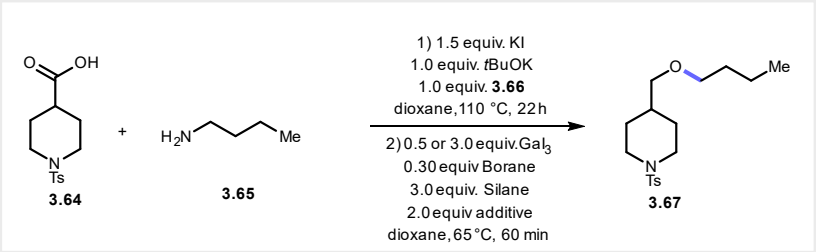

Table 3.8 Color coordinated table of reagents and concentrations.

name	molarity	color
Ester	0.1	#f9dd25
Gallium Iodide	0.3	#fbd324
Gallium iodide 0.5 equiv	0.05	#6300a7
Triphenylborane	0.03	#5b01a5
Trimesitylborane	0.03	#fa9e3b
Additive blank	0.1	#2a0593
CHLOROTRIMETHYLSILANE	0.2	#7a02a8
TRIMETHYL BORATE	0.2	#2c0594
HCl in dioxane 4 molar	0.1	#da5a6a
Sodium tetraphenylborate	0.01	#fdcb26
Sodium tetrakis[3,5-bis(trifluoromethyl)phenyl]borate	0.005	#e56b5d

Reagents	Solvent	Cstock (M)	Vdose (µL)	Wells	Order Added
Gallium (III) Iodide	Dioxane	0.9	25	A,B 1-6	1
Gallium (III) Iodide	Dioxane	0.9	25	C,D 1-6	1
Triphenylborane	Dioxane	0.12	25	A,C 1-6	2
3.71	Dioxane	0.12	25	B,D 1-6	2
Blank	Dioxane	0.12	25	A,B,C,D, 1	3
TMSCl	Dioxane	0.6	25	A,B,C,D, 2	3
B(OMe)3	Dioxane	0.6	25	A,B,C,D, 3	3
HCl in dioxane	Dioxane	0.6	25	A,B,C,D, 4	3
Sodium tetraphenylborate	Dioxane	0.6	25	A,B,C,D, 5	3
sodium tetrakis (3,5-CF3 phenyl)borate	Dioxane	0.6	25	A,B,C,D, 6	3
3.70 ester solution	Dioxane	0.3	25	All	4
diphenylsilane	Dioxane	0.9	25	All	5

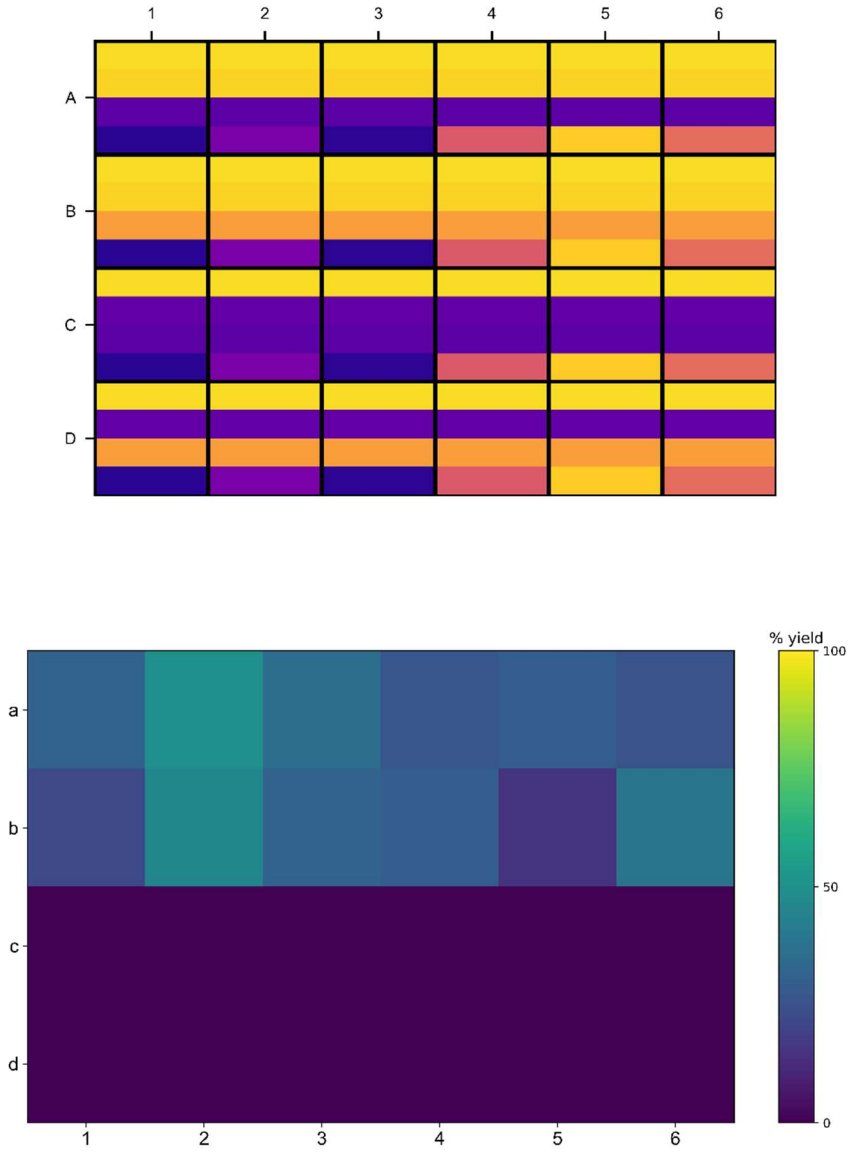

Figure 3.20 Results of screen examining 6 additives, 2 boranes, and 2 gallium loadings.

3.4.4.5 Screen examining 6 silyl halides and 4 boranes.

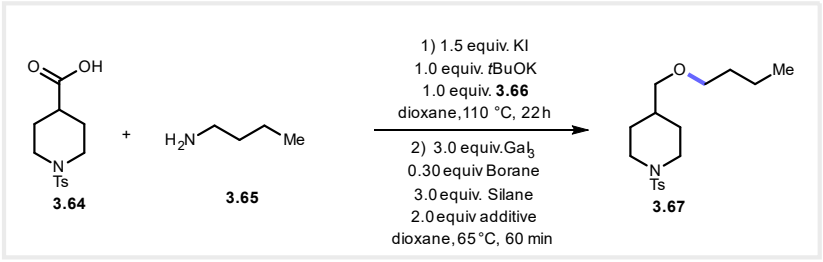

Table 3.9 Color coordinated table of reagents and concentrations.

name	molarity	color
Gallium Iodide	0.25	#e06363
Triphenylborane	0.025	#6c00a8
TRIS(PENTAFLUOROPHENYL)BORANE	0.025	#c5407e
tri-mesityl borane	0.025	#f99a3e
Ester solution	0.1	#f7e225
Bromotrimethylsilane	0.2	#e56b5d
CHLOROTRIMETHYLSILANE	0.2	#ca457a
Chlorotriethylsilane	0.2	#c23c81
dichlorodimethylsilane	0.2	#41049d
Trimethoxychlorosilane	0.2	#7e03a8
Additive blank	0.1	#e26561
borane blank	0.1	#8305a7
Diphenylsilane	0.3	#fdae32

Reagents	Solvent	Cstock (M)	Vdose (µL)	Wells	Order Added
Gallium (III) Iodide	Dioxane	1.2	20	All	1
triphenylborane	Dioxane	1.2	20	A 1-6	2
3.68	Dioxane	0.15	20	B 1-6	2
3.71	Dioxane	0.15	20	C 1-6	2
Blank	Dioxane	0.15	20	D 1-6	2
TMSBr	Dioxane	0.8	20	A,B,C,D, 1	3
TMSCl	Dioxane	0.8	20	A,B,C,D, 2	3
TESCl	Dioxane	0.8	20	A,B,C,D, 3	3
Si(Me)2Cl2	Dioxane	0.8	20	A,B,C,D, 4	3
3.72	Dioxane	0.8	20	A,B,C,D, 5	3
Additive Blank	Dioxane	0.8	20	A,B,C,D, 6	3
3.70 ester solution	Dioxane	0.4	20	All	4
diphenylsilane	Dioxane	1.2	20	All	5

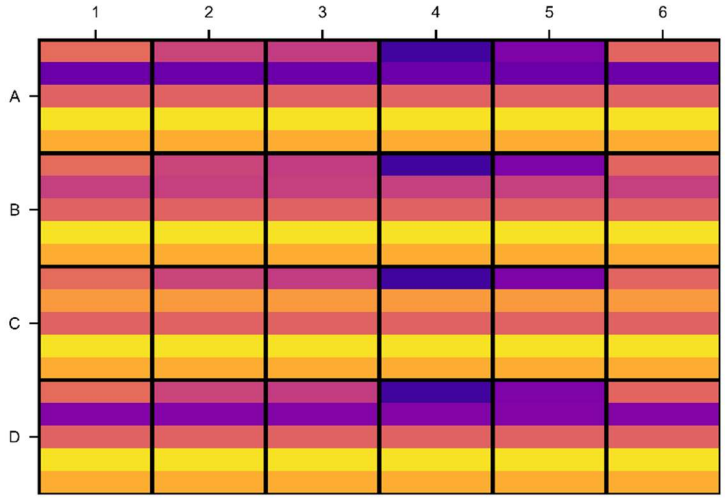

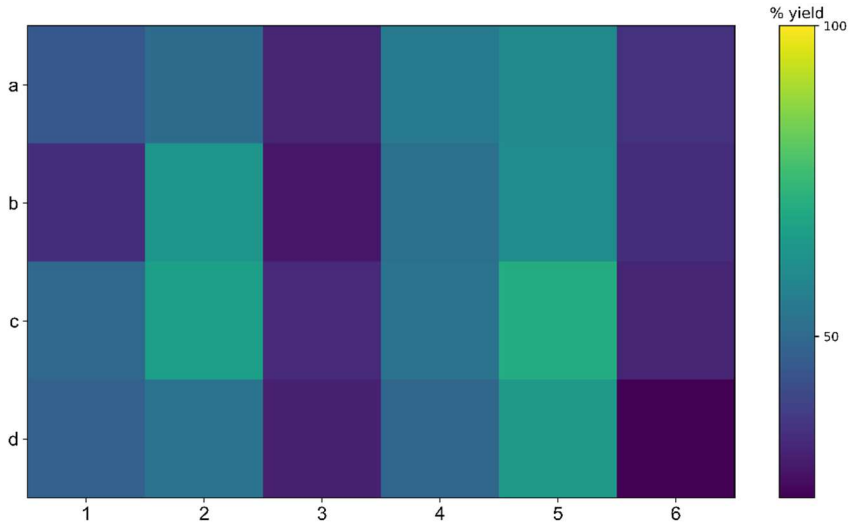

Figure 3.21 Results of screen examining 6 silyl halides and 4 boranes.

3.4.4.6 Screen examining 4 solvents and 6 silanes.

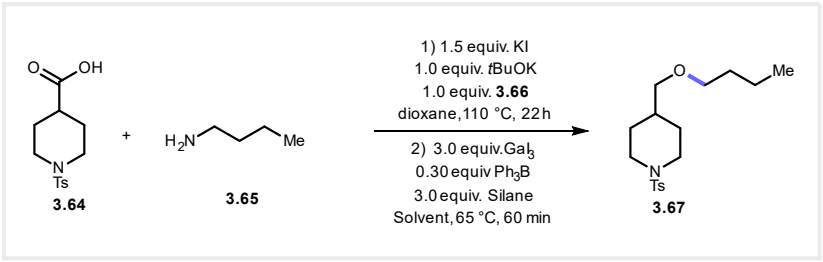

Table 3.10 Color coordinated table of reagents and concentrations.

name	molarity	color
Phenylsilane	0.2	#be3885
Diphenylsilane	0.3	#f8e125
triethylsilane	0.4	#e06363
1,1,3,3-tetramethyldisiloxane	0.3	#5601a4
diethylsilane	0.3	#f2f227
dimethylphenylsilane	0.4	#fa9c3c
Ester Solution	0.1	#ed7a52
Gallium Iodide	0.3	#6e00a8
Triphenylborane	0.03	#910ea3
Phenylsilane	0.2	#be3885
Diphenylsilane	0.3	#f8e125
triethylsilane	0.4	#e06363
1,1,3,3-tetramethyldisiloxane	0.3	#5601a4
diethylsilane	0.3	#f2f227
dimethylphenylsilane	0.4	#fa9c3c
Ester Solution	0.1	#ed7a52
Gallium Iodide	0.3	#6e00a8
Triphenylborane	0.03	#910ea3
Phenylsilane	0.2	#be3885
Diphenylsilane	0.3	#f8e125
triethylsilane	0.4	#e06363
1,1,3,3-tetramethyldisiloxane	0.3	#5601a4
diethylsilane	0.3	#f2f227
dimethylphenylsilane	0.4	#fa9c3c
Ester Solution	0.1	#ed7a52
Gallium Iodide	0.3	#6e00a8
Triphenylborane	0.03	#910ea3
Phenylsilane	0.2	#be3885
Diphenylsilane	0.3	#f8e125
triethylsilane	0.4	#e06363
1,1,3,3-tetramethyldisiloxane	0.3	#5601a4
diethylsilane	0.3	#f2f227
dimethylphenylsilane	0.4	#fa9c3c
Ester Solution	0.1	#ed7a52
Gallium Iodide	0.3	#6e00a8
Triphenylborane	0.03	#910ea3

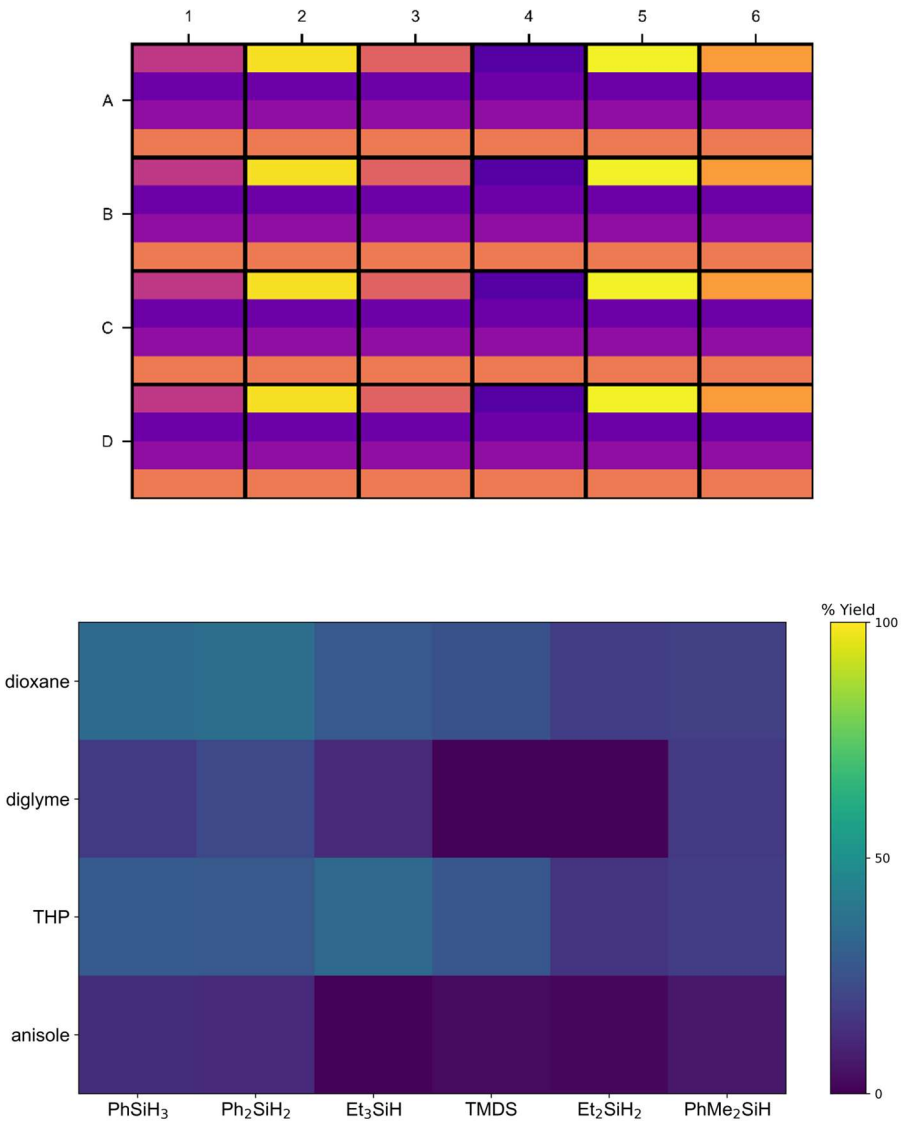

Figure 3.22 Results of screen examining 4 solvents and 6 silanes.

3.4.4.7 Screen examining 16 Lewis Acids at 3 loadings and 2 cocatalysts.

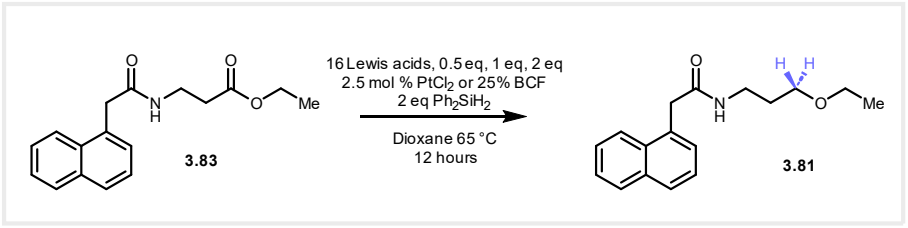

Table 3.11 Reagents used in amide selectivity screen

Reagents	Solvent	Cstock (M)	Vdose (µL)	Wells	Order Added
GaCl3 (3 equiv)	Dioxane	1.2	25	A 1,3	1
PdCl2 (2 equiv)	Dioxane	0.8	25	B 1,3	1
AgNO3(2 equiv)	Dioxane	0.8	25	C 1,3	1
AuCl (2 equiv)	Dioxane	0.8	25	D 1,3	1
BiCl3 (2 equiv)	Dioxane	0.8	25	E 1,3	1
RuCl3 (2 equiv)	Dioxane	0.8	25	F 1,3	1
InCl3 (2 equiv)	Dioxane	0.8	25	G 1,3	1
FeCl2 (2 equiv)	Dioxane	0.8	25	H 1,3	1
Co(acac)3 (2 equiv)	Dioxane	0.8	25	A 2,4	1
AlCl3 (2 equiv)	Dioxane	0.8	25	B 2,4	1
NiCl2 (2 equiv)	Dioxane	0.8	25	C 2,4	1
FeCl3 (2 equiv)	Dioxane	0.8	25	D 2,4	1
ZrCl4 (2 equiv)	Dioxane	0.8	25	E 2,4	1
ZnCl2 (2 equiv)	Dioxane	0.8	25	F 2,4	1
CuCl (2 equiv)	Dioxane	0.8	25	G 2,4	1
MnCl2 (2 equiv)	Dioxane	0.8	25	H 2,4	1
GaCl3 (1.5 equiv)	Dioxane	0.6	25	A 5,7	1
PdCl2 (1 equiv)	Dioxane	0.4	25	B 5,7	1
AgNO3(1 equiv)	Dioxane	0.4	25	C 5,7	1
AuCl (1 equiv)	Dioxane	0.4	25	D 5,7	1
BiCl3 (1 equiv)	Dioxane	0.4	25	E 5,7	1
RuCl3 (1 equiv)	Dioxane	0.4	25	F 5,7	1
InCl3 (1 equiv)	Dioxane	0.4	25	G 5,7	1
FeCl2 (1 equiv)	Dioxane	0.4	25	H 5,7	1
Co(acac)3 (1 equiv)	Dioxane	0.4	25	A 6,8	1
AlCl3 (1 equiv)	Dioxane	0.4	25	B 6,8	1
NiCl2 (1 equiv)	Dioxane	0.4	25	C 6,8	1
FeCl3 (1 equiv)	Dioxane	0.4	25	D 6,8	1
ZrCl4 (1 equiv)	Dioxane	0.4	25	E 6,8	1
ZnCl2 (1 equiv)	Dioxane	0.4	25	F 6,8	1
CuCl (1 equiv)	Dioxane	0.4	25	G 6,8	1
MnCl2 (1 equiv)	Dioxane	0.4	25	H 6,8	1
GaCl3 (0.75 equiv)	Dioxane	0.3	25	A 9,11	1
PdCl2 (0.5 equiv)	Dioxane	0.2	25	B 9,11	1
AgNO3(0.5 equiv)	Dioxane	0.2	25	C 9,11	1
AuCl (0.5 equiv)	Dioxane	0.2	25	D 9,11	1
BiCl3 (0.5 equiv)	Dioxane	0.2	25	E 9,11	1
RuCl3 (0.5 equiv)	Dioxane	0.2	25	F 9,11	1
InCl3 (0.5 equiv)	Dioxane	0.2	25	G 9,11	1
FeCl2 (0.5 equiv)	Dioxane	0.2	25	H 9,11	1
Co(acac)3 (0.5 equiv)	Dioxane	0.2	25	A 10,12	1
AlCl3 (0.5 equiv)	Dioxane	0.2	25	B 10,12	1
NiCl2 (0.5 equiv)	Dioxane	0.2	25	C 10,12	1
FeCl3 (0.5 equiv)	Dioxane	0.2	25	D 10,12	1
ZrCl4 (0.5 equiv)	Dioxane	0.2	25	E 10,12	1
ZnCl2 (0.5 equiv)	Dioxane	0.2	25	F 10,12	1
CuCl (0.5 equiv)	Dioxane	0.2	25	G 10,12	1
MnCl2 (0.5 equiv)	Dioxane	0.2	25	H 10,12	1
3.68	Dioxane	0.1	25	-H 1,2,5,6,9,1	2
PtCl2	Dioxane	0.04	25	H 3,4,7,8,11,	2
3.83	Dioxane	0.4	25	All	3
diphenylsilane	Dioxane	0.8	25	All	4

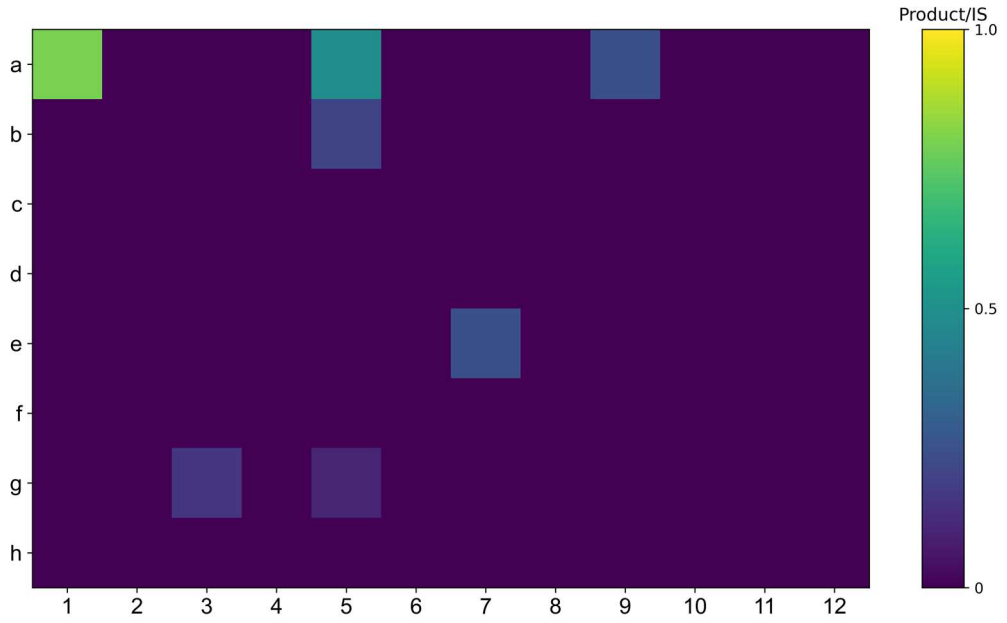

Figure 3.23 Results of amide selectivity screen

3.4.5 Extended optimization data

All reactions were performed according to general procedure 3.4. Assay yields of the ester reaction were collected via LCMS before starting the ether step. Assay yields were collected again after the ether reduction step. The major products of the reaction are **3.67** (ether), **3.70** (ester) or **3.113** (alcohol).

Table 3.12 Optimization of solvent, concentration, and ester step promoter.

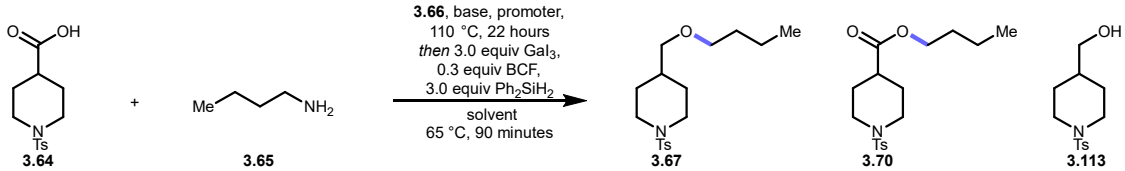

3.64 + **3.65** → **3.67** + **3.70** + **3.113**

entry	base	Promoter	Concentration (step 1)	Concentration (step 2)	Solvent	LC yield ether	Pre-reduction LC yield ester	Post-reduction LC yield ester
1	KOtBu	KI	0.3 M	0.1 M	dioxane	40%	70%	ND
2	KOtBu	KBr	0.3 M	0.1 M	dioxane	35%	65%	ND
3	DIPEA	KI	0.3 M	0.1 M	dioxane	35%	63%	ND
4	KOtBu	KI	0.3 M	0.1 M	MeCN	ND	55%	55%
5	KOtBu	KI	0.3 M	0.1 M	$CF_3C_6H_5$	20%	45%	20%
6	KOtBu	KI	0.3 M	0.1 M	Pyridine	ND	ND	ND
7	KOtBu	KI	0.3 M	0.1 M	DCE	25%	48%	22%
8	KOtBu	KI	0.3 M	0.3 M	dioxane	40%	70%	48%
9	KOtBu	KI	0.1 M	0.1 M	dioxane	28%	40%	ND
10	KOtBu	KI	0.3 M	0.05 M	dioxane	36%	72%	5%

Table 3.13 Extended optimization of gallium source, boron source, and ligand.

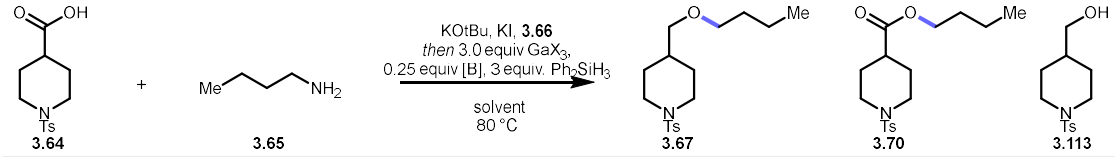

3.64 3.65 3.67 3.70 3.113

entry	Ga source	Boron Source	Ligand	LC yield ether	post-reduction LC yield ester
1	GaI_3	Mes_3B	None	45%	ND
2	GaOTf	Mes_3B	None	Trace	75%
3	GaI_3	BCF	None	42%	ND
4	GaI_3	BF_3	None	15%	ND
5	GaI_3	$B(OMe)_3$	None	20%	30%
6	GaI_3	$PhB(OH)_2$	None	25%	25%
7	GaI_3	KI	None	20%	54%
8	GaI_3	KI	PCy_3	ND	72%
9	GaI_3	KI	L1	ND	76%
10	GaI_3	KI	L2	ND	70%

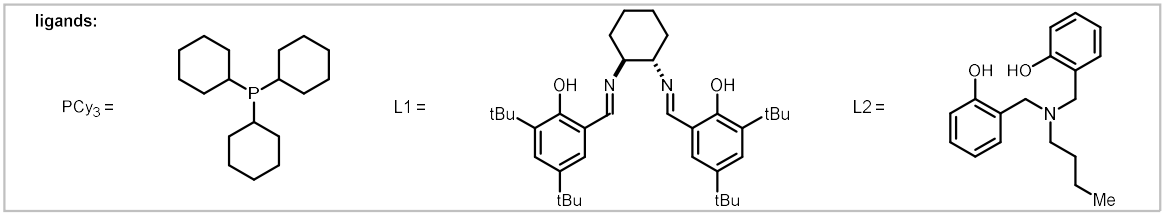

3.4.6 NMRs of mechanistic studies

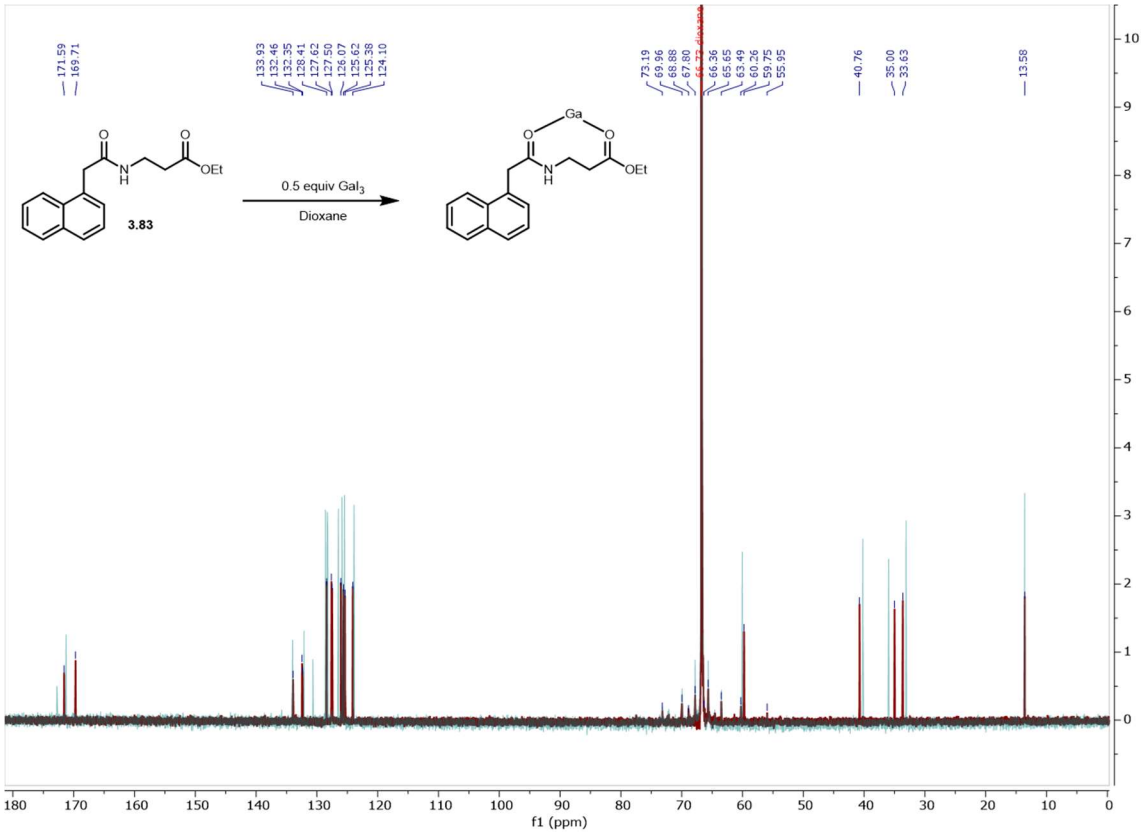

Spectrum 3.4 ^{13}C NMR of Compound **3.83** with and without 0.5 equiv of GaI_3. The darker color is the base compound and lighter color is with gallium added.

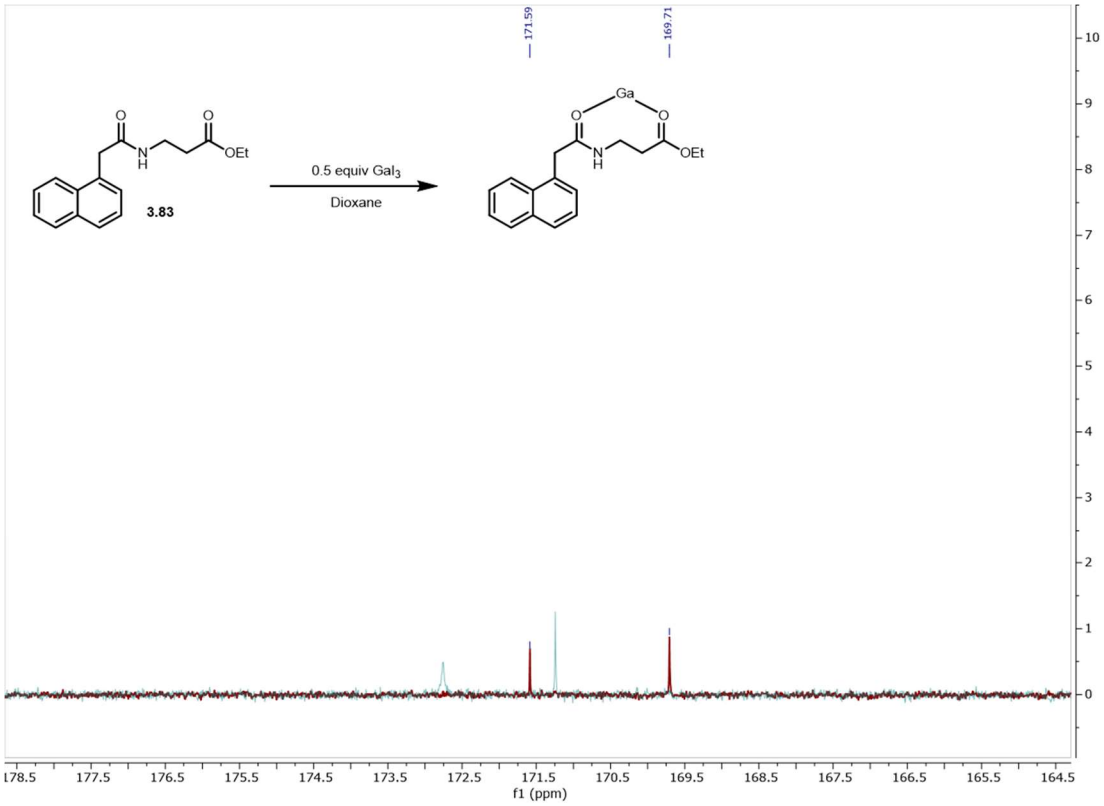

Spectrum 3.5 ^{13}C NMR of Compound **3.83** with and without 0.5 equiv of GaI_3 zoomed in on carbonyl region. The darker color is the base compound and lighter color is with gallium added.

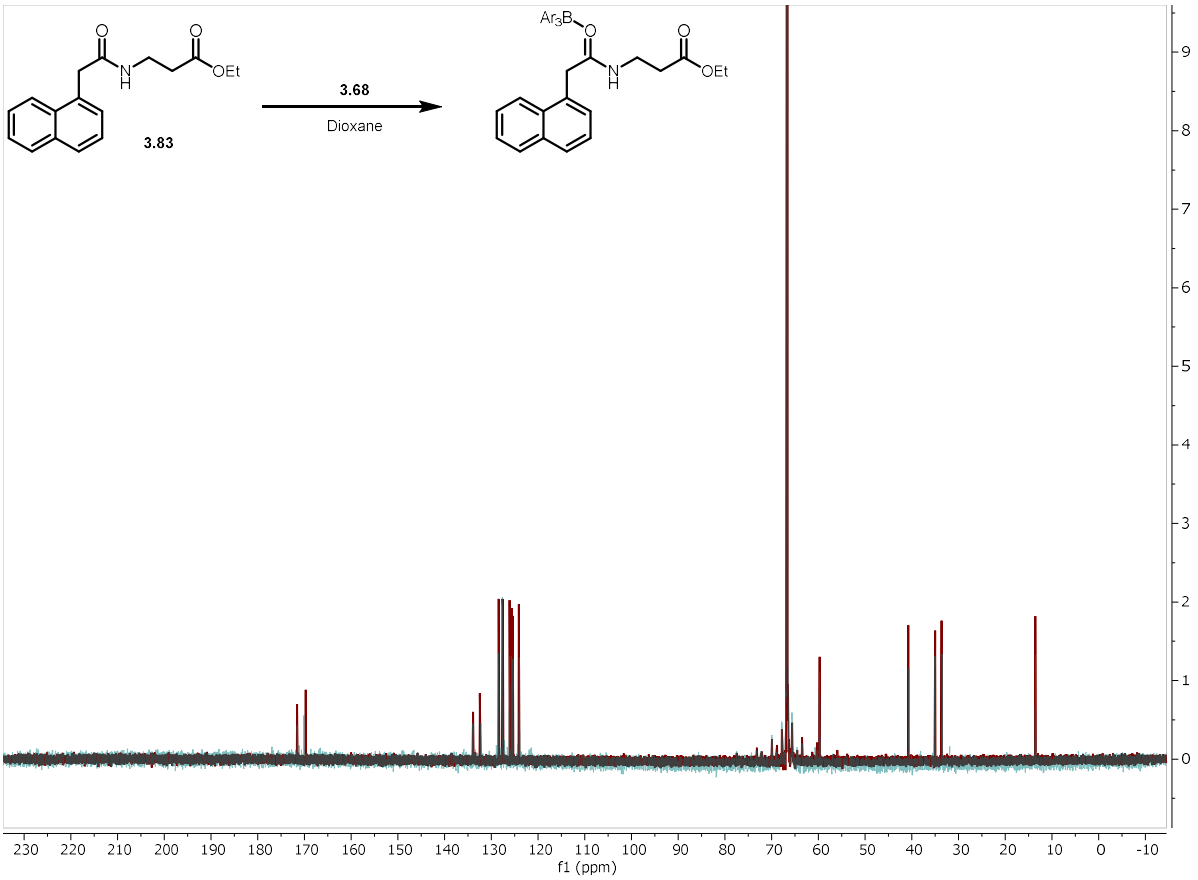

Spectrum 3.6 ^{13}C NMR of Compound **3.83** with and without 0.25 equiv of **3.68**. The darker color is the base compound and lighter color is with **3.68** added.

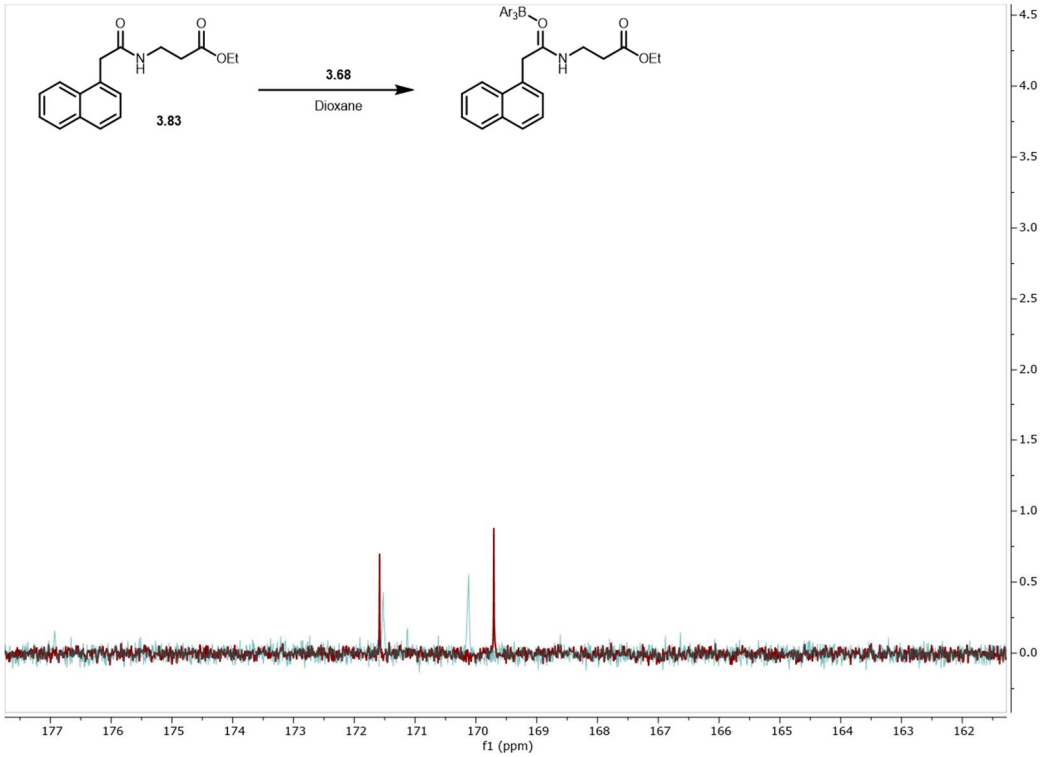

Spectrum 3.7 ^{13}C NMR of Compound **3.83** with and without 0.25 equiv of **3.68** zoomed in on the carbonyl region. The darker color is the base compound and lighter color is with **3.68** added.

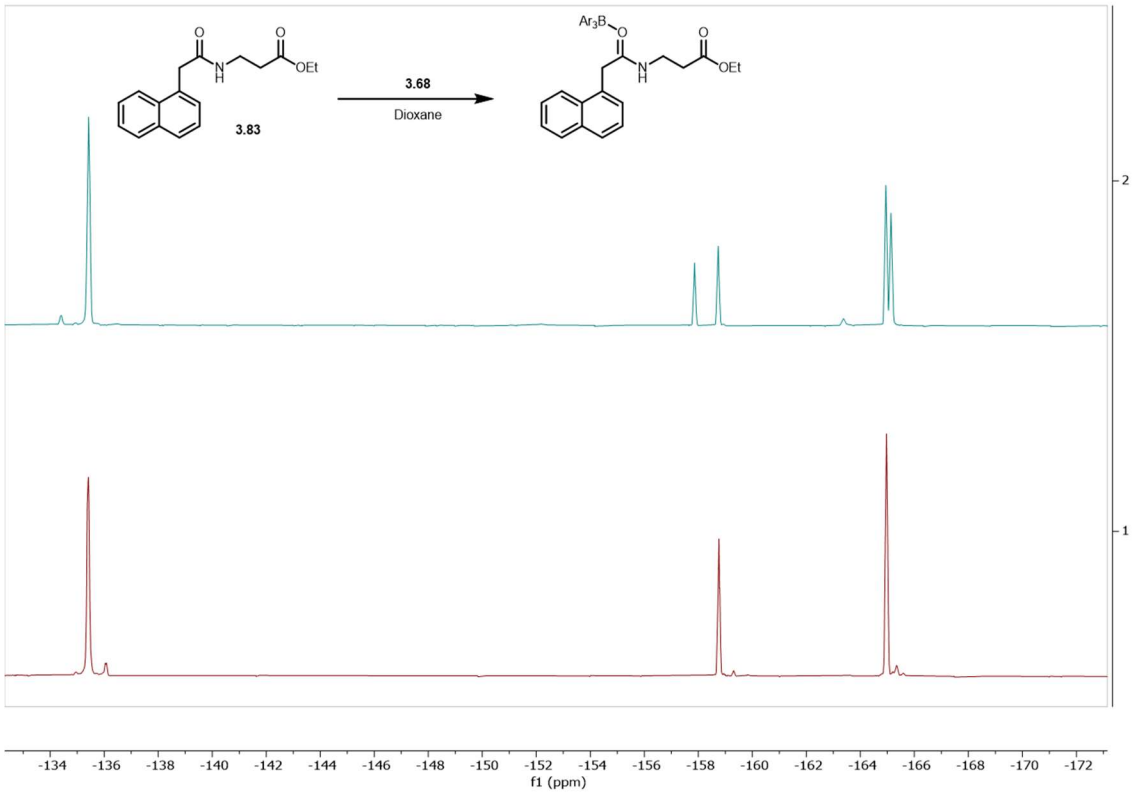

Spectrum 3.8 ^{19}F NMR of Compound **3.68** with and without **3.83**. The darker color is the base compound and lighter color is with **3.83** added.

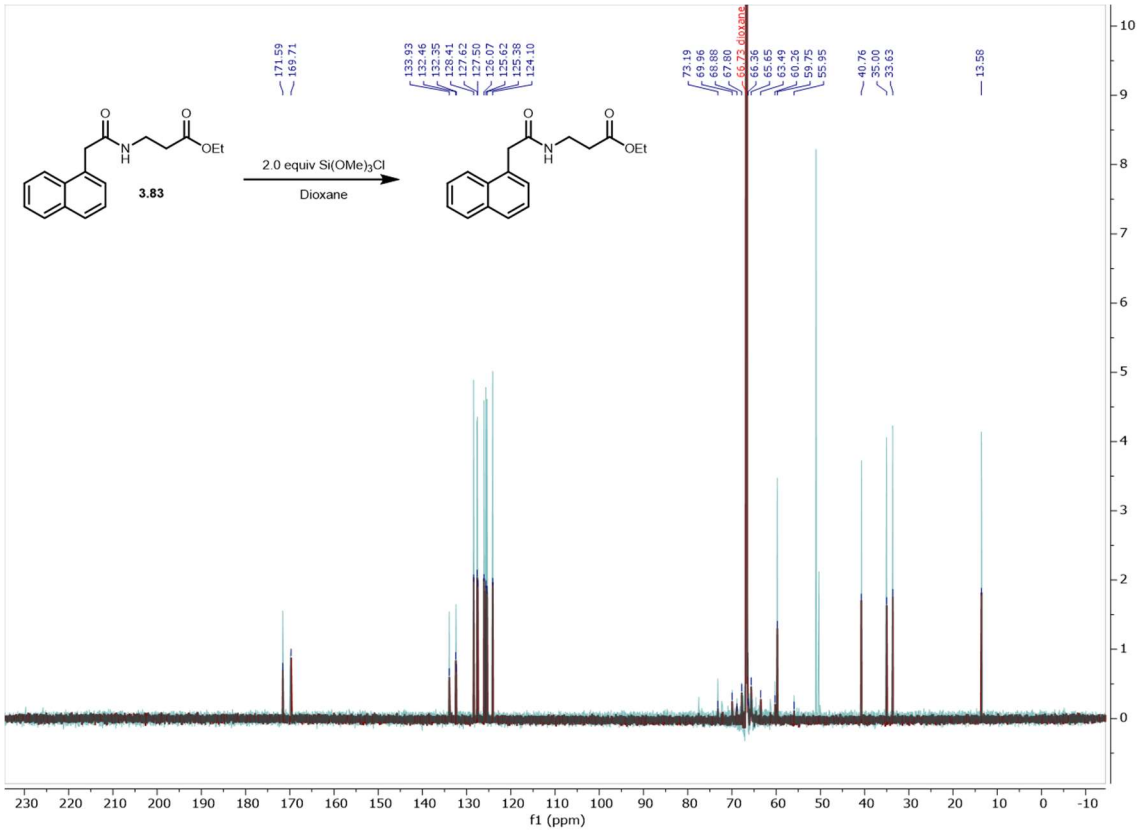

Spectrum 3.9 ^{13}C NMR of Compound **3.83** with and without 2.0 equiv of **3.72**. zoomed in on the carbonyl region. The darker color is the base compound and lighter color is with **3.72** added.

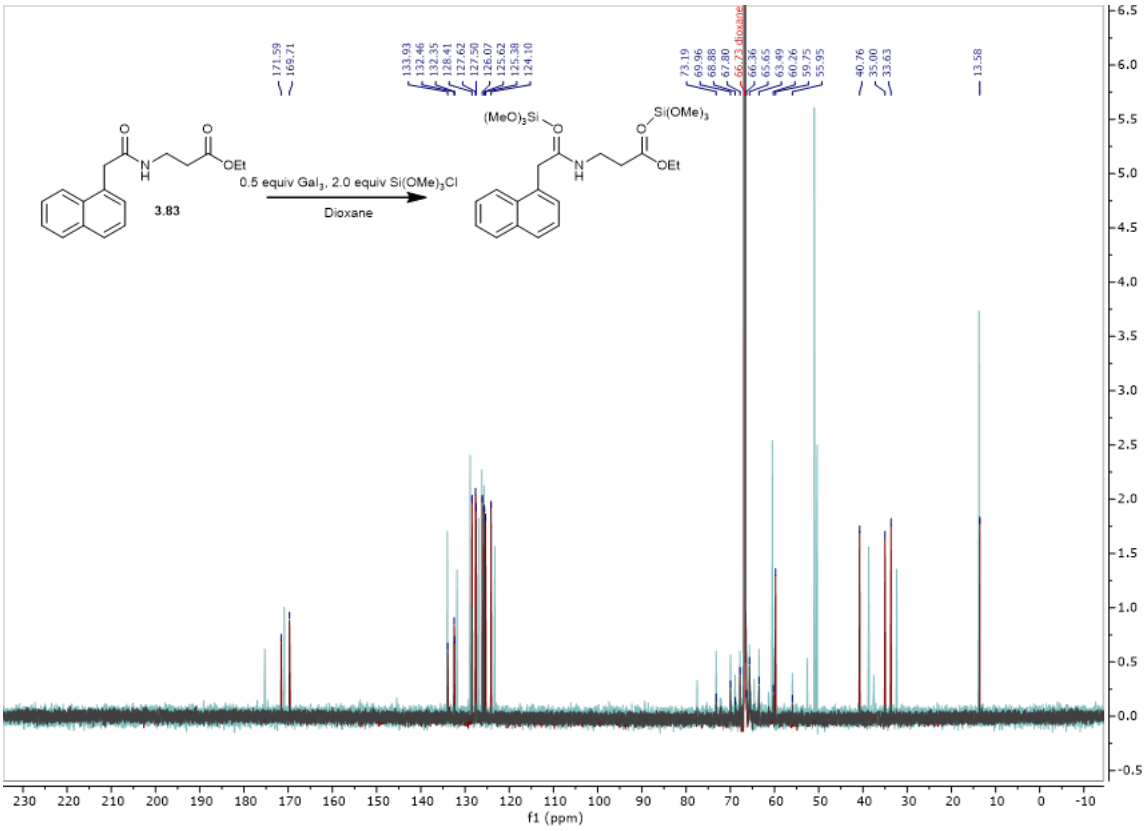

Spectrum 3.10 ^{13}C NMR of Compound **3.83** with and without 2.0 equiv of **3.72** and 0.5 equiv GaI_3. The darker color is the base compound and lighter color is with reagents added.

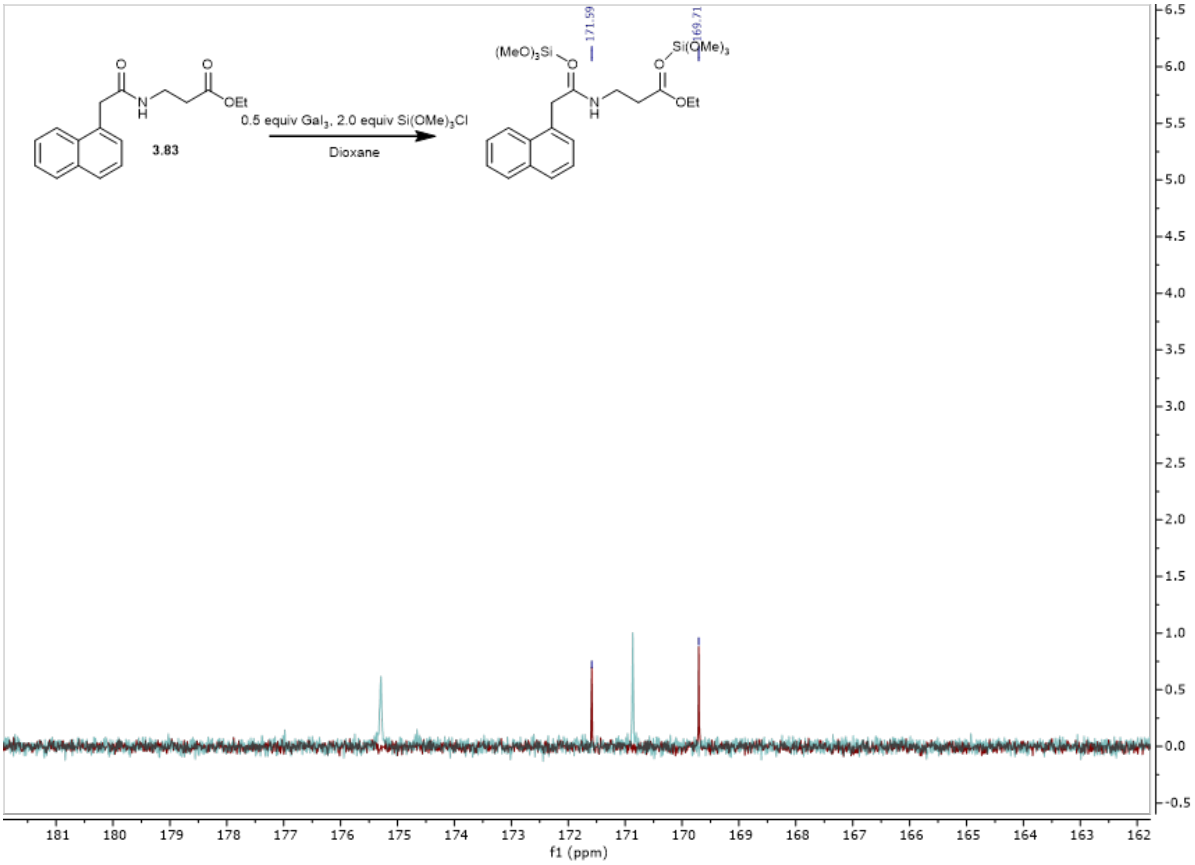

Spectrum 3.11 ^{13}C NMR of Compound **3.83** with and without 2.0 equiv of **3.72** and 0.5 equiv GaI_3 zoomed in on the carbonyl region. The darker color is the base compound and lighter color is with reagents added.

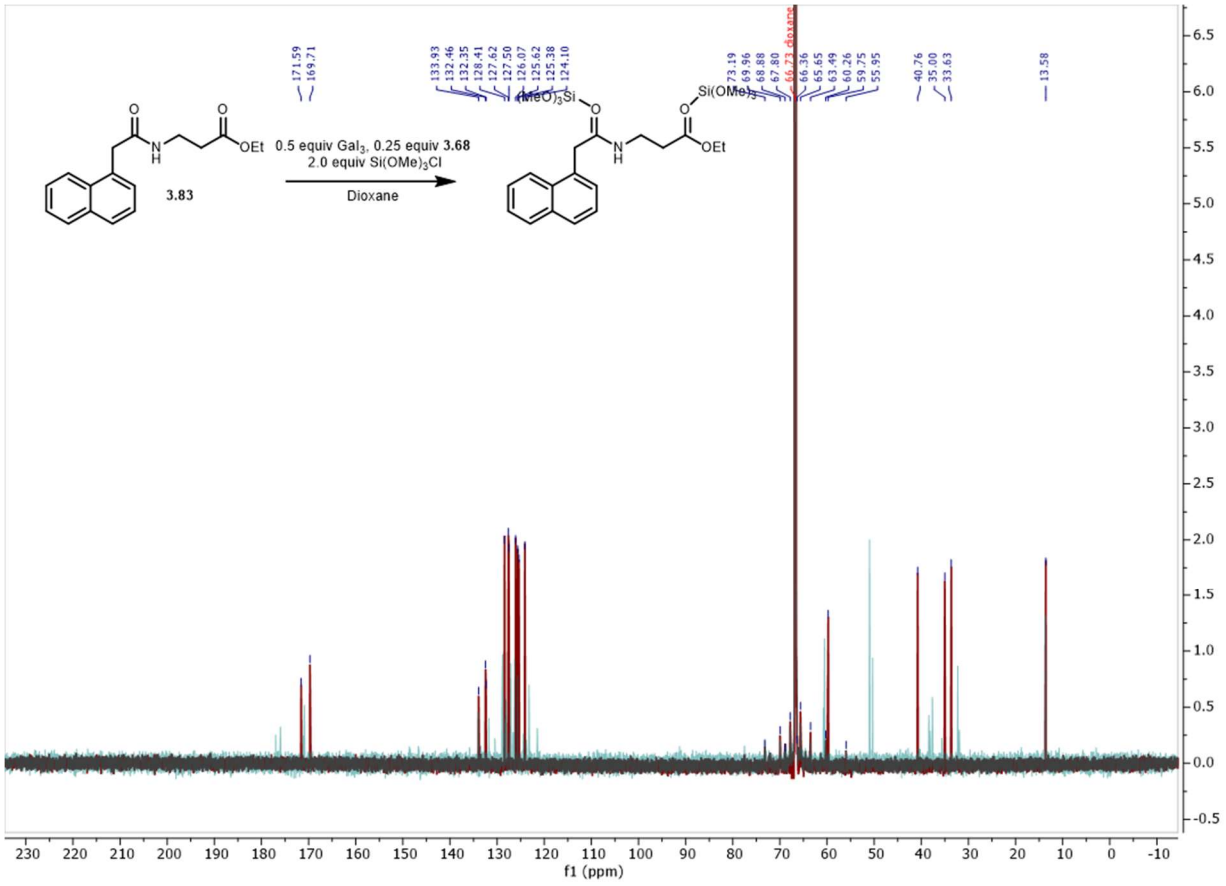

Spectrum 3.12 ^{13}C NMR of Compound **3.83** with and without 0.25 equiv **3.68**, 2.0 equiv of **3.72** and 0.5 equiv GaI_3. The darker color is the base compound and lighter color is with reagents added.

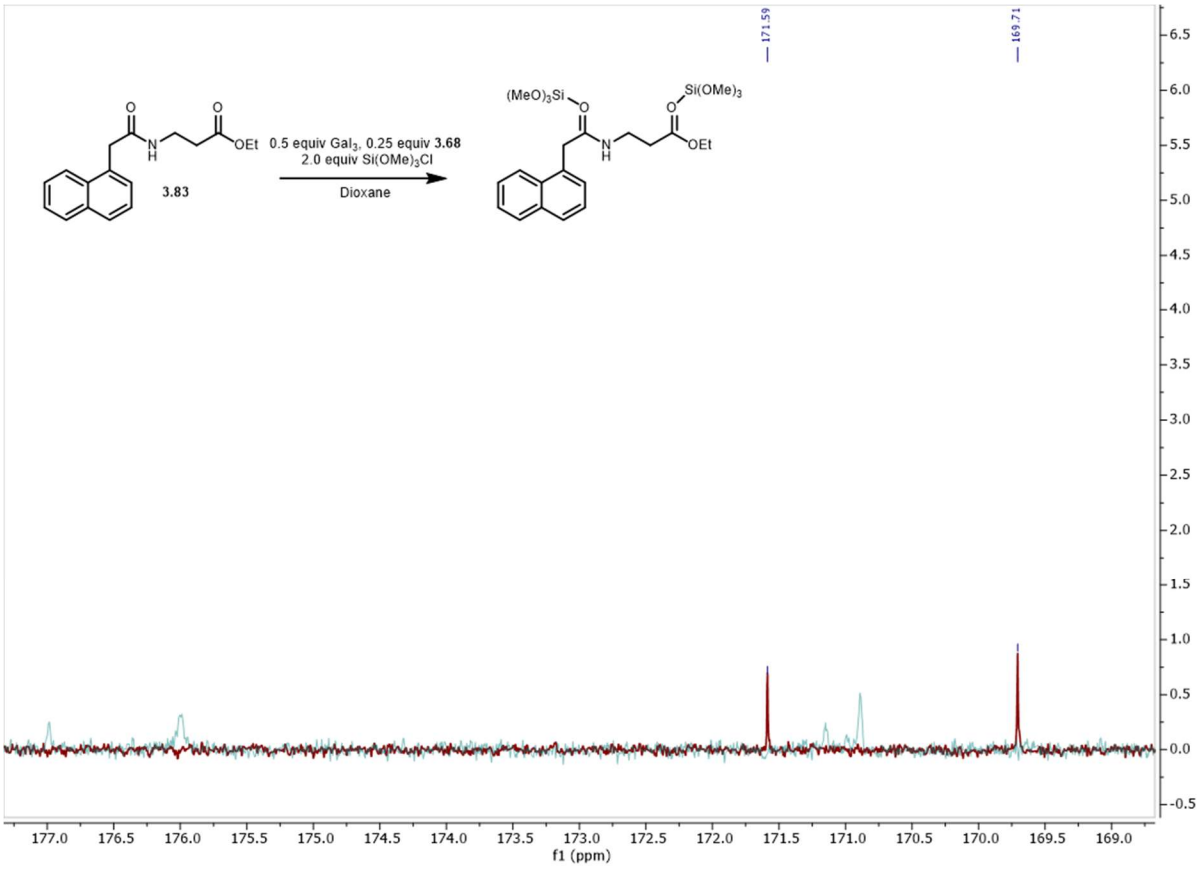

Spectrum 3.13 ^{13}C NMR of Compound **3.83** with and without 0.25 equiv **3.68**, 2.0 equiv of **3.72** and 0.5 equiv GaI_3 zoomed in on the carbonyl region. The darker color is the base compound and lighter color is with reagents added.

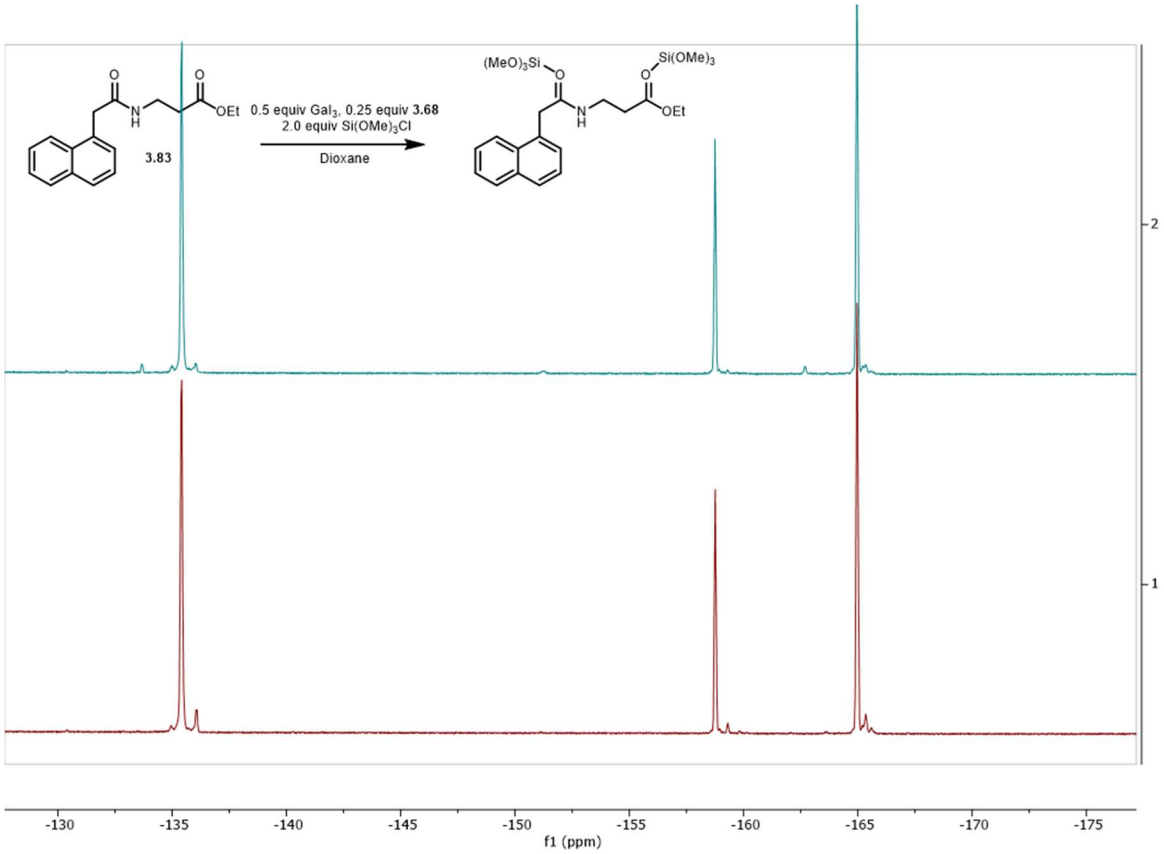

Spectrum 3.14 ^{19}F NMR of Compound **3.83** with and without 0.25 equiv **3.68**, 2.0 equiv of **3.72** and 0.5 equiv GaI_3. The darker color is the base compound and lighter color is with reagents added.

3.4.7 Discovery and optimization of a platinum based pyridinium salt-acid reductive etherification.

The initial discovery of this reaction was via platinum-based catalysis from the pyridinium salt and acid. These conditions were discovered to work for benzylic pyridinium salts, and somewhat for primary, however the structure reactivity relationship was discovered to be quite flat and optimization attempts were abandoned in favor of the gallium-based conditions.

3.4.7.1 Screen examining 6 Lewis acids, 2 silanes, +/- trifluoracetic acid.

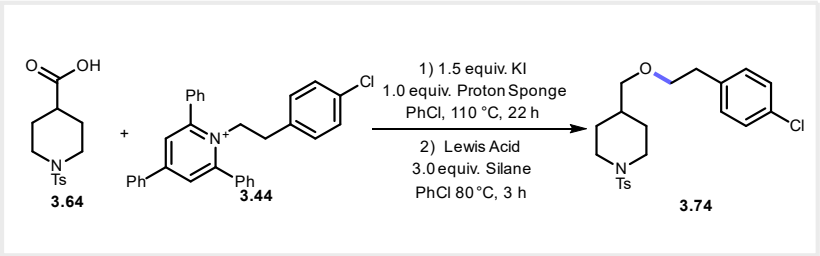

Table 3.14 Color coordinated table of reagents and concentrations.

name	molarity	color
INDIUM(III) BROMIDE	0.015	#b83289
SCANDIUM(III) TRIFLATE	0.015	#5502a4
ALUMINUM CHLORIDE	0.015	#8405a7
TRIS(PENTAFLUOROPHENYL)BORANE\	0.015	#48039f
PLATINUM(II) CHLORIDE	0.015	#ce4b75
TETRABUTYLAMMONIUM FLUORIDE HYDRATE	1.5	#b83289
TFA blank	0.1	#41049d
Trifluoroacetic Acid	0.15	#99159f
triethylsilane	0.3	#de6164
Phenylsilane	0.3	#8e0ca4
Ester solution	0.1	#f68d45

Reagents	Solvent	Cstock (M)	Vdose (µL)	Wells	Order Added
Indium (III) Bromide	Chlorobenzene	0.2	25	A,B,C,D 1	1
Scandium (III) Triflate	Chlorobenzene	0.2	25	A,B,C,D 2	1
Aluminum Chloride	Chlorobenzene	0.2	25	A,B,C,D 3	1
3.68	Chlorobenzene	0.2	25	A,B,C,D 4	1
platinum (II) chloride	Chlorobenzene	0.05	25	A,B,C,D 5	1
tetrabutyl ammonium fluoride	Chlorobenzene	0.3	25	A,B,C,D 6	1
Acid blank	Chlorobenzene	0.3	25	A,C 1-6	2
trifluoro acetic acid	Chlorobenzene	0.3	25	B,D 1-6	2
triethylsilane	Chlorobenzene	0.9	25	A,B 1-6	3
phenylsilane	Chlorobenzene	0.6	25	C,D 1-6	3
Ester solution	Chlorobenzene	0.3	25	All	4

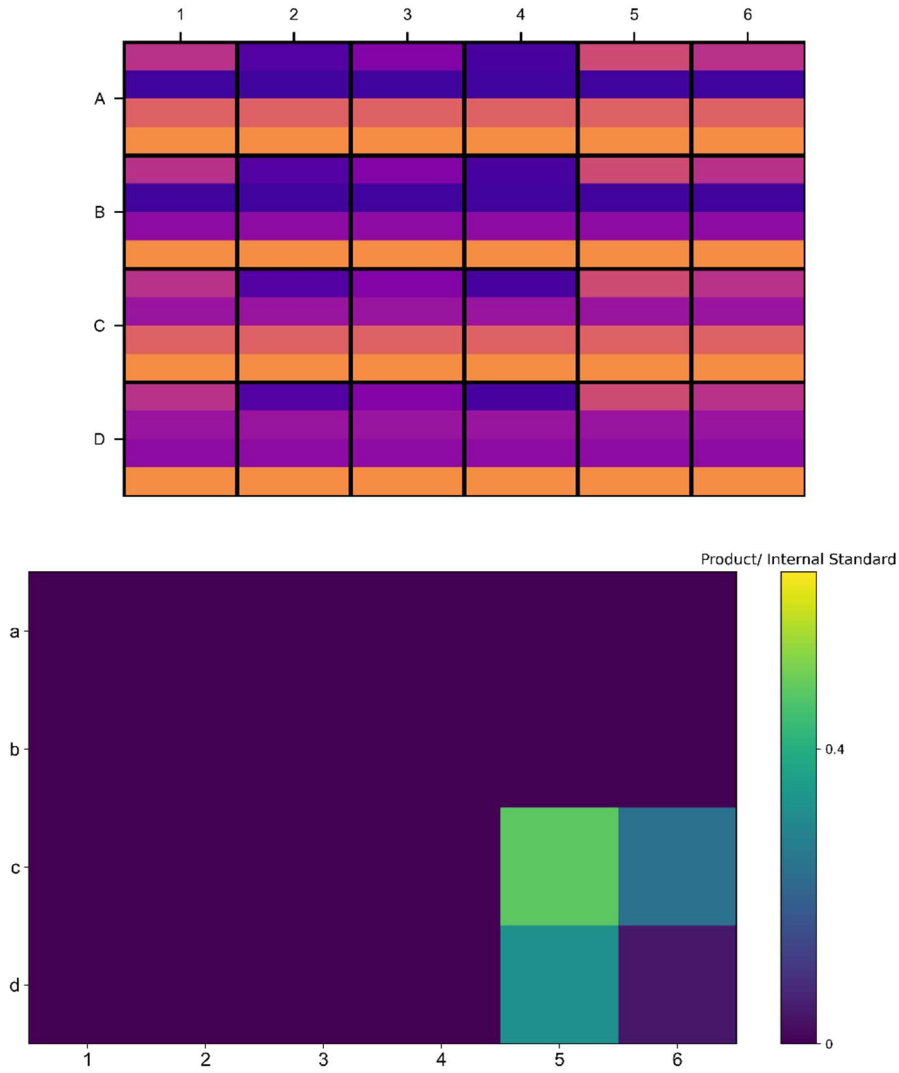

Figure 3.24 Results of screen examining 6 Lewis acids, 2 silanes, +/- trifluoracetic acid. Platinum chloride and tetrabutylammonium fluoride (TBAF) produced ether product in combination with phenylsilane.

3.4.7.2 Remote access ligand and silane screen for platinum catalyzed reductive etherification.

This screen was conducted when limitations on the number of people allowed in lab were in place during COVID. To continue research, we conducted a remote access screen where Dr. Sam Zhang was in lab to load the robot with the necessary reagents, and I controlled the Opentrons from my laptop.

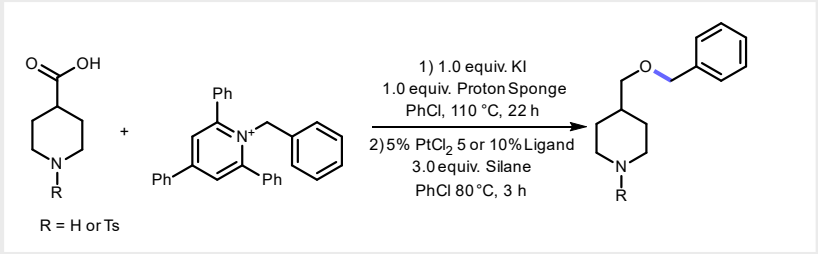

name	molarity	color
N-tosyl isonipectoic acid	0.1	#9511a1
isonipecotic acid	0.1	#9613a1
benzyl kat salt	0.1	#fdab33
PLATINUM(II) CHLORIDE, 99.99+%	0.01	#fbd724
DPPF	0.01	#5002a2
1,2-BIS(DICYCLOHEXYLPHOSPHINO)ETHANE, 98%	0.01	#ca457a
1,2-BIS(DIPHENYLPHOSPHINO)BENZENE 98%	0.01	#8707a6
(R)-BINAP	0.01	#4b03a1
BrettPhos	0.01	#fba238
2-DI-TERT-BUTYLPHOSPHINO-2',4',6'-TRIISOPROPYLBIPHENYL, 97%	0.01	#5c01a6
2-DICYCLOHEXYLPHOSPHINO-2',4',6'-TRIISOPROPYLBIPHENYL, 97%	0.01	#eb7655
ICYCLOHEXYLPHOSPHINO-2',6'-DIISOPROPOXYBIPHENYL, 95% [RUPHOS]	0.01	#c43e7f
AlPhos	0.01	#e4695e
CyJohnPhos	0.01	#c33d80
4,6-BIS(DIPHENYLPHOSPHINO)PHENOXAZINE, 97%	0.01	#48039f
LPHOSPHINO)3,6-DIMETHOXY-2',4',6'-TRIISOPROPYL-1,1'-BIPHENYL, 96%	0.01	#9a169f
(2-BIPHENYLYL)DI-TERT-BUTYLPHOSPHINE, 97%	0.01	#e76f5a
TRI-O-TOLYLPHOSPHINE	0.01	#f2844b
TRI-TERT-BUTYLPHOSPHINE, 98%	0.01	#d14e72
TRIPHENYLPHOSPHINE, 99%	0.01	#e26660
TRIS(4-TRIFLUOROMETHYLPHENYL)PHOSPHINE, 97%	0.01	#fa9c3c
1,3-BIS(DIPHENYLPHOSPHINO)PROPANE, 98.0+%	0.01	#fcd225
ligand blank	0.1	#fdc229
XANTPHOS, 97%	0.01	#f1814d
(OXYDI-2,1-PHENYLENE)BIS(DIPHENYLPHOSPHINE), 98%	0.01	#fec029
CATACXIUM A, 95%	0.01	#fcd225
Me4tButylXphos	0.01	#d9586a
ligand blank 2	0.1	#feba2c
Diphenylsilane	0.3	#d24f71
Phenylsilane, 97+%, Thermo Scientificâ€šÃ¢Ã¢	0.3	#3e049c

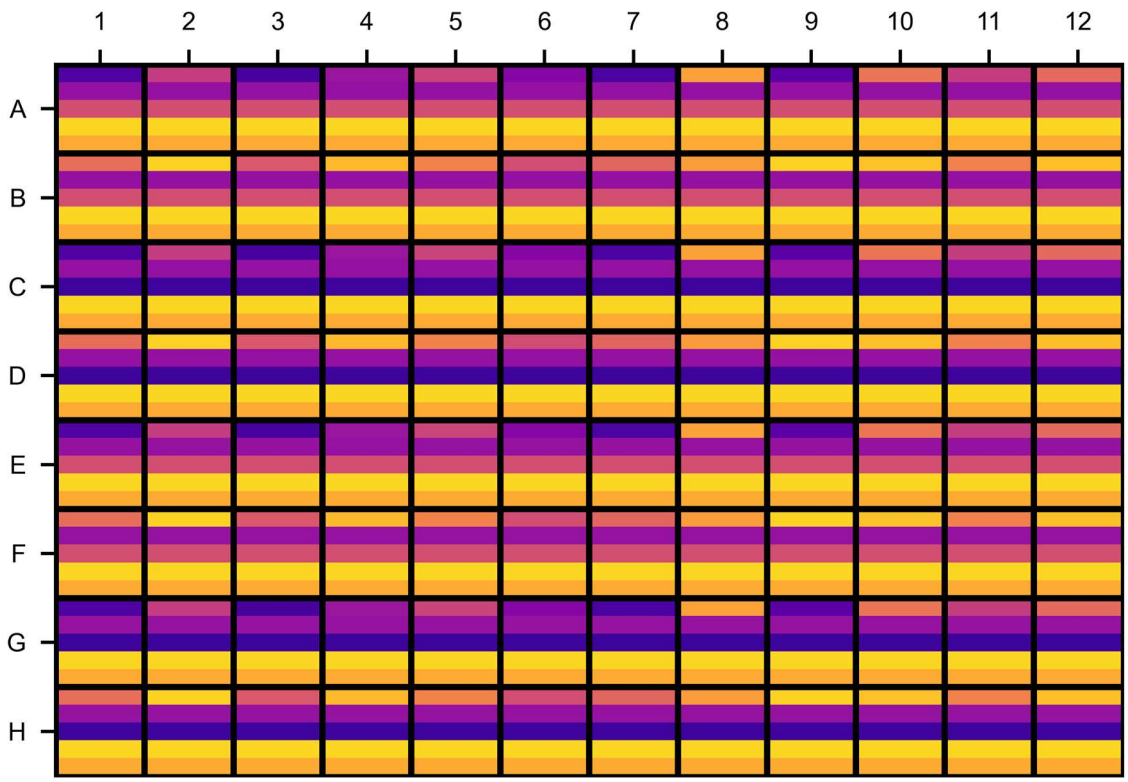
1
2
3
4
5
6
7
8
9
10
11
12
A
B
C
D
E
F
G
H

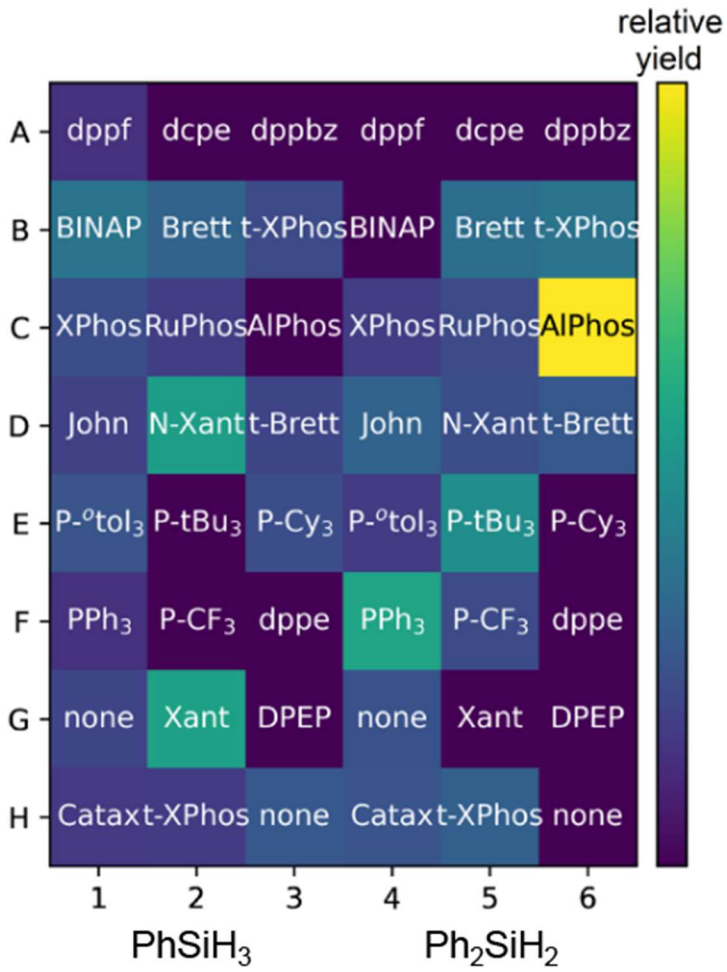

Figure 3.25 Results of remote access ligand/silane screen. Please note only product **3.114** was observed so only half of the heatmap is displayed.

3.4.7.3 Scale up of remote access screen.

Upon scaleup of the best results from the screen it was revealed the major product was actually enol ether **3.115** which has an M-2 mass. Subsequent attempts to reduce this to **3.114** failed.

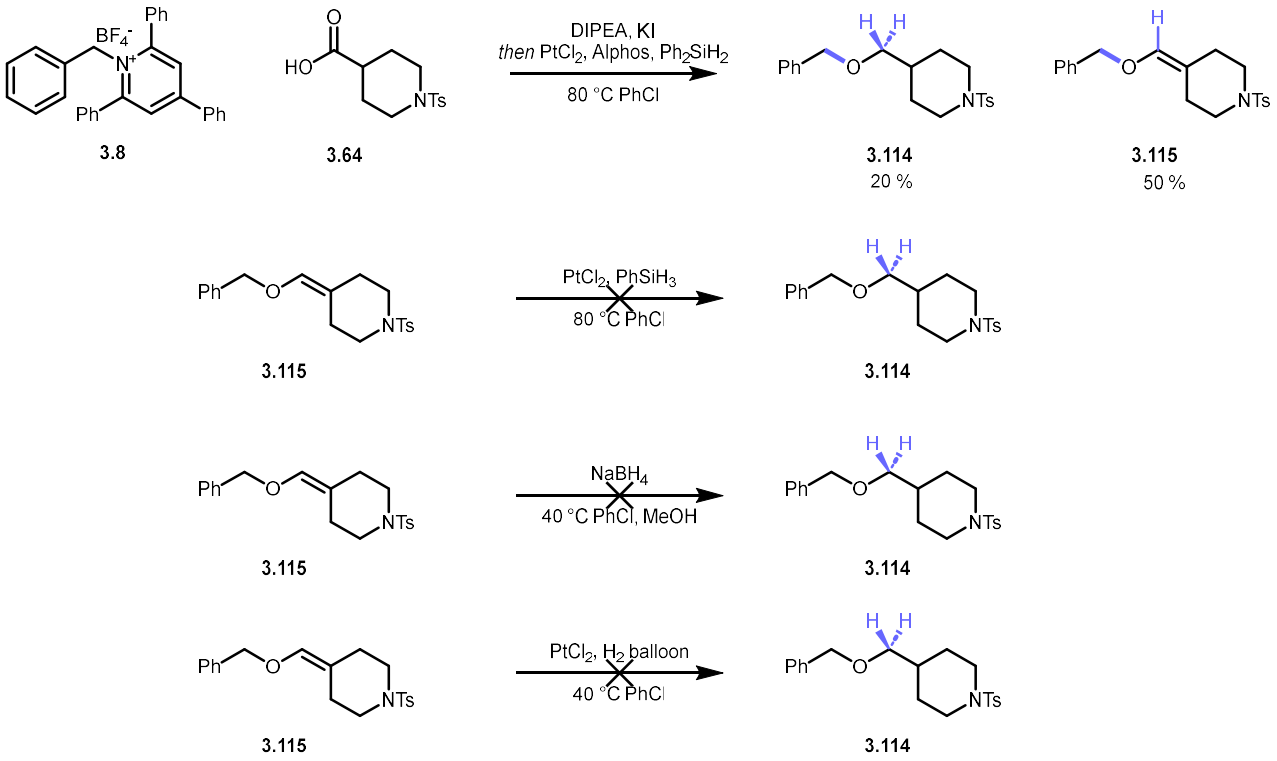

Scheme 3.6 Results of remote access scaleup and subsequent attempts to reduce enol ether.

3.4.7.4 Optimization of platinum based reductive etherification.

Table 3.15 Optimizing platinum source, loading, ligand, silane, and concentration.

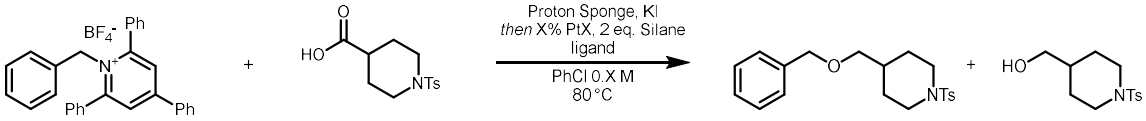

entry	Platinum Salt	Silane	Ligand	Concentration	NMR yield ether (isolated)	NMR yield alcohol
1	$PtCl_2$ (10%)	$PhSiH_3$	None	0.3	61%	35%
2	PtO_2 (10%)	$PhSiH_3$	None	0.3	55%	33%
3	$Pt(COD)Me_2$ (10%)	$PhSiH_3$	None	0.3	62%	34%
4	$PtCl_2$ (20%)	$PhSiH_3$	None	0.3	42%	52%
5	$PtCl_2$ (1%)	$PhSiH_3$	None	0.3	32%	26%
6	$PtCl_2$ (3%)	$PhSiH_3$	None	0.3	62%	35%
7	$PtCl_2$ (3%)	$PhSiH_3$	PPh_3	0.3	20%	73%
8	$PtCl_2$ (3%)	Ph_2SiH_2	None	0.3	21%	10%
9	$PtCl_2$ (3%)	Ph_2SiH_2	PPh_3	0.3	33%	12%
10	$PtCl_2$ (3%)	TMDS	None	0.3	trace	trace
11	$PtCl_2$ (3%)	$PhSiH_3$	None	0.1	40%	48%
12	$PtCl_2$ (3%)	$PhSiH_3$	PPh_3	0.5	55%	37%

Table 3.16 Optimization of ester promoter, base, and solvent as well as investigating the effects of additives.

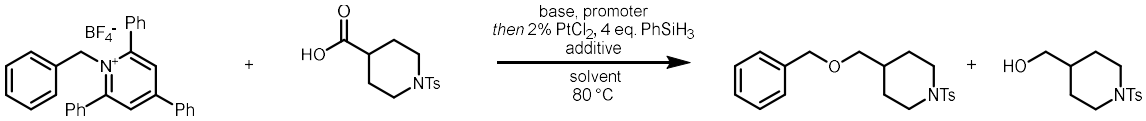

entry	base	Promoter	solvent	additive	NMR yield ether (isolated)	NMR yield alcohol
1	Proton Sponge	KI	PhCl	None	61% (59%)	35%
2	Proton Sponge	BMDM	PhCl	None	Trace	Trace
3	Proton Sponge	KI	DMF	None	0%	0%
4	DIPEA	KI	PhCl	None	61% (60%)	35%
5	DIPEA	KI	PhCl	Water 2 eq	58%	38%
6	DIPEA	KI	PhCl	TMSOTf	59%	37%
7	DIPEA	KI	PhCl	TBAF	40%	54%
8	DIPEA	KI	Dioxane	None	40%	48%
9	DIPEA	KI	Diglyme	None	30%	60%
10	DIPEA	KI	$PhCF_3$	None	65%	37%

additives:

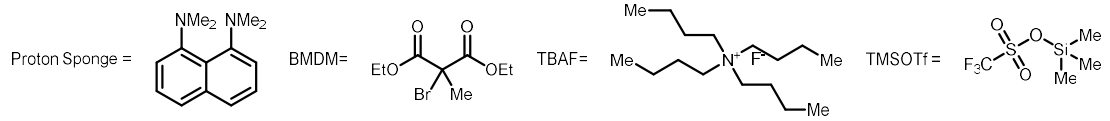

3.4.8 Comparison of gallium and platinum-based conditions.

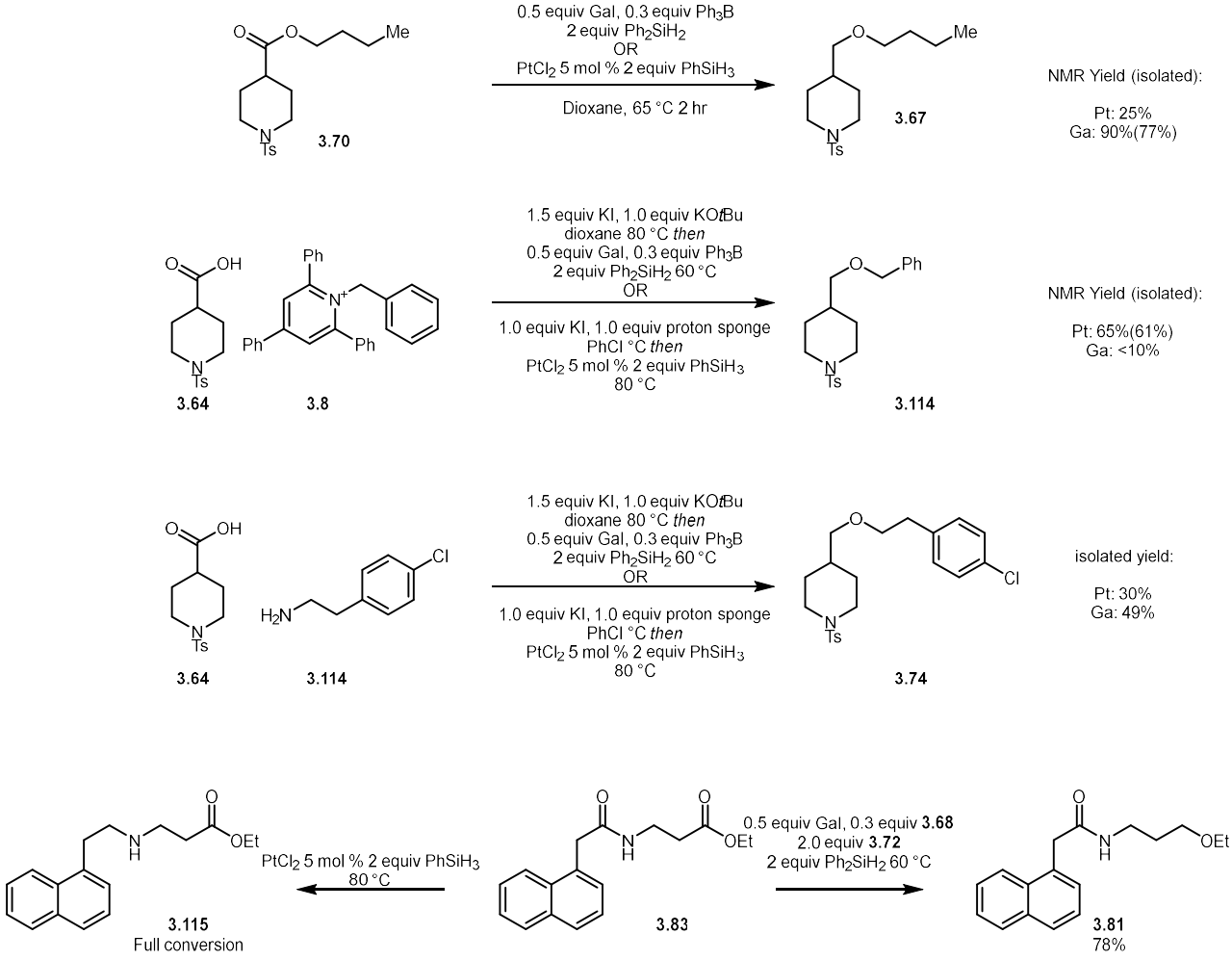

Scheme 3.7 Comparison of Gallium and Platinum based reduction conditions. Gallium is selective for esters and outperforms platinum in non-benzylic esters.

3.4.9 Deaminative amine–phenol etherification optimization

For entries **1-12** all reagents were added in a single step to try and perform a single step operation. This was met with some success on simpler substrates, but on the more complex drug molecules, yields were unacceptable as a single step operation, and a two-step protocol was developed (entries 13-16)

Table 3.17 Optimization of a two-step deaminative phenolic etherification protocol.

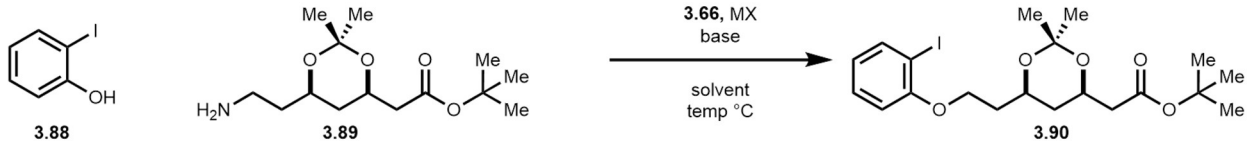

entry	MX	Base	Solvent	Temperature (°C)	NMR yield ether
1	KI	K_2CO_3	Dioxane	110	40%
2	KI	K_2CO_3	DMA	110	15%
3	KBr	K_2CO_3	Dioxane	110	35%
4	KBr	K_2CO_3	DMA	110	14%
5	CsI	K_2CO_3	Dioxane	110	37%
6	CsI	K_2CO_3	DMA	110	18%
7	KI	KOtBu	Dioxane	110	12%
8	KI	LiOtBu	Dioxane	110	10%
9	KI	Cs_2CO_3	Dioxane	110	15%
10	KI	KOtBu	DMA	110	trace
11	KI	LiOtBu	DMA	110	trace
12	KI	Cs_2CO_3	DMA	110	11%
13	KI	K_2CO_3	Dioxane	110 *then* 80	45%
14	KI	K_2CO_3	DMA	110 *then* 80	50%
15	KI	K_2CO_3	1:1 Dioxane:DMA	110 *then* 80	50%
16	KI	K_2CO_3	Dioxane *then* DMA	110 *then* 80	64%

3.4.10 Characterization of alkyl ether products.

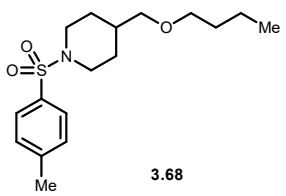

4-(butoxymethyl)-1-tosylpiperidine (3.68)

3.68 was prepared on a 0.2 mmol scale from butyl amine (**3.65)** and **3.64** according to general procedure 3.4 to give 41.9 mg (63%) of a white solid after purification with EtOAc/hexanes.

R_f = 0.32 in 25:75 EtOAc:hexanes

^{1}H NMR (499 MHz, cdcl$_3$) δ 7.64 (d, *J* = 8.3 Hz, 2H), 7.31 (d, *J* = 8.5 Hz, 2H), 3.82 – 3.74 (m, 2H), 3.35 (t, *J* = 6.6 Hz, 2H), 3.20 (d, *J* = 6.5 Hz, 2H), 2.43 (s, 3H), 2.23 (td, *J* = 11.9, 2.6 Hz, 2H), 1.77 (dd, *J* = 13.7, 3.6 Hz, 2H), 1.55 – 1.46 (m, 3H), 1.38 – 1.27 (m, 4H), 0.89 (t, *J* = 7.4 Hz, 3H).

^{13}C NMR (126 MHz, cdcl$_3$) δ 143.5, 134.5, 129.7, 127.9, 77.4, 77.2, 76.9, 75.3, 71.1, 46.3, 35.9, 31.9, 28.7, 21.7, 19.5, 14.0.

HRMS (ESI) Calculated $C_{17}H_{28}NO_3S^+$ $[M+H]^+$: 326.1784, Found 326.1777.

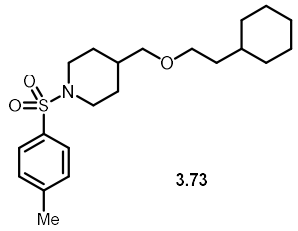

3.73

4-((2-cyclohexylethoxy)methyl)-1-tosylpiperidine (3.73)

3.73 was prepared on a 0.2 mmol scale from 2-cyclohexylethylamine and **3.64** according to general procedure 3.4 to give 41.0 mg (55%) of a white solid after purification with EtOAc/hexanes.

R_f = 0.25 in 25:75 EtOAc:hexanes

^{1}H NMR (401 MHz, CDC$_3$) δ 7.64 (d, *J* = 8.2 Hz, 2H), 7.31 (d, *J* = 8.0 Hz, 2H), 3.78 (d, *J* = 11.6 Hz, 2H), 3.38 (t, *J* = 6.7 Hz, 2H), 3.19 (d, *J* = 6.5 Hz, 2H), 2.43 (s, 3H), 2.23 (td, *J* = 11.9, 2.2 Hz, 2H), 1.76 (d, *J* = 11.2 Hz, 2H), 1.66 (d, *J* = 10.0 Hz, 4H), 1.55 – 1.45 (m, 1H), 1.41 (q, *J* = 6.8 Hz, 2H), 1.33 (tt, *J* = 11.5, 5.9 Hz, 3H), 1.19 (dt, *J* = 19.4, 11.0 Hz, 4H), 0.97 – 0.77 (m, 3H).

^{13}C NMR (101 MHz, CDC$_3$) δ 143.3, 133.4, 129.5, 127.7, 77.3, 77.0, 76.7, 75.2, 69.2, 46.1, 37.0, 35.7, 34.7, 33.3, 28.6, 26.6, 26.3, 21.5.

HRMS (ESI) Calculated $C_{21}H_{34}NO_3S^+$ $[M+H]^+$: 380.2245, Found 380.2250

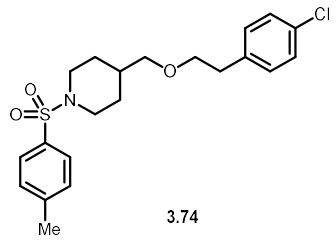

3.74

4-((4-chlorophenethoxy)methyl)-1-tosylpiperidine (3.74)

3.74 was prepared on a 0.2 mmol scale from 2-(4-chlorophenyl)ethylamine and **3.64** according to general procedure 3.4 to give 40.0 mg (49%) of a white solid after purification with EtOAc/hexanes.

R_f = 0.23 in 25:75 EtOAc:hexanes

^{1}H NMR (400 MHz, $CDCl_3$) δ 7.63 (d, *J* = 8.3 Hz, 2H), 7.32 (d, *J* = 8.4 Hz, 2H), 7.23 (d, *J* = 8.4 Hz, 2H), 7.11 (d, *J* = 8.4 Hz, 2H), 3.77 (dt, *J* = 11.0, 2.4 Hz, 2H), 3.55 (t, *J* = 6.8 Hz, 2H), 3.21 (d, *J* = 6.4 Hz, 2H), 2.79 (t, *J* = 6.8 Hz, 2H), 2.43 (s, 3H), 2.20 (td, *J* = 11.9, 2.6 Hz, 2H), 1.76 – 1.67 (m, 2H), 1.52 – 1.40 (m, 1H), 1.30 (qd, *J* = 12.4, 4.4 Hz, 2H).

^{13}C NMR (101 MHz, $CDCl_3$) δ 143.5, 137.7, 133.3, 132.1, 130.4, 129.7, 128.5, 127.8, 75.4, 71.81, 46.2, 35.8, 35.7, 28.6, 21.7.

HRMS (ESI) Calculated $C_{21}H_{27}ClNO_3S^+$ $[M+H]^+$: 408.1395, Found 408.1392

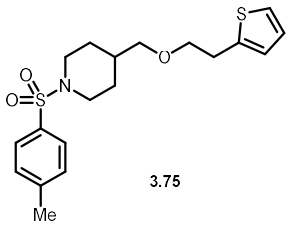

3.75

3.75 was prepared on a 0.05 mmol scale from **3.111** according to general procedure 3.5 using **3.71** to give 12.8 mg (68%) of a yellow oil after purification with EtOAc/hexanes.

R_f = 0.25 in 30:70 EtOAc:hexanes

^{1}H NMR (499 MHz, $CDCl_3$) δ 7.64 (d, *J* = 8.3 Hz, 2H), 7.32 (d, *J* = 8.0 Hz, 2H), 7.12 (dd, *J* = 5.2, 1.2 Hz, 1H), 6.91 (dd, *J* = 5.1, 3.4 Hz, 1H), 6.81 (dd, *J* = 3.4, 1.1 Hz, 1H), 3.78 (dt, *J* = 11.3, 2.9 Hz, 2H), 3.60 (t, *J* = 6.6 Hz, 2H), 3.26 (d, *J* = 6.4 Hz, 2H), 3.04 (td, *J* = 6.6, 0.9 Hz, 2H), 2.43 (s, 3H), 2.23 (td, *J* = 11.9, 2.6 Hz, 2H), 1.77 (dd, *J* = 13.7, 3.7 Hz, 2H), 1.56 – 1.45 (m, 1H), 1.34 (qd, *J* = 11.9, 4.2 Hz, 2H).

^{13}C NMR (126 MHz, $CDCl_3$) δ 143.4, 141.3, 134.3, 129.6, 127.7, 126.6, 125.1, 123.7, 75.3, 71.6, 46.1, 35.7, 30.4, 28.5, 21.5.

HRMS (ESI) Calculated $C_{19}H_{25}NO_3S_2^+$ $[M+H]^+$: 379.1276, Found 379.1277.

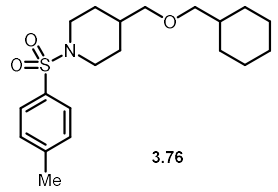

3.76

4-((cyclohexylmethoxy)methyl)-1-tosylpiperidine (3.76)

3.76 was prepared on a 0.2 mmol scale from cyclohexylmethylamine and **3.64** according to general procedure 3.4 to give 34.8 mg (48%) of a clear oil after purification with EtOAc/hexanes.

R_f = 0.30 in 25:75 EtOAc:hexanes

^{1}H NMR (499 MHz, $CDCl_3$) δ 7.64 (d, *J* = 8.3 Hz, 2H), 7.31 (d, *J* = 7.9 Hz, 2H), 3.78 (dt, *J* = 11.5, 2.2 Hz, 2H), 3.19 (d, *J* = 6.4 Hz, 2H), 3.14 (d, *J* = 6.5 Hz, 2H), 2.43 (s, 3H), 2.23 (td, *J* = 11.9, 2.6 Hz, 2H), 1.76 (dd, *J* = 13.4, 3.4 Hz, 2H), 1.72 – 1.61 (m, 6H), 1.57 – 1.43 (m, 1H), 1.33 (qd, *J* = 12.0, 4.2 Hz, 2H), 1.28 – 1.06 (m, 3H), 0.93 – 0.82 (m, 2H).

^{13}C NMR (126 MHz, $CDCl_3$) δ 143.5, 134.5, 129.7, 127.9, 75.4, 46.3, 38.2, 35.8, 30.2, 28.7, 26.76, 26.0, 21.7.

HRMS (ESI) Calculated $C_{20}H_{32}NO_3S^+$ $[M+H]^+$: 366.2097, Found 366.2097.

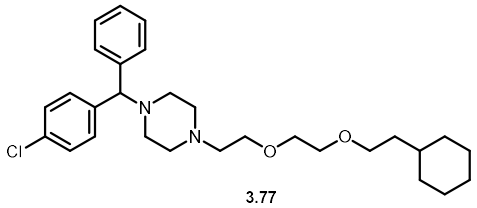

3.77

1-((4-chlorophenyl)(phenyl)methyl)-4-(2-(2-(2-cyclohexylethoxy)ethoxy)ethyl)piperazine (3.77)

3.77 was prepared on a 0.2 mmol scale from 2-cyclohexylethylamine and cetirizine via a modified general procedure 3.4 where an extra 1.5 equiv of GaI_3 was used to give 40.7 mg (42%) of a white solid after purification by preparative HPLC.

^{1}H NMR (499 MHz, $CDCl_3$) δ 7.26 – 7.23 (m, 5H), 7.22 (d, *J* = 4.5 Hz, 4H), 4.02 (s, 1H), 3.74 – 3.69 (m, 2H), 3.54 – 3.49 (m, 2H), 3.43 (t, *J* = 4.6 Hz, 2H), 3.33 (t, *J* = 7.1 Hz, 4H), 3.00 (t, *J* = 4.7 Hz, 2H), 2.87 (t, *J* = 11.8 Hz, 2H), 2.72 (d, *J* = 13.1 Hz, 2H), 2.07 (d, *J* = 12.8 Hz, 3H), 1.64 – 1.49 (m, 6H), 1.28 (q, *J* = 7.0 Hz, 3H), 1.18 (tdd, *J* = 14.0, 6.8, 3.4 Hz, 2H), 1.08 (dd, *J* = 8.3, 2.4 Hz, 2H), 0.77 (qd, *J* = 11.4, 3.5 Hz, 2H).

^{13}C NMR (126 MHz, $CDCl_3$) δ 133.5, 129.2, 129.1, 128.7, 128.0, 127.3, 74.6, 70.5, 69.6, 69.4, 64.9, 53.5, 48.0, 37.0, 34.6, 33.3, 26.4, 26.2.

HRMS (ESI) Calculated $C_{29}H_{42}ClN_2O_2^+$ $[M+H]^+$: 485.2929, Found 485.2932

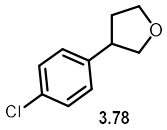

3.78

3.78 was prepared on a 0.2 mmol scale from baclofen via a modified general procedure 3.4 where DIPEA was used instead of KO*t*-Bu was used to give 24.8 mg (68%) of a clear oil after purification with EtOAc/hexanes.

R_f = 0.65 in 15:85 EtOAc:hexanes

^{1}H NMR (499 MHz, $CDCl_3$) δ 7.27 (d, *J* = 13.1 Hz, 2H), 7.18 (d, *J* = 8.5 Hz, 2H), 4.11 (t, *J* = 8.1 Hz, 1H), 4.06 (td, *J* = 8.4, 4.6 Hz, 1H), 3.91 (q, *J* = 8.0 Hz, 1H), 3.70 (dd, *J* = 8.5, 7.2 Hz, 1H), 3.38 (p, *J* = 7.7 Hz, 1H), 2.36 (dtd, *J* = 12.4, 7.8, 4.6 Hz, 1H), 1.96 (dq, *J* = 12.4, 7.9 Hz, 1H).

^{13}C NMR (126 MHz, $CDCl_3$) δ 141.5, 132.4, 128.8, 128.7, 74.7, 68.6, 44.5, 34.8.

Did not ionize on UPLC-MS

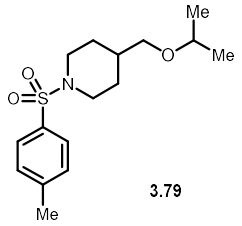

3.79

4-(isopropoxymethyl)-1-tosylpiperidine (3.79)

3.79 was prepared on a 0.2 mmol scale from **3.64** and isopropylamine according to general procedure 3.4 to give 16.8 mg (27%) of a clear oil after purification with EtOAc/hexanes.

^{1}H NMR (401 MHz, $CDCl_3$) δ 7.64 (d, *J* = 8.0 Hz, 2H), 7.31 (d, *J* = 7.8 Hz, 2H), 3.79 (d, *J* = 11.3 Hz, 2H), 3.48 (dt, *J* = 11.8, 6.1 Hz, 1H), 3.21 (d, *J* = 6.2 Hz, 2H), 2.43 (s, 3H), 2.23 (t, *J* = 10.7 Hz, 2H), 1.78 (d, *J* = 13.5 Hz, 2H), 1.49 – 1.41 (m, 1H), 1.37 – 1.25 (m, 3H), 1.10 (d, *J* = 6.1 Hz, 6H).

^{13}C NMR (151 MHz, $CDCl_3$) δ 143.3 133.3, 129.5, 127.7, 72.5, 71.7, 46.1, 36.0, 28.6, 22.0, 21.5.

LRMS (UPLC) Calculated $C_{16}H_{26}NO_3S^+$ $[M+H]^+$: 312, Found 312

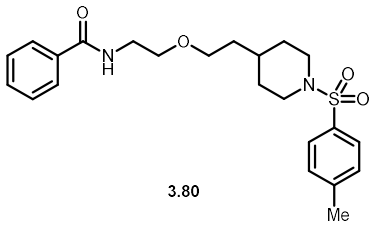

3.80

***N*-(2-(2-(1-tosylpiperidin-4-yl)ethoxy)ethyl)benzamide (3.80)**

3.80 was prepared on a 0.10 mmol scale from **3.112** according to general procedure 3.5 using **3.68** to give 29.5 mg (69%) of a white solid after purification with EtOAc.

R_f = 0.28 in 100:0 EtOAc:hexanes

^{1}H NMR (499 MHz, $CDCl_3$) δ 7.69 (d, *J* = 7.0 Hz, 2H), 7.60 (d, *J* = 8.3 Hz, 2H), 7.48 (t, *J* = 7.4 Hz, 1H), 7.37 (t, *J* = 7.8 Hz, 2H), 7.31 (d, *J* = 8.0 Hz, 2H), 6.49 (t, *J* = 5.5 Hz, 1H), 3.71 (d, *J* = 11.4 Hz, 2H), 3.57 (q, *J* = 5.5 Hz, 2H), 3.52 (t, *J* = 5.1 Hz, 2H), 3.45 (t, *J* = 6.4 Hz, 2H), 2.44 (s, 3H), 2.17 (t, *J* = 11.5 Hz, 2H), 1.70 (d, *J* = 9.5 Hz, 2H), 1.49 (q, *J* = 6.0 Hz, 2H), 1.32 – 1.25 (m, 3H).

^{13}C NMR (126 MHz, $CDCl_3$) δ 167.8, 143.6, 134.4, 133.1, 131.7, 129.7, 128.7, 127.8, 126.9, 69.3, 68.6, 46.5, 39.8, 35.7, 32.4, 31.6, 21.6.

LRMS (UPLC) Calculated $C_{23}H_{31}N_2O_4S^+$ $[M+H]^+$: 431, Found 431

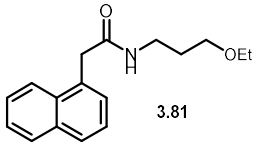

3.81

N-(3-ethoxypropyl)-2-(naphthalen-1-yl)acetamide (3.81)

3.81 was prepared on a 0.20 mmol scale from **3.83** according to general procedure 3.5 using **3.68** to give 42.1 mg (78 %) of a white solid after purification with EtOAc.

^{1}H NMR (400 MHz, $CDCl_3$) δ 7.96 – 7.89 (m, 1H), 7.89 – 7.83 (m, 1H), 7.81 (d, *J* = 8.2 Hz, 1H), 7.56 – 7.45 (m, 2H), 7.44 (dd, *J* = 8.2, 7.0 Hz, 1H), 7.37 (dd, *J* = 7.0, 1.3 Hz, 1H), 5.92 (s,

1H), 3.97 (s, 2H), 3.27 – 3.17 (m, 4H), 3.12 (q, *J* = 7.0 Hz, 2H), 1.55 (p, *J* = 6.0 Hz, 2H), 0.89 (t, *J* = 7.0 Hz, 3H).

^{13}C NMR (101 MHz, $CDCl_3$) δ 171.2, 134.0, 132.2, 131.2, 128.9, 128.6, 126.8, 126.3, 125.8, 123.90, 77.5, 77.2, 76.8, 69.0, 66.2, 41.9, 38.3, 28.9, 15.0.

HRMS (ESI) Calculated $C_{17}H_{22}NO_2^+$ $[M+H]^+$: 272.1645, Found 272.1655

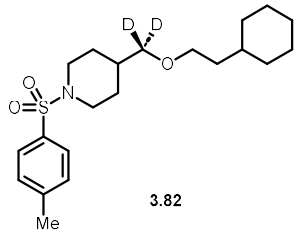

3.82

4-((2-cyclohexylethoxy)methyl-*d2*)-1-tosylpiperidine (3.82)

3.79 was prepared on a 0.10 mmol scale from **3.64** and 2-cyclohexylethylamine according to a modified general procedure 3.4 using deuterated phenylsilane[61] to give 17.1 mg (45%) of a clear oil after purification with EtOAc/hexanes.

^{1}H NMR (600 MHz, cdcl$_3$) δ 7.64 (d, *J* = 8.2 Hz, 2H), 7.31 (d, *J* = 8.0 Hz, 2H), 3.78 (d, *J* = 11.6 Hz, 2H), 3.38 (t, *J* = 6.8 Hz, 2H), 2.43 (s, 3H), 2.24 (td, *J* = 11.9, 2.3 Hz, 2H), 1.76 (d, *J* = 11.0 Hz, 2H), 1.66 (d, *J* = 10.7 Hz, 5H), 1.48 (ddt, *J* = 11.7, 6.8, 3.5 Hz, 1H), 1.41 (q, *J* = 6.8 Hz, 2H), 1.32 (qd, *J* = 12.4, 4.1 Hz, 3H), 1.25 – 1.08 (m, 4H), 0.94 – 0.83 (m, 2H).

^{13}C NMR (151 MHz, cdcl$_3$) δ 143.31, 133.32, 129.54, 127.69, 77.21, 77.00, 76.79, 69.12, 46.12, 37.06, 35.50, 34.63, 33.34, 28.53, 26.57, 26.27, 21.51.

LRMS (UPLC) Calculated $C_{21}H_{32}D_2NO_3S^+$ $[M+H]^+$: 382, Found 382

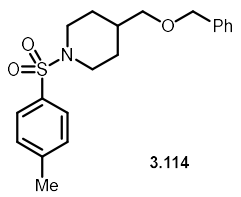

3.114

4-((benzyloxy)methyl)-1-tosylpiperidine (3.114)

3.114 was prepared on a 0.20 mmol scale according to general procedure from **3.65** and **3.8** via general procedure 3.6 to give 43.8 mg (61%) of a clear oil after purification with EtOAc/hexanes.

R_f = 0.38 in 25:75 EtOAc:hexanes

^{1}H NMR (499 MHz, $CDCl_3$) δ 7.64 (d, *J* = 8.3 Hz, 2H), 7.39 – 7.30 (m, 4H), 7.29 – 7.27 (m, 2H), 4.46 (s, 2H), 3.78 (dt, *J* = 11.5, 2.7 Hz, 2H), 3.28 (d, *J* = 6.5 Hz, 2H), 2.43 (s, 3H), 2.24 (td, *J* = 12.0, 2.6 Hz, 2H), 1.84 – 1.76 (m, 2H), 1.35 (qd, *J* = 12.0, 4.2 Hz, 2H).

^{13}C NMR (126 MHz, $CDCl_3$) δ 143.5, 138.5, 133.5, 129.7, 128.5, 127.9, 127.8, 127.7, 74.7, 73.2, 46.3, 35.9, 28.7, 21.7.

HRMS (ESI) Calculated $C_{20}H_{26}NO_3S^+$ $[M+H]^+$: 360.1628, Found 360.1625

3.4.11 Characterization of phenolic ether products

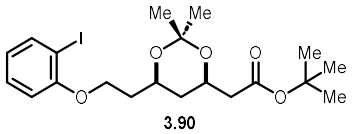

3.90

***tert*-butyl 2-((4*R*,6*R*)-6-(2-(2-iodophenoxy)ethyl)-2,2-dimethyl-1,3-dioxan-4-yl)acetate**

3.90 was prepared on a 0.2 mmol scale from 2-iodophenol and *tert*-butyl 2-((4*R*,6*R*)-6-(2-aminoethyl)-2,2-dimethyl-1,3-dioxan-4-yl)acetate via general procedure 3.7 to give 61.0 mg (64%) of a clear oil after purification with EtOAc/hexanes.

^{1}H NMR (499 MHz, $CDCl_3$) δ 7.76 (dd, *J* = 7.8, 1.6 Hz, 1H), 7.28 (ddd, *J* = 8.2, 7.3, 1.6 Hz, 1H), 6.82 (dd, *J* = 8.2, 1.3 Hz, 1H), 6.70 (td, *J* = 7.6, 1.3 Hz, 1H), 4.30 (qdd, *J* = 11.8, 5.2, 2.4 Hz, 2H), 4.14 (td, *J* = 8.8, 4.8 Hz, 1H), 4.12 – 4.04 (m, 1H), 2.44 (dd, *J* = 15.1, 7.2 Hz, 1H), 2.32 (dd, *J* = 15.1, 6.0 Hz, 1H), 2.04 – 1.87 (m, 2H), 1.67 (dt, *J* = 12.7, 2.5 Hz, 1H), 1.46 (s, 3H), 1.44 (s, 9H), 1.36 (s, 3H), 1.34 – 1.23 (m, 1H).

^{13}C NMR (126 MHz, $CDCl_3$) δ 170.4, 157.6, 139.5, 129.6, 122.6, 112.3, 99.0, 86.8, 80.7, 66.4, 65.7, 65.0, 42.9, 36.8, 35.9, 30.2, 28.3, 20.0

HRMS (ESI) Calculated $C_{20}H_{29}INaO_5^+$ $[M+Na]^+$: 499.0952, Found 499.0944

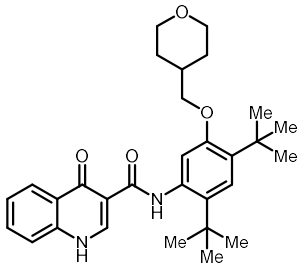

3.91

_N_-(2,4-di-tert-butyl-5-((tetrahydro-2_H_-pyran-4-yl)methoxy)phenyl)-4-oxo-1,4-dihydroquinoline-3-carboxamide (3.91)

Compound **3.91** was prepared on a 0.20 mmol scale from ivacaftor and 4-tetrahydropyranyl methanamine via general procedure 3.7 to give 39.2 mg (40%) of a white solid after purification by preparative LC.

^{1}H NMR (400 MHz, $CDCl_3$) δ 11.91 (s, 1H), 8.87 (s, 1H), 8.59 (dd, *J* = 8.3, 1.6 Hz, 1H), 7.76 (ddd, *J* = 8.7, 7.1, 1.6 Hz, 1H), 7.55 – 7.46 (m, 2H), 7.27 (s, 2H), 7.15 (s, 1H), 4.13 (d, *J* = 7.2

Hz, 2H), 3.91 (dd, *J* = 11.5, 3.8 Hz, 2H), 3.26 (td, *J* = 11.1, 2.6 Hz, 2H), 2.16 (s, 1H), 1.56 – 1.42 (m, 13H), 1.38 (s, 9H).

^{13}C NMR (101 MHz, $CDCl_3$) δ 176.8, 153.5, 148.7, 139.3, 134.0, 133.2, 133.2, 132.8, 128.1, 128.0, 125.4, 125.1, 125.1, 116.4, 116.0, 111.5, 67.2, 59.7, 34.9, 34.8, 34.5, 31.0, 30.4, 29.8.

HRMS (ESI) Calculated $C_{30}H_{39}N_2O_4^+$ $[M+H]^+$: 491.2904, Found 491.2914

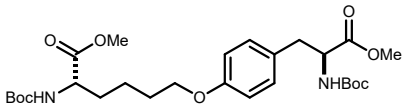

3.92

methyl (*S*)-2-((*tert*-butoxycarbonyl)amino)-6-(4-((*S*)-2-((*tert*-butoxycarbonyl)amino)-3-methoxy-3-oxopropyl)phenoxy)hexanoate (3.92)

Compound **3.92** was prepared on a 0.10 mmol scale from N-α-Boc lysine methyl ester hydrochloride and boc tyrosine methyl ester via general procedure 3.7 to give 18.6 mg (35%) of a white solid after purification by preparative LC.

^{1}H NMR (400 MHz, $CDCl_3$) δ 7.01 (d, *J* = 8.4 Hz, 2H), 6.79 (d, *J* = 8.5 Hz, 2H), 5.03 (d, *J* = 8.5 Hz, 1H), 4.95 (d, *J* = 8.1 Hz, 1H), 4.53 (q, *J* = 6.6 Hz, 1H), 4.32 (q, *J* = 6.3 Hz, 1H), 3.91 (t, *J* = 6.3 Hz, 2H), 3.74 (s, 3H), 3.71 (s, 3H), 3.01 (t, *J* = 6.8 Hz, 2H), 1.84 (dd, *J* = 20.4, 7.5 Hz, 2H), 1.76 – 1.62 (m, 4H), 1.53 (q, *J* = 7.8 Hz, 1H), 1.44 (s, 10H), 1.42 (s, 9H).

^{13}C NMR (101 MHz, $CDCl_3$) δ 172.6, 158.2, 130.4, 128.0, 114.6, 79.9, 67.5, 54.7, 53.5, 52.5, 52.4, 37.6, 32.7, 31.7, 28.9, 28.5, 22.2.

HRMS (ESI) Calculated $C_{27}H_{42}N_2NaO_9^+$ $[M+Na]^+$: 561.2783, Found 561.2763

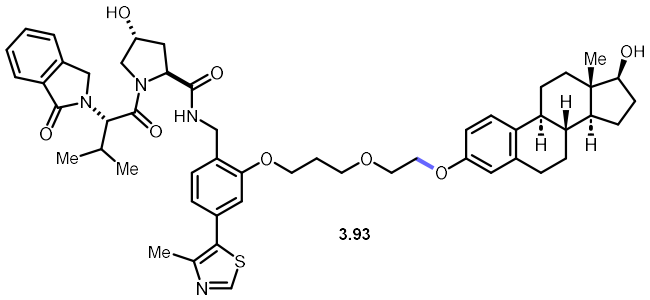

(*2S*,*4R*)-4-hydroxy-*N*-(2-(3-(2-(((*8R*,*9S*,*13S*,*14S*,*17S*)-17-hydroxy-13-methyl-7,8,9,11,12,13,14,15,16,17-decahydro-*6H*-cyclopenta[*a*]phenanthren-3-yl)oxy)ethoxy)propoxy)-4-(4-methylthiazol-5-yl)benzyl)-1-((*S*)-3-methyl-2-(1-oxoisoindolin-2-yl)butanoyl)pyrrolidine-2-carboxamide (3.93)

Compound **3.93** was prepared on a 0.10 mmol scale from (*8R*,*9S*,*13S*,*14S*,*17S*)-3-(2-(2-aminoethoxy)ethoxy)-13-methyl-7,8,9,11,12,13,14,15,16,17-decahydro-*6H*-cyclopenta[*a*]phenanthren-17-ol hydrochloride and estradiol via general procedure 3.7 to give 22.5 mg (25%) of a white solid after purification by preparative LC.

^{1}H NMR (499 MHz, $CDCl_3$) δ 8.73 (s, 1H), 7.79 (d, *J* = 7.6 Hz, 1H), 7.54 (td, *J* = 7.5, 1.1 Hz, 1H), 7.44 (dd, *J* = 12.0, 7.9 Hz, 2H), 7.32 (dd, *J* = 9.6, 6.8 Hz, 2H), 7.16 (d, *J* = 8.6 Hz, 1H), 6.97 (dd, *J* = 7.7, 1.6 Hz, 1H), 6.91 (d, *J* = 1.6 Hz, 1H), 6.68 (dd, *J* = 8.6, 2.8 Hz, 1H), 6.61 (d, *J* = 2.7 Hz, 1H), 4.77 (d, *J* = 6.3 Hz, 1H), 4.74 (s, 1H), 4.65 (t, *J* = 7.9 Hz, 1H), 4.53 (d, *J* = 5.8 Hz, 1H), 4.51 – 4.45 (m, 2H), 4.44 (d, *J* = 6.1 Hz, 1H), 4.16 (td, *J* = 6.2, 1.9 Hz, 2H), 4.09 (t, *J* = 4.5 Hz, 2H), 3.82 (dd, *J* = 5.6, 4.0 Hz, 2H), 3.78 (t, *J* = 6.0 Hz, 2H), 3.73 (t, *J* = 8.5 Hz, 1H), 3.64 (dd, *J* = 11.5, 3.5 Hz, 1H), 3.50 (s, 2H), 2.80 (dd, *J* = 12.7, 6.2 Hz, 2H), 2.54 (s, 3H), 2.41 (dt, *J* = 11.0, 6.5 Hz, 2H), 2.30 (ddd, *J* = 13.5, 10.0, 5.5 Hz, 4H), 2.22 – 2.15 (m, 7H), 2.15 – 2.07 (m, 1H), 2.08 – 2.00 (m, 2H), 1.94 (dt, *J* = 12.5, 3.3 Hz, 1H), 1.89 – 1.82 (m, 1H), 1.72 – 1.64 (m, 1H),

1.49 (ddd, *J* = 20.8, 12.0, 5.5 Hz, 2H), 1.42 – 1.13 (m, 8H), 0.90 (dd, *J* = 6.6, 3.6 Hz, 6H), 0.77 (s, 3H).

^{13}C NMR (126 MHz, $CDCl_3$) δ 170.4, 170.3, 169.6, 156.8, 156.6, 150.5, 142.1, 138.0, 132.9, 132.0, 131.8, 131.6, 129.4, 128.0, 127.9, 126.5, 126.3, 123.8, 122.9, 121.5, 114.6, 112.1, 112.1, 81.9, 70.0, 69.6, 67.9, 67.4, 65.1, 58.7, 58.4, 55.9, 50.0, 47.5, 43.9, 43.2, 38.9, 38.8, 36.7, 35.6, 30.9, 30.6, 29.8, 29.6, 28.7, 27.2, 26.3, 23.1, 19.1, 19.0, 15.9, 11.1.

HRMS (ESI) Calculated $C_{52}H_{65}N_4O_8S^+$ $[M+H]^+$: 945.4518, Found 945.4506

3.4.12 Characterization of alkyl halide products.

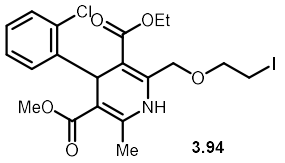

3.94

3-ethyl 5-methyl 4-(2-chlorophenyl)-2-((2-iodoethoxy)methyl)-6-methyl-1,4-dihydropyridine-3,5-dicarboxylate (3.94)

Compound **3.94** was prepared on a 0.20 mmol scale from amlodipine besylate and potassium iodide via general procedure 3.8 to give 74.7 mg (72%) of a yellow oil after purification with EtOAc/hexanes.

R_f = 0.65 in 25:75 EtOAc:hexanes

^{1}H NMR (499 MHz, $CDCl_3$) δ 7.39 (dd, *J* = 7.8, 1.7 Hz, 1H), 7.24 (d, *J* = 8.4 Hz, 2H), 7.15 (t, *J* = 7.5 Hz, 1H), 7.08 – 7.03 (m, 1H), 5.42 (s, 1H), 4.80 (q, *J* = 16.1 Hz, 2H), 4.05 (tt, *J* = 10.7, 5.4

Hz, 2H), 3.82 (qt, *J* = 11.0, 5.9 Hz, 2H), 3.63 (s, 3H), 3.38 (t, *J* = 5.9 Hz, 2H), 2.39 (s, 3H), 1.19 (t, *J* = 7.1 Hz, 3H).

^{13}C NMR (126 MHz, $CDCl_3$) δ 168.0, 167.2, 145.7, 144.9, 144.0, 132.4, 131.5, 129.3, 127.4, 126.9, 104.0, 101.6, 71.1, 67.6, 59.8, 50.8, 37.2, 19.6, 14.3, 3.6.

HRMS (ESI) Calculated $C_{20}H_{24}ClIN_4O_5^+$ $[M+H]^+$: 520.0382, Found 520.0388

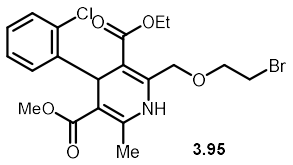

3.95

Compound **3.95** was prepared on a 0.20 mmol scale from amlodipine besylate and potassium bromide via general procedure 3.8 to give 81.1 mg (86%) of a yellow oil after purification with EtOAc/hexanes.

R_f = 0.65 in 25:75 EtOAc:hexanes

^{1}H NMR (400 MHz, $CDCl_3$) δ 7.38 (dd, *J* = 7.8, 1.7 Hz, 1H), 7.25 (s, 1H), 7.23 (dd, *J* = 7.9, 1.4 Hz, 1H), 7.14 (td, *J* = 7.5, 1.4 Hz, 1H), 7.04 (ddd, *J* = 7.8, 1.7, 0.0 Hz, 1H), 5.41 (s, 1H), 4.76 (dd, *J* = 16.2, 11.5 Hz, 2H), 4.04 (qt, *J* = 7.2, 3.6 Hz, 2H), 3.96 – 3.82 (m, 2H), 3.61 (s, 3H), 3.59 (t, *J* = 5.3 Hz, 2H), 2.36 (s, 3H), 1.18 (t, *J* = 7.1 Hz, 3H).

^{13}C NMR (101 MHz, $CDCl_3$) δ 168.1, 167.3, 145.8, 145.1, 144.2, 132.5, 131.6, 129.4, 127.5, 127.0, 104.1, 101.7, 71.1, 67.9, 60.0, 51.0, 37.4, 37.3, 31.3, 19.64, 19.62, 14.4.

HRMS (ESI) Calculated $C_{20}H_{24}ClBrN_4O_5^+$ $[M+H]^+$: 472.0521, Found 472.0519

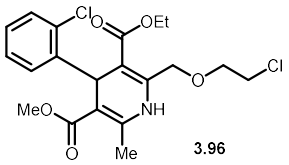

3.96

Compound **3.96** was prepared on a 0.20 mmol scale from amlodipine besylate and lithium chloride via general procedure 3.8 to give 30.8 mg (36%) of a yellow oil after purification with EtOAc/hexanes.

R_f = 0.63 in 25:75 EtOAc:hexanes

^{1}H NMR (400 MHz, $CDCl_3$) δ 7.38 (dd, *J* = 7.7, 1.7 Hz, 1H), 7.23 (dd, *J* = 8.0, 1.4 Hz, 3H), 7.14 (td, *J* = 7.5, 1.4 Hz, 1H), 7.04 (td, *J* = 7.6, 1.7 Hz, 1H), 5.41 (s, 1H), 4.79 (dd, *J* = 16.1, 14.8 Hz, 2H), 4.05 (tt, *J* = 7.1, 3.7 Hz, 2H), 3.91 – 3.76 (m, 2H), 3.74 (t, *J* = 4.7 Hz, 2H), 3.62 (s, 3H), 2.35 (s, 3H), 1.19 (t, *J* = 7.1 Hz, 3H).

^{13}C NMR (101 MHz, $CDCl_3$) δ 168.1, 167.4, 145.8, 145.1, 144.2, 132.5, 131.6, 129.4, 127.5, 127.0, 104.1, 101.8, 71.4, 68.0, 60.0, 50.9, 43.5, 37.4, 37.4, 19.6, 14.4.

HRMS (ESI) Calculated $C_{20}H_{24}Cl_2N_4O_5^+$ $[M+H]^+$: 428.1026, Found 428.1016

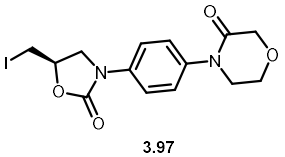

3.97

(*R*)-4-(4-(5-(iodomethyl)-2-oxooxazolidin-3-yl)phenyl)morpholin-3-one (3.97)

Compound **3.97** was prepared on a 0.20 mmol scale from (*S*)-4-(4-(5-(aminomethyl)-2-oxooxazolidin-3-yl)phenyl)morpholin-3-one and KI via general procedure 3.8 to give 54.5 mg (68%) of a yellow oil after purification with EtOAc/hexanes.

R_f = 0.27 in 100:0 EtOAc:hexanes

^{1}H NMR (499 MHz, $CDCl_3$) δ 7.60 (d, *J* = 8.9 Hz, 2H), 7.36 (d, *J* = 8.9 Hz, 2H), 4.74 (tdd, *J* = 8.4, 5.9, 3.9 Hz, 1H), 4.34 (s, 2H), 4.18 (t, *J* = 8.9 Hz, 1H), 4.04 (dd, *J* = 5.6, 4.5 Hz, 2H), 3.80 (dd, *J* = 9.2, 6.0 Hz, 1H), 3.75 (dd, *J* = 9.9, 5.2 Hz, 3H), 3.48 (dd, *J* = 10.4, 3.9 Hz, 1H), 3.37 (dd, *J* = 10.4, 8.2 Hz, 1H).

^{13}C NMR (126 MHz, $CDCl_3$) δ 166.80, 136.51, 126.23, 119.15, 71.19, 68.57, 64.11, 51.01, 49.65, 5.97.

HRMS (ESI) Calculated $C_{14}H_{16}IN_2O_4^+$ $[M+H]^+$: 403.0149, Found 403.0132

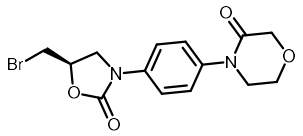

3.98

(*R*)-4-(4-(5-(bromomethyl)-2-oxooxazolidin-3-yl)phenyl)morpholin-3-one (3.98)

Compound **3.98** was prepared on a 0.20 mmol scale from (*S*)-4-(4-(5-(aminomethyl)-2-oxooxazolidin-3-yl)phenyl)morpholin-3-one and KBr via general procedure 3.8 to give 52.6 mg (75%) of a yellow oil after purification with EtOAc/hexanes.

R_f = 0.25 in 100:0 EtOAc:hexanes

^{1}H NMR (499 MHz, $CDCl_3$) δ 7.60 (d, *J* = 9.0 Hz, 2H), 7.36 (d, *J* = 8.9 Hz, 2H), 4.97 – 4.80 (m, 1H), 4.34 (s, 2H), 4.18 (t, *J* = 8.9 Hz, 1H), 4.04 (dd, *J* = 5.6, 4.5 Hz, 2H), 3.93 (dd, *J* = 9.2, 5.8 Hz, 1H), 3.76 (dd, *J* = 5.9, 4.2 Hz, 2H), 3.65 (dd, *J* = 10.8, 3.8 Hz, 1H), 3.57 (dd, *J* = 10.8, 7.4 Hz, 1H).

^{13}C NMR (126 MHz, $CDCl_3$) δ 166.8, 153.8, 137.4, 136.5, 126.2, 119.1, 70.6, 68.6, 64.1, 49.6, 49.2, 32.5.

HRMS (ESI) Calculated $C_{14}H_{16}BrN_2O_4^+$ $[M+H]^+$: 355.0288, Found 355.0231

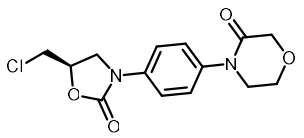

3.99

(*R*)-4-(4-(5-(chloromethyl)-2-oxooxazolidin-3-yl)phenyl)morpholin-3-one (3.99)

Compound **3.99** was prepared on a 0.20 mmol scale from (*S*)-4-(4-(5-(aminomethyl)-2-oxooxazolidin-3-yl)phenyl)morpholin-3-one and LiCl via general procedure 3.8 to give 20.0 mg (32%) of a yellow oil after purification with EtOAc/hexanes.

R_f = 0.22 in 100:0 EtOAc:hexanes

^{1}H NMR (499 MHz, $CDCl_3$) δ 7.59 (d, *J* = 8.6 Hz, 3H), 7.36 (d, *J* = 8.7 Hz, 2H), 4.88 (ddd, *J* = 9.8, 7.7, 4.9 Hz, 1H), 4.34 (s, 2H), 4.16 (t, *J* = 9.0 Hz, 1H), 4.04 (dd, *J* = 5.6, 4.5 Hz, 2H), 3.96 (dd, *J* = 9.1, 5.7 Hz, 1H), 3.84 – 3.69 (m, 4H).

^{13}C NMR (126 MHz, $CDCl_3$) δ 154.0, 137.5, 136.7, 126.4, 119.3, 71.0, 68.7, 64.2, 49.8, 48.3, 44.7

HRMS (ESI) Calculated $C_{14}H_{16}ClN_2O_4^+$ $[M+H]^+$: 311.0793, Found 311.0793

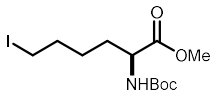

3.100

methyl (*S*)-2-((*tert*-butoxycarbonyl)amino)-6-iodohexanoate (3.100)

Compound **3.100** was prepared on a 0.20 mmol scale from boc lysine methyl ester hydrochloride and KI via general procedure 3.8 to give 34.8 mg (47%) of a yellow oil after purification with EtOAc/hexanes.

R_f = 0.35 in 25:75 EtOAc:hexanes

^{1}H NMR (499 MHz, $CDCl_3$) δ 5.03 (d, *J* = 8.0 Hz, 1H), 4.32 (q, *J* = 14.4, 7.5, 6.9 Hz, 1H), 3.76 (s, 3H), 3.18 (t, *J* = 6.9 Hz, 2H), 1.84 (qp, *J* = 14.2, 7.4 Hz, 4H), 1.71 – 1.60 (m, 1H), 1.53 – 1.41 (m, 11H).

^{13}C NMR (126 MHz, $CDCl_3$) δ 173.1, 155.3, 80.0, 53.1, 52.3, 32.7, 31.7, 28.3, 26.2, 6.1.

HRMS (ESI) Calculated $C_{12}H_{22}INaNO_4^+$ $[M+H]^+$: 394.0486, Found 394.0455

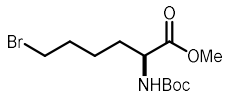

3.101

methyl (*S*)-2-((*tert*-butoxycarbonyl)amino)-6-bromohexanoate (3.101)

Compound **3.100** was prepared on a 0.20 mmol scale from **3.51** and KBr via general procedure 3.8 to give 27.0 mg (42%) of a yellow oil after purification with EtOAc/hexanes.

R_f = 0.30 in 25:75 EtOAc:hexanes

^{1}H NMR (499 MHz, $CDCl_3$) δ 5.02 (d, *J* = 8.4 Hz, 1H), 4.31 (q, *J* = 13.0, 6.9 Hz, 1H), 3.75 (s, 3H), 3.39 (t, *J* = 6.7 Hz, 2H), 1.96 – 1.77 (m, 4H), 1.70 – 1.59 (m, 1H), 1.55 – 1.47 (m, 2H), 1.44 (s, 9H).

^{13}C NMR (126 MHz, $CDCl_3$) δ 173.0, 155.4, 80.0, 53.1, 52.3, 33.2, 32.0, 31.9, 28.3, 23.8.

HRMS (ESI) Calculated $C_{12}H_{22}BrNaNO_4^+$ $[M+H]^+$: 346.0624, Found 346.0622

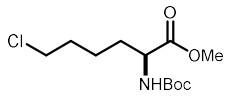

3.102

methyl (*S*)-2-((*tert*-butoxycarbonyl)amino)-6-chlorohexanoate (3.102)

Compound **3.102** was prepared on a 0.20 mmol scale from boc lysine methyl ester hydrochloride and LiCl via general procedure 3.8 to give 12.3 mg (22%) of a yellow oil after purification with EtOAc/hexanes.

R_f = 0.30 in 25:75 EtOAc:hexanes

^{1}H NMR (499 MHz, $CDCl_3$) δ 5.02 (d, *J* = 8.2 Hz, 1H), 4.31 (q, *J* = 7.4 Hz, 1H), 3.74 (s, 3H), 3.52 (t, *J* = 6.5 Hz, 2H), 1.89 – 1.71 (m, 3H), 1.72 – 1.60 (m, 1H), 1.56 – 1.45 (m, 2H), 1.44 (s, 9H).

^{13}C NMR (126 MHz, $CDCl_3$) δ 173.3, 80.1, 53.3, 52.5, 44.7, 32.2, 32.1, 28.5, 22.7.

HRMS (ESI) Calculated $C_{12}H_{22}ClNaNO_4^+$ $[M+H]^+$: 302.1130, Found 302.1133

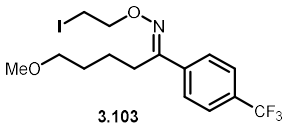

3.103

(*E*)-5-methoxy-1-(4-(trifluoromethyl)phenyl)pentan-1-one O-(2-iodoethyl) oxime (3.103)

Compound **3.103** was prepared on a 0.20 mmol scale from **3.55** and KI via a modified general procedure 3.8 where DMA was used as a solvent to give 80.0 mg (92%) of a tan solid after purification with EtOAc/hexanes.

R_f = 0.75 in 20:80 EtOAc:hexanes

^{1}H NMR (499 MHz, cdcl$_3$) δ 7.74 (d, *J* = 8.2 Hz, 3H), 7.62 (d, *J* = 7.9 Hz, 4H), 4.42 (t, *J* = 6.8 Hz, 4H), 3.44 – 3.36 (m, 6H), 2.81 (t, *J* = 7.5 Hz, 2H), 1.70 – 1.59 (m, *J* = 3.3 Hz, 7H).

^{13}C NMR (126 MHz, cdcl$_3$) δ 158.32, 138.86, 131.13, 126.08 (q, *J* = 197.7 Hz), 125.40 (q, *J* = 3.8 Hz), 122.90, 74.24, 72.25, 58.60, 29.59, 26.35, 23.19, 2.88.

^{19}F NMR (376 MHz, cdcl$_3$) δ -62.77.

HRMS (ESI) Calculated $C_{15}H_{20}F_3INO_2^+$ $[M+H]^+$: 430.0485, Found 430.0485

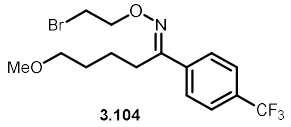

3.104

(*E*)-5-methoxy-1-(4-(trifluoromethyl)phenyl)pentan-1-one O-(2-bromoethyl) oxime (3.104)

Compound **3.104** was prepared on a 0.20 mmol scale from **3.55** and KBr via a modified general procedure 3.8 where DMA was used as a solvent to give 67.8 mg (89%) of a tan solid after purification with EtOAc/hexanes.

R_f = 0.75 in 20:80 EtOAc:hexanes

^{1}H NMR (499 MHz, cdcl$_3$) δ 7.74 (d, *J* = 8.1 Hz, 1H), 7.62 (d, *J* = 7.9 Hz, 1H), 4.47 (t, *J* = 6.2 Hz, 2H), 3.62 (t, *J* = 6.2 Hz, 2H), 3.42 – 3.36 (m, 2H), 3.32 (s, 3H), 2.84 – 2.78 (m, 2H), 1.69 – 1.58 (m, 3H).

^{13}C NMR (126 MHz, cdcl$_3$) δ 158.58, 139.01, 126.08 (q, *J* = 197.7 Hz), 125.40 (q, *J* = 3.8 Hz), 73.69, 72.40, 58.74, 30.21, 29.71, 26.45, 23.29.

^{19}F NMR (376 MHz, cdcl$_3$) δ -62.77.

HRMS (ESI) Calculated $C_{15}H_{20}F_3BrNO_2^+$ $[M+H]^+$: 382.0624, Found 382.0630

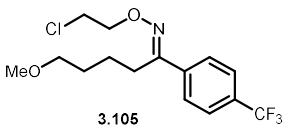

3.105

(*E*)-5-methoxy-1-(4-(trifluoromethyl)phenyl)pentan-1-one O-(2-chloroethyl) oxime (3.105)

Compound **3.105** was prepared on a 0.20 mmol scale from **3.55** and LiCl via a modified general procedure 3.8 where DMA was used as a solvent to give 23.7 mg (35%) of a tan solid after purification with EtOAc/hexanes.

R_f = 0.75 in 20:80 EtOAc:hexanes

^{1}H NMR (499 MHz, cdcl$_3$) δ 7.74 (d, *J* = 7.8 Hz, 2H), 7.62 (d, *J* = 8.2 Hz, 2H), 4.41 (t, *J* = 5.9 Hz, 2H), 3.78 (t, *J* = 5.8 Hz, 2H), 3.38 (t, *J* = 6.5 Hz, 1H), 3.32 (s, 3H), 2.81 (t, *J* = 7.3 Hz, 2H), 1.80 – 1.45 (m, 4H).

^{13}C NMR (126 MHz, cdcl$_3$) δ 158.41, 138.86, 131.13, 130.87, 126.08 (q, *J* = 197.7 Hz), 125.40 (q, *J* = 3.8 Hz), 122.90, 73.74, 72.23, 58.57, 42.27, 29.51, 26.26, 23.09.

^{19}F NMR (470 MHz, cdcl$_3$) δ -62.79.

HRMS (ESI) Calculated $C_{15}H_{20}F_3ClNO_2^+$ $[M+H]^+$: 338.1129, Found 338.1135

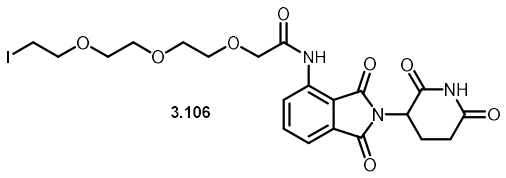

3.106

2-(2-(2-(2-iodoethoxy)ethoxy)ethoxy)-*N*-(2-(2,6-dioxopiperidin-3-yl)-1,3-dioxoisoindolin-4-yl)acetamide (3.106)

Compound **3.106** was prepared on a 0.05 mmol scale from 2-(2-(2-(2-Aminoethoxy)ethoxy)ethoxy)-*N*-(2-(2,6-dioxopiperidin-3-yl)-1,3-dioxoisoindolin-4-yl)acetamide hydrochloride, and KI via a modified general procedure 3.8 where **3.66** was replaced with 2,4,6-tris(4-(trifluoromethyl)phenyl)pyrylium tetrafluoroborate to give 23.0 mg (80%) of a white solid after purification with EtOAc.

^{1}H NMR (499 MHz, $CDCl_3$) δ 10.46 (s, 1H), 8.86 (d, *J* = 8.4 Hz, 1H), 8.25 (s, 1H), 7.73 (t, *J* = 7.9 Hz, 1H), 7.58 (d, *J* = 7.3 Hz, 1H), 4.96 (dd, *J* = 12.4, 5.4 Hz, 1H), 4.22 (s, 2H), 3.87 – 3.79 (m, 5H), 3.73 (t, *J* = 6.8 Hz, 2H), 3.71 – 3.68 (m, 2H), 3.68 – 3.62 (m, 2H), 3.24 (t, *J* = 6.8 Hz, 2H), 2.98 – 2.87 (m, 1H), 2.86 – 2.70 (m, 2H), 2.21 – 2.13 (m, 1H).

^{13}C NMR (126 MHz, $CDCl_3$) δ 170.9, 169.6, 168.6, 167.9, 166.9, 136.9, 136.5, 131.5, 125.4, 119.0, 116.3, 72.1, 71.7, 71.2, 70.9, 70.7, 70.3, 49.4, 31.5, 22.8, 3.1.

HRMS (ESI) Calculated $C_{21}H_{25}IN_3O_8^+$ $[M+H]^+$: 574.0681, Found 574.0688

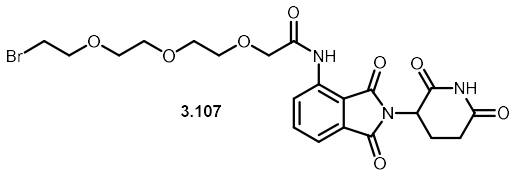

3.107

2-(2-(2-(2-bromoethoxy)ethoxy)ethoxy)-*N*-(2-(2,6-dioxopiperidin-3-yl)-1,3-dioxoisoindolin-4-yl)acetamide (3.107)

Compound **3.107** was prepared on a 0.05 mmol scale from 2-(2-(2-(2-Aminoethoxy)ethoxy)ethoxy)-*N*-(2-(2,6-dioxopiperidin-3-yl)-1,3-dioxoisoindolin-4-

yl)acetamide hydrochloride, and KBr via a modified general procedure 3.8 where **3.66** was replaced with 2,4,6-tris(4-(trifluoromethyl)phenyl)pyrylium tetrafluoroborate to give 23.0 mg (80%) of a white solid after purification with EtOAc.

^{1}H NMR (499 MHz, $CDCl_3$) δ 10.47 (s, 1H), 8.87 (d, *J* = 8.4 Hz, 1H), 8.32 (s, 1H), 7.74 (t, *J* = 7.9 Hz, 1H), 7.59 (d, *J* = 7.3 Hz, 1H), 4.97 (dd, *J* = 12.4, 5.3 Hz, 1H), 4.22 (s, 2H), 3.83 (q, *J* = 1.7 Hz, 4H), 3.80 (t, *J* = 6.2 Hz, 3H), 3.75 (t, *J* = 5.8 Hz, 1H), 3.73 – 3.70 (m, 3H), 3.70 – 3.66 (m, 3H), 3.62 (t, *J* = 5.8 Hz, 1H), 3.46 (t, *J* = 6.2 Hz, 2H), 2.96 – 2.71 (m, 4H), 2.21 – 2.13 (m, 1H).

^{13}C NMR (126 MHz, $CDCl_3$) δ 170.8, 169.4, 168.4, 167.9, 166.8, 136.8, 136.3, 131.4, 125.3, 118.8, 116.1, 71.6, 71.4, 71.2, 71.1, 70.71, 70.69, 70.6, 70.5, 49.2, 42.8, 31.4, 30.4, 22.7.

HRMS (ESI) Calculated $C_{21}H_{25}BrN_3O_8^+$ $[M+H]^+$: 526.0820, Found 526.0833

3.5 NMR spectra of compounds.

3.5.1 NMR spectra for Esterification Reaction

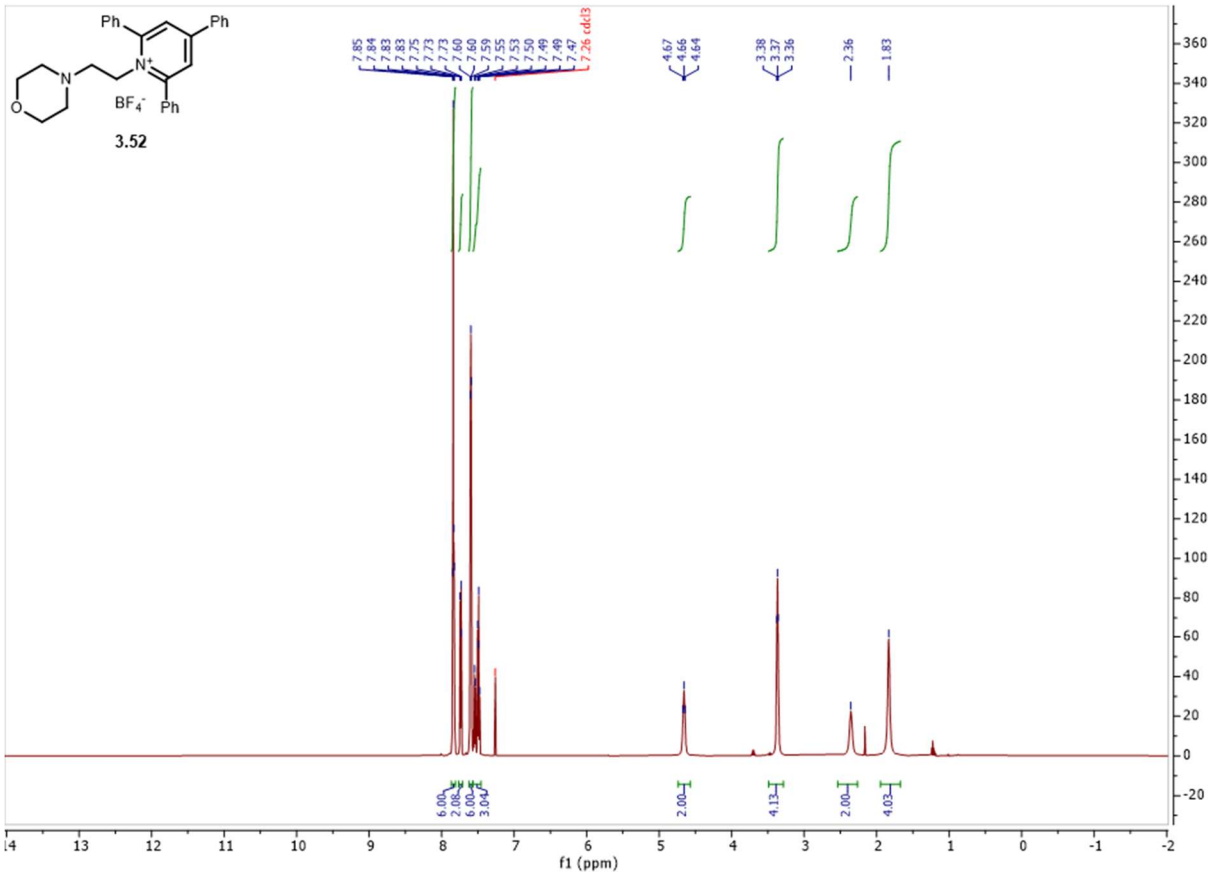

Spectrum 3.15 ^{1}H NMR of compound **3.52**

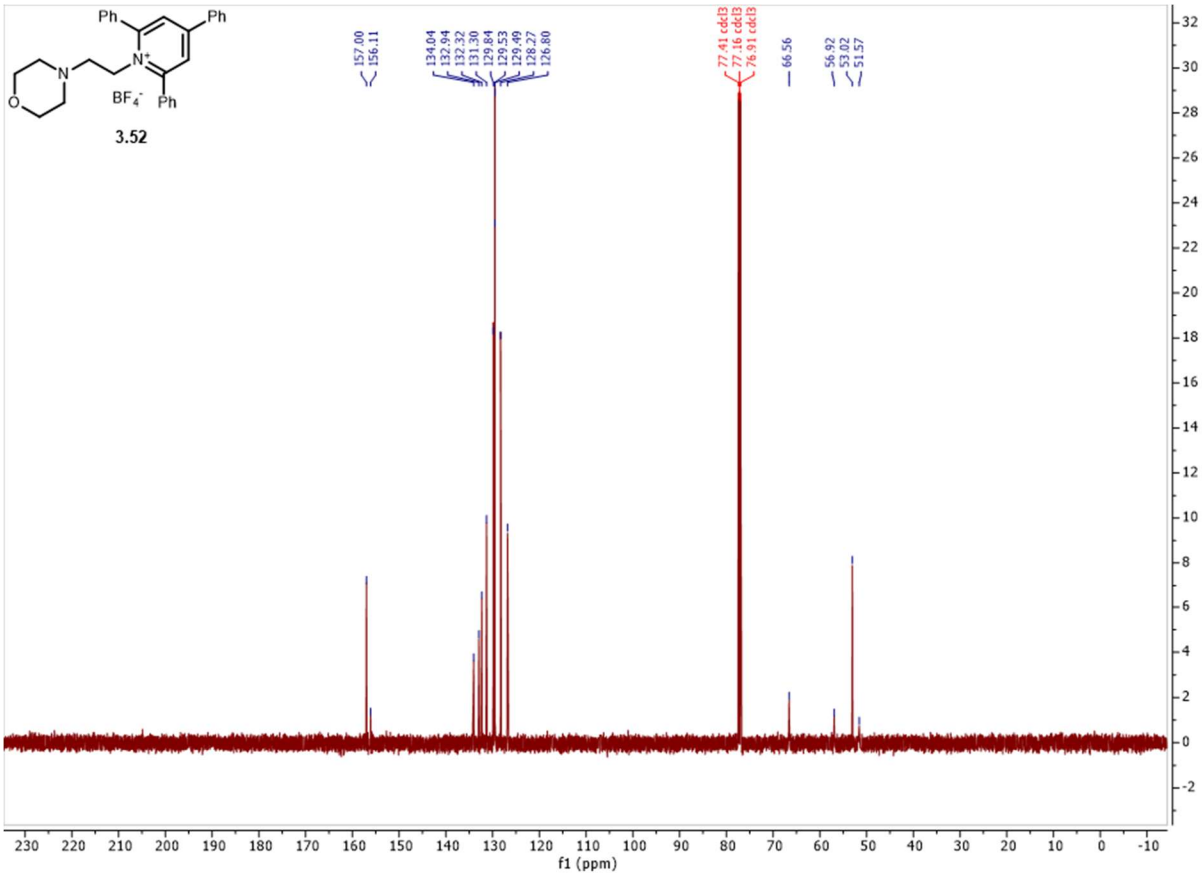

Spectrum 3.16 ^{13}C NMR of compound **3.52**

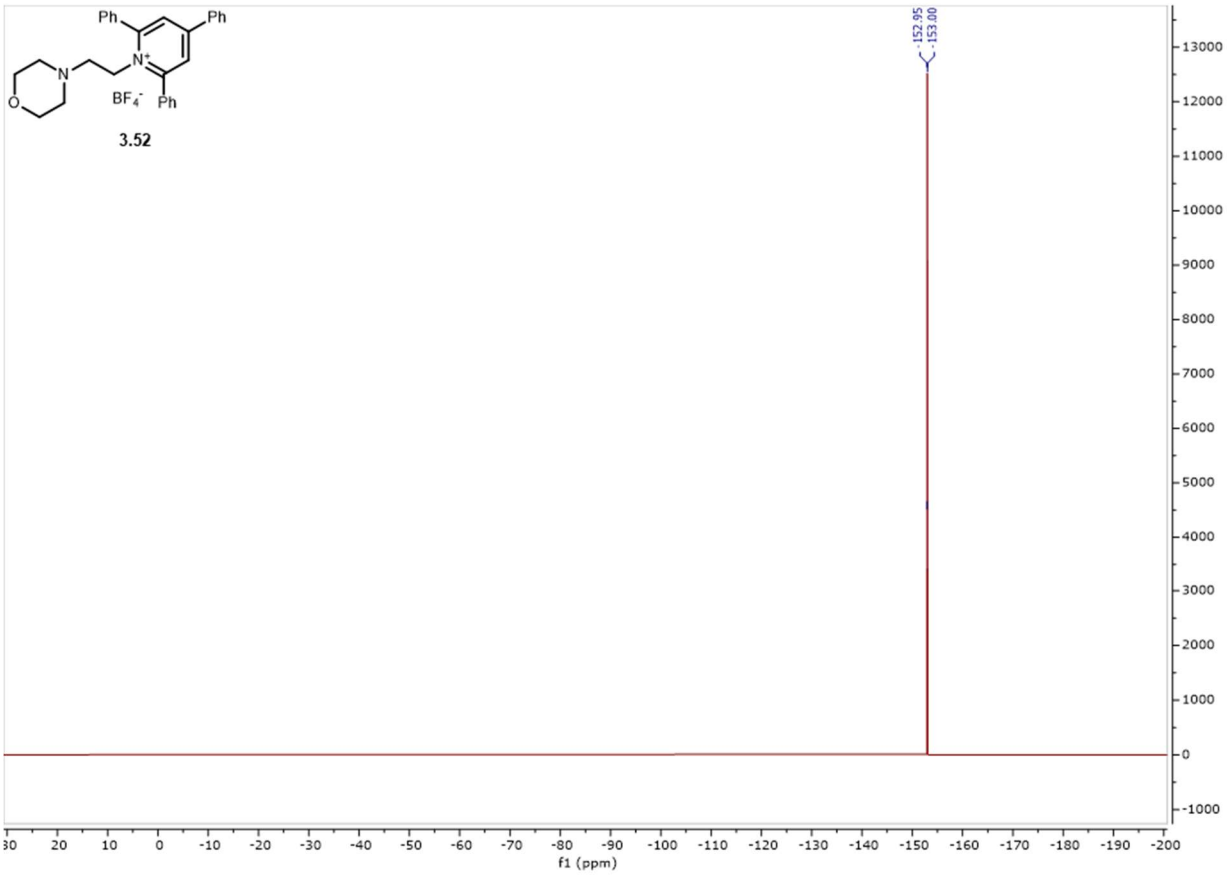

Spectrum 3.17 ^{19}F NMR of compound **3.52**

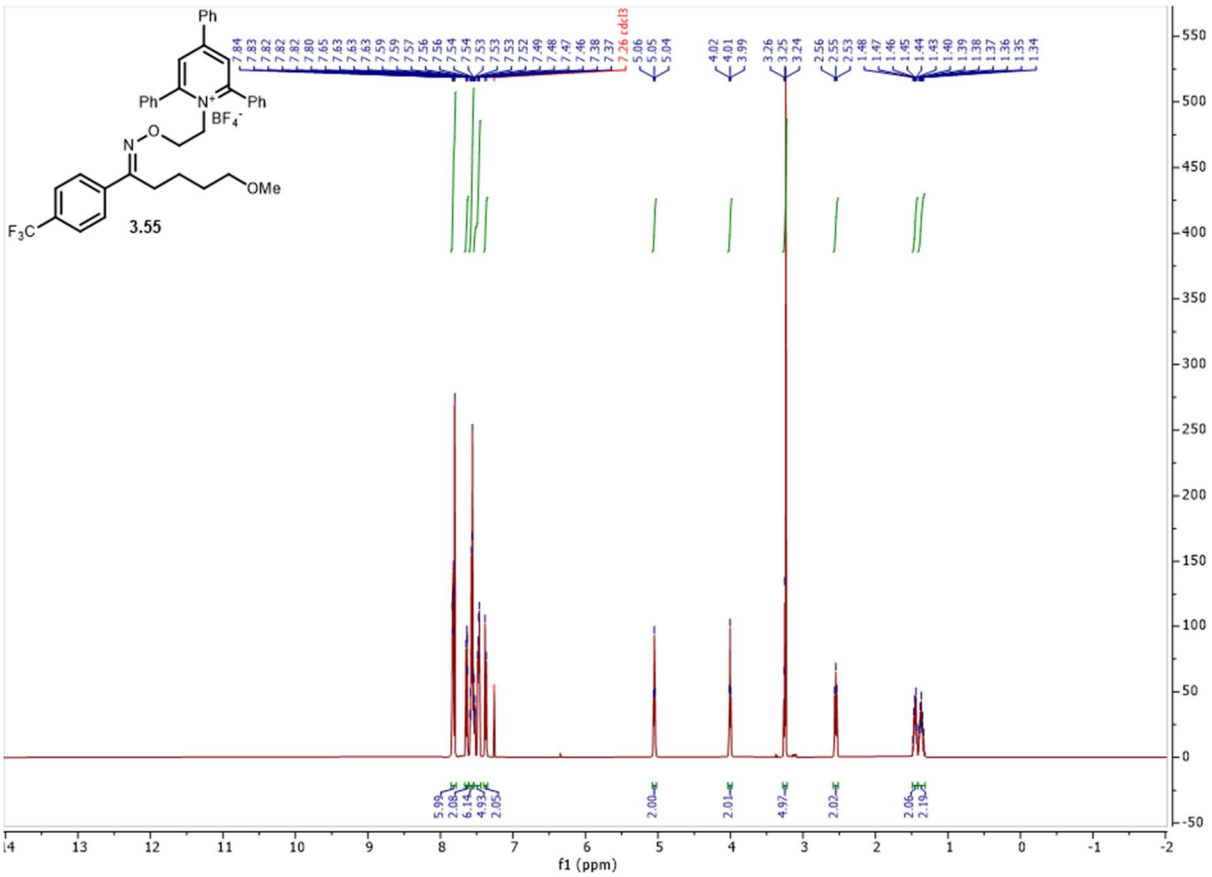

Spectrum 3.18 ^{1}H NMR of compound **3.55**

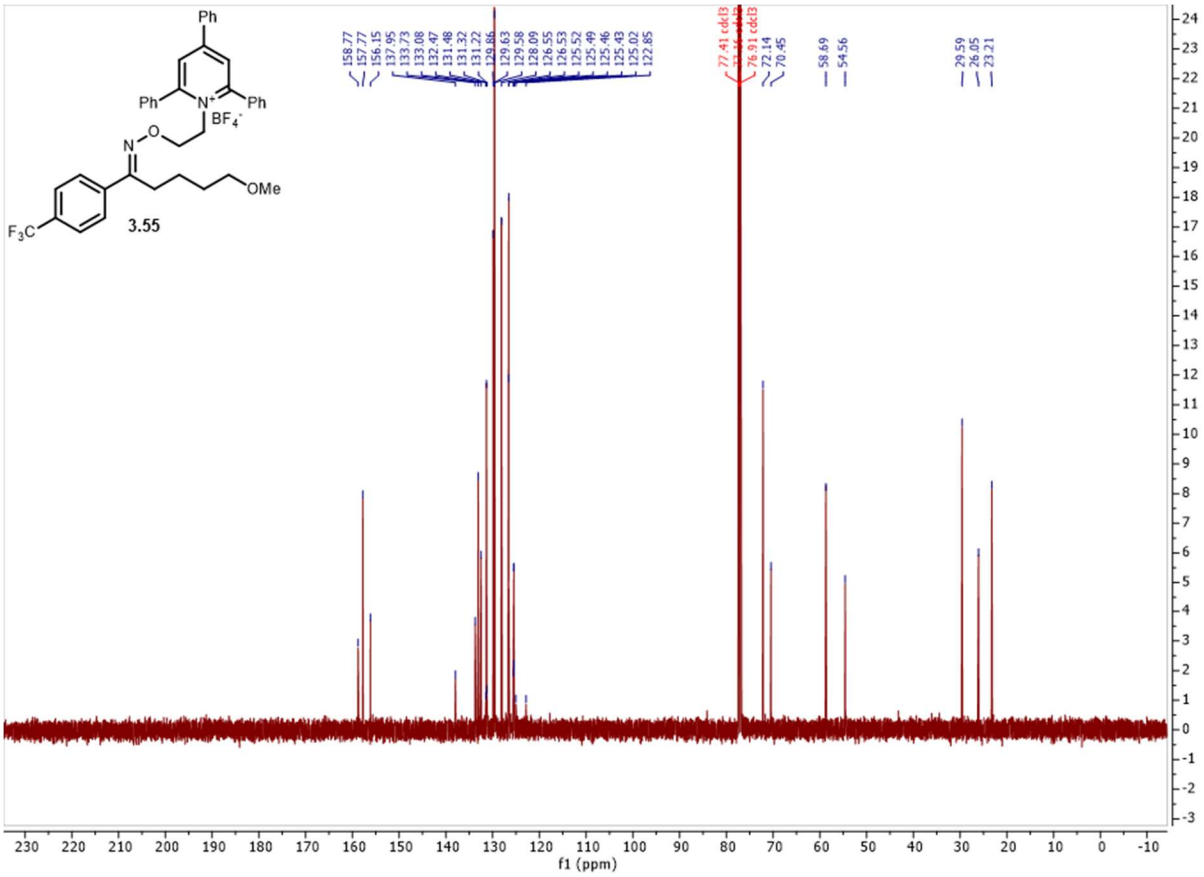

Spectrum 3.19 ^{13}C NMR of compound **3.55**

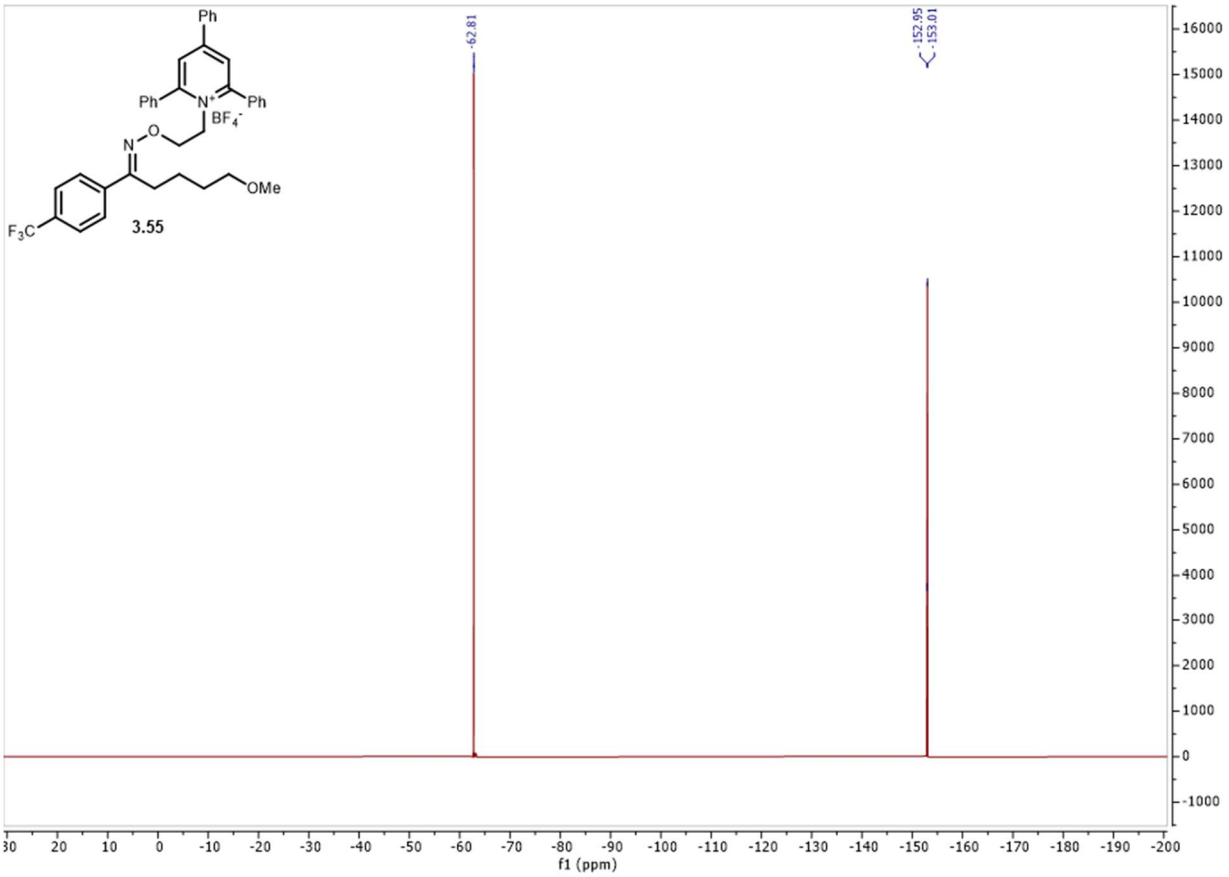

Spectrum 3.20 ^{19}F NMR of compound **3.55**

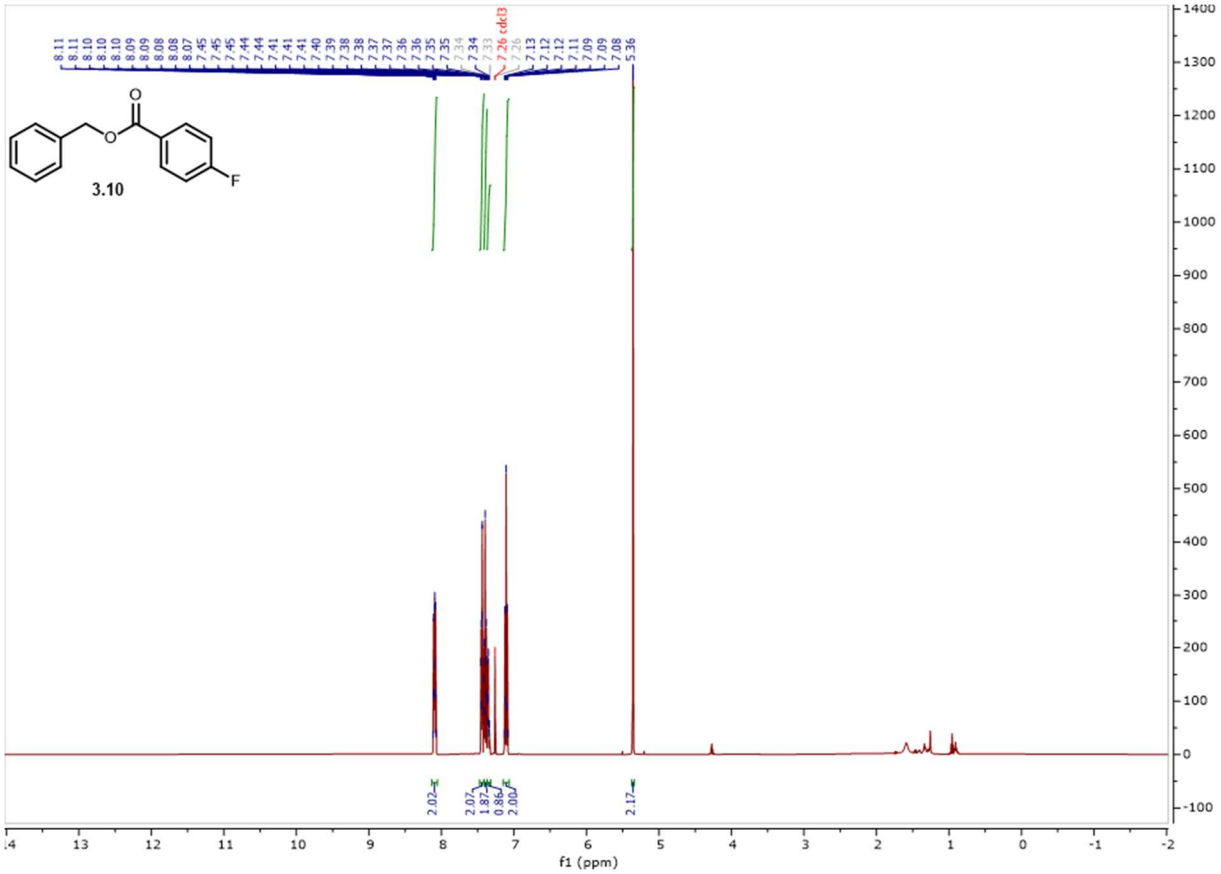

Spectrum 3.21 ^{1}H NMR of compound **3.10**

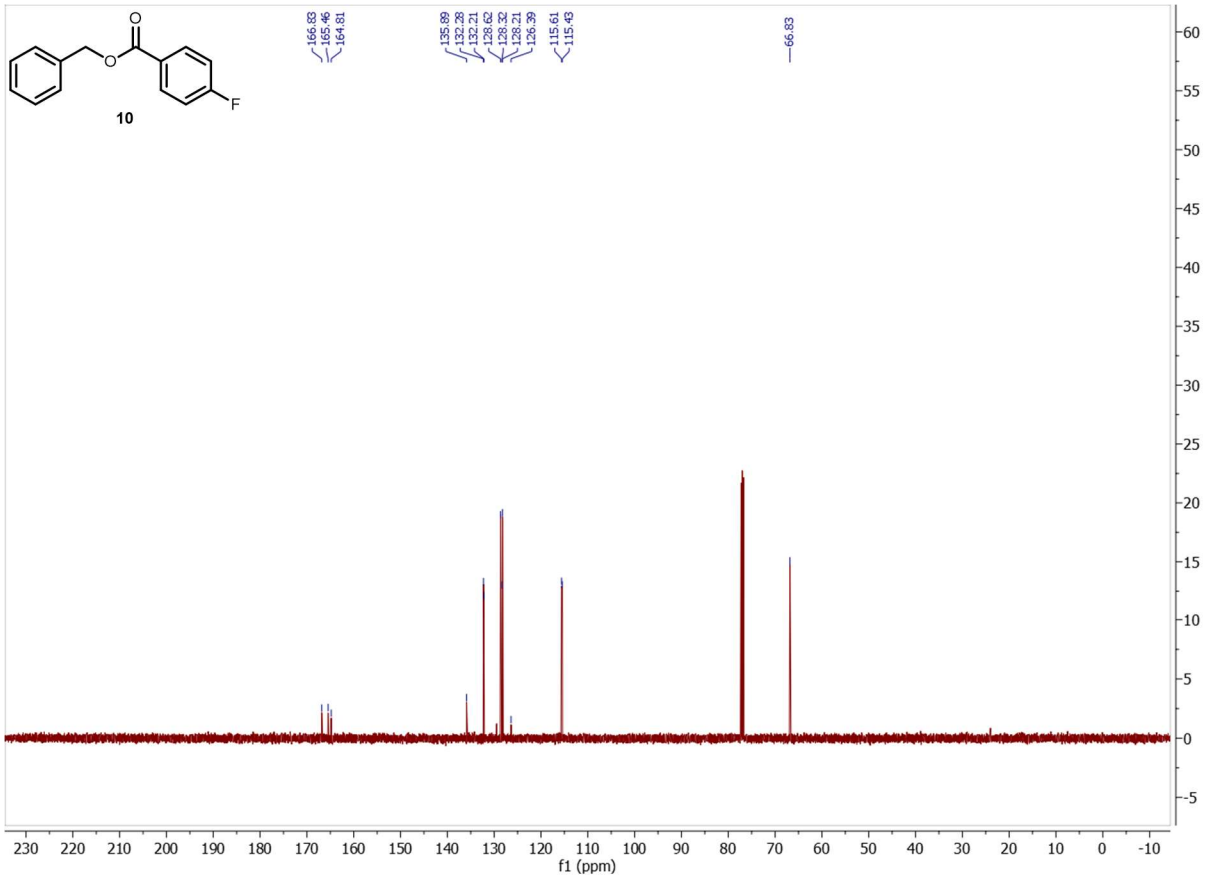

Spectrum 3.22 ^{13}C NMR of compound **3.10**

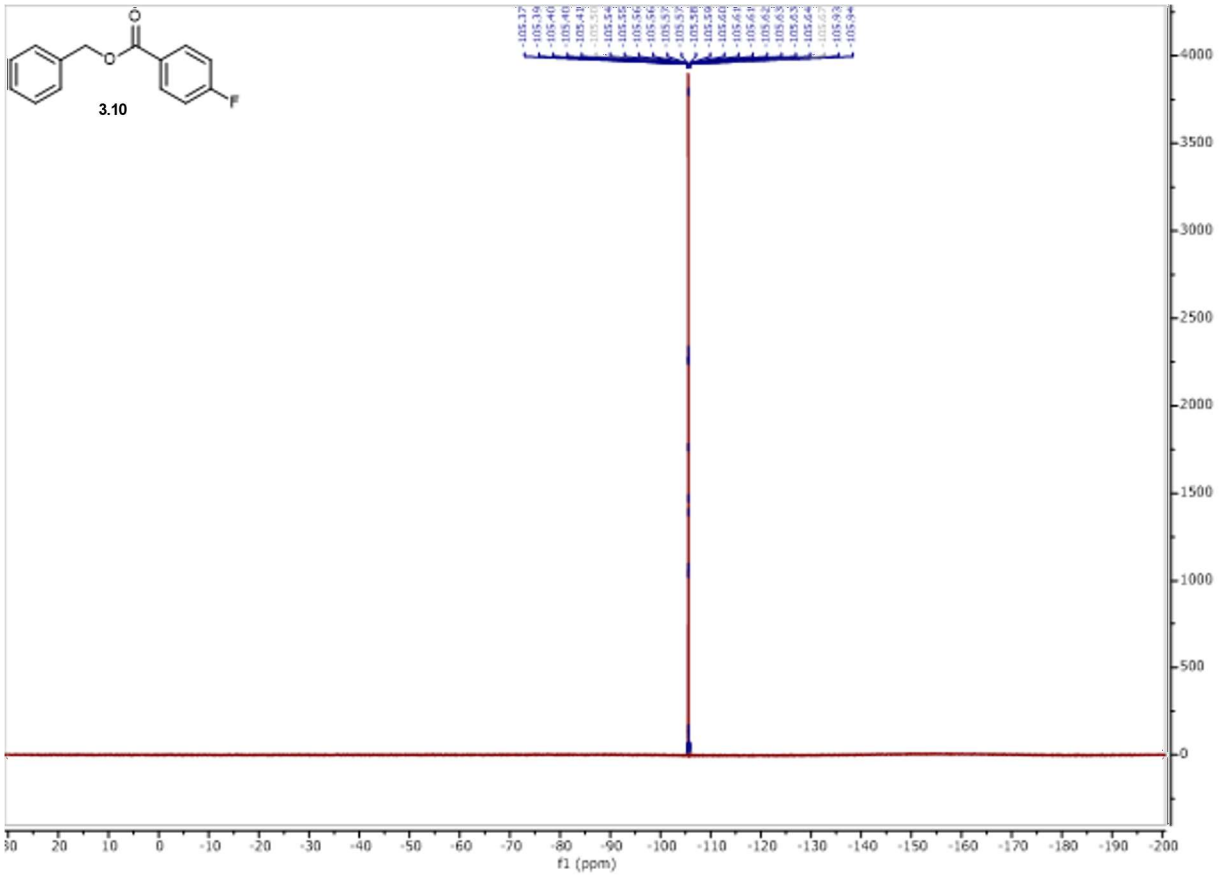

Spectrum 3.23 ^{19}F NMR of compound **3.10**

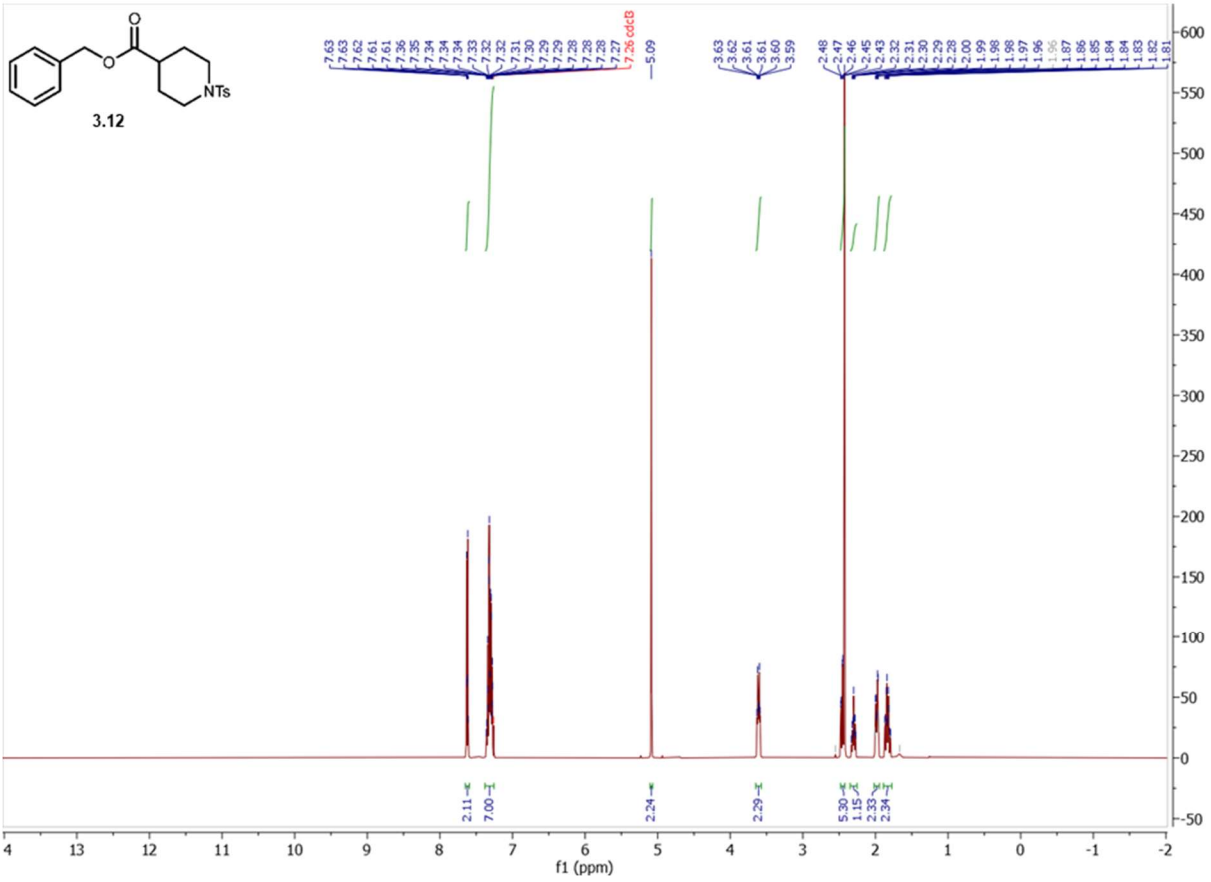

Spectrum 3.24 ^{1}H NMR of compound **3.12**

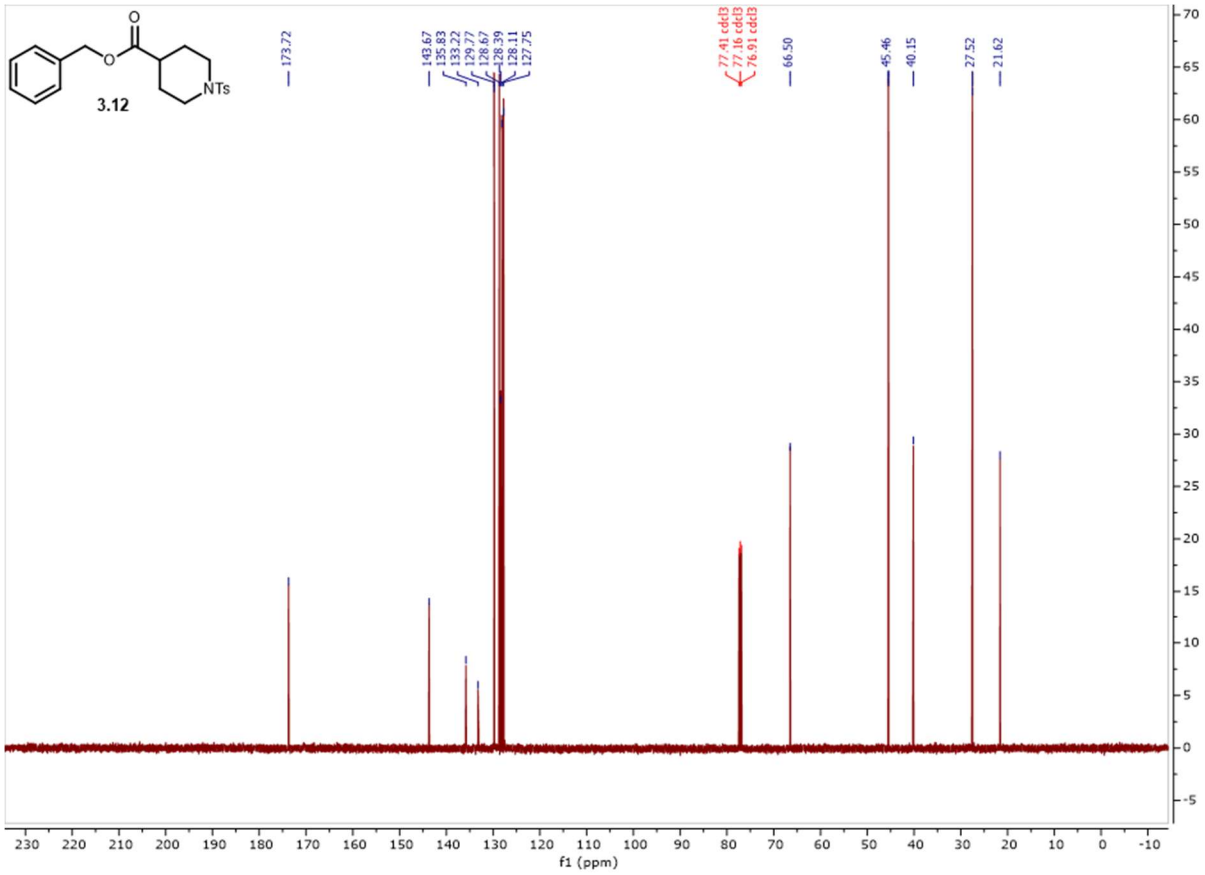

Spectrum 3.25 ^{13}C NMR of compound **3.12**

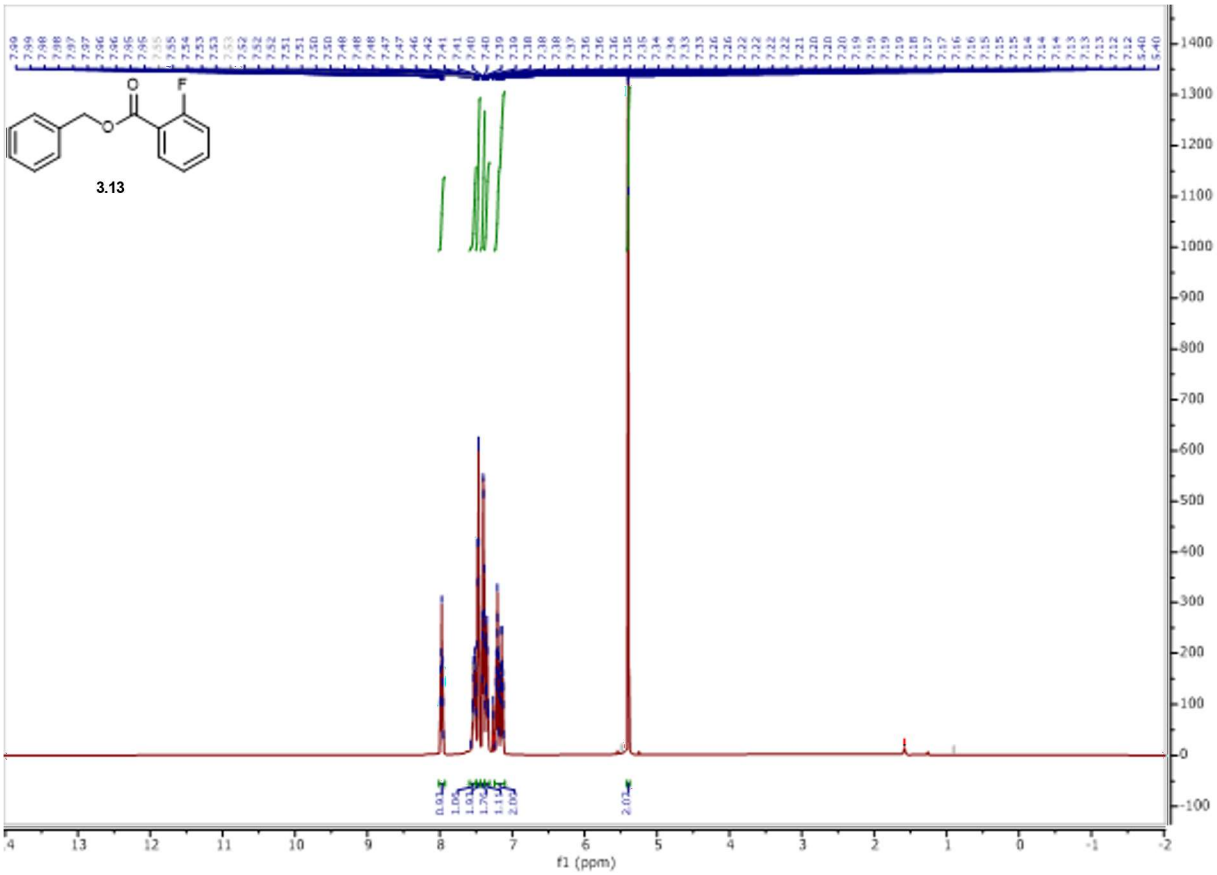

Spectrum 3.26 ^{1}H NMR of compound **3.13**

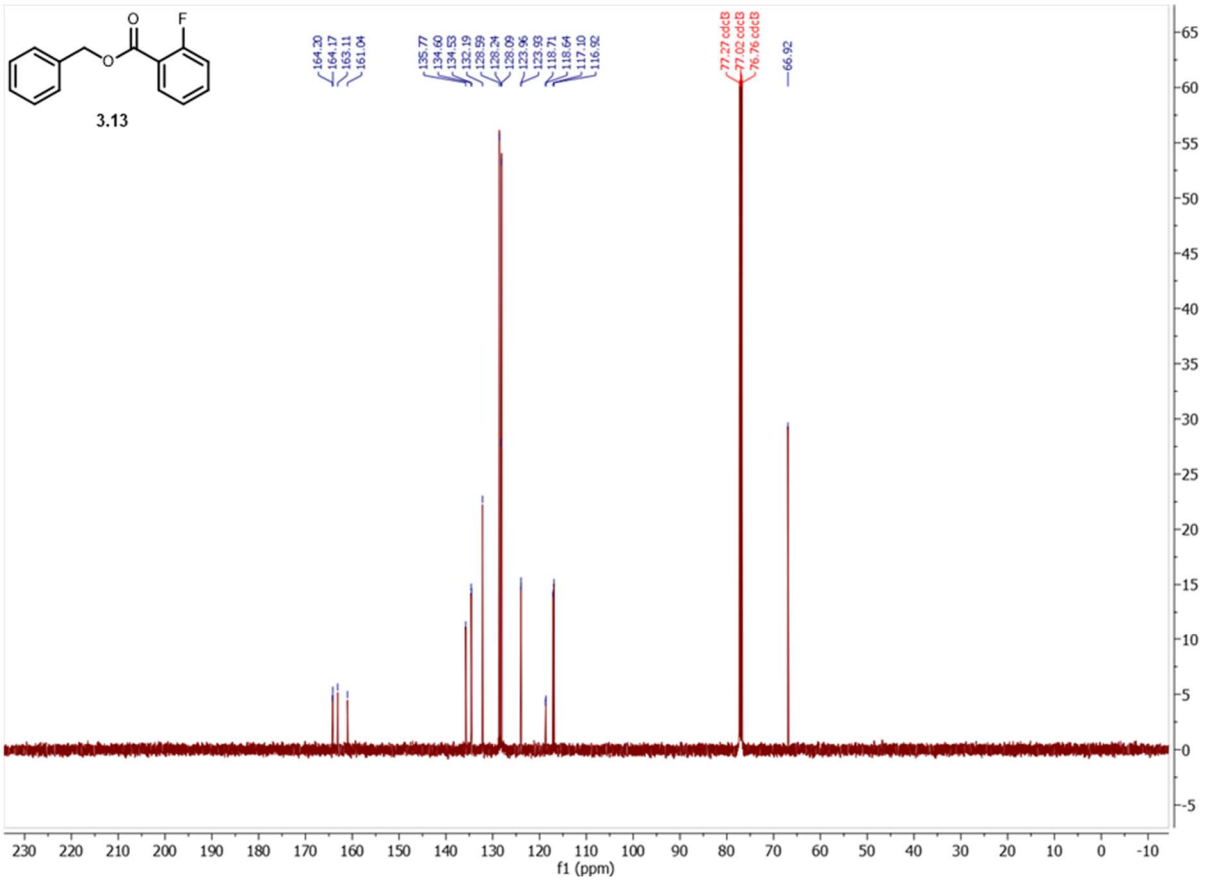

Spectrum 3.27 ^{13}C NMR of compound **3.13**.

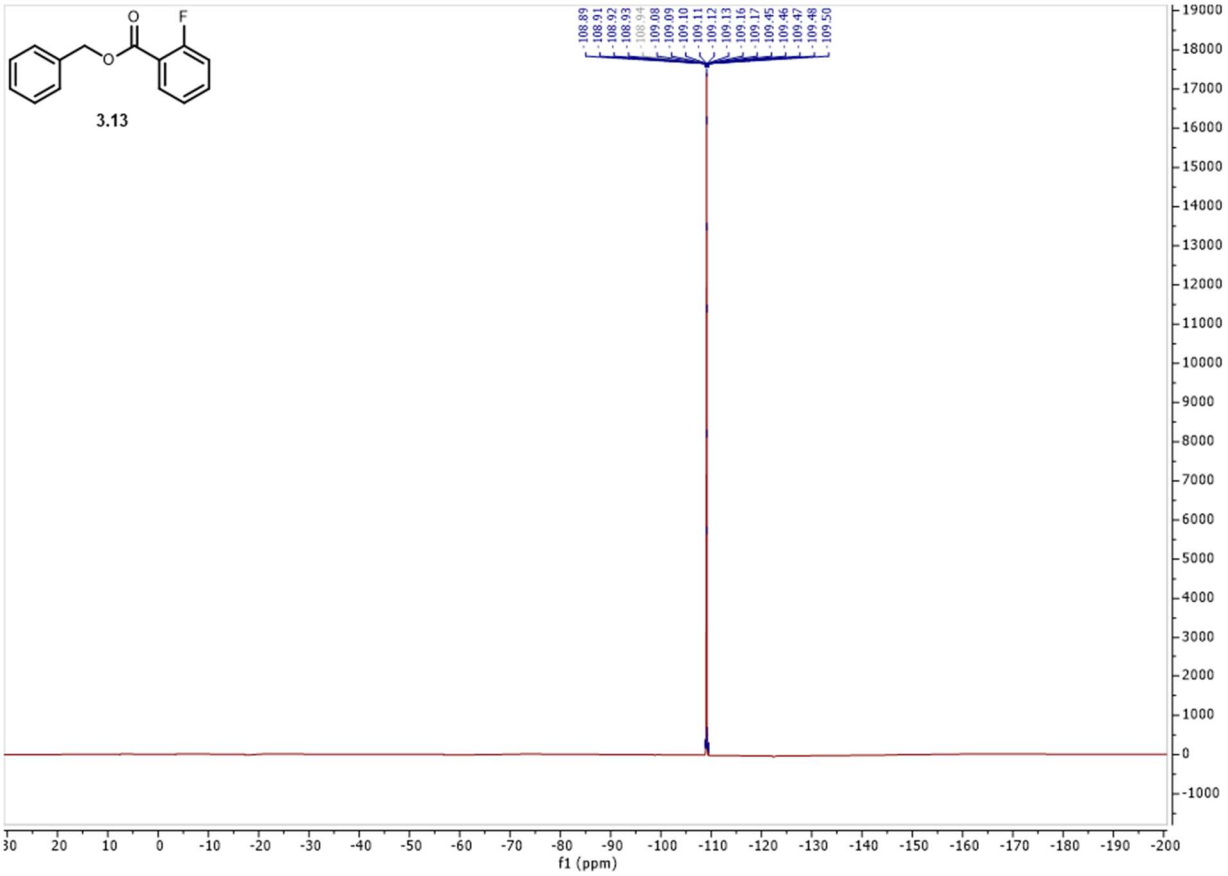

Spectrum 3.28 ^{19}F NMR of compound **3.13**.

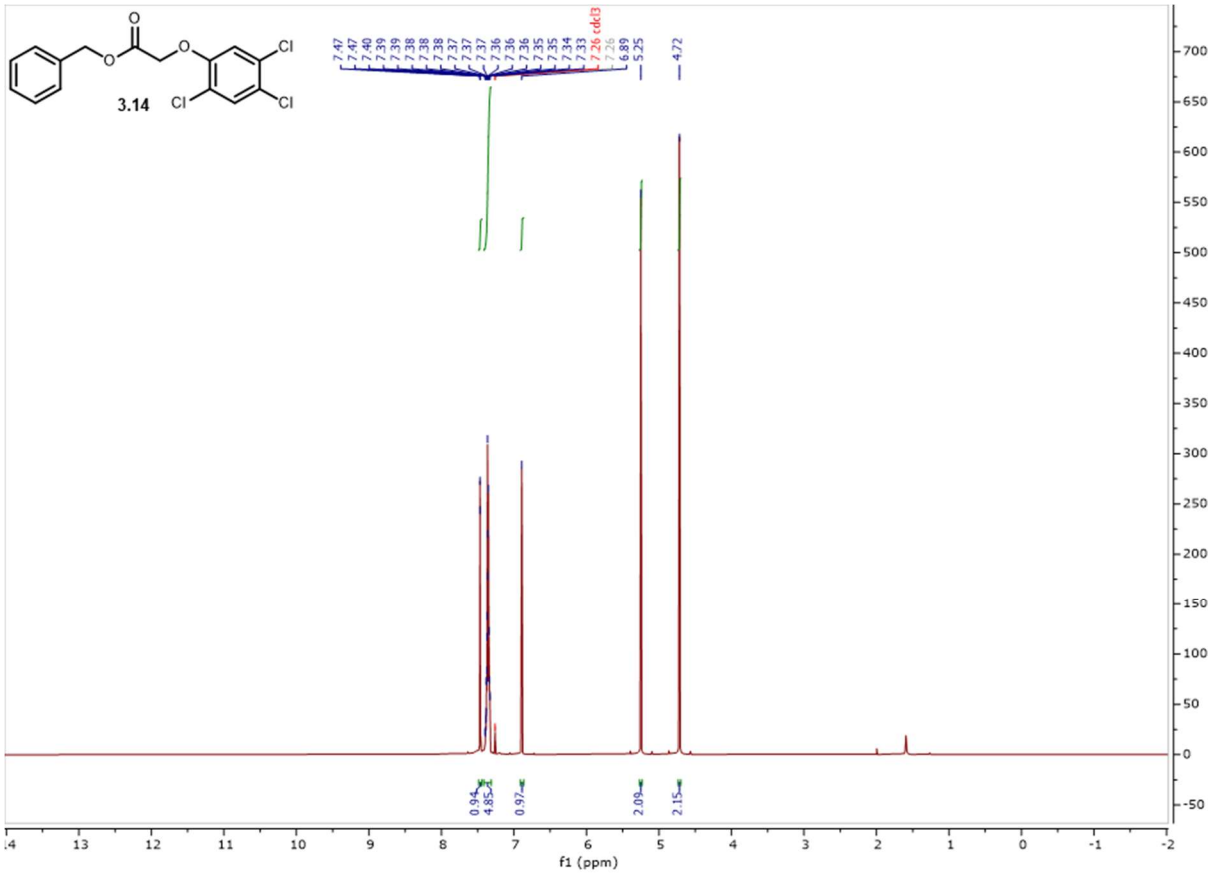

Spectrum 3.29 ^{1}H NMR of compound **3.14**

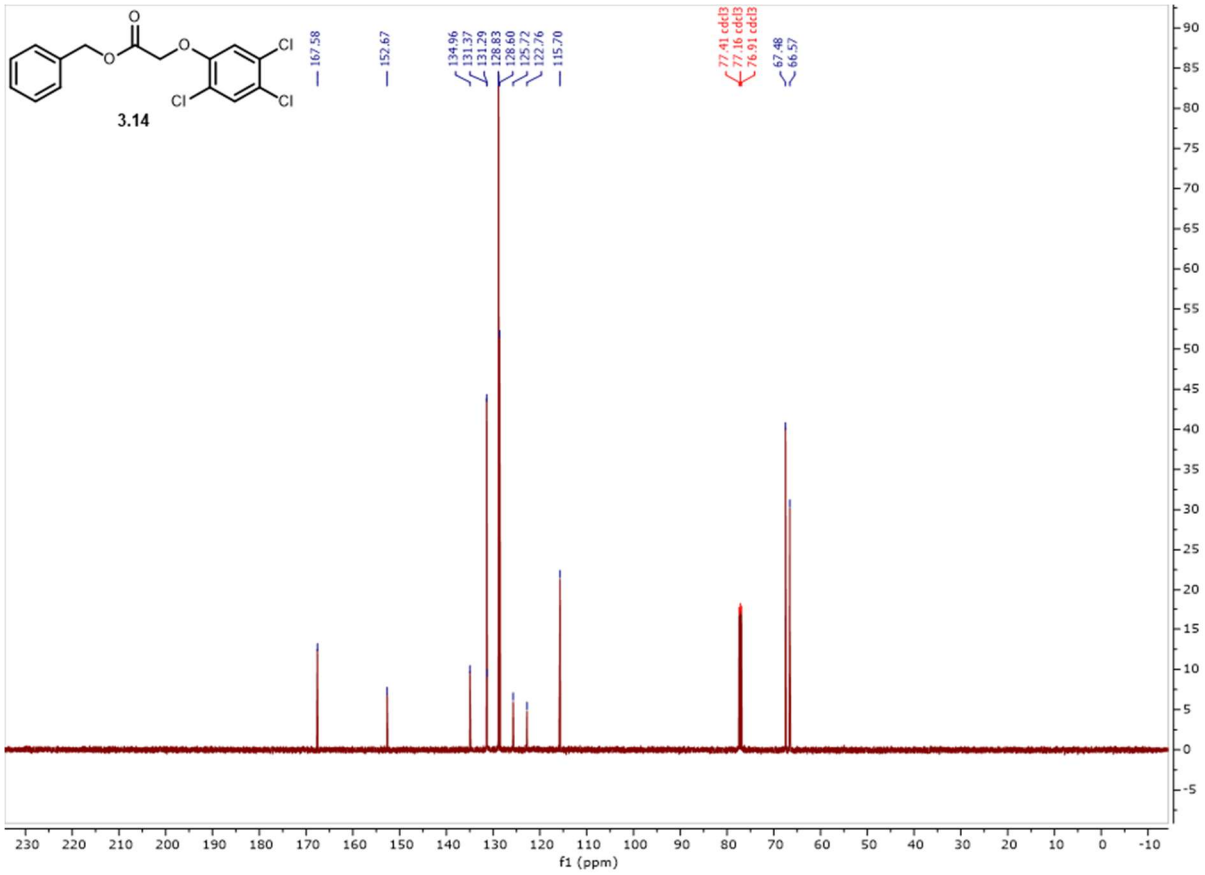

Spectrum 3.30 ^{13}C NMR of compound **3.14**.

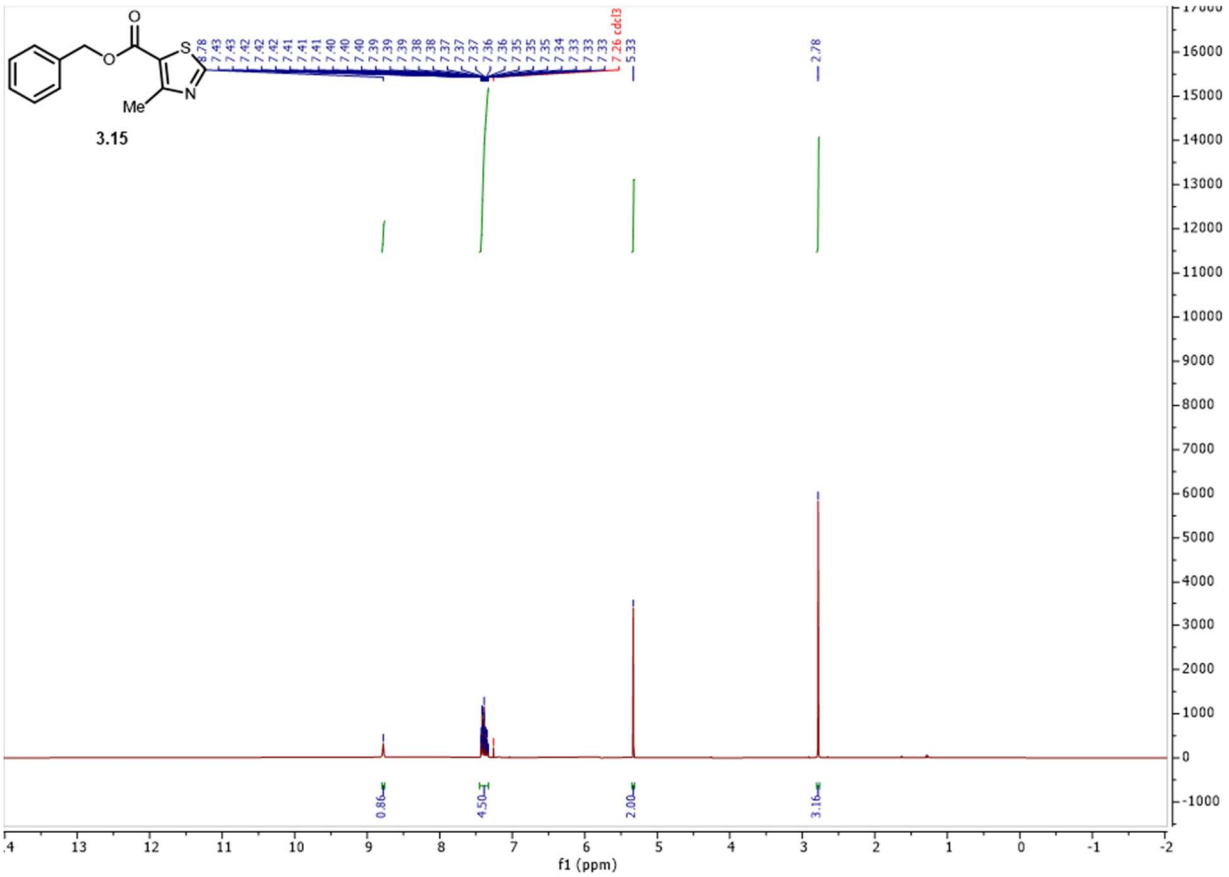

Spectrum 3.31 ^{1}H NMR of compound **3.15**.

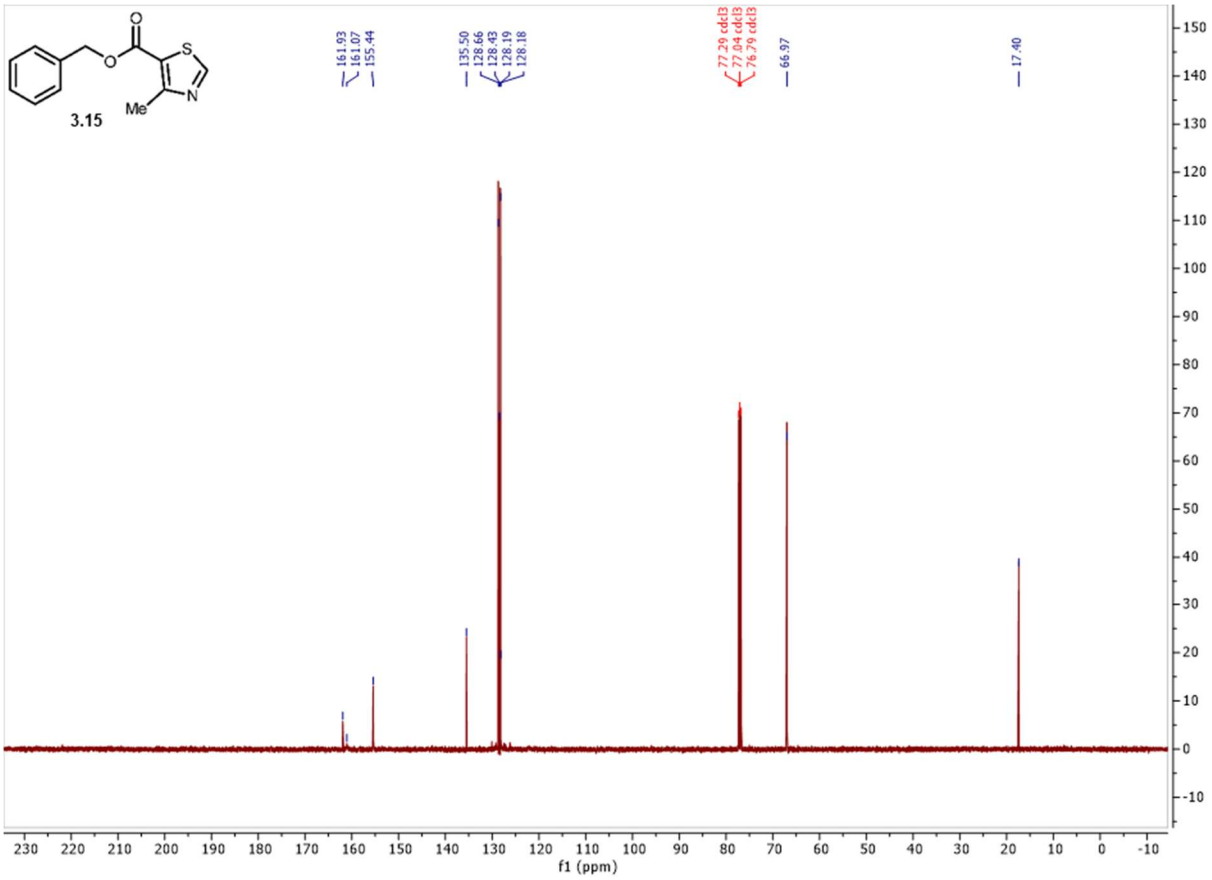

Spectrum 3.32 ^{13}C NMR of compound **3.15**.

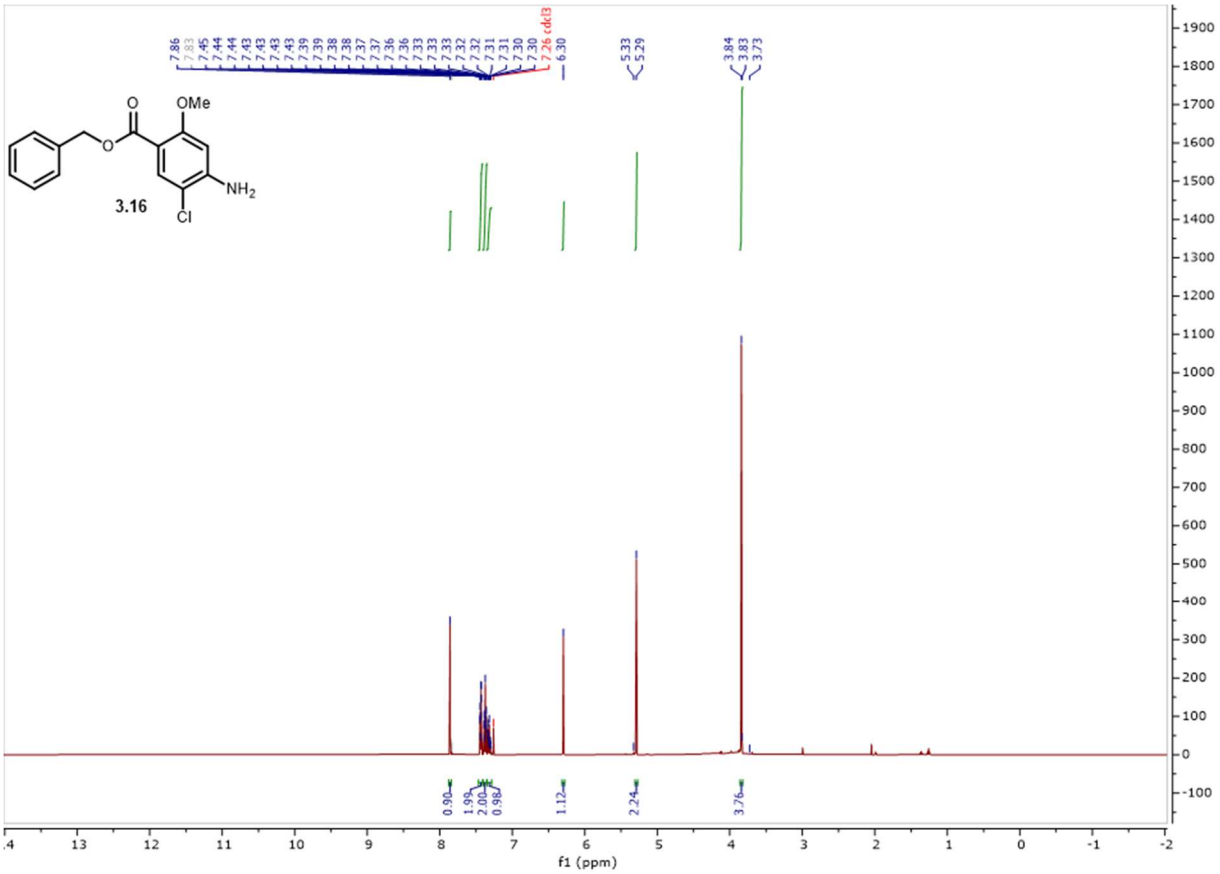

Spectrum 3.33 ^{1}H NMR of compound **3.16**.

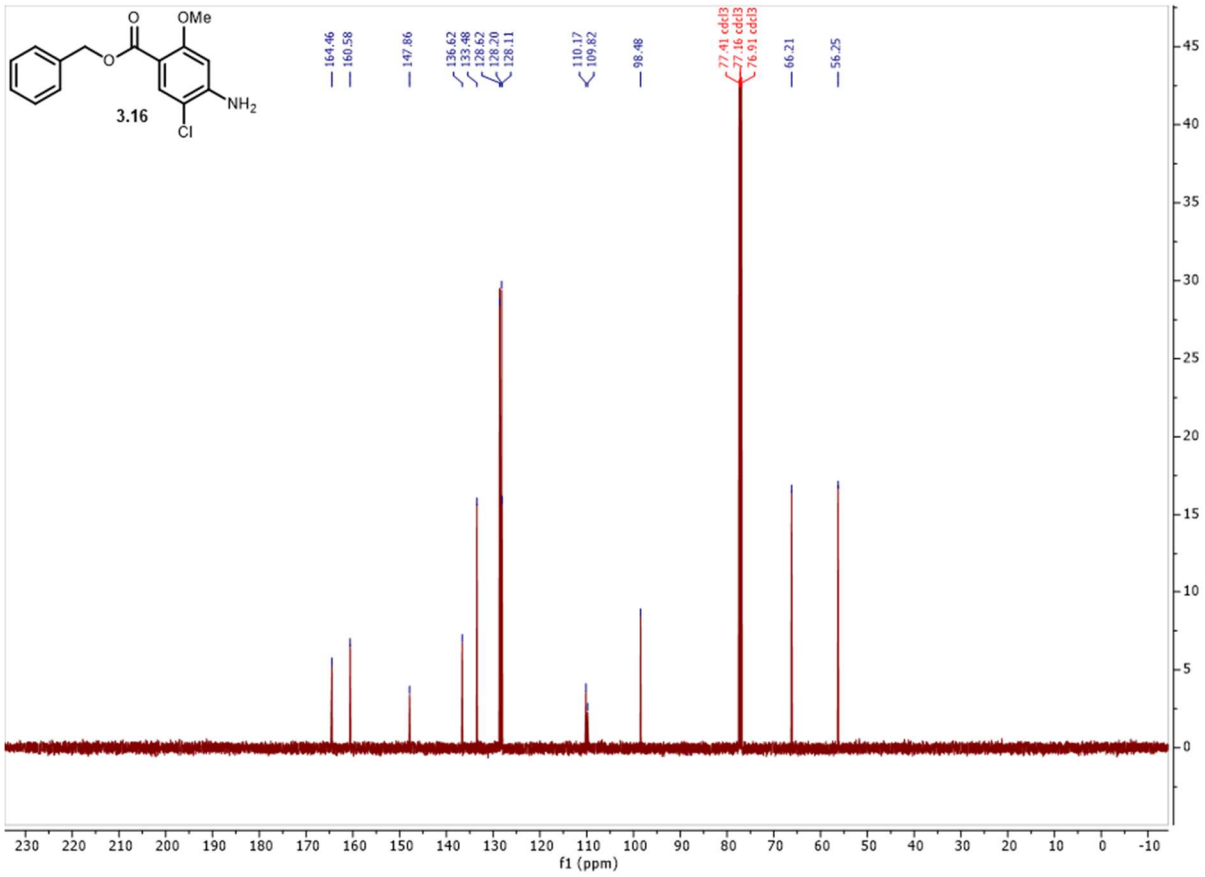

Spectrum 3.34 ^{13}C NMR of compound **3.16**.

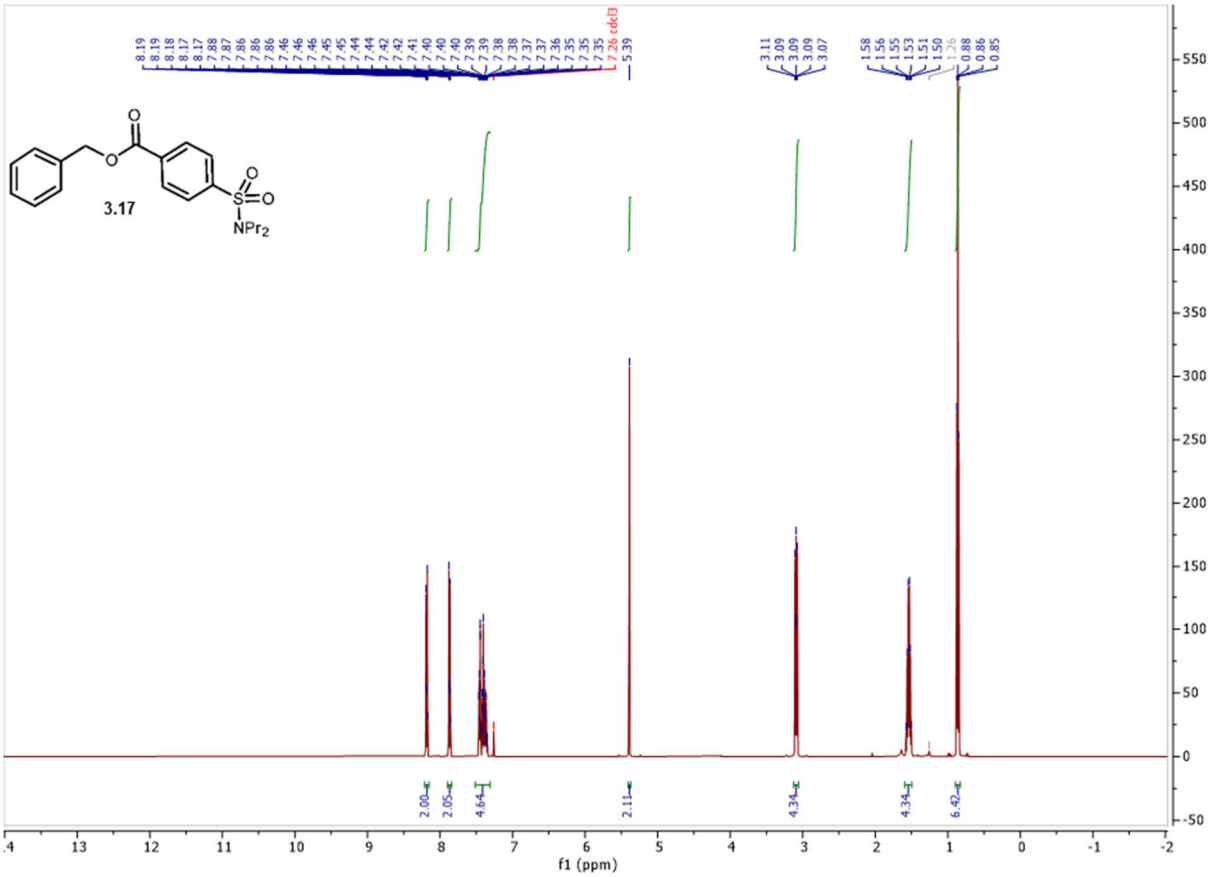

Spectrum 3.35 ^{1}H NMR of compound **3.17**.

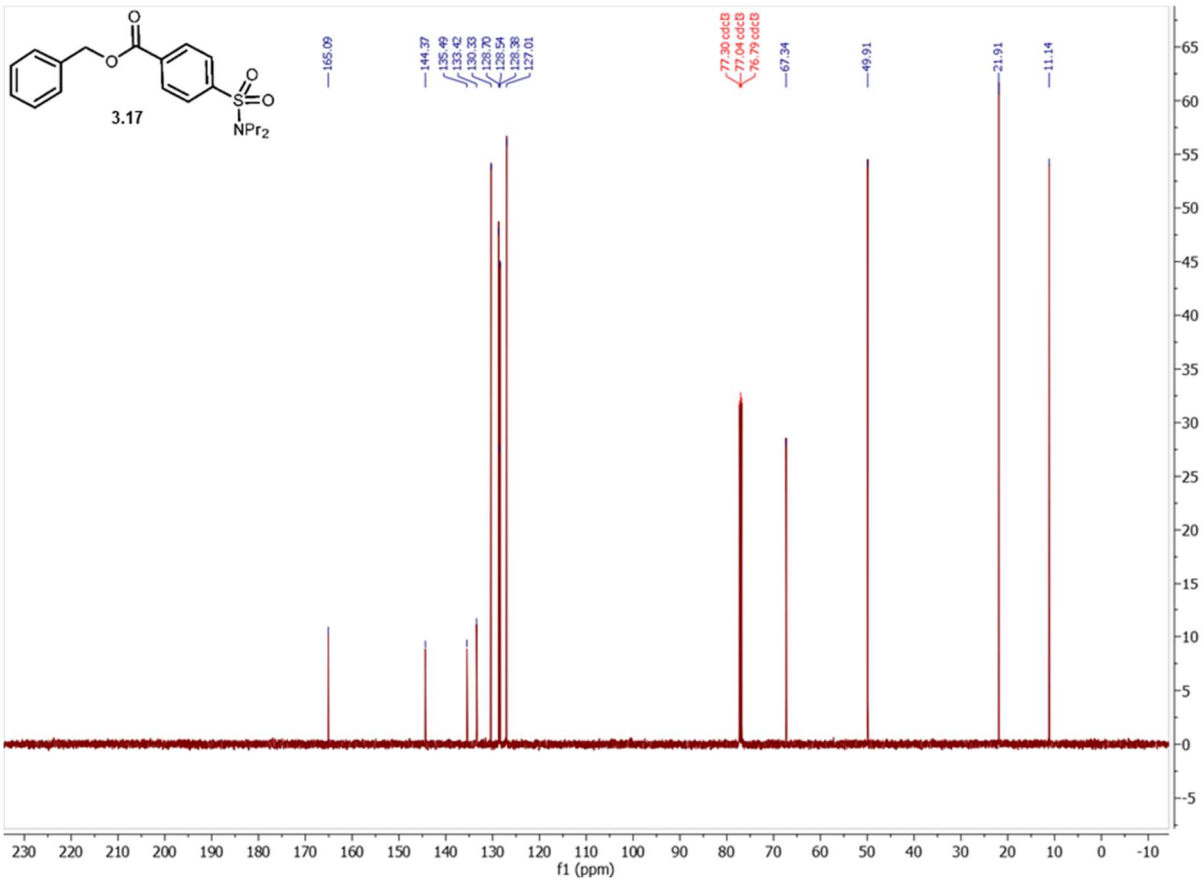

Spectrum 3.36 ^{13}C NMR of compound **3.17**.

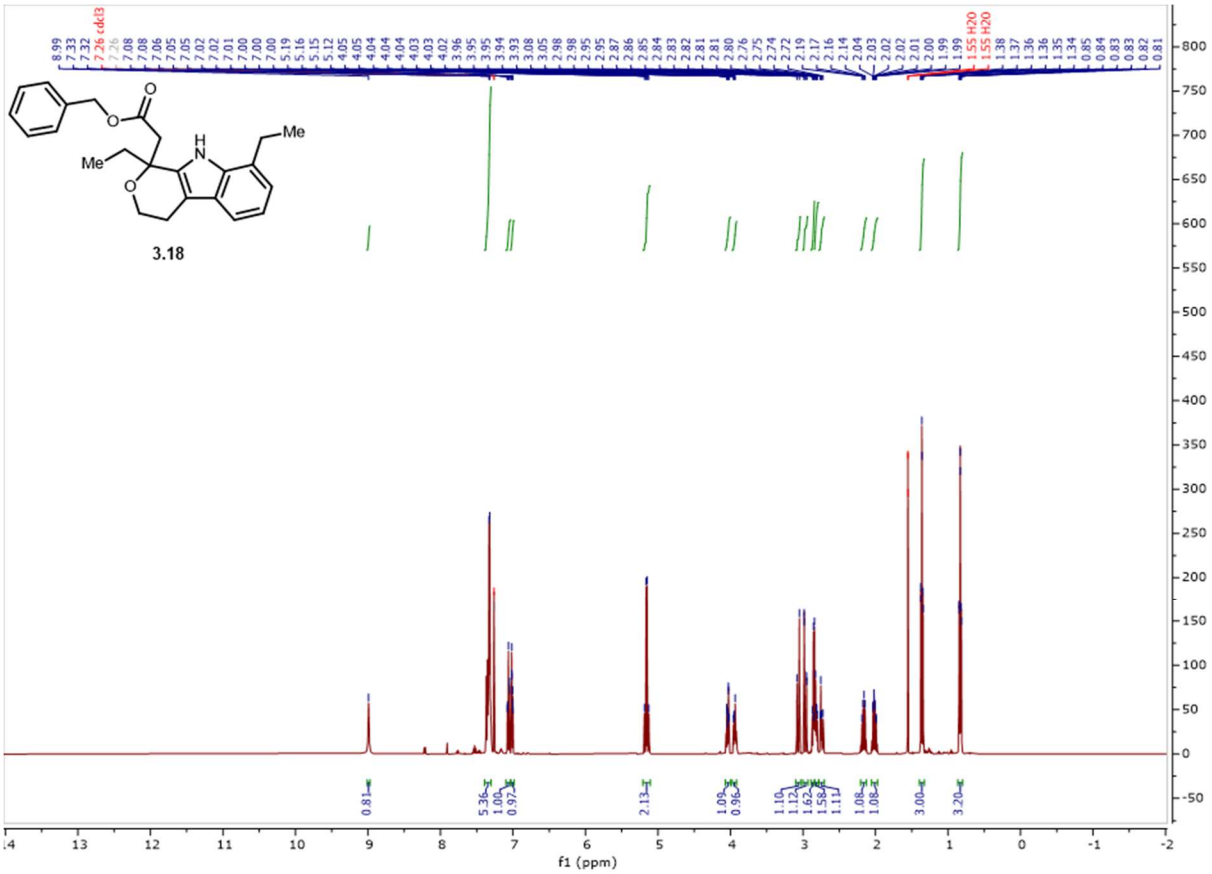

Spectrum 3.37 ^{1}H NMR of compound **3.18**.

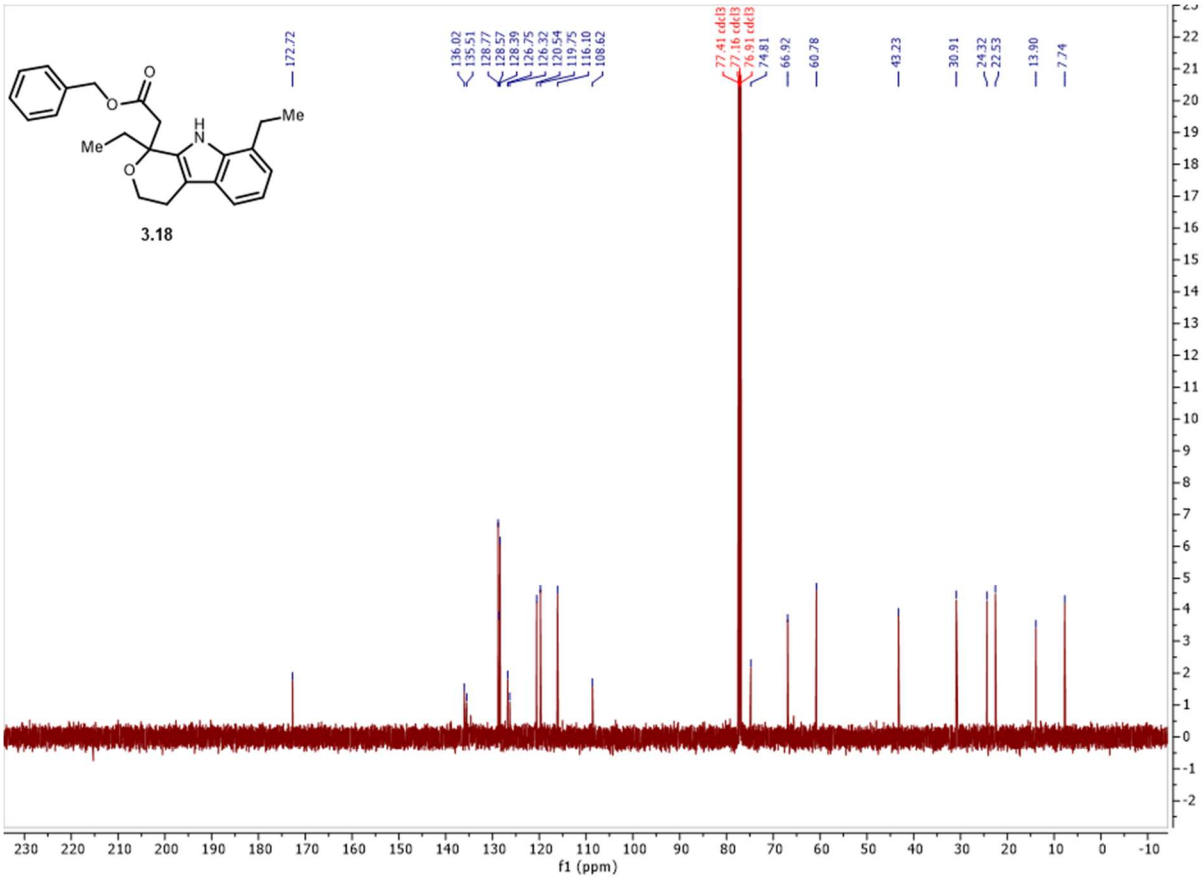

Spectrum 3.38 ^{13}C NMR of compound **3.18**.

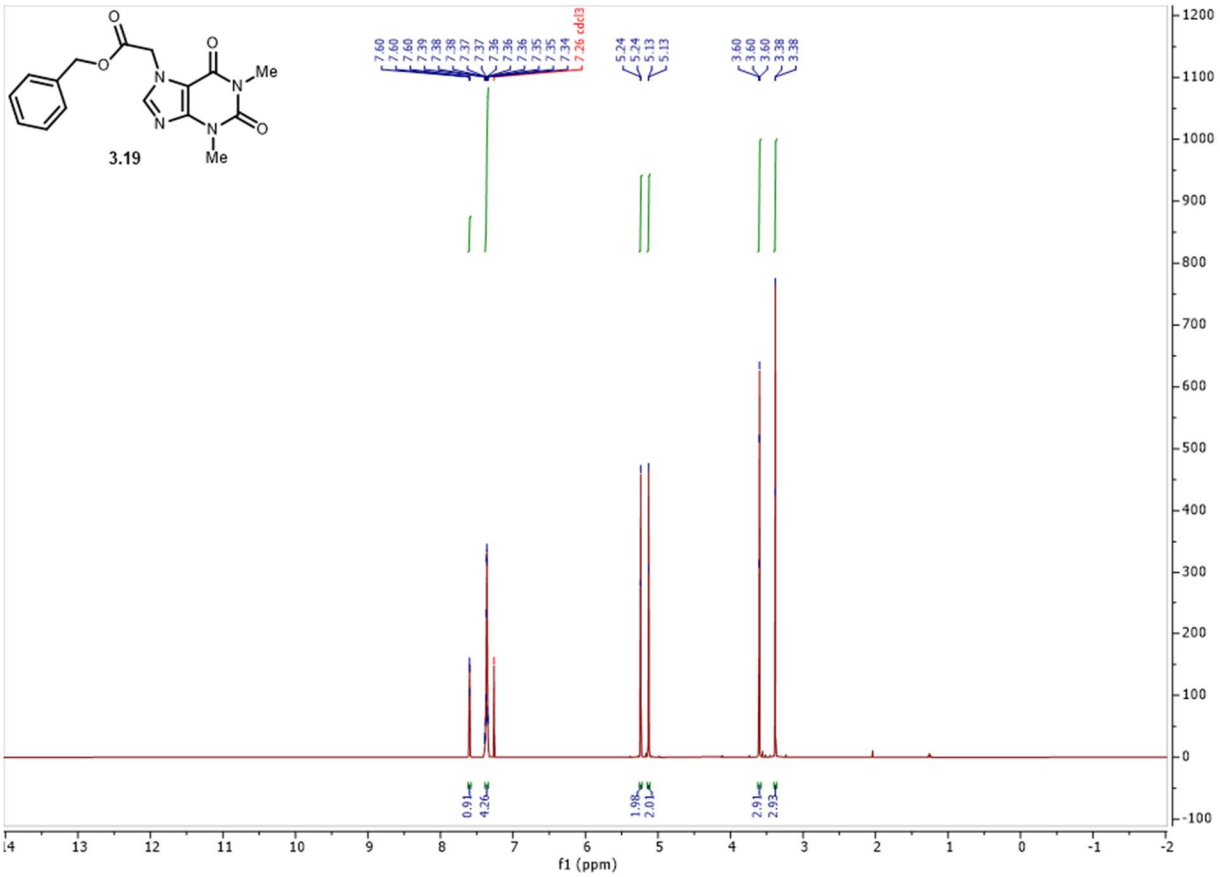

Spectrum 3.39 ^{1}H NMR of compound **3.19**.

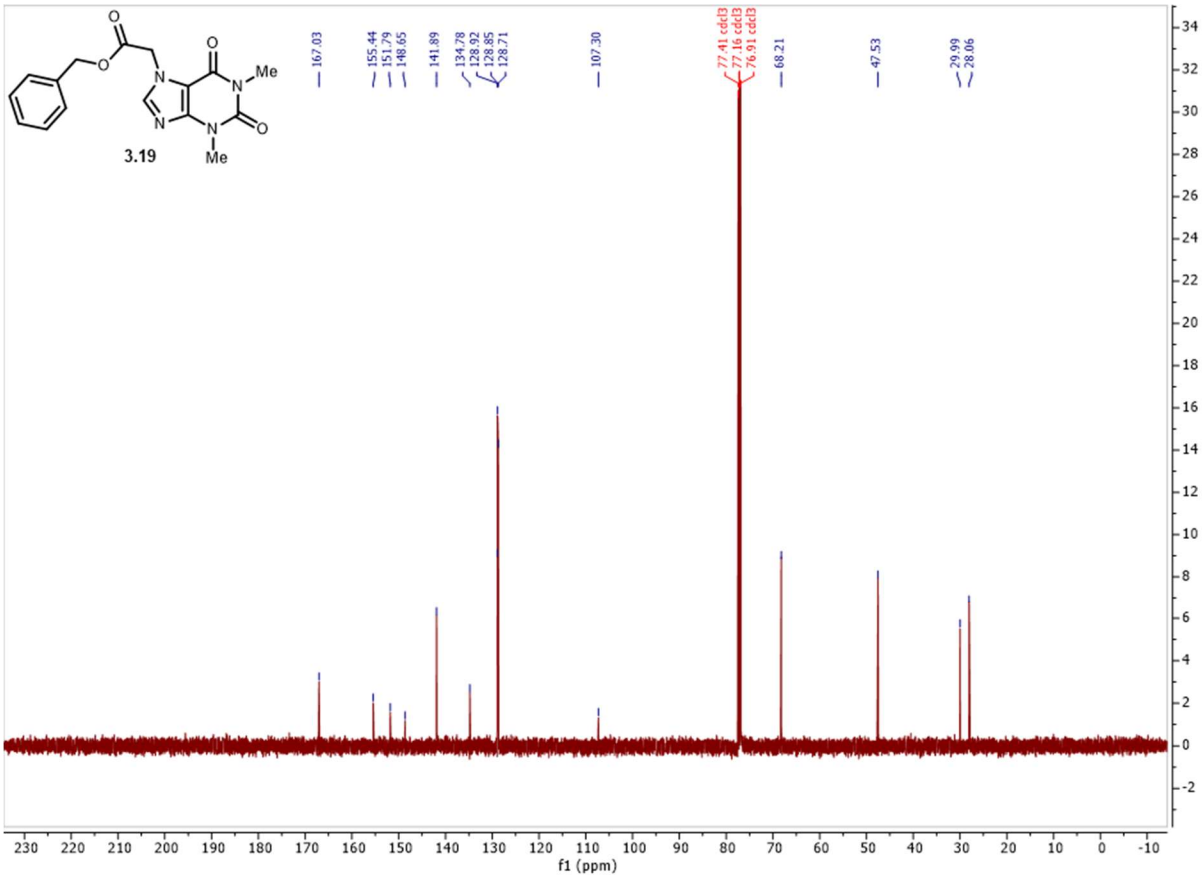

Spectrum 3.40 ^{13}C NMR of compound **3.19**.

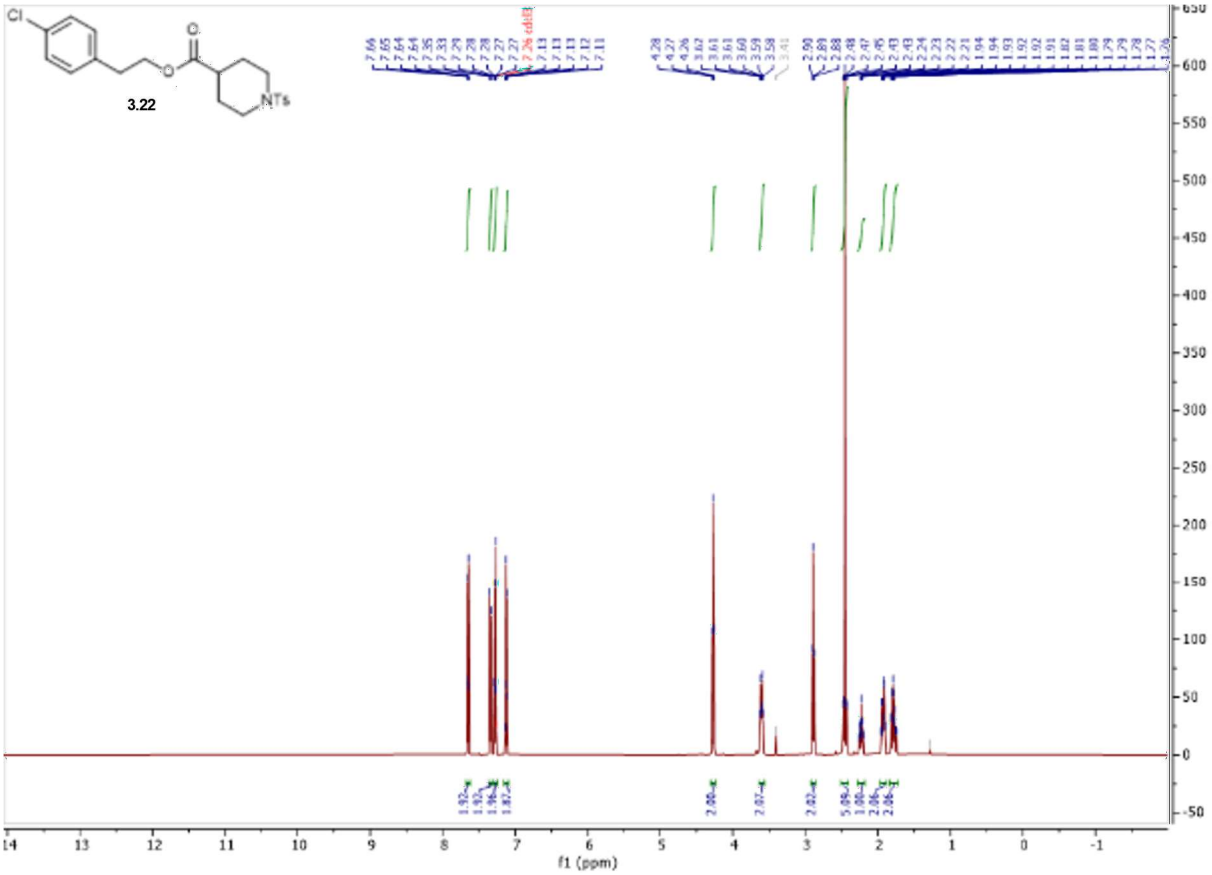

Spectrum 3.41 ^{1}H NMR of compound **3.22**.

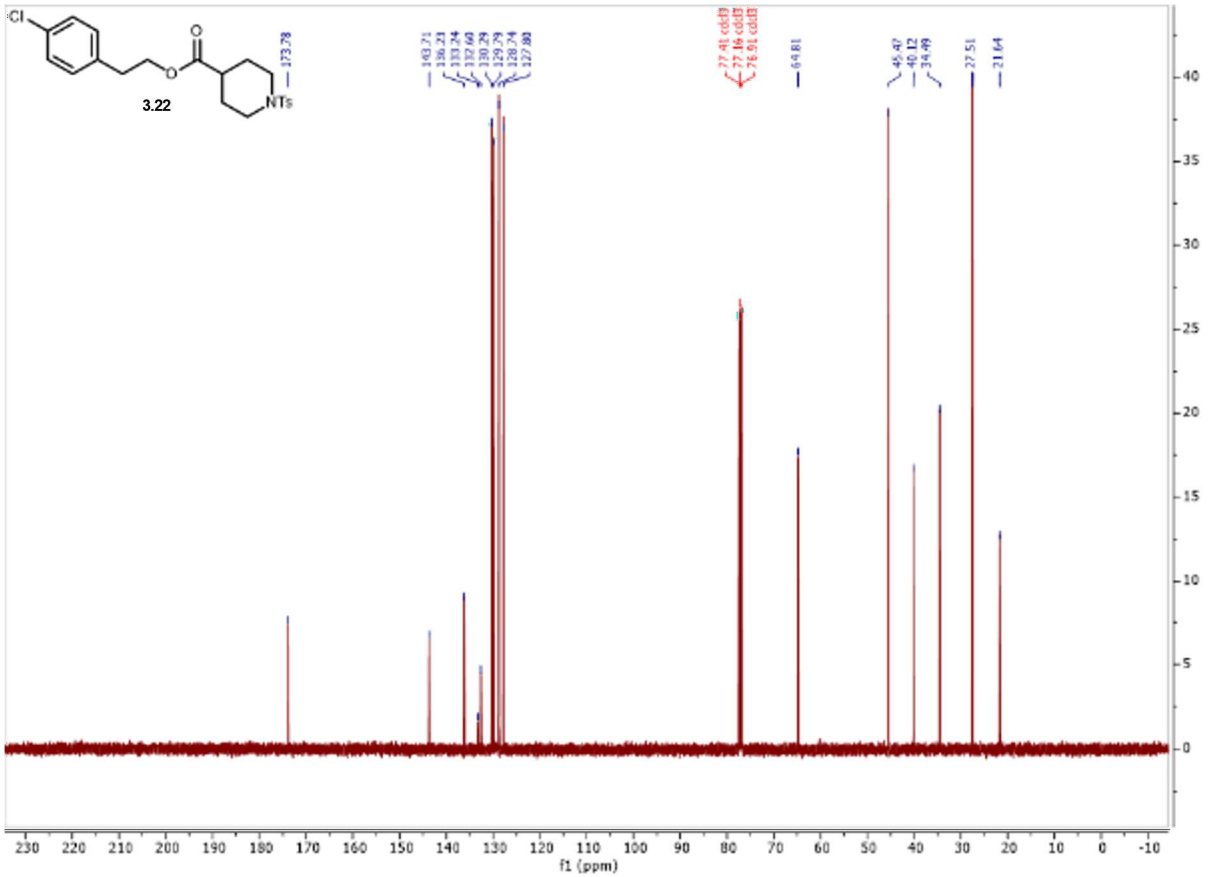

Spectrum 3.42 ^{13}C NMR of compound **3.22**.

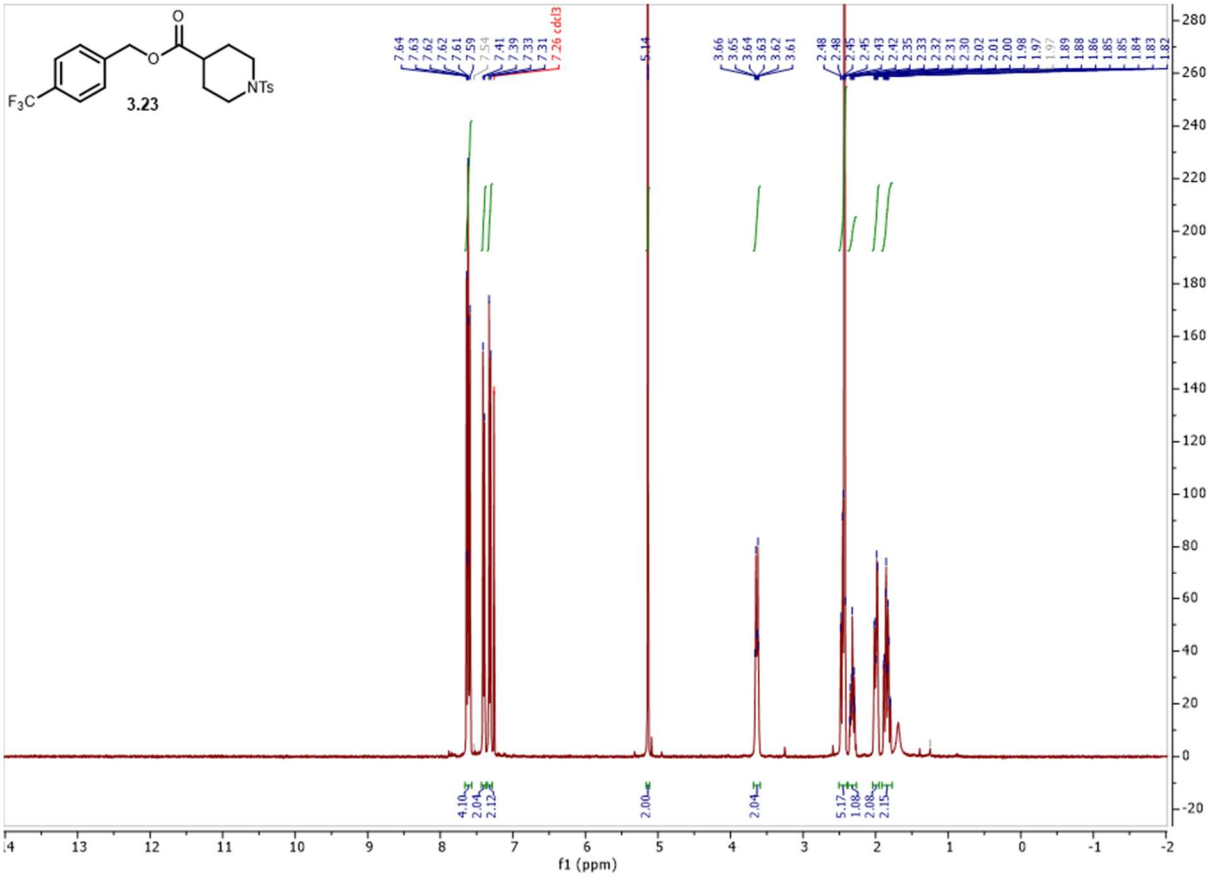

Spectrum 3.43 ^{1}H NMR of compound **3.23**

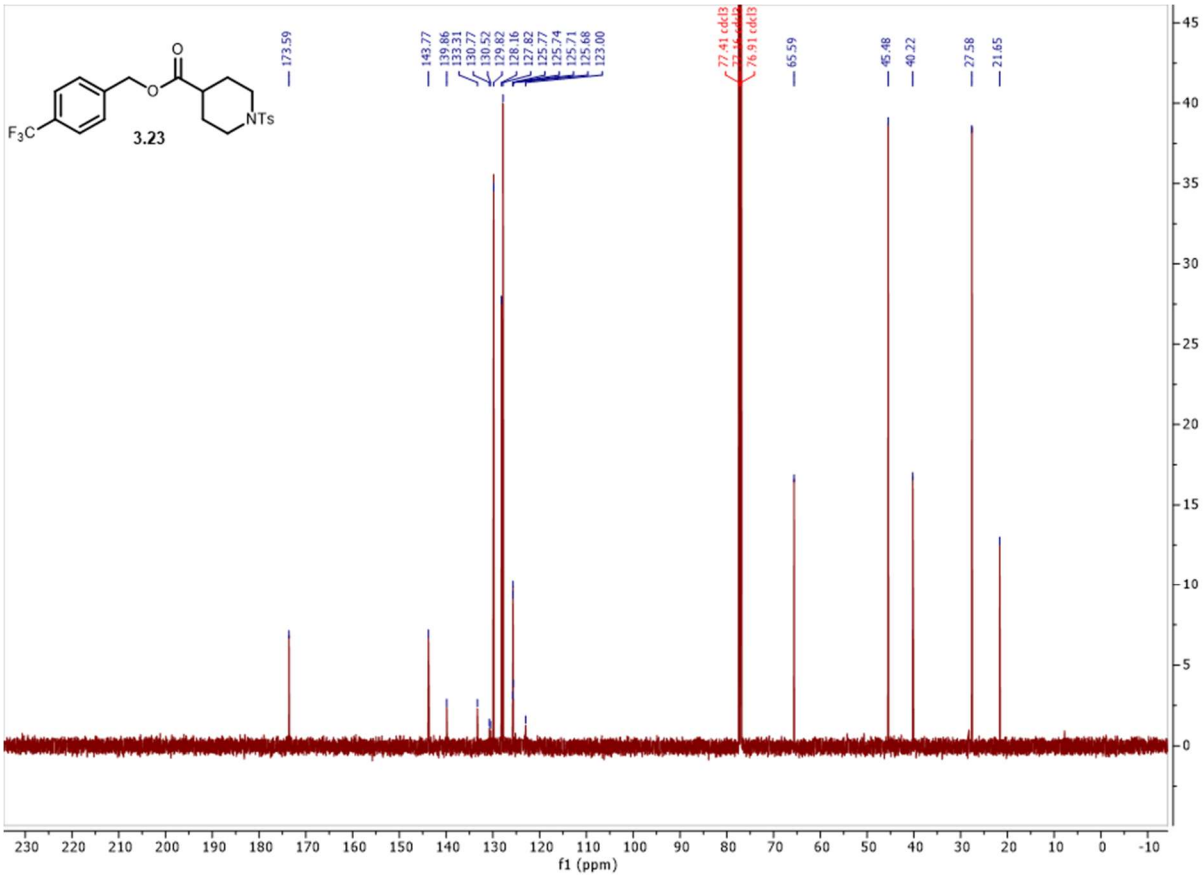

Spectrum 3.44 ^{13}C NMR of compound **3.23**.

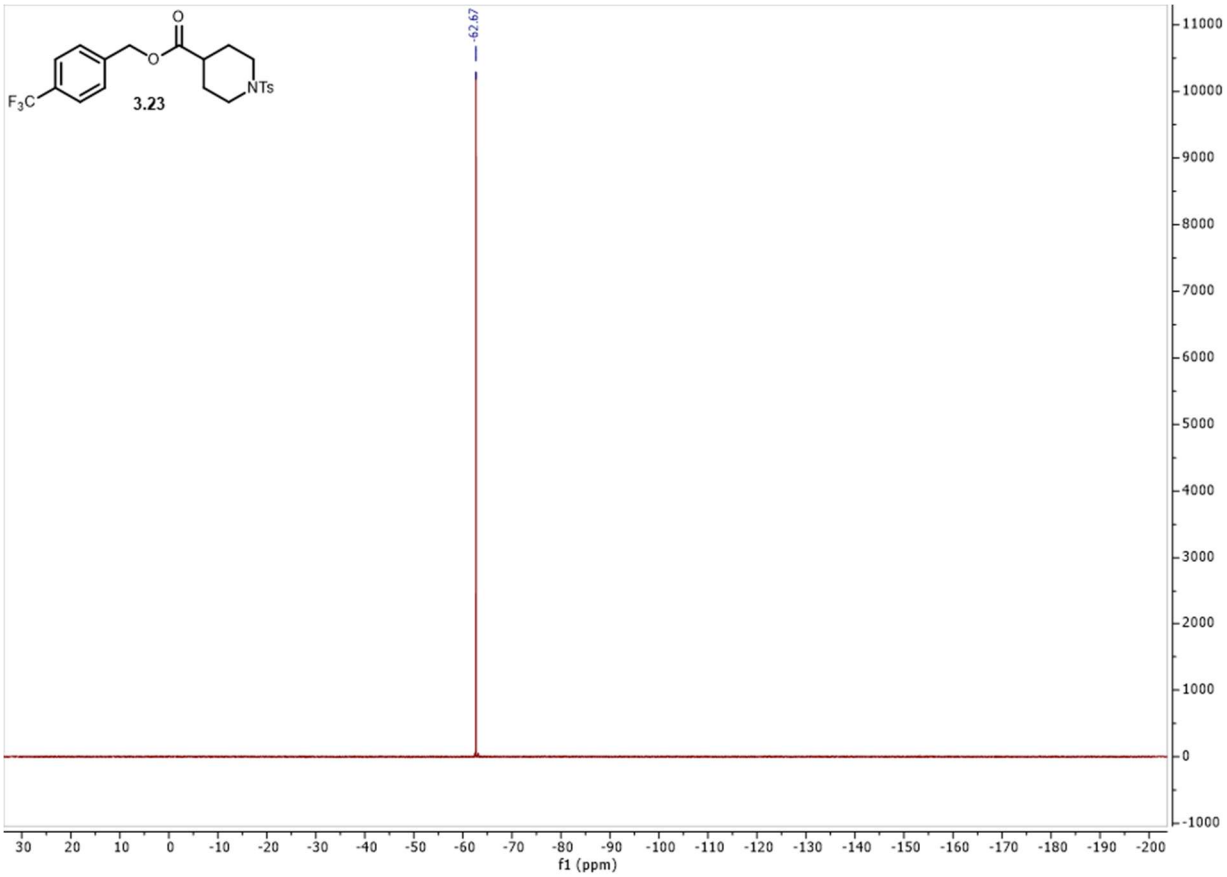

Spectrum 3.45 ^{19}F NMR of compound **3.23**.

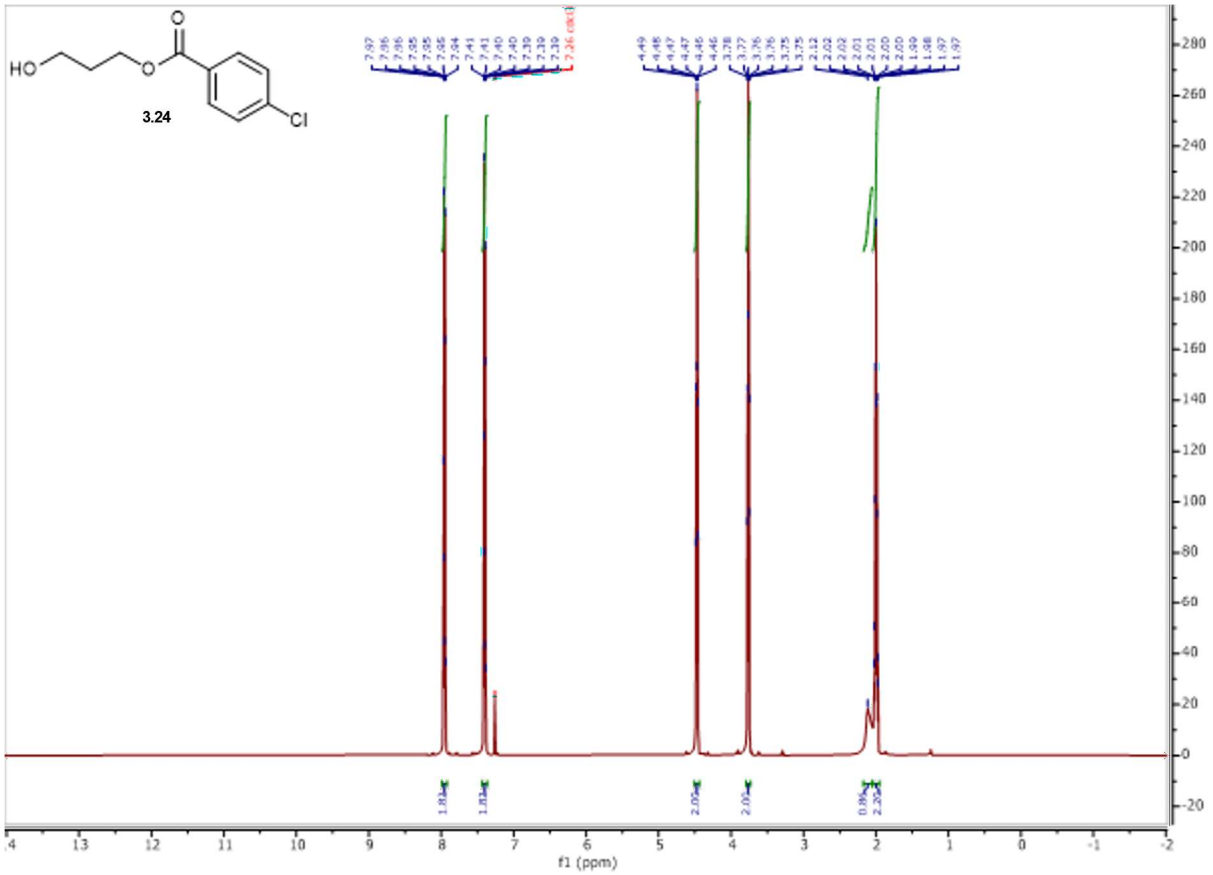

Spectrum 3.46 ^{1}H NMR of compound **3.24**.

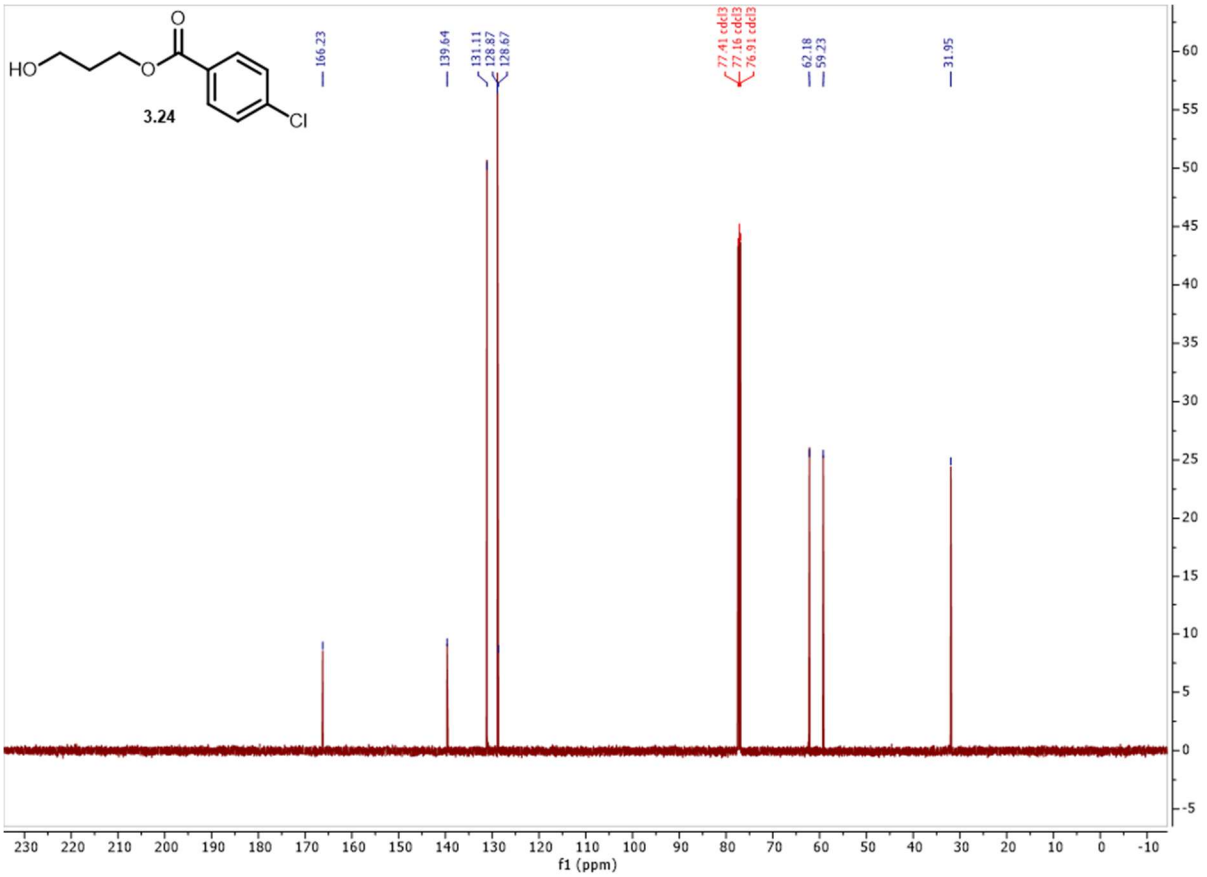

Spectrum 3.47 ^{13}C NMR of compound of **3.24**.

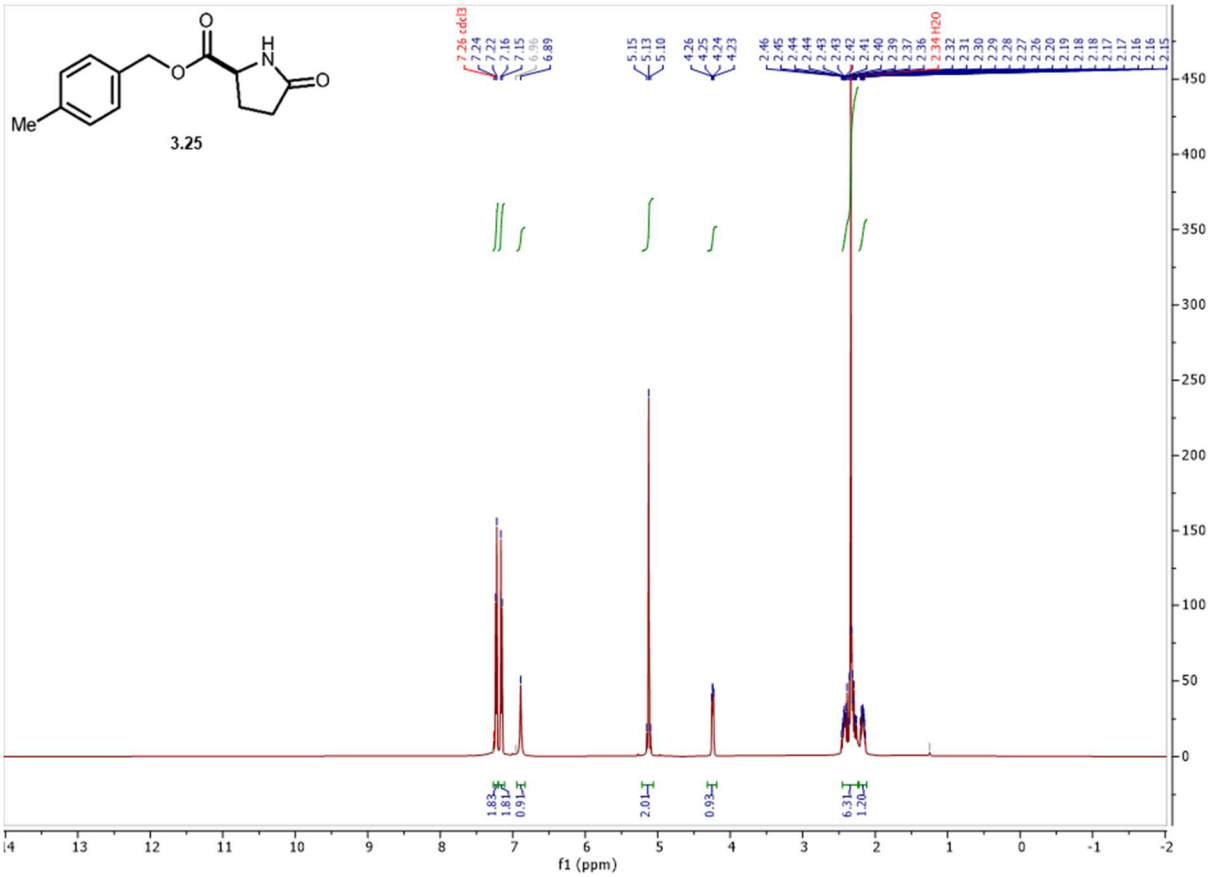

Spectrum 3.48 ^{1}H NMR of compound **3.25**.

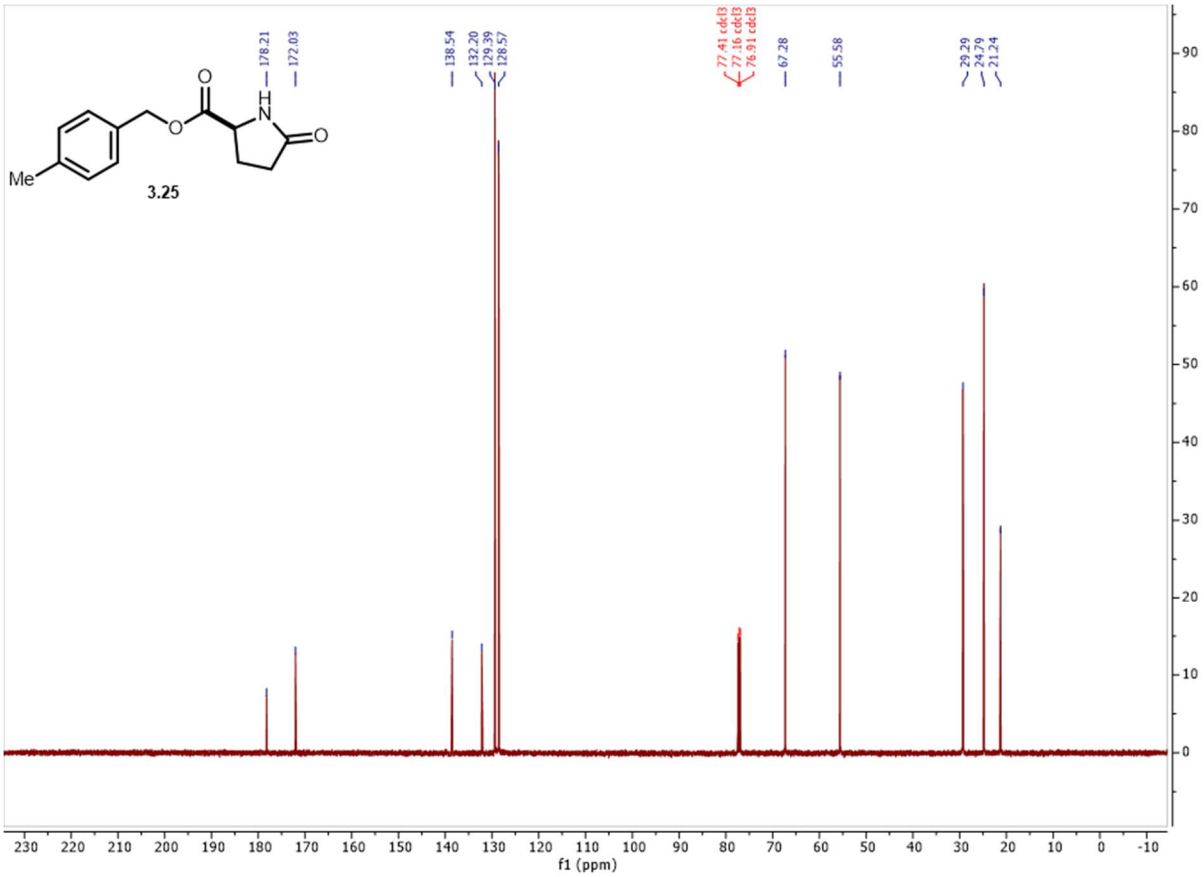

Spectrum 3.49 ^{13}C NMR of compound **3.25**.

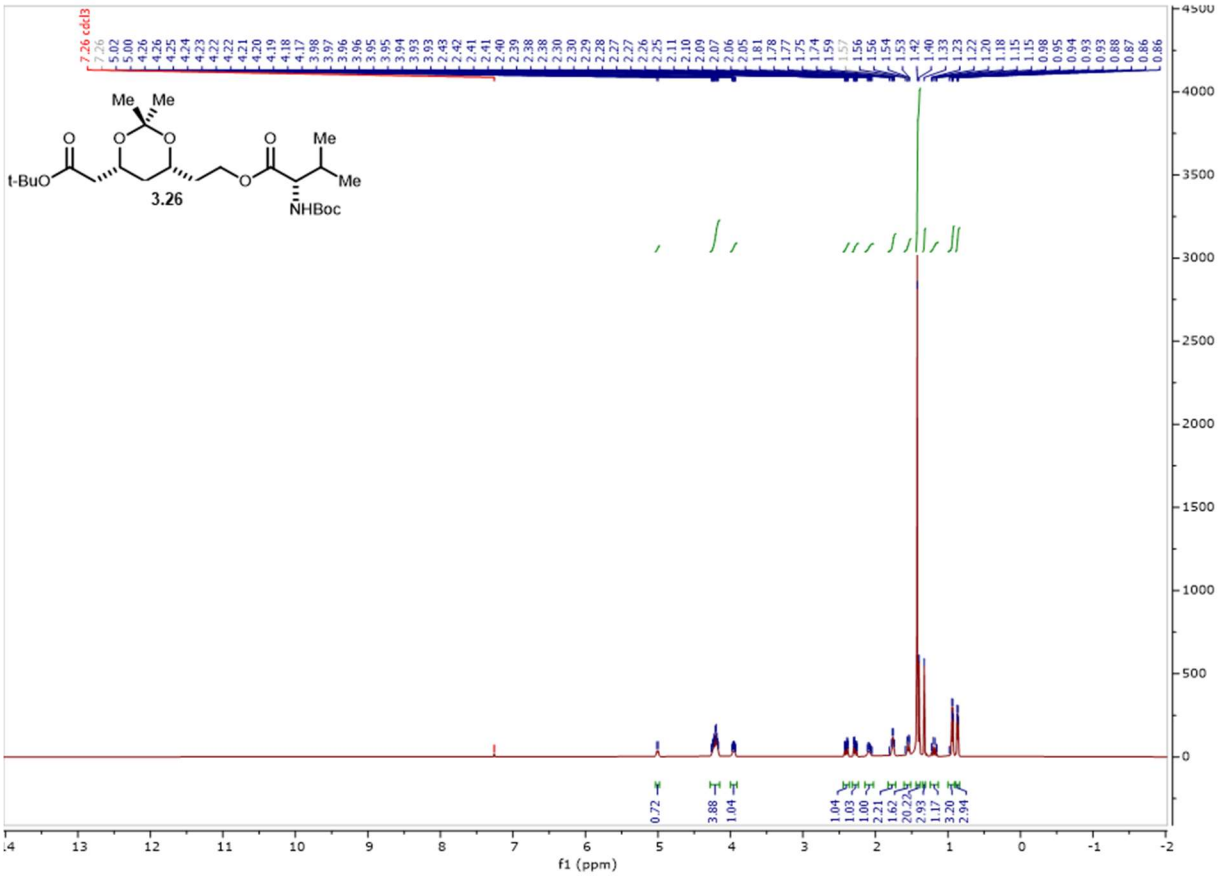

Spectrum 3.50 ^{1}H NMR of compound **3.26**.

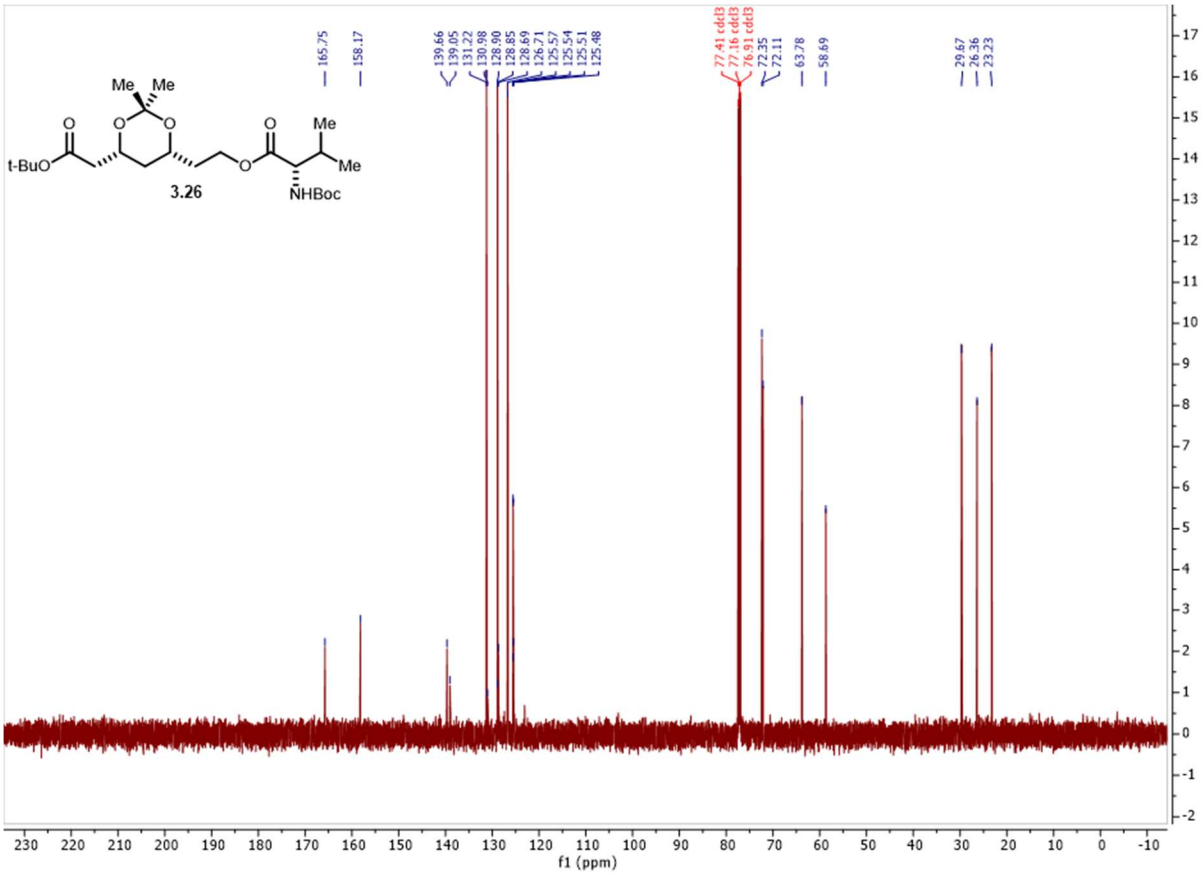

Spectrum 3.51 ^{13}C NMR of compound **3.26**.

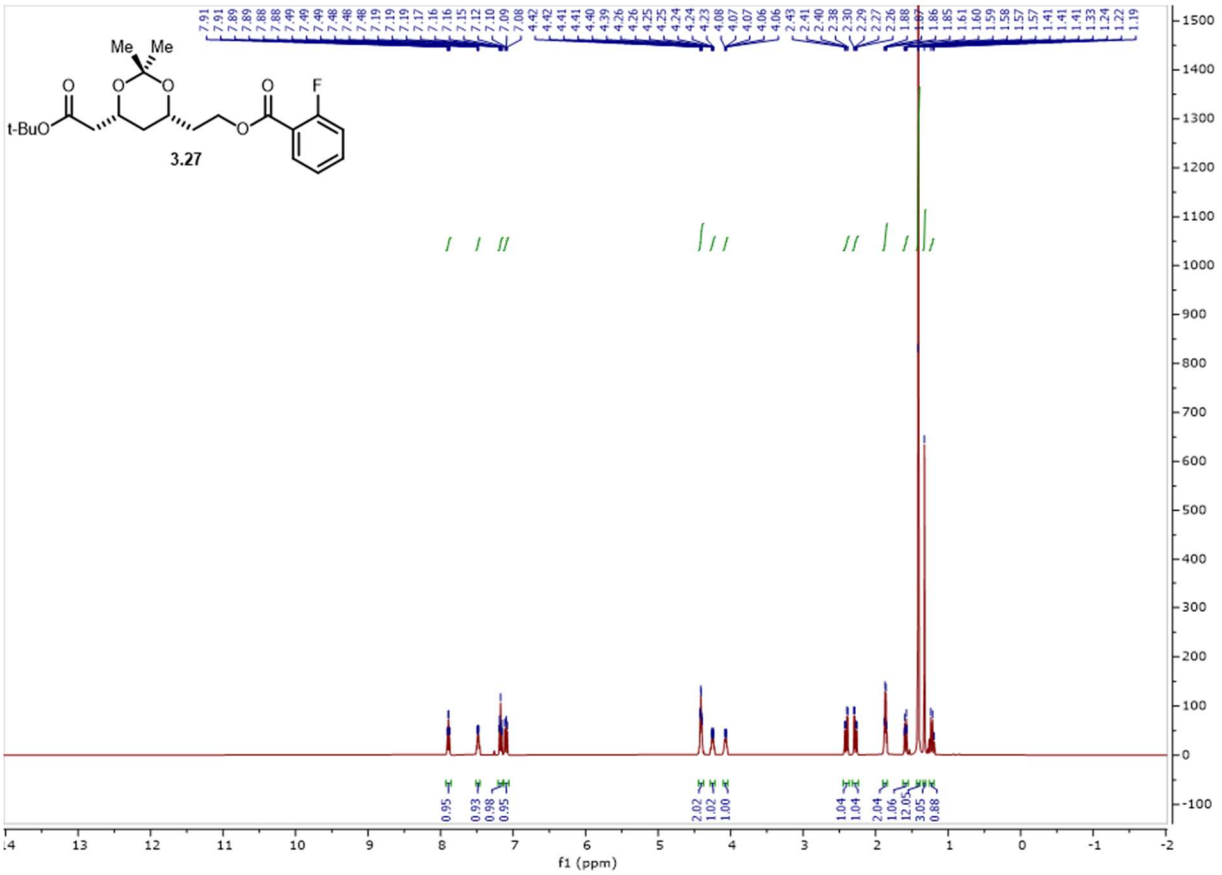

Spectrum 3.52 ^{1}H NMR of compound **3.27**.

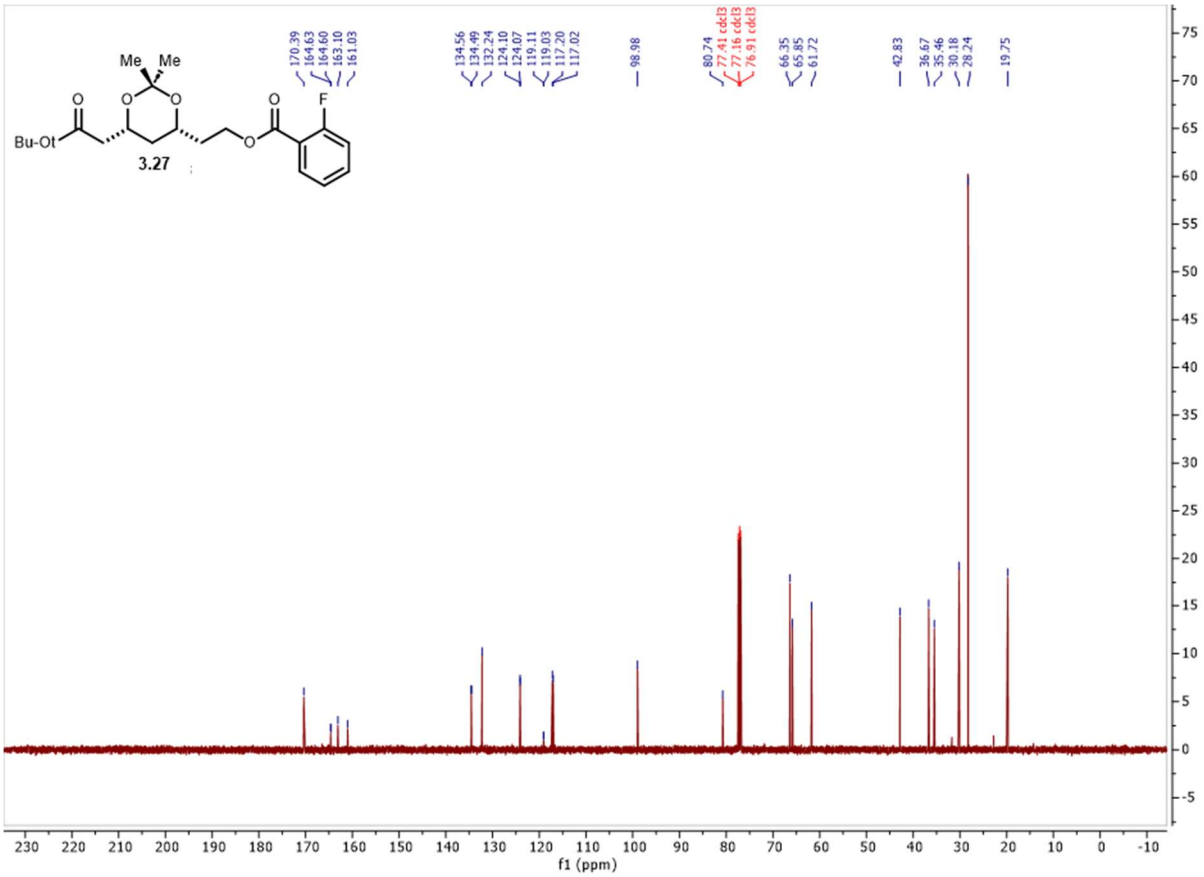

Spectrum 3.53 ^{13}C NMR of compound **3.27**.

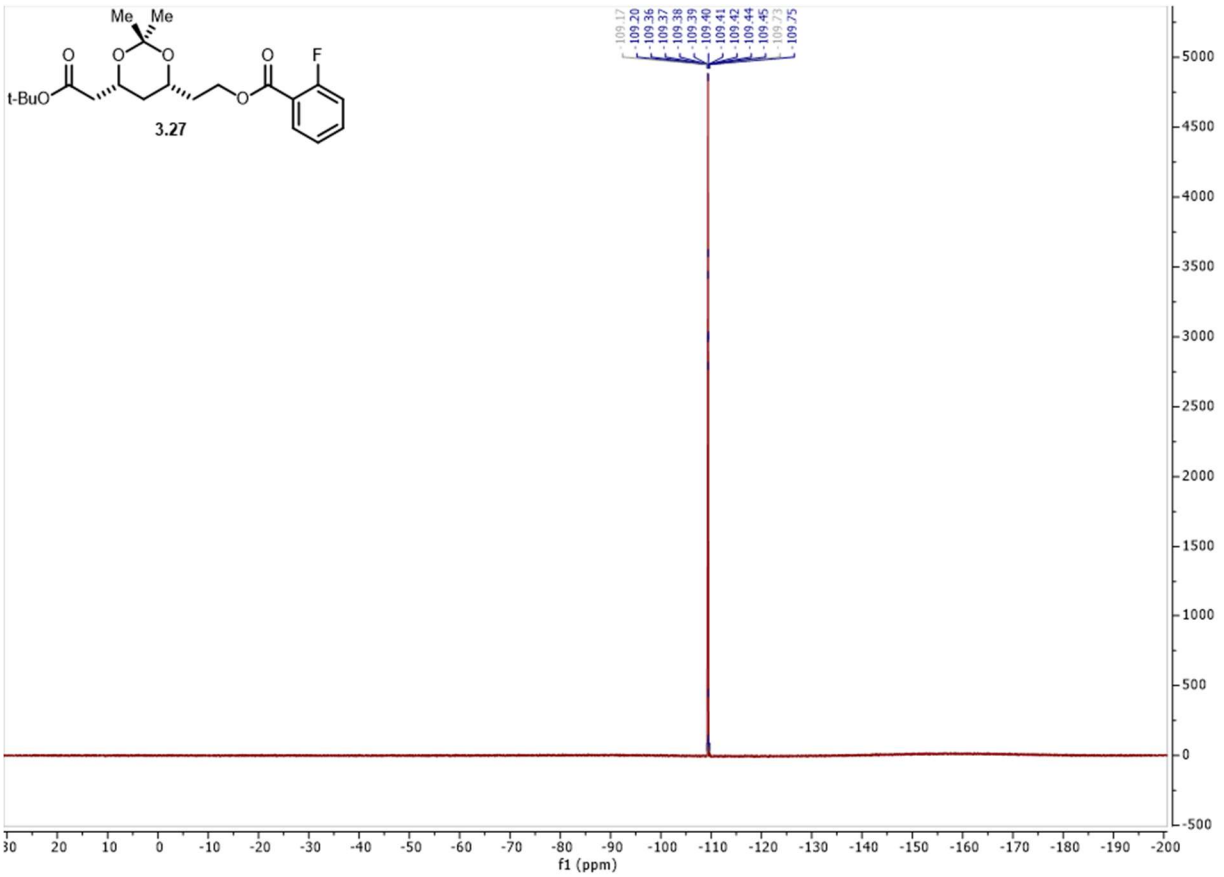

Spectrum 3.54 ^{19}F NMR of compound **3.27**.

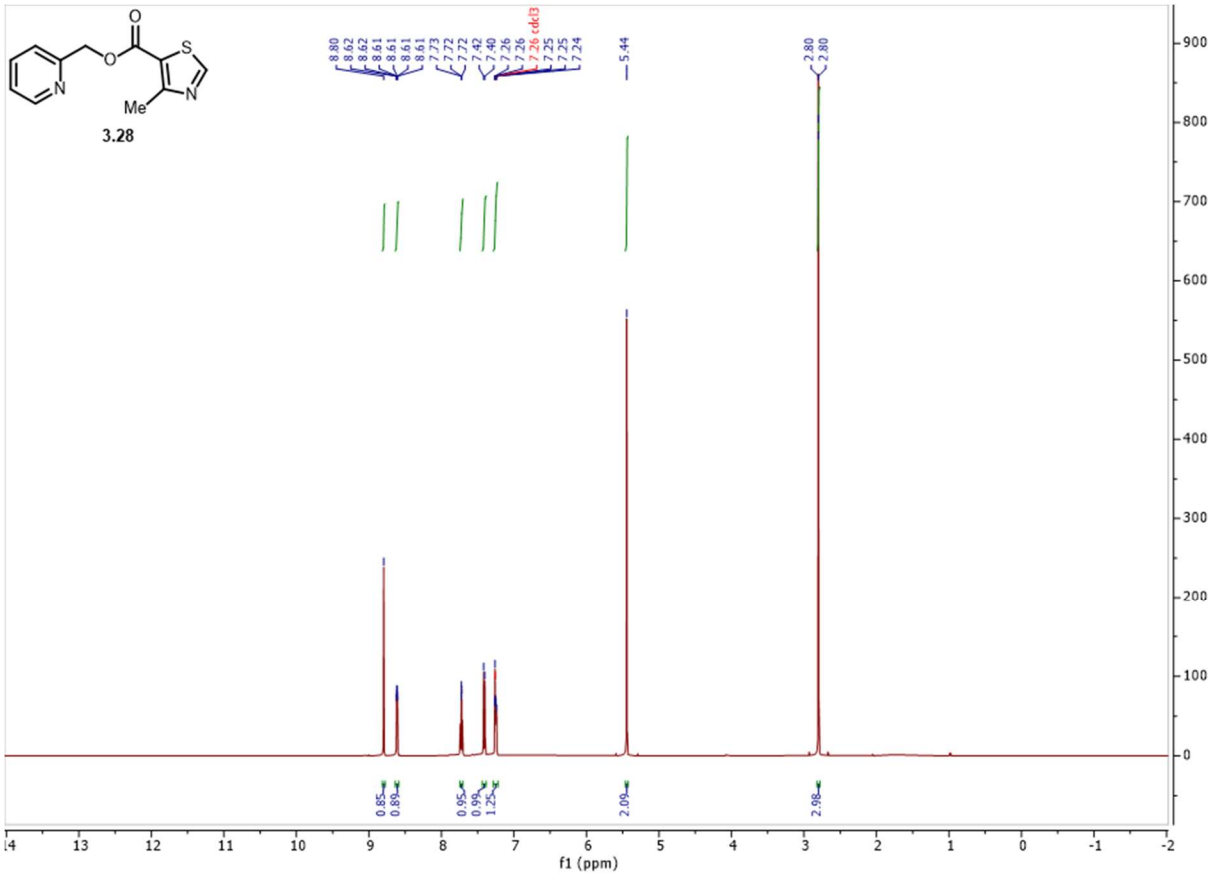

Spectrum 3.55 ^{1}H NMR of compound **3.28**.

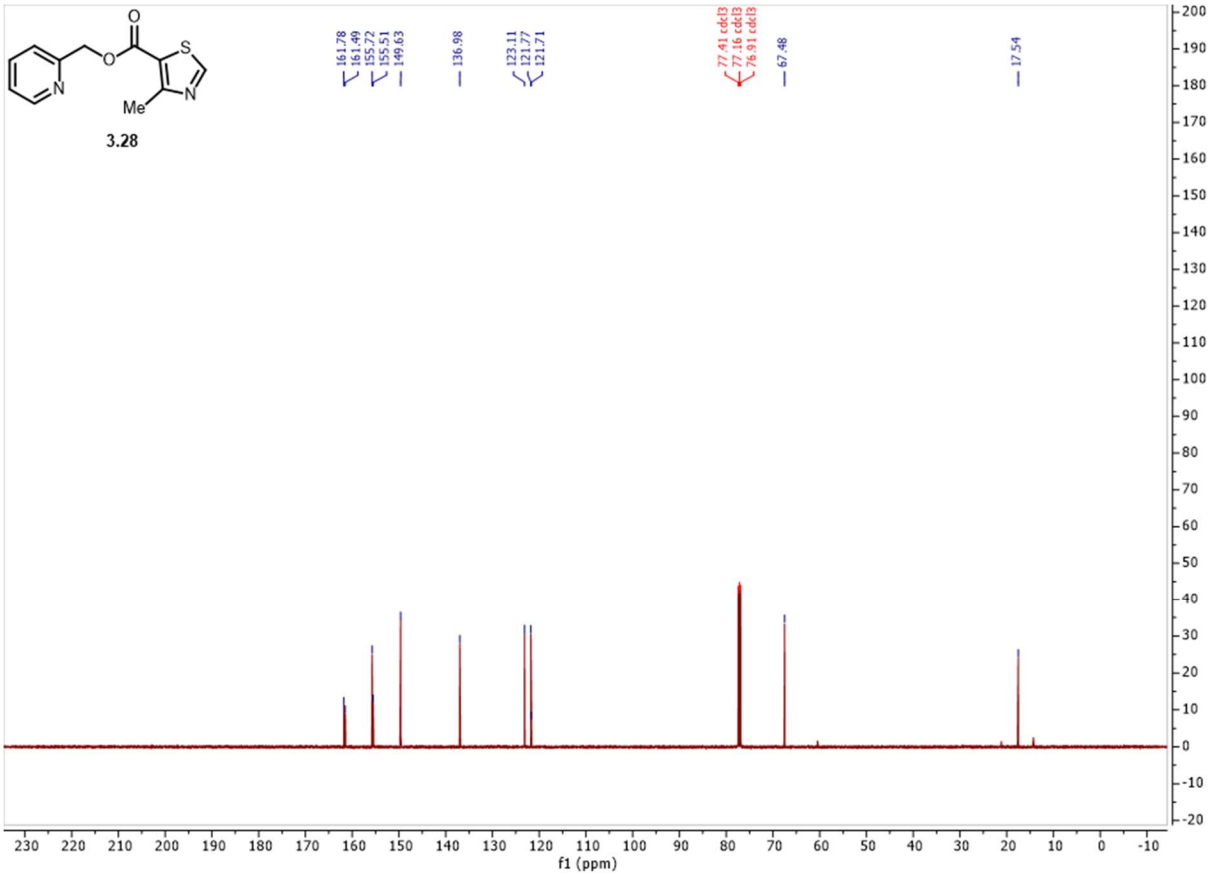

Spectrum 3.56 ^{13}C NMR of compound of **3.28**.

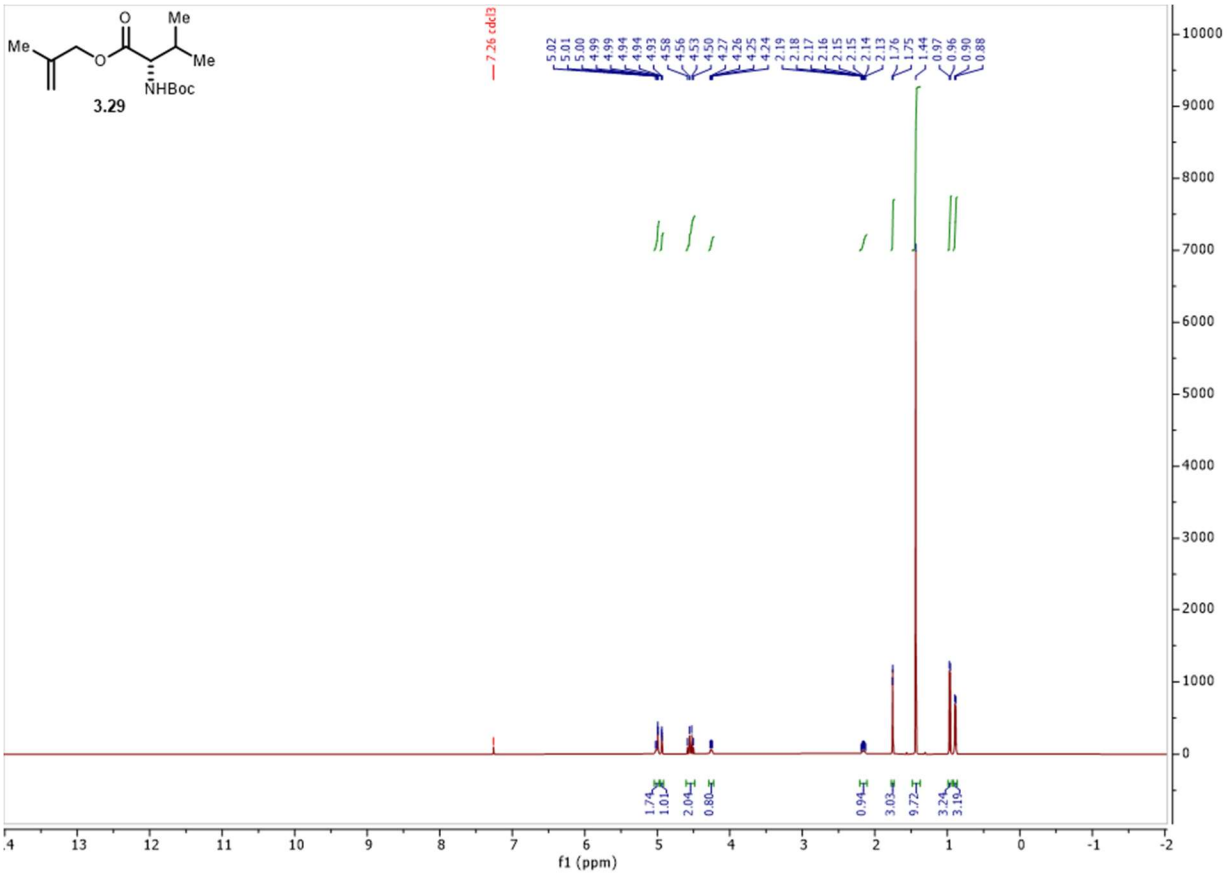

Spectrum 3.57 ^{1}H NMR of compound **3.29**.

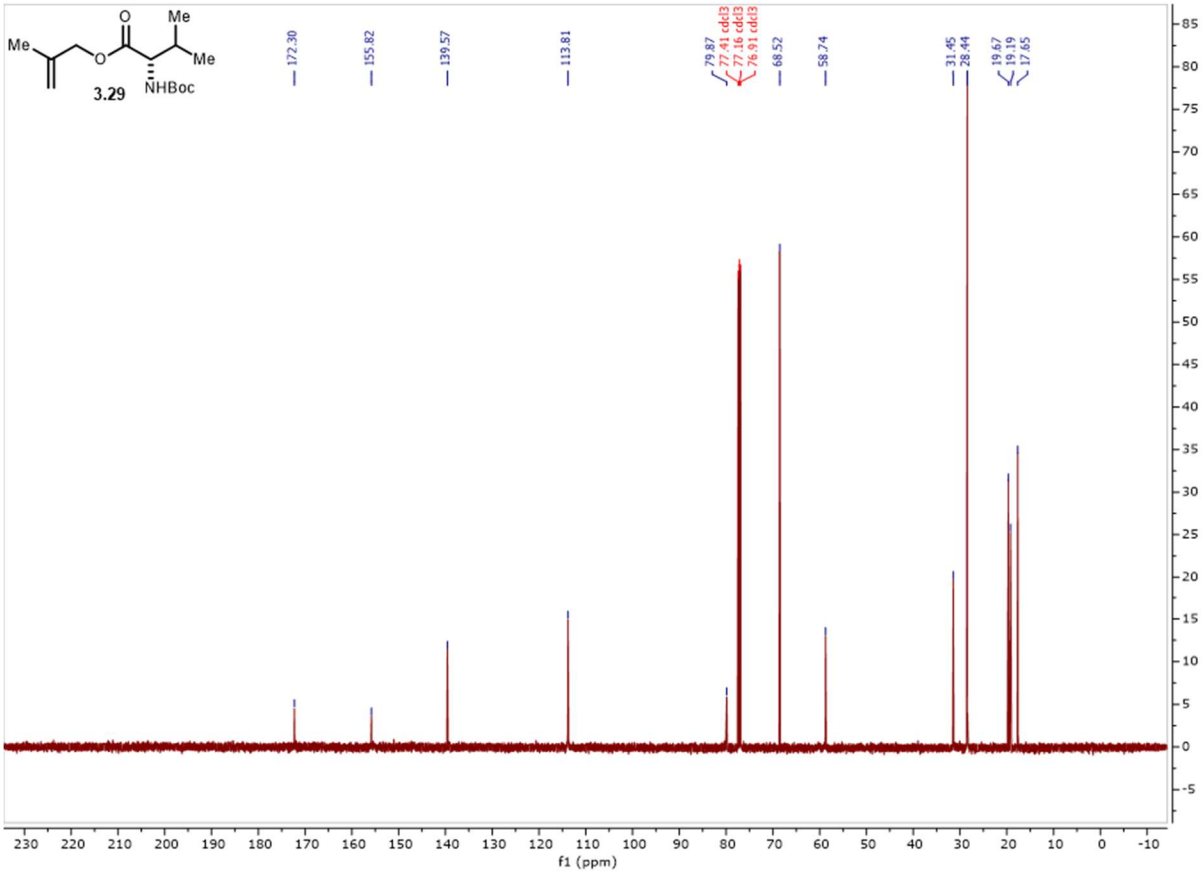

Spectrum 3.58 ^{13}C NMR of compound **3.29**.

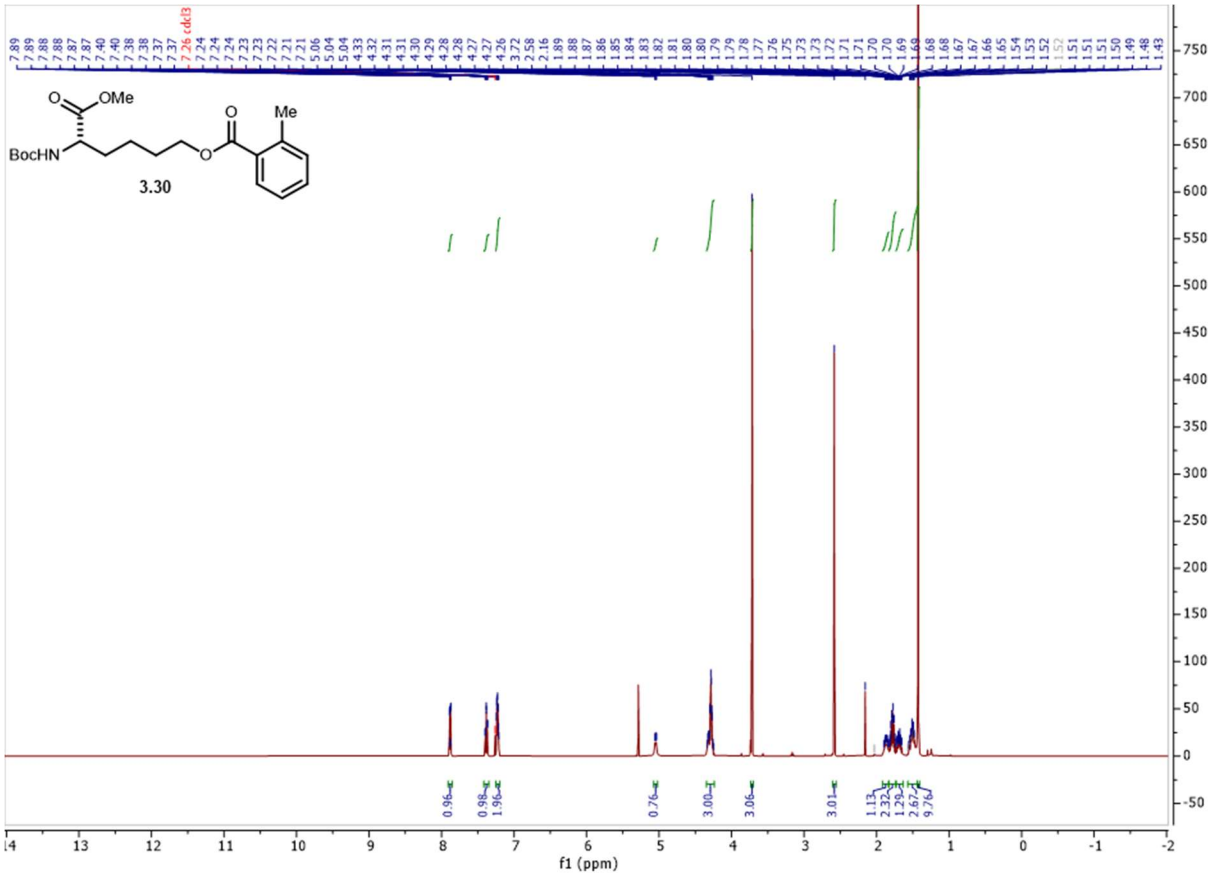

Spectrum 3.59 ^{1}H NMR of compound **3.30**.

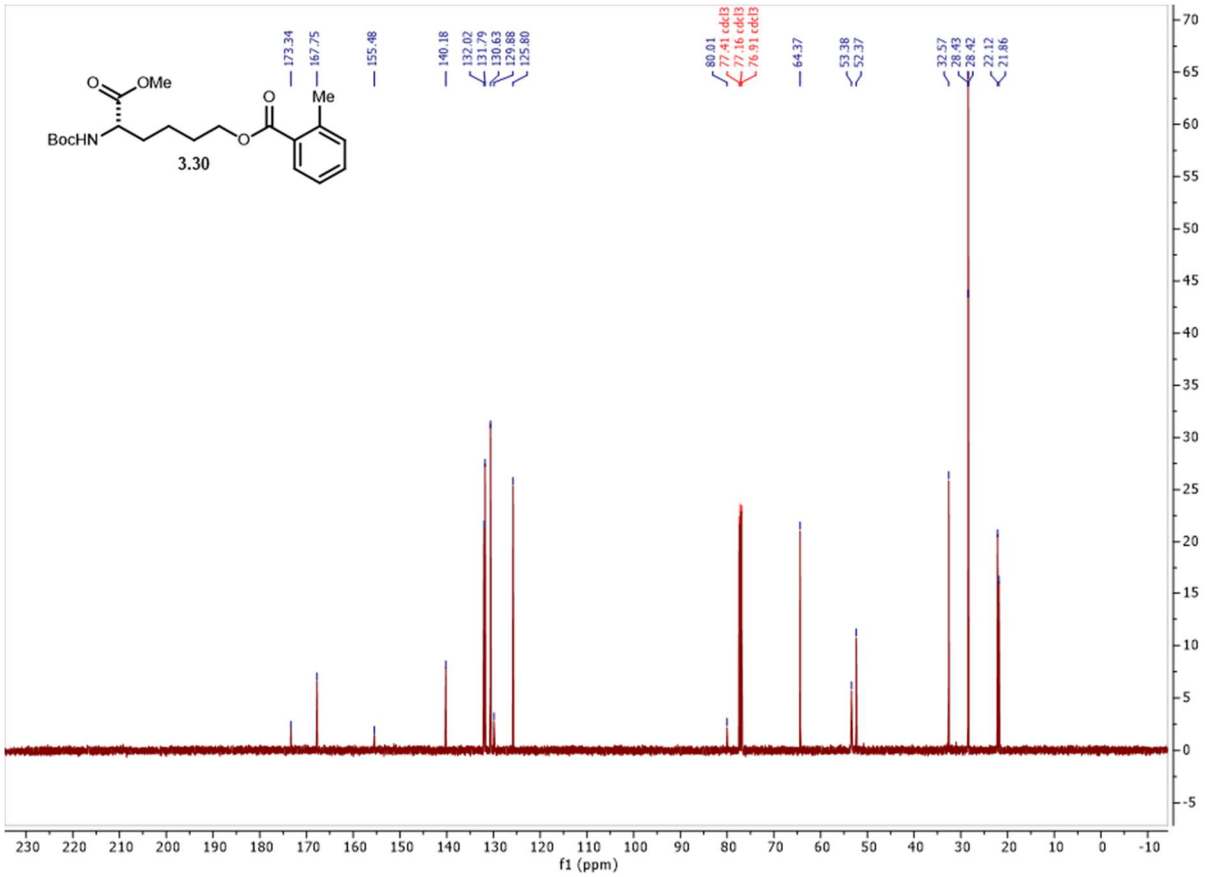

Spectrum 3.60 ^{13}C NMR of compound **3.30**.

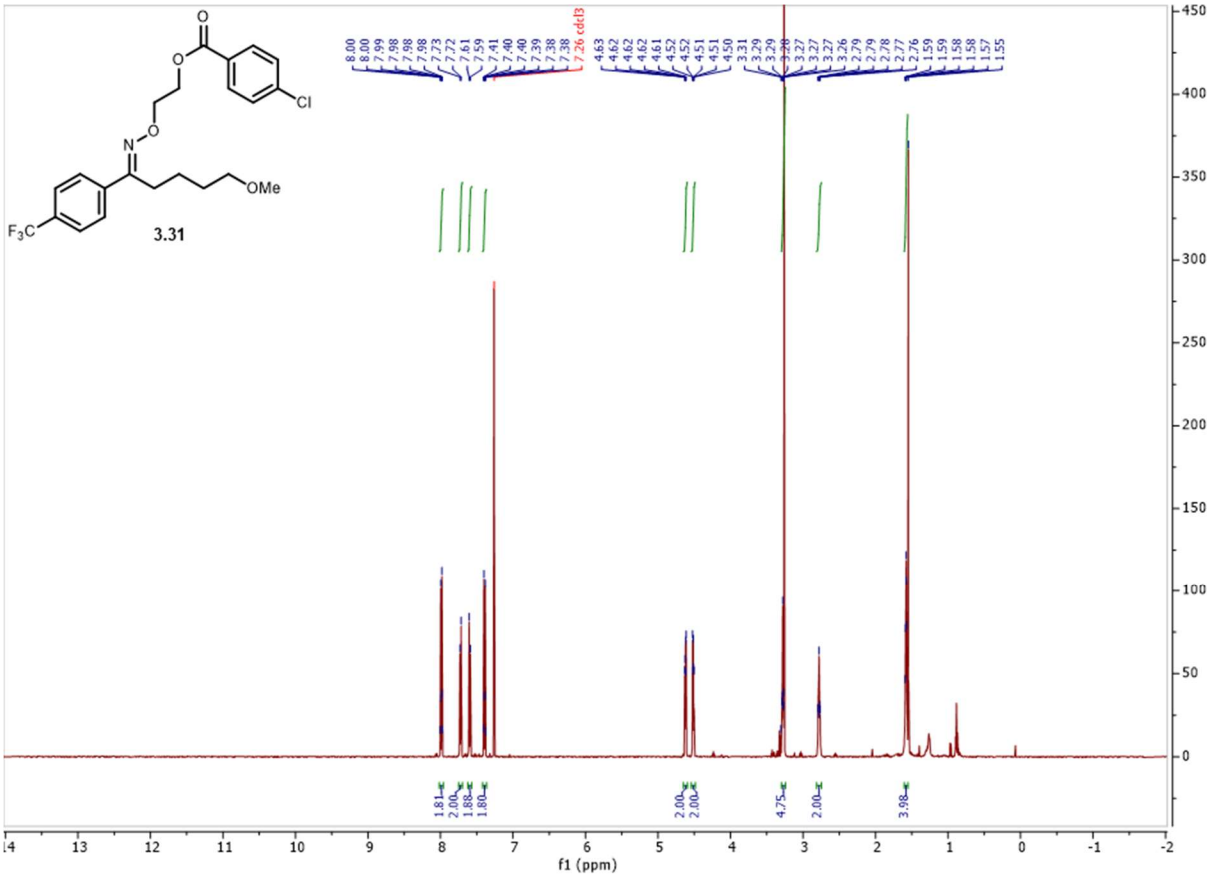

Spectrum 3.61 ^{1}H NMR of compound **3.31**.

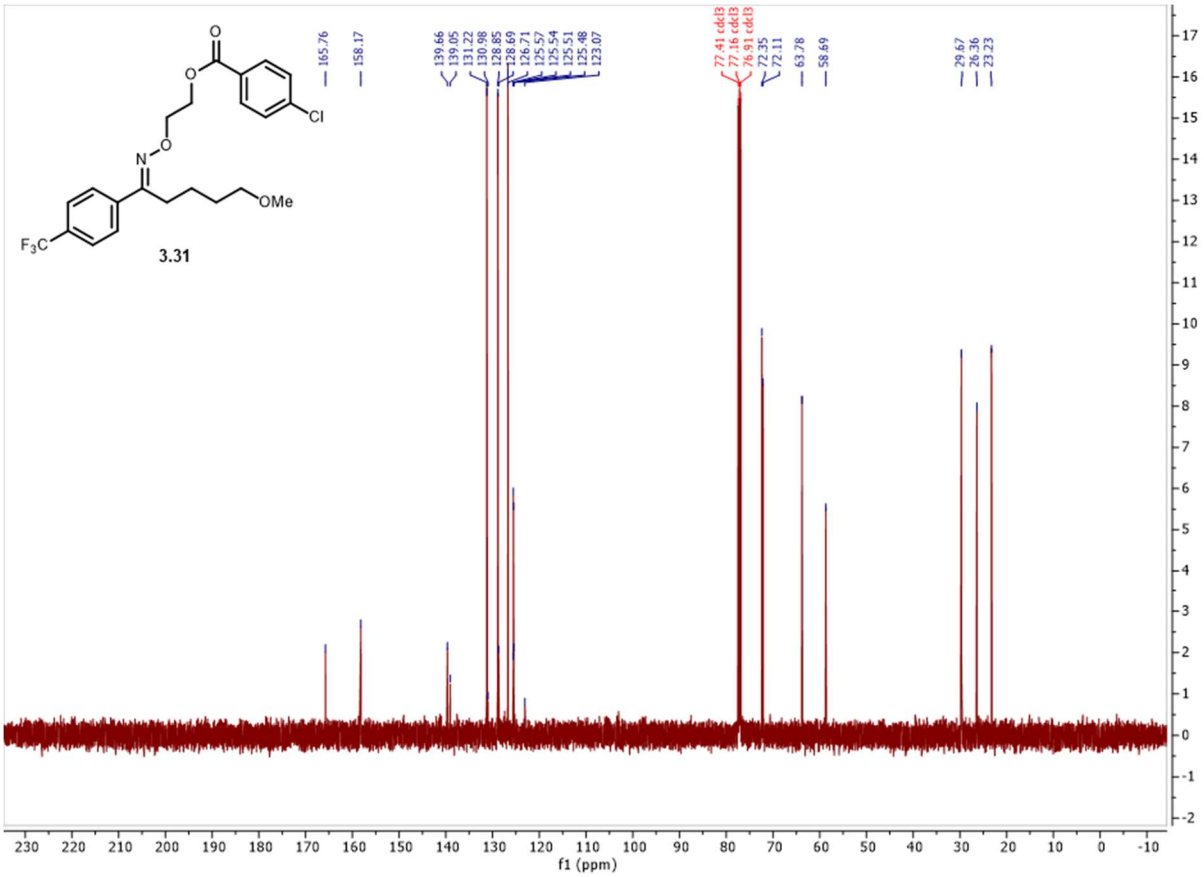

Spectrum 3.62 ^{13}C NMR of compound of **3.31**.

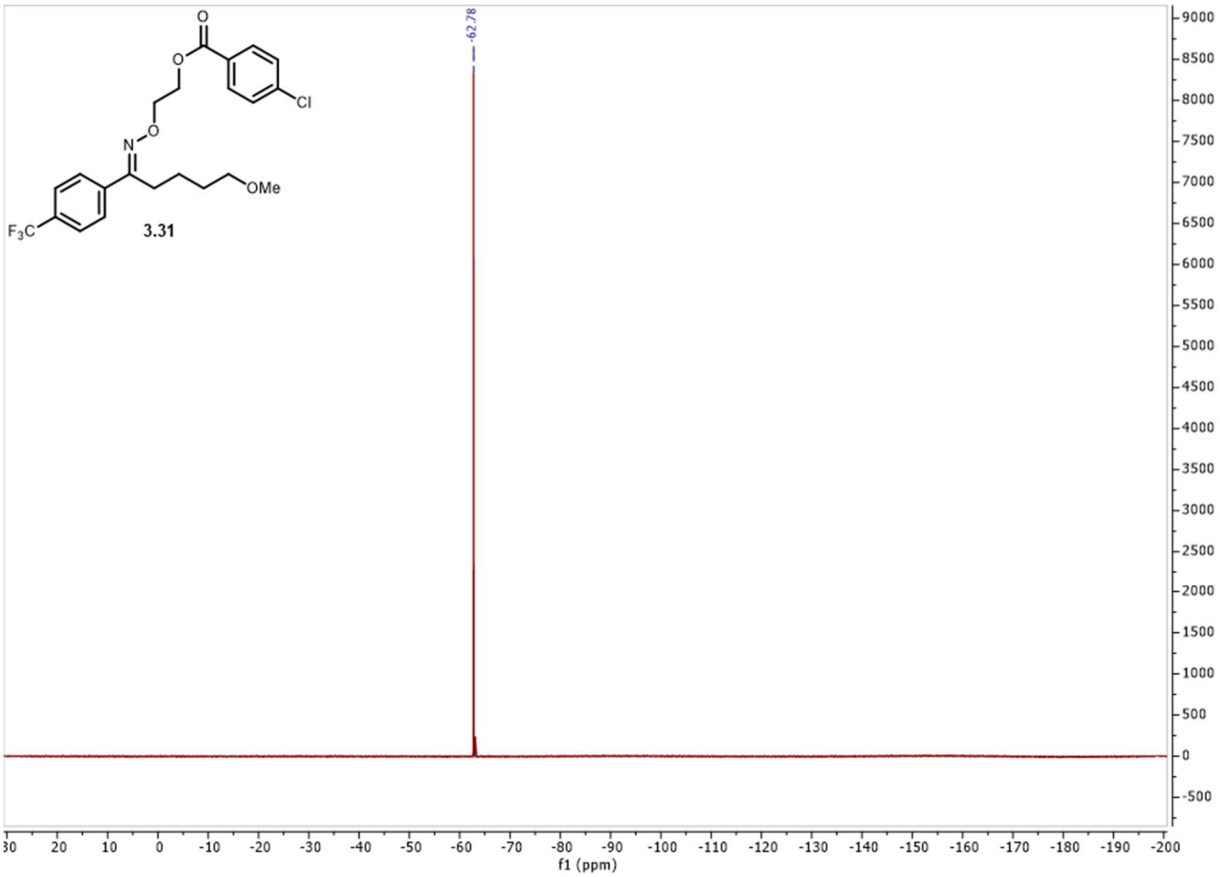

Spectrum 3.63 ^{19}F NMR of compound **3.31**.

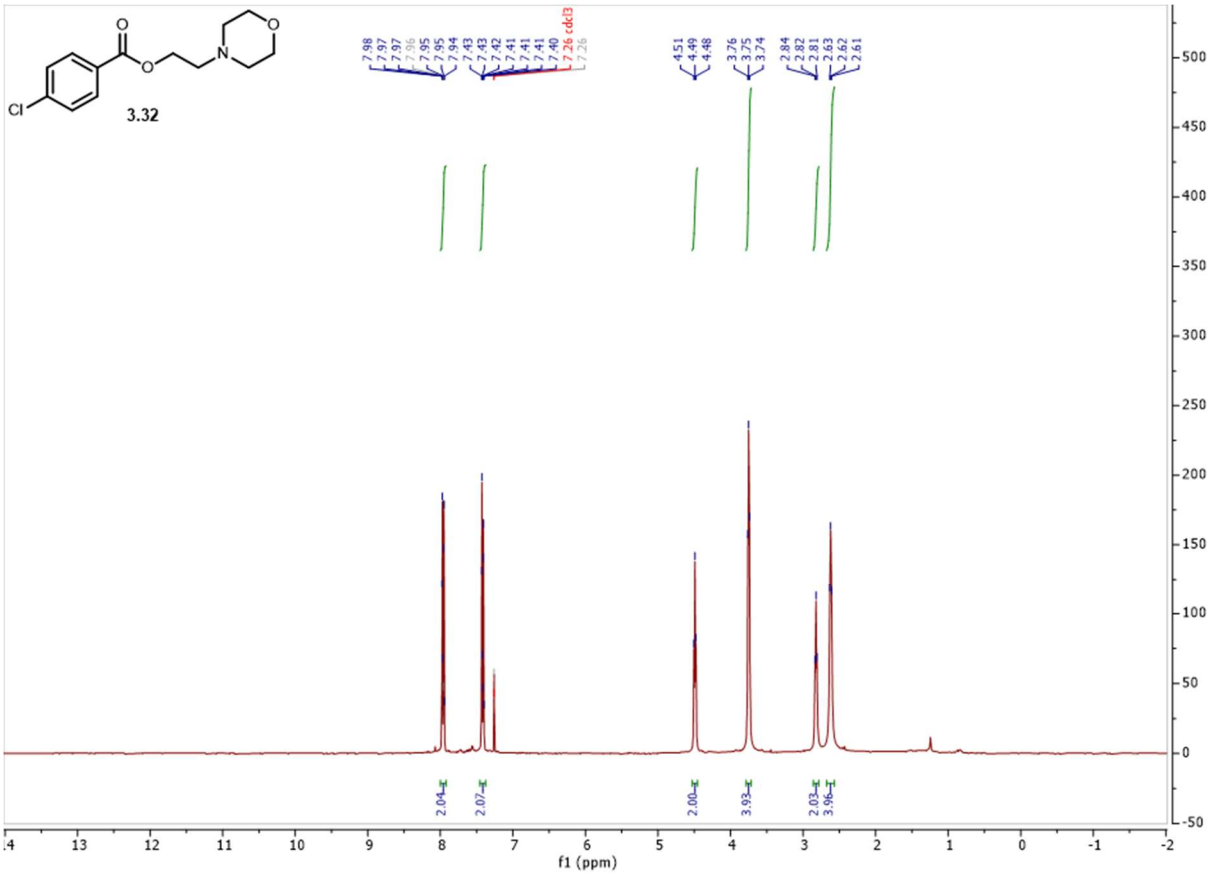

Spectrum 3.64 ^{1}H NMR of compound **3.32**.

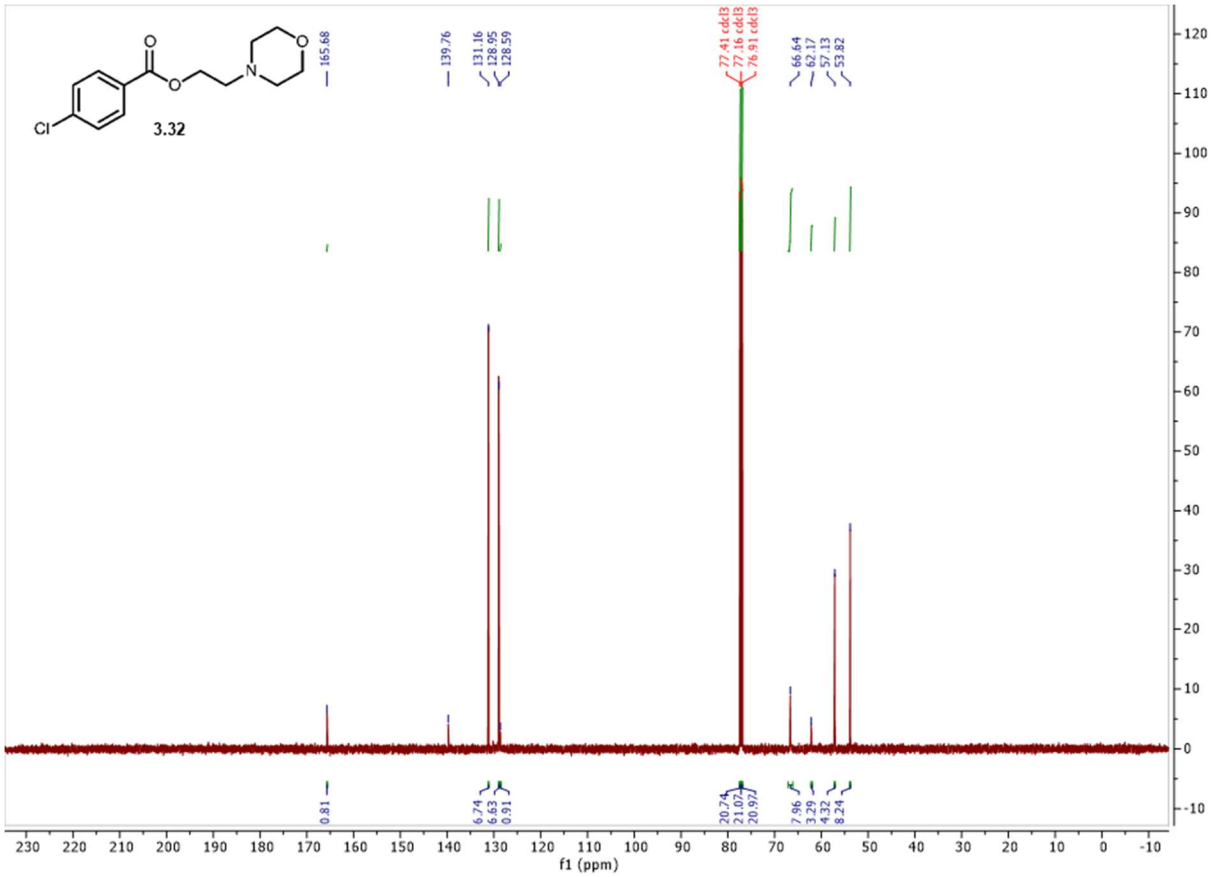

Spectrum 3.65 ^{13}C NMR of compound **3.32**.

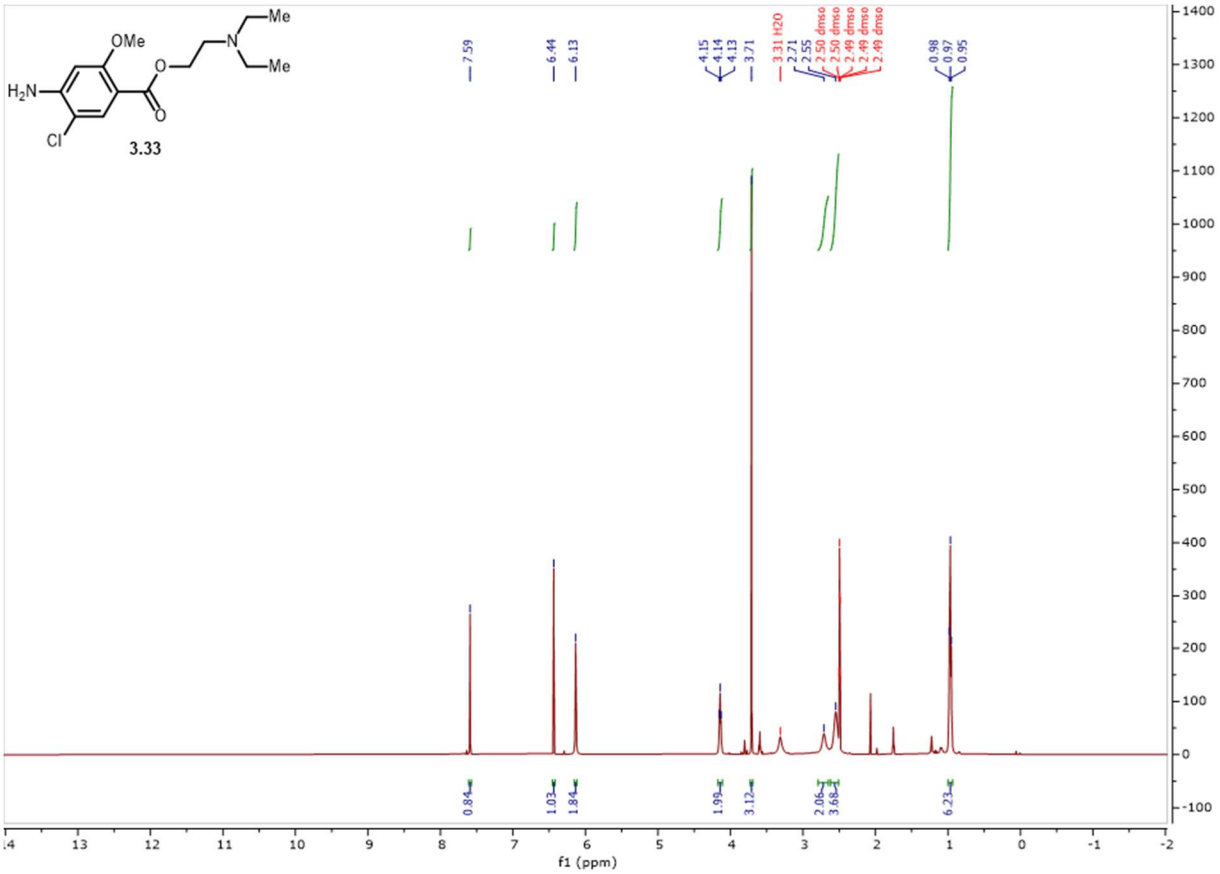

Spectrum 3.66 ^{1}H NMR of compound **3.33**

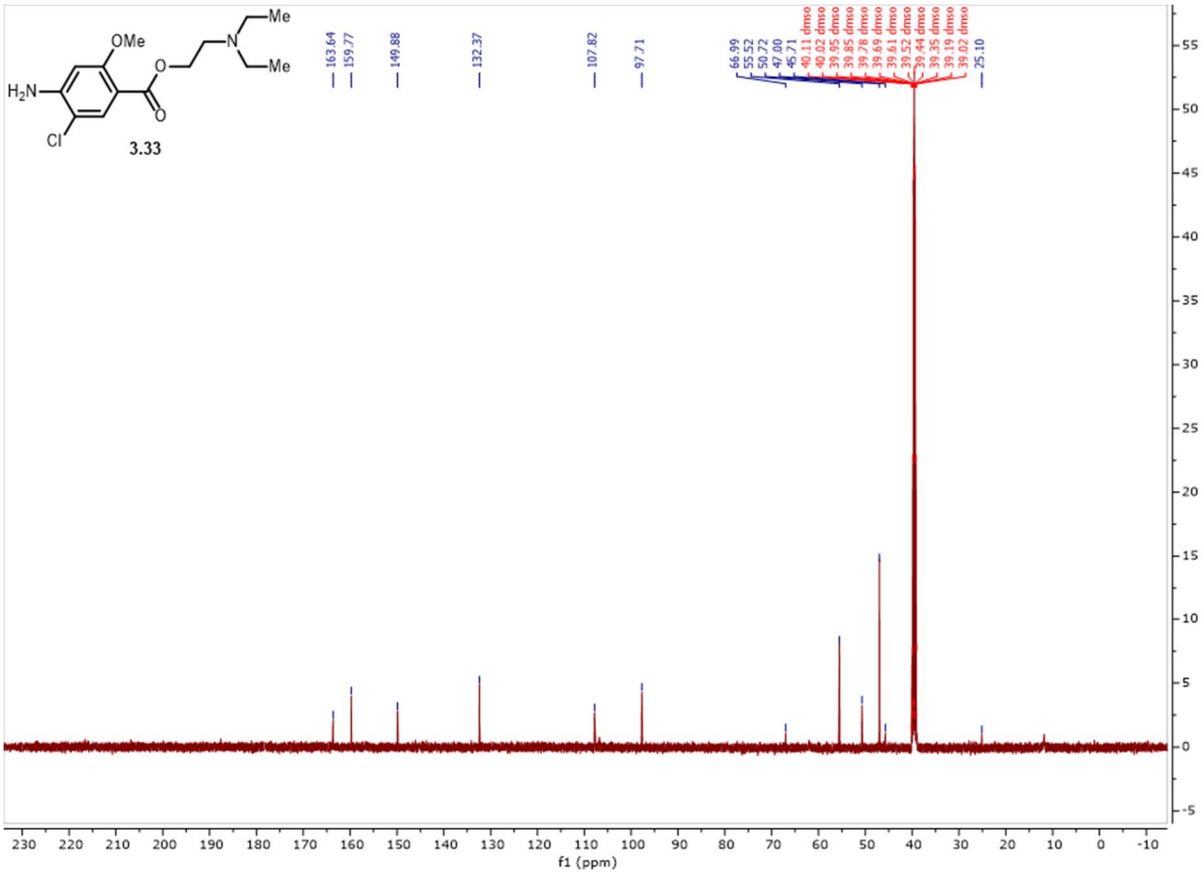

Spectrum 3.67 ^{13}C NMR of compound **3.33**.

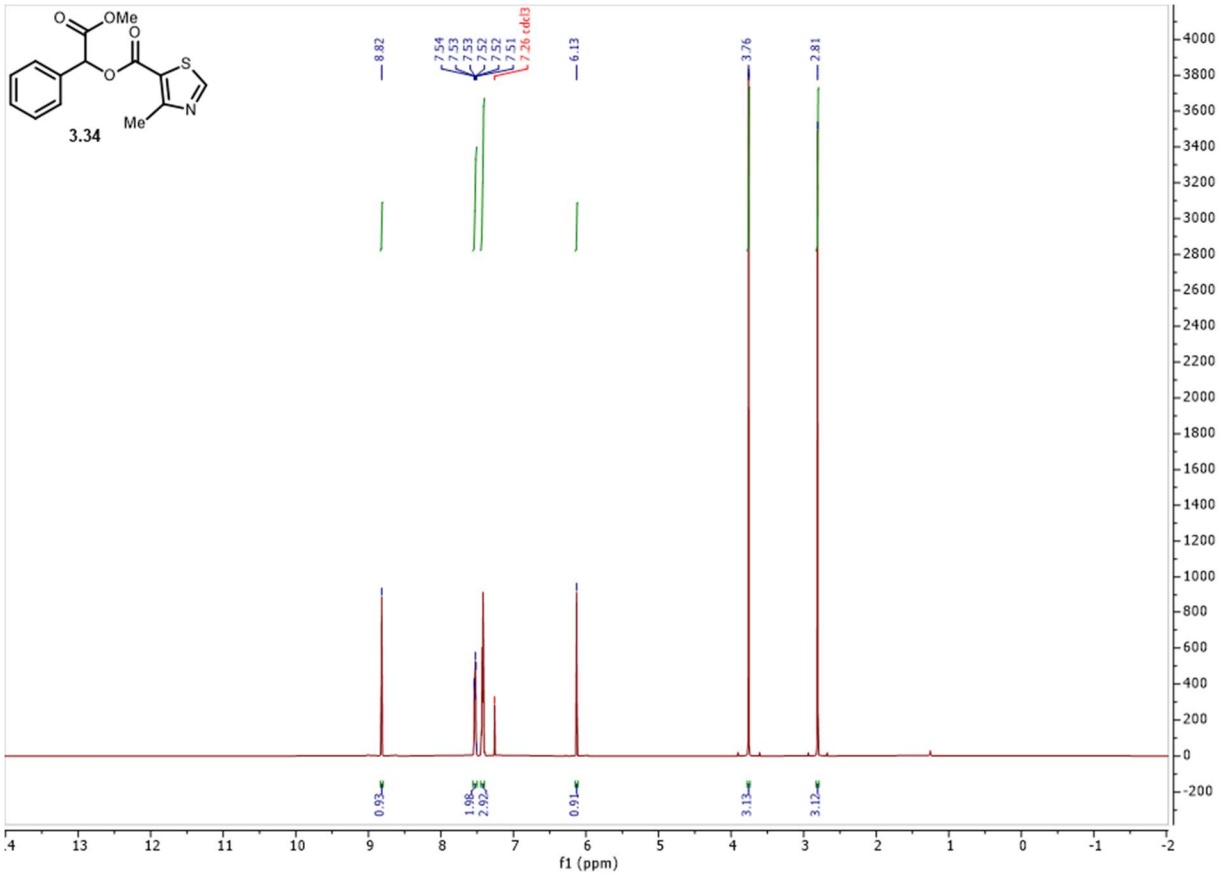

Spectrum 3.68 ^{1}H NMR of compound **3.34**.

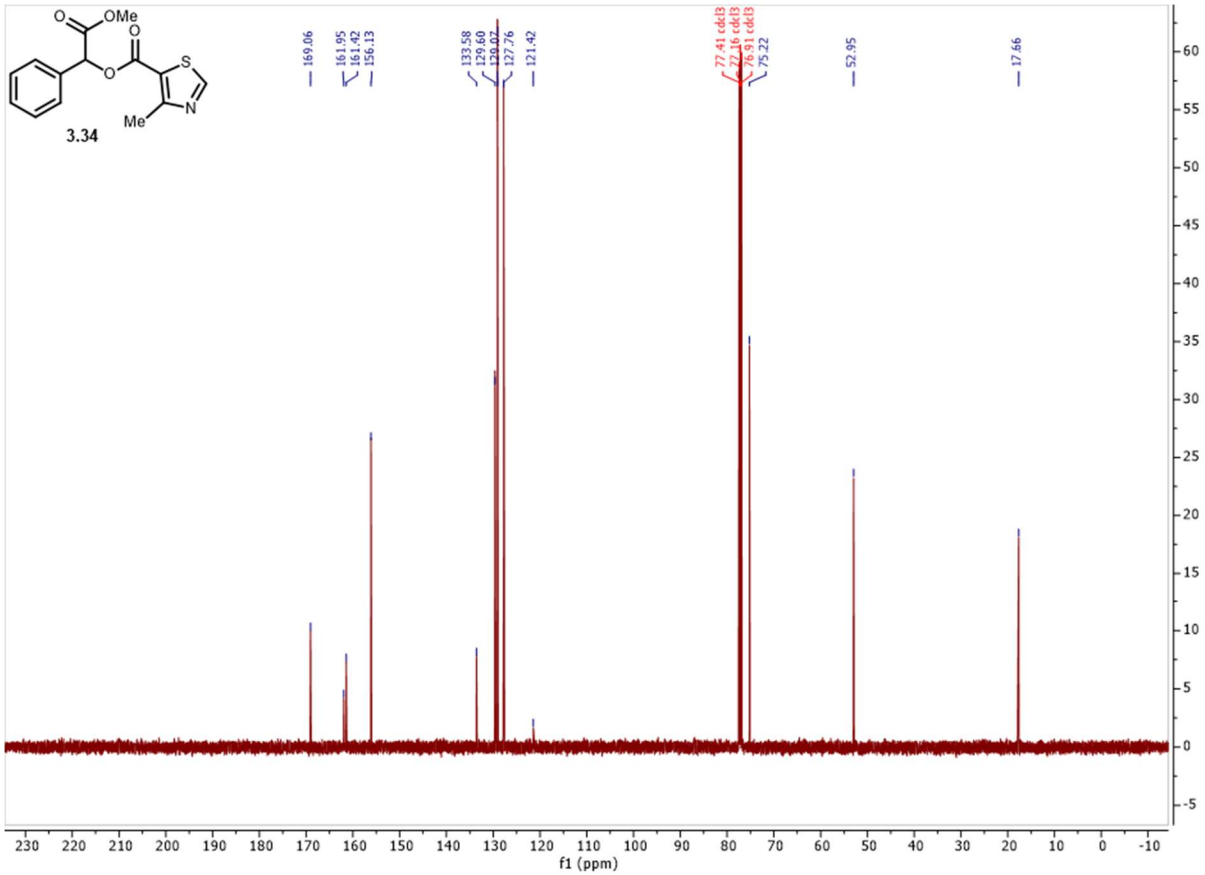

Spectrum 3.69 ^{13}C NMR of compound **3.34**.

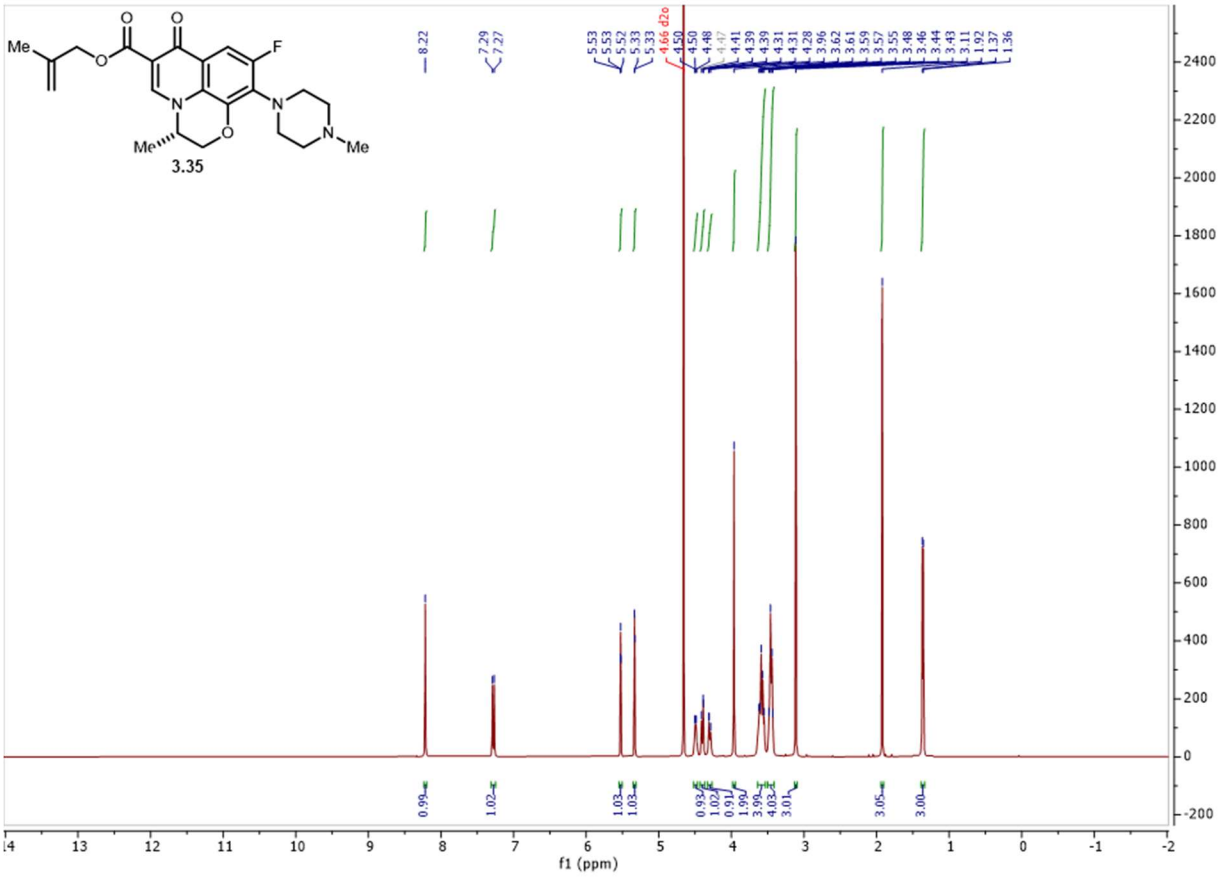

Spectrum 3.70 ^{1}H NMR of compound **3.35**.

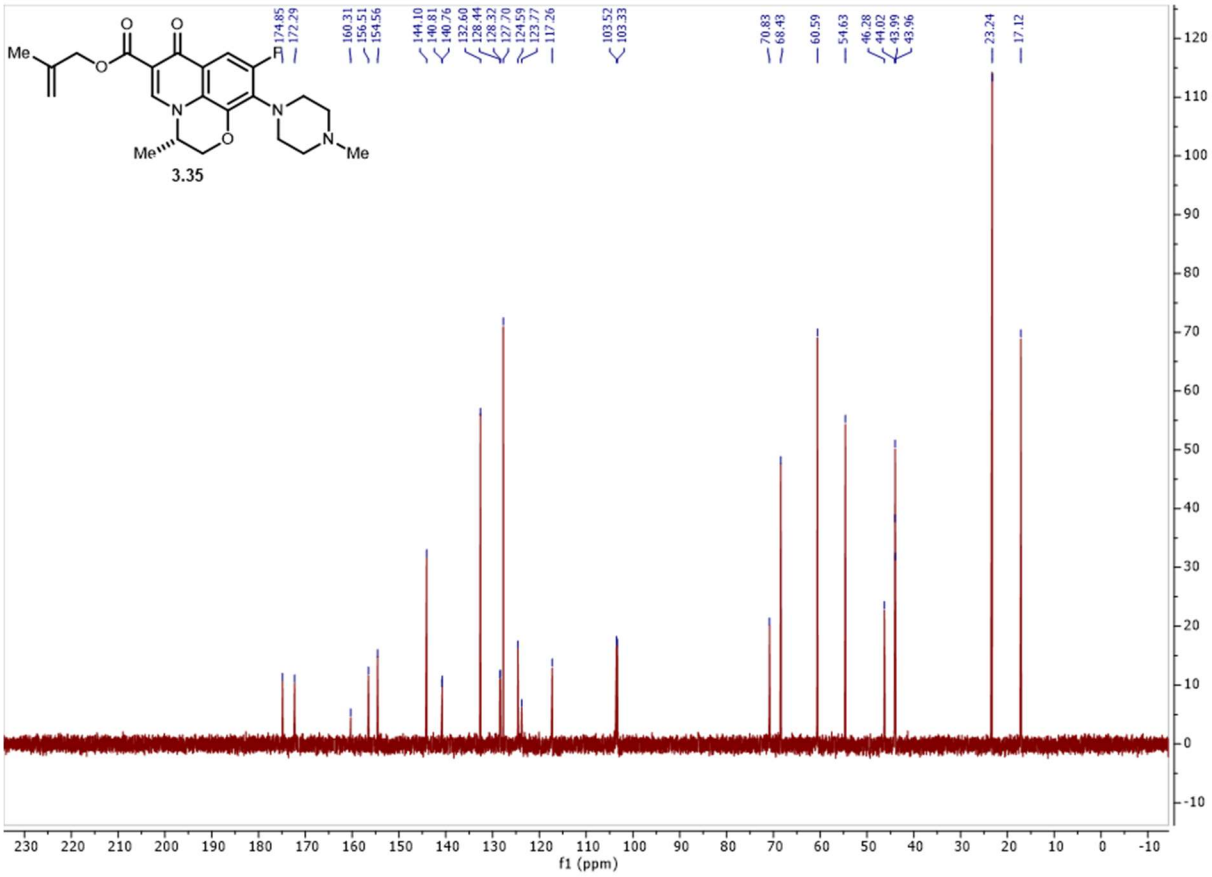

Spectrum 3.71 ^{13}C NMR of compound **3.35**.

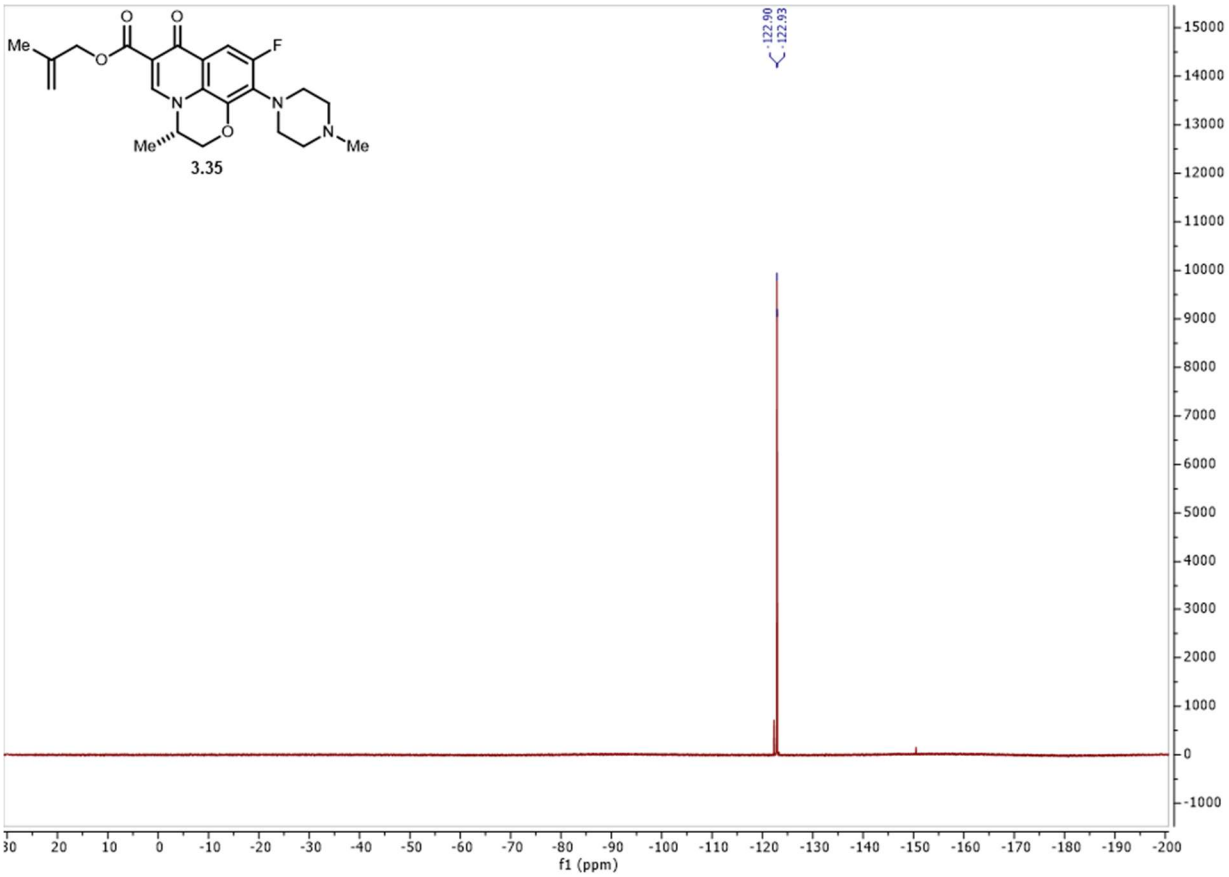

Spectrum 3.72 ^{19}F NMR of compound **3.35**.

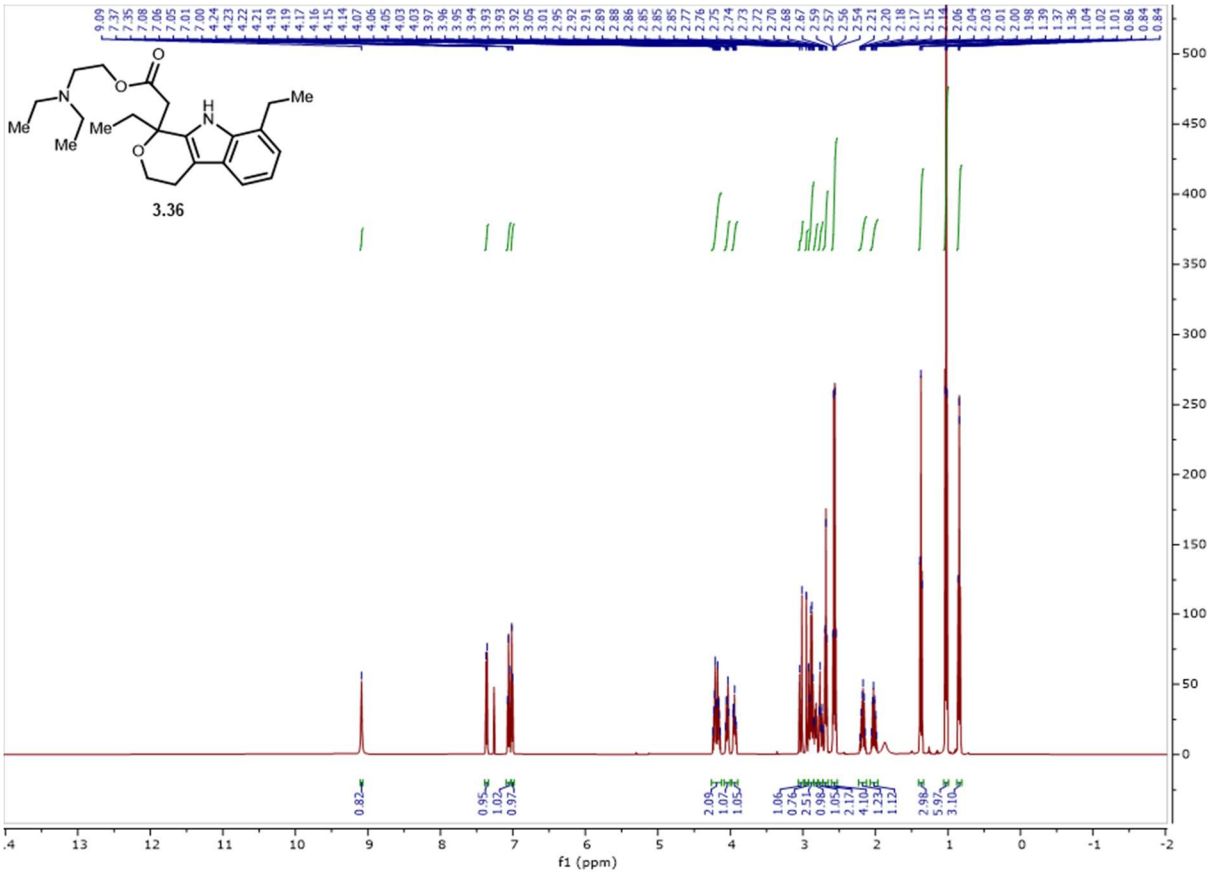

Spectrum 3.73 ^{1}H NMR of compound **3.36**.

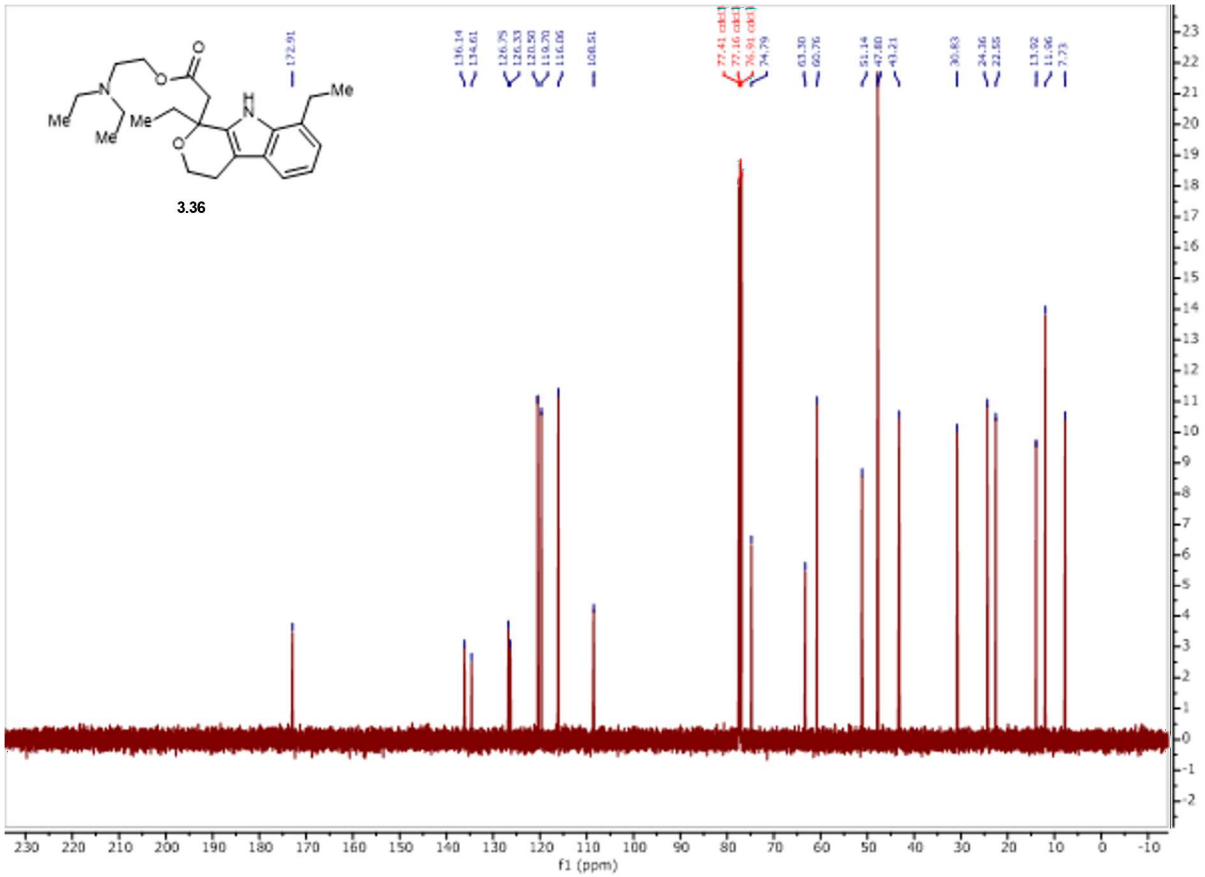

Spectrum 3.74 ^{13}C NMR of compound **3.36**.

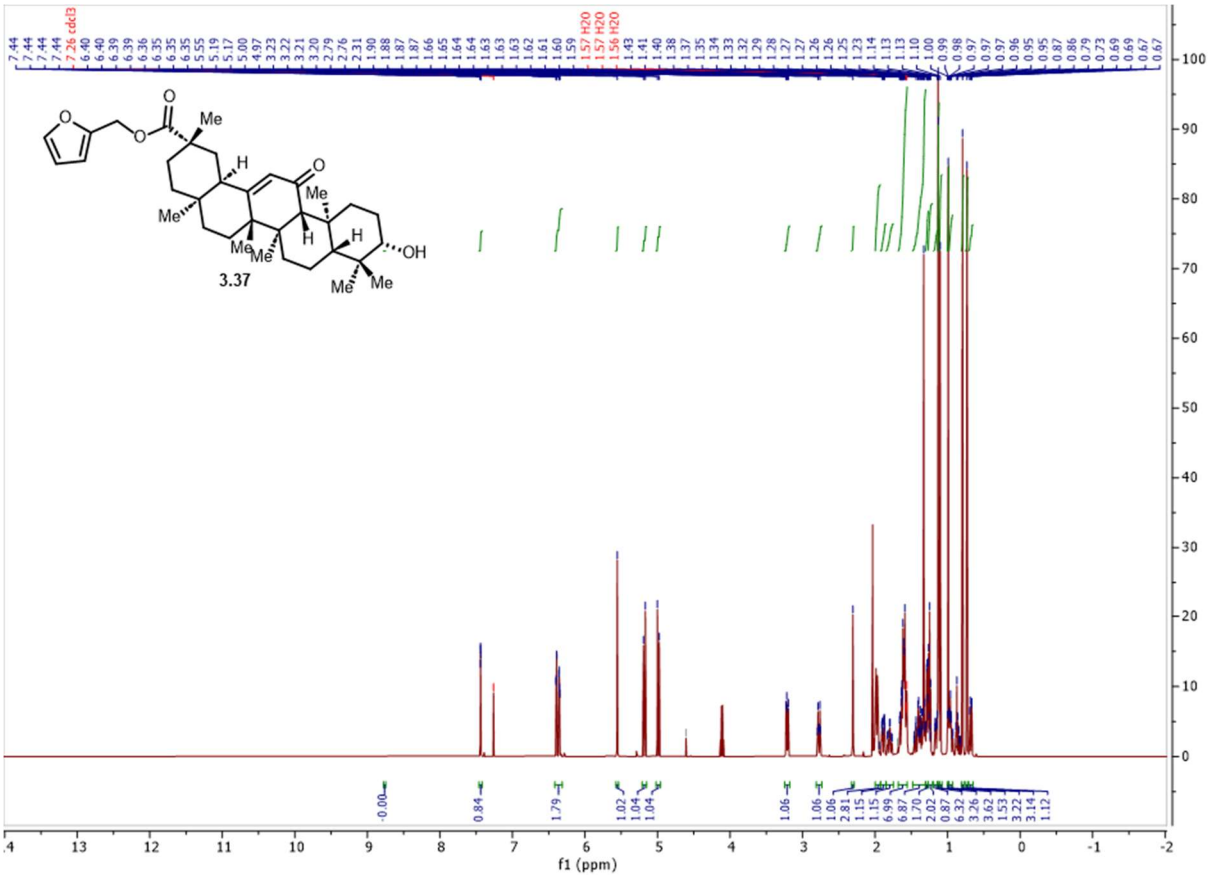

Spectrum 3.75 ^{1}H NMR of compound **3.37**.

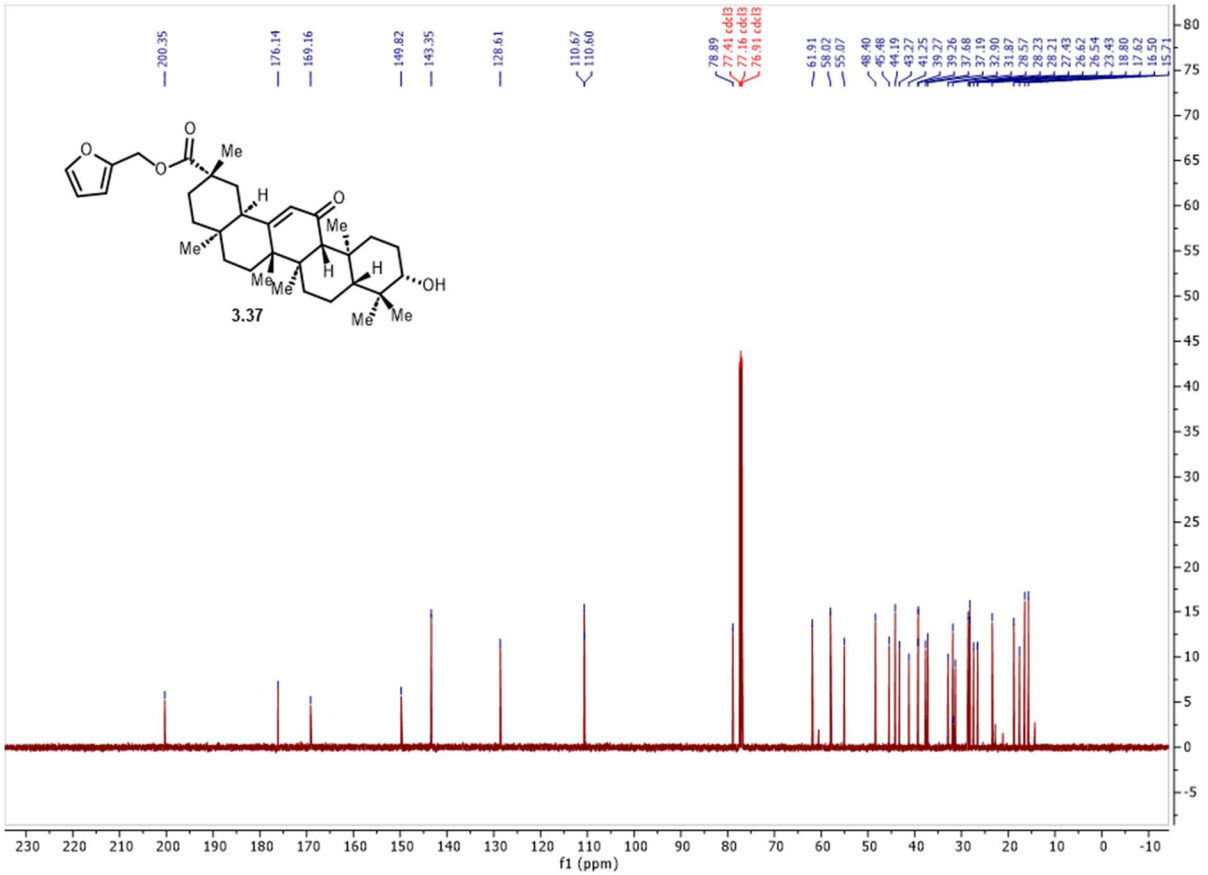

Spectrum 3.76 ^{13}C NMR of compound **3.37**.

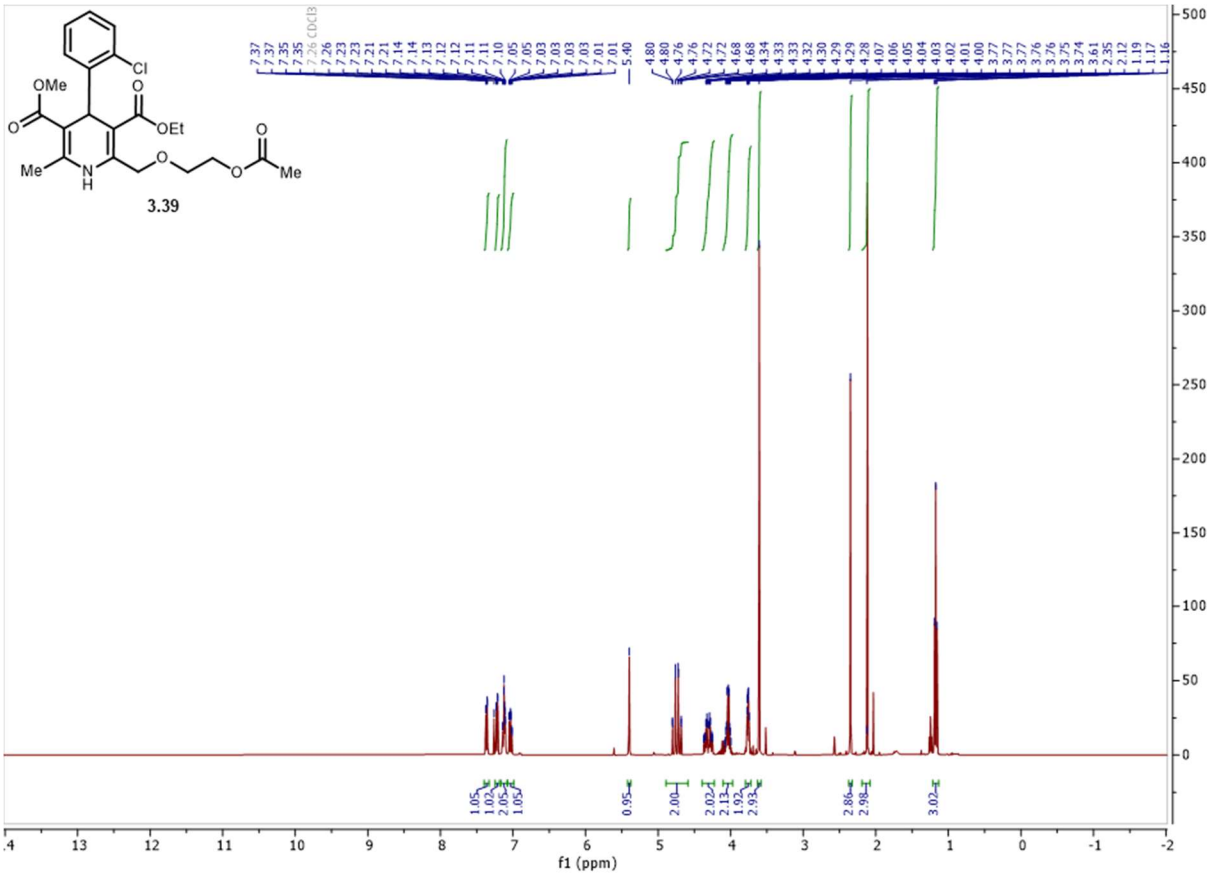

Spectrum 3.77 ^{1}H NMR of compound **3.39**.

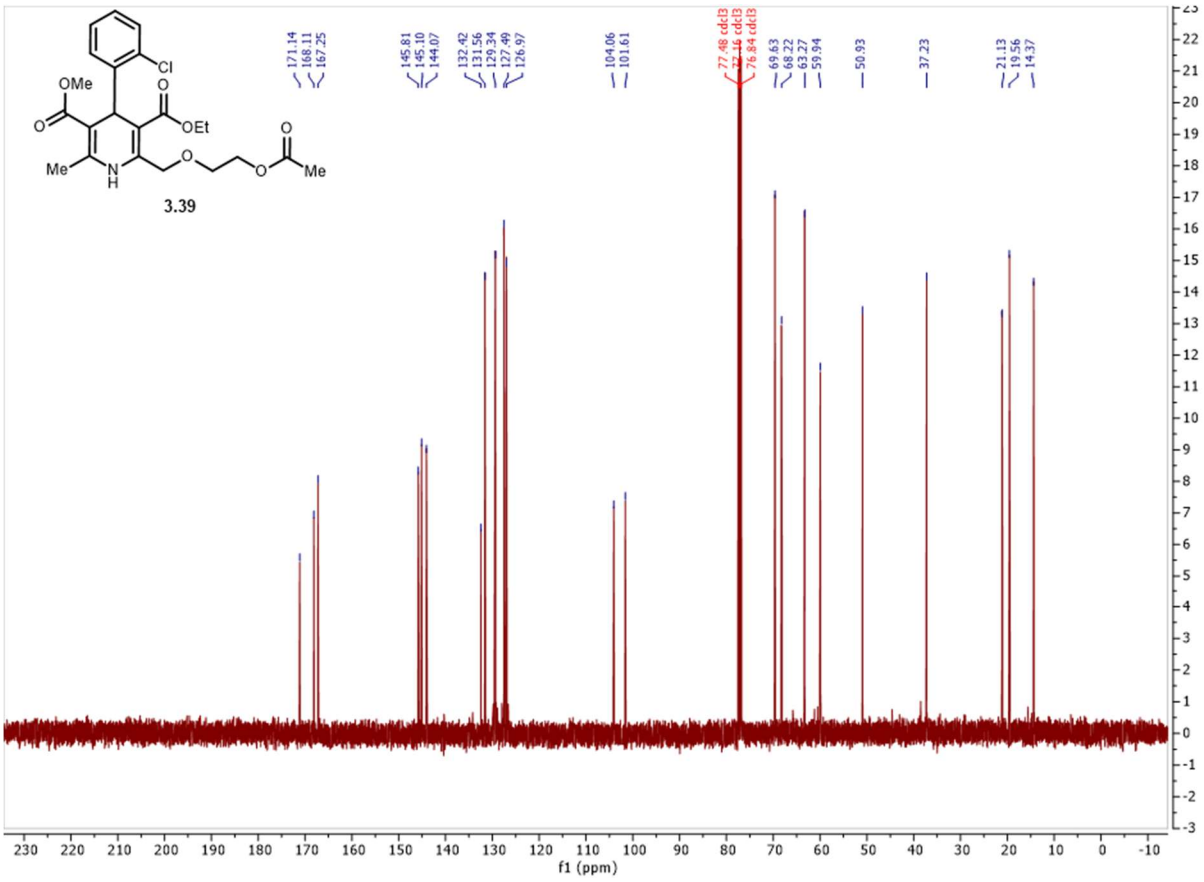

Spectrum 3.78 ^{13}C NMR of compound **3.39**.

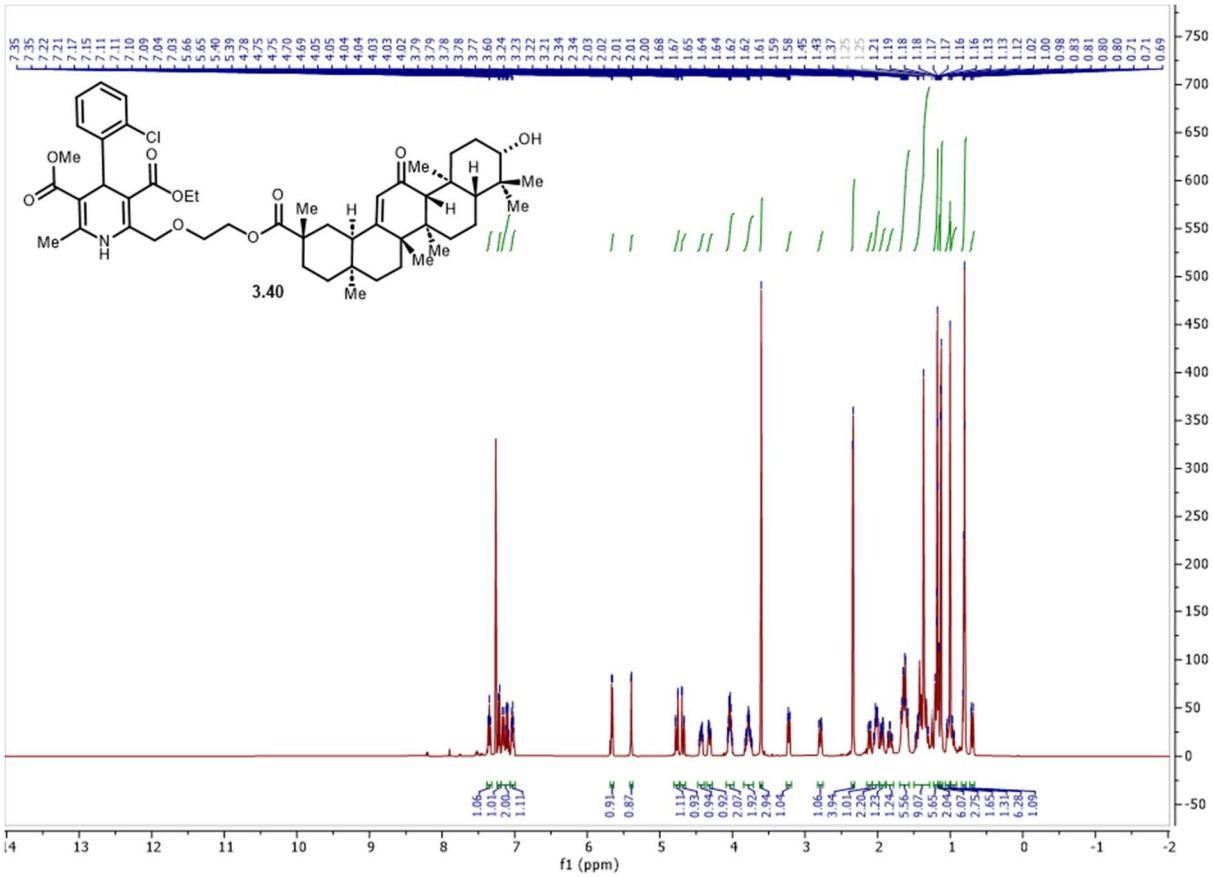

Spectrum 3.79 ^{1}H NMR of compound **3.40**.

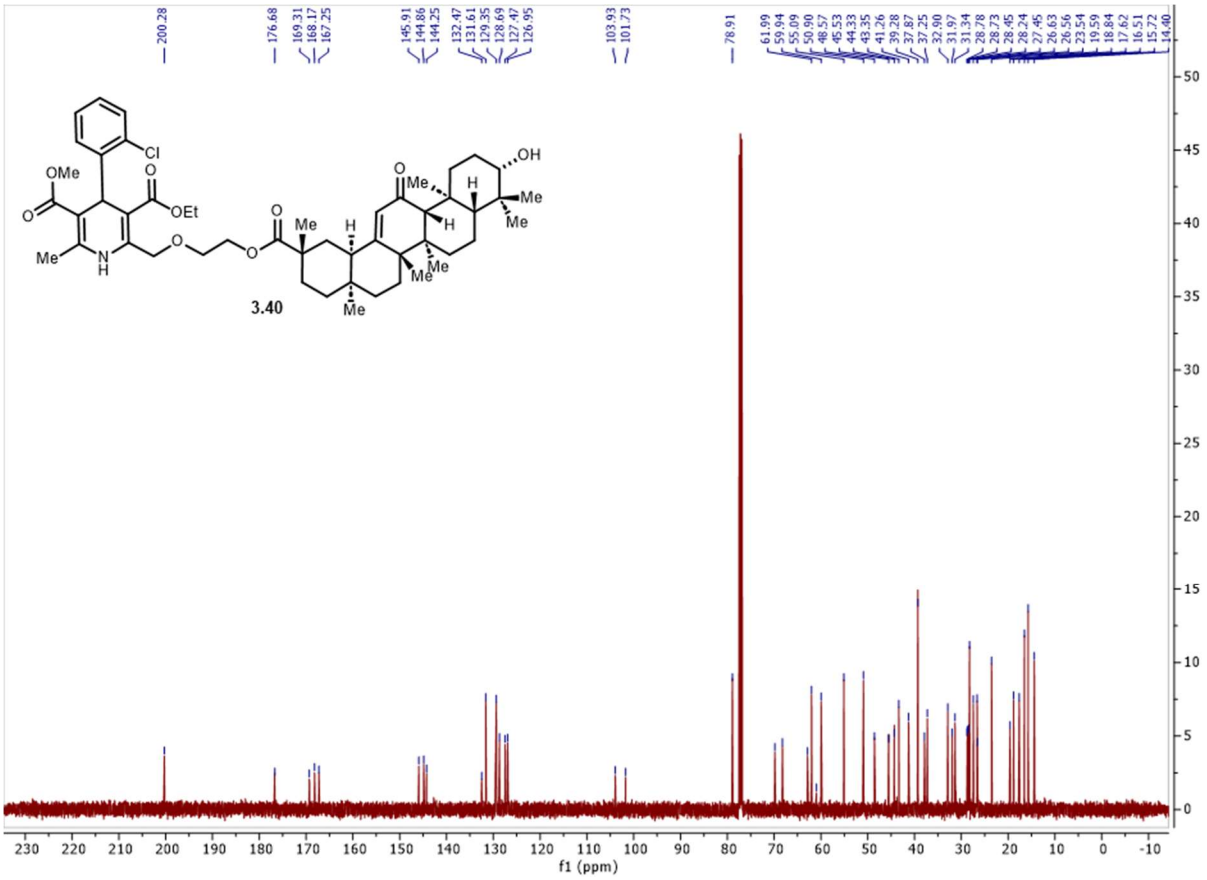

Spectrum 3.80 ^{13}C NMR of compound **3.40**

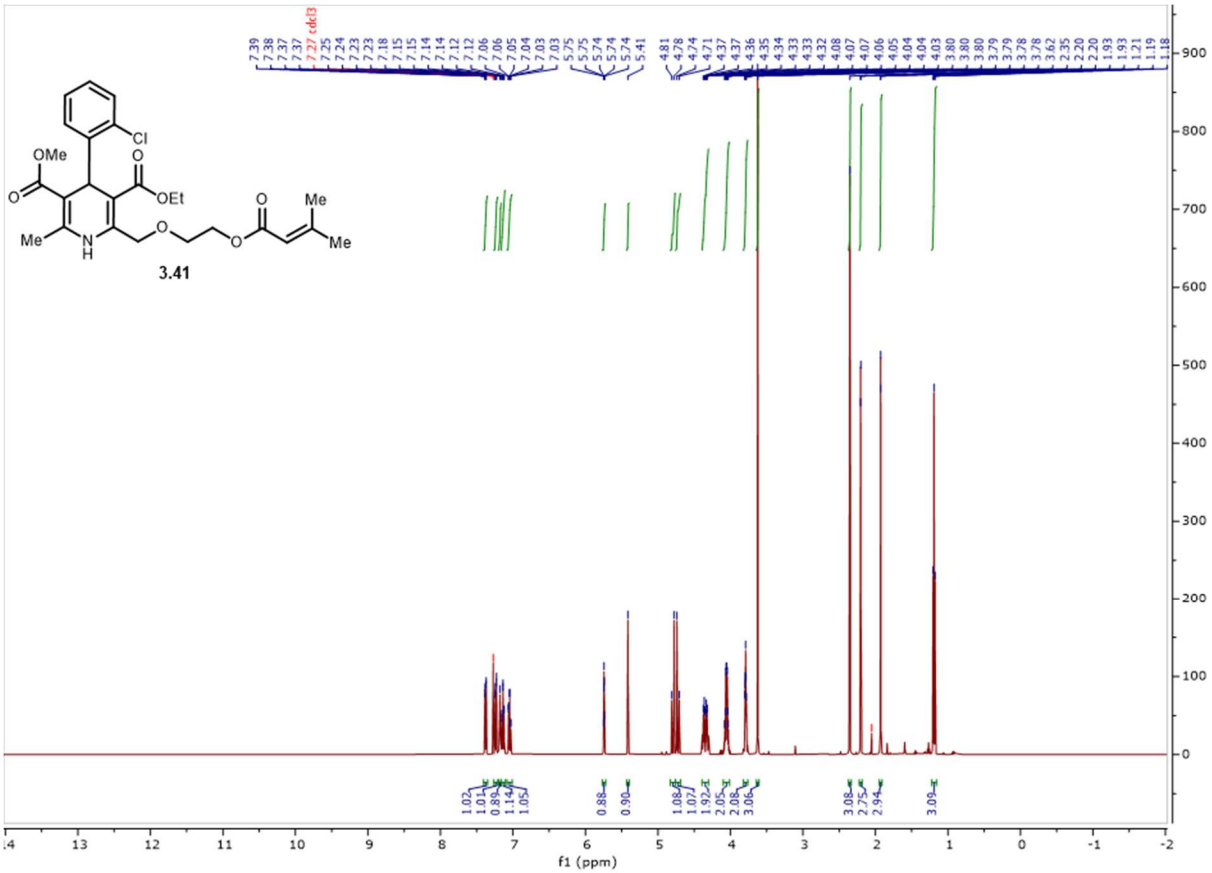

Spectrum 3.81 ^{1}H NMR of compound **3.41**

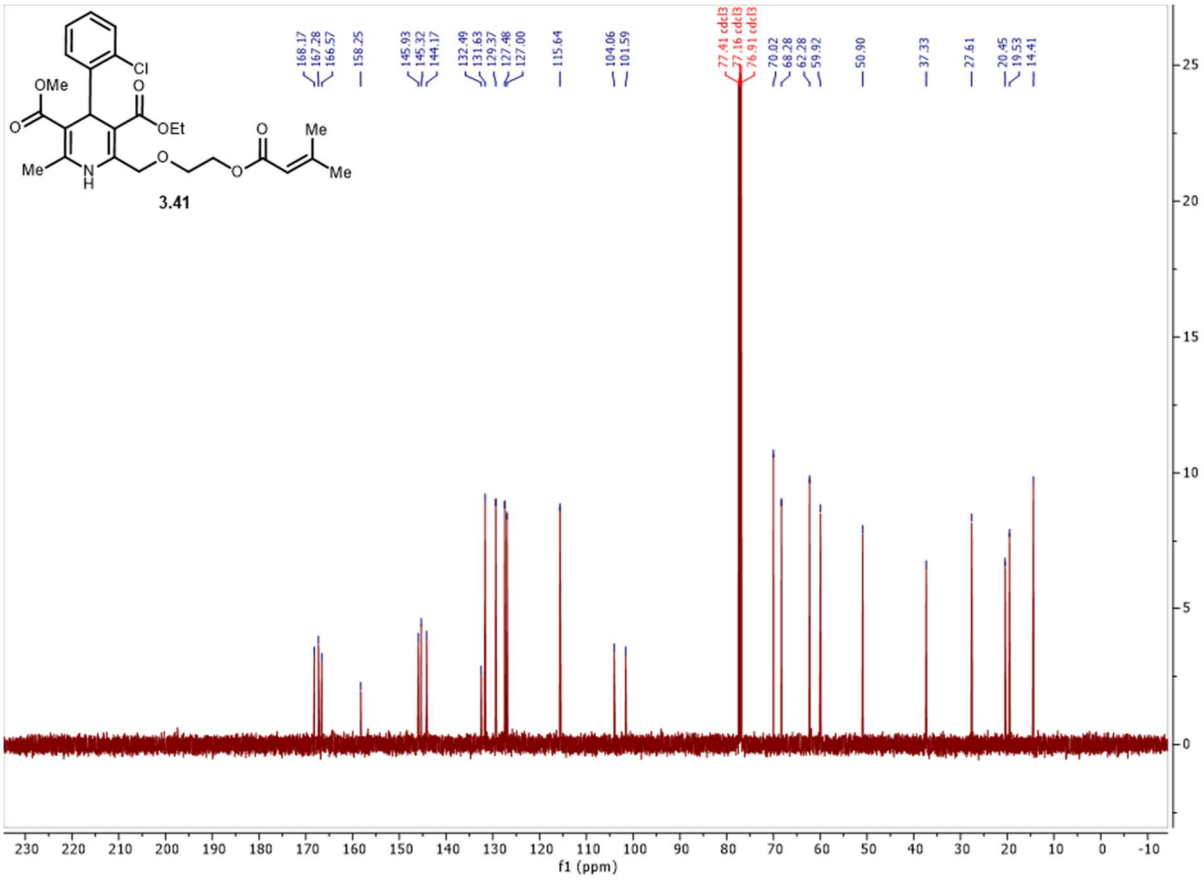

Spectrum 3.82 ^{13}C NMR of compound **3.41**.

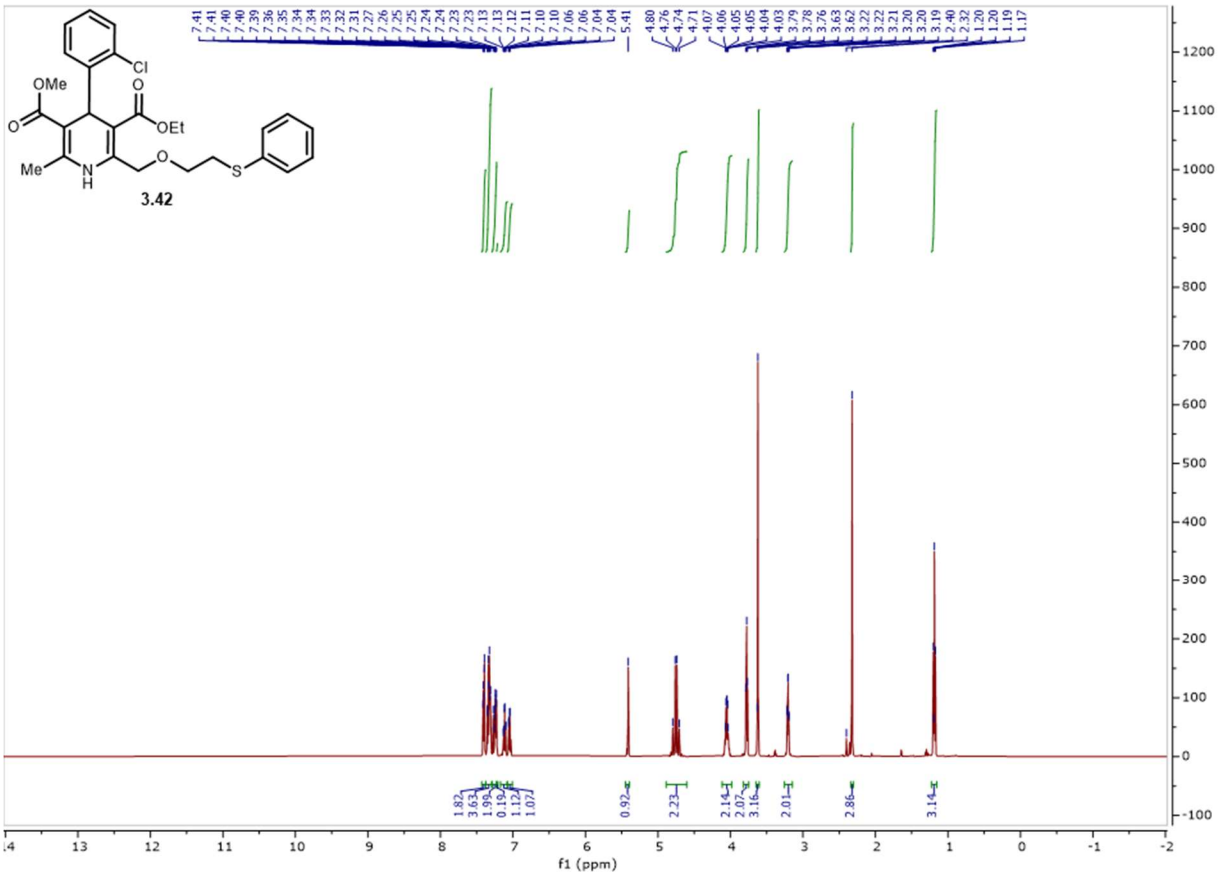

Spectrum 3.83 ^{1}H NMR of **3.42**.

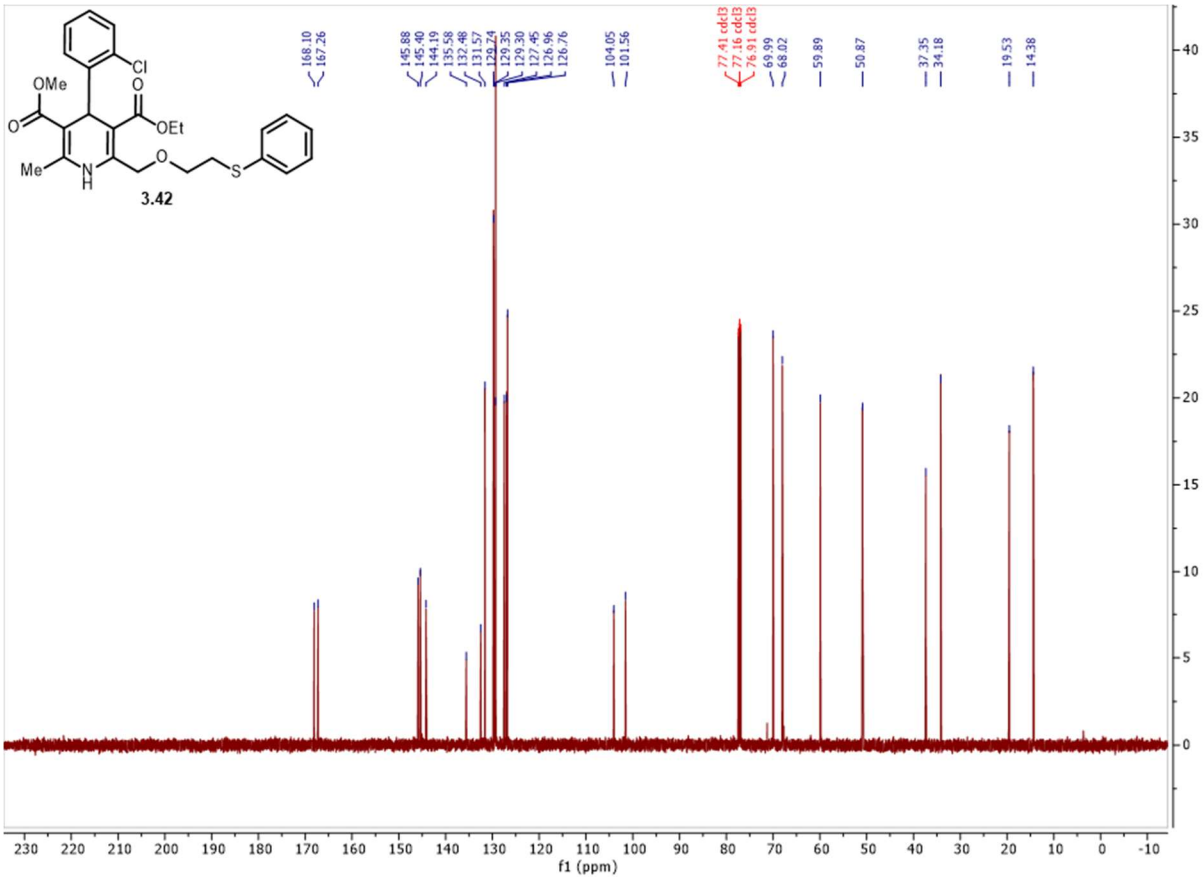

Spectrum 3.84 ^{13}C NMR of compound **3.42**.

3.5.2 NMR Spectra for etherification reaction

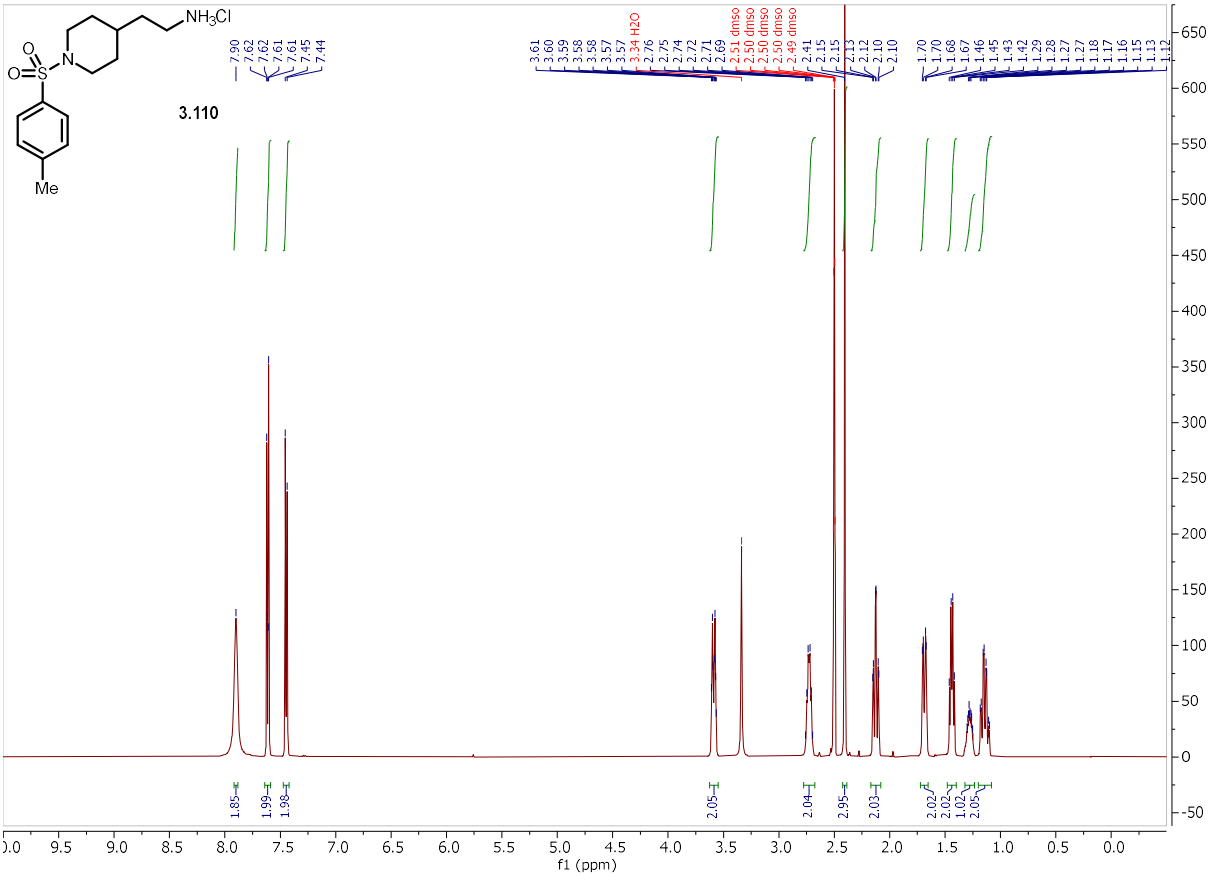

Spectrum 3.85 ^{1}H NMR of **3.110**.

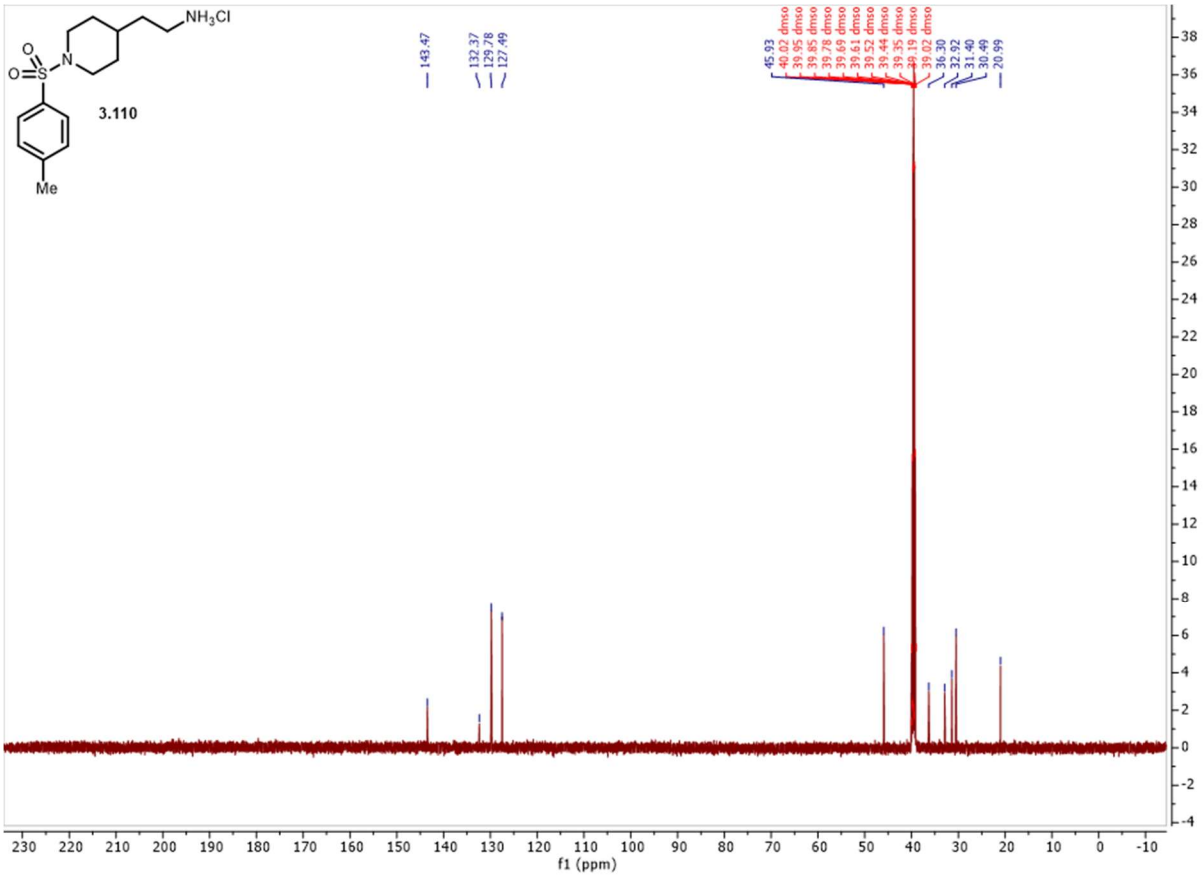

Spectrum 3.86 ^{13}C NMR of **3.111**

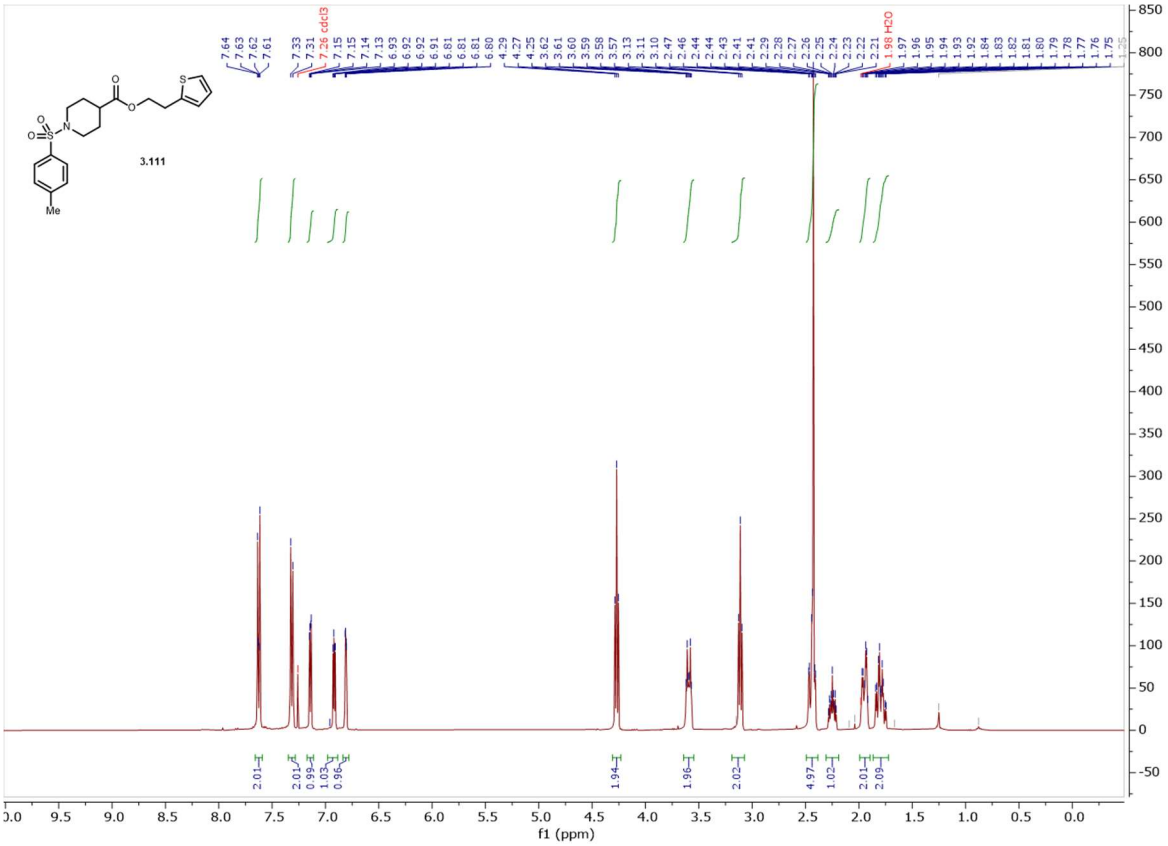

Spectrum 3.87 ^{1}H NMR of **3.111**.

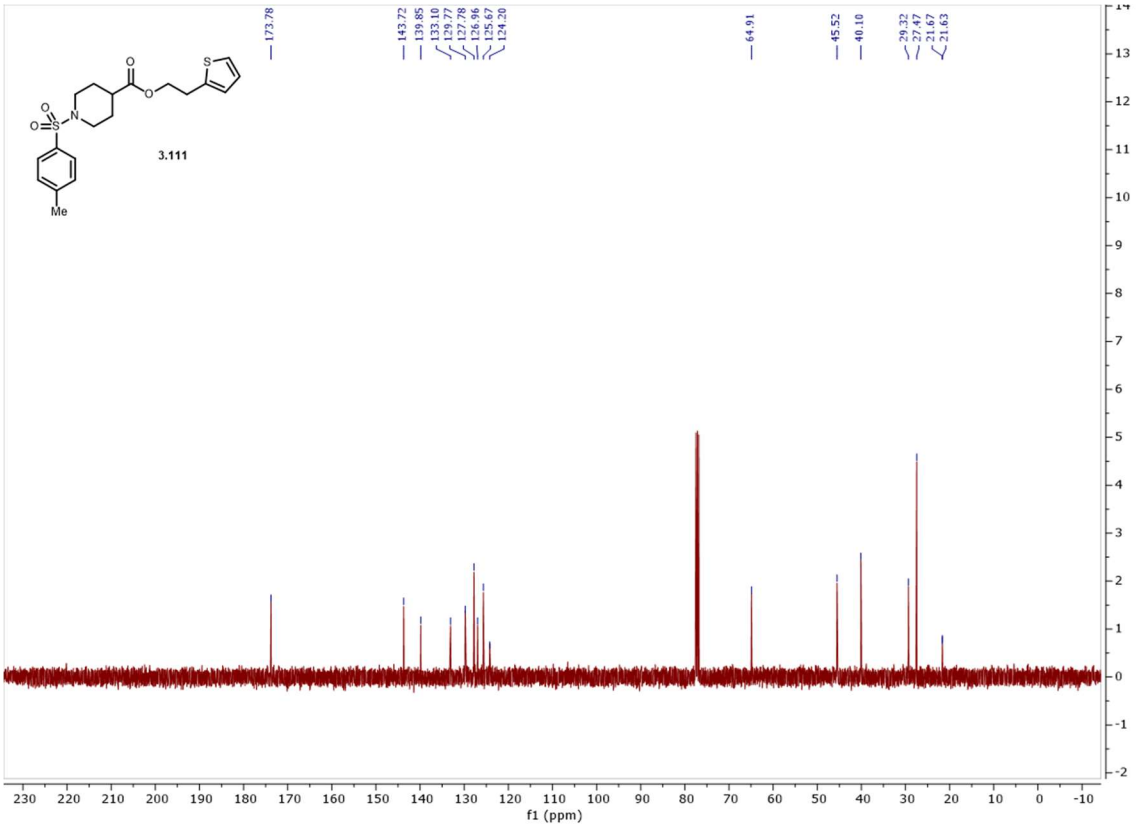

Spectrum 3.88 ^{13}C NMR of **3.111**.

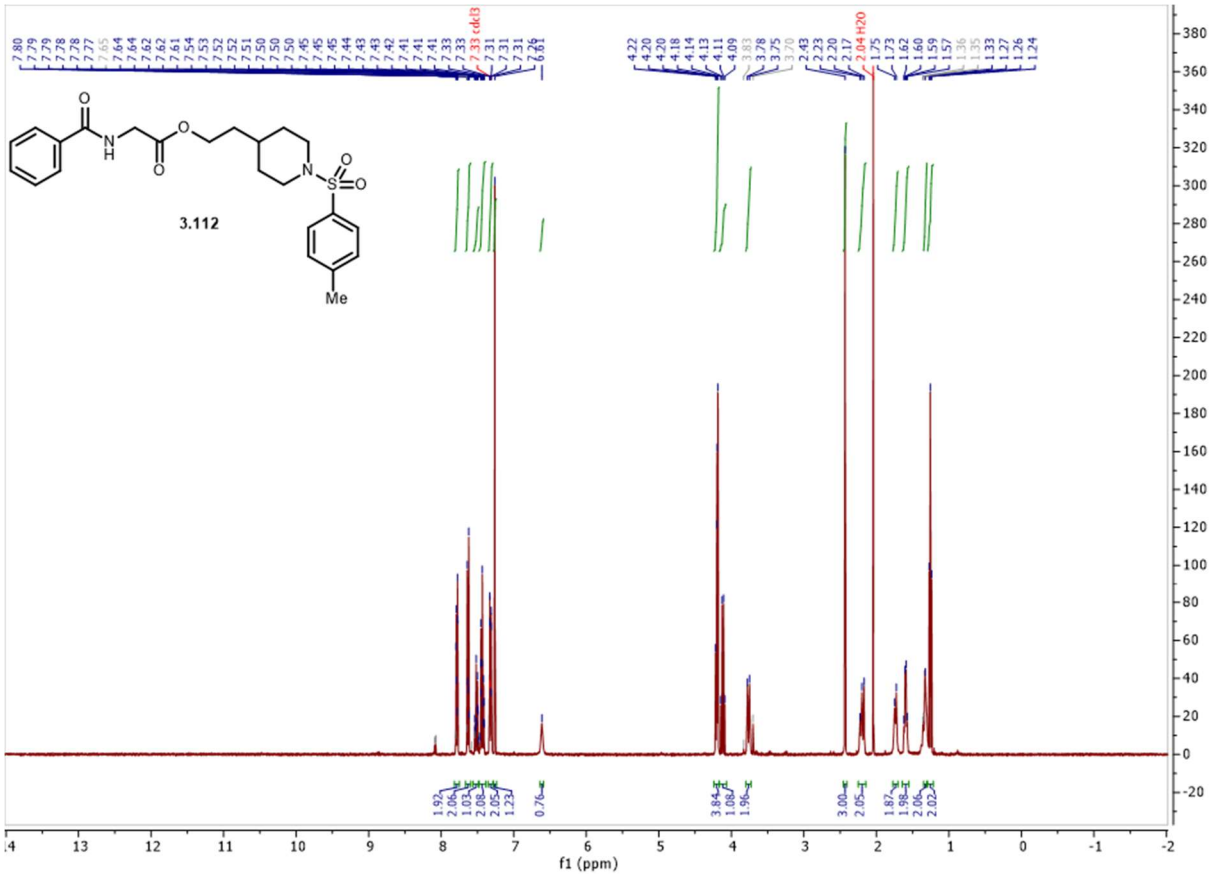

Spectrum 3.89 ^{1}H NMR of **3.112**.

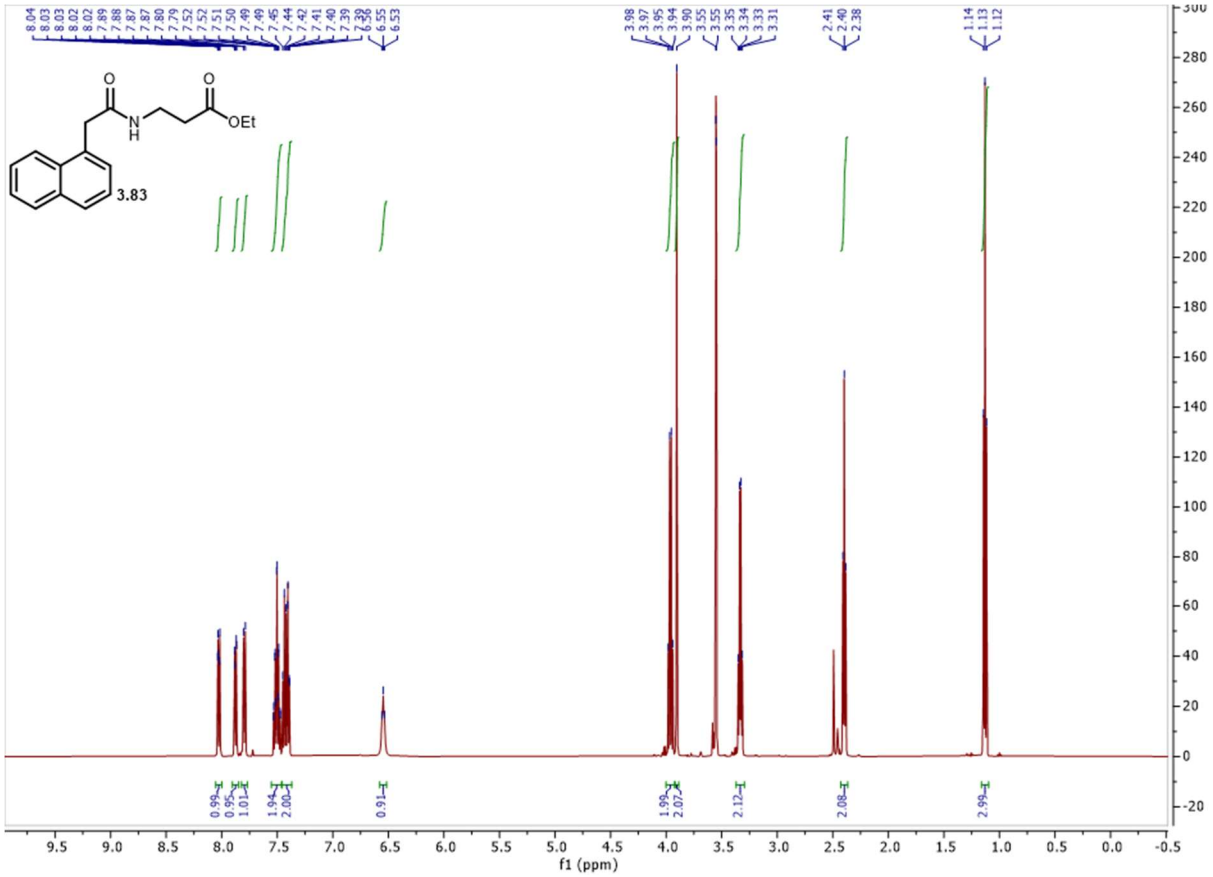

Spectrum 3.90 ^{1}H NMR of **3.83**.

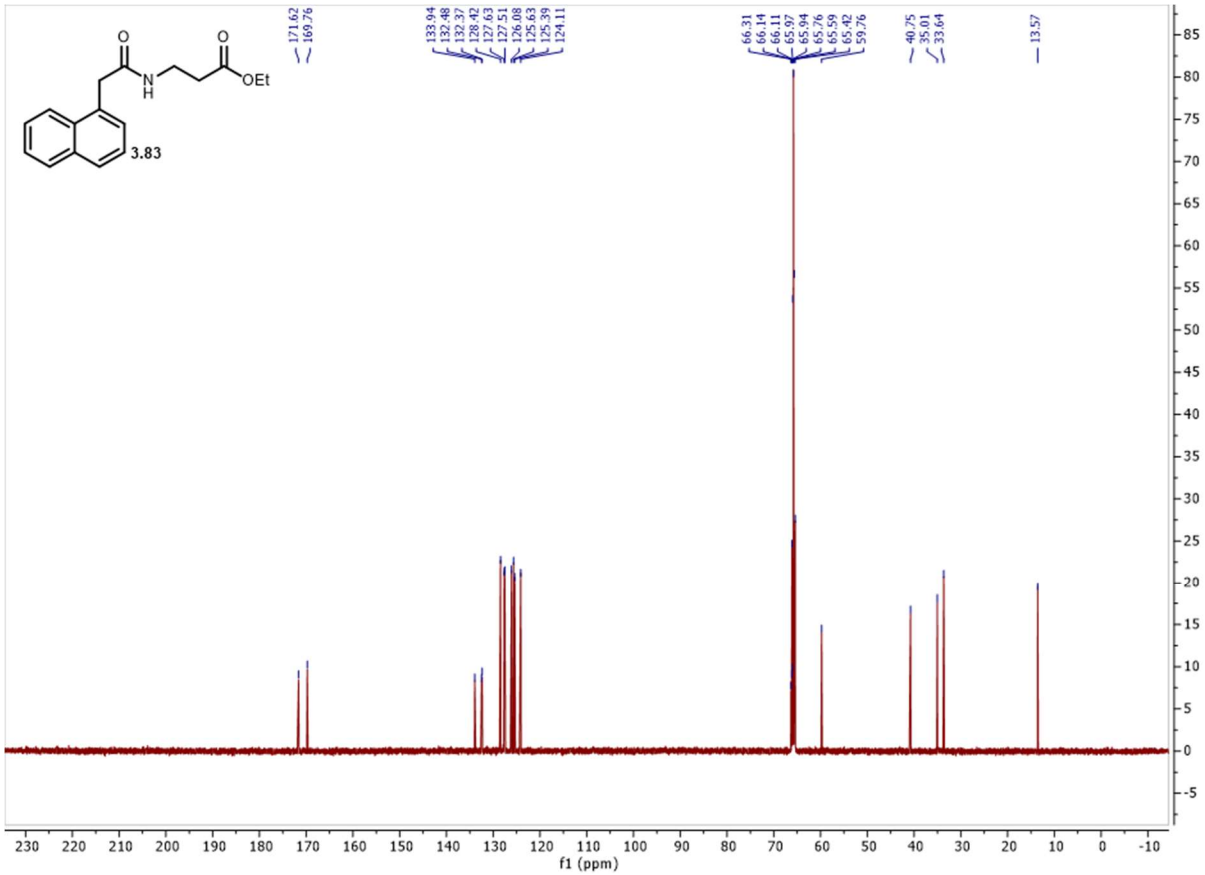

Spectrum 3.91 ^{13}C NMR of **3.83**.

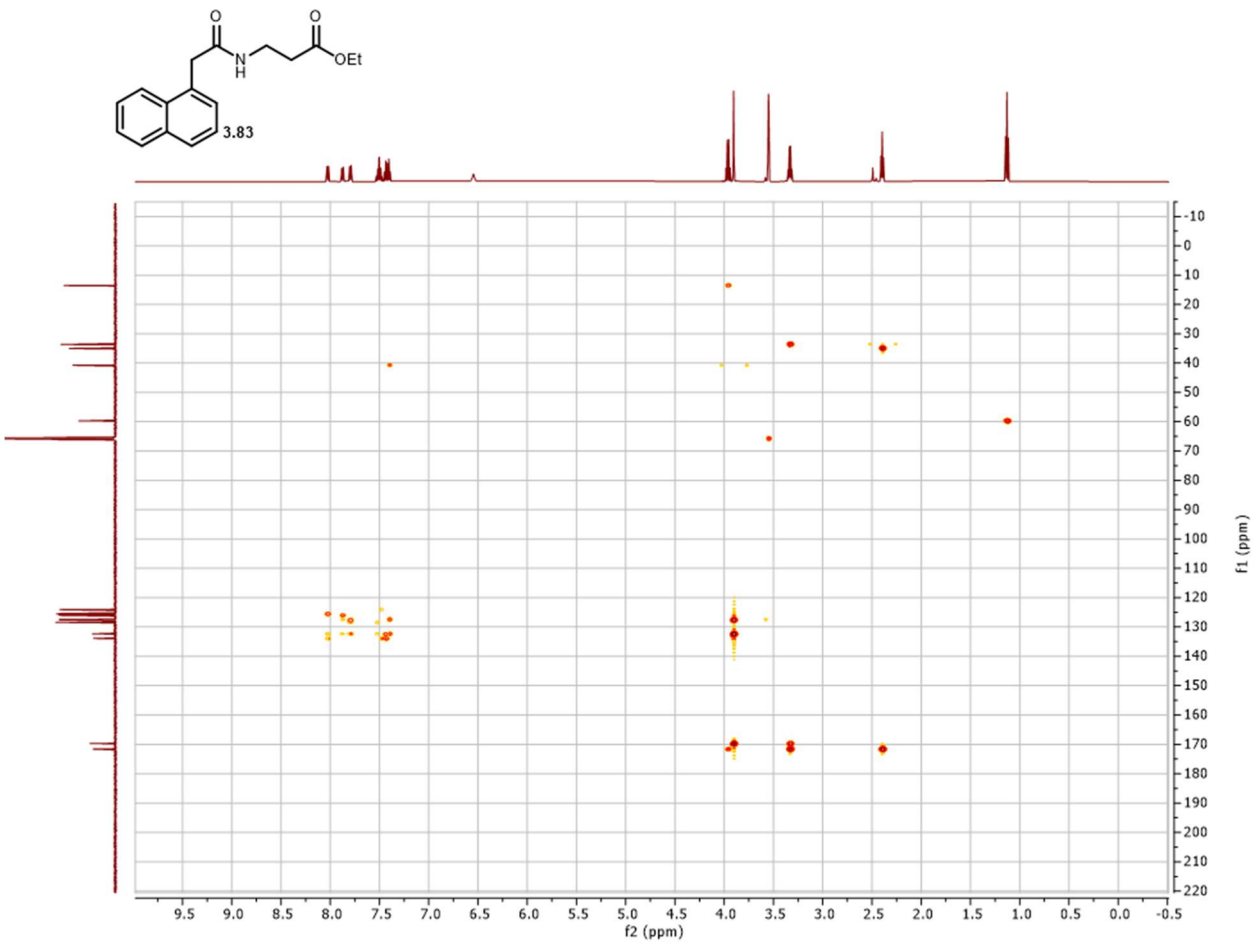

Spectrum 3.92 HMBC of **3.83**.

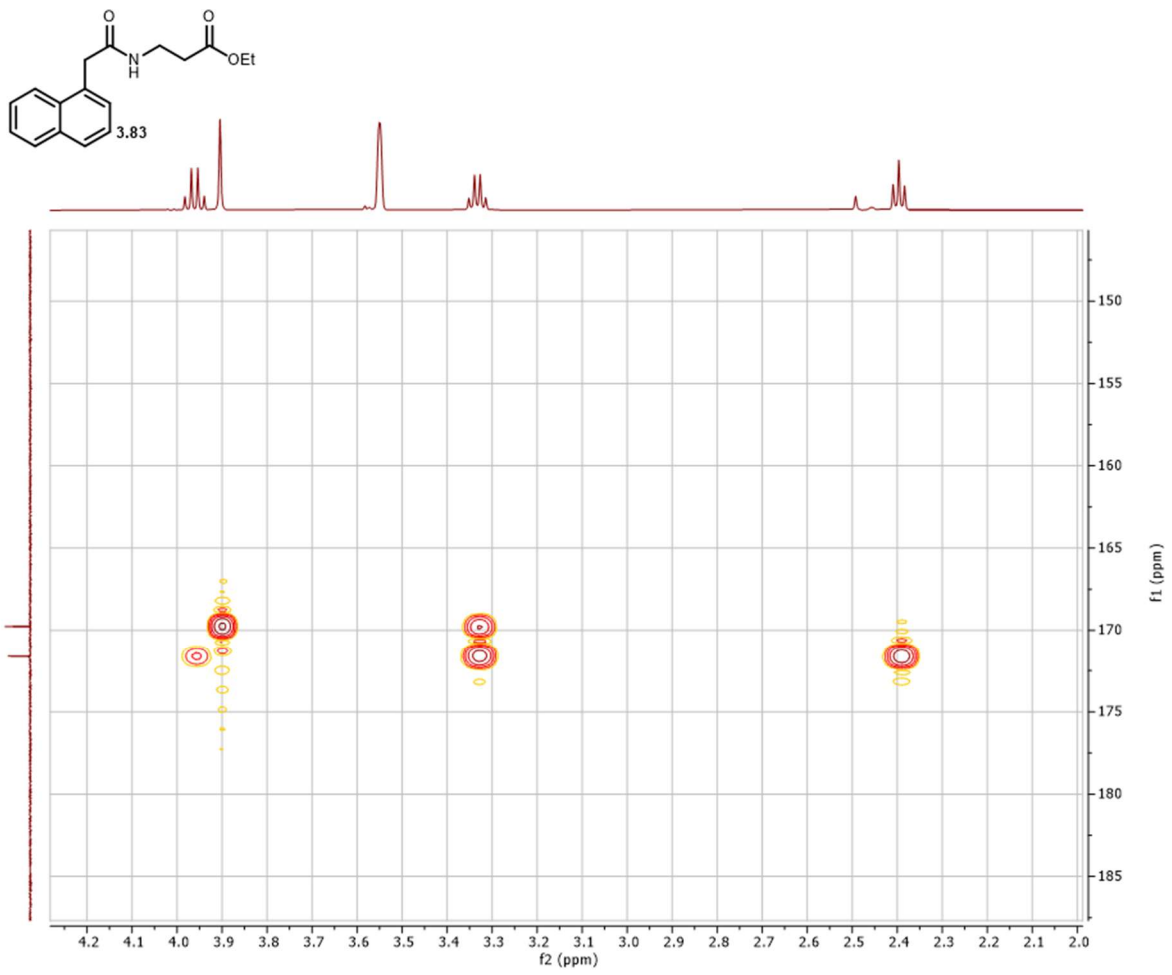

Spectrum 3.93 HMBC of **3.83** zoomed in on carbonyl carbon and ester proton region.

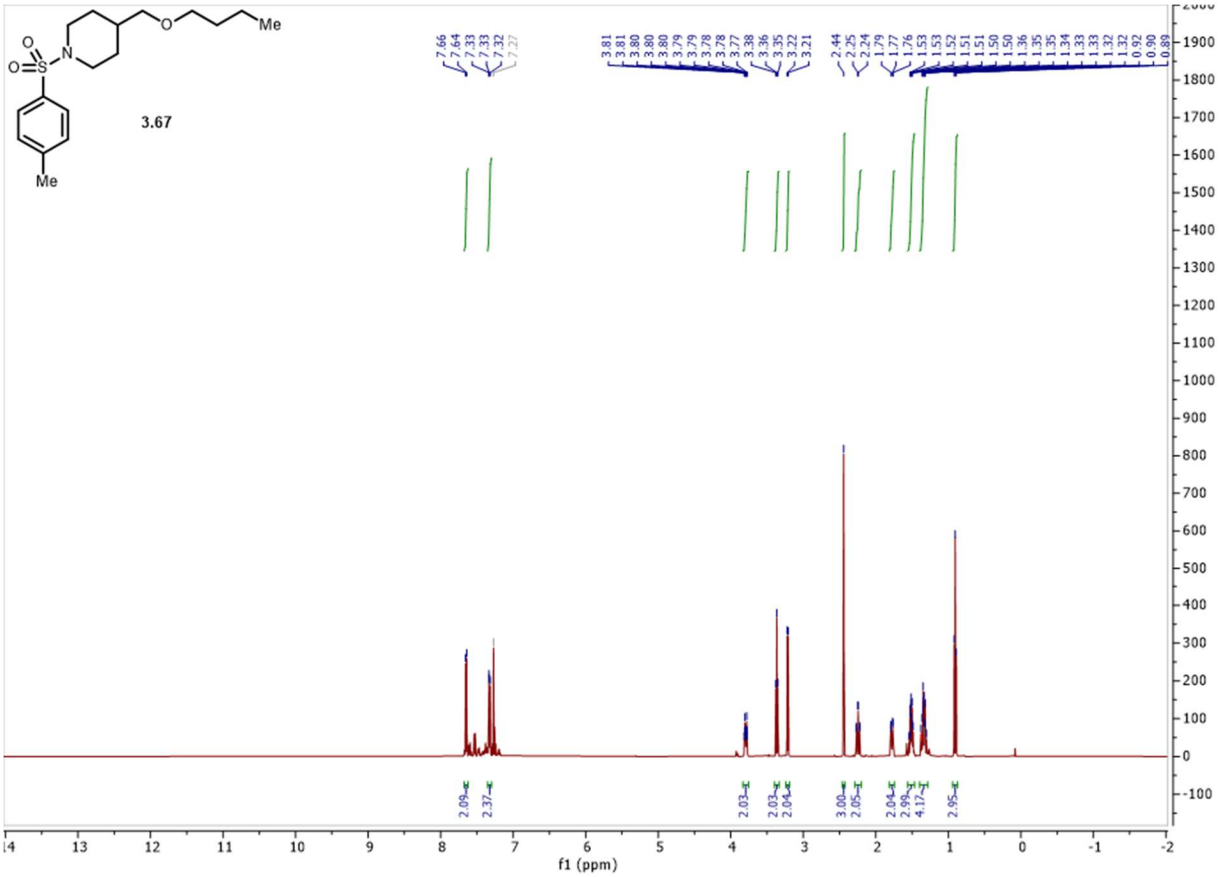

Spectrum 3.94 ^{1}H NMR of **3.67**.

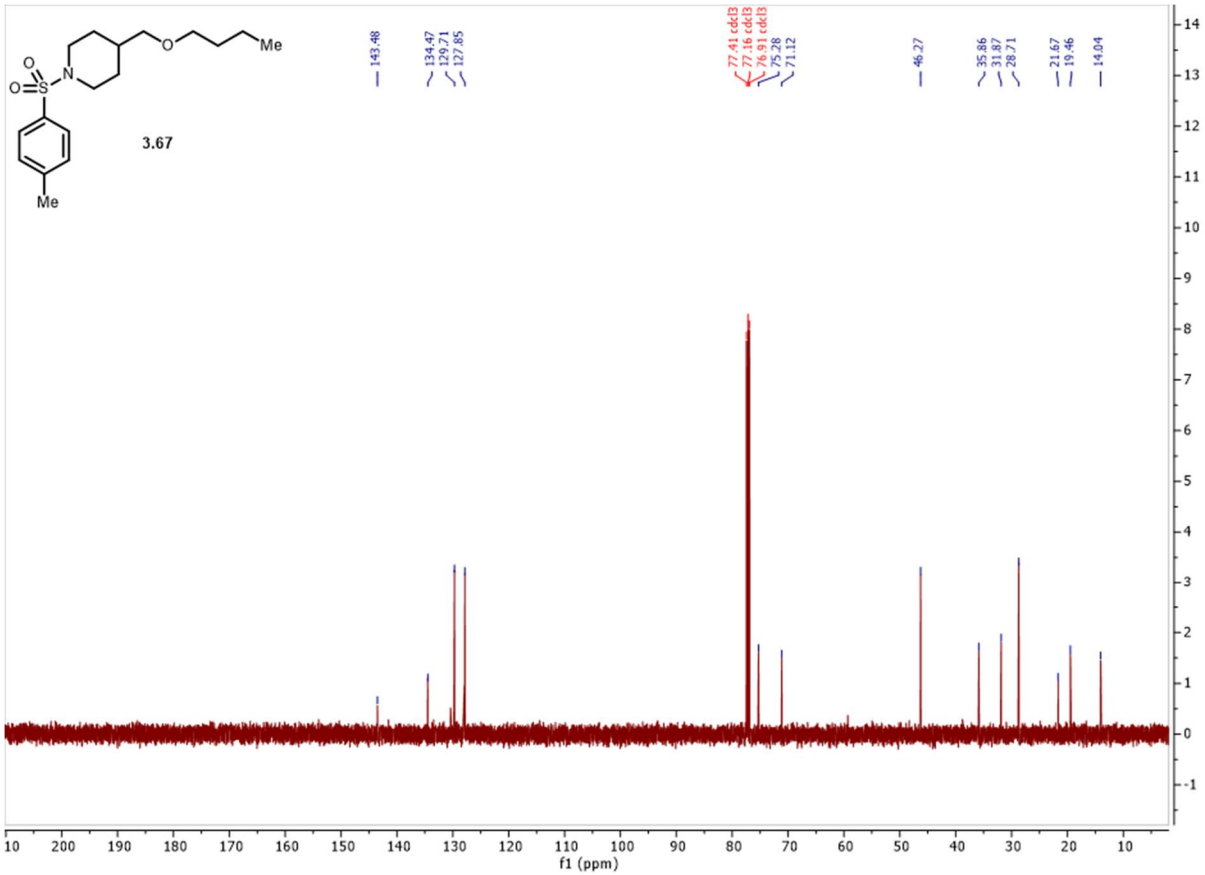

Spectrum 3.95 ^{13}C NMR of **3.67**.

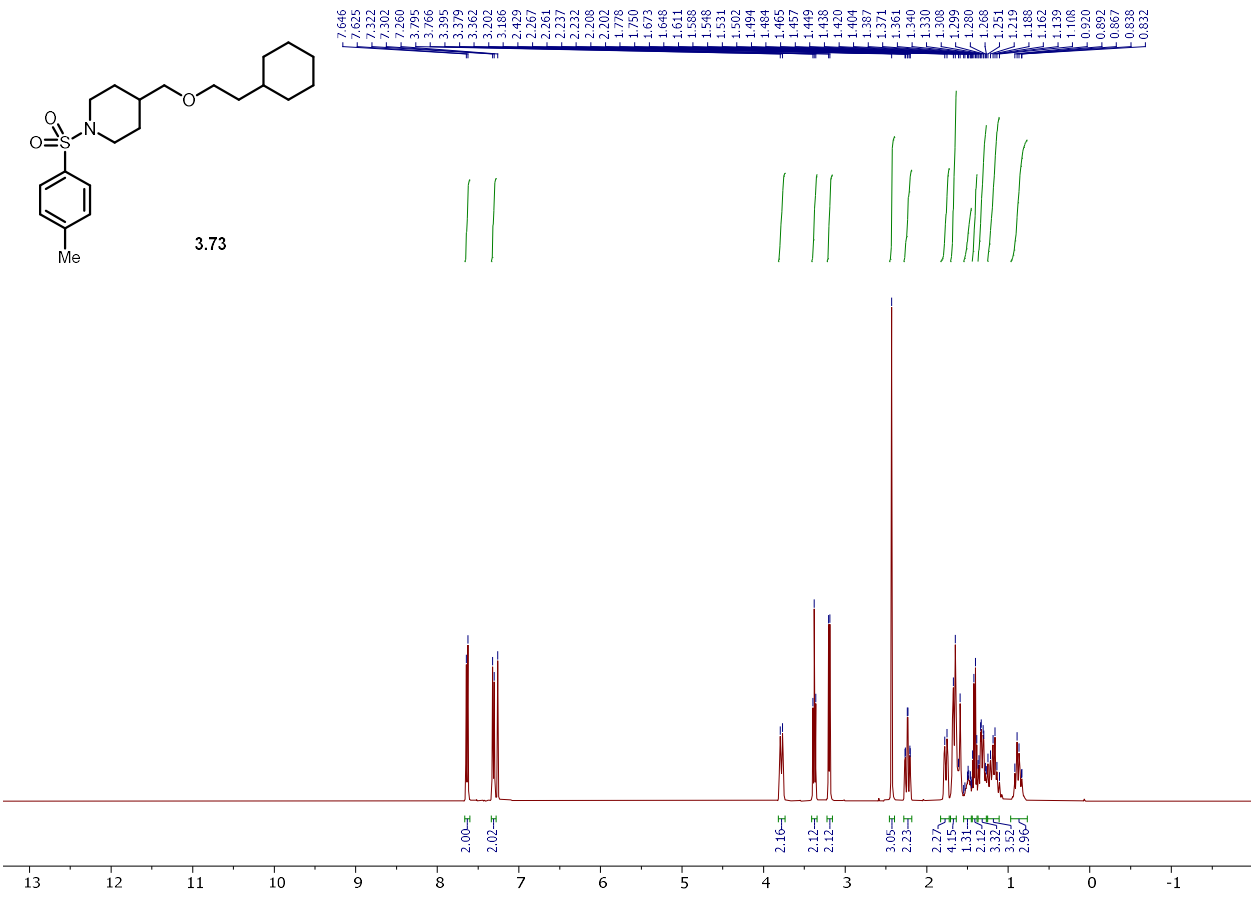

Spectrum 3.96 ^{1}H NMR of **3.73**.

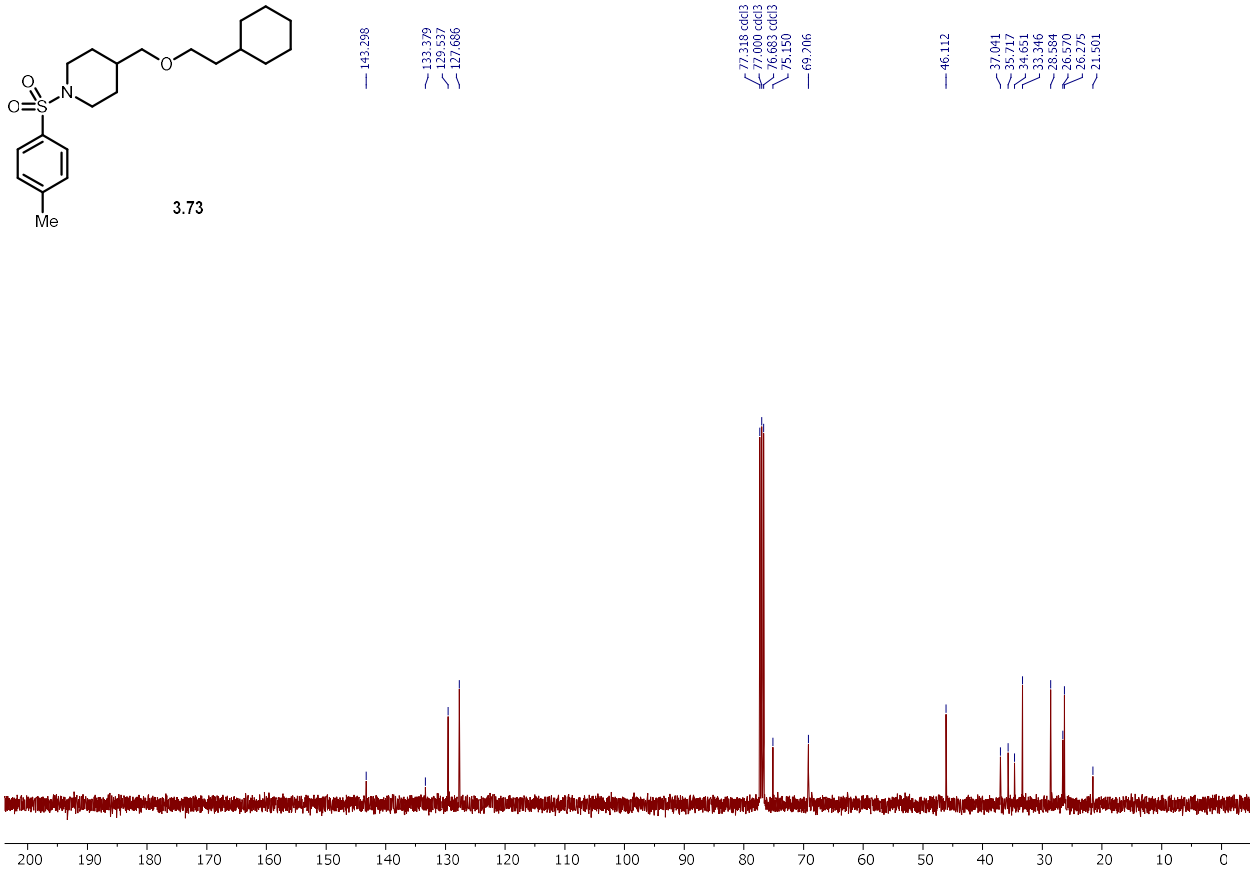

Spectrum 3.97 ^{13}C NMR of **3.73**.

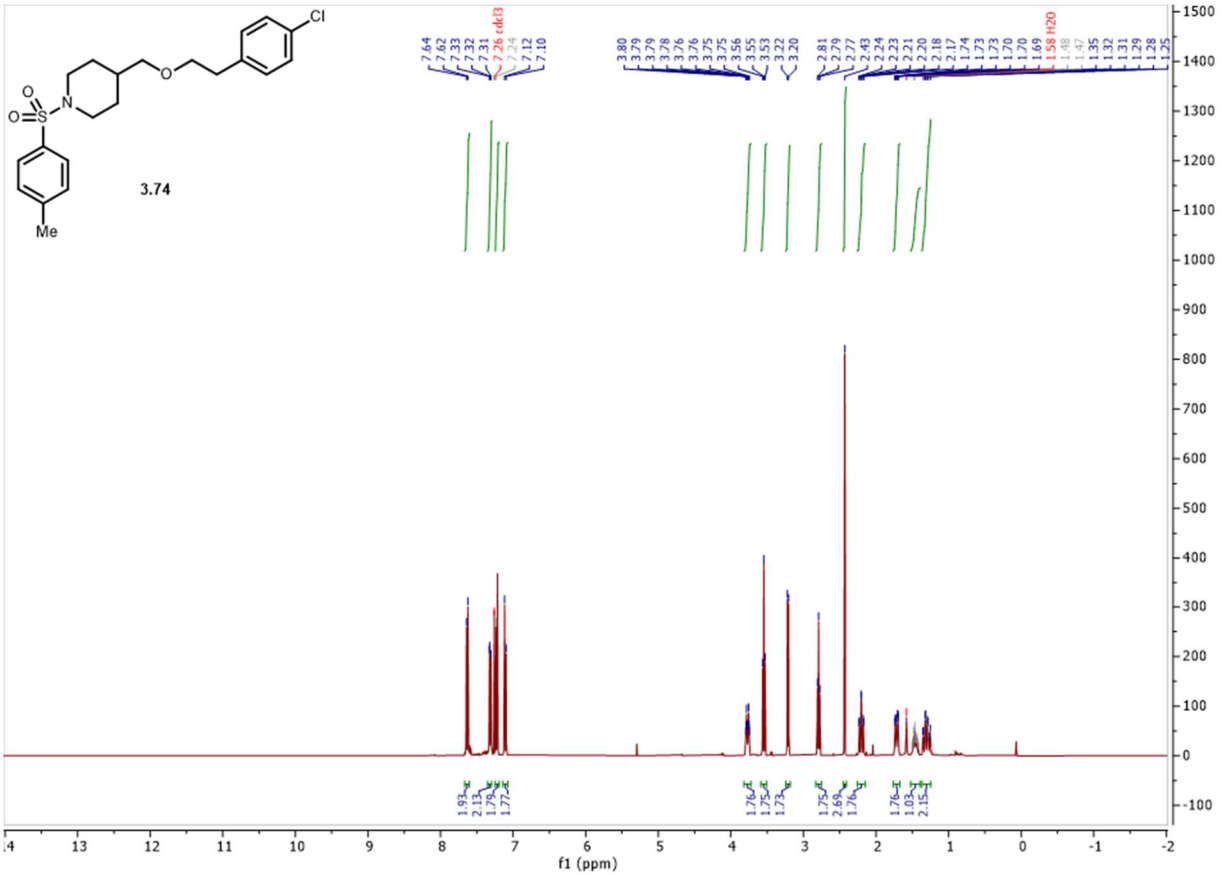

Spectrum 3.98 ^{1}H NMR of **3.74**.

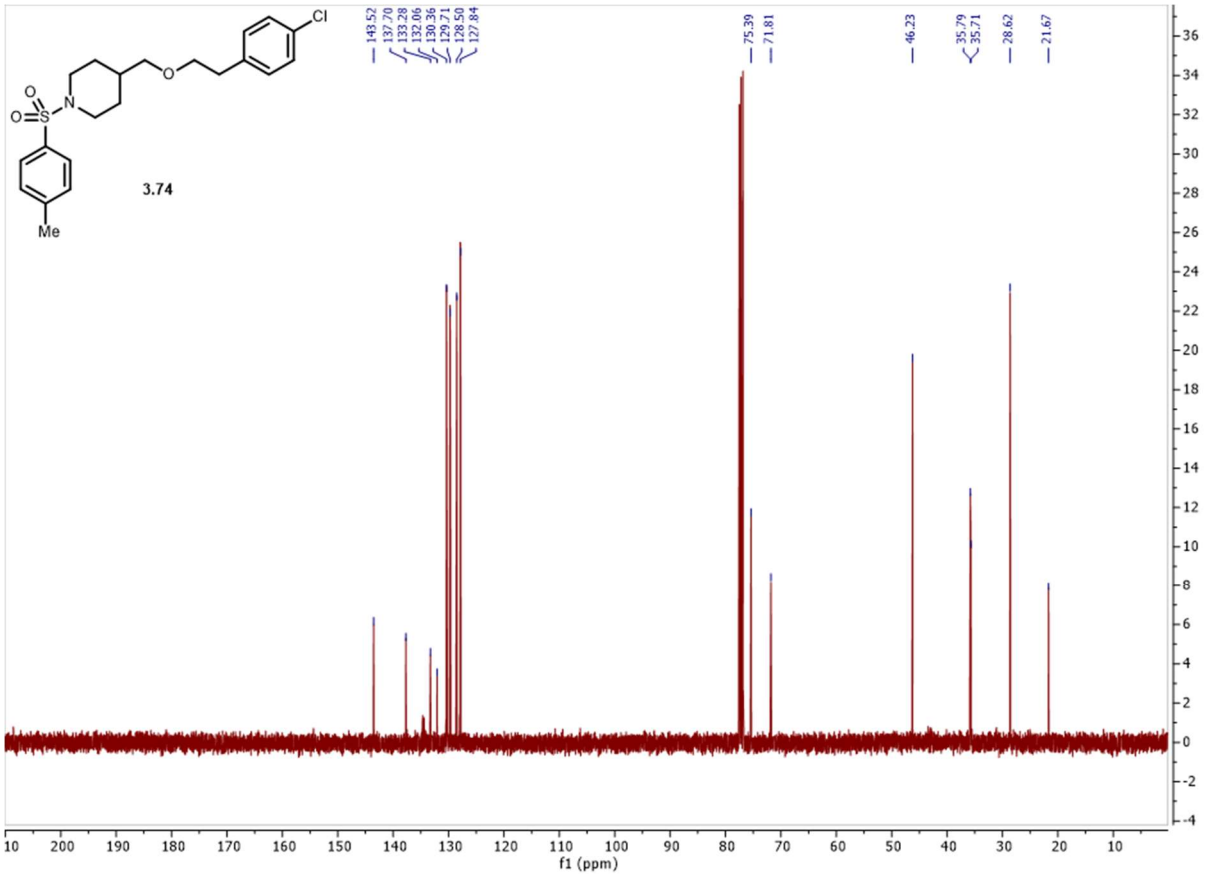

Spectrum 3.99 ^{13}CNMR of **3.74**.

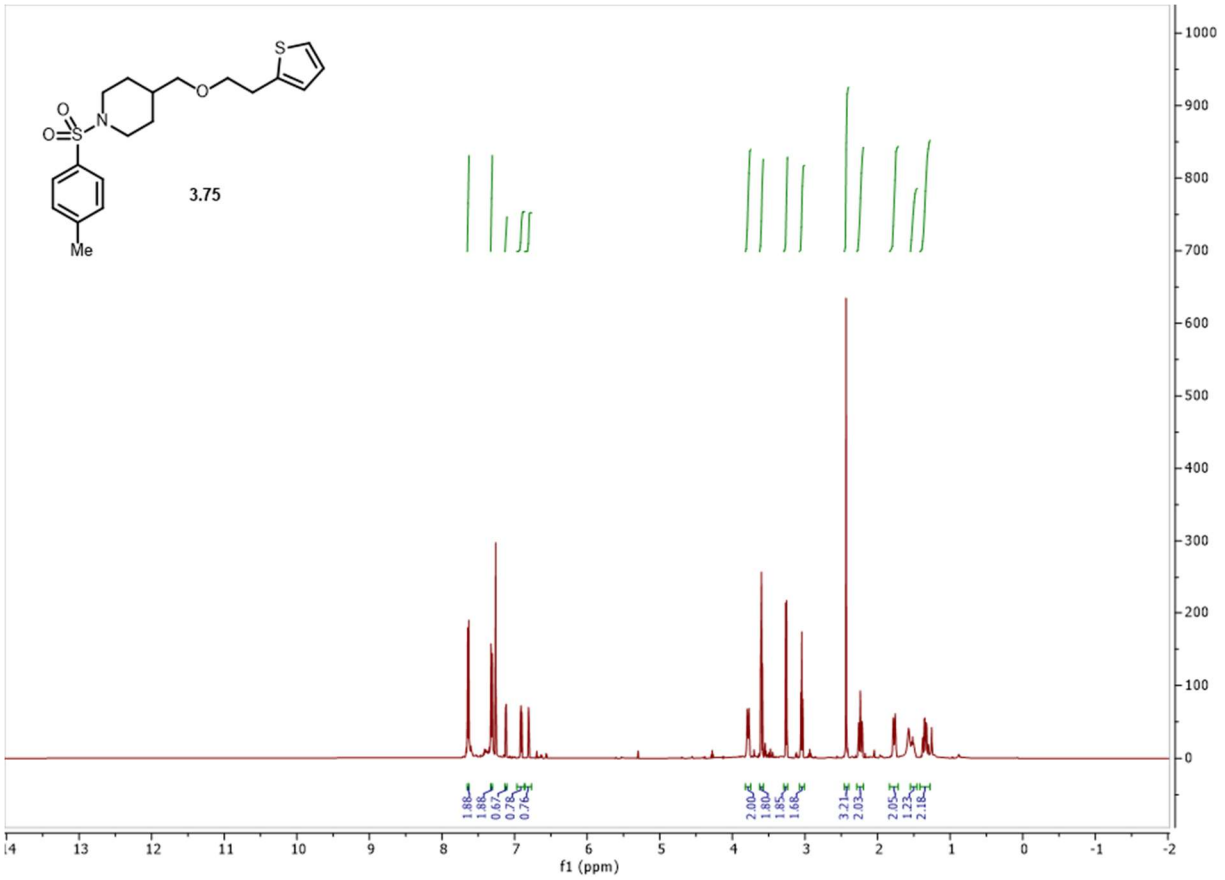

Spectrum 3.100 ^{1}H NMR of **3.75**.

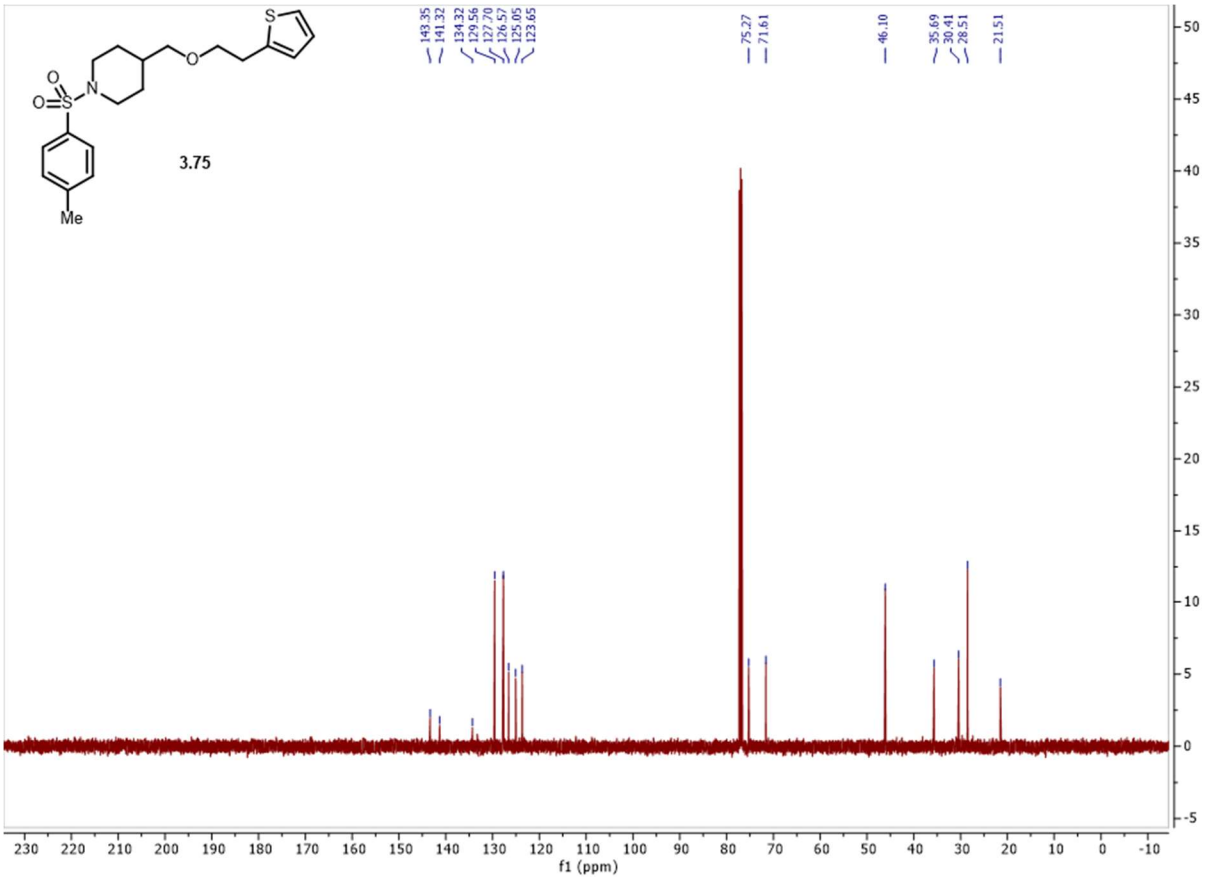

Spectrum 3.101 ^{13}C NMR of **3.75**.

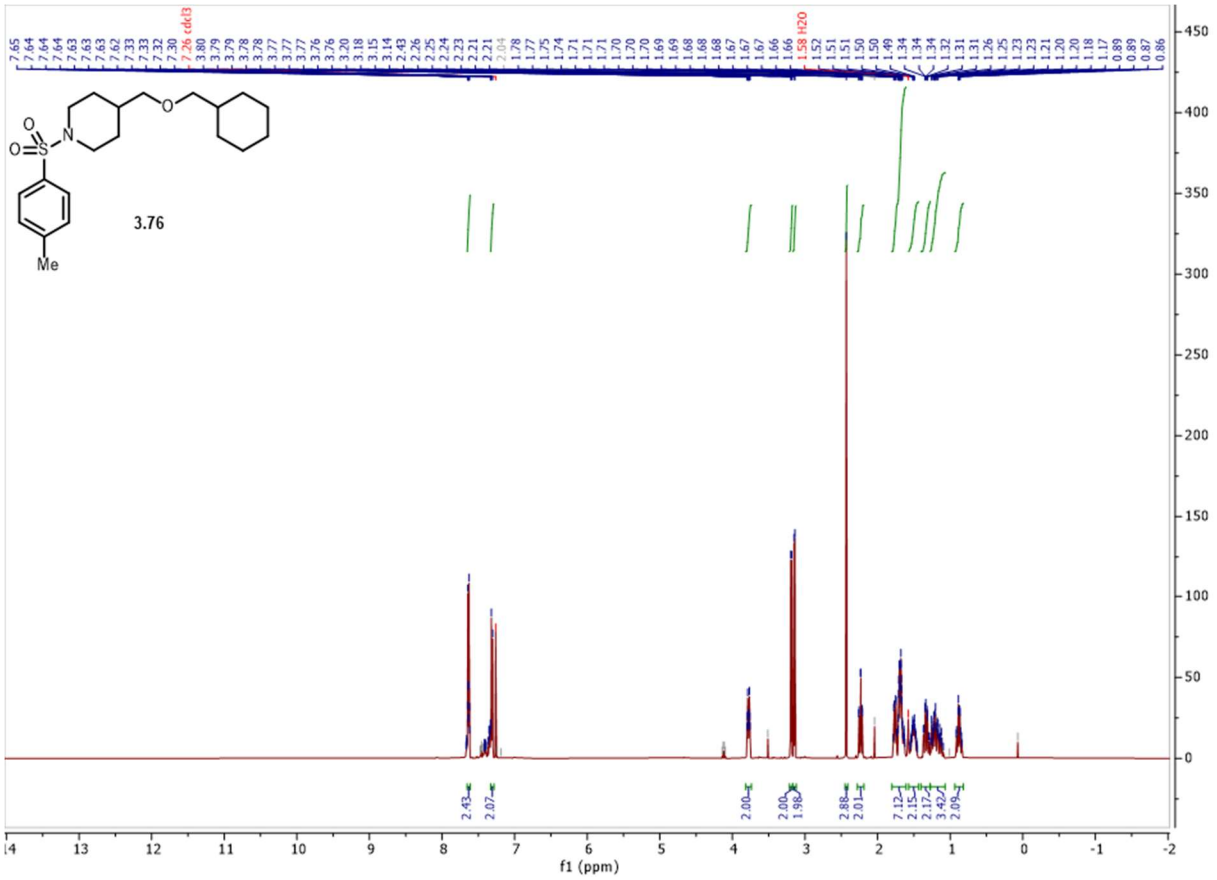

Spectrum 3.102 ^{1}H NMR of **3.76**.

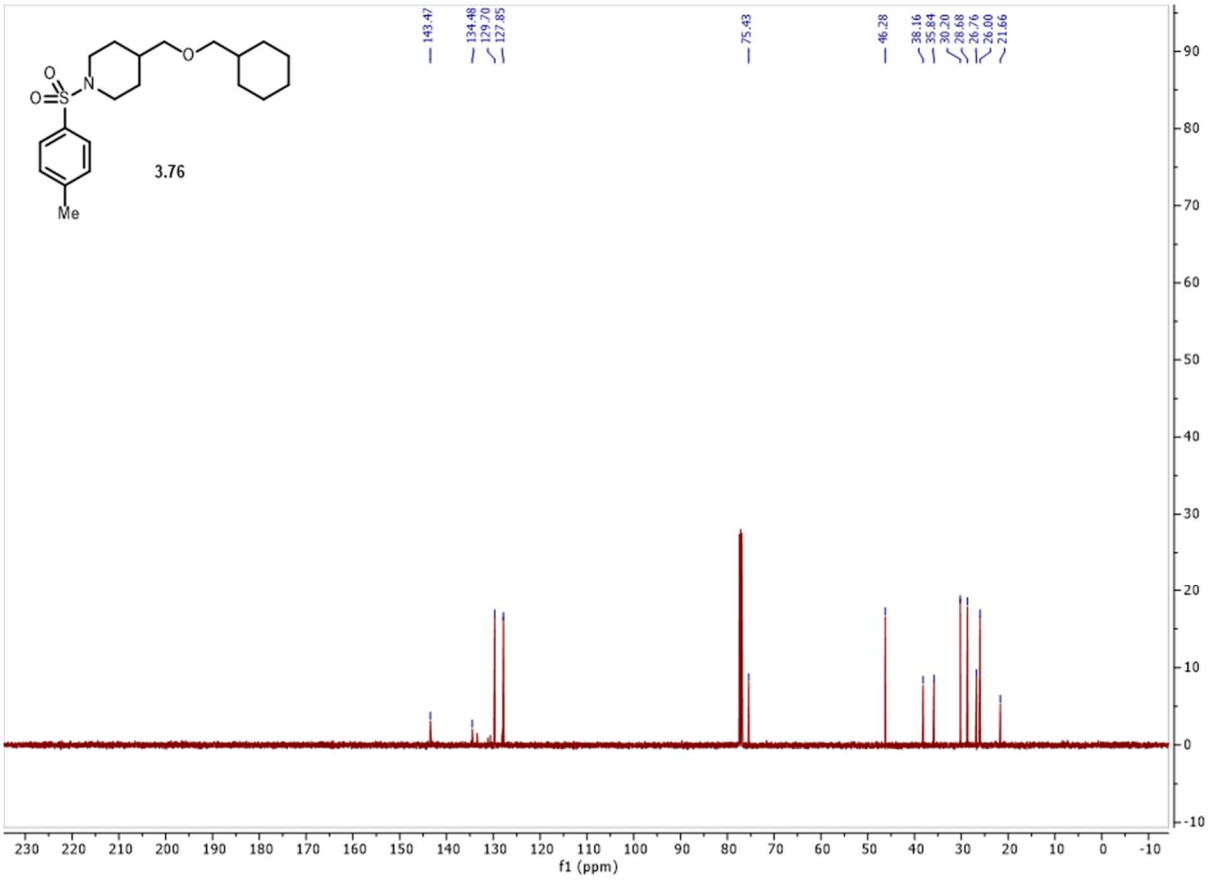

Spectrum 3.103 ^{13}C NMR of **3.76**.

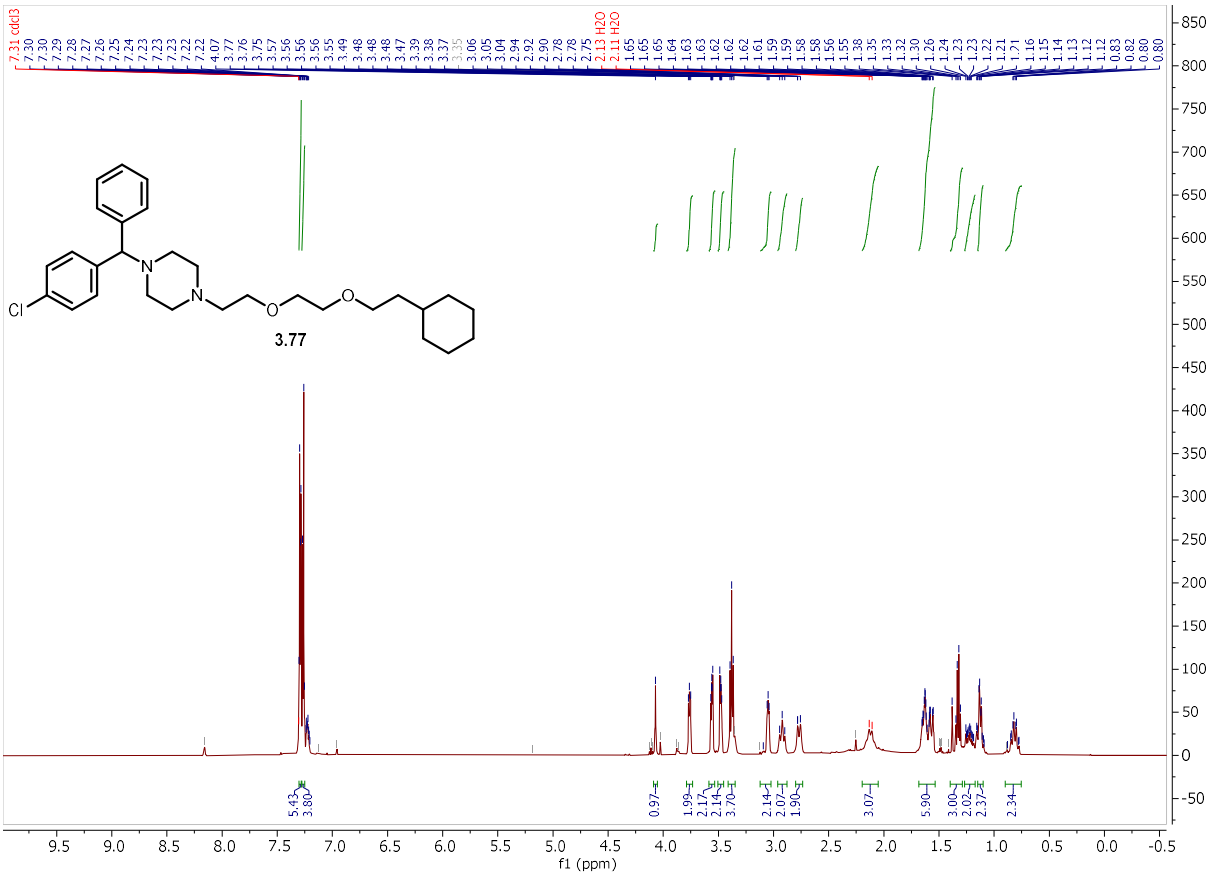

Spectrum 3.104 ^{1}H NMR of **3.77**.

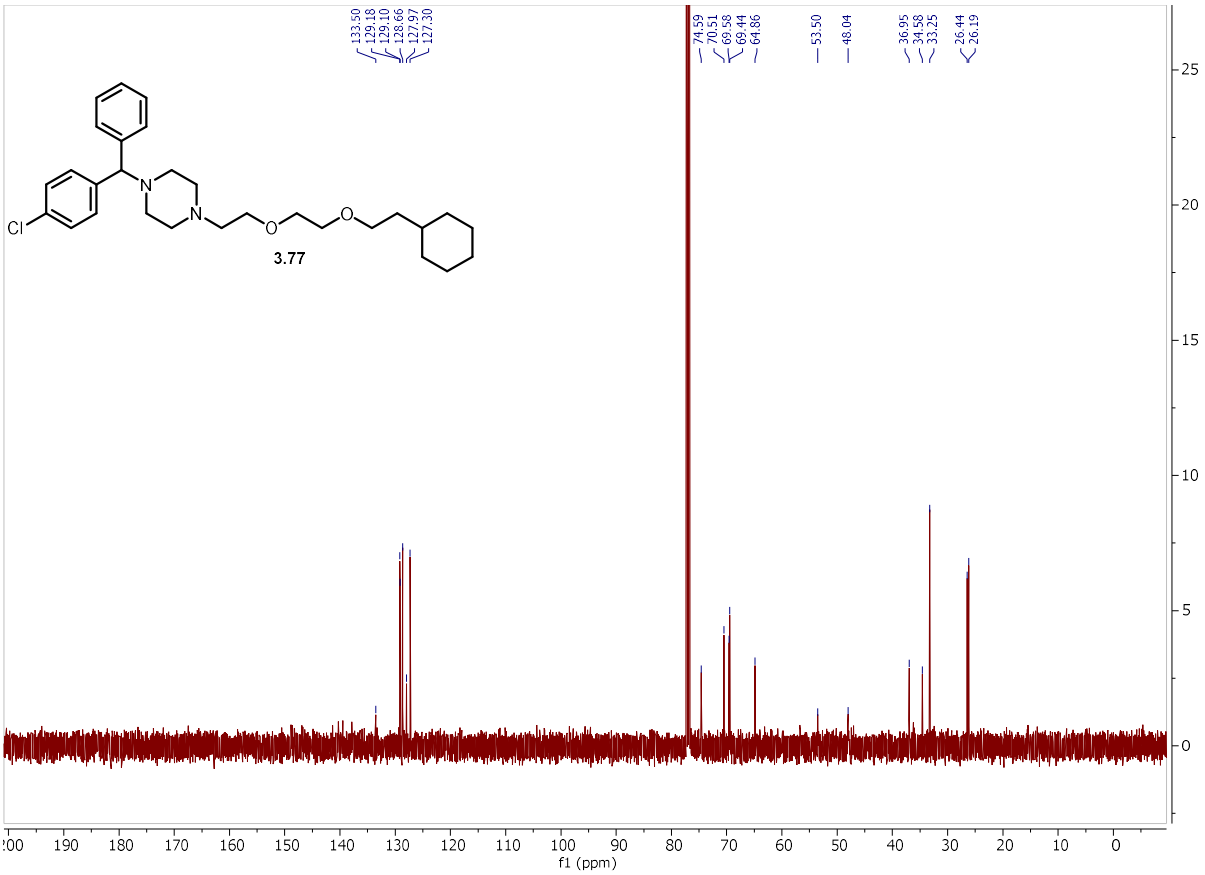

Spectrum 3.105 ^{13}C NMR of **3.77**.

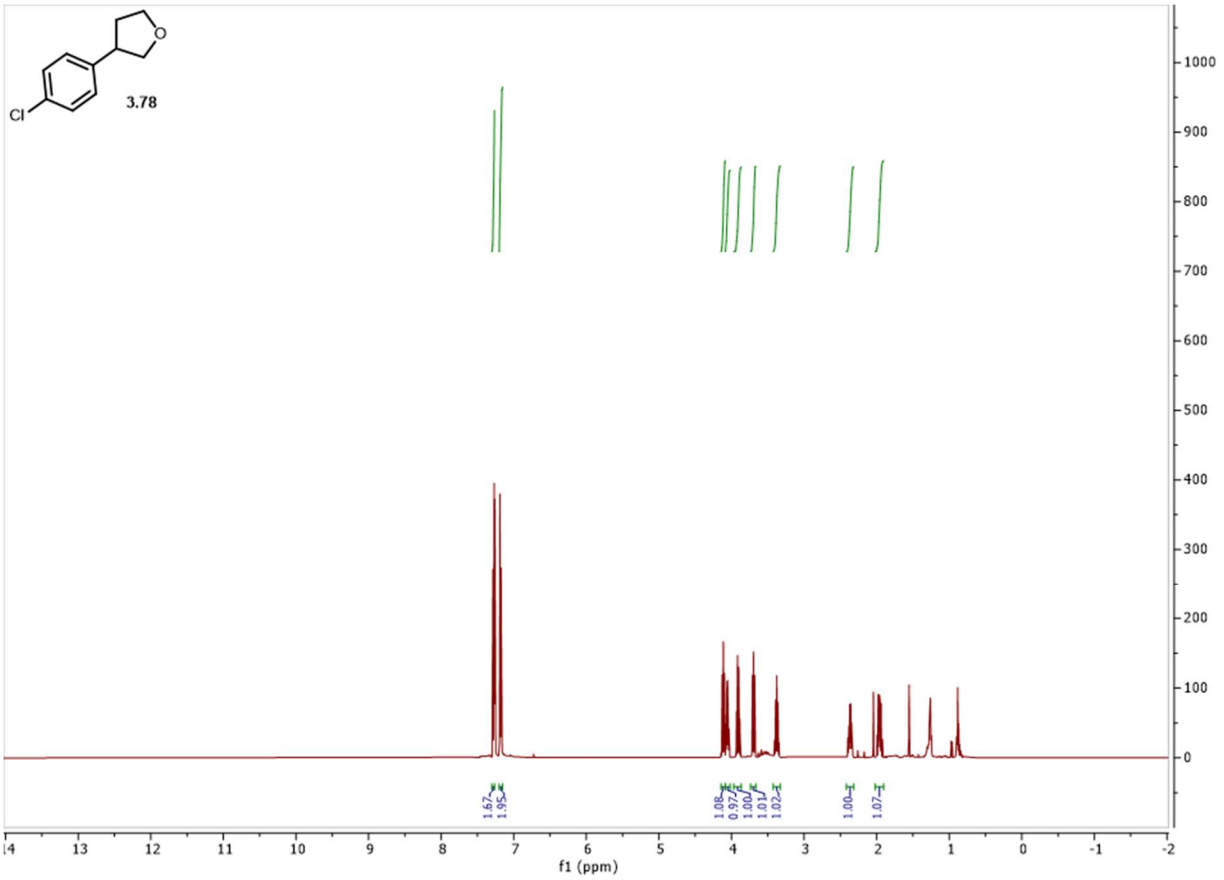

Spectrum 3.106 ^{1}H NMR of **3.78**.

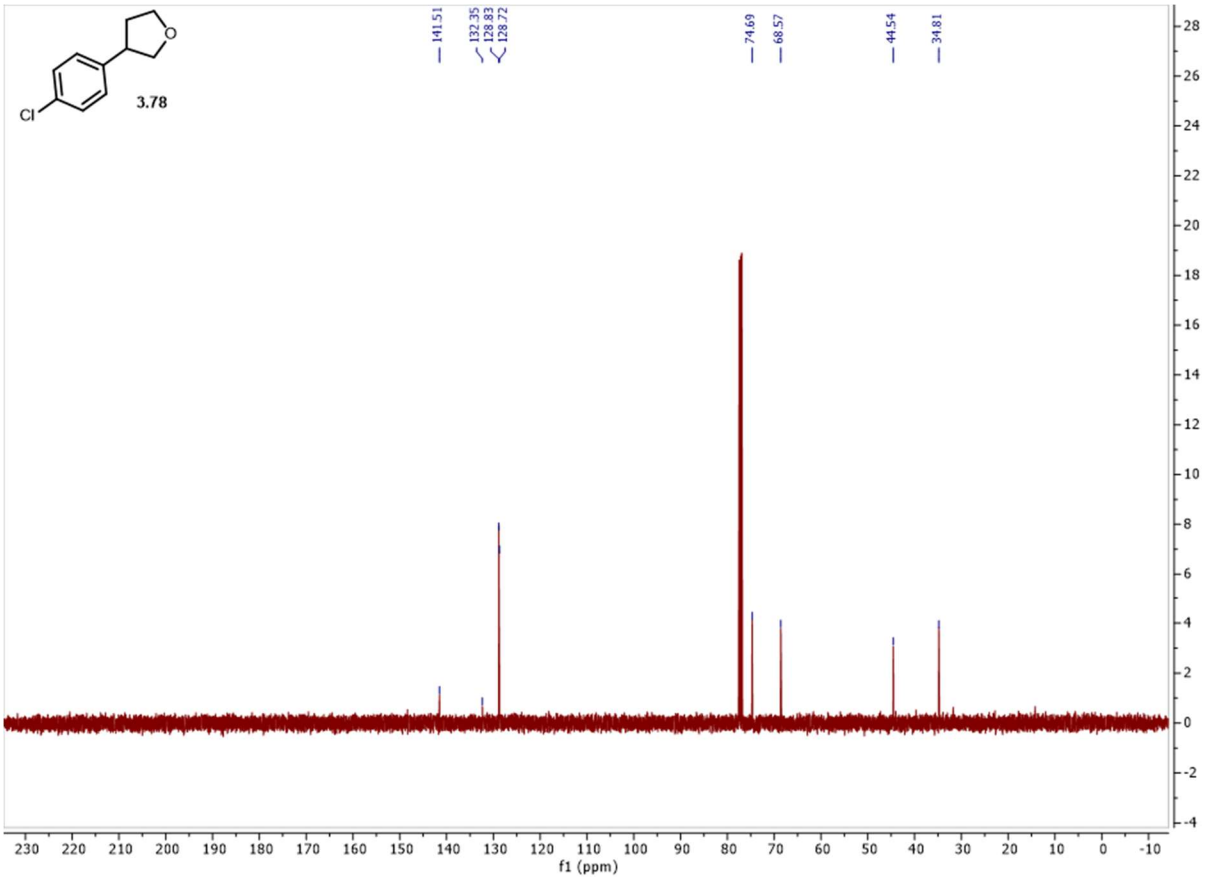

Spectrum 3.107 ^{13}C NMR of **3.78**.

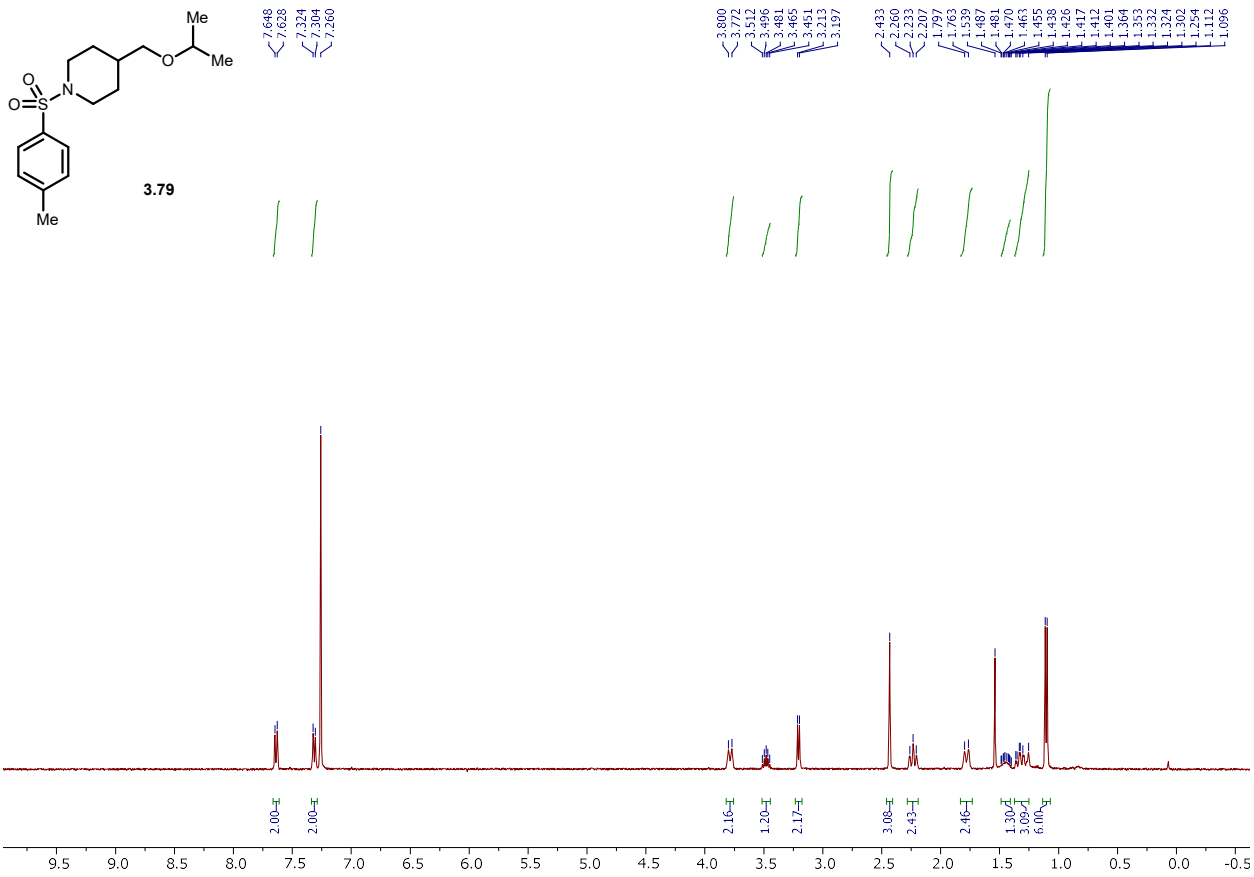

Spectrum 3.108 ^{1}H NMR of **3.79**.

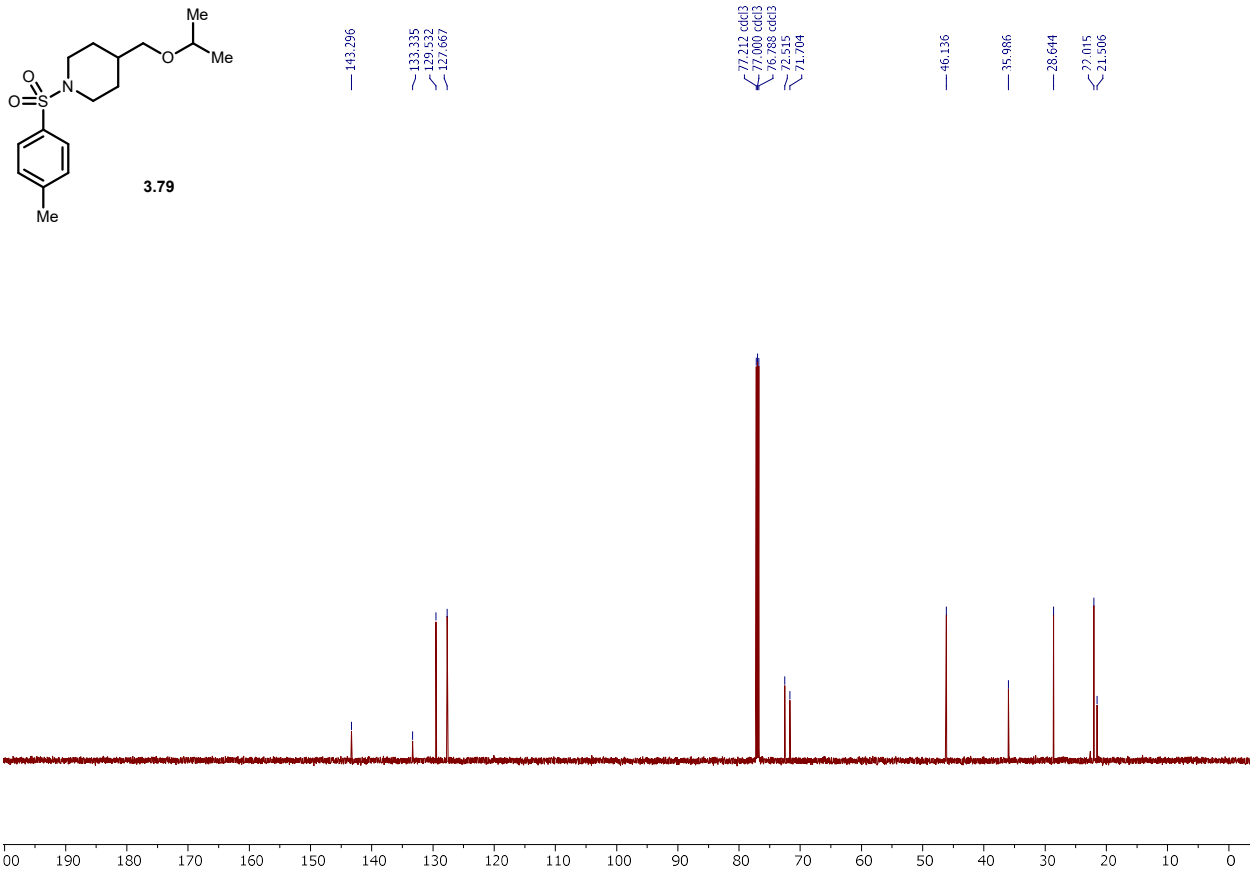

Spectrum 3.109 ^{13}C NMR of **3.79**.

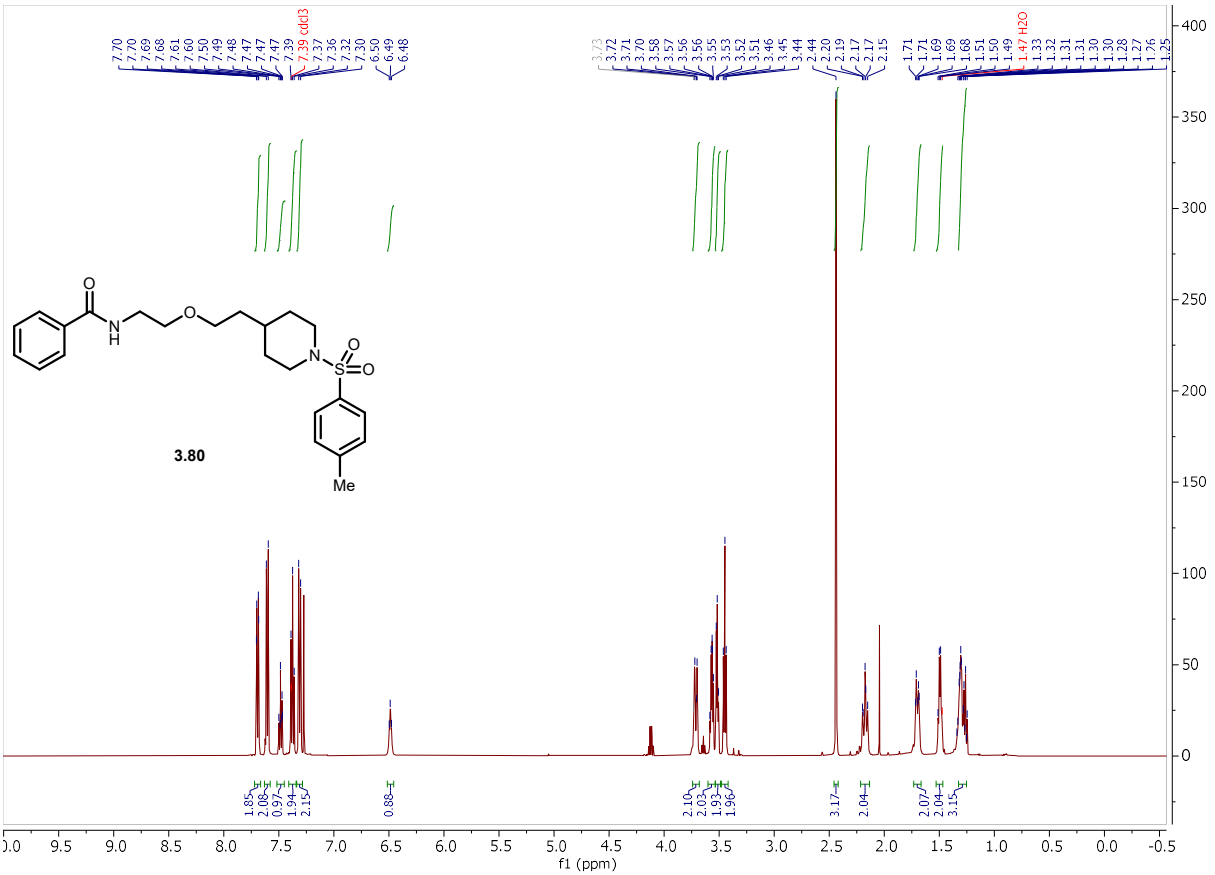

Spectrum 3.110 ^{1}H NMR of **3.80**.

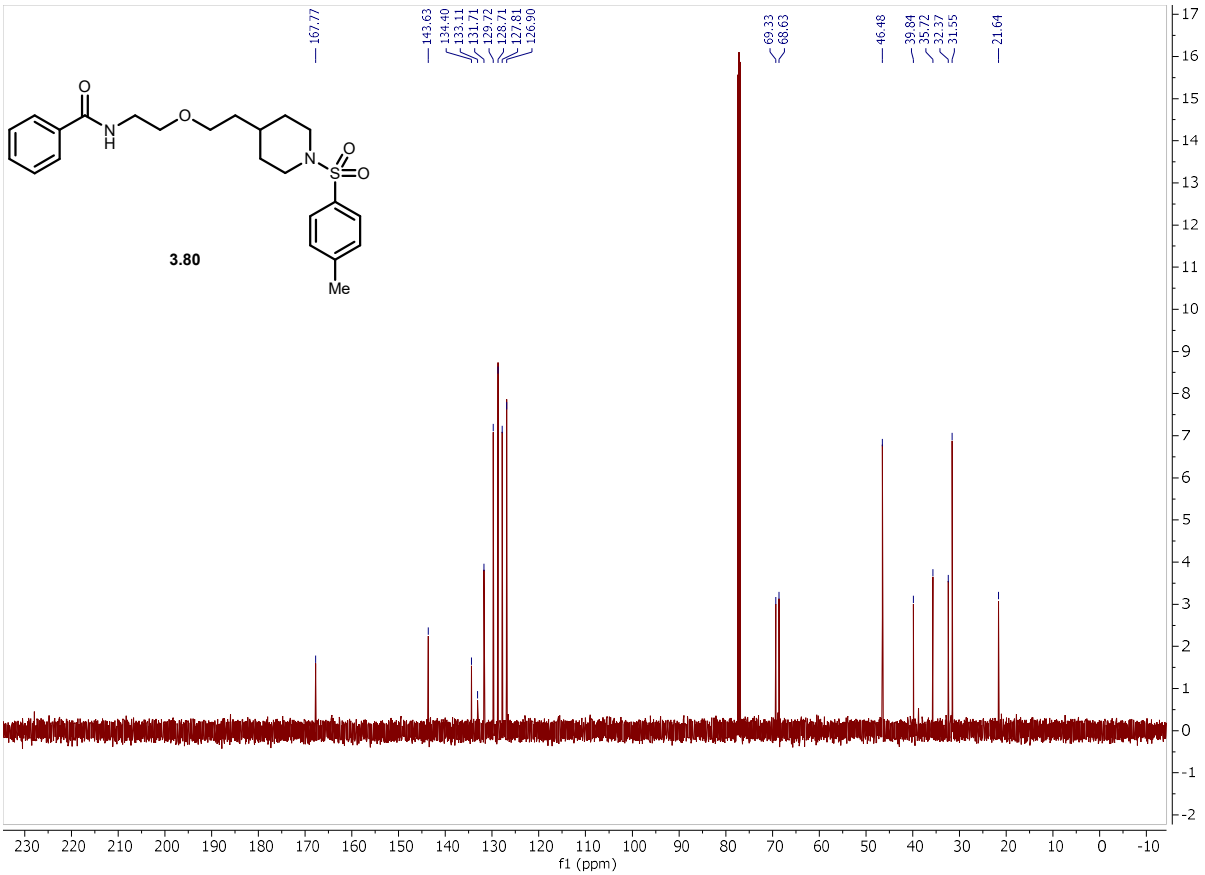

Spectrum 3.111 ^{13}C NMR of **3.80**

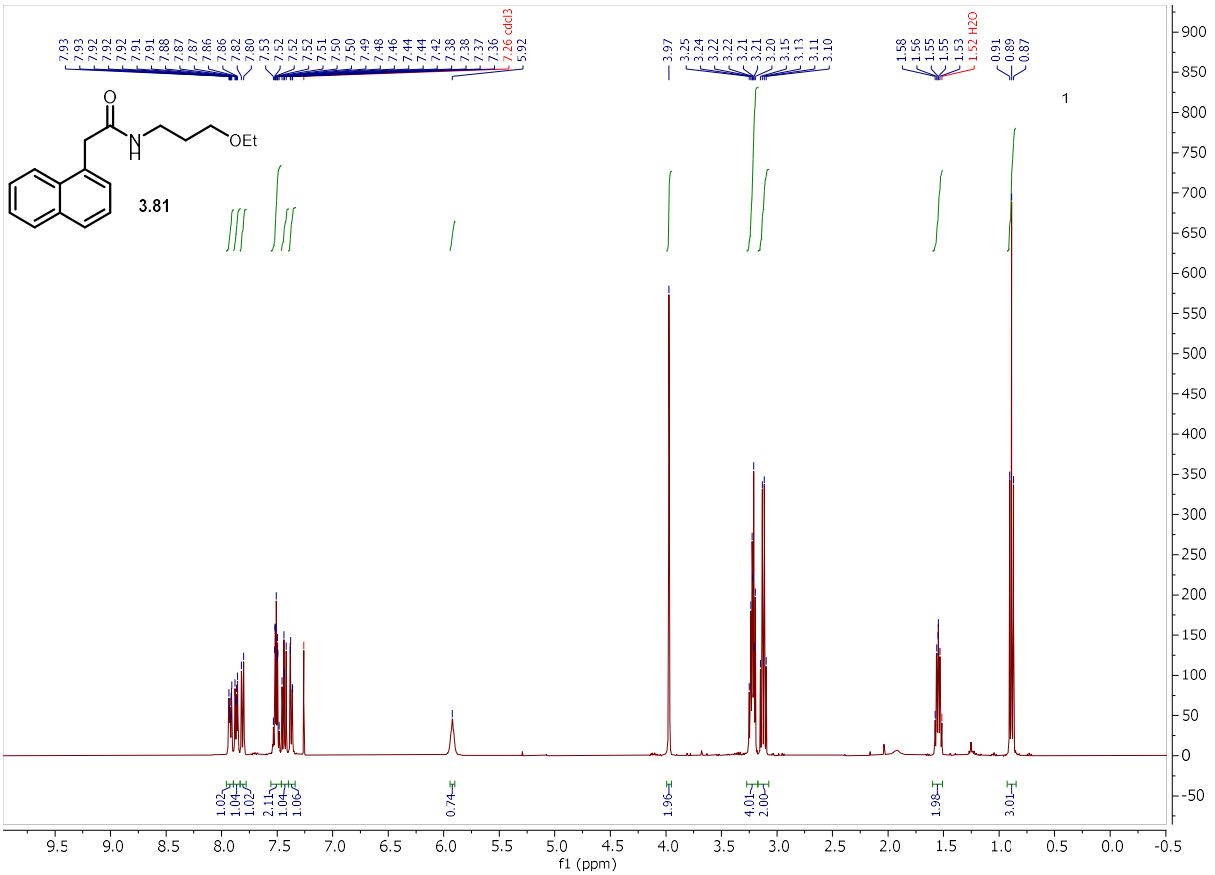

Spectrum 3.112 ^{1}H NMR of **3.81**

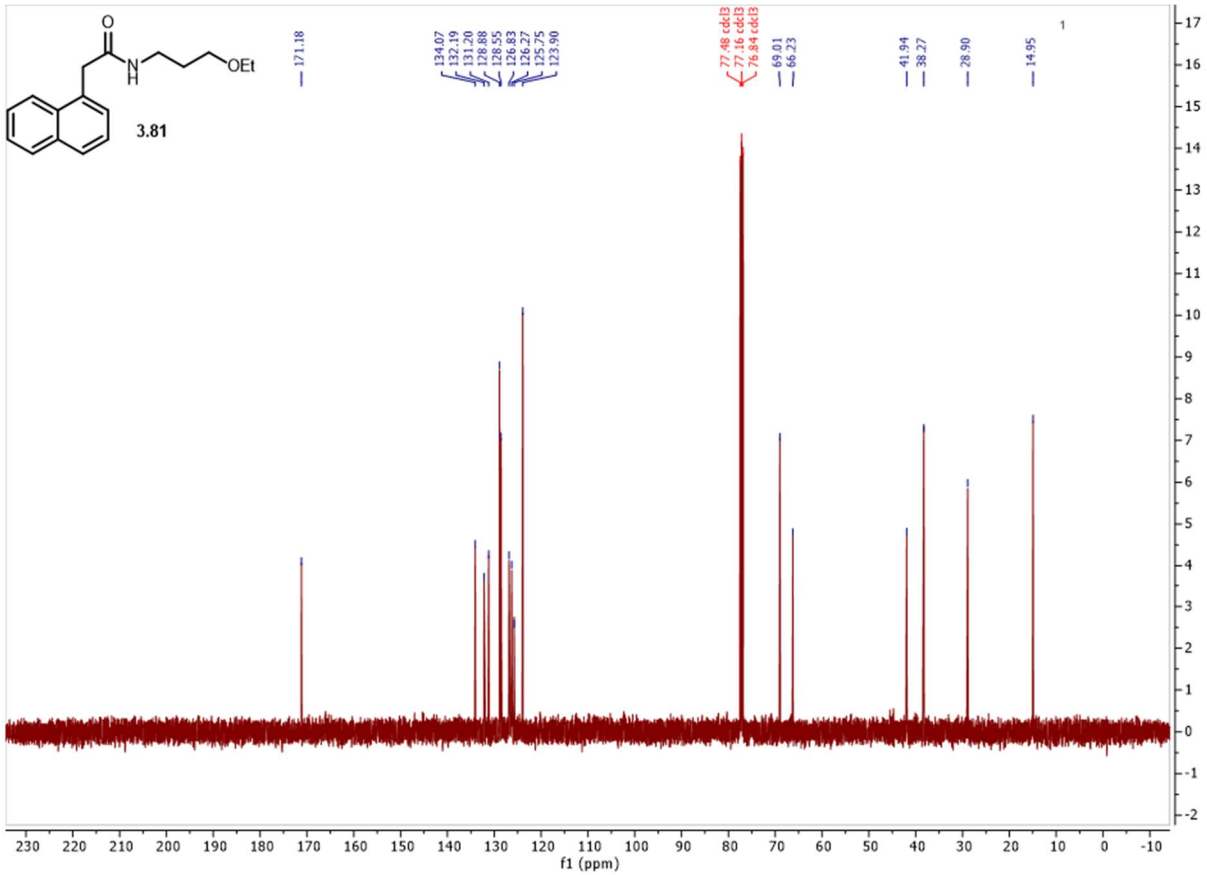

Spectrum 3.113 ^{13}C NMR of **3.81**.

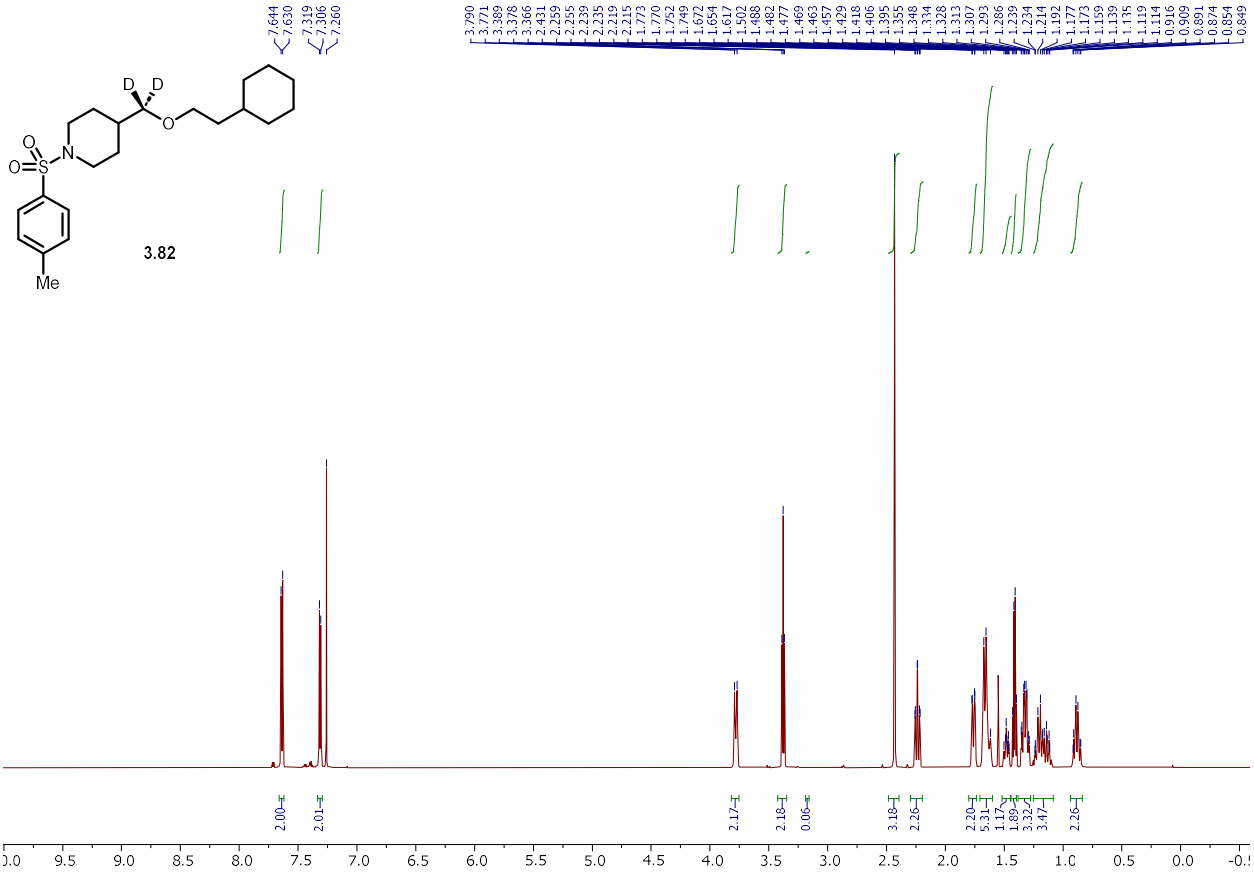

Spectrum 3.114 ^{1}H NMR of **3.82**.

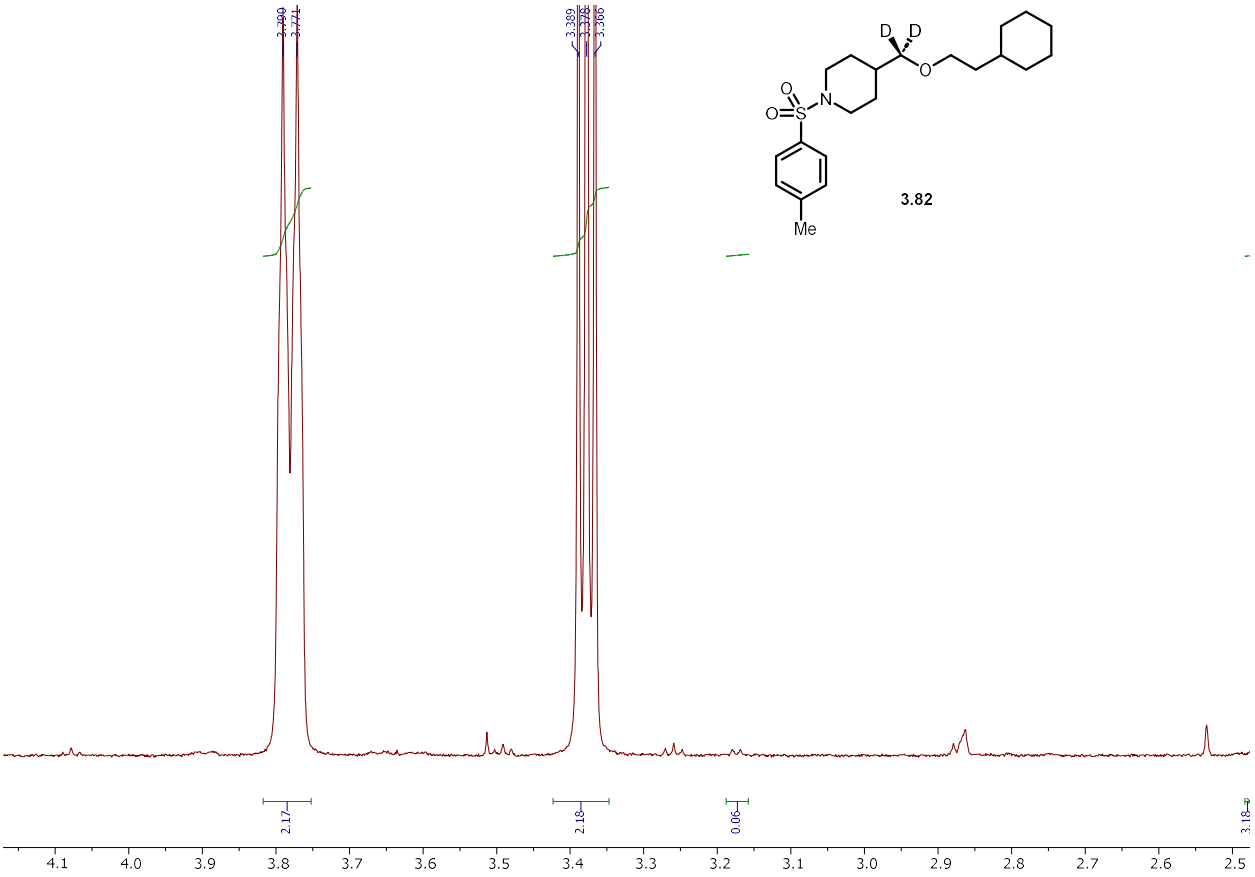

Spectrum 3.115 Zoomed in ^{1}H NMR of **3.82** where CD_2 would be. The H's at 3.17 integrate to ~3% of what they would if it were full H incorporation.

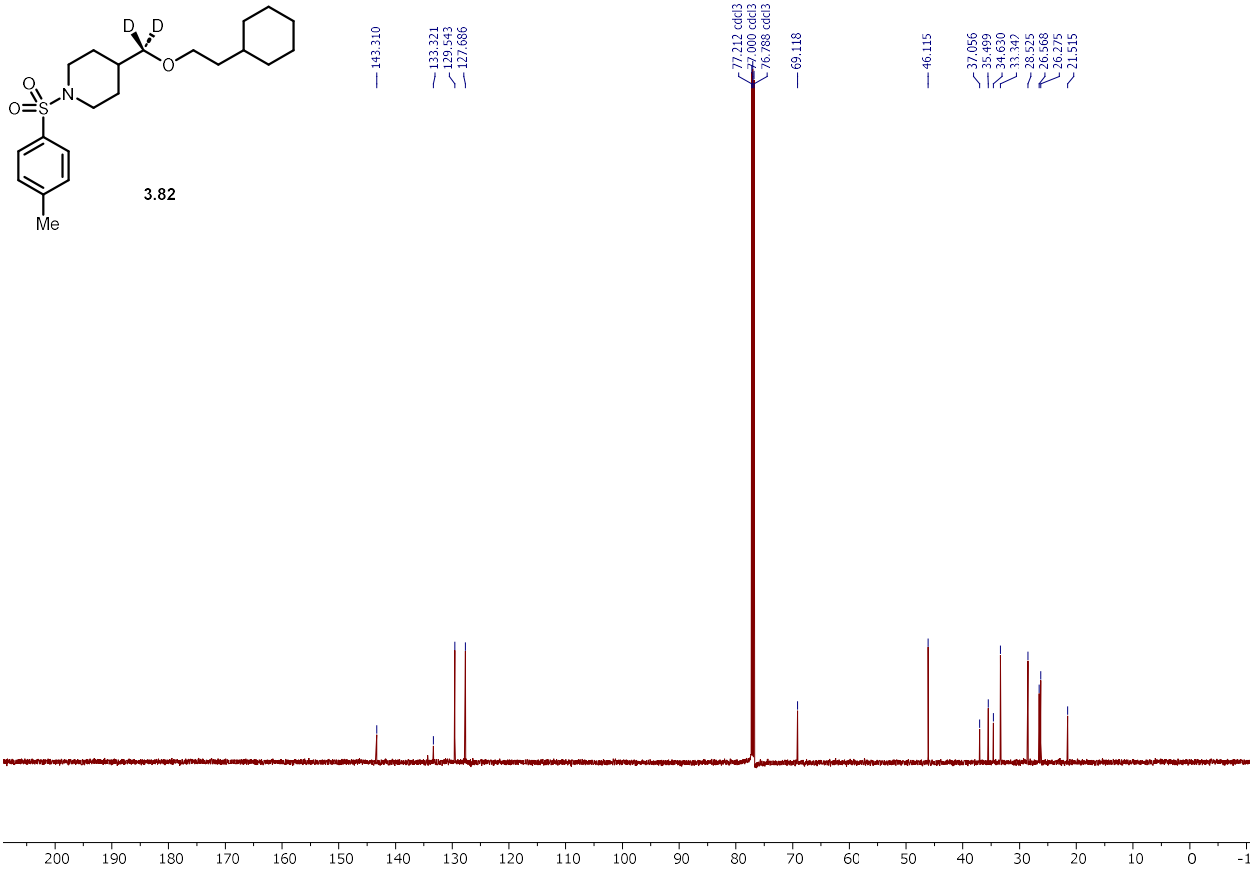

Spectrum 3.116 ^{13}C NMR of **3.82**.

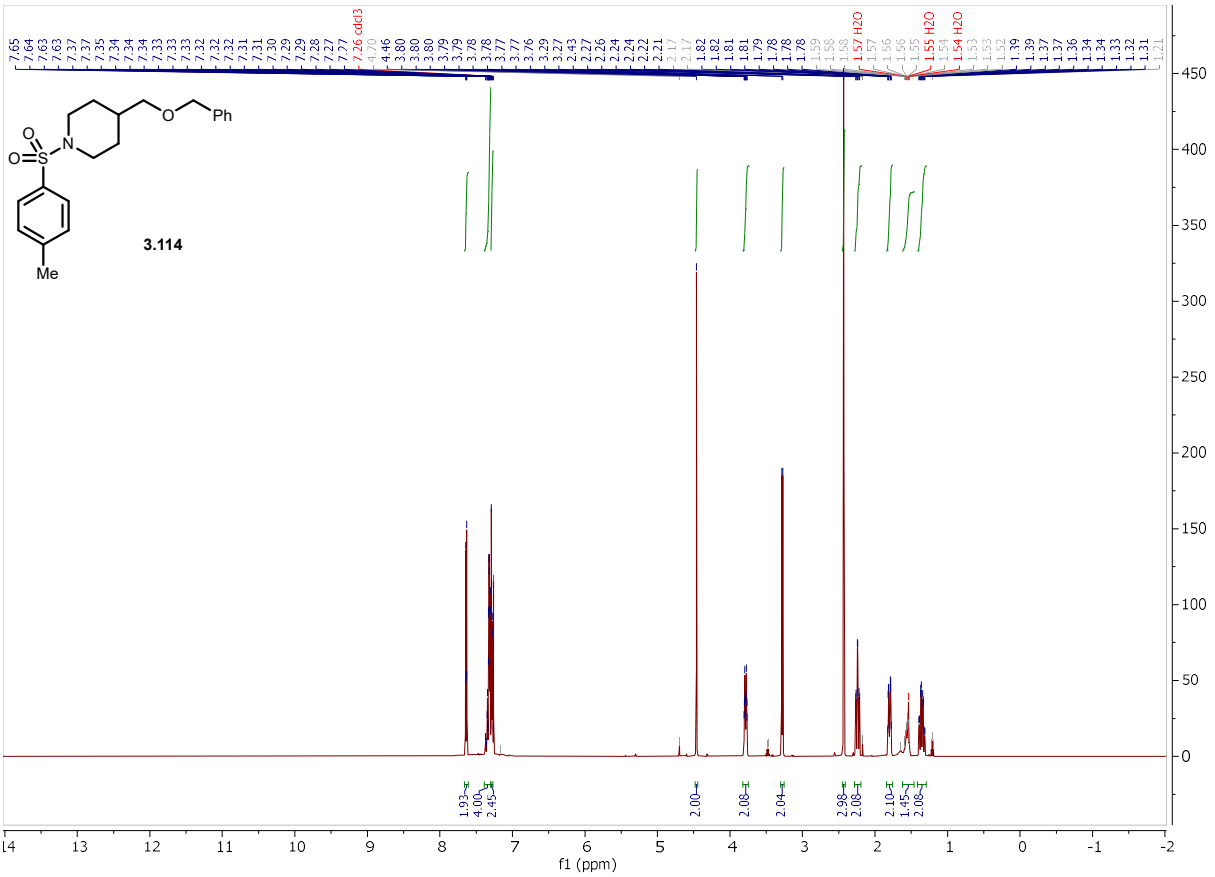

Spectrum 3.117 ^{1}H NMR of **3.114**

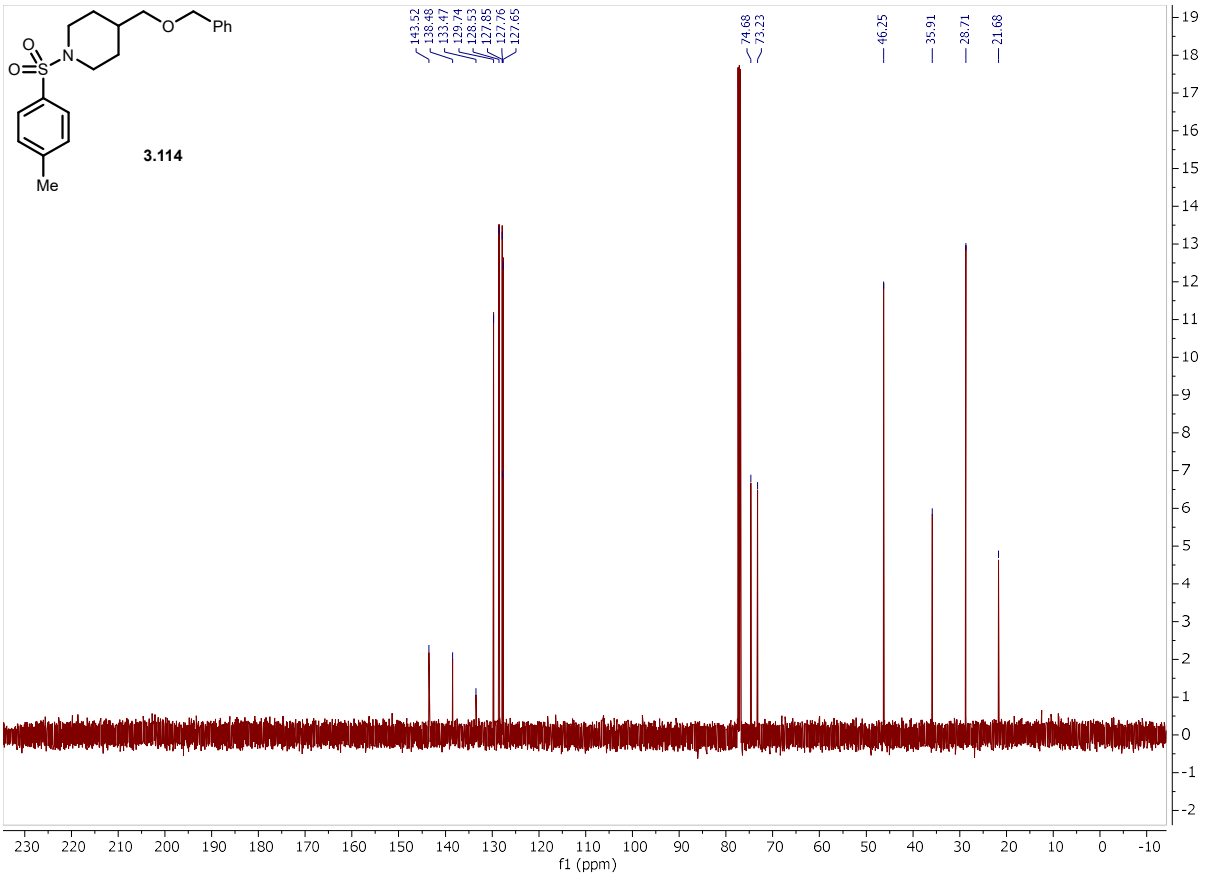

Spectrum 3.118 ^{13}C NMR of **3.114**.

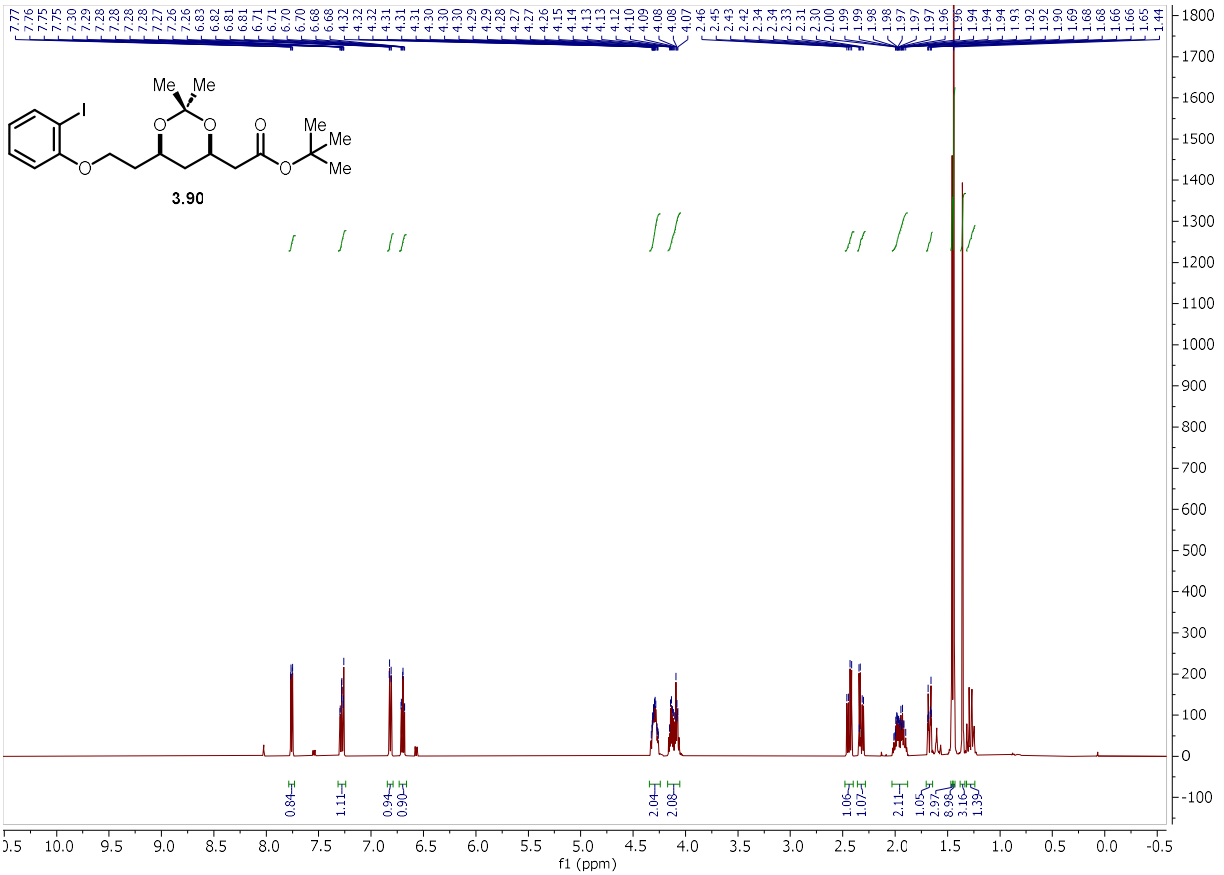

Spectrum 3.119 ^{1}H NMR of **3.90**.

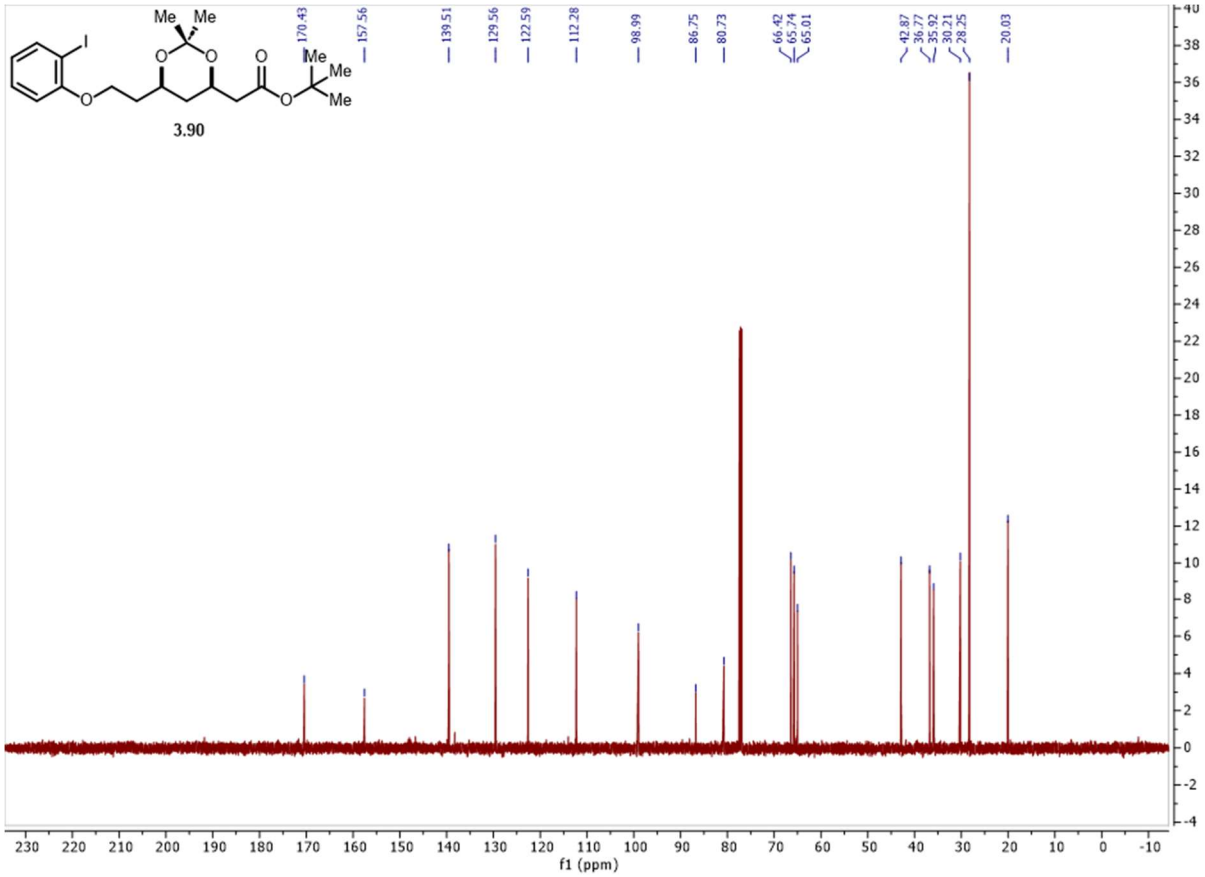

Spectrum 3.120 ^{13}C NMR of **3.90**.

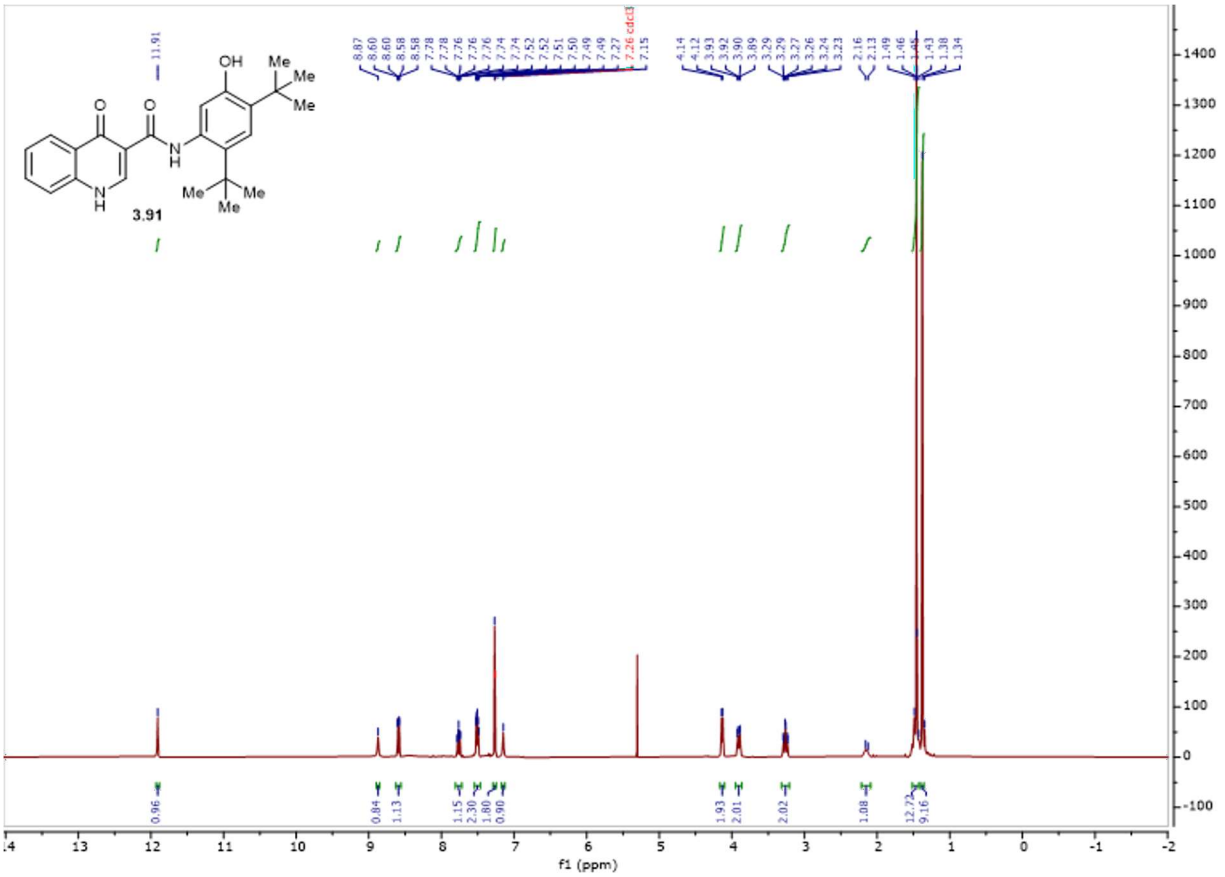

Spectrum 3.121 ^{1}H NMR of **3.91**.

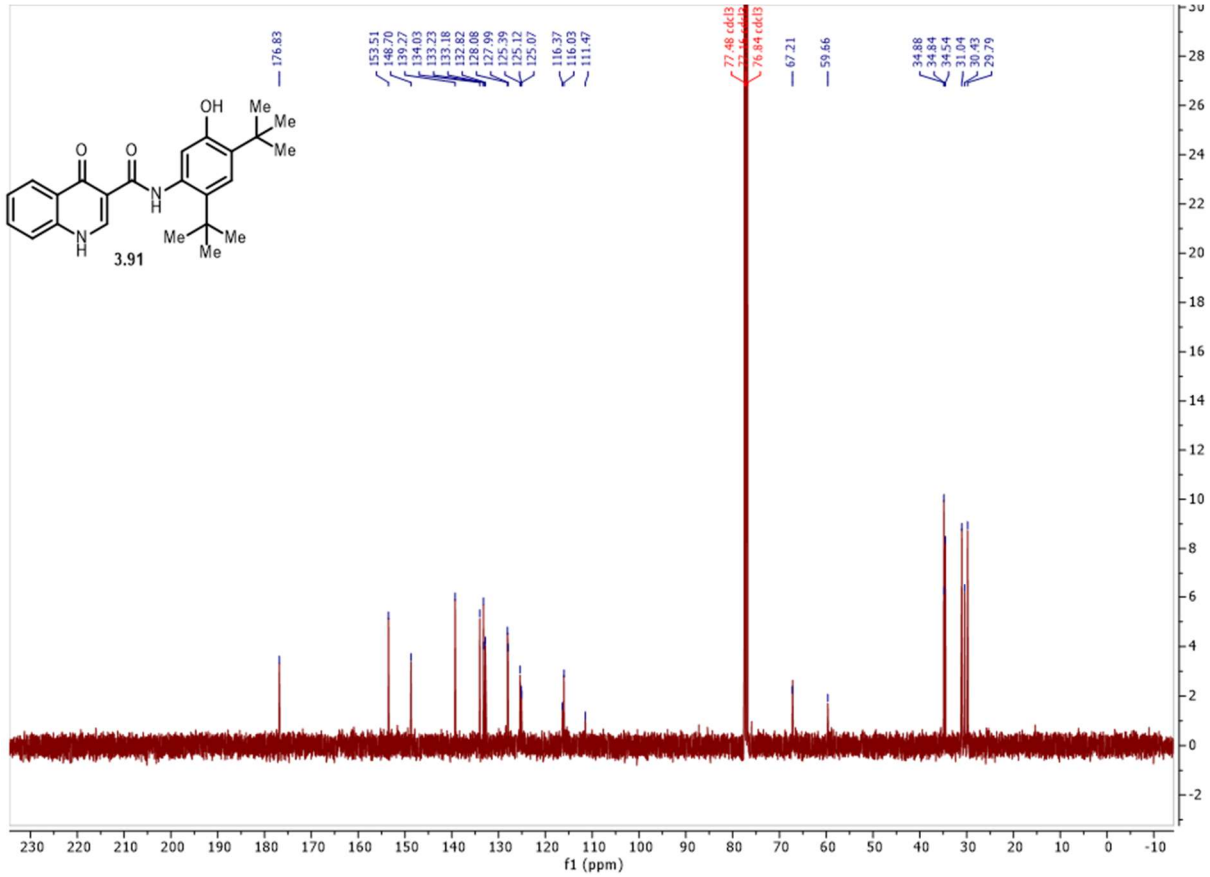

Spectrum 3.122 ^{13}C NMR of **3.91**.

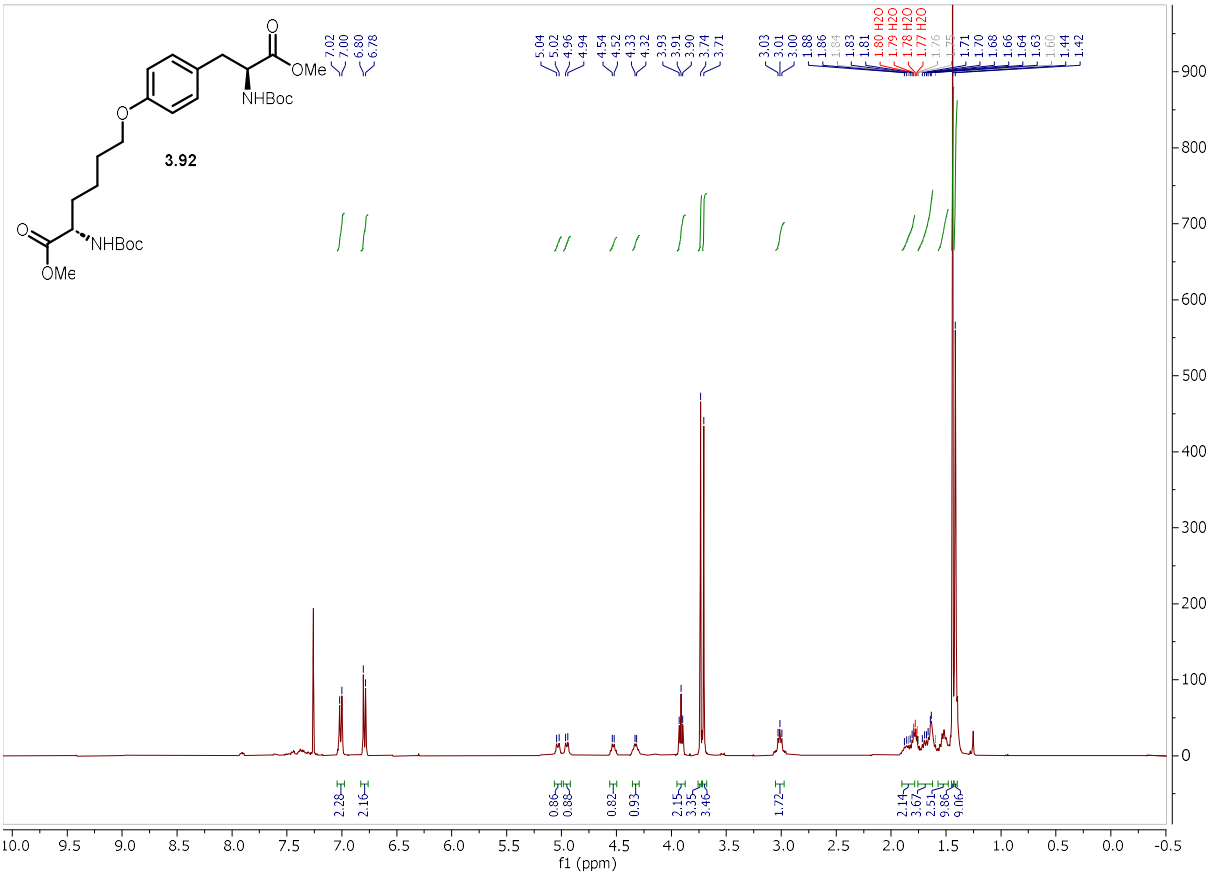

Spectrum 3.123 ^{1}H NMR of **3.92**.

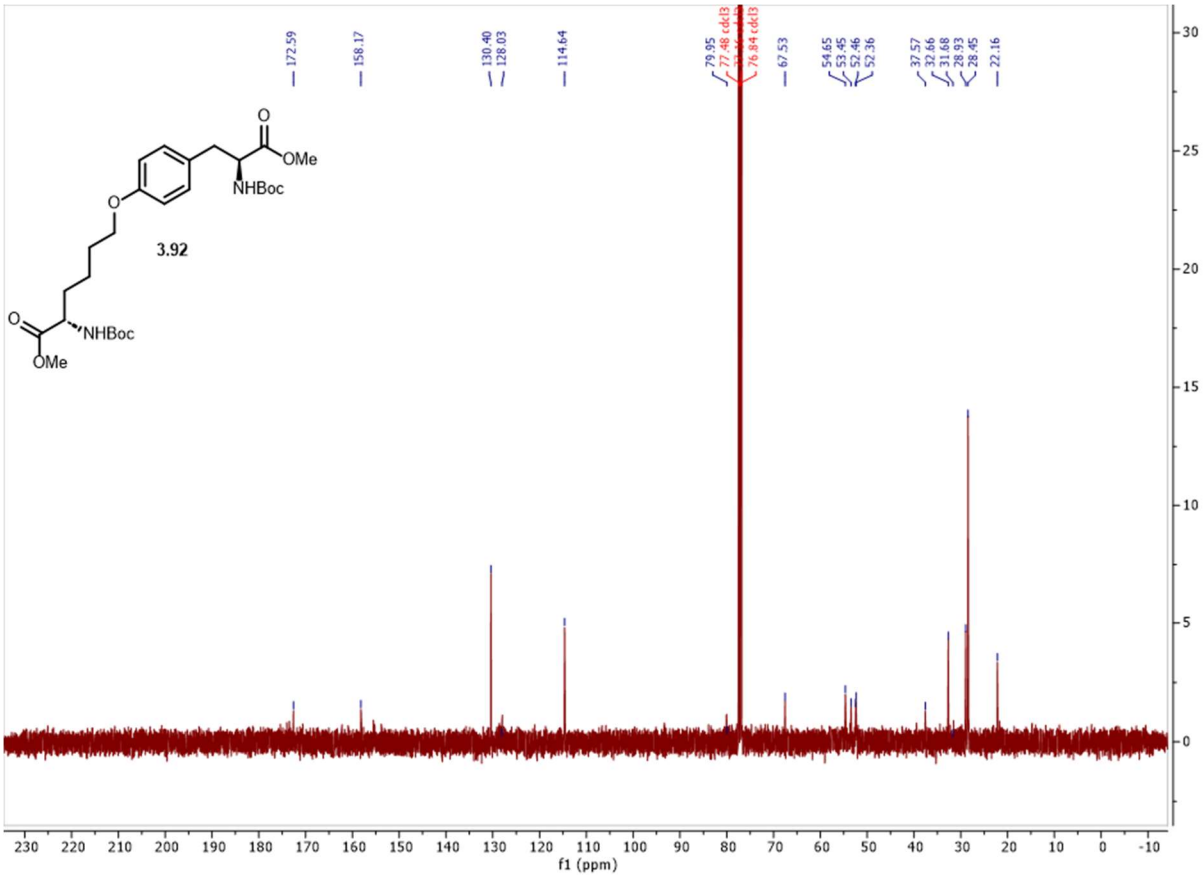

Spectrum 3.124 ^{13}C NMR of **3.92**.

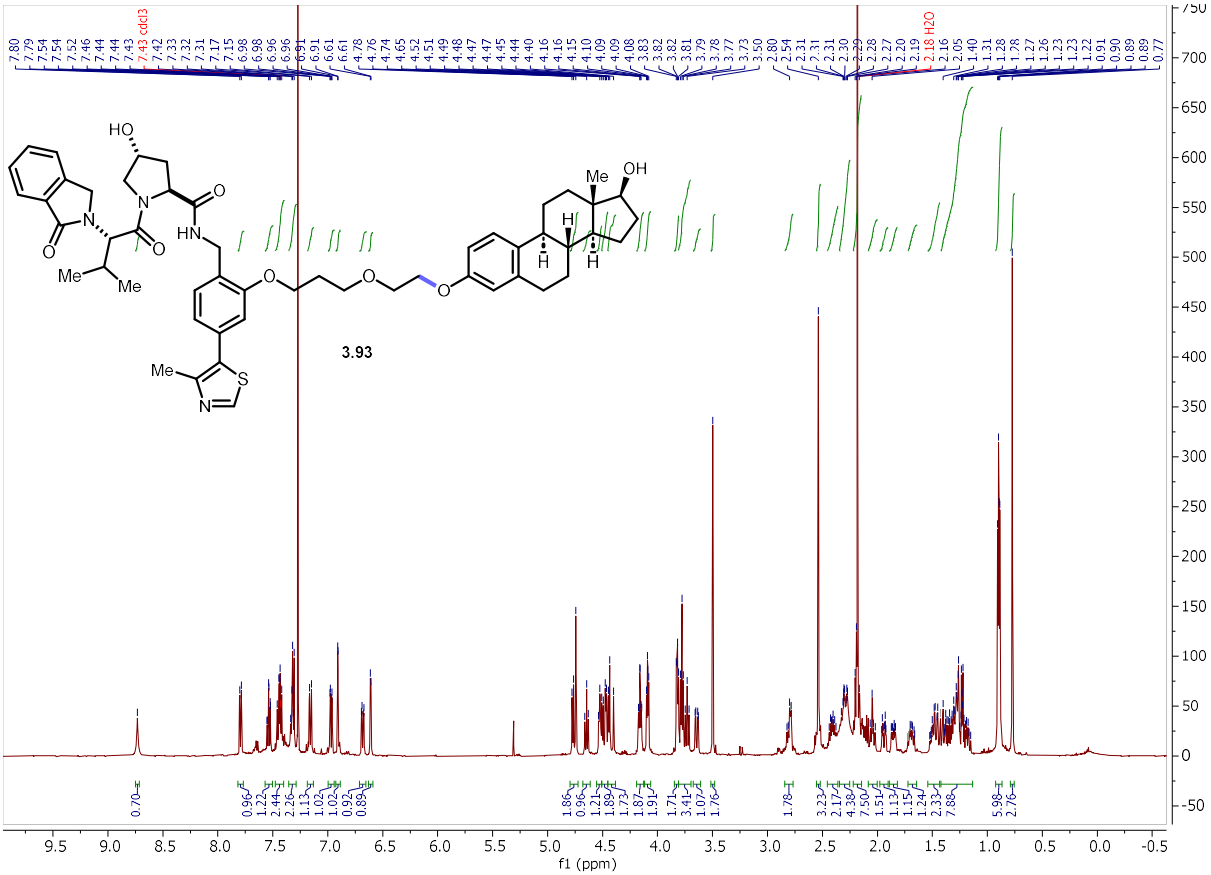

Spectrum 3.125 ^{1}H NMR of **3.93**.

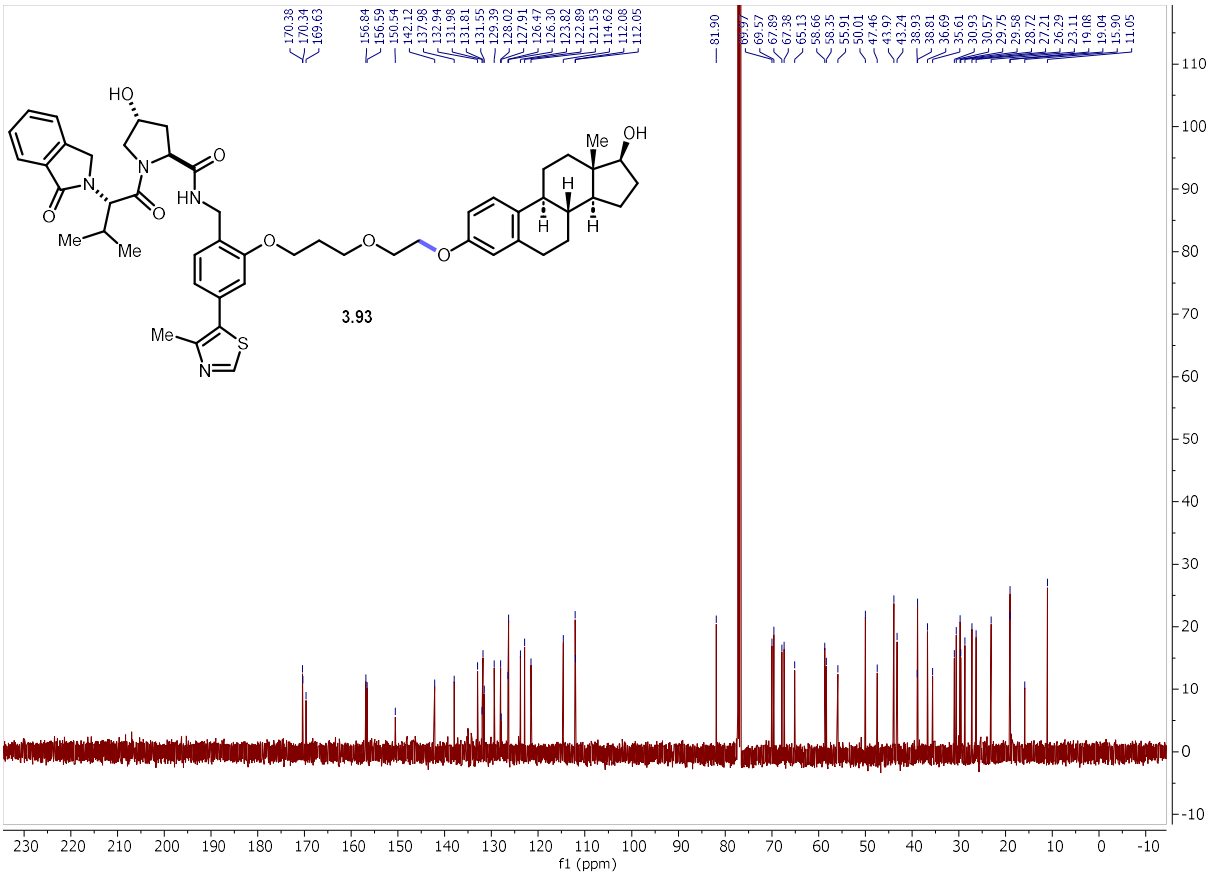

Spectrum 3.126 ^{13}C NMR of **3.93**.

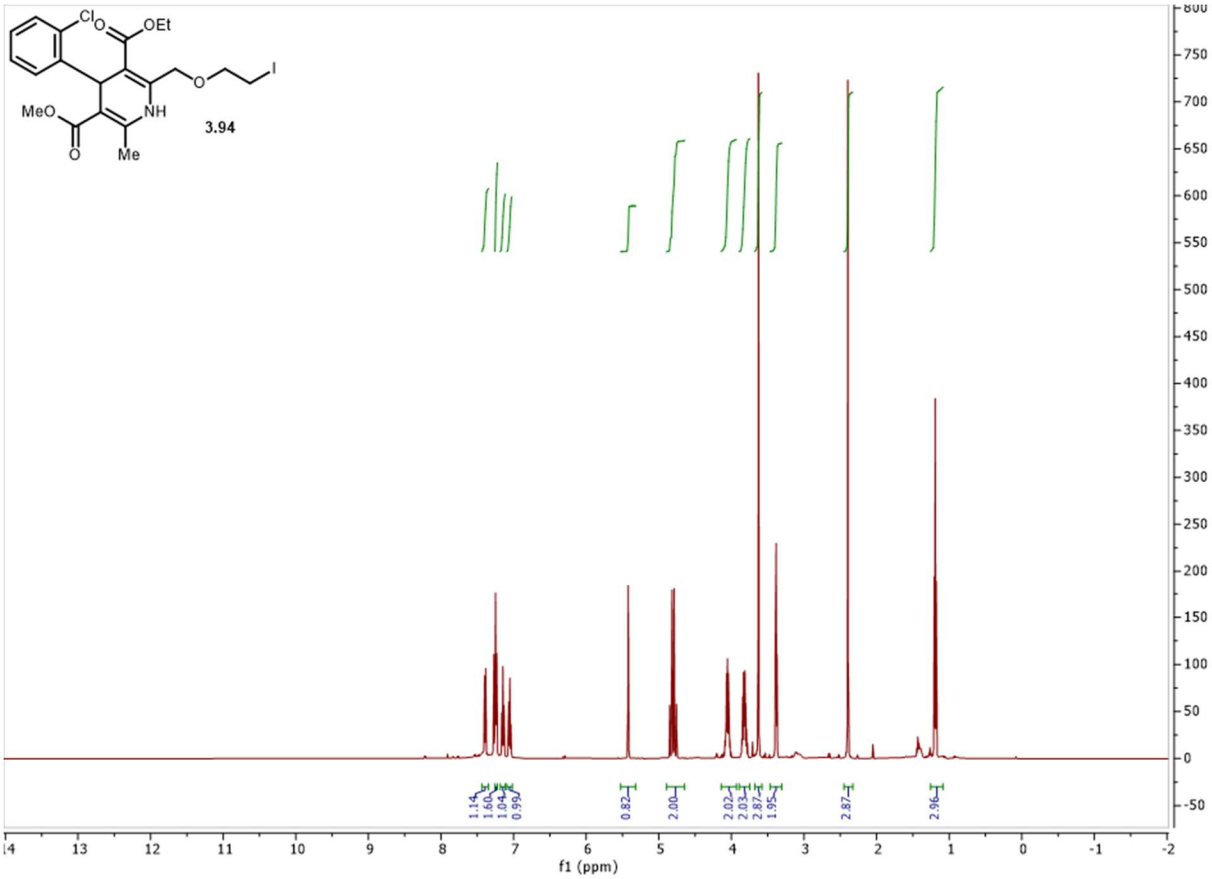

Spectrum 3.127 ^{1}H NMR of **3.94**

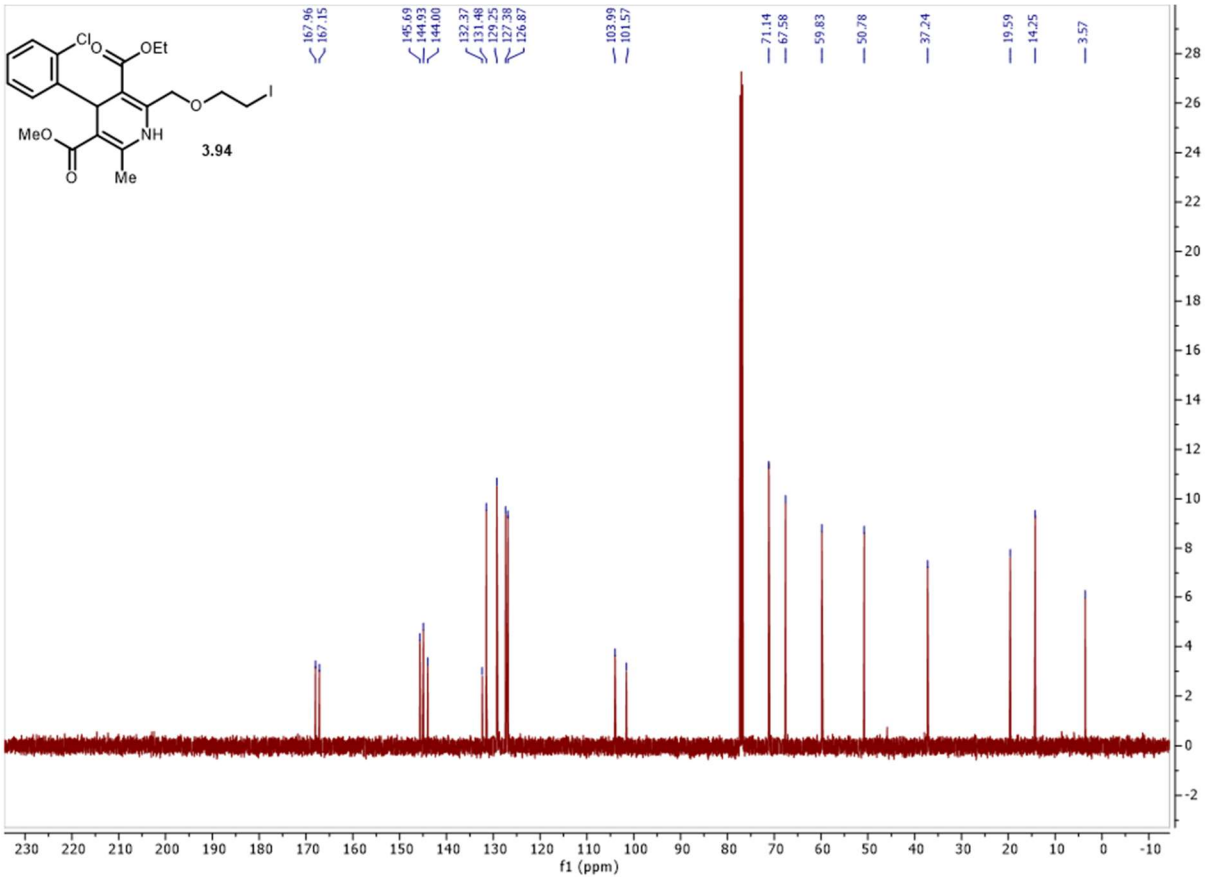

Spectrum 3.128 ^{13}C NMR of **3.94**.

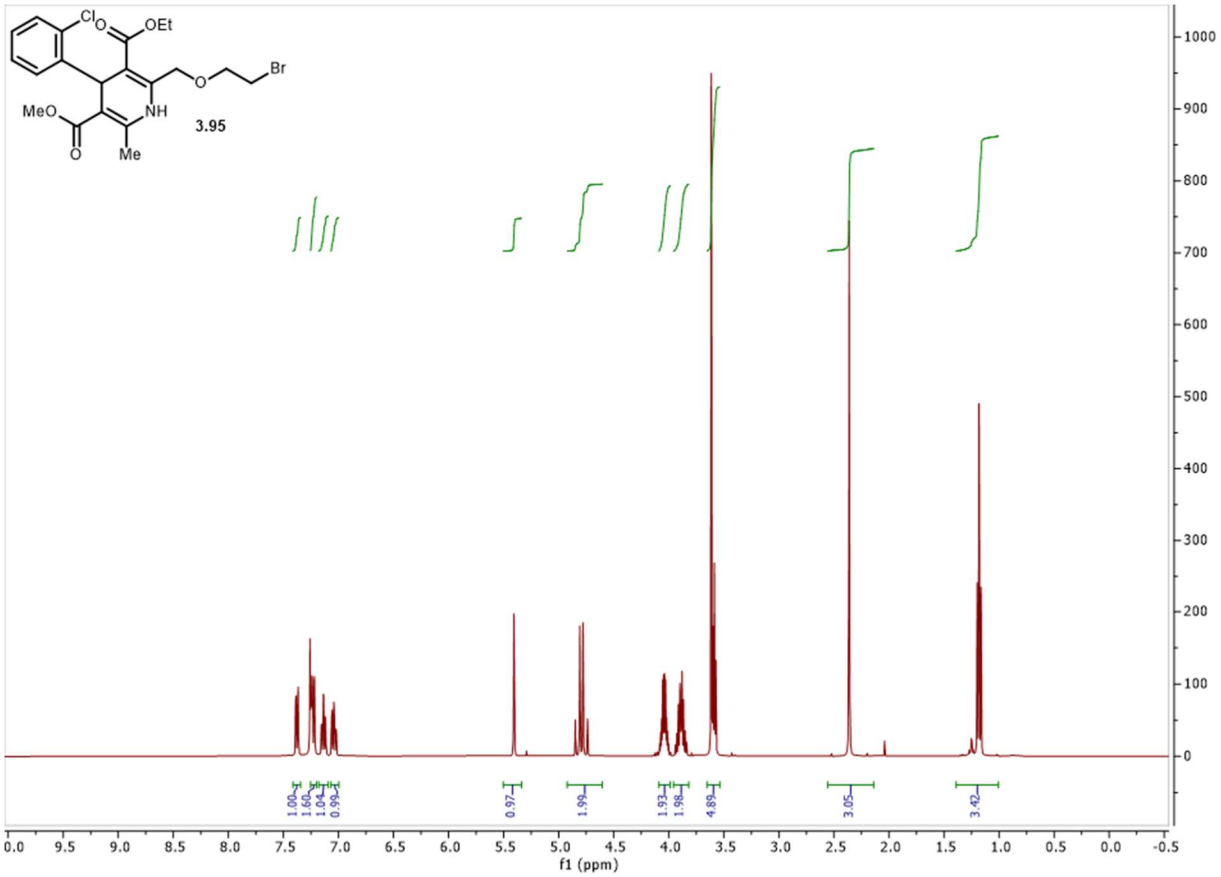

Spectrum 3.129 ^{1}H NMR of **3.95.**

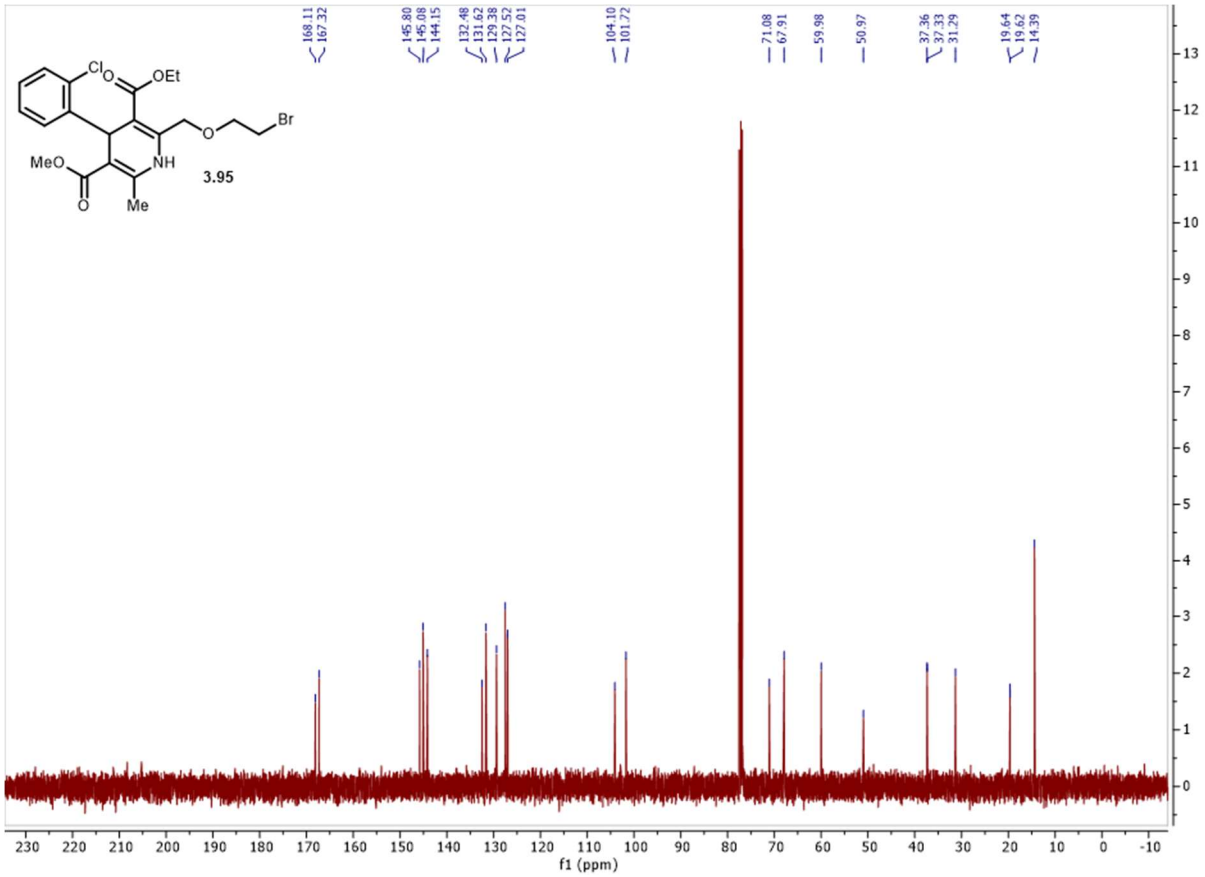

Spectrum 3.130 ^{13}C NMR of **3.95**.

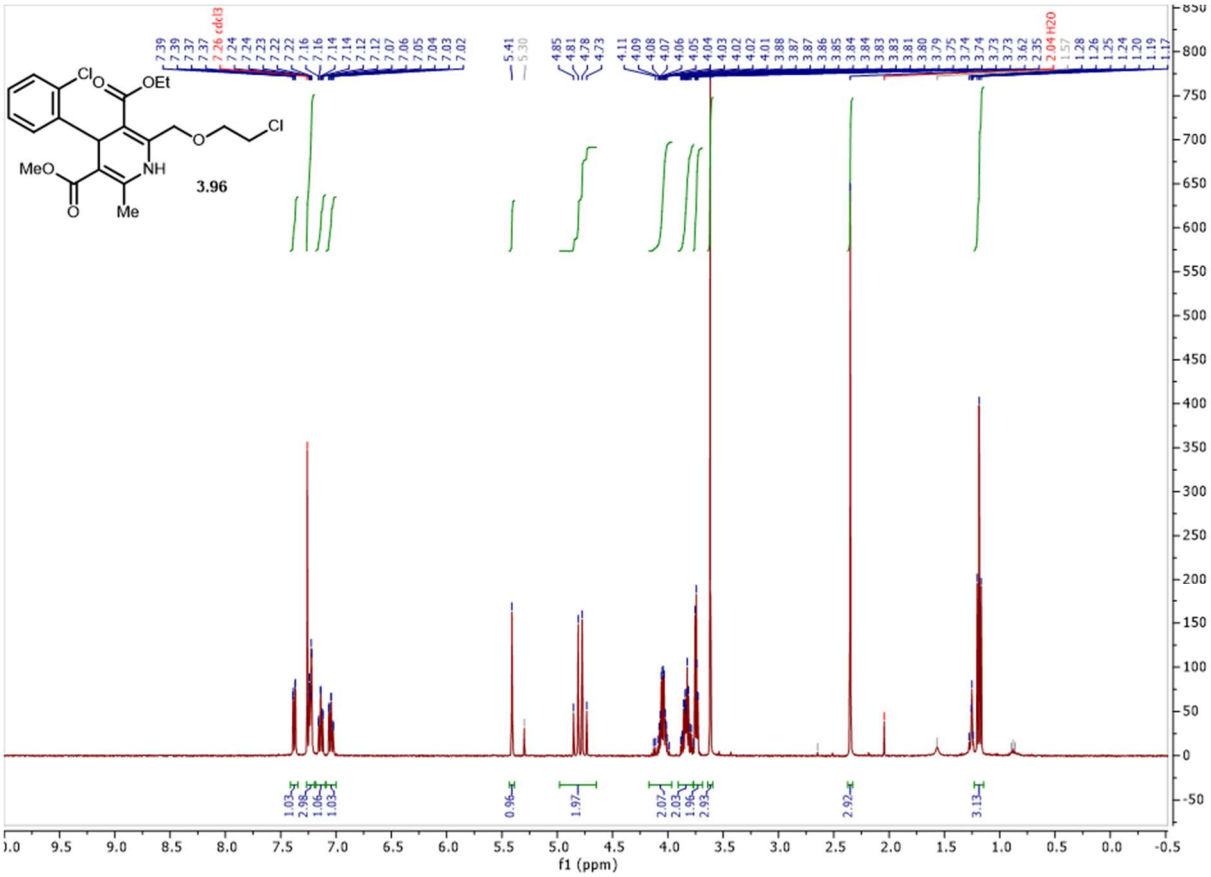

Spectrum 3.131 ^{1}H NMR of **3.96**.

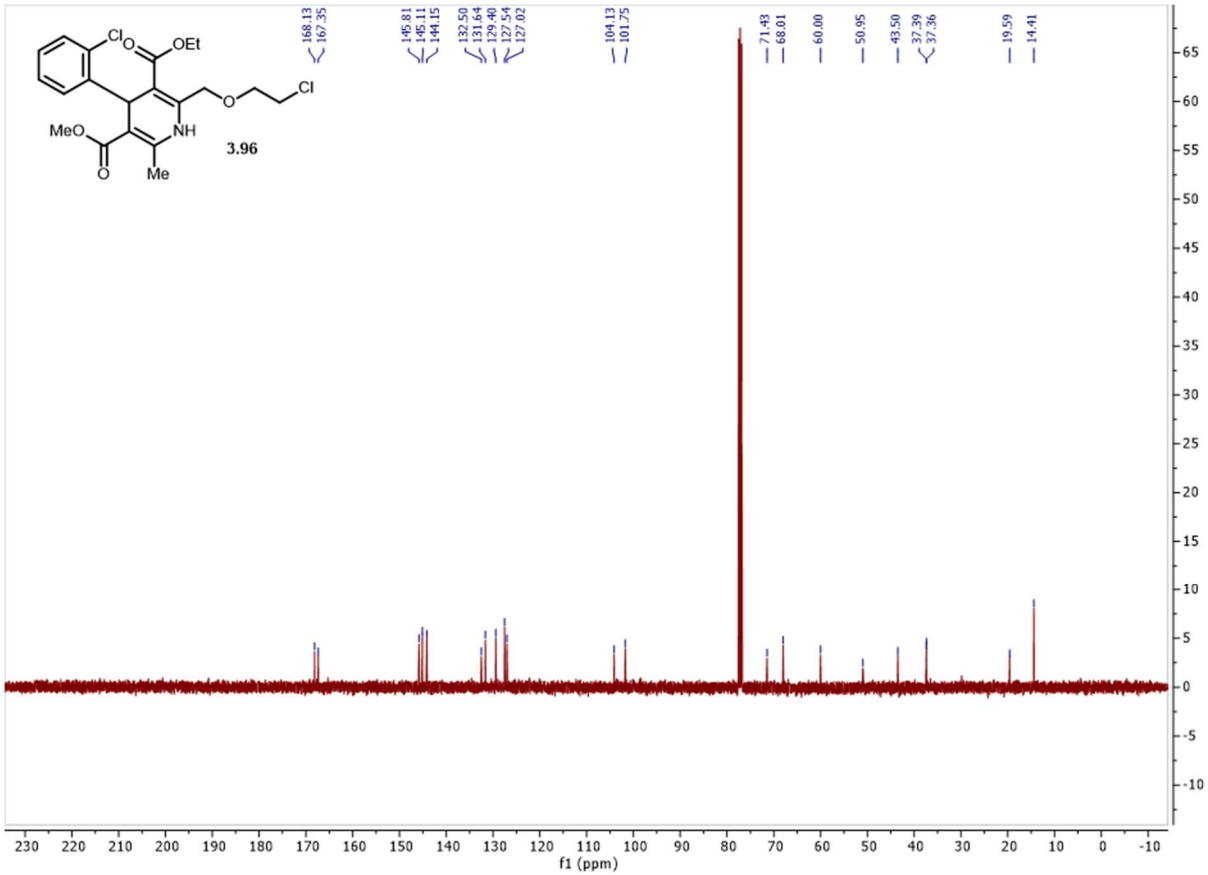

Spectrum 3.132 ^{13}C NMR of **3.96**.

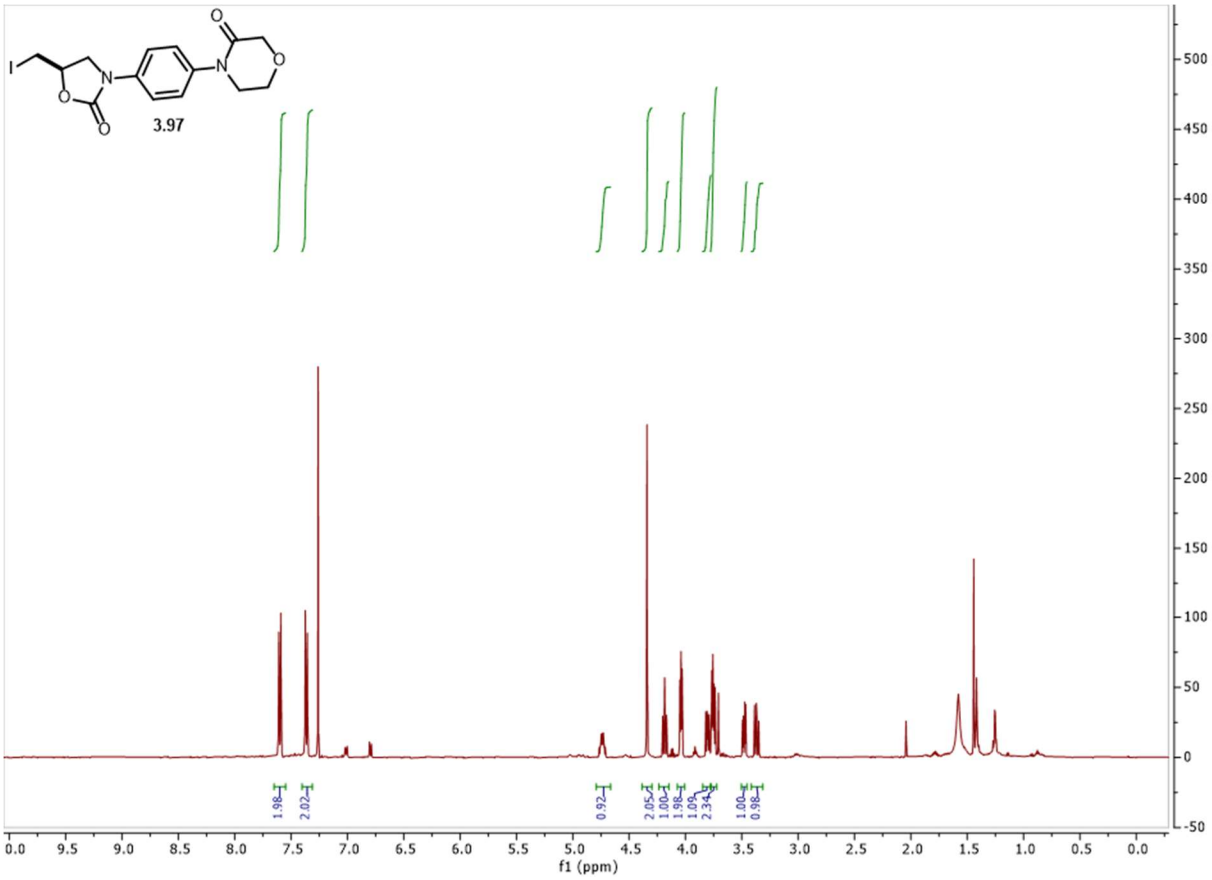

Spectrum 3.133 ^{1}H NMR of **3.97**.

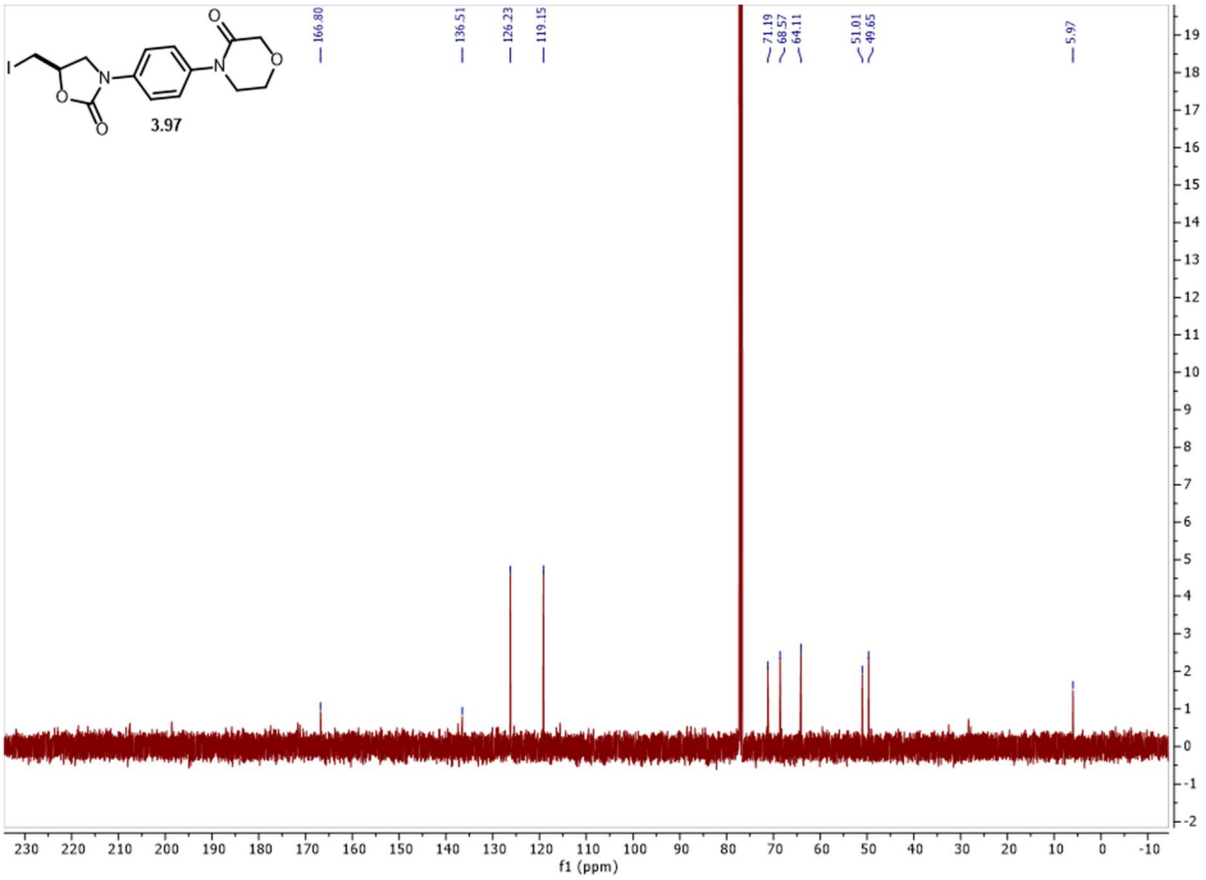

Spectrum 3.134 ^{13}C NMR of **3.97**.

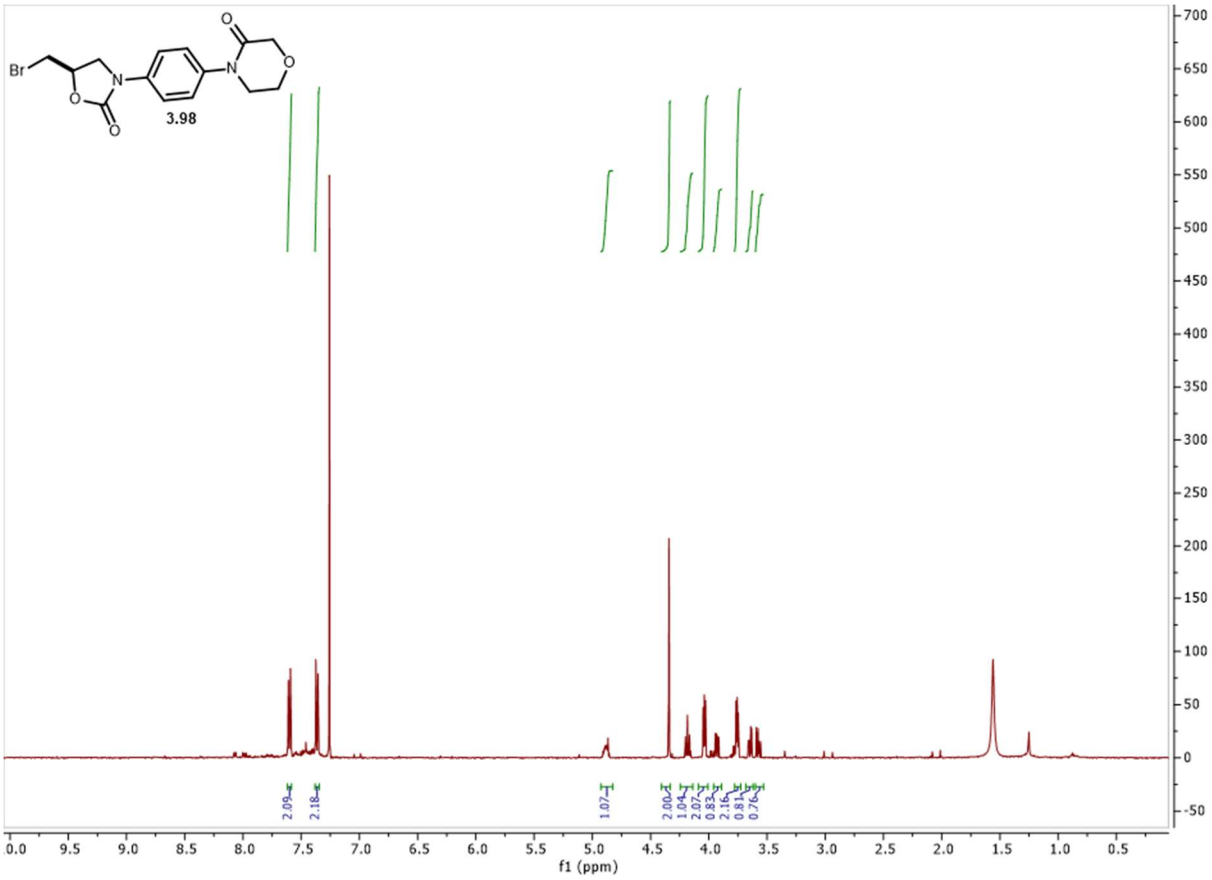

Spectrum 3.135 ^{1}H NMR of **3.98**.

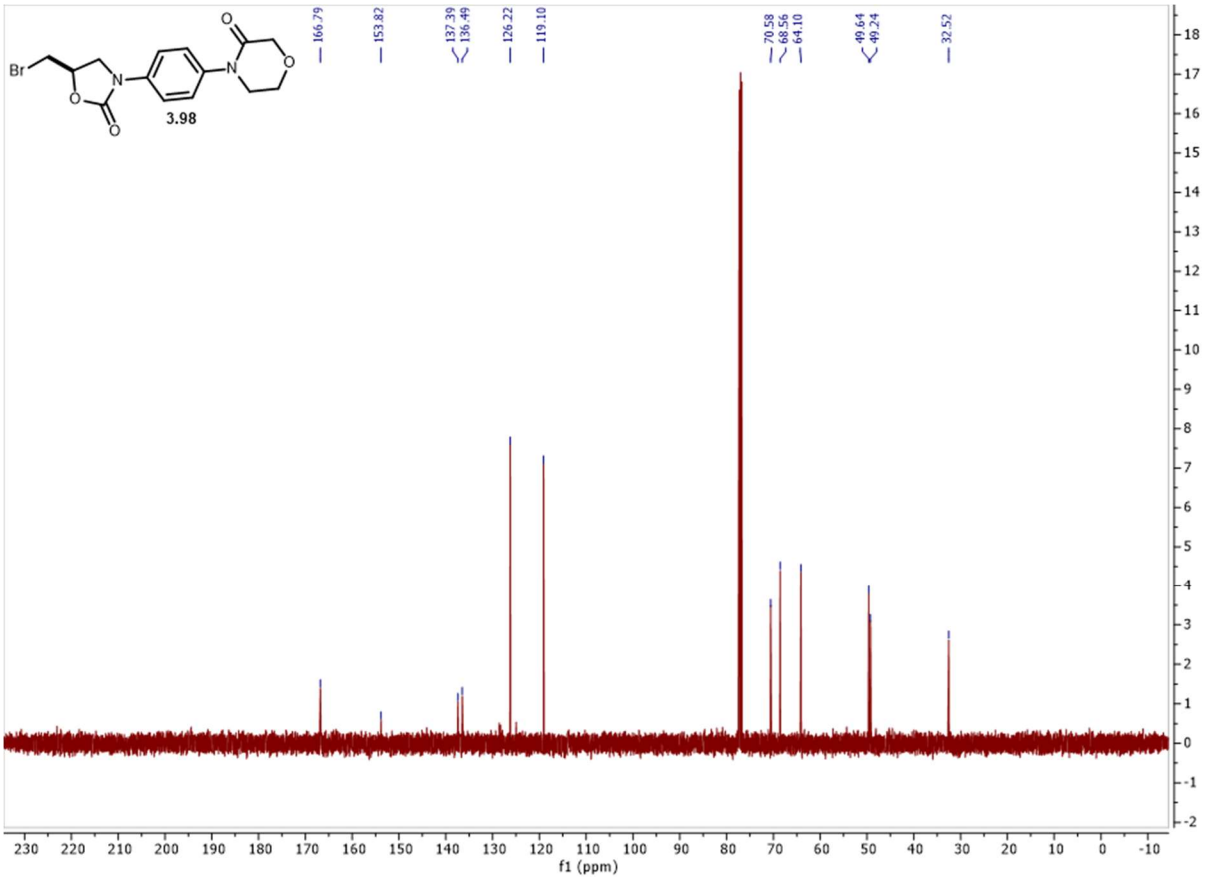

Spectrum 3.136 ^{13}C NMR of **3.98**.

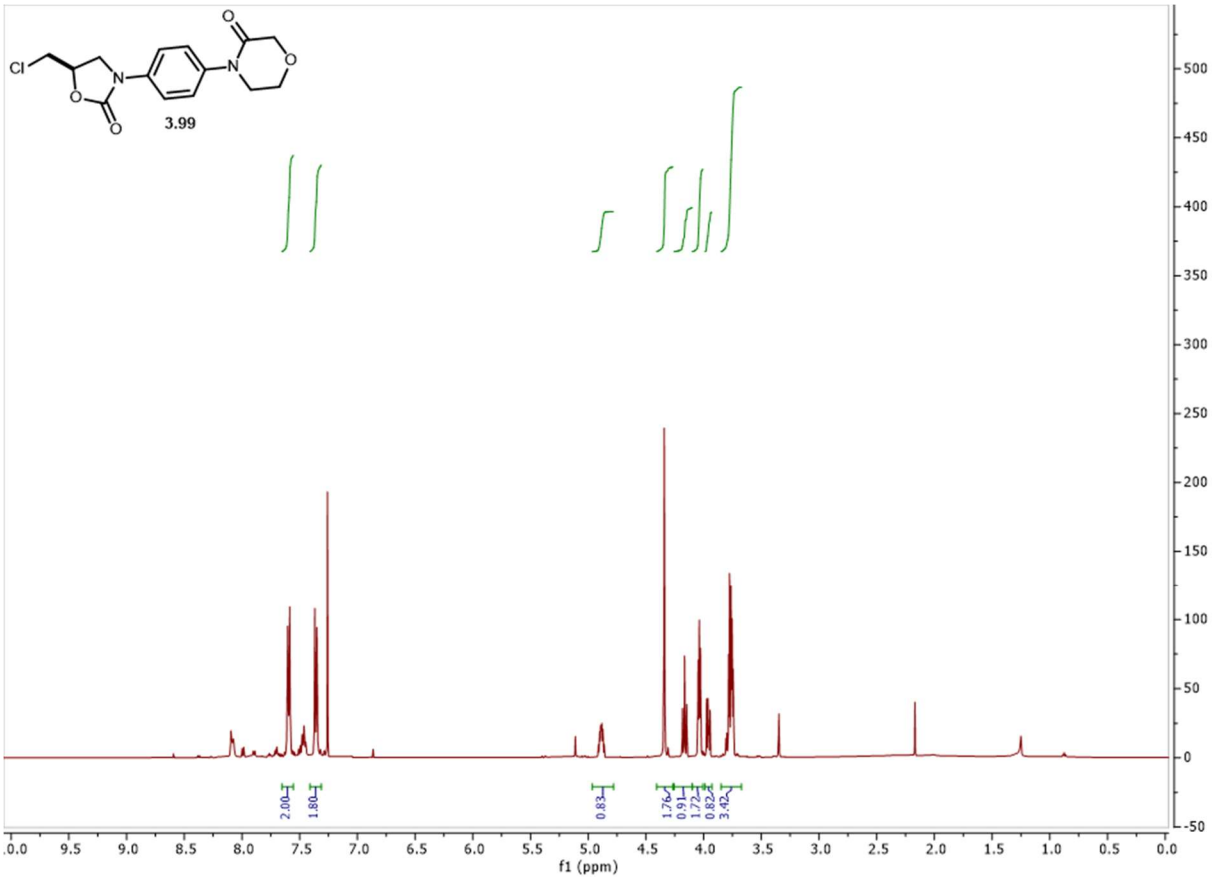

Spectrum 3.137 ^{1}H NMR of **3.99**.

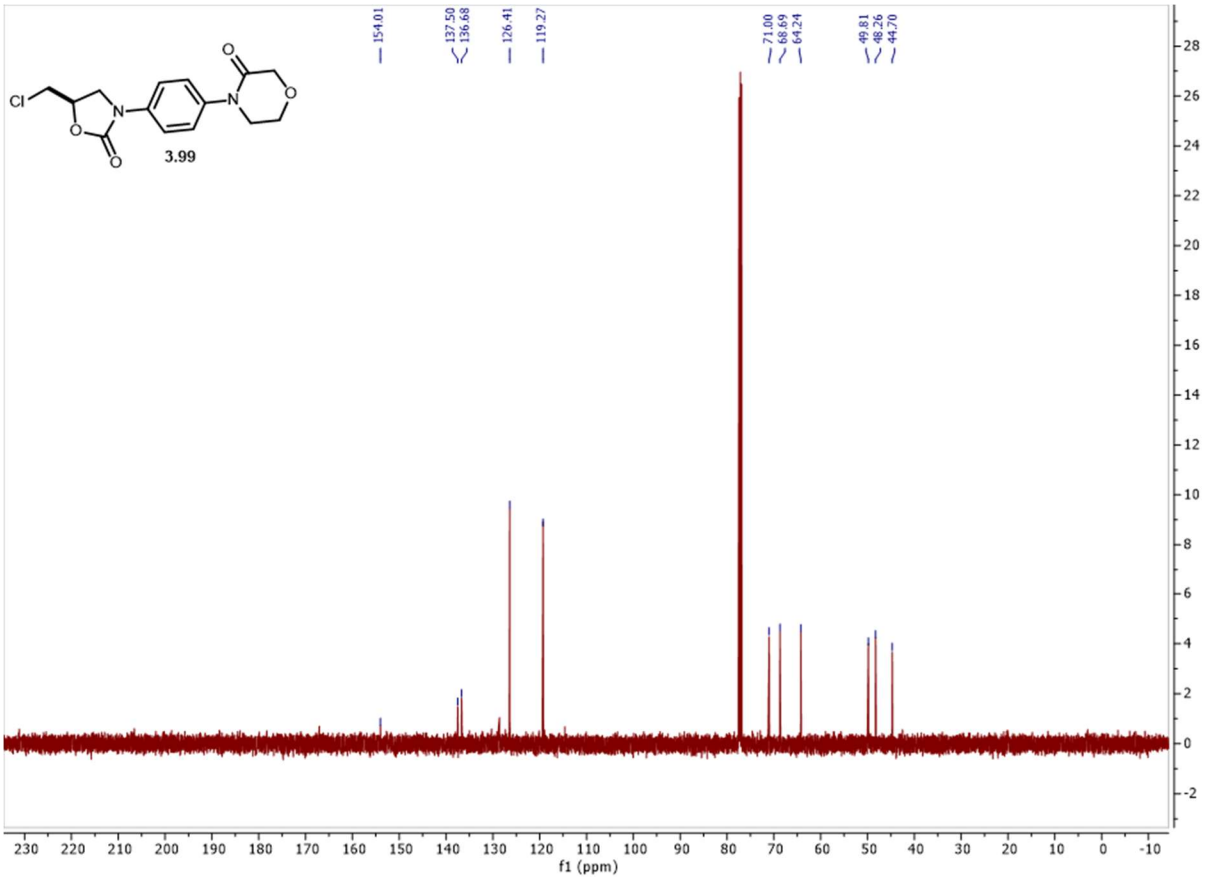

Spectrum 3.138 ^{13}C NMR of **3.99**.

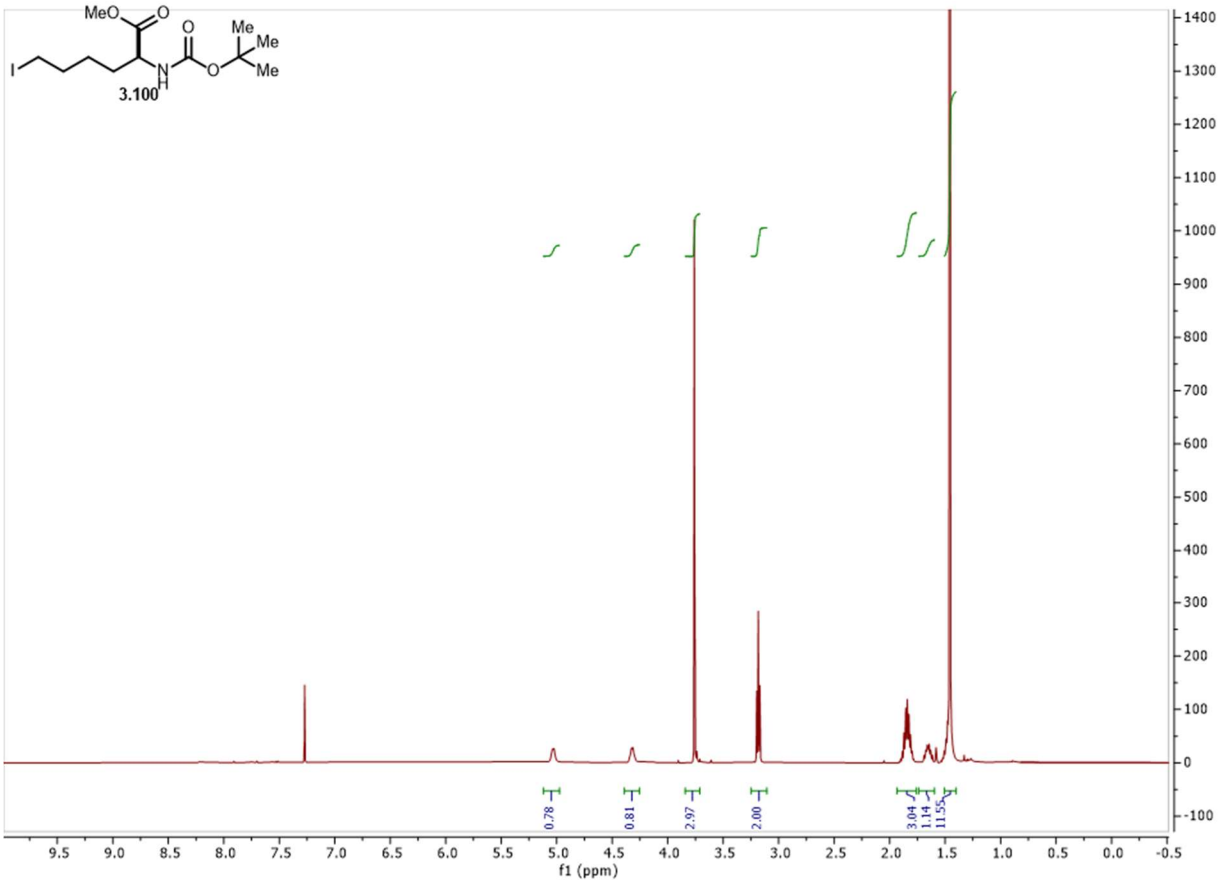

Spectrum 3.139 ^{1}H NMR of **3.100**.

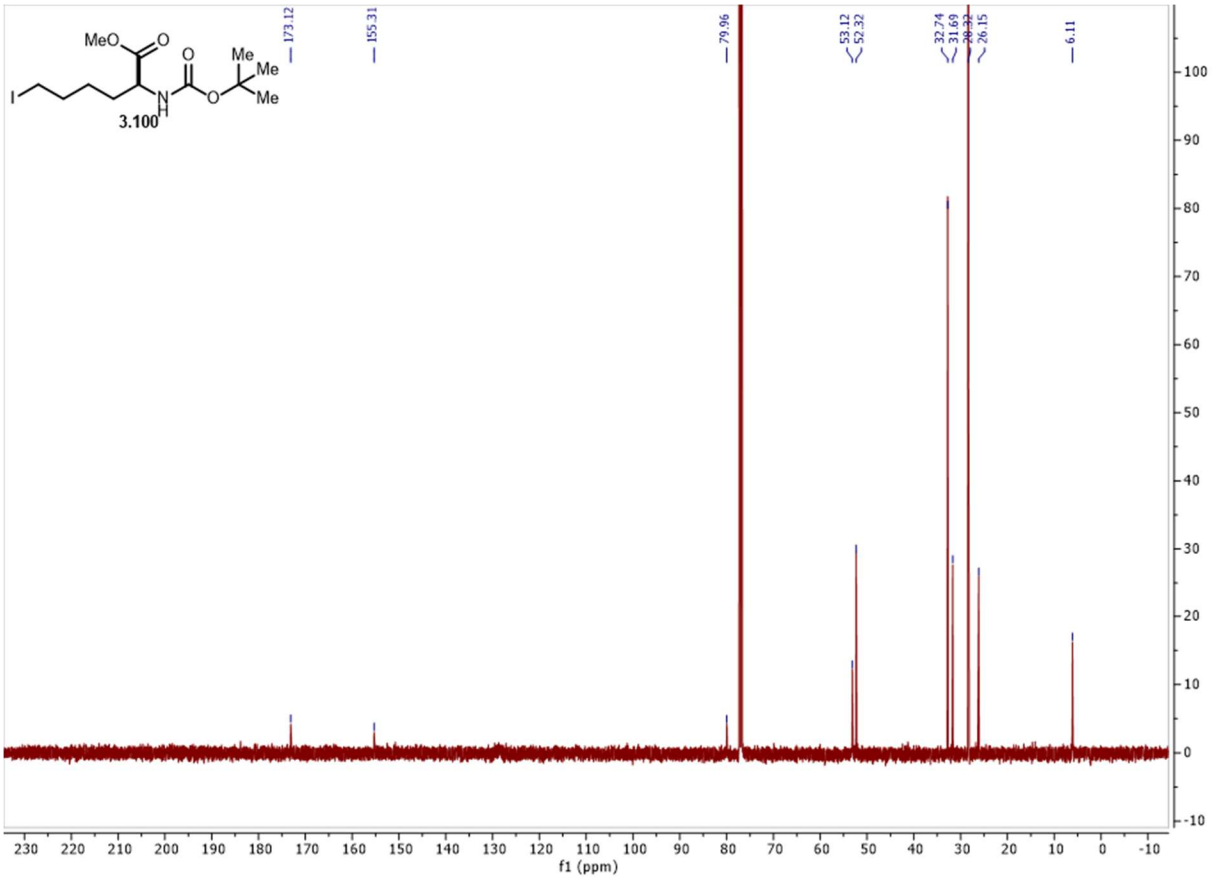

Spectrum 3.140 ^{13}C NMR of **3.100**.

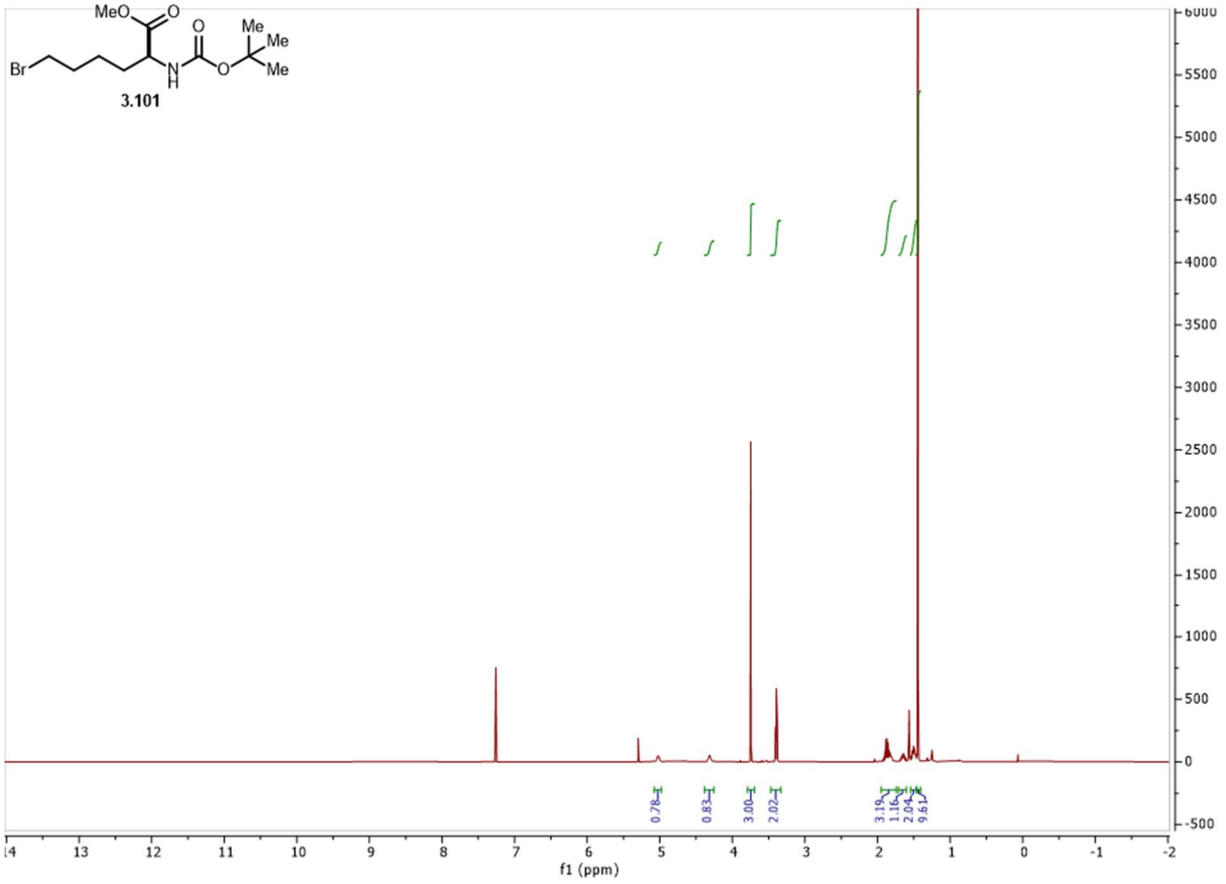

Spectrum 3.141 ^{1}H NMR of **3.101**.

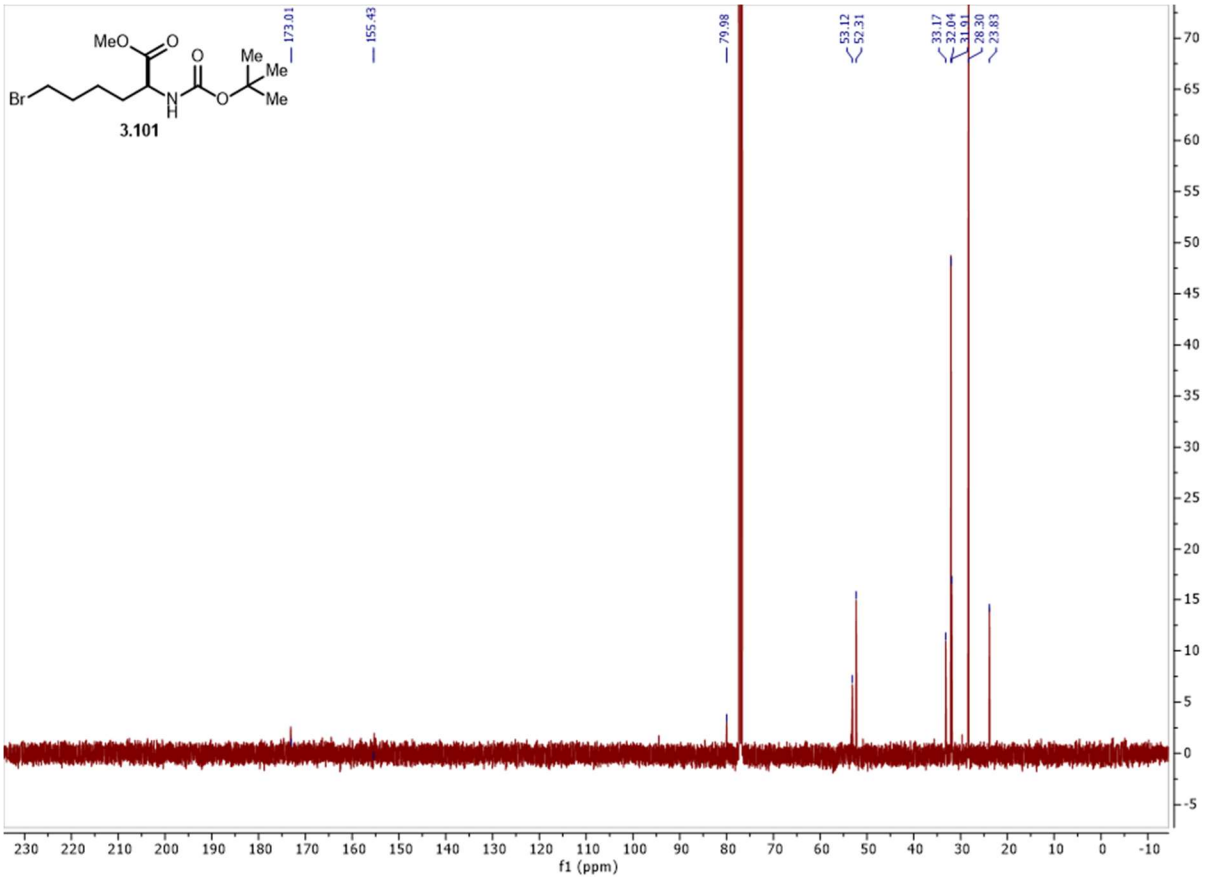

Spectrum 3.142 ^{13}C NMR of **3.101**.

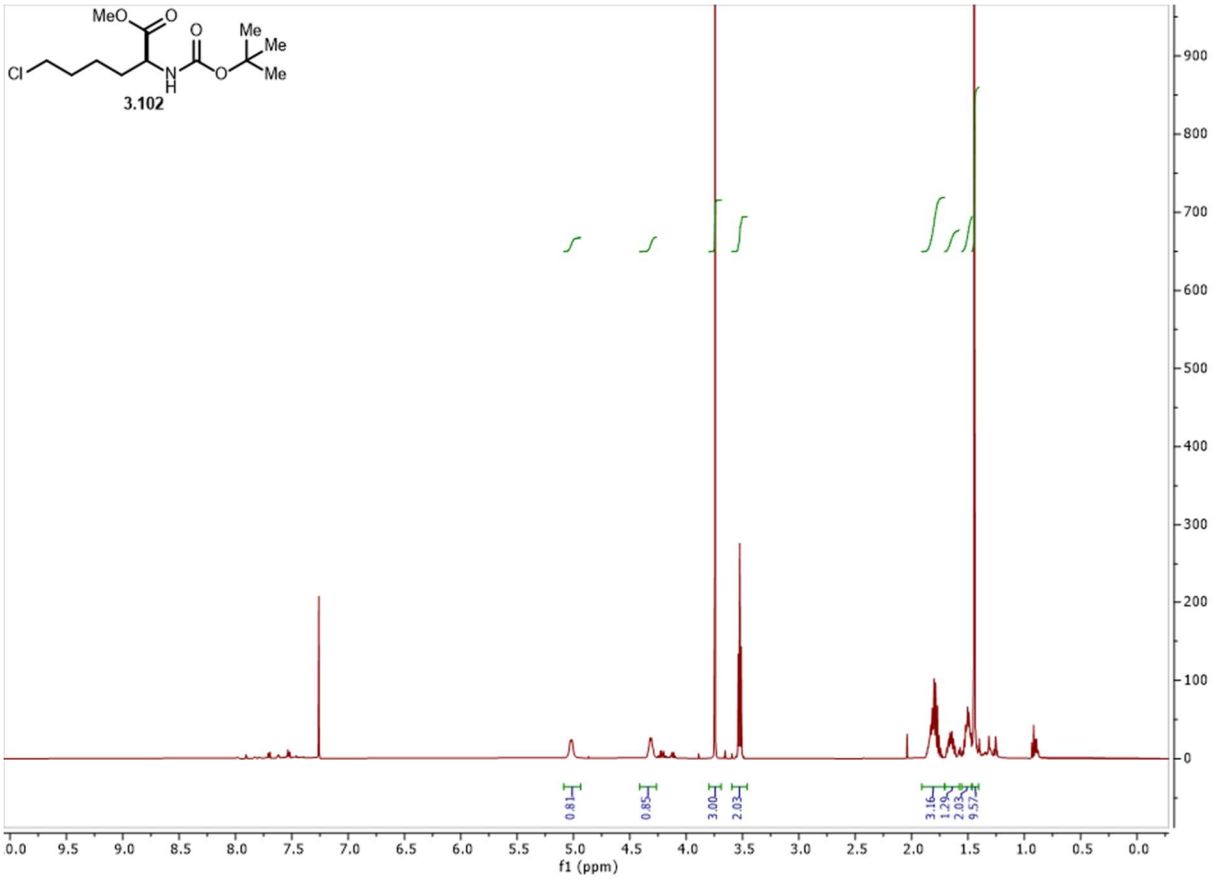

Spectrum 3.143 ^{1}H NMR of **3.102**.

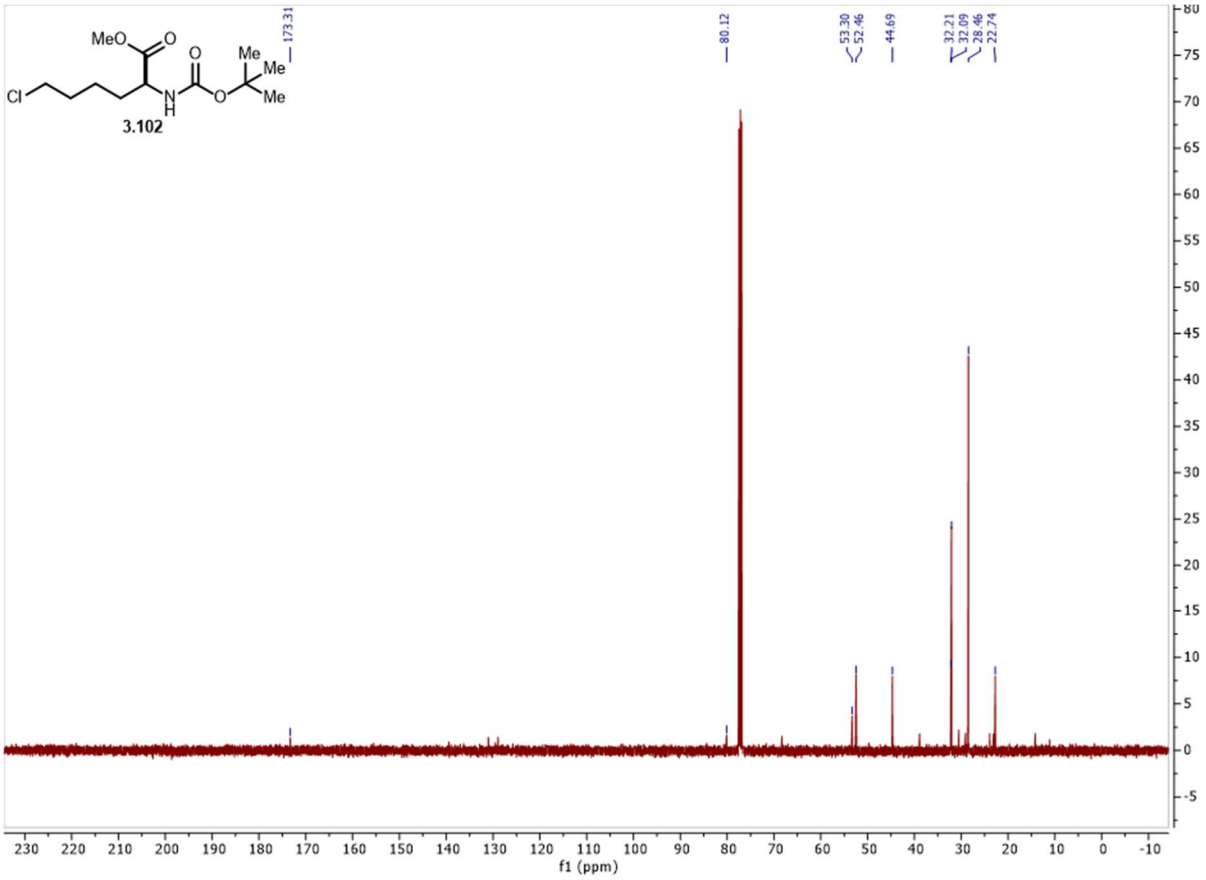

Spectrum 3.144 ^{13}C NMR of **3.102**.

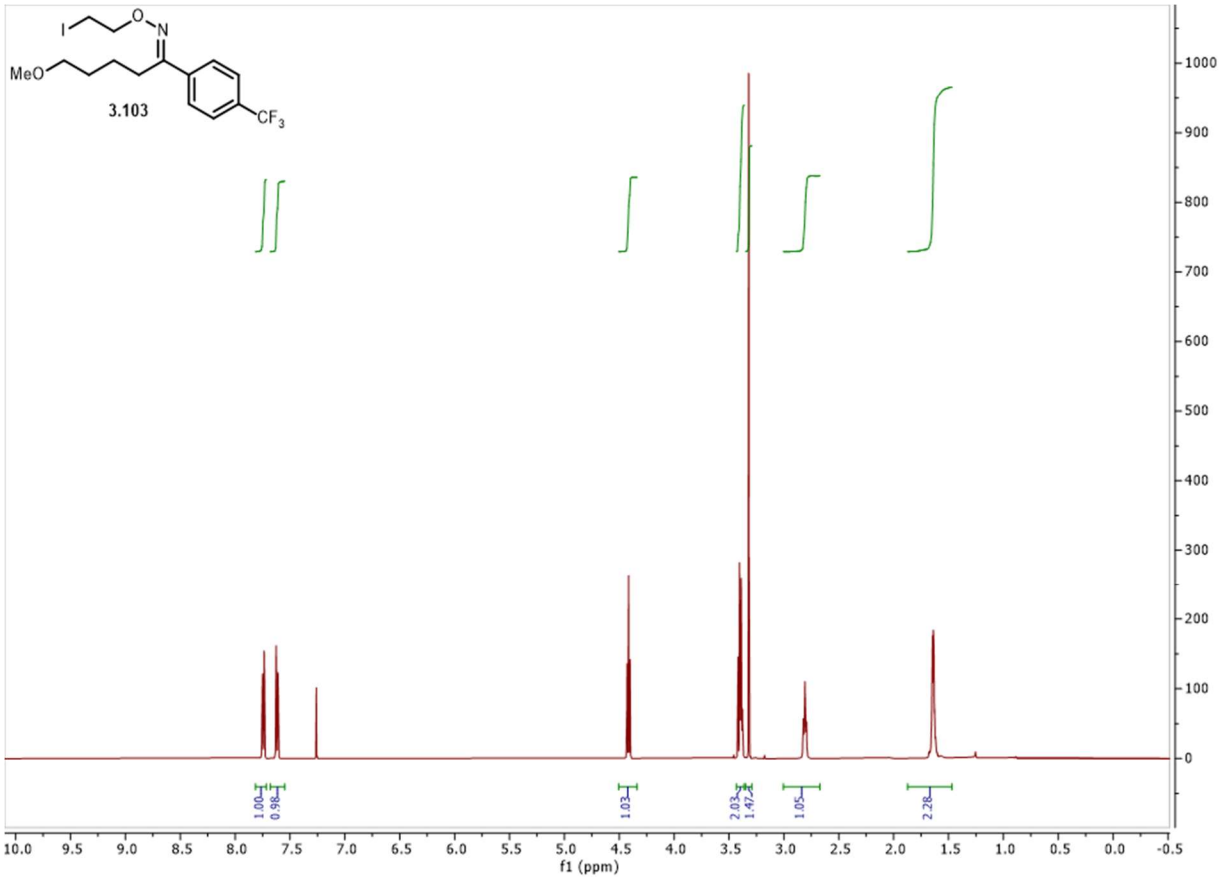

Spectrum 3.145 ^{1}H NMR of **1.103**.

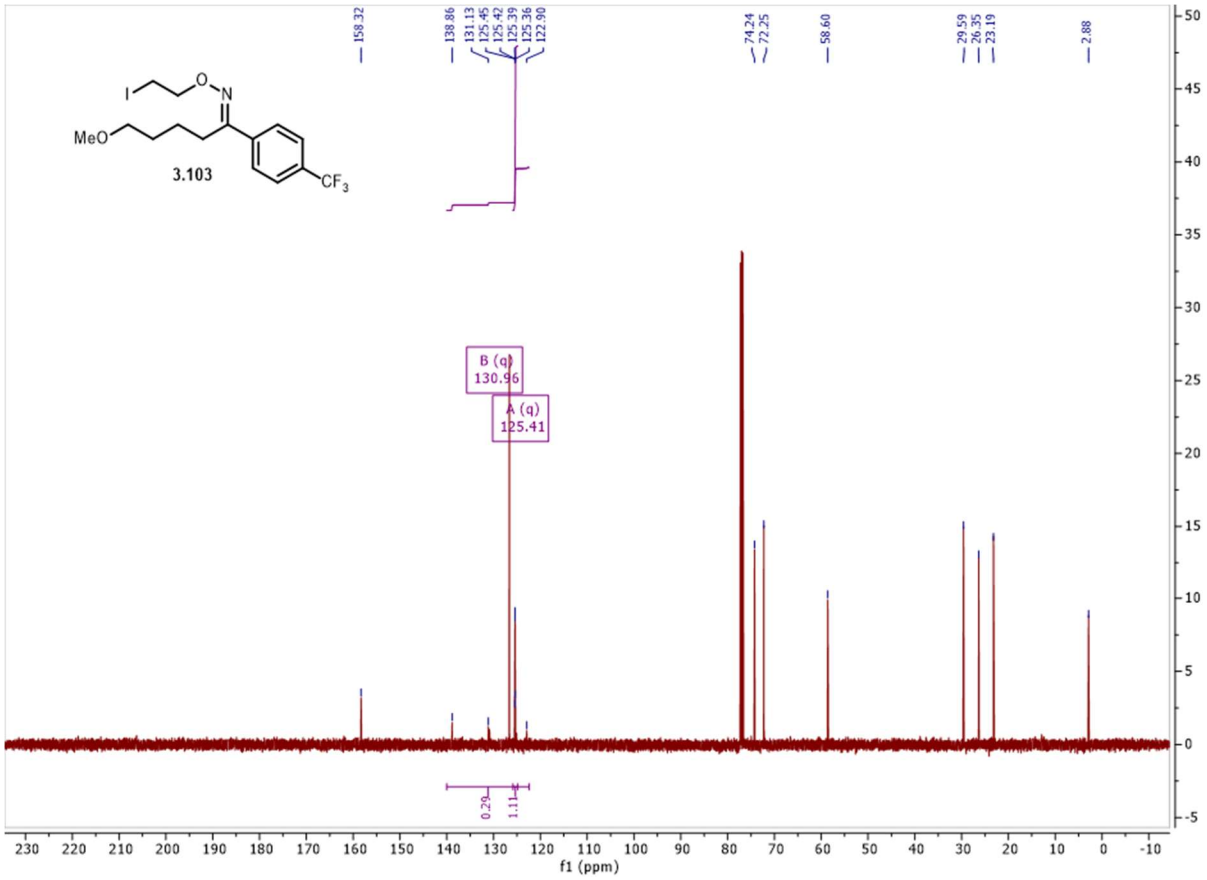

Spectrum 3.146 ^{13}C NMR of **1.103**.

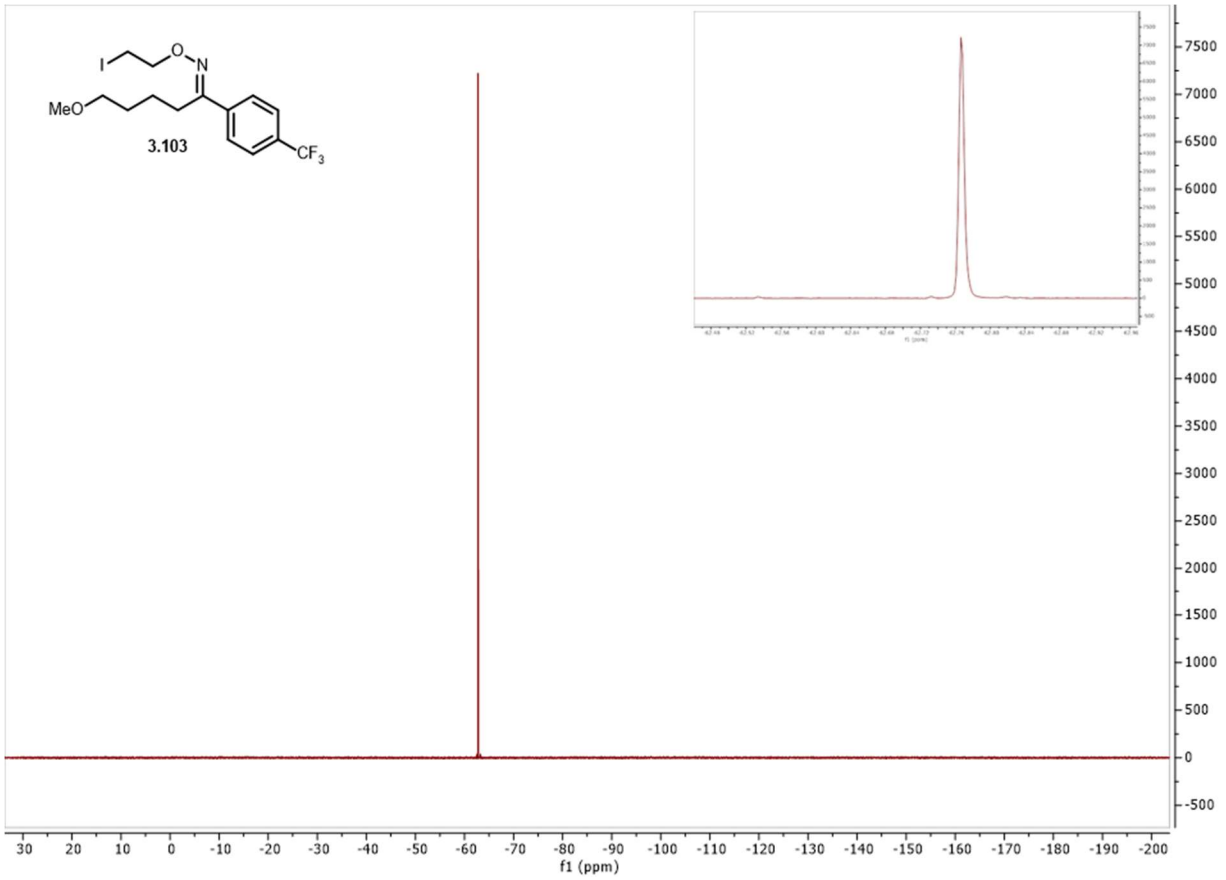

Spectrum 3.147 ^{19}F NMR of **3.103**.

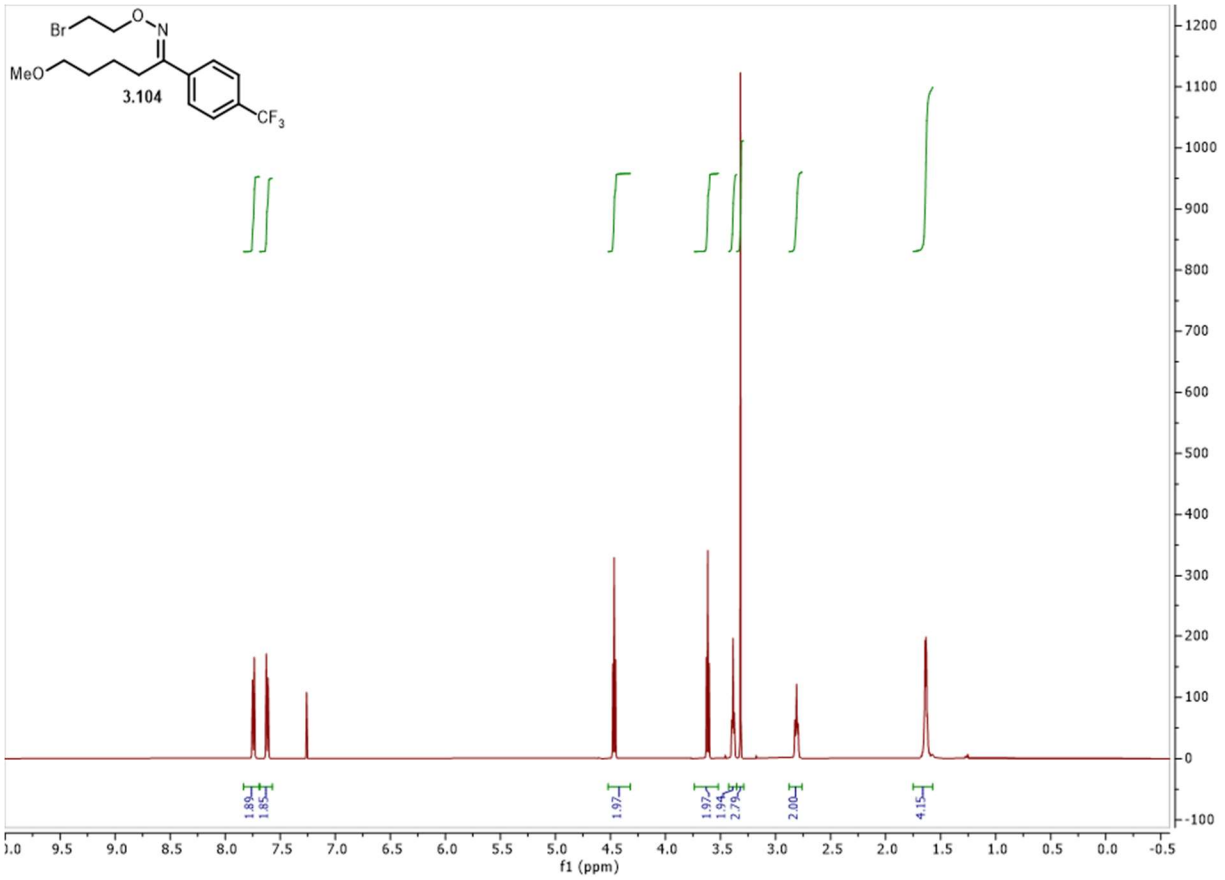

Spectrum 3.148 ^{1}H NMR of **3.104**.

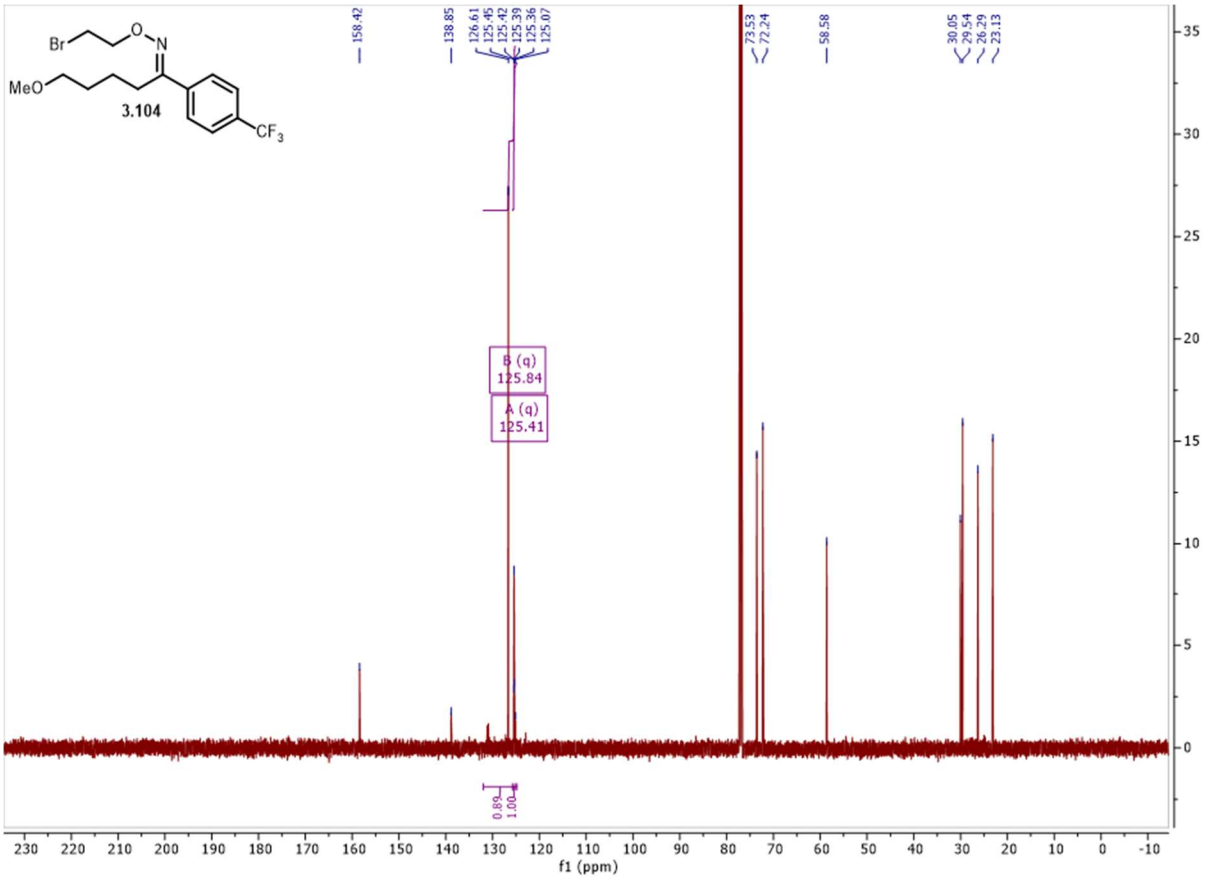

Spectrum 3.149 ^{13}C NMR of **3.104**.

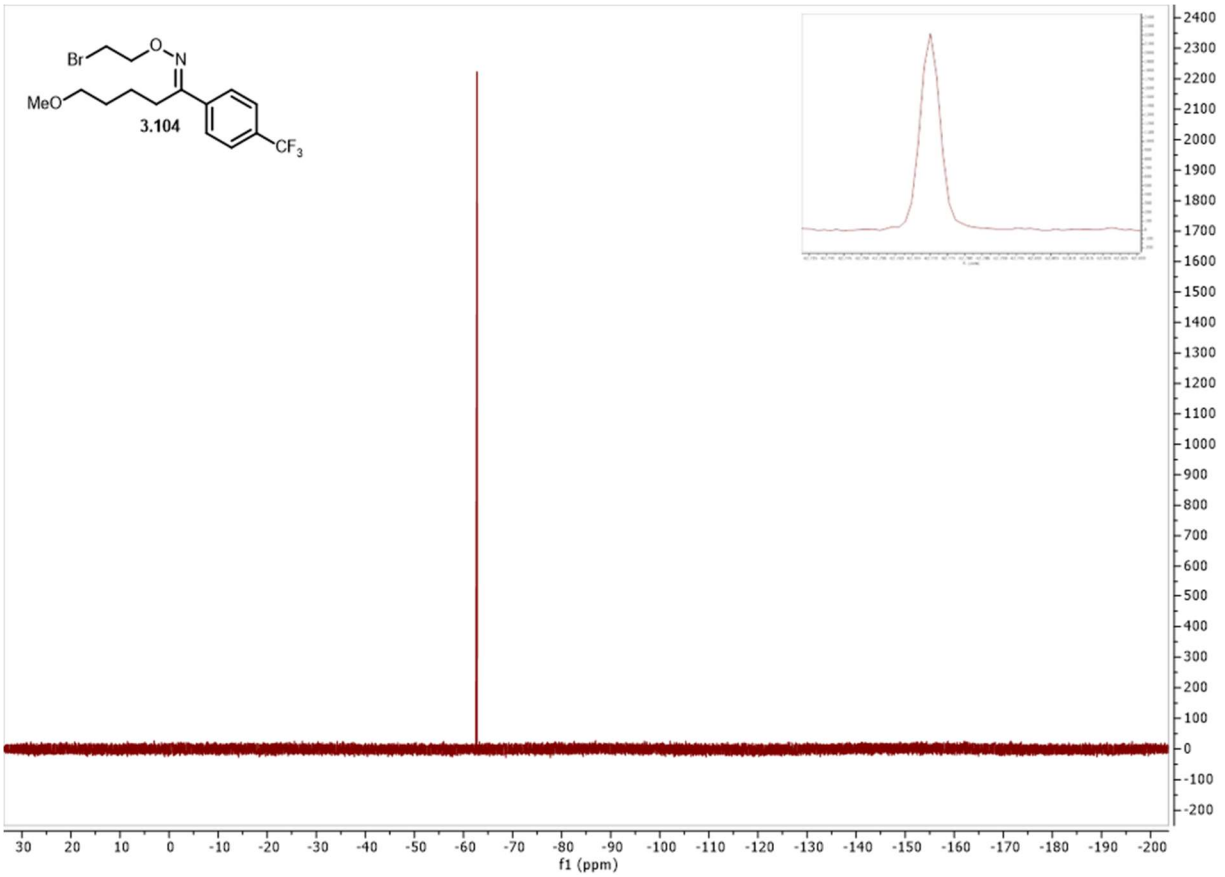

Spectrum 3.150 ^{19}F NMR of **3.104**.

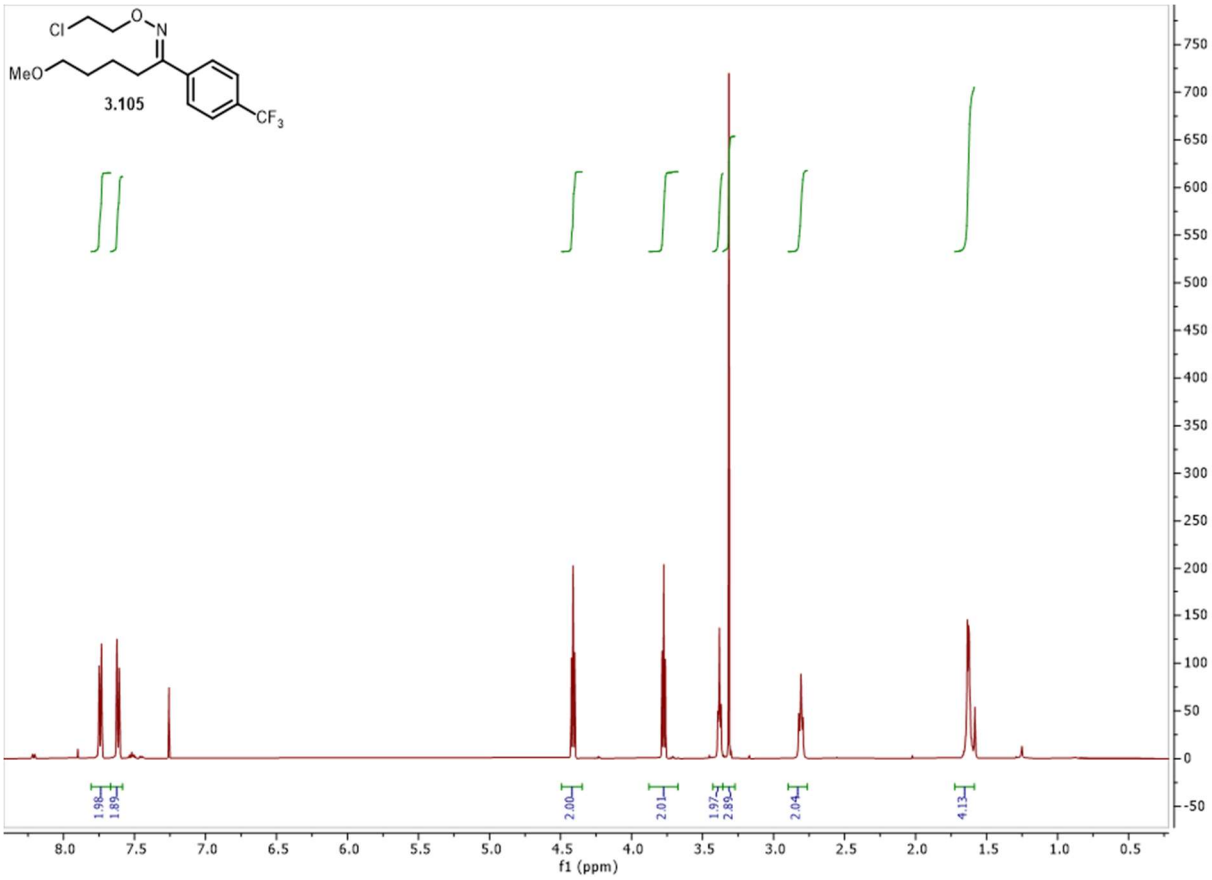

Spectrum 3.151 ^{1}H NMR of **3.105**.

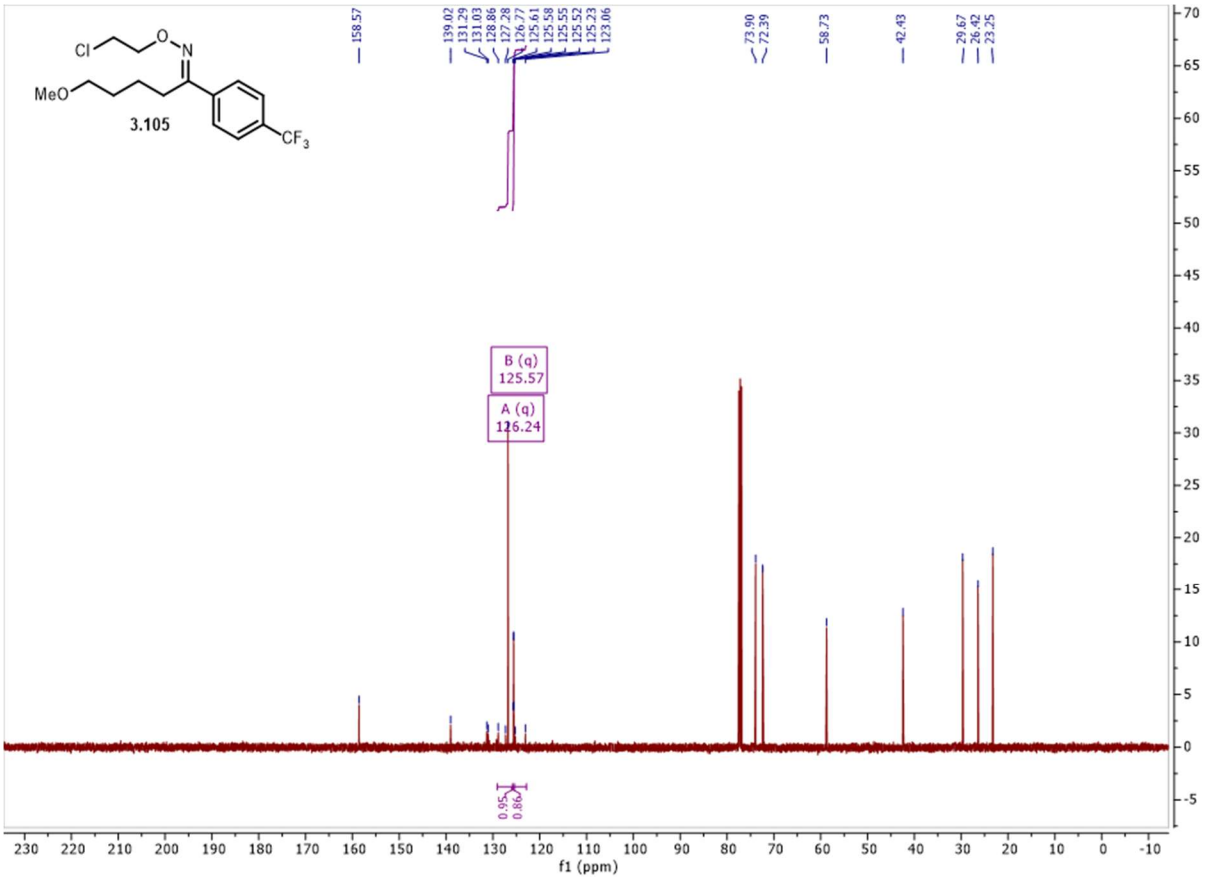

Spectrum 3.152 ^{13}C NMR of **3.105**.

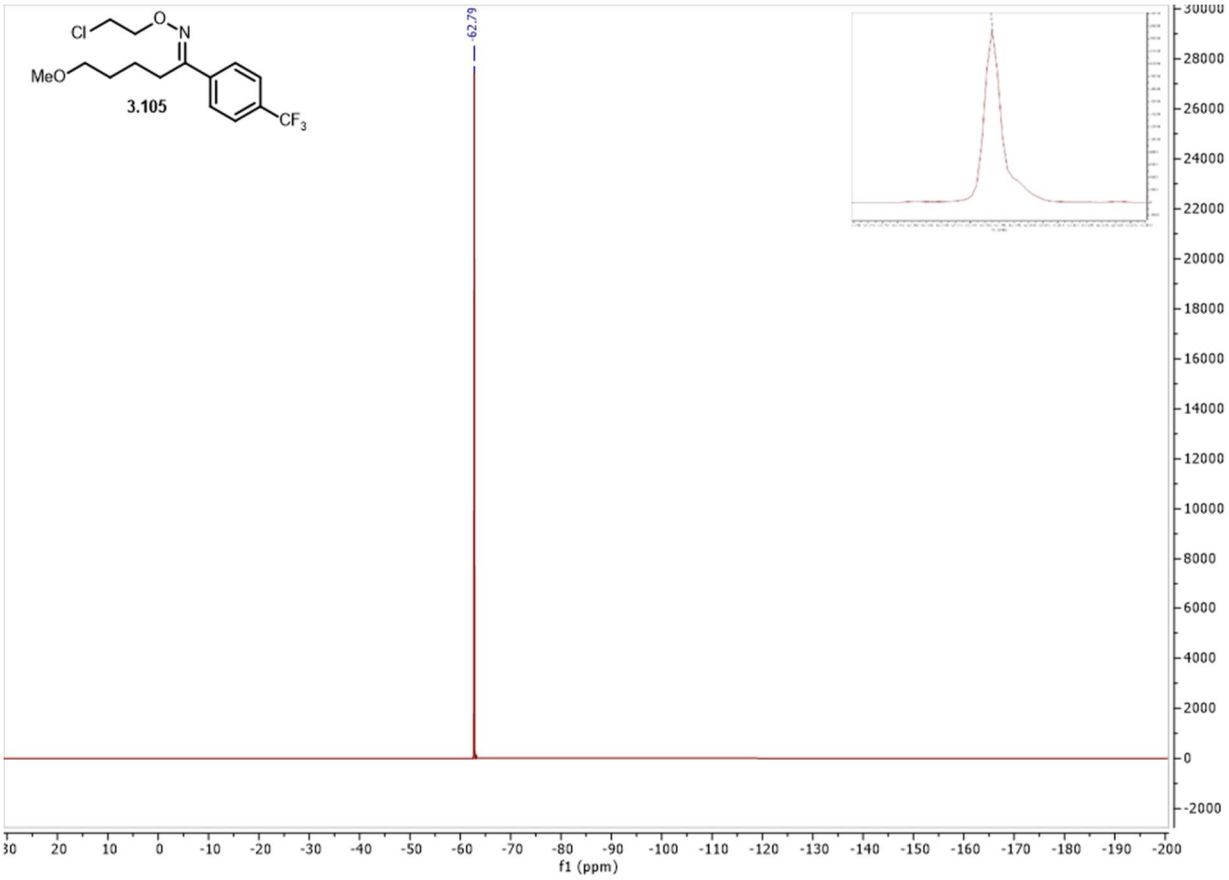

Spectrum 3.153 ^{19}F NMR of **3.105**.

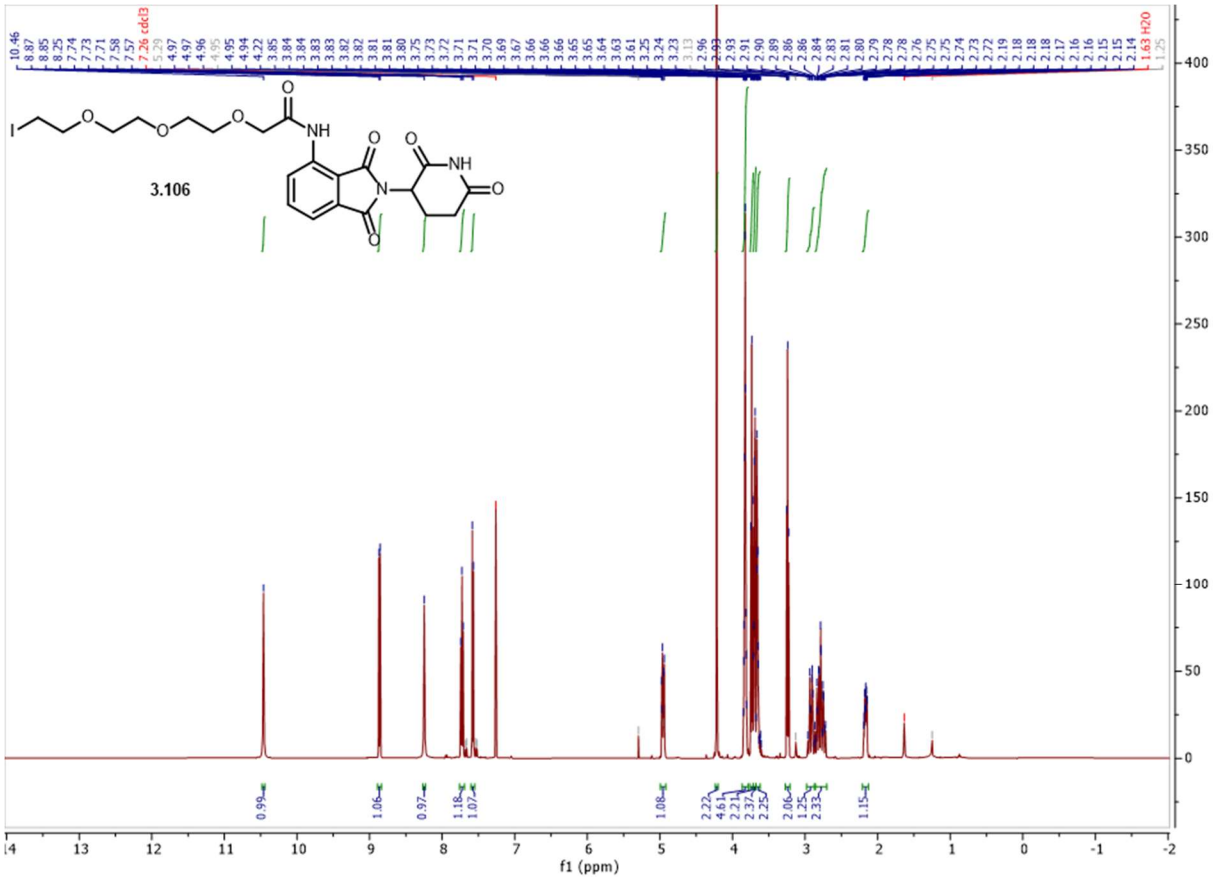

Spectrum 3.154 ^{1}H NMR of **3.106**.

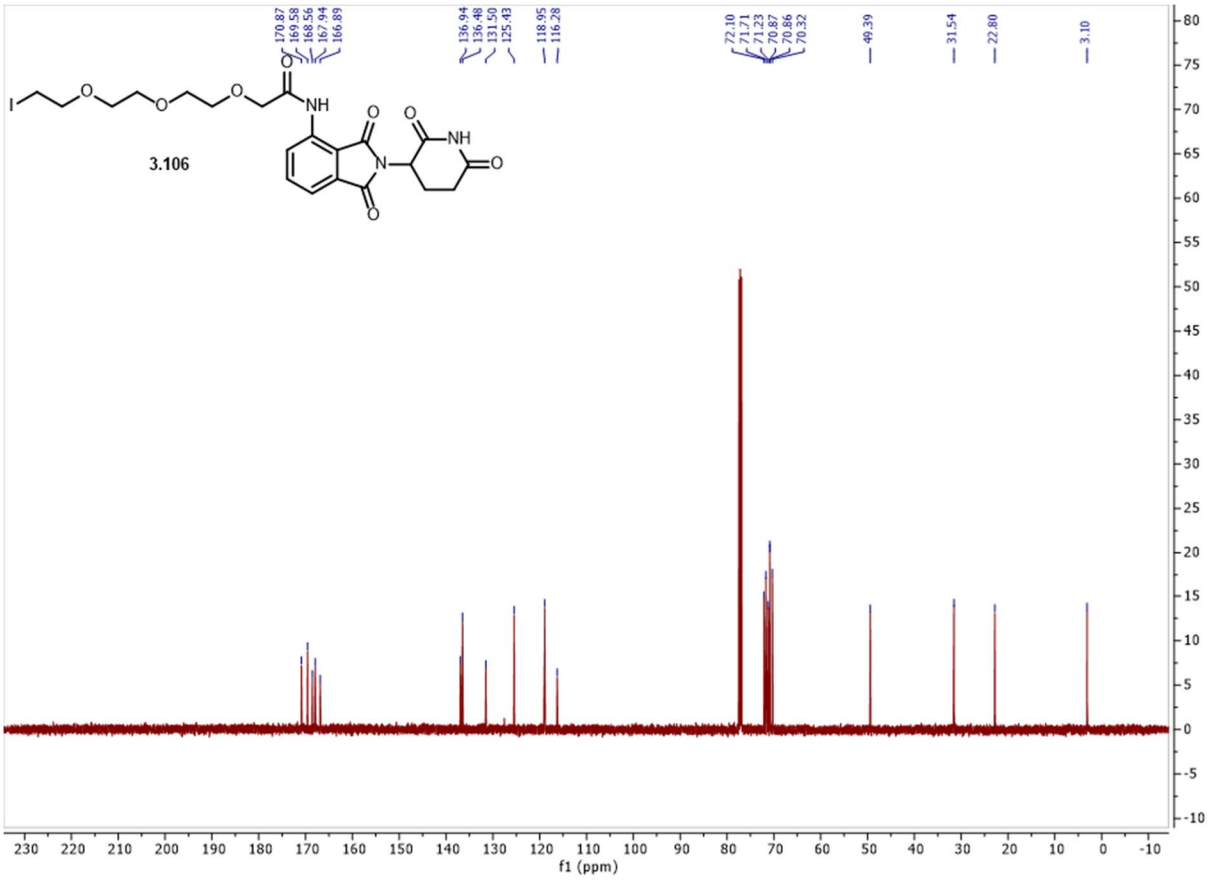

Spectrum 3.155 ^{13}C NMR of **3.106**.

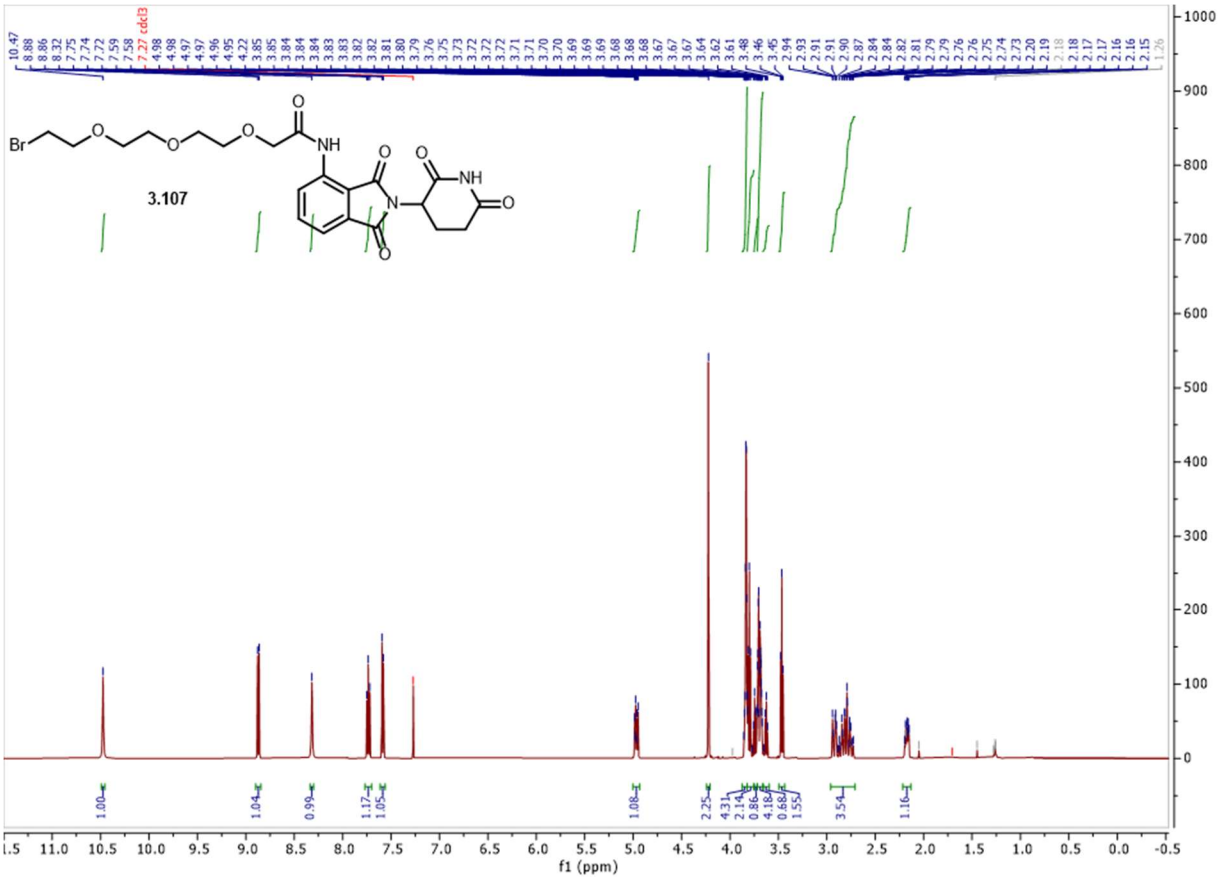

Spectrum 3.156 ^{1}H NMR of **3.107**.

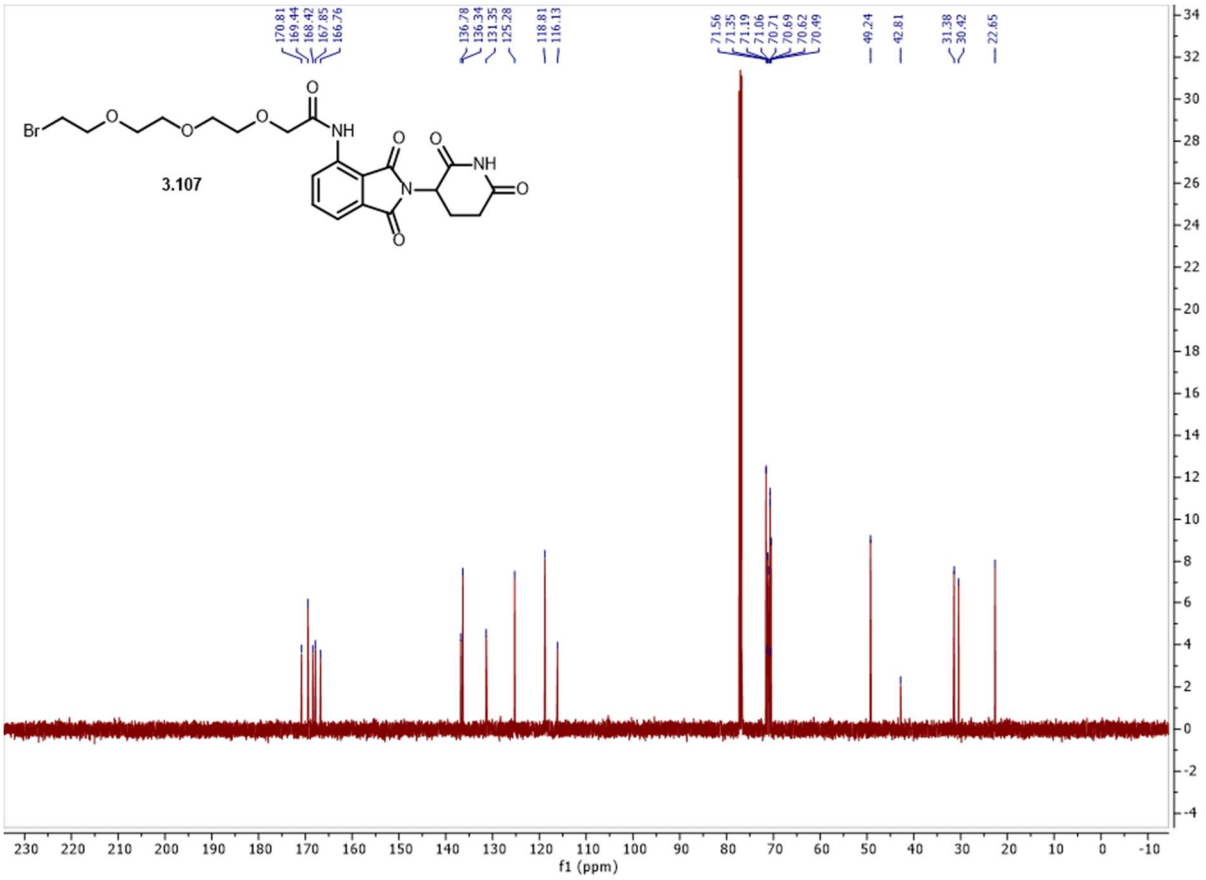

Spectrum 3.157 ^{13}C NMR of **3.107**.

3.6 References

(1) Wang, Y.; Haight, I.; Gupta, R.; Vasudevan, A. What Is in Our Kit? An Analysis of Building Blocks Used in Medicinal Chemistry Parallel Libraries. *J. Med. Chem.* **2021**, *64* (23), 17115–17122. https://doi.org/10.1021/acs.jmedchem.1c01139.

(2) Grygorenko, O. O.; Volochnyuk, D. M.; Vashchenko, B. V. Emerging Building Blocks for Medicinal Chemistry: Recent Synthetic Advances. *European Journal of Organic Chemistry* **2021**, *2021* (47), 6478–6510. https://doi.org/10.1002/ejoc.202100857.

(3) Lyu, J.; Wang, S.; Balius, T. E.; Singh, I.; Levit, A.; Moroz, Y. S.; O'Meara, M. J.; Che, T.; Algaa, E.; Tolmachova, K.; Tolmachev, A. A.; Shoichet, B. K.; Roth, B. L.; Irwin, J. J. Ultra-Large Library Docking for Discovering New Chemotypes. *Nature* **2019**, *566* (7743), 224–229. https://doi.org/10.1038/s41586-019-0917-9.

(4) Boström, J.; Brown, D. G.; Young, R. J.; Keserü, G. M. Expanding the Medicinal Chemistry Synthetic Toolbox. *Nature Reviews Drug Discovery* **2018**, *17* (10), 709–727. https://doi.org/10.1038/nrd.2018.116.

(5) Mahjour, B.; Shen, Y.; Liu, W.; Cernak, T. A Map of the Amine–Carboxylic Acid Coupling System. *Nature* **2020**, *580* (7801), 71–75. https://doi.org/10.1038/s41586-020-2142-y.

(6) Basch, C. H.; Liao, J.; Xu, J.; Piane, J. J.; Watson, M. P. Harnessing Alkyl Amines as Electrophiles for Nickel-Catalyzed Cross Couplings via C–N Bond Activation. *J. Am. Chem. Soc.* **2017**, *139* (15), 5313–5316. https://doi.org/10.1021/jacs.7b02389.

(7) Kennedy, S. H.; Dherange, B. D.; Berger, K. J.; Levin, M. D. Skeletal Editing through Direct Nitrogen Deletion of Secondary Amines. *Nature* **2021**, *593* (7858), 223–227. https://doi.org/10.1038/s41586-021-03448-9.

(8) Ghiazza, C.; Faber, T.; Gómez-Palomino, A.; Cornella, J. Deaminative Chlorination of Aminoheterocycles. *Nature Chemistry* **2022**, *14* (1), 78–84. https://doi.org/10.1038/s41557-021-00812-0.

(9) Ashley, M. A.; Rovis, T. Photoredox-Catalyzed Deaminative Alkylation via C–N Bond Activation of Primary Amines. *J. Am. Chem. Soc.* **2020**, *142* (43), 18310–18316. https://doi.org/10.1021/jacs.0c08595.

(10) Klein, V. G.; Bond, A. G.; Craigon, C.; Lokey, R. S.; Ciulli, A. Amide-to-Ester Substitution as a Strategy for Optimizing PROTAC Permeability and Cellular Activity. *J. Med. Chem.* **2021**, *64* (24), 18082–18101. https://doi.org/10.1021/acs.jmedchem.1c01496.

(11) E. Fischer; Speier, A. Darstellung Der Ester. *Berichte der deutschen chemischen Gesellschaft* **1898**, *28*, 3252–3258.

(12) Shen, Y.; Mahjour, B.; Cernak, T. Development of Copper-Catalyzed Deaminative Esterification Using High-Throughput Experimentation. *Communications Chemistry* **2022**, *5* (1), 83. https://doi.org/10.1038/s42004-022-00698-0.

(13) Zhang, Z.; Cernak, T. The Formal Cross-Coupling of Amines and Carboxylic Acids to Form Sp3–Sp3 Carbon–Carbon Bonds. *Angewandte Chemie International Edition* **2021**, *60* (52), 27293–27298. https://doi.org/10.1002/anie.202112454.

(14) Klauck, F. J. R.; James, M. J.; Glorius, F. Deaminative Strategy for the Visible-Light-Mediated Generation of Alkyl Radicals. *Angewandte Chemie International Edition* **2017**, *56* (40), 12336–12339. https://doi.org/10.1002/anie.201706896.

(15) Wu, J.; Grant, P. S.; Li, X.; Noble, A.; Aggarwal, V. K. Catalyst-Free Deaminative Functionalizations of Primary Amines by Photoinduced Single-Electron Transfer. *Angewandte Chemie International Edition* **2019**, *58* (17), 5697–5701. https://doi.org/10.1002/anie.201814452.

(16) Sun, S.-Z.; Cai, Y.-M.; Zhang, D.-L.; Wang, J.-B.; Yao, H.-Q.; Rui, X.-Y.; Martin, R.; Shang, M. Enantioselective Deaminative Alkylation of Amino Acid Derivatives with Unactivated Olefins. *J. Am. Chem. Soc.* **2022**, *144* (3), 1130–1137. https://doi.org/10.1021/jacs.1c12350.

(17) Yi, J.; Badir, S. O.; Kammer, L. M.; Ribagorda, M.; Molander, G. A. Deaminative Reductive Arylation Enabled by Nickel/Photoredox Dual Catalysis. *Org. Lett.* **2019**, *21* (9), 3346–3351. https://doi.org/10.1021/acs.orglett.9b01097.

(18) Yue, H.; Zhu, C.; Shen, L.; Geng, Q.; Hock, K. J.; Yuan, T.; Cavallo, L.; Rueping, M. Nickel-Catalyzed C–N Bond Activation: Activated Primary Amines as Alkylating Reagents in Reductive Cross-Coupling. *Chem. Sci.* **2019**, *10* (16), 4430–4435. https://doi.org/10.1039/C9SC00783K.

(19) Wu, J.; He, L.; Noble, A.; Aggarwal, V. K. Photoinduced Deaminative Borylation of Alkylamines. *J. Am. Chem. Soc.* **2018**, *140* (34), 10700–10704. https://doi.org/10.1021/jacs.8b07103.

(20) Gruntz, U.; Katritzky, A. R.; Kenny, D. H.; Rezende, M. C.; Sheikh, H. Pyridines as Leaving Groups in Synthetic Transformations: Conversion of Amines into Esters. *J. Chem. Soc., Chem. Commun.* **1977**, No. 20, 701–701. https://doi.org/10.1039/C39770000701.

(21) Katritzky, A. R.; Marson, C. M. Pyrylium Mediated Transformations of Primary Amino Groups into Other Functional Groups. New Synthetic Methods (41). *Angewandte Chemie International Edition in English* **1984**, *23* (6), 420–429. https://doi.org/10.1002/anie.198404201.

(22) Hu, J.; Wang, G.; Li, S.; Shi, Z. Selective C−N Borylation of Alkyl Amines Promoted by Lewis Base. *Angewandte Chemie International Edition* **2018**, *57* (46), 15227–15231. https://doi.org/10.1002/anie.201809608.

(23) Pitzer, L.; Schäfers, F.; Glorius, F. Rapid Assessment of the Reaction-Condition-Based Sensitivity of Chemical Transformations. *Angewandte Chemie International Edition* **2019**, *58* (25), 8572–8576. https://doi.org/10.1002/anie.201901935.

(24) Antimicro. https://github.com/AntiMicro/antimicro.

(25) *Pikpng*. https://www.pikpng.com/pngvi/hJwiiw_xbox-clipart-ps4-controller-xbox-controller-template-png-download/.

(26) Katritzky, A. R.; Horvath, K.; Plau, B. Reductive Deamination of Primary Amines. *J. Chem. Soc., Perkin Trans. 1* **1980**, No. 0, 2554–2560. https://doi.org/10.1039/P19800002554.

(27) Liao, J.; Basch, C. H.; Hoerrner, M. E.; Talley, M. R.; Boscoe, B. P.; Tucker, J. W.; Garnsey, M. R.; Watson, M. P. Deaminative Reductive Cross-Electrophile Couplings of Alkylpyridinium Salts and Aryl Bromides. *Org. Lett.* **2019**, *21* (8), 2941–2946. https://doi.org/10.1021/acs.orglett.9b01014.

(28) Ramón Malet; Marcial Moreno-Mañas; Roser Pleixats. A Concise Preparation of H3-Allylpalladium Tetrafluoroborates from N-Allylpyridinium Tetrafluoroborates. *Anales de Quimica* **1996**, *92* (1), 25–30.

(29) Zhang, C.-S.; Bao, L.; Chen, K.-Q.; Wang, Z.-X.; Chen, X.-Y. Photoinduced α-Alkenylation of Katritzky Salts: Synthesis of β,γ-Unsaturated Esters. *Org. Lett.* **2021**, *23* (5), 1577–1581. https://doi.org/10.1021/acs.orglett.0c04287.

(30) Katritzky, A. R.; Burgess, K.; Patel, R. C. Pyridiniums as Potential Synthetic Substitutes for Nitrogen Mustards. *Journal of Heterocyclic Chemistry* **1982**, *19* (4), 741–745. https://doi.org/10.1002/jhet.5570190408.

(31) Liao, J.; Guan, W.; Boscoe, B. P.; Tucker, J. W.; Tomlin, J. W.; Garnsey, M. R.; Watson, M. P. Transforming Benzylic Amines into Diarylmethanes: Cross-Couplings of Benzylic Pyridinium Salts via C–N Bond Activation. *Org. Lett.* **2018**, *20* (10), 3030–3033. https://doi.org/10.1021/acs.orglett.8b01062.

(32) Nyfeler, E.; Renaud, P. Decarboxylative Radical Azidation Using MPDOC and MMDOC Esters. *Org. Lett.* **2008**, *10* (5), 985–988. https://doi.org/10.1021/ol702832x.

(33) Corey, E. J. General Methods for the Construction of Complex Molecules. **1967**, *14* (1), 19–38. https://doi.org/10.1351/pac196714010019.

(34) Shennan, B. D. A.; Berheci, D.; Crompton, J. L.; Davidson, T. A.; Field, J. L.; Williams, B. A.; Dixon, D. J. Branching out: Redox Strategies towards the Synthesis of Acyclic α-Tertiary Ethers. *Chem. Soc. Rev.* **2022**, *51* (14), 5878–5929. https://doi.org/10.1039/D1CS00669J.

(35) Chen, T.; Xiong, H.; Yang, J.-F.; Zhu, X.-L.; Qu, R.-Y.; Yang, G.-F. Diaryl Ether: A Privileged Scaffold for Drug and Agrochemical Discovery. *J. Agric. Food Chem.* **2020**, *68* (37), 9839–9877. https://doi.org/10.1021/acs.jafc.0c03369.

(36) Wu, D.; Hernández, W. Y.; Zhang, S.; Vovk, E. I.; Zhou, X.; Yang, Y.; Khodakov, A. Y.; Ordomsky, V. V. In Situ Generation of Brønsted Acidity in the Pd-I Bifunctional Catalysts for Selective Reductive Etherification of Carbonyl Compounds under Mild Conditions. *ACS Catal.* **2019**, *9* (4), 2940–2948. https://doi.org/10.1021/acscatal.8b04925.

(37) Biermann, U.; Metzger, J. O. Synthesis of Ethers by GaBr3-Catalyzed Reduction of Carboxylic Acid Esters and Lactones by Siloxanes. *ChemSusChem* **2014**, *7* (2), 644–649. https://doi.org/10.1002/cssc.201300627.

(38) Williamson, A. W. XXII.—On Etherification. *Q. J. Chem. Soc.* **1852**, *4* (3), 229–239. https://doi.org/10.1039/QJ8520400229.

(39) Zhao, C.; Sojdak, C. A.; Myint, W.; Seidel, D. Reductive Etherification via Anion-Binding Catalysis. *J. Am. Chem. Soc.* **2017**, *139* (30), 10224–10227. https://doi.org/10.1021/jacs.7b05832.

(40) Fu, J.; Vaughn, Z.; Nolting, A. F.; Gao, Q.; Yang, D.; Schuster, C. H.; Kalyani, D. Diastereoselective Reductive Etherification Via High-Throughput Experimentation: Access to Pharmaceutically Relevant Alkyl Ethers. *J. Org. Chem.* **2023**, *88* (19), 13454–13465. https://doi.org/10.1021/acs.joc.3c00822.

(41) Sakai, N.; Moriya, T.; Konakahara, T. An Efficient One-Pot Synthesis of Unsymmetrical Ethers: A Directly Reductive Deoxygenation of Esters Using an InBr3/Et3SiH Catalytic System. *J. Org. Chem.* **2007**, *72* (15), 5920–5922. https://doi.org/10.1021/jo070814z.

(42) Das, S.; Li, Y.; Junge, K.; Beller, M. Synthesis of Ethers from Esters via Fe-Catalyzed Hydrosilylation. *Chem. Commun.* **2012**, *48* (87), 10742–10744. https://doi.org/10.1039/C2CC32142D.

(43) Xu, S.; Boschen, J. S.; Biswas, A.; Kobayashi, T.; Pruski, M.; Windus, T. L.; Sadow, A. D. Mild Partial Deoxygenation of Esters Catalyzed by an Oxazolinylborate-Coordinated Rhodium Silylene. *Dalton Trans.* **2015**, *44* (36), 15897–15904. https://doi.org/10.1039/C5DT02844B.

(44) Sakoda, K.; Yamaguchi, S.; Mitsudome, T.; Mizugaki, T. Selective Hydrodeoxygenation of Esters to Unsymmetrical Ethers over a Zirconium Oxide-Supported Pt–Mo Catalyst. *JACS Au* **2022**, *2* (3), 665–672. https://doi.org/10.1021/jacsau.1c00535.

(45) Ramachandran, P. V.; Alawaed, A. A.; Hamann, H. J. Catalyst- and Stoichiometry-Dependent Deoxygenative Reduction of Esters to Ethers or Alcohols with Borane–Ammonia. *Org. Lett.* **2023**, *25* (37), 6902–6906. https://doi.org/10.1021/acs.orglett.3c02643.

(46) Sakai, N.; Usui, Y.; Moriya, T.; Ikeda, R.; Konakahara, T. One-Pot Sequential Synthesis of Ethers from an Aliphatic Carboxylic Acid and an Alcohol by Indium-Catalyzed Deoxygenation of an Ester. *European Journal of Organic Chemistry* **2012**, *2012* (24), 4603–4608. https://doi.org/10.1002/ejoc.201200552.

(47) Sakai, N.; Usui, Y.; Ikeda, R.; Konakahara, T. Indium-Catalyzed Reductive Esterification of a Carboxylic Acid: Sequential Preparation of an Ester and Symmetrical Ether. *Advanced Synthesis & Catalysis* **2011**, *353* (18), 3397–3401. https://doi.org/10.1002/adsc.201100524.

(48) Liu, L.; Tang, Y.; Wang, K.; Huang, T.; Chen, T. Transition-Metal-Free and Base-Promoted Carbon–Heteroatom Bond Formation via C–N Cleavage of Benzyl Ammonium Salts. *J. Org. Chem.* **2021**, *86* (5), 4159–4170. https://doi.org/10.1021/acs.joc.0c02992.

(49) McGrath, A.; Zhang, R.; Shafiq, K.; Cernak, T. Repurposing Amine and Carboxylic Acid Building Blocks with an Automatable Esterification Reaction. *Chem. Commun.* **2023**, *59* (8), 1026–1029. https://doi.org/10.1039/D2CC05670D.

(50) Sakai, N.; Moriya, T.; Konakahara, T. An Efficient One-Pot Synthesis of Unsymmetrical Ethers: A Directly Reductive Deoxygenation of Esters Using an InBr3/Et3SiH Catalytic System. *J. Org. Chem.* **2007**, *72* (15), 5920–5922. https://doi.org/10.1021/jo070814z.

(51) Hart, A.; Kelley, S. A.; Harless, T.; Hood, J. A.; Tagert, M.; Pigza, J. A. An Efficient Method for the Reductive Conversion of Acyclic Esters to Ethers via a TMS-Protected Acetal. *Tetrahedron Letters* **2017**, *58* (31), 3024–3027. https://doi.org/10.1016/j.tetlet.2017.06.043.

(52) Yato, M.; Homma, K.; Ishida, A. Reduction of Carboxylic Esters to Ethers with Triethyl Silane in the Combined Use of Titanium Tetrachloride and Trimethylsilyl Trifluoromethanesulfonate. *Tetrahedron* **2001**, *57* (25), 5353–5359. https://doi.org/10.1016/S0040-4020(01)00420-3.

(53) Rysak, V.; Dixit, R.; Trivelli, X.; Merle, N.; Agbossou-Niedercorn, F.; Vanka, K.; Michon, C. Catalytic Reductive Deoxygenation of Esters to Ethers Driven by Hydrosilane Activation through Non-Covalent Interactions with a Fluorinated Borate Salt. *Catal. Sci. Technol.* **2020**, *10* (14), 4586–4592. https://doi.org/10.1039/D0CY00775G.

(54) Todtz, S. R.; Schneider, C. W.; Malakar, T.; Anderson, C.; Koska, H.; Zimmerman, P. M.; Devery, J. J. I. Controlling Catalyst Behavior in Lewis Acid-Catalyzed Carbonyl-Olefin Metathesis. *J. Am. Chem. Soc.* **2023**, *145* (24), 13069–13080. https://doi.org/10.1021/jacs.3c01508.

(55) Di Martino, R. M. C.; Maxwell, B. D.; Pirali, T. Deuterium in Drug Discovery: Progress, Opportunities and Challenges. *Nature Reviews Drug Discovery* **2023**, *22* (7), 562–584. https://doi.org/10.1038/s41573-023-00703-8.

(56) Gudz, A.; Payne, P. R.; Gagné, M. R. Phosphines as Silylium Ion Carriers for Controlled C–O Deoxygenation: Catalyst Speciation and Turnover Mechanisms. *Organometallics* **2017**, *36* (20), 4047–4053. https://doi.org/10.1021/acs.organomet.7b00689.

(57) Zoppi, V.; Hughes, S. J.; Maniaci, C.; Testa, A.; Gmaschitz, T.; Wieshofer, C.; Koegl, M.; Riching, K. M.; Daniels, D. L.; Spallarossa, A.; Ciulli, A. Iterative Design and Optimization of Initially Inactive Proteolysis Targeting Chimeras (PROTACs) Identify VZ185 as a Potent, Fast, and Selective von Hippel–Lindau (VHL) Based Dual Degrader Probe of BRD9 and BRD7. *J. Med. Chem.* **2019**, *62* (2), 699–726. https://doi.org/10.1021/acs.jmedchem.8b01413.

(58) Dherange, B. D.; Yuan, M.; Kelly, C. B.; Reiher, C. A.; Grosanu, C.; Berger, K. J.; Gutierrez, O.; Levin, M. D. Direct Deaminative Functionalization. *J. Am. Chem. Soc.* **2023**, *145* (1), 17–24. https://doi.org/10.1021/jacs.2c11453.

(59) Logvinenko, I. G.; Kondratov, I. S.; Pridma, S. O.; Tolmachova, N. A.; Morev, R. N.; Dolovanyuk, V. G.; Boretskyi, A. L.; Stepaniuk, R. O.; Trofymchuk, S. A.; Mück-Lichtenfeld, C.; Daniliuc, C. G.; Haufe, G. Synthesis and Physical Chemical Properties of CF3O-Containg Secondary Amines—Perspective Building Blocks for Drug Discovery. *Journal of Fluorine Chemistry* **2022**, *257–258*, 109990. https://doi.org/10.1016/j.jfluchem.2022.109990.

(60) Tcyrulnikov, S.; Cai, Q.; Twitty, J. C.; Xu, J.; Atifi, A.; Bercher, O. P.; Yap, G. P. A.; Rosenthal, J.; Watson, M. P.; Kozlowski, M. C. Dissection of Alkylpyridinium Structures to Understand Deamination Reactions. *ACS Catal.* **2021**, *11* (14), 8456–8466. https://doi.org/10.1021/acscatal.1c01860.

(61) Wang, D.; Xue, X.-S.; Houk, K. N.; Shi, Z. Mild Ring-Opening 1,3-Hydroborations of Non-Activated Cyclopropanes. *Angewandte Chemie International Edition* **2018**, *57* (51), 16861–16865. https://doi.org/10.1002/anie.201811036.

Chapter 4 The Biological Impact of Alternative Amine–Acid Coupling Reactions[8]

This chapter focuses on the applications of the work developed in the last chapter. In the first part of the chapter, amine–acid coupling reactions are developed and applied to generate derivatives of the PROTAC dbet1. The biological activity of these products is explored, and computational studies performed to rationalize some of the observed activity.

The second part of this chapter details synthesizing derivatives of fluorescein using amine–acid couplings. The products of these reactions are then imaged in cells and their organelle distribution profile is studied.

4.1 Diverse Amine-Acid Coupling Reactions Modulate the Potency of BRD4 PROTACs[9]

4.1.1 Introduction

The ability to covalently unite two molecules is critical to studies in proximity-induced pharmacology, medicinal chemistry, polymer chemistry, chemical biology, antibody-drug fusion and other diverse bioconjugation applications. Recently, the emergence of proteolysis targeting chimeras (PROTACs) as a powerful therapeutic modality has highlighted the role that the linker composition has not only on the activity, but also the bulk physicochemical properties of these

[8] The first portion of this chapter submitted as a preprint to ChemRxiv: McGrath, A.; Huang, H.; Brazeau, J.-F.; Zhang, Z.; Vellore, N. A.; Zhu, L.; Shi, Z.; Venable, J. D.; Gelin, C.; Cernak, T. Diverse Amine-Acid Coupling Reactions Modulate the Potency of BRD4 PROTACs. *ChemRxiv* **2023**. DOI:10.26434/chemrxiv-2023-bh0d1.

[9] This work was done in collaboration with Janssen Pharmaceuticals. Dr. Rose Zhang performed some of the initial optimization studies for the alkylation reaction. Dr Haiyan Huang synthesized compounds **4.3**, **4.5**, **4.19**, **4.23**, and **4.53** All other chemistry optimization and compound synthesis was performed by me. I performed the chemoinformatic exercises. Scientists at Janssen performed all assays and MD simulations.

protein degraders.[1–6] PROTACs are heterobifunctional ligands that contain a ligand to recruit an E3 ubiquitin ligase, a ligand to bind the protein of interest (POI), and a linker conjoining the two ligands, leading to event driven pharmacology that is catalytic and agnostic of receptor occupancy.[7] As such, PROTACs have a unique ability to eliminate "undruggable" protein targets. The explosion of interest in PROTACs has led to an extensive, commercially available toolkit of linker and E3 ligase binding building blocks, many of which terminate in an amine or carboxylic acid. The amide reaction is one of the most popular methods for linking two molecules together and has been broadly used in the development of PROTACs.[8,9] Other tactics include esterification[10], click chemistry,[11] S_NAr,[12] Buchwald–Hartwig coupling,[13] among other new methods.[14,15] Each of these methods represents a powerful way to unite the POI and E3 ligase pair, but often requires multi-step synthesis to install an alternative reactive functional group on one or both binders. Recently, we have shown that amines and carboxylic acids can be united in many ways beyond the amide connection, with each amine–acid coupling transformation imparting a distinct physicochemical footprint on the product.[16–21] Given that the linker moiety may affect degradation efficiency as well as absorption, distribution, metabolism and excretion (ADME) properties such as permeability of PROTACs,[22] we sought to explore new reactions that would expand access to diverse linkages between a POI and E3 ligase ligands, and examine the influence of the linker changes on the biological activity of certain final PROTACs.

Conventionally, when a primary amine and carboxylic acid are coupled together[23], the resultant amide motif bears one hydrogen bond donor (HBD) along with two hydrogen bond acceptors (HBA) and a neutral charge. In this manner, the transformation itself can be viewed as leaving a physicochemical footprint on the product. However, if the conditions used in the

reaction are modified and an ester is produced instead, the HBD is removed from the product. It follows that the functional outcome of a molecule is dependent not only upon the building blocks used to create it but also the transformation used to unite these fragments which are intertwined with the selected reaction conditions. In this way, shifts in the composition and arrangement of atoms allow for a fine tuning of the property space accessible from just two building blocks by changing reaction conditions.[17] We have developed transformations that couple amines and acids into esters,[18,19] alkanes,[20,21] and ketones.[21] The application of complementary amine–acid coupling transformations to assemble PROTACs is particularly intriguing, considering the important role that the linker design itself may play on properties. Herein, we developed a suite of amine–acid PROTACs linking reactions that produced either an amide, ester, amine, alkane, or ketone linkage using the well-studied bromodomain inhibitor JQ1 **1** and cereblon (CRBN) binding pomalidomide derived amine **2** to yield derivatives **4**–**7** of the classic PROTAC dBET1 (**3**) (Figure 4.1).[24] Our suite of heterobifunctional degraders, accessed from these two starting materials was expanded upon by applying the same transformations to a von Hippel-Lindau (VHL) targeting amine. The resultant compounds span a range of physicochemical and pharmacological properties.

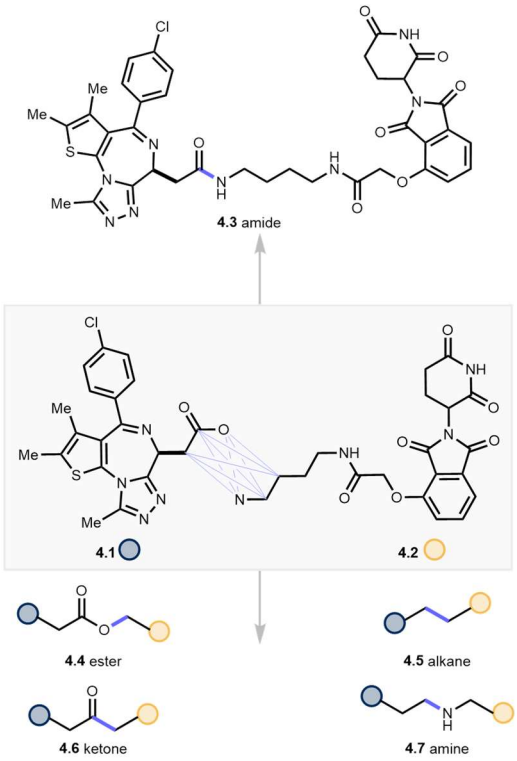

Figure 4.1 Diverse amine–acid couplings on **1** and **2** can produce amide (**3**), ester (**4**), alkane (**5**), ketone (**6**), or amine (**7**), congeners.

4.1.2 Chemoinformatic analysis of commercially available PROTACs

When 80 possible transformations[16] were applied on **4.1** and a suite of commercially available CRBN recruiting amines *in silico*, a diverse property space emerged. The properties of these molecules, including molecular weight, LogP, formal charge, and polar surface area (PSA) were calculated and compared for the 80 possible transformations using a t-Distributed Stochastic Neighbor Embedding (tSNE) (Figure 4.2). This analysis revealed the amide (purple) and amine (yellow) transformations in general occupy their own chemical space, suggesting these transformations impart a larger effect on the overall properties of the molecule. Comparatively, the ester (pink), alkane (red), and ketone (orange) overlap in chemical space, indicating these transformations exert a more nuanced effect on the property space occupied by the products. This is further exemplified by the incorporation of basic amines into the linker portion of the

starting amine (c.f. orange dots in the yellow space). Notable inaccessible pockets (grey) of this space that remain include transformations that retain the carboxylic acid or incorporate rearrangements (See Supporting Information), representing synthetic methods that may be possible to investigate in the future. However, these four new transformations cover a breadth of space and offer new structure activity relationships from the same two building blocks.

4.1.3 HTE optimization of PROTAC amine–acid couplings

Our studies initiated with a campaign to identify diverse reaction conditions for linking **4.1** and **4.2** that would produce PROTAC molecules **4.3**–**7**. We used miniaturized high throughput experimentation (HTE), which has emerged as a powerful tool in the navigation of reaction space.[25–28] In addition to allowing a rapid assessment of the interplay of multiple reaction variables, the use of miniature glass vials allows for conservation of precious starting materials,[29] such as partial PROTAC building blocks. HTE investigation of the four targeted amine–acid coupling transformations esterification, alkylation, ketonylation, or amination was conducted surveying 24 unique reaction conditions each. Reactions were performed on less than 10 μmol scale of starting material **4.2** per well (Figure 2a).

Automatable amine–acid esterification reactions have been developed by our lab for both alkyl[19] and aryl amines.[18] In the alkyl amine setting, the esterification proceeds via activation of the alkyl amine as its triphenylpyridinium salt[30] and aging with a carboxylic acid in the presence of *N,N*-diispropylethylamine (DIPEA) and potassium iodide (KI). When **4.1** and the pyridinium salt of **4.2** were subjected to these conditions, the desired ester was observed alongside an undesired isobaric compound presumed to be from imine N-alkylation (See Experimental). Thus, a 24-well reaction array examining different promoter additives and bases was performed to identify alternative reaction conditions for the formation of desired ester **4.4** (Figure 4.2, B). In

general, stronger bases facilitated the formation of the desired ester product. For instance, potassium *tert*-butoxide yielded **4.4** as the exclusive product whereas lutidine exclusively formed the undesired adduct. DIPEA and triethylamine (TEA) gave mixtures of both the desired product and the undesired adduct. Potassium bromide (KBr) and bromomethyldiethyl malonate facilitated the reaction as additives, but in lower yield than KI or sodium iodide (NaI). The best performing conditions used KI and potassium *tert*-butoxide and gave **4.4** in 53% assay yield and 54% isolated yield. This protocol complements multi-step synthesis methods to access ester-linked PROTACs via total synthesis.[10]

To access the alkane and ketone linked products, we explored nickel-catalyzed reductive cross-couplings conditions. Recent methods employing nickel as the metal catalyst have emerged as a powerful tool to link pyridinium salts[31–35] and activated carboxylic acids for the formation of alkanes or ketones[36–39], and we hypothesized that a reducing nickel system would best facilitate the formation of alkane (**4.5**) and ketone (**4.6**) targets. We began our investigation through coupling acyl fluoride **4.8** (Figure 4.3), generated *in-situ* from **4.1** using tetramethylfluoroformamidinium hexafluorophosphate (TFFH) and proton sponge, and **4.10** (pyridinium salt of **4.2**). Subjecting these coupling partners to nickel (II) bromide•glyme ($NiBr_2$•DME), 4,4-di-*tert*-butylbipyridine (dtbpy), and elemental manganese produced alkane product **4.5**. A thorough investigation of the interplay of imide additives (Experimental)[40], nickel sources, ligands, and Brønsted acid additives (Figure 4.2, C) was conducted. We found that hydantoin increased alkane formation whereas the inclusion of Brønsted acids was detrimental. $NiBr_2$•DME, and dtbpy were observed to be the optimal catalyst and ligand combination giving **4.5** in 38% assay yield.

In our investigation of ligands to synthesize alkane **4.5**, we observed a ligand change occasionally yielded mixtures of **4.5** and ketone **4.6** (see Experimental). Based on these observations we hypothesized we could access **4.6** through careful selection of catalyst, ligand and additive. Thorough investigation revealed we should explore other activation strategies (see Experimental). For substrates derived from **4.1**, we determined acyl carbonates to be a viable activating group.[38] Subsequently, JQ1 (**4.1**) was activated *in situ* by using dimethyldicarbonate (DMDC). After determining our optimal activating group, we investigated the use of imides, Brønsted acids, and ligands (Figure 4.2, D). We found the ligand (*Z*)-*N*-cyanopicolinimidamide (PyCamCN) maximized the yield of **4.6,** whereas dtbpy gave alkane **4.5** exclusively. Notably, in contrast to our findings in the C–C coupling of **4.1** and **4.2**, the use of imide additives hindered ketone formation while triethylammonium hydrochloride (NEt_3•HCl) was found to increase the yield. We selected *in situ* activation of **4.1** with DMDC and catalyzed ketonylation with nickel (II) acetylacetonate $Ni(acac)_2$, PyCamCN, and NEt_3•HCl as optimal conditions to deliver **4.6** in 36 % assay yield.

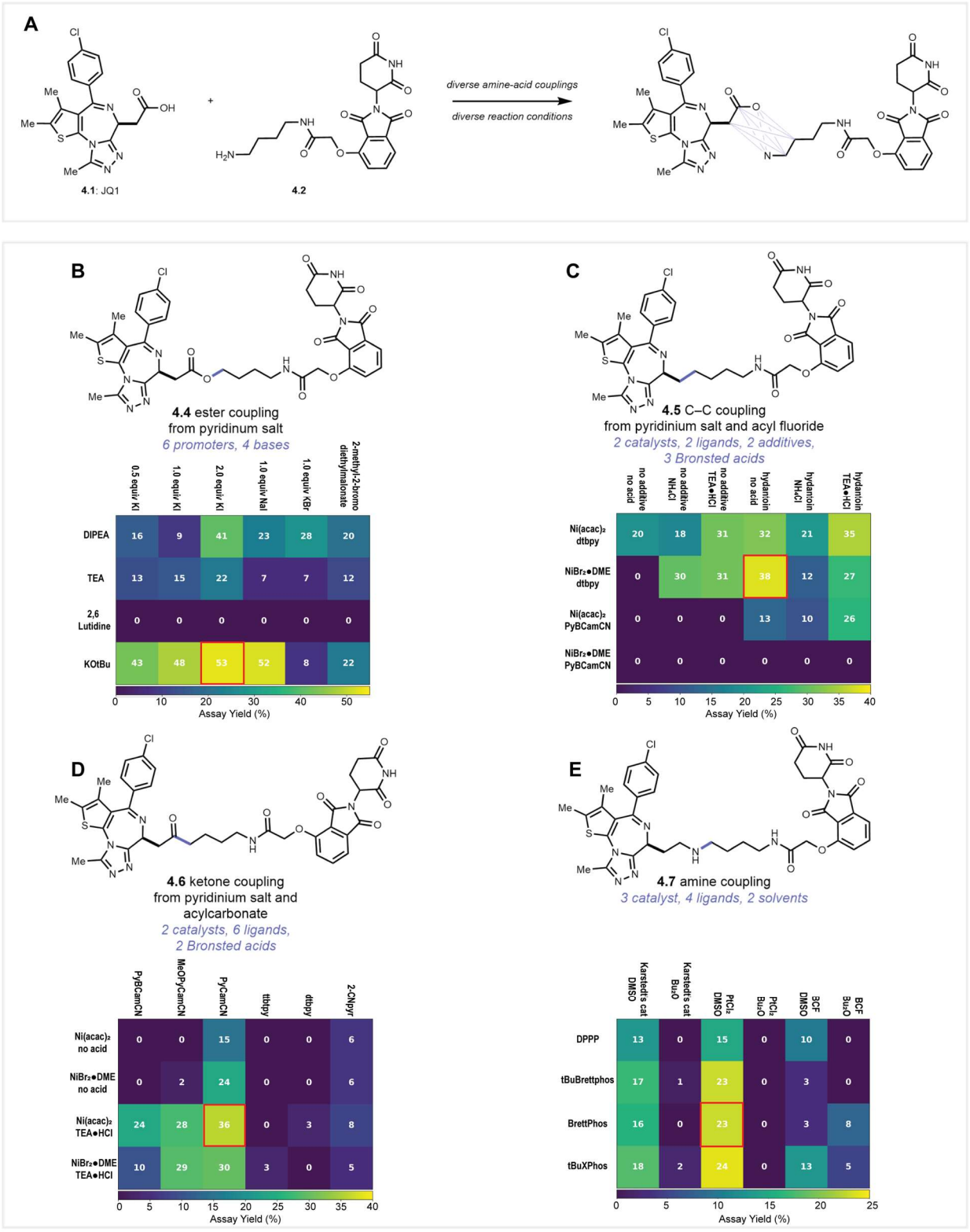

Figure 4.2 (A) Developing diverse reaction conditions to produce ester, amine, alkane, and ketone-linked analogs of amide dBET1 (**4.3**) using high-throughput experimentation. Assay yields were determined by UPLC-MS. (B) Ester array conditions: 10 μmol of **4.1** (1.0 equiv), **4.10** (1.0 equiv), base (1.0 equiv) and additive (equiv listed) per well.

(C) Alkane array conditions: 5 μmol (2.0 equiv) of **4.8**, **4.10** (1.0 equiv), nickel catalyst (40 mol%), ligand (40 mol %), imide additive (2.0 equiv), Brønsted acid (2.0 equiv), and manganese (4.0 equiv) per well. (D) Ketone array conditions: 5 μmol (2.0 equiv) of **4.9**, **4.10** (1.0 equiv), nickel catalyst (40 mol%), ligand (40 mol %), additive (2.0 equiv), and manganese (4.0 equiv) per well. (E) Amine array conditions: 15 μmol **4.1** (1.5 equiv), **4.2** (1.0 equiv), catalysts (5 mol %), ligand (10 mol %), and phenylsilane (4 equiv) per well. All wells contain 100 μL of solvent. PyBCamCN = (2*Z*,6*Z*)-N′2,N′6-Dicyanopyridine-2,6-bis(carboximidamide), MeOPyCamCN = 4-methoxy-N-cyanopicolinimidamide PyCamCN = N-cyanopicolinimidamide, ttbtpy = 4,4′,4″-Tri-tert-Butyl-2,2′:6′,2″-terpyridine, dtbpy = 4,4-di-tert-butylbipyridine, 2CNPyr = 2-cyanopyridine, Karstedt's cat = Platinum(0)-1,3-divinyl-1,1,3,3-tetramethyldisiloxane complex.

4.1.3.1 Ligand effects in nickel catalyzed coupling reaction outcomes

We were intrigued by the rapid decarbonylation of the acyl fluoride **4.8** to give alkane product **4.5** as opposed to ketone product **4.6** when subjected to nickel and dtbpy, in contrast to literature reports (Figure 4.3).[36] This may be due to subtle changes in electronics of the substrate having a profound impact on the rate of decarbonylation in nickel catalyzed reactions.[21] Mechanistic investigations in our lab and others[21,37,41,42] have highlighted that subtle effects govern the decarbonylation event in nickel-catalyzed reductive cross-couplings. In addition, ligands may also play a role in governing the kinetics of decarbonylation; when the acyl carbonate of **4.1** and pyridinium salt of **4.2** were subjected to $NiBr_2$•DME and dtbpy, only the decarbonylated alkyl coupling product **4.5** was observed albeit in lower yield. To further probe this effect, we investigated other amine and carboxylic acid coupling partners under our reaction conditions (see Experimental). In general, we have discovered that selectivity for C–C coupling is consistent in the case of primary pyridinium salts whereas only the ketone product is observed when using secondary pyridinium salts. The rapid decarbonylation is also observed in carboxylic acids containing α β-diphenyl imine group. Further investigations into this effect are ongoing in our lab.

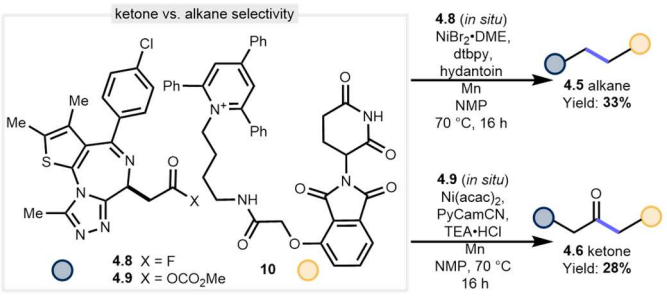

Figure 4.3 A change in ligand switches the selectivity for the synthesized product. Reactions conducted using **4.8** or **4.9** (2.0 equiv), **4.10** (1.0 equiv), nickel catalyst and ligand (40 mol % each), additive (2.0 equiv), and manganese (4.0 equiv) at 0.025 M.

4.1.3.2 A selective amine–acid reductive amination

We next turned our attention to the formal reductive amination between **4.1** and **4.2**. Based upon literature precedent[43,44], we believed the desired reactivity could be achieved using either platinum-based catalysis or *tris*(pentafluorophenyl)borane (BCF). BCF in dibutylether (Bu_2O) produced a trace amount of desired amine **4.7** along with amide **4.3** and recovered starting material, and no reduction of the amide bond or four other carbonyls. Further investigation of solvent effect demonstrated that DMSO outperforms other polar aprotic solvents (see Experimental) suggesting that the effect is not entirely solubility driven. Based upon these data we planned a screen investigating solvents, catalysts, and ligands. Three catalysts (two platinum and BCF), and four phosphine ligands, were surveyed by HTE using DMSO or dibutyl ether as solvent. Our observations confirmed that DMSO is essential to achieving reactivity with these complex substrates, which contrasts reports on simpler substrates.[43–45] Additionally, platinum catalysis outperformed boron catalysis with platinum (II) chloride being an optimal catalyst and BrettPhos as a preferred ligand.

To further explore the scope of the reductive amination reaction we applied our optimized condition to an array of six amines including four partial PROTACs (**4.2**, **4.11**–**13**), two linker type molecules (**4.14**, **4.15**) (Figure 4.4, A) and four pharmaceutically relevant

carboxylic acids (**4.1**, **4.16**–**18**) (Figure 4b). Since we have seen that CRBN targeting ligands such as **4.2** and **4.11** generally perform better in pure DMSO, and other systems perform better using a mixture of DMSO and dioxane, we settled on 30% DMSO in dioxane as a balance. These conditions appear broadly applicable to late-stage derivatization as we saw product formed in every well (Figure 4.4, C). This is remarkable as the reaction performs in the presence of functionalities such as alcohols (**4.12**,**4.13**), acetonides (**4.17**), a dihydrouracil (**4.11**), and an indole (**4.16**). Additionally, the reaction works on aliphatic as well as benzylic acids. To assess the performance of the reaction we isolated products from four wells on a 0.1 mmol scale (**4.19**–**22**) (Figure 4.4, D). In each of these reactions, we did not observe reduction of other carbonyls present in the molecule. These results as well as control experiments leaving the amine out (see Experimental) suggest a pathway where an aldehyde intermediate plays a dominant role as opposed to amide formation and subsequent reduction.[43,44,46] A second scope screen and subsequent scale up of several amines was performed (see Experimental). The ester, alkane, and ketone transformations as well as the amide coupling were also applied to this library (see Experimental).

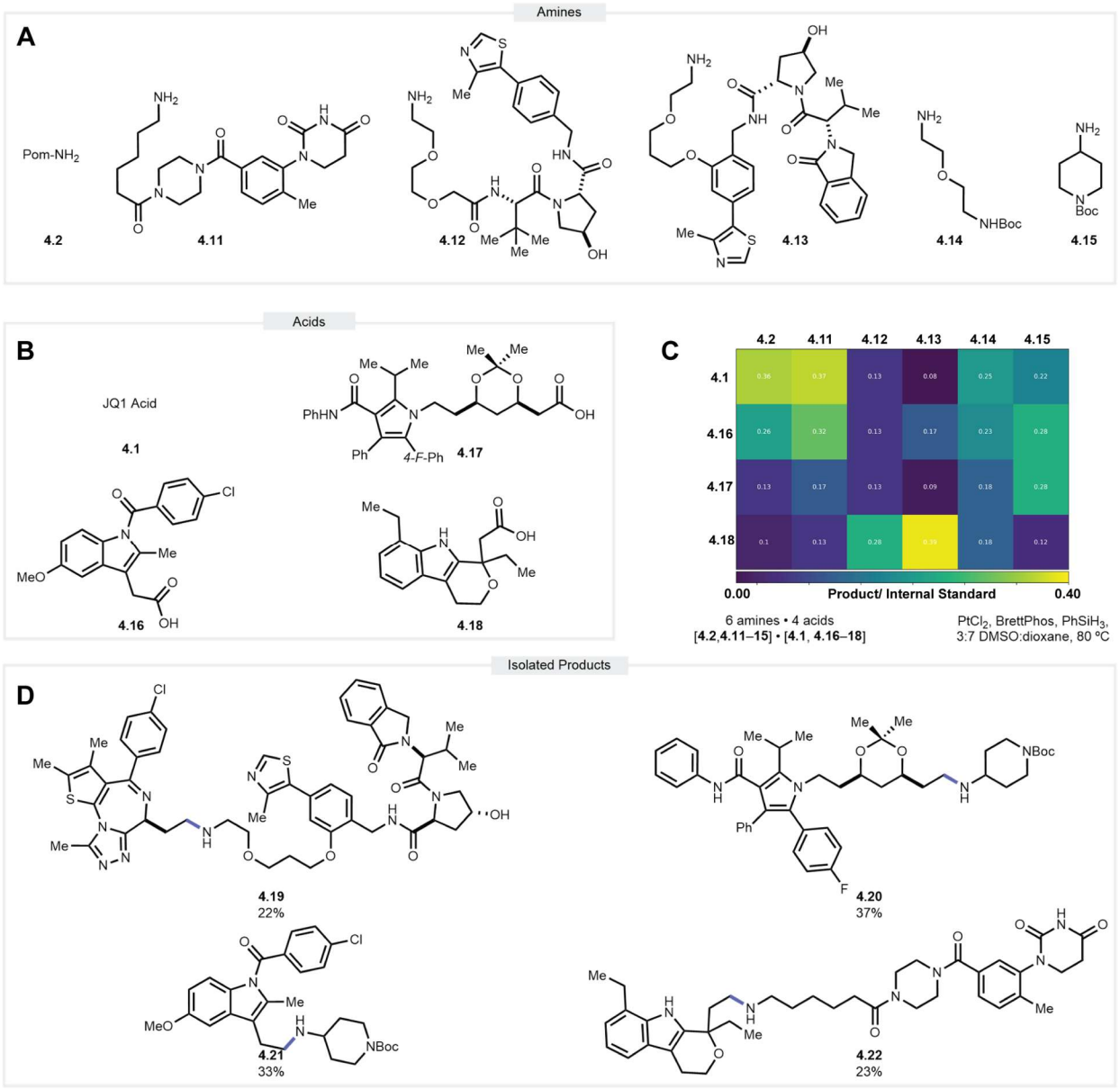

Figure 4.4 Reductive amination conditions applied to a library of (A) 6 amines and (B) 4 acids. All reactions conducted using 10 µmol of amine (1.0 equiv) and 15 µmol of acid (1.5 equiv), $PtCl_2$ (5 mol %), BrettPhos (10 mol %) and $PhSiH_3$ (5.0 equiv) at 0.1 M. (C) Results of the screen (D) Scale up of select compounds on 0.100 mmol scale relative to the amine starting material.

4.1.4 Scale up and isolation of PROTACs.

With optimized conditions for each transformation, we turned our attention towards the scale up and isolation of each compound in practically useful amounts (0.1 mmol scale) (Figure

4.5, A). Due to the immense interest in using VHL as an E3 ligase as a complementary approach to protein degradation, we applied our conditions to VHL targeting amine **4.13**.[3,4,47] We observed similar reactivity trends despite incorporating new functional groups with the potential to interfere. Scale up of our conditions was found to correlate well with assay yield for each transformation and delivered both the CRBN and VHL based PROTACs in acceptable yield. Our amide conditions (see Experimental) yielded compound **4.3** in 73% and compound **4.23** in 47% yields respectively. Applying our esterification conditions to each substrate yielded ester **4.4** in 54% and ester **4.24** in 36% yields. Further, a one-pot protocol (see Experimental) was developed to give **4.4** directly from **4.1** and **4.2** in 28% yield. A slightly modified protocol using two equivalents of base was applied to the HCl salt **4.13** to give **4.24** in 25% yield. Applying our alkane conditions yielded **4.5** in 33% and **4.25** in 20% yields respectively. Application of our ketone conditions yielded **4.6** and **4.26** in 28% and 19% yields. Finally, our conditions for reductive amination yielded **7** in 23% yield. It was found it was necessary to adjust the solvent to 10% DMSO in dioxane to achieve optimal reactivity for the synthesis of **4.19**. This adjustment furnished **4.19** in 23% yield. It is of note that we did not observe opening of the glutarimide ring under any of our reaction conditions.[48,49] With nine new dBET1 analogs in hand, calculations were performed on each molecule to demonstrate that we can effectively modulate the properties of each final PROTAC by changes to the linker composition (Figure 5, B & D). While bulk properties are determined by choice of building blocks (**4.2** vs **4.13**), each transformation imparts its own effect on the overall properties of the molecule with removal of the hydrogen bond donor (amide/amine to ester/alkane/ketone) having the greatest impact in this investigation (see Experimental for labels).

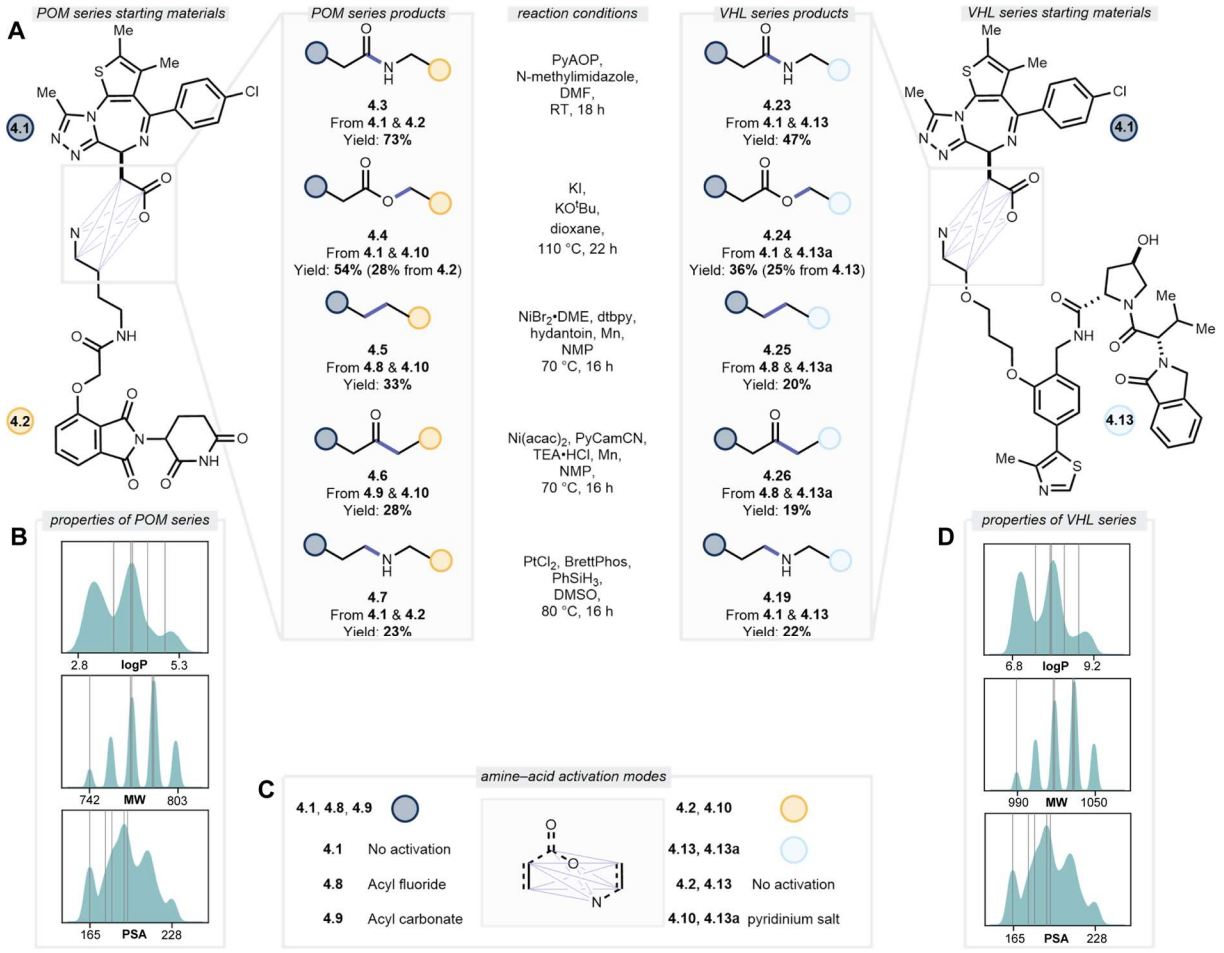

Figure 4.5 (A) Five transformations applied to **4.1** & **4.2** (POM), as well as **4.1** and **4.13** (VHL)**.** All reactions conducted at 0.100 mmol scale relative to the amine. Amide conditions: **4.1** and **4.2** (1.0 equiv), PyAOP (1.0 equiv), and N-methylimidazole (1.0 equiv) in 1.0 mL of solvent (0.1 M). Ester reaction conditions: **4.1** and **4.10** (1.0 equiv), KI (2.0 equiv), and KO^{t}Bu (1.0 equiv) in 1.0 mL solvent (0.1 M). CC and Ketone conditions: **4.1** (2.0 equiv), **4.2** (1.0 equiv), nickel catalyst (40 mol%), ligand (40 mol %), additive (2.0 equiv), and manganese (4.0 equiv) in 2.0 mL solvent 0.05 M. Amine conditions: **4.1** (1.5 equiv) and **2** (1.0 equiv) $PtCl_2$ (5 mol %), BrettPhos (10 mol %) and $PhSiH_3$ (5.0 equiv). (B) Chemoinformatic analysis of **4.3**-**7**. (C) methods used to activate the amine or acid coupling partner (D) Chemoinformatic analysis of **4.19**, **4.23**-**26**.

4.1.5 Biological activity of PROTAC derivatives

Having established conditions to scale up and isolate the 10 BRD4 PROTACs (**4.3**–**7**, **4.19**, **4.23**–**26**), in vitro profiling in our primary biological assays to assess BRD4 degradation was initiated. We tested both CRBN-based PROTACs **4.3–7** as well as VHL (**4.19**, **4.23**–**26**) using HEK293 cells to readout endogenous BRD4 degradation DC_{50} and D_{max} values.[50] In addition, to separate on target BRD4 degradation from general cell toxicity, Cell Titer Glo

(CTG) was also conducted (see Experimental). Within the CRBN-BRD4 PROTAC series, we observed several molecules with more efficient BRD4 degradation than dBET1 (**4.3**) (Figure 4.6, A; Table 4.1). The ester **4.4**, alkane **4.5** and ketone **4.6** were more potent than amide **4.3**, with DC_{50} values of 5.4 nM, 10.8 nM, 9.2 nM, and 95.0 nM, respectively (Table 4.1). Comparable target degradation to amide **4.3** (D_{max} 80%), was observed for **4.4**, **4.5**, and **4.6** (83%, 76% and 85% at 24 h). Conversely, the amine analog **4.7** was not successful at degrading BRD4 with a DC_{50} of > 11 µM. In general, the VHL-based PROTACs **4.19**, **4.23**–**26**, follow the same trend in BRD4 degradation as observed for the four linkages compared to the CRBN series (see Figure 4.6, B), albeit DC_{50} values are higher and D_{max} values lower. VHL ester **4.24** and ketone **4.26** are the most efficient degraders of BRD4 in the set, with DC_{50} values of 27.3 nM and 13.4 nM (D_{max} values of 80% and 79%, respectively) (Table 4.1). VHL alkane **4.25** has a 21-fold higher DC_{50} and diminished D_{max} value relative to CRBN alkane **4.5**, likely due to reduced binding to BRD4 and VHL protein (see Figure 4.37,38 in Experimental).

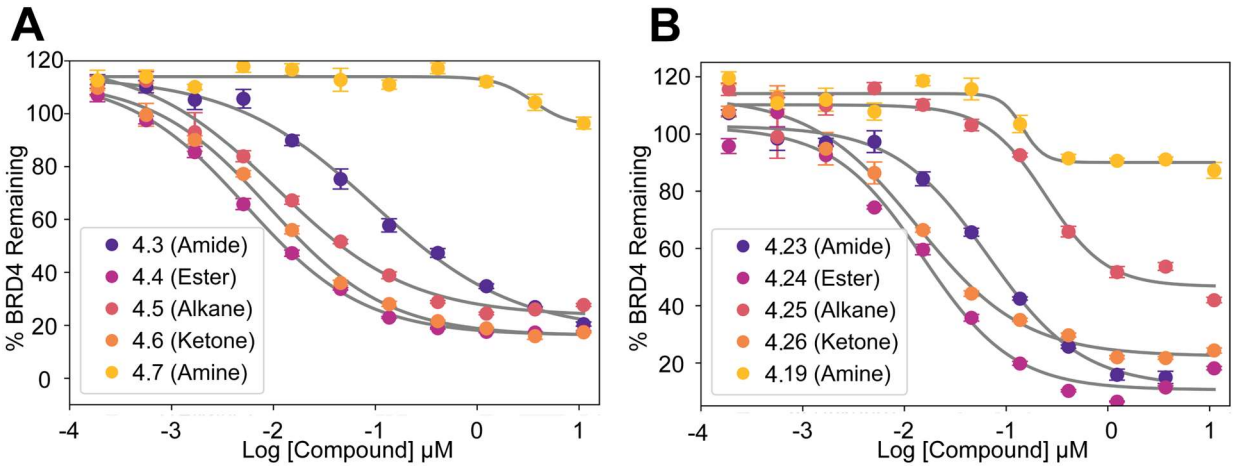

Figure 4.6 BRD4 HTRF Degradation Assay: (A) CRBN series degradation curves (**4.3**-**7**). (B) VHL series degradation curves (**4.19**, **4.23**-**26**).

Table 4.1 Table of experimental physicochemical properties and BRD4 HTRF degradation values. Values reported are the mean ± SEM of a single experiment in quadruplicate.

E3 Ligase	Linker Type (#)	MW	CHI $LogD_{7.4}$	BRD4 HTRF degradation DC_{50} (nM)	BRD4 HTRF degradation D_{max} (%)
CRBN	amide (**4.3**)	785	2.16	95.0 ± 7.2	80
CRBN	ester (**4.4**)	786	2.68	5.4± 1.0	83
CRBN	alkane (**4.5**)	742	2.81	10.8 ± 0.9	76
CRBN	ketone (**4.6**)	770	2.57	9.2 ± 1.0	85
CRBN	amine (**4.7**)	771	1.66	>11,000	2
VHL	amide (**4.23**)	1033	2.78	68.3 ± 6	87
VHL	ester (**4.24**)	1034	3.25	15.8 ± 1.5	89
VHL	alkane (**4.25**)	990	3.38	228.0 ± 16.7	58
VHL	ketone (**4.26**)	1018	3.16	13.4 ± 0.9	79
VHL	amine (**4.19**)	1019	2.30	11,000	14

To understand the observed BRD4 degradation results that arose from subtle changes to the linker, we measured target engagement of the heterobifunctional degraders to BRD4 protein and the corresponding E3 ligase (Table 4.2). Binding affinity of the PROTACs to BRD4 **4.3**–**7** was assessed in a BRD4-BD1 biochemical probe displacement assay to bromodomain BD1. E3 ligase engagement was evaluated in a cellular CRBN or VHL nanoBRET (Bioluminescence Resonance Energy Transfer) assay dependent on the PROTAC synthesized. The cellular nanoBRET target engagement assay was used as a surrogate to examine PROTAC cellular permeability.[51] The assay was performed in both live and permeabilized (lytic) cells and intracellular availability was determined by calculating the relative binding affinity (RBA).[52]

Table 4.2 Target engagement for CRBN analogs (**4.3**-**7**) assessed by BRD4-BD1 HTRF displacement assay and cellular nanoBRET CRBN-tracer assay in live and permeabilized conditions. Values reported are the mean ± SEM of a single experiment in triplicate for the BRD4—BD1 HTRF assay. Values reported are the mean ± SEM of a single experiment containing five technical replicates for the cellular nanoBRET CRBN-tracer assay.

Linker Type (#)	BRD4-BD1 HTRF (nM)	nanoBRET Live (nM)	nanoBRET Permeabilized (nM)	nanoBRET RBA
amide (**4.3**)	16.0 ± 1.1	528.5 ± 35.0	86.3 ± 4.8	6.1
ester (**4.4**)	2.3 ± 0.1	263.7 ± 7.6	68.8 ± 4.4	2.4
alkane (**4.5**)	66.9 ± 1.1	503.5 ± 19.9	120.7 ± 14.2	4.2
ketone (**4.6**)	24.2 ± 0.9	421.8 ± 21.1	107.1 ± 15.9	3.9
amine (**4.7**)	453.2 ± 18.4	11272 ± 1992.7	102.0 ± 4.9	110.5

Table 4.2 shows the data for the five CRBN-BRD4 PROTACs using amide **4.3** as a benchmark, which has a BRD4 affinity of 16.0 nM, and CRBN binding of 528.5 nM (live cells) and 86.3 nM (permeabilized cells). Of the newly synthesized analogs, ester **4.4**, alkane **4.5**, and ketone **4.6** maintain binding with IC_{50} values of 2.2, 66.9, and 24.2 nM for BRD4, respectively. Notably removal of the carbonyl moiety in alkane **4.5** does not result in a significant loss in BRD4 affinity (Table 2). Looking at the RBA values, a decrease is seen for ester **4.4**, alkane **4.5**, and ketone **4.6**, (RBA: 2.4, 4.2, and 3.9, respectively, relative to **4.3**). This is possibly because these three analogs have higher LogD, correlating with an anticipated increase in permeability. All three of these analogs have the HBD N–H group seen in amide **4.3** removed. The SAR trend observed for BRD4 degradation has **4.4**–**6** as the most potent degraders and the improvement in permeability and BRD4 affinity may be an explanation for the observed degradation. VHL degraders **4.19**, **4.23**–**26** occupy less drug-like space due to their higher molecular weight and larger number of HBD but still show the same rank order in BRD4 target engagement and improved RBA values (see Experimental). However, the lower VHL affinity in live cell nanoBRET for **4.19**, **4.23**–**26** may explain the rightward shift in DC_{50} values (Table 4.1). High degradation efficacy of BRD4 is retained by VHL PROTACs with D_{max} ranging from 58–83%. Amine **4.7** shows a greater than 100-fold difference in IC_{50} between the live and permeabilized cells and this can be attributed to the presence of the basic amine in the linker. Additionally, the BRD4 potency of amine **7** is 453 nM compared to 15 nM for amide **4.3**.

4.1.6 Computational investigation into the effects of alternative amine–acid couplings or BRD4 binding

To understand the differences in binding affinity of highly potent versus poor binders, molecular dynamic simulations of BRD4-BD1 in the presence of amide **4.3**, ester **4.4**, and amine

4.7 were conducted in explicit solvent conditions. Sampled conformations from the 250-ns MD simulations are shown in Figure 4.7 (initial pose is shown in red and final in blue). Based on the simulations, both amide **4.3** and ester **4.4** maintain key interactions with the BRD4 binding site. In contrast, amine **4.7,** due to presence of a charged linker, interacts with Asp144 and engages in an intramolecular hydrogen bond with the azepine moiety on the POI portion during the course of the simulation (see Experimental for 2D interaction diagram). These observed interactions significantly alter the conformation of amine **4.7** as seen during MD simulation (Figure 4.7). Furthermore, the BRD4-BD1 protein near the binding region of the amine **4.7** displays significantly higher root-mean-square fluctuation (RMSF) compared to amide **4.3** or ester **4.7** compounds. This instability of the amine **4.7** interaction with BRD4 along with conformational preference could influence productive ternary complex formation and contribute to the lower observed degradation.

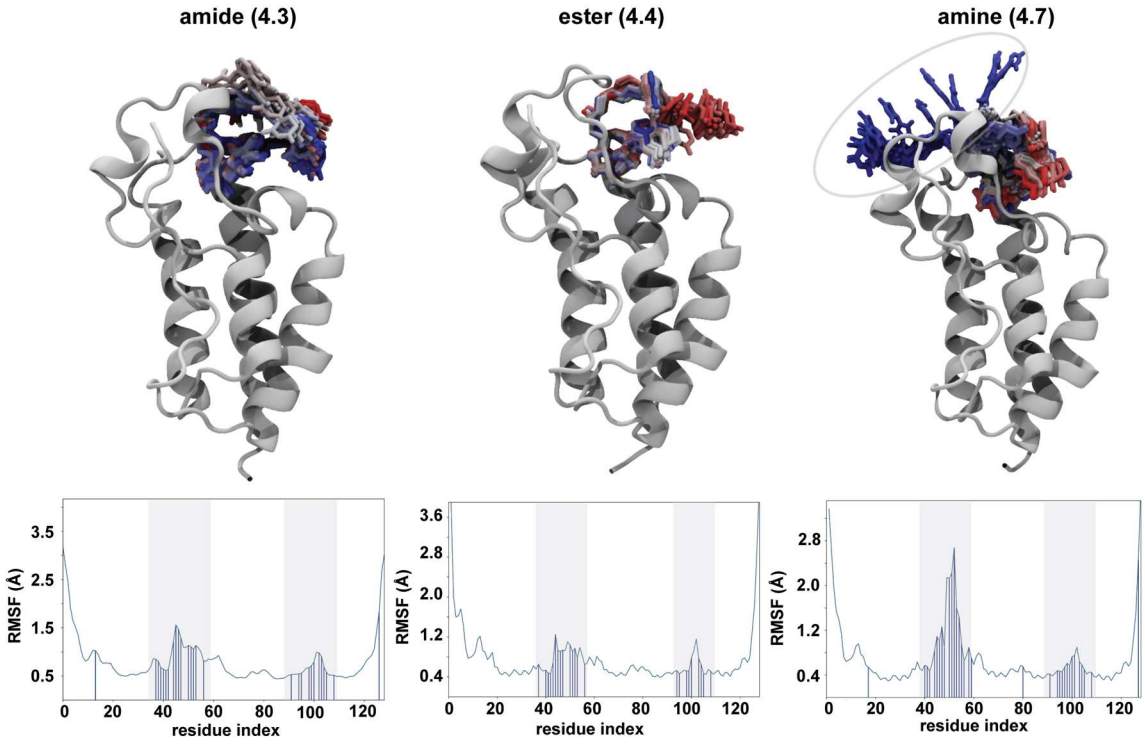

Figure 4.7 Molecular dynamic simulations of PROTACs **4.3**, **4.4**, and **4.7** bound to the BRD4-BD1 crystal structure. Time-lapse snapshots from 250-ns simulations are shown overlaid and depicted using color changes from red to blue indicating initial to final binding pose.

4.1.7 Conclusions

In conclusion, by harnessing the power of HTE we have developed four unique transformations, esterification, alkylation, ketonylation, and amination to quickly access a suite of BRD4 degraders with modifications to the linker. Importantly these adjustments to the linker connectivity have been achieved using JQ-1 as the target binding moiety and several types of E3 ligase recruiters. The ester, ketone, and alkane transformations all removed the HBD moiety imparted by the amide transformation, leading to higher LogD values, and increased cellular permeability. This is contrasted by the amine, which retains the hydrogen bond donor and has a significantly lower LogD due to its charge and is less permeable. The structural changes also affect binding with removal of the carbonyl having the largest effect. Computational studies

indicate this change is not tolerated in amine 7. These combined effects lead to more potent degraders when the amide is exchanged for an ester, alkane, or ketone, but ineffective degraders when exchanged for an amine. Given the impact new transformations have on the properties and of PROTACs, there is a need to develop new amine–acid couplings that perform on densely functionalized PROTACs.

4.2 Experimental data for Diverse Amine-Acid Coupling Reactions Modulate the Potency of BRD4 PROTACs

4.2.1 General information

All reactions were conducted in oven- or flame-dried glassware under an atmosphere of nitrogen unless stated otherwise. Reactions were set up in an MBraun LABmaster Pro Glove Box (H_2O level <0.1 ppm, O_2 level <0.1 ppm), or using standard Schlenk technique with a glass vacuum manifold connected to an inlet of dry nitrogen gas. N-methylpyrrolidinone was purchased as anhydrous and degassed by sparging overnight with nitrogen. Other solvents were purchased as anhydrous and used as received. Reagents were purchased from Sigma Aldrich, Alfa Aesar, Oakwood Chemical, Ambeed, or TCI Chemical. All chemicals were used as received. Glass1-dram (Fisherbrand™ parts No. 03-339-21B) or 2-dram vials (Fisherbrand™ parts No. 03-339-21D or ChemGlass #CG-4912-02) were used as reaction vessels, fitted with standard screwcaps (#03- 452-225 or #03-452-300) or with Teflon-coated silicone septa (#CG-4910-02 or CG-4910-02), and magnetic stir bars (Fisher Scientific #14-513-93 or #14-513-65; stirbars.com #SBM-0803-MIC or #SBM-1003-MIC).

^{1}H NMR spectra were recorded on a Varian MR-500 MHz, Varian MR-400 MHz, Bruker DPX, DRX, or AV spectrometers. Chemical shifts are reported in parts per million (ppm) and the spectra are calibrated to the resonance resulting from incomplete deuteration of the solvent

($CDCl_3$: 7.26 ppm; DMSO-d6: 2.50 ppm, qn; MeOD-d4: 3.31 ppm, qn; Acetonitrile-d3: 1.94 ppm, qn). ^{13}C NMR spectra were recorded on the same spectrometers with complete proton decoupling. Chemical shifts are reported in ppm with the solvent resonance as the internal standard ($CDCl_3$: 77.16 ppm, t; DMSO-d6: 39.52 ppm, sept; MeOD-d4: 49.00 ppm, sept, Acetonitrile-d3 1.39 ppm, m, 128.39 ppm, s.)). Data are reported using the abbreviations: app = apparent, s = singlet, d = doublet, t = triplet, q = quartet, p = pentet, h = hextet, m = multiplet, comp = complex, br = broad. Coupling constant(s) are reported in Hz. ^{19}F NMR spectra were recorded on the same spectrometers as above. ^{13}C and ^{19}F signals are singlets unless otherwise stated. ^{1}H-COSY, HSQC and HMBC were used where appropriate to facilitate structural determination.

High resolution mass spectrometry data (HRMS) were obtained on an Agilent 6230 TOF LC/MS equipped with ESI detector in positive mode and on a Micromass AutoSpec Ultima Magnetic Sector instrument with EI detector in positive mode. Reaction analysis was typically performed by thin-layer chromatography on silica gel or using a Waters I-class ACQUITY UPLC-MS (Waters Corporation, Milford, MA, USA) equipped with in-line photodiode array detector (PDA), evaporative light scattering detector (ELSD) and QDa mass detector (Both ESI positive and negative ionization mode). Typically, 0.1 μL sample injections were taken from acetonitrile solutions of reaction mixtures or products (~1 mg/mL). A partial loop injection mode was used with the needle placement at 2.0 mm from bottom of the wells and a 0.2 μL air gap at pre-aspiration and post-aspiration. Column used: Waters Cortecs UPLC C18+ column, 2.1mm × 50 mm with (Waters S5 #186007114) with Waters Cortecs UPLC C18+ VanGuard Pre-column 2.1mm × 5 mm (Waters #186007125), Mobile Phase A: 0.1 % formic acid in Optima LC/MS-grade water, Mobile Phase B: 0.1% formic acid in Optima LC/MS-grade MeCN. Flow rate: 0.8

mL/min. Column temperature: 45 °C. The PDA sampling rate was 20 points/sec. The QDa detector monitored m/z 150-750 with a scan time of 0.06 seconds and a cone voltage of 30 V. The ELSD had a gain of 750, data rate of 10 pps, time constant "normal" 0.2000 sec, a gas pressure of 40.0 psi, with the nebulizer in cooling mode at 75% power level and the drift tube temperature set to 50 °C. The PDA detector range was between 210 nm – 400 nm with a resolution of 1.2 nm. 2 minute and 8-minute methods were used. The method gradients are below: 2 min method, 0 min: 0.8 mL/min, 95% 0.1% formic acid in water/5% 0.1% formic acid in acetonitrile; 1.5 min: 0.8 mL/min, 0.1% 0.1% formic acid in water/99.9% 0.1% formic acid in acetonitrile; 1.91 min: 0.8 mL/min, 95% 0.1% formic acid in water/5% 0.1% formic acid in acetonitrile. 8 min method, 0 min: 0.8 mL/min, 95% 0.1% formic acid in water/5% 0.1% formic acid in acetonitrile; 7.5 min: 0.8 mL/min, 0.1% 0.1% formic acid in water/99.9% 0.1% formic acid in acetonitrile; 7.91 min: 0.8 mL/min, 95% 0.1% formic acid in water/5% 0.1% formic acid in acetonitrile.

Flash chromatography was performed on silica gel (230 – 400 Mesh, Grade 60) under a positive pressure of Nitrogen. Thin Layer Chromatography was performed on 25 μm TLC Silica gel 60 F254 glass plates purchased from Fisher Scientific (part number: S07876). Visualization was performed using ultraviolet light (254 and 365 nm) and/or potassium permanganate ($KMnO_4$) stain. Reverse-phase prep-HPLC was performed on a Teledyne ISCO CombiFlash® EZ Prep (RediSep Prep C18, 100 Å, 5 μm, 150 mm × 20 mm (part no. 692203810) using 0.1% formic acid in water and 0.1% formic acid in acetonitrile eluent.

4.2.2 General Procedures

4.2.2.1 General Procedure 4.1: Synthesis of non-pomalidomide based Katritzky salts.[53]

A flame dried 2-dram vial equipped with a Teflon-coated stir bar was charged with amine or amine HCl salt (1.1 equiv). This was suspended/dissolved in ethanol (2.0 mL/mmol amine) and if starting from HCl salt triethylamine added (2.2 equiv). The suspension was stirred at room temperature for 30 minutes and 500 rpm followed by the addition of triphenylpyrylium tetrafluoroborate (1.0 equiv). The resultant red solution was stirred at 60 °C and 500 rpm for 16 hours. Upon cooling to room temperature, the reaction was diluted with DCM (40 mL/mmol amine), and washed with aqueous hydrochloric acid (0.5 M, 20 mL/mmol amine) The organic layer was separated, dried over sodium sulfate, filtered, and concentrated *in vacuo*. The residue was reconstituted in DCM (2.5 mL/mmol amine) and added dropwise to a vigorously stirred flask of diethyl ether (12 mL/ mmol amine). This suspension was stirred at 1000 rpm for 30 minutes, filtered, washed with diethyl ether, and dried under high vacuum to give the desired Katritzky salt.

4.2.2.2 General procedure 4.2: Procedure for HTE screen preparation

Stock solutions, or suspensions, were prepared as shown in the heatmap preparation table. In an inert atmosphere glovebox, all non-OEB-3b reagents were weighed and dissolved or suspended in anhydrous solvent to achieve their listed concentrations in table. Stock solutions of reagents were stirred until either a clear solution or a uniform slurry was achieved. A 24-well aluminum microvial (Analytical Sales & Services cat. no. 25243) was equipped with oven-dried shell vials (Analytical Sales & Services cat. no. 884001). A parylene-coated stir dowel (Analytical Sales & Services cat. no. 13258) was then added to each vial, and the apparatus moved into the glovebox. Stock solutions were dosed to the appropriate shell vials according to the plate map shown in table using single channel micropipetters. If catalyst/ligand combinations

were screened, these were dosed into the vials first and stirred for 30 minutes before dosing of the remaining reagents. The microvial plate was sealed, removed from the glove box, and stirred on a hot plate with heating at the indicated temperature for planned reaction time. The reactions were quenched by opening the reaction block and adding 400 μL of a 7 mg/mL caffeine in methanol solution as an internal standard. Reactions were then stirred for 5 minutes at room temperature and 1000 rpm. Using six channels of an eight channel micropipetter, from each reaction, a 50 μL aliquot of the quenched reaction mixture was added into a 96-well polypropylene collection plate (Analytical Sales & Services cat. no. 17P687). The solvent was evaporated by blowing nitrogen down on the analytical plate. Acetonitrile (600 μL) was added and mixed by pipetting up and down. The reactions were then analyzed by UPLCMS. The Product/Internal Standard value was produced by measuring the UV absorbance of desired product relative to the caffeine internal standard.

General procedure 4.2 alkane & ketone addendum:

For the alkane and ketone forming reactions, the carboxylic acid required activation. This was done *in situ* either via an acyl fluoride or an acyl carbonate. For the acyl fluoride 1 equivalent of proton sponge and 1 equivalent of Tetramethylfluoroformamidinium hexafluorophosphate (TFFH) relative to the acid were weighed into the same vial. This mixture was stirred at 500 rpm in NMP for 30 minutes before dosing. For acyl carbonates 1.5 equivalents of dimethyldicarbonate with respect to the acid were dosed into a n-methyl pyrrolidinone (NMP) solution of the acid and stirred for 30 minutes before dosing. Additionally, all Katritzky salts were pre-stirred with manganese for 5 minutes prior to dosing. All other steps are the same as general procedure **4.2**.

4.2.2.3 General Procedure 4.3 Alkane/Ketone singleton optimization:

In a nitrogen filled glovebox, an oven dried two-dram vial (vial A), equipped with a Teflon-coated stir bar, was charged with nickel source (5 μmol**,** 40 mol %, unless otherwise indicated)**,** ligand (5 μmol, 40 mol%, unless otherwise indicated) and dry solvent (200 μL for 0.025 M reactions). This was stirred at 500 rpm for 30 min. Outside of the glove box two oven dried 2-dram vials, equipped with Teflon-coated stir bars, one (vial B) was charged with **4.10** (10 mg, 12.5 μmol, 1.0 equiv). Another (vial C) was charged with **4.1** (10 mg, 50 μmol, 2.0 equiv, unless otherwise indicated). These two vials (vial B and C) were then transferred into the glove box. NMP (200 μL for 0.025 M reactions) was added to the vial C followed by addition of either dimethyldicarbonate (1.5 equiv relative to acid) or proton sponge (1 equiv) and TFFH (1.0 equiv of each relative to acid). Vial C was stirred at 500 rpm for 20 minutes before the mixture was transferred into vial A. To vial B was added dry NMP (100 μL for 0.025 M reaction), and manganese (5.5 mg, 100 μmol, 4.0 equiv, unless otherwise indicated). This vial was stirred at 700 rpm for two minutes and the reaction mixture was transferred to vial A. If present, the additive was added to the vial before it was capped, sealed with electrical tape, removed from the glovebox, and heated at the indicated temperature at 800 rpm for 14 hours.

4.2.2.4 General procedure 4.4 amine singleton optimization with catalyst/acid prestir:

A stock solution of catalyst was prepared in flame dried one–dram vial, equipped with a Teflon coated stir bar. Inside the glovebox the vial was charged with Platinum II Chloride (1.7 mg, 6.2 μmol, 10x5 mol%), and BrettPhos (6.7 mg, 12.4 μmol, 10x10 mol%). This was suspended in 100 μL of the desired solvent (usually dioxane) and stirred at for 30 minutes at 40 °C and 500 rpm. The yellow solution was cooled to room temperature and had phenylsilane (unless otherwise indicated, 77 μL, 620 μmol, 10x5 equiv) (**CAUTION Exothermic)** added and

18 µL of solution was quickly transferred to a vial containing **4.1** (7.5 mg, 18 µmol, 1.5 equiv) dissolved/suspended in 100 µL the desired solvent. This was stirred at 80 °C and 500 rpm for 15 minutes (unless otherwise indicated) and transferred to a vial containing **4.2** (5.0 mg, 12 µmol, 1.0 equiv). This was heated at 80 °C (unless otherwise indicated) and 500 rpm overnight. The next morning the reaction was quenched with 400 µL of 7mg/mL caffeine in methanol solution and each reaction analyzed via LC/MS.

4.2.2.5 General procedure 4.5 amine singleton optimization without catalyst/acid prestir

A stock solution of catalyst was prepared in flame dried one–dram vial, equipped with a Teflon coated stir bar. Inside the glovebox the vial was charged with Platinum II Chloride (1.7 mg, 6.2 µmol, 10x5 mol%), and BrettPhos (6.7 mg, 12.4 µmol, 10x10 mol%). This was suspended in 100 µL of the desired solvent (usually dioxane) and stirred at for 30 minutes at 40 °C and 500 rpm. The yellow solution was cooled to room temperature and had phenylsilane (77 µL, 620 µmol, 10x5 equiv) (**CAUTION Exothermic)** added and 18 µL of solution was quickly transferred to a vial containing **4.2 or equivalent amount of salt** (5.0 mg, 12 µmol, 1.0 equiv) and **4.1** (7.5 mg, 18 µmol, 1.5 equiv) dissolved/suspended in 100 µL the desired solvent. This was heated at 80 °C (unless otherwise indicated) and 500 rpm overnight. The next morning the reaction was quenched with 400 µL of 7mg/mL caffeine in methanol solution and each reaction analyzed via LC/MS.

4.2.2.6 General Procedure 4.6 synthesis of amide products:

A flamed-dried two-dram vial, equipped with a Teflon-coated stir bar, was charged JQ1 (40.0 mg, 0.1 mmol, 1 equiv) and PyAOP (52.1 mg, 0.1 mmol, 1 equiv). To this vial was added dry DMF (0.5 mL) followed by N-methyl imidazole (8.2 µL, 0.1 mmol, 1 equiv). The resulting homogeneous solution was stirred at ambient temperature for 10 min. To another flamed-dried

two-dram vial was added amine HCl salt (0.1 mmol, 1 equiv) and N-methyl imidazole (12.3 µL, 0.15 mmol, 1.5 equiv) before the addition of DMF (0.5 mL). The amine mixture was then transferred to the first vial. The combined homogeneous solution was stirred at ambient temperature for 14 hours. Upon completion of the reaction the reaction was worked up and purified as described.

4.2.2.7 General Procedure 4.7 synthesis of ester products:

An oven dried two-dram vial, equipped with a Teflon-coated stir bar, was charged with Katritzky salt (0.10 mmol, 1.0 equiv), carboxylic acid (0.10 mmol, 1.0 equiv), potassium *tert*-butoxide (11.2 mg, 0.10 mmol, 1.0 equiv), and finely ground potassium iodide (32.0 mg, 0.20 mmol, 2.0 equiv). The vial was then capped, evacuated, and refilled with N_2 three times. 1.00 mL of dioxane was added to the reaction vessel via syringe, and the reaction heated at 110 °C for 22 hours at a stir rate of 500 rpm. Upon completion, the reaction was filtered through a celite plug and washed with DCM. The filtrate was evaporated *in vacuo* and purified as described.

4.2.2.8 General Procedure 4.8 one pot synthesis of ester products:

An oven dried two-dram vial, equipped with a Teflon-coated stir bar, was charged with amine hydrochloride salt (0.10 mmol, 1.0 equiv), triphenyl pyrylium tetrafluoroborate (39.6 mg, 0.10 mmol, 1.0 equiv), carboxylic acid (0.10 mmol, 1.0 equiv), potassium *tert*-butoxide (22.4 mg, 0.20 mmol, 2.0 equiv), and finely ground potassium iodide (32.0 mg, 0.20 mmol, 2.0 equiv). The vial was then capped, evacuated, and refilled with N_2 three times. 1.00 mL of dioxane was added to the reaction vessel via syringe, and the reaction heated at 110 °C for 22 hours at a stir rate of 500 rpm. Upon completion, the reaction was filtered through a celite plug and washed with DCM. The filtrate was evaporated *in vacuo* and purified as described.

4.2.2.9 General Procedure 4.9 synthesis of amine products:

In a nitrogen filled glovebox, an oven dried one-dram vial, equipped with a Teflon-coated stir bar, was charged with Platinum (II) chloride (1.3 mg, 0.005 mmol, 0.05 equiv) and Brettphos (5.3 mg, 0.01 mmol, 0.01 equiv). 100 μL of 1:1 dioxane:DMSO was added, and the solution stirred for 20 minutes at 30 °C and 300 rpm. Outside of the glovebox, an additional oven dried one-dram vial, equipped with a Teflon-coated stir bar, was charged with amine (0.1 mmol, 1.0 equiv) and carboxylic acid (0.15 mmol, 1.5 equiv). 900 μL of solvent was added. The catalyst solution was removed from the glovebox, cooled to room temperature, and phenylsilane (61 μL, 0.5 mmol, 5.0 equiv) added via syringe. **Note the solution will bubble vigorously and generate hydrogen gas.** The yellow solution was transferred via syringe to the amine/acid vial which was subsequently heated at 70°C for 16 hours and a stir rate of 500 rpm. Upon completion, the reaction was worked up and purified as described.

4.2.2.10 General Procedure 4.10 synthesis of alkane products:

In a nitrogen filled glovebox, an oven dried two-dram vial, equipped with a Teflon-coated stir bar, was charged with $NiBr_2$*glyme (12 mg, 0.04 mmol, 0.40 equiv), dtbpy (10.7 mg, 0.04 mmol, 0.40 equiv), and 800 μL of NMP (vial A). This was stirred wat 500 rpm for 30 min. During this time, an oven dried two-dram vial, equipped with a Teflon-coated stir bar, was charged with Katritzky salt (0.10 mmol, 1.0 equiv) (vial B). Another oven dried two-dram vial, equipped with a Teflon-coated stir bar, was charged with acid (0.20 mmol, 2.0 equiv), proton sponge (42.8 mg, 0.20 mmol, 2.0 equiv), and TFFH (52.8 mg, 0.20 mmol, 2.0 equiv) (Vial C). These vials were transferred to the glovebox. Vial C had 800 μL of NMP added and was stirred for 20 minutes followed by addition into vial A. To vial C was added 400 μL of NMP and manganese (22 mg, 0.40 mmol, 4.0 equiv,). This vial was stirred at 700 rpm for two minutes and

transferred to vial A. Vial A was sealed with electrical tape, removed from the glovebox, and heated at 70 °C and 800 rpm for 14 hours. Upon completion, the reaction was filtered through a pad of celite using 30 mL of ethyl acetate. The filtrate was washed with 20 mL of saturated sodium sulfate. The organic layer was collected, dried with sodium sulfate, and concentrated *in vacuo*. Purification was achieved as described.

4.2.2.11 General Procedure 4.11 synthesis of JQ1 based ketone products:

In a nitrogen filled glovebox, an oven dried two-dram vial, equipped with a Teflon-coated stir bar, was charged with Nickel(II) bis(acetylacetonate) (12.5 mg, 0.04 mmol, 0.40 equiv), (Z)-N'-cyanopicolinimidamide (5.8 mg, 0.04 mmol, 0.40 equiv), and 800 µL of NMP (vial A). This was stirred at 500 rpm for 30 min. During this time, an oven dried two-dram vial, equipped with a Teflon-coated stir bar, was charged with Katritzky salt (0.10 mmol, 1.0 equiv) (vial B). Another oven dried two-dram vial, equipped with a Teflon-coated stir bar, was charged with acid (0.20 mmol, 2.0 equiv) (vial C). These vials were transferred to the glovebox. Vial C had 800 µL of NMP and dimethyldicarbonate (32.2 µL, 40.2 mg, 0.30 mmol, 3.0 equiv) and was stirred at 500 rpm for 20 minutes followed by addition into vial A. To vial B was added 400 µL of NMP and manganese (22 mg, 0.40 mmol, 4.0 equiv,). This vial was stirred at 700 rpm for two minutes and transferred to vial A. Triethyl amine hydrochloride (28 mg, 0.20 mmol, 2.0 equiv) was added to the vial and it was capped, sealed with electrical tape, removed from the glovebox, and heated at 70 °C & 800 rpm for 14 hours. Upon completion, the reaction was filtered through a pad of celite using 30 mL of ethyl acetate. The filtrate was washed with 20 mL of saturated sodium sulfate. The organic layer was collected, dried with sodium sulfate, and concentrated *in vacuo*. Purification was achieved as described.

4.2.3 Preparation of starting materials

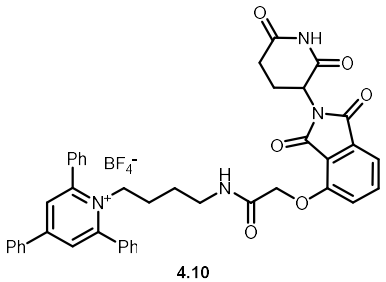

4.10

1-(4-(2-((2-(2,6-dioxopiperidin-3-yl)-1,3-dioxoisoindolin-4-yl)oxy)acetamido)butyl)-2,4,6-triphenylpyridin-1-ium tetrafluoroborate (4.10)

A flame dried 2-dram vial equipped with a Teflon-coated stir bar was charged with **4.2** (400.0 mg, 1.0 mmol, 1.0 equiv), triphenylpyrylium tetrafluoroborate (396.2 mg, 1.0 mmol, 1.0 equiv), and powdered 4Å molecular sieves (400 mg). This was suspended/dissolved in dichloromethane (DCM) (4.0 mL) and triethylamine added (151.7 mg, 209 µL, 1.50 mmol, 1.5 equiv). The suspension was stirred for one hour followed by the addition of acetic acid (126 mg, 120 µL, 2.10 mmol, 2.1 equiv). The resultant red solution was stirred at room temperature and 500 rpm for 16 hours. Upon completion, the reaction was filtered through a pad of celite and washed with DCM (40 mL). This was washed with aqueous hydrochloric acid (0.5 molar, 20 mL) The organic layer was separated, dried over sodium sulfated, and removed *in vacuo*. The residue was reconstituted in DCM (2.5 mL) and added dropwise to a vigorously stirred flask of diethyl ether (12 mL). This suspension was stirred at 1000 rpm for 30 minutes, filtered, washed with diethyl ether, and dried to give the desired Katritzky salt as a pale-yellow powder 260 mg (51.7% yield).

^{1}H NMR (499 MHz, $CDCl_3$) δ 8.56 (s, ^{1}H), 7.86 (s, 2H), 7.82 – 7.77 (m, 4H), 7.75 (d, *J* = 2.0 Hz, ^{1}H), 7.74 – 7.68 (m, 2H), 7.54 – 7.43 (m, 9H), 7.37 (t, *J* = 6.8 Hz, 1H), 7.19 (d, *J* = 8.4 Hz, 1H), 4.97 (dd, *J* = 12.1, 5.6 Hz, 1H), 4.55 (s, 2H), 4.45 (t, *J* = 8.0 Hz 2H), 2.87 (q, *J* = 6.7 Hz, 2H), 2.83 – 2.67 (m, 3H), 2.16 –2.09 (m, 1H), 1.53 (p, *J* = 9.2 Hz, 2H), 1.02 (p, *J* = 7.1 Hz, 2H).

^{13}C NMR (126 MHz, $CDCl_3$) δ 171.4, 168.5, 167.1, 166.8, 166.1, 156.7, 155.8, 154.8, 137.2, 134.0, 133.6, 132.8, 132.3, 131.2, 129.9, 129.5, 129.2, 128.3, 126.9, 120.3, 118.3, 117.5, 68.3, 54.6, 49.4, 37.8, 31.4, 27.2, 26.1, 22.6, 8.8.

^{19}F NMR (470 MHz, $CDCl_3$) δ -152.3, -152.4.

HRMS (ESI) Calculated $C_{42}H_{37}N_4O_6^+$ $[M\text{-}BF_4]^+$: 693.2708, Found 693.2711.

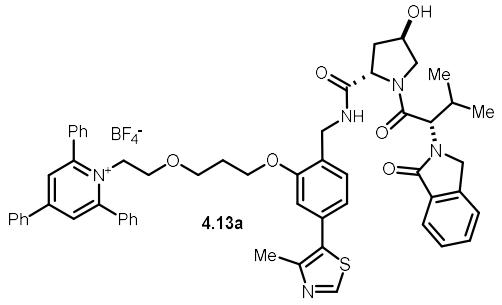

1-(2-(3-(2-(((2*S*,4*R*)-4-hydroxy-1-((*S*)-3-methyl-2-(1-oxoisoindolin-2-yl)butanoyl)pyrrolidine-2-carboxamido)methyl)-5-(4-methylthiazol-5-yl)phenoxy)propoxy)ethyl)-2,4,6-triphenylpyridin-1-ium tetrafluoroborate (4.13a)

4.13a was prepared from the HCl salt of **4.13** on a 0.53 mmol scale via general procedure 4.1 to give 351 mg (64.0%) of a pale-yellow solid.

^{1}H NMR (499 MHz, $CDCl_3$) δ 8.39 (s, 1H), 7.58 (s, 2H), 7.52 (d, *J* = 8.1 Hz, 4H), 7.45 (d, *J* = 7.1 Hz, 2H), 7.42 (dd, *J* = 7.5, 1.4 Hz, 1H), 7.28 – 7.20 (m, 7H), 7.20 – 7.12 (m, 4H), 7.08 (d, *J* = 7.2 Hz, 2H), 7.03 (d, *J* = 7.7 Hz, 1H), 7.01 – 6.97 (m, 1H), 6.68 (dd, *J* = 7.7, 1.5 Hz, 1H), 6.43 (d, *J* = 1.6 Hz, 1H), 4.55 (t, *J* = 5.8 Hz, 2H), 4.47 (d, *J* = 10.9 Hz, 1H), 4.41 – 4.30 (m, 2H), 4.18 (dt, *J* = 9.6, 6.2 Hz, 2H), 4.11 – 4.02 (m, 2H), 3.98 (dt, *J* = 11.4, 1.9 Hz, 1H), 3.53 (t, *J* = 6.0 Hz, 2H), 3.41 (d, *J* = 3.8 Hz, 1H), 3.39 (d, *J* = 3.7 Hz, 1H), 3.00 (dt, *J* = 11.5, 5.9 Hz, 4H), 2.20 (s, 3H), 2.06 (ddt, *J* = 12.0, 10.5, 4.4 Hz, 2H), 1.86 – 1.78 (m, 1H), 1.59 (p, *J* = 6.2 Hz, 2H), 0.63 (d, *J* = 6.5 Hz, 3H), 0.54 (d, *J* = 6.6 Hz, 3H).

^{13}C NMR (126 MHz, $CDCl_3$) δ 171.0, 170.2, 169.3, 157.4, 156.4, 155.9, 150.4, 148.4, 142.1, 133.8, 133.0, 132.4, 132.0, 131.9, 131.8, 131.6, 131.2, 129.8, 129.5, 129.4, 129.0, 128.2, 128.0, 126.5, 123.8, 123.0, 121.8, 111.9, 69.9, 67.7, 67.5, 64.5, 58.9, 58.6, 56.0, 54.1, 47.5, 38.6, 36.6, 29.1, 29.0, 19.1, 19.1, 19.1, 16.2

^{19}F NMR (470 MHz, $CDCl_3$) δ -152.7, -152.8.

HRMS (ESI) Calculated $C_{57}H_{58}N_5O_6S^+$ $[M\text{-}BF_4]^+$: 940.4102, Found 940.4110.

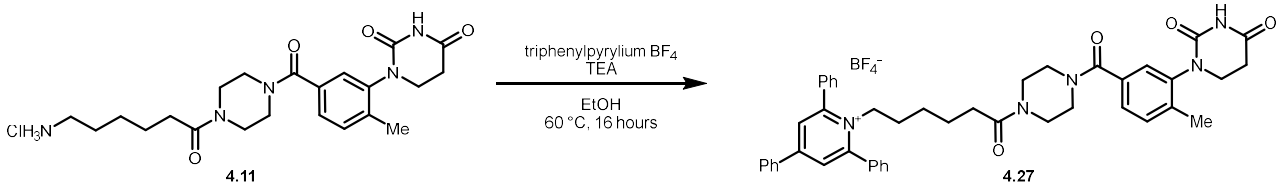

Scheme 4.1 synthesis of **4.27**.

1-(6-(4-(3-(2,4-dioxotetrahydropyrimidin-1(2H)-yl)-4-methylbenzoyl)piperazin-1-yl)-6-oxohexyl)-2,4,6-triphenylpyridin-1-ium tetrafluoroborate (4.27)

4.27 was prepared from **4.11** salt on a 0.48 mmol scale via general procedure 4.1 to give 272 mg (70.2%) of an orange solid.

^{1}H NMR (499 MHz, $CDCl_3$) δ 8.81 – 8.73 (m, 1H), 8.43 (t, *J* = 4.8 Hz, 3H), 7.87 (d, *J* = 5.7 Hz, 2H), 7.82 – 7.73 (m, 6H), 7.72 (q, *J* = 6.2, 4.6 Hz, 3H), 7.60 (q, *J* = 3.1 Hz, 6H), 7.56 – 7.48 (m, 4H), 7.33 – 7.28 (m, 2H), 4.41 (d, *J* = 8.9 Hz, 2H), 3.85 (s, 1H), 3.79 – 3.21 (m, 9H), 2.81 (q, *J* = 8.4, 6.6 Hz, 2H), 2.27 (d, *J* = 3.6 Hz, 3H), 2.08 – 1.93 (m, 2H), 1.48 (t, *J* = 10.2 Hz, 2H), 1.14 (t, *J* = 9.1 Hz, 2H), 0.80 (t, *J* = 8.9 Hz, 2H).

^{13}C NMR (126 MHz, $CDCl_3$) δ 169.5, 156.7, 156.6, 138.1, 134.0, 132.8, 132.4, 131.7, 131.3, 129.9, 129.9, 129.5, 129.2, 128.9, 128.3, 126.9, 126.9, 126.5, 66.0, 55.0, 45.3, 32.4, 31.6, 25.8, 23.8, 18.1, 15.4.

^{19}F NMR (470 MHz, $CDCl_3$) δ -152.3, -152.4.

HRMS (ESI) Calculated $C_{45}H_{46}N_5O_4^+$ [M-BF_4]$^+$: 720.3544, Found 720.3547.

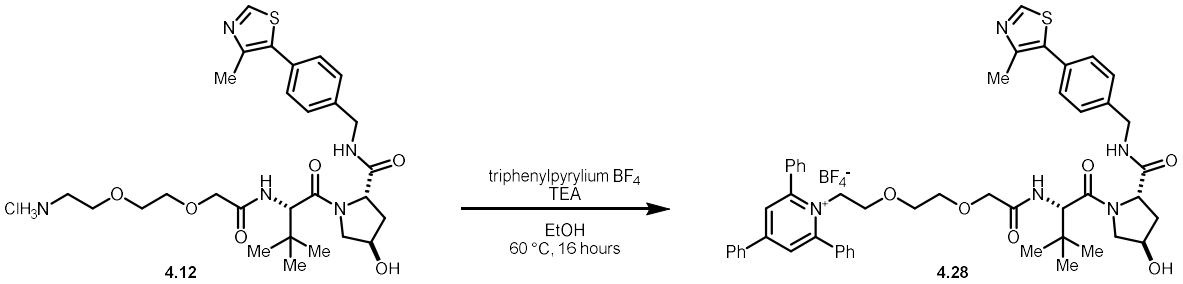

Scheme 4.2 synthesis of **4.28**

1-(2-(2-(2-(((S)-1-((2S,4R)-4-hydroxy-2-((4-(4-methylthiazol-5-yl)benzyl)carbamoyl)pyrrolidin-1-yl)-3,3-dimethyl-1-oxobutan-2-yl)amino)-2-oxoethoxy)ethoxy)ethyl)-2,4,6-triphenylpyridin-1-ium tetrafluoroborate (4.28)

4.28 was prepared from the HCl salt of **4.12** on a 0.35 mmol scale via general procedure 4.1 to give 217 mg (65.1%) of a white solid.

^{1}H NMR (500 MHz, $CDCl_3$) δ 8.66 (s, 1H), 7.85 (s, 2H), 7.77 (m, ,5H), 7.61 – 7.44 (m, 10H), 7.35 (d, *J* = 8.0 Hz, 2H), 7.24 (d, *J* = 8.2 Hz, 2H), 7.00 (d, *J* = 9.1 Hz, 1H), 5.03 (dt, *J* = 14.8, 6.5 Hz, 1H), 4.83 (dt, *J* = 14.9, 4.8 Hz, 1H), 4.75 (t, *J* = 8.3 Hz, 1H), 4.55 – 4.48 (m, 3H), 4.41 (dd, *J* = 15.4, 5.8 Hz, 1H), 3.92 (d, *J* = 11.1 Hz, 1H), 3.87 (d, *J* = 14.9 Hz, 1H), 3.67 (dd, *J* = 11.1, 3.6 Hz, 1H), 3.55 (d, *J* = 14.9 Hz, 1H), 3.47 – 3.43 (m, 1H), 3.41 – 3.16 (m, 5H), 2.47 (s, 3H), 0.91 (s, 9H).

^{13}C NMR (126 MHz, $CDCl_3$) δ 171.8, 171.3, 170.4, 168.6, 157.6, 155.9, 150.3, 148.4, 138.9, 133.9, 133.2, 132.4, 132.0, 131.2, 130.5, 129.9, 129.5, 129.4, 129.3, 128.2, 127.9, 126.6, 71.1, 70.5, 70.5, 70.4, 68.8, 60.5, 59.2, 57.0, 56.8, 54.4, 43.0, 37.5, 36.6, 29.8, 26.6, 21.2, 16.2, 14.3

^{19}F NMR (470 MHz, $CDCl_3$) δ -151.7, -151.8.

HRMS (ESI) Calculated $C_{51}H_{56}N_5O_6S^+$ $[M\text{-}BF_4]^+$: 866.3946, Found 866.3953.

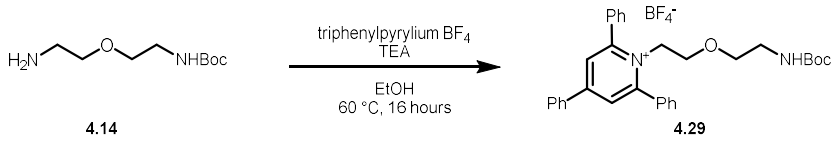

4.14 4.29

Scheme 4.3 synthesis **4.29**.

1-(2-(2-((tert-butoxycarbonyl)amino)ethoxy)ethyl)-2,4,6-triphenylpyridin-1-ium tetrafluoroborate (4.29)

4.29 was prepared from tert-butyl (2-(2-aminoethoxy)ethyl)carbamate (**4.14**) on a 1.00 mmol scale via general procedure 4.1 to give 420 mg (72.2%) of a white solid.

^{1}H NMR (499 MHz, $CDCl_3$) δ 7.90 (dd, J = 3.2, 1.6 Hz, 2H), 7.81 (ddt, J = 9.9, 7.8, 1.9 Hz, 6H), 7.65 – 7.52 (m, 9H), 4.86 (t, J = 5.8 Hz, 2H), 4.50 (s, 1H), 3.28 (t, J = 4.7 Hz, 2H), 3.10 (q, J = 5.4, 4.6 Hz, 4H), 1.40 (s, 9H).

^{13}C NMR (126 MHz, $CDCl_3$) δ 157.6, 156.2, 134.0, 133.1, 132.4, 131.3, 129.9, 129.6, 129.6, 128.3, 126.7, 70.2, 67.8, 54.1, 40.0, 28.5.

^{19}F NMR (470 MHz, $CDCl_3$) δ -153.0, -153.1.

HRMS (ESI) Calculated $C_{32}H_{35}N_2O_3^+$ $[M\text{-}BF_4]^+$: 495.2642, Found 495.2627.

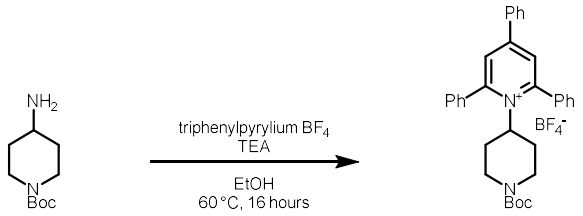

4.15 4.30

Scheme 4.4 Synthesis of **4.30**

1-(1-(tert-butoxycarbonyl)piperidin-4-yl)-2,4,6-triphenylpyridin-1-ium tetrafluoroborate (4.30)

4.30 was prepared on a 2.00 mmol scale from tert-butyl 4-aminopiperidine-1-carboxylate (**4.15**) via general procedure 4.1 to give 613 mg (53%) of a white solid.

^{1}H NMR (500 MHz, $CDCl_3$) δ 7.82 (s, 2H), 7.74 (m, 6H), 7.65 – 7.44 (m, 9H), 3.92 (m, 2H), 2.07 (m, 4H), 1.58 (s, 1H), 1.31 (s, 9H).

^{13}C NMR (126 MHz, $CDCl_3$) δ 157.3, 155.6, 154.3, 134.1, 133.8, 132.2, 131.2, 129.8, 129.4, 129.1, 128.4, 28.4.

^{19}F NMR (470 MHz, $CDCl_3$) δ -152.8, -152.8.

The spectra are consistent with the literature.[35]

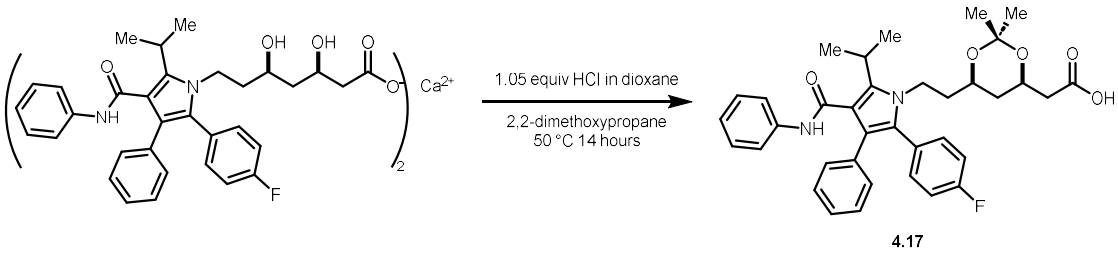

Scheme 4.5 synthesis of **4.17**.

To an oven dried 100 mL round bottom flask charged with a Teflon coated stir bar was added atorvastatin calcium (575 mg, 0.50 mmol, 0.5 equiv). A rubber septum was fitted, and the flask evacuated and refilled under a nitrogen atmosphere 3x. To the flask was added 30.0 mL of 2,2-dimethyoxypropane and 10.0 mL of acetone followed by HCl in dioxane (4 molar, 300 µL, 1.20 mmol, 1.20 equiv). The solution was stirred for 14 hours at 50 °C and 300 rpm. After cooling to room temperature, the reaction was concentrated *in vacuo* and reconstituted in DCM. This was purified by column chromatography 0à30% acetone in DCM to give 375 mg (62.9%) of **17** as a white solid.

R_f: 0.5 (streak, depends on concentration) in 85:15 DCM:acetone

^{1}H NMR (499 MHz, $CDCl_3$) δ 7.23 – 7.13 (m, 8H), 7.07 (d, *J* = 8.0 Hz, 2H), 6.99 (td, *J* = 8.5, 3.4 Hz, 3H), 6.87 (s, 1H), 4.20 (dtd, *J* = 13.1, 6.4, 2.3 Hz, 1H), 4.09 (ddd, *J* = 15.2, 10.0, 5.5 Hz, 1H), 3.84 (ddd, *J* = 14.5, 9.9, 6.3 Hz, 1H), 3.70 (d, *J* = 5.2 Hz, 1H), 3.57 (hept, *J* = 7.0 Hz, 1H), 2.53 (dd, *J* = 15.9, 6.9 Hz, 1H), 2.39 (dd, *J* = 15.9, 5.8 Hz, 1H), 1.74 – 1.60 (m, 2H), 1.53 (d, *J* = 7.1 Hz, 6H), 1.35 (dt, *J* = 10.0, 2.4 Hz, 1H), 1.32 (s, 3H), 1.07 (q, *J* = 11.9 Hz, 1H).

^{13}C NMR (126 MHz, $CDCl_3$) δ 175.2, 165.1, 162.4 (d, *J* = 247.8 Hz), 141.6, 138.4, 134.7, 133.3 (d, *J* = 8.1 Hz), 130.6, 128.9, 128.8, 128.4 (d, *J* = 3.3 Hz), 128.4, 126.7, 123.7, 122.0, 119.8, 115.5 (d, *J* = 21.5 Hz), 115.4, 99.1, 67.2, 66.5, 65.6, 41.0, 40.9, 38.0, 35.9, 30.0, 26.2, 21.9, 21.7, 19.8.

^{19}F NMR (470 MHz, $CDCl_3$) δ -113.6.

The spectra are consistent with the literature.[54]

4.2.4 Calibration curves of 4.3–7

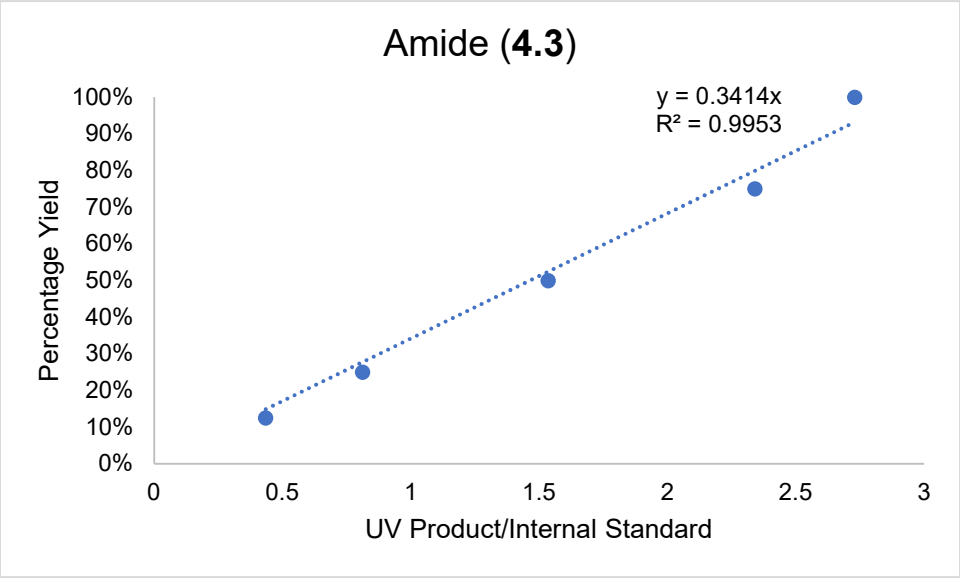

Figure 4.8 Calibration curve of UV integration of **4.3** relative to **0.70 mg/mL** caffeine internal standard.

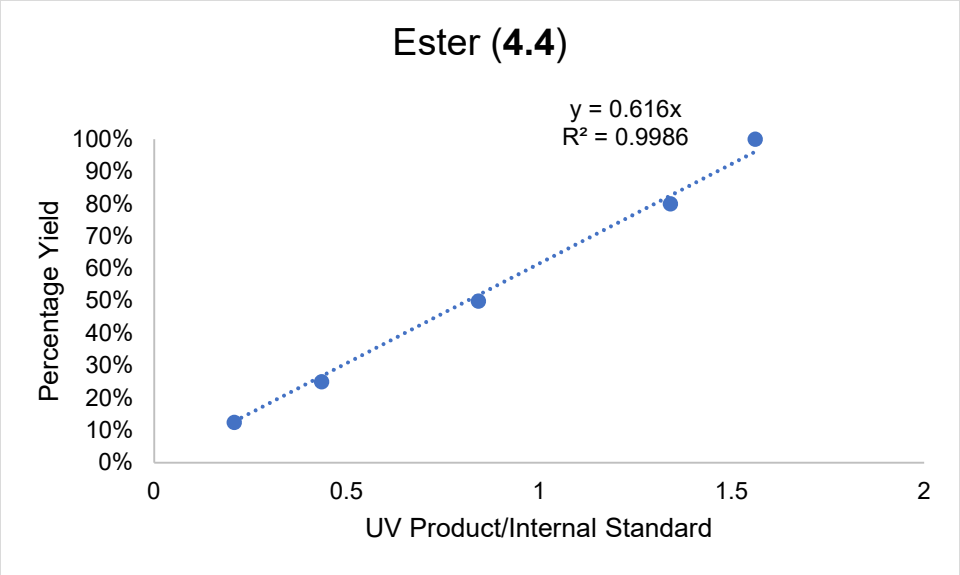

Figure 4.9: Calibration curve of UV integration of **4.4** relative to 0.70 mg/mL caffeine internal standard

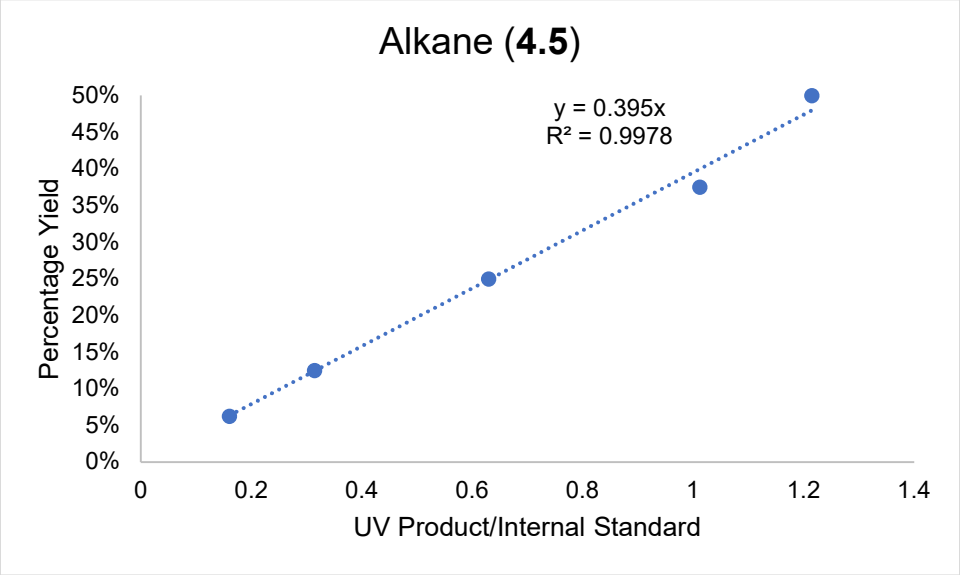

Figure 4.10: Calibration curve of UV integration of **4.5** relative to 0.70 mg/mL caffeine internal standard

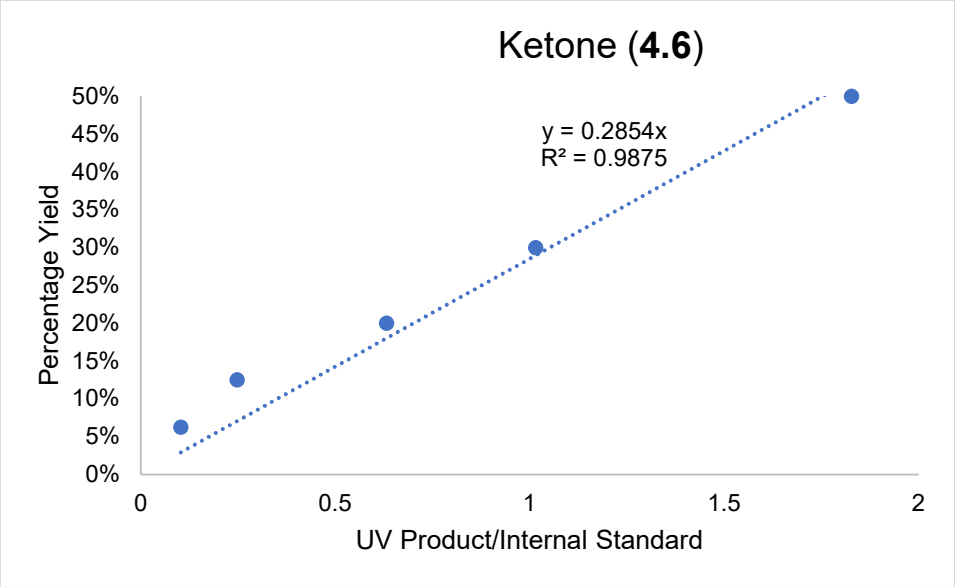

Figure 4.11: Calibration curve of UV integration of **4.6** relative to 0.70 mg/mL caffeine internal standard

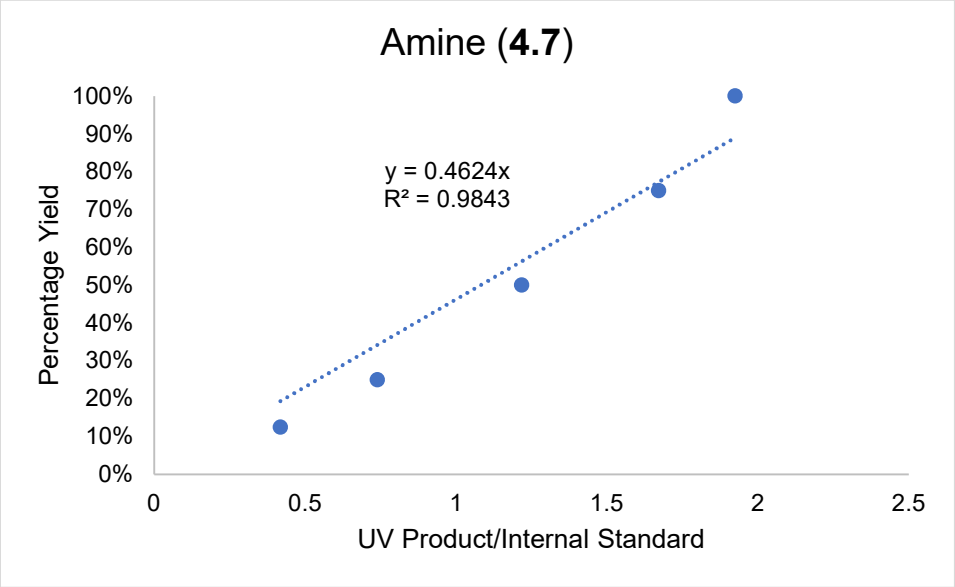

Figure S4.12: Calibration curve of UV integration of **4.7** relative to 0.70 mg/mL caffeine internal standard

4.2.5 Amide optimization screen 3 coupling agents, 4 bases, +/- DMAP:

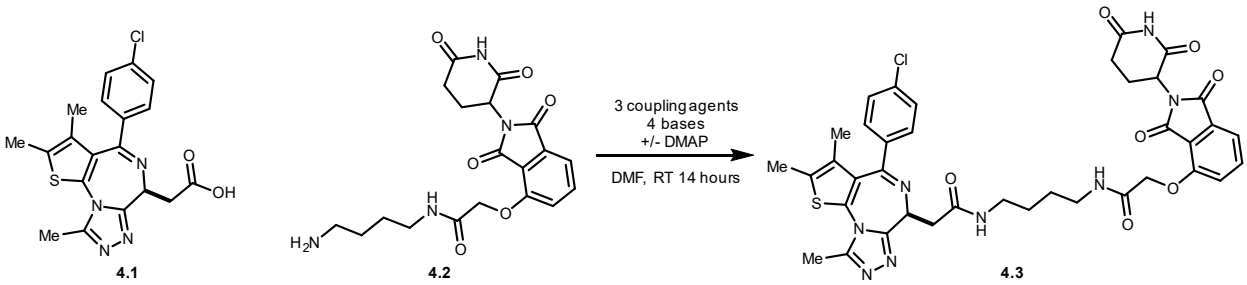

4.1 4.2 4.3

Table 4.3 Recipe for amide optimization screen. HATU = 1-[Bis(dimethylamino)methylene]-1H-1,2,3-triazolo[4,5-b]pyridinium 3-oxide hexafluorophosphate, HCTU = O-(1H-6-Chlorobenzotriazole-1-yl)-1,1,3,3-tetramethyluronium hexafluorophosphate, PyAOP = (7-Azabenzotriazol-1-yloxy)tripyrrolidinophosphonium hexafluorophosphate, EDC = N-Ethyl-N′-(3-dimethylaminopropyl)carbodiimide, HOBt = hydroxybenzotriazole, DMAP = N,N-Dimethylpyridin-4-amine. Reactions run at 0.1 M.

Reagents	Solvent	C_{stock} (M)	V_{dose} (µL)	Wells	Order Added
JQ1 Acid (4.1)	DMF	0.50	20	All	1
N,N-diisopropylethylamine	DMF	1.00	20	A,B,C,D, 1&2	2
1-methylimidazole	DMF	1.00	20	A,B,C,D, 3&4	2
2,6-lutidine	DMF	1.00	20	A,B,C,D, 5&6	2
HATU	DMF	0.50	20	A, 1-6	3
HCTU	DMF	0.50	20	B, 1-6	3
PyAOP	DMF	0.50	20	C, 1-6	3
EDC & HOBt	DMF	0.50/0.50	20	D, 1-6	3
DMAP	DMF	0.10	20	A,B,C,D, 1,3,5	4
DMAP Blank	DMF	solvent	20	A,B,C,D, 2,4,6	4
Pom partial protac (4.2)	DMF	0.50	20	All	5

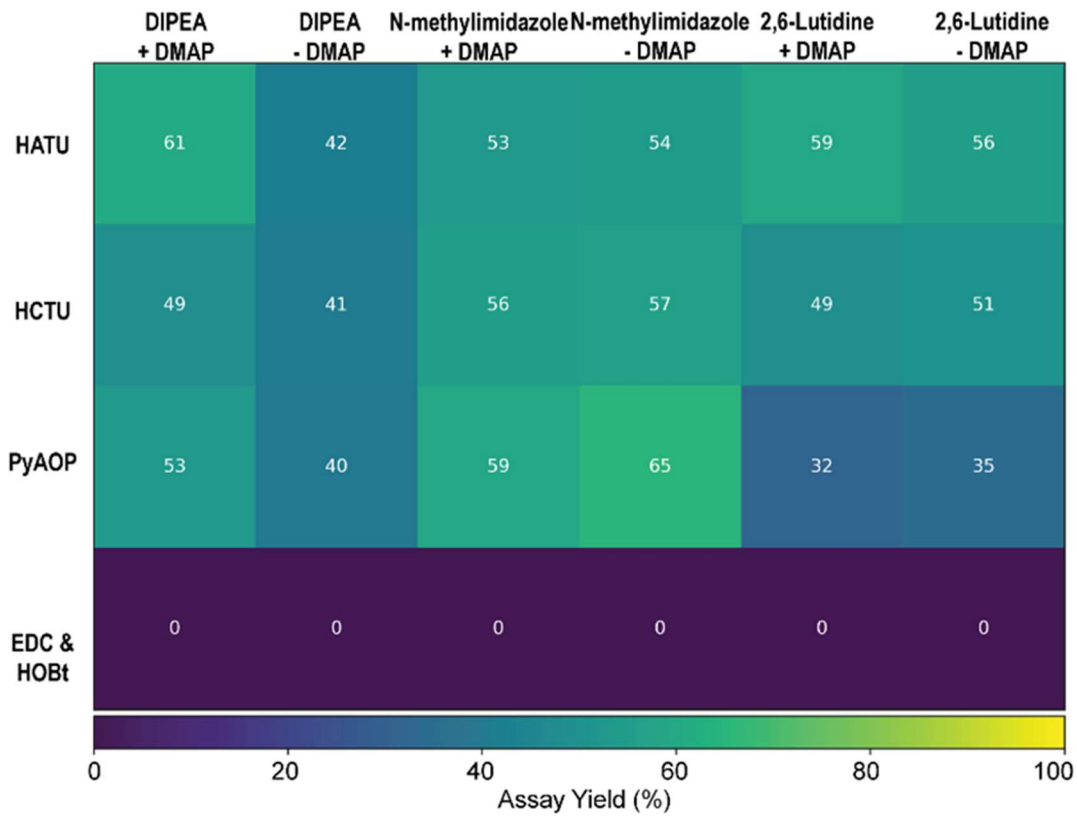

Figure 4.13 Results of amide optimization screen.

4.2.6 Ester Optimization Screen 6 promoters, 4 bases.

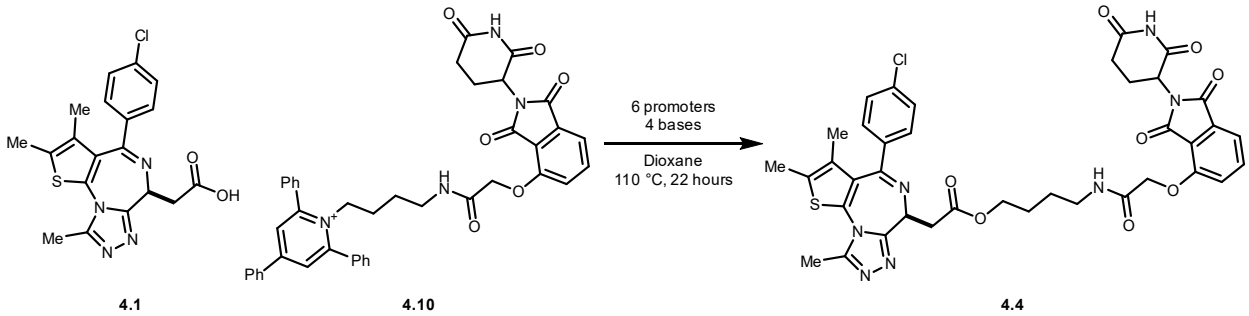

4.1 4.10 4.4

Table 4.4 Ester optimization screen recipe. Reactions run at 0.1 M.

Reagents	Solvent	C_{stock} (M)	V_{dose} (µL)	Wells	Order Added
JQ1 Acid (4.1)	dioxane	0.40	25	All	1
N,N-diisopropylethylamine	dioxane	0.40	25	A, 1-6	2
triethylamine	dioxane	0.40	25	B, 1-6	2
2,6-lutidine	dioxane	0.40	25	C, 1-6	2
potassium *tert*-butoxide	dioxane	0.40	25	D, 1-6	2
potassium iodide 0.5 equiv	dioxane	0.20	25	A,B,C,D, 1	3
potassium iodide 1.0 equiv	dioxane	0.40	25	A,B,C,D, 2	3
potassium iodide 2.0 equiv	dioxane	0.80	25	A,B,C,D, 3	3
sodium iodide	dioxane	0.40	25	A,B,C,D, 4	3
potassium bromide	dioxane	0.4	25	A,B,C,D, 5	3
2-bromo-2-methyl diethylmalonate	dioxane	0.08	25	A,B,C,D, 6	3
Pom Katritzky Salt (4.10)	dioxane	0.4	25	All	4

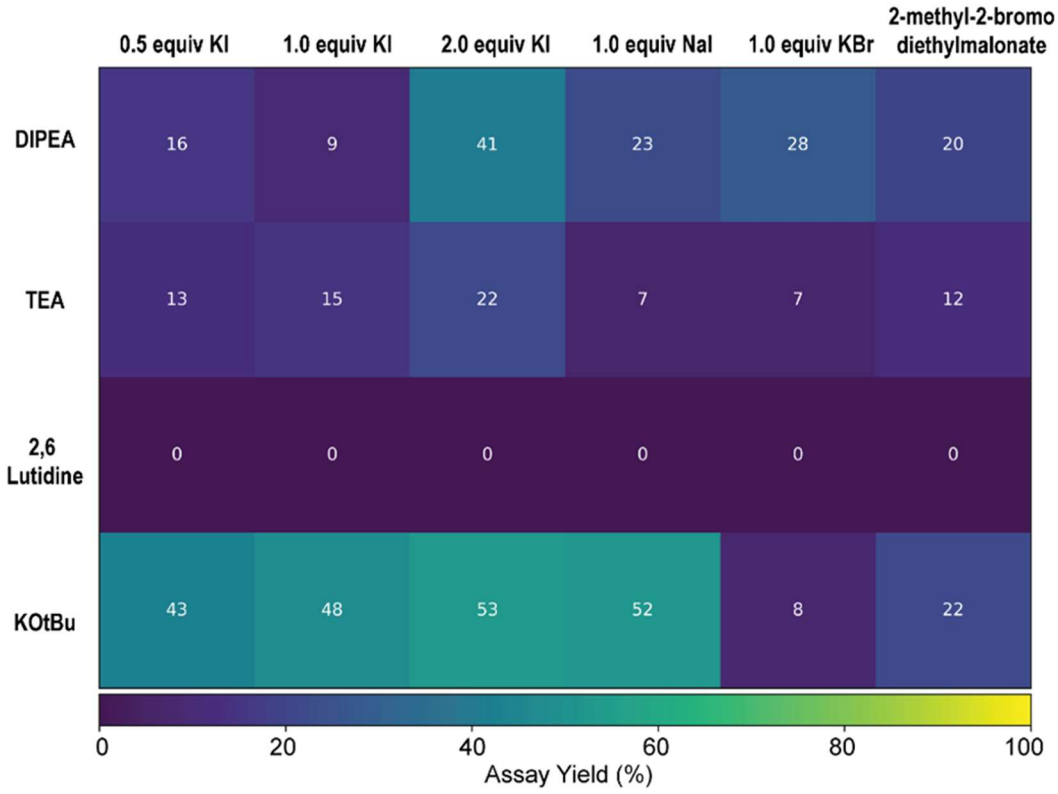

Figure 4.14 Results of ester optimization screen for desired product (4.4).

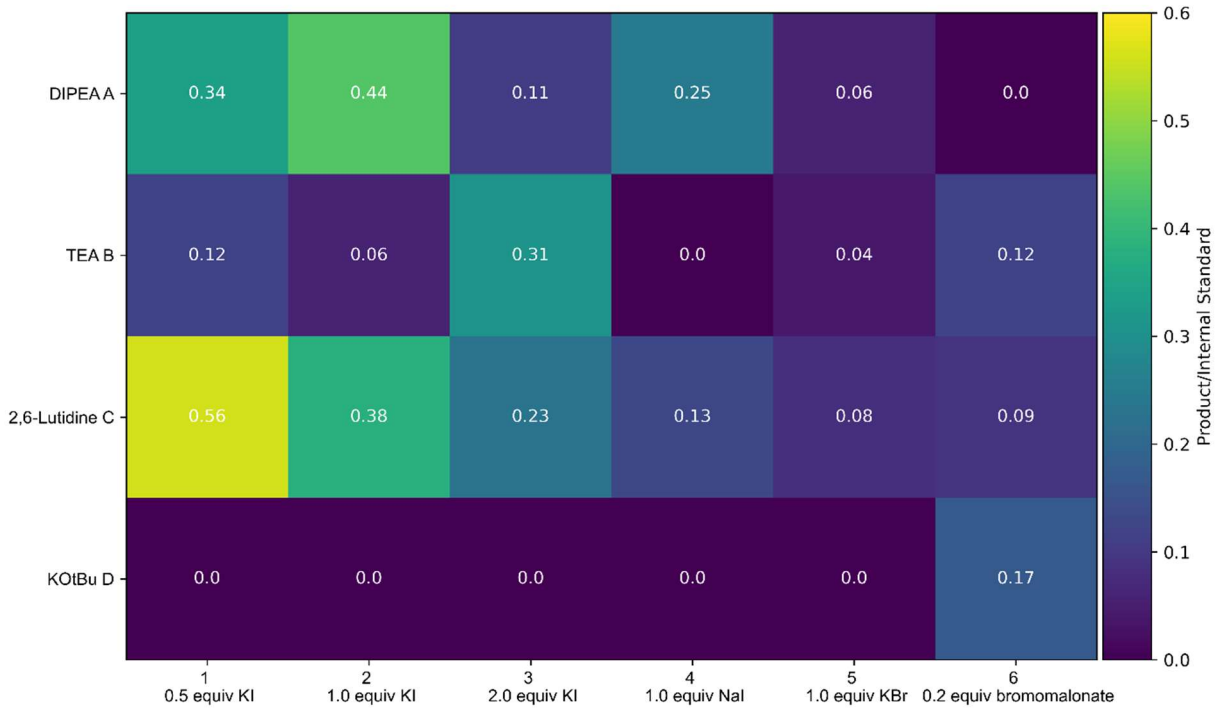

Figure 4.15 Product/internal standard results of ester optimization screen for isobaric byproduct.

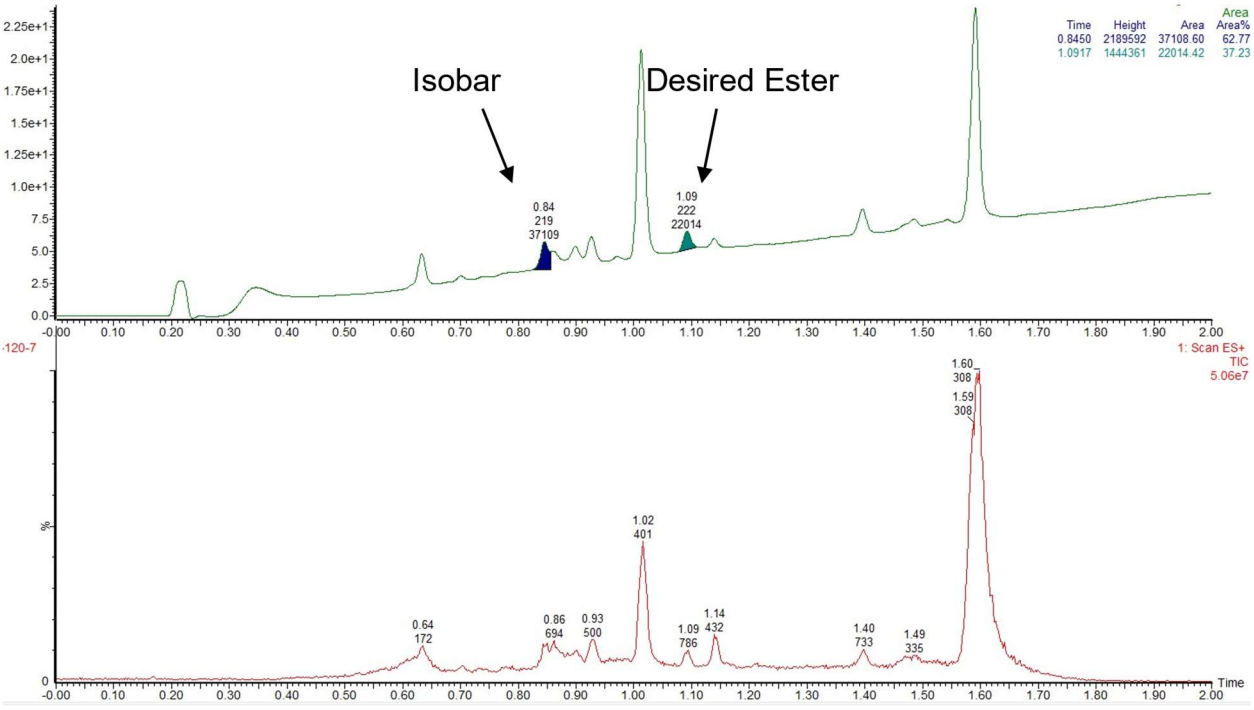

Figure 4.16 LC trace of esterification reaction using DIPEA. Two isobaric products.

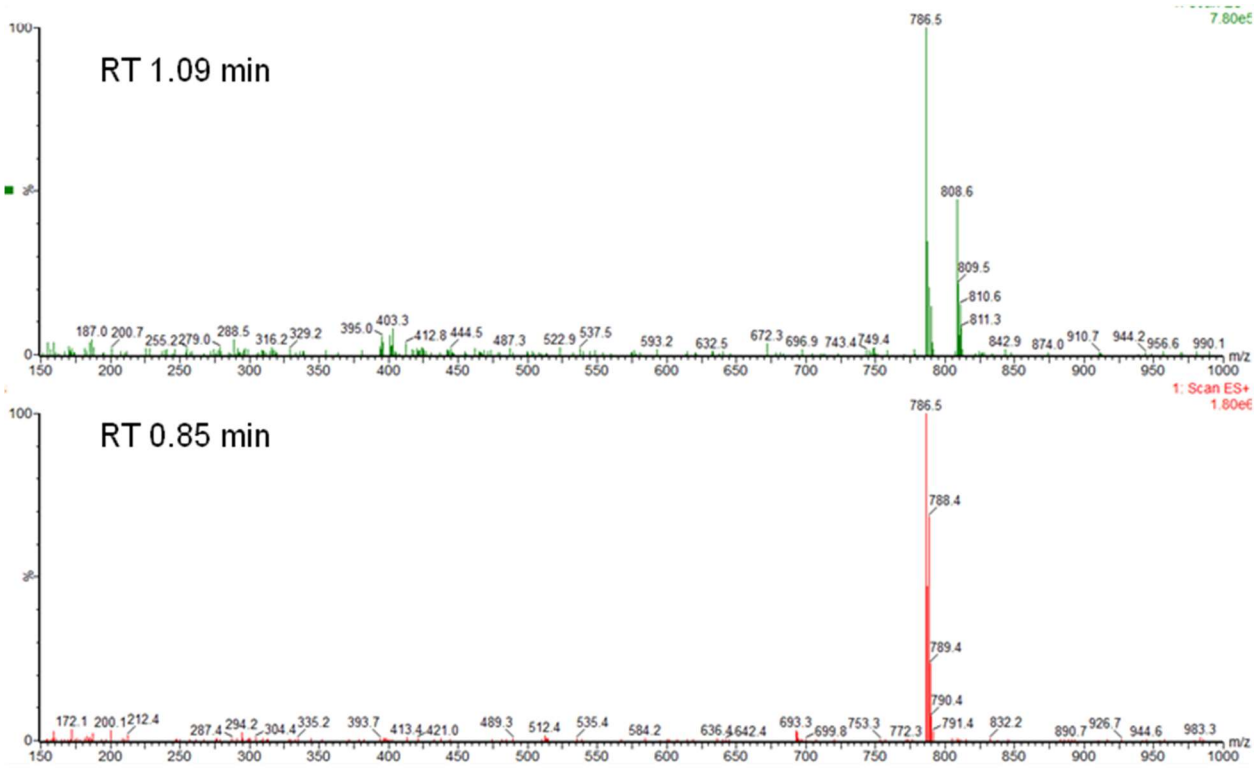

Figure 4.17 Mass spectra of ester (1.09 min) and isobar (0.85 min). The ester ionizes significantly as M+Na whereas the isobar which presumably exists as a persistent cation does not.

4.2.7 Alkane Optimization screen 8 additives, 3 Lewis acids.

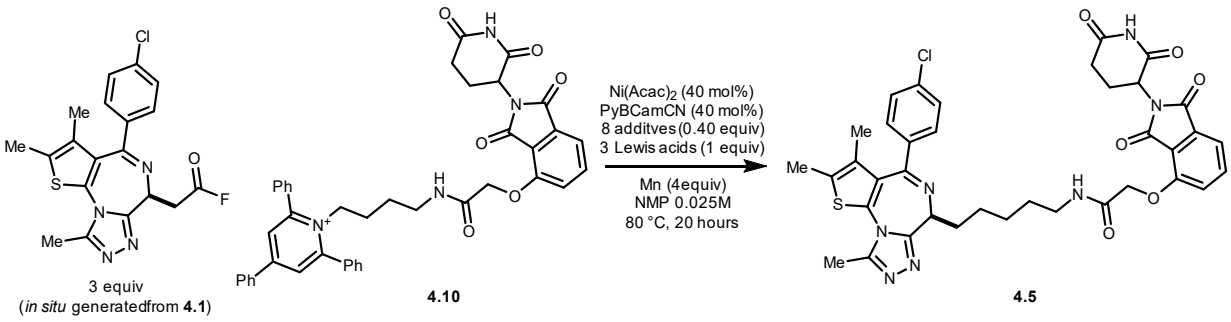

Table 4.5 Recipe for a screen investigating the effect of imide and Lewis Acid additives on alkane product. Reactions run at 0.025 M. PyBCamCN = (2Z,6Z)-N'2-N'6-dicyanopyridine-2,6-bis(carboximidamide).

Reagents	Solvent	C_{stock} (M)	V_{dose} (µL)	Wells	Order Added
Nickel(II) Acetylacetonate/PyBCamCN	NMP	0.06/0.06	17	All	1
Additive Blank	NMP	N/A	17	A, 1,3,5	2
Hydantoin	NMP	0.06	17	A, 2,4,6	2
Succinimide	NMP	0.06	17	B, 1,3,5	2
Hexahydrophthalimide	NMP	0.06	17	B, 2,4,6	2
Phthalimide	NMP	0.06	17	C, 1,3,5	2
3-methyl-3-phenylsuccinimide	NMP	0.06	17	C, 2,4,6	2
N-methylhydantoin	NMP	0.06	17	D, 1,3,5	2
Phenytoin	NMP	0.06	17	D, 2,4,6	2
JQ1 Acyl Fluoride **(4.8)**	NMP	0.45	17	All	3
Pom Katritzky Salt **(4.10)**	NMP	0.15	17	All	4
Manganese	NMP	1.80	17	All	5
No Lewis Acid	NMP	N/A	17	A,B,C,D 1&2	6
Ruthenium (III) Chloride	NMP	0.15	17	A,B,C,D 3&4	6
Gallium Chloride	NMP	0.15	17	A,B,C,D 5&6	6

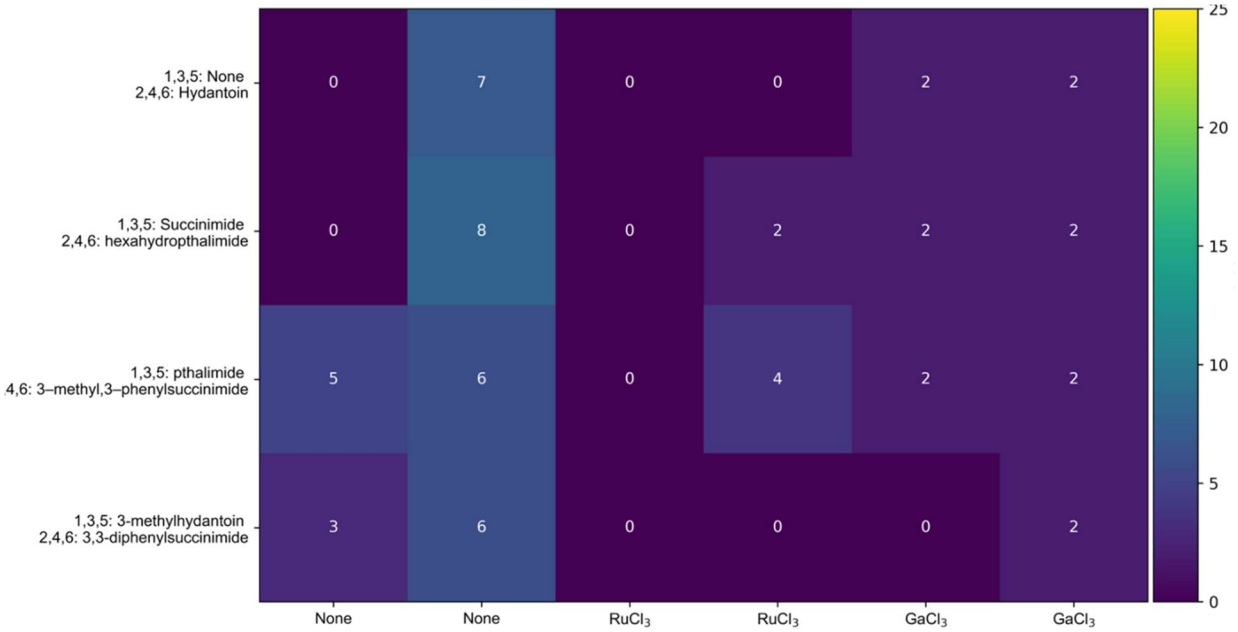

Figure 4.18 Results of screen examining the effect of imide additives and Lewis Acids. Assay yields are scaled to 25% for clarity.

4.2.8 Additional alkane screen 2 Nickel Sources, 2 Ligands, 3 Bronsted acids, +/- Hydantoin

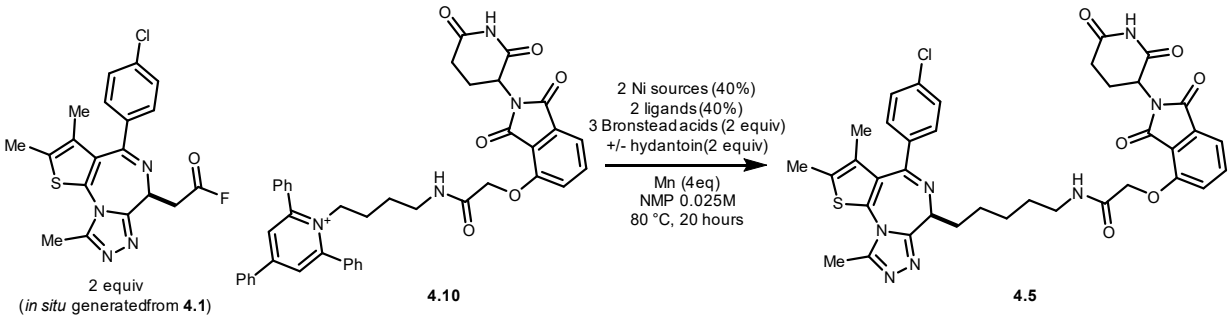

Table 4.6 Recipe for alkane optimization screen. PyBCamCN = (2Z,6Z)-N'2-N'6-dicyanopyridine-2,6-bis(carboximidamide), Dtbpy = 4,4'-di-tert-butyl bipyridine. Reactions run at 0.025 M.

Reagents	Solvent	Cstock (M)	Vdose (µL	Wells	Order Added
Nickel(II) Acetylacetonate	NMP	0.06	17	A,C 1-6	1
Nickel(II) bromide glyme	NMP	0.06	17	B,D 1-6	2
PyBCamCN	NMP	0.06	17	A.B 1-6	2
dtbpy	NMP	0.06	17	C,D 1-6	3
additive blank	NMP	blank	17	A,B,C,D 1-3	3
Hydantoin	NMP	0.18	17	A,B,C,D 4-6	3
JQ1 acyl fluori **(4.8)**	NMP	0.3	17	all	4
Pom Katritzky salt **(4.10)** Mn	NMP	0.15/0.60	17	all	5
acid blank	NMP	blank	17	A,B,C,D 1&4	5
ammonium hcloride	NMP	0.24	17	A,B,C,D 2&5	5
triethyl amine hydrochloride	NMP	0.24	17	A,B,C,D 3&6	5

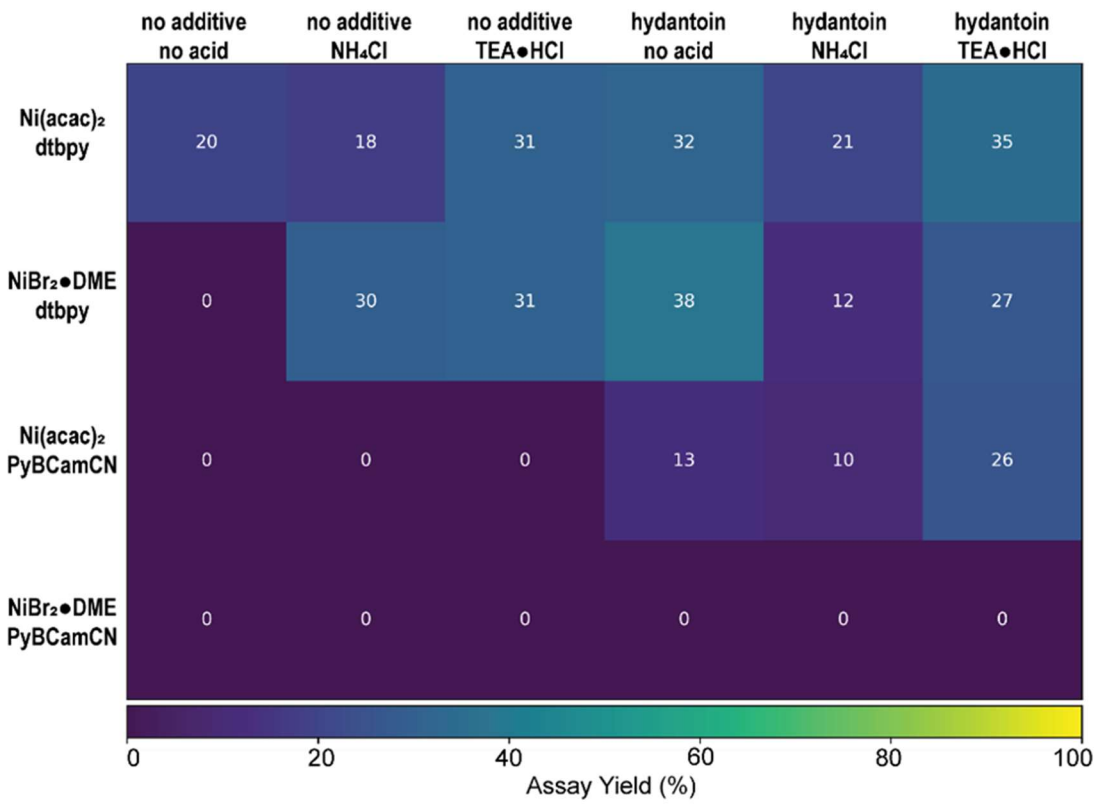

Figure 4.19 Results of Alkane optimization screen. Dtbpy = 4,4'-*di-tert*-butyl bipyridine, PyBCamCN = (2*Z*,6*Z*)-N'2-N'6-dicyanopyridine-2,6-bis(carboximidamide).

4.2.9 Ketone optimization screen 2 Ligands 3 Additives, 4 Bronsted acids.

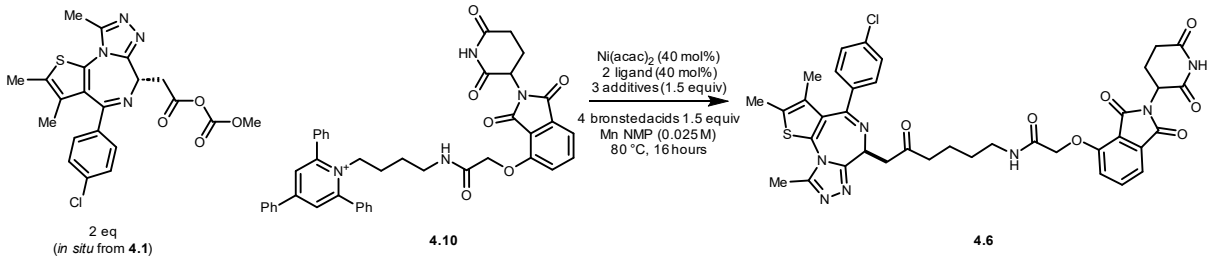

Table 4.7 Ketone optimization screen recipe. All reactions run at 0.025 M. Dtbpy = 4,4'-*di-tert*-butyl bipyridine, PyBCamCN = (2*Z*,6*Z*)-N'2-N'6-dicyanopyridine-2,6-bis(carboximidamide).

Reagents	Solvent	C_{stock} (M)	V_{dose} (µL)	Wells	Order Added
Nickel(II) Acetylacetonate/dtbpy	NMP	0.05/0.05	20	A,B,C,D 1-3	1
Nickel(II) Acetylacetonate/PyBCamCN	NMP	0.05/0.05	20	A,B,C,D 4-6	1
Additive Blank	NMP	N/A	20	A,B,C,D 1&4	2
Hydantoin	NMP	0.20	20	A,B,C,D 2&5	2
Phthalimide	NMP	0.20	20	A,B,C,D 3&6	2
JQ1 Acyl carbonate **(4.9)**	NMP	0.25	20	All	3
Pom Katritzky Salt **(4.10)** Manganese	NMP	0.125/0.50	20	All	4
Bronsted Acid Blank	NMP	0.45	20	A, 1-6	5
Ammonium Chloride	NMP	0.06	20	B, 1-6	5
Triethylamine hydrochloride	NMP	0.06	20	C, 1-6	5
hydrogen chloride in dioxane	20:1 NMP:dioxane	0.20	20	D, 1-6	5

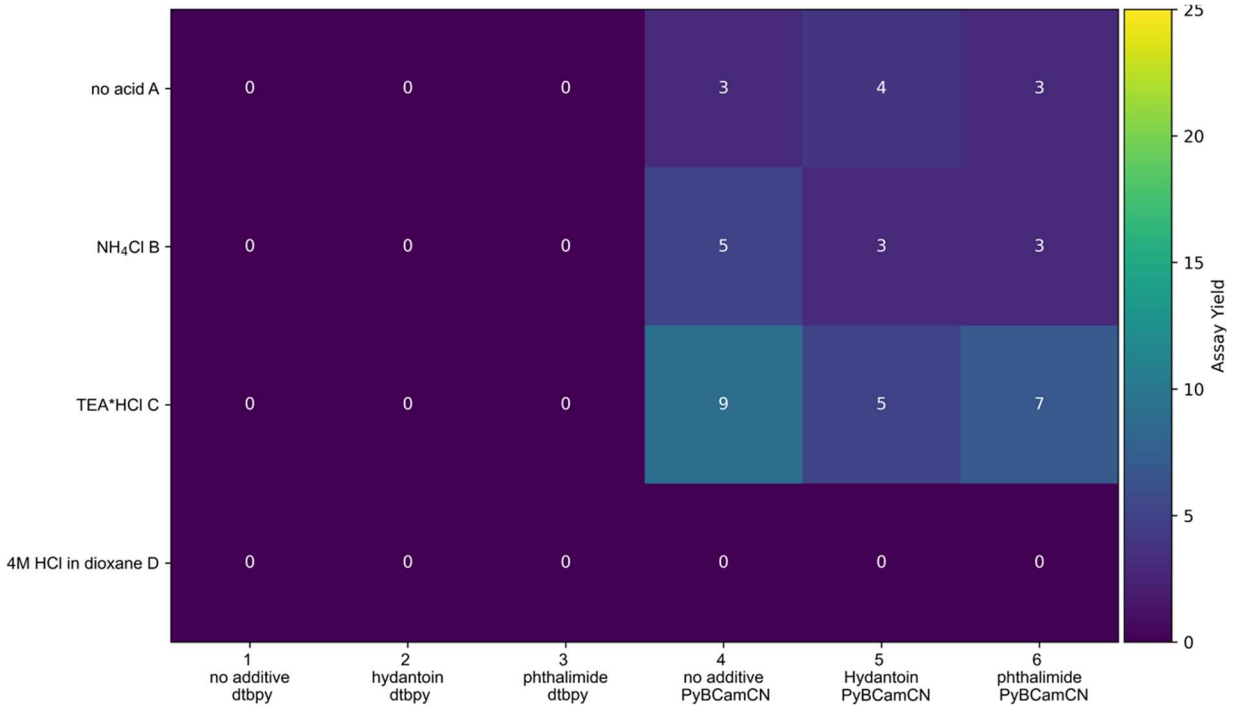

Figure 4.20 Results of ketone optimization screen investigating Bronsted Acids and imide additives. Assay yields are scaled to 25% for clarity. Dtbpy = 4,4'-*di-tert*-butyl bipyridine, PyBCamCN = (2*Z*,6*Z*)-N'2-N'6-dicyanopyridine-2,6-bis(carboximidamide).

4.2.10 Ketone optimization 2 Nickel sources, 6 ligands, 2 additives

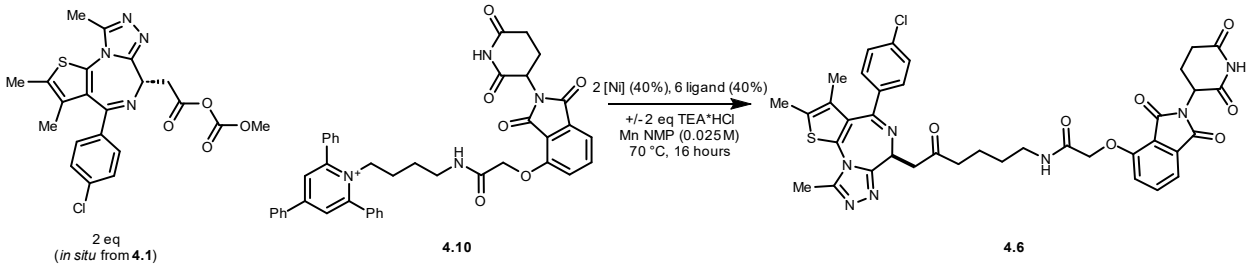

Table 4.8 Recipe for ketone optimization screen. Reactions run at 0.025 M.

Reagents	Solvent	C_{stock} (M)	V_{dose} (µL)	Wells	Order Added
Nickel(acac)$_2$	NMP	0.06	20	A,C 1-6	1
$NiBr_2$*dimethoxyethane	NMP	0.06	20	B,D 1-6	1
(2Z,6Z)-N'2,N'6-dicyanopyridine-2,6-bis(carboximidamide)	NMP	0.06	20	A,B,C,D 1	2
N-cyano-4-methoxy-picolinimidamide	NMP	0.06	20	A,B,C,D 2	2
(Z)-N'-cyanopicolinimidamide	NMP	0.06	20	A,B,C,D 3	2
4,4',4"-tri-tert-butyl-2,2':6',2"terpyridine, 97%	NMP	0.06	20	A,B,C,D 4	2
4,4'-di-tert-butyl-2,2'-dipyridyl, 98%	NMP	0.06	20	A,B,C,D 5	2
2-cyanopyridine	NMP	0.12	20	A,B,C,D 6	2
JQ1 methyl carbonate **(4.9)**	NMP	0.3	20	All	3
Pom Katritzky salt **(4.10)** Mn	NMP	.15 / 0.60	20	All	4
acid blank	NMP	blank	20	A,B 1-6	5
triethyl amine hydrochloride	NMP	0.24	20	C,D 1-6	5

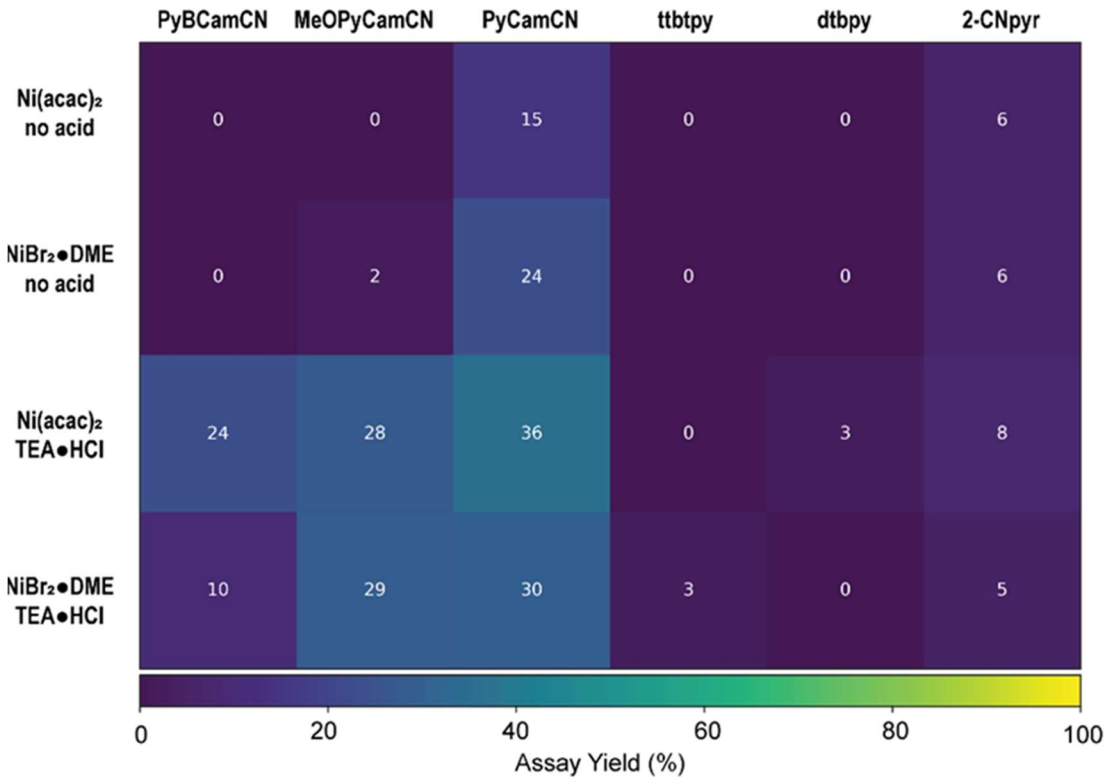

Figure 4.21 Results of ketone optimization screen. PyBCamCN = (2Z,6Z)-N′2,N′6-Dicyanopyridine-2,6-bis(carboximidamide), MeOPyCamCN = 4-methoxy-N-cyanopicolinimidamide PyCamCN = N-cyanopicolinimidamide, ttbtpy = 4,4′,4″-Tri-tert-Butyl-2,2′:6′,2″-terpyridine**,** dtbpy = 4,4-di-tert-butylbipyridine, 2CNPyr = 2-cyanopyridine

4.2.11 Amine Product optimization screen: 3 catalysts, 4 ligands, 2 solvents.

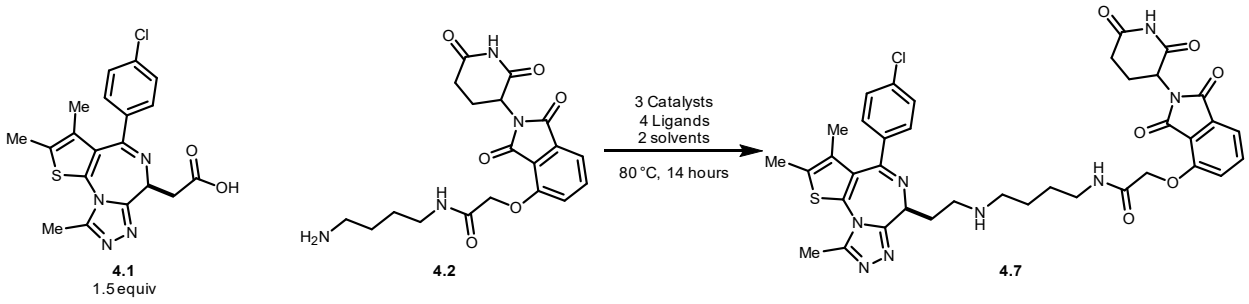

Table 4.9 Recipe of amine optimization screen. PtC_{l2} = platinum II chloride, $^{n}Bu_2O$ = di-*n*-butyl ether, DMSO = dimethyl sulfoxide. Reactions run at 0.1 M.

Reagents	Solvent	C_{stock} (M)	V_{dose} (µL)	Wells	Order Added
Karstedt's Catalyst	DMSO	0.025	20	A,B,C,D, 1	1
Karstedt's Catalyst	$^{n}Bu_2O$	0.025	20	A,B,C,D, 2	1
$PtCl_2$	DMSO	0.025	20	A,B,C,D, 3	1
$PtCl_2$	$^{n}Bu_2O$	0.025	20	A,B,C,D, 4	1
Trispentafluorophenylborane	DMSO	0.025	20	A,B,C,D, 5	1
Trispentafluorophenylborane	$^{n}Bu_2O$	0.025	20	A,B,C,D, 6	1
diphenylphosphinopropane	DMSO	0.0125	20	A, 1,3	2
diphenylphosphinopropane	$^{n}Bu_2O$	0.0125	20	A, 2,4	2
tert-butyl Brettphos	DMSO	0.025	20	B, 1,3,5	2
tert-butyl Brettphos	$^{n}Bu_2O$	0.025	20	B, 2,4,6	2
Brettphos	DMSO	0.025	20	C, 1,3,5	2
Brettphos	$^{n}Bu_2O$	0.025	20	C, 2,4,6	2
tert-butyl Xphos	DMSO	0.025	20	D, 1,3,5	2
tert-butyl Xphos	$^{n}Bu_2O$	0.025	20	D, 2,4,6	2
Ligand blank	DMSO	solvent	20	A, 5	2
Ligand blank	$^{n}Bu_2O$	solvent	20	A, 6	2
Phenylsilane	DMSO	2.00	20	A, B, C, D, 1,3,5	3
Phenylsilane	$^{n}Bu_2O$	2.00	20	A, B, C, D, 2,4,6	3
JQ1 Acid **(4.1)**	DMSO	0.75	20	A, B, C, D, 1,3,5	4
JQ1 Acid **(4.1)**	$^{n}Bu_2O$	0.75	20	A, B, C, D, 2,4,6	4
Pom amine **(4.2)**	DMSO	0.50	20	A, B, C, D, 1,3,5	5
Pom amine **(4.2)**	$^{n}Bu_2O$	0.50	20	A, B, C, D, 2,4,6	5

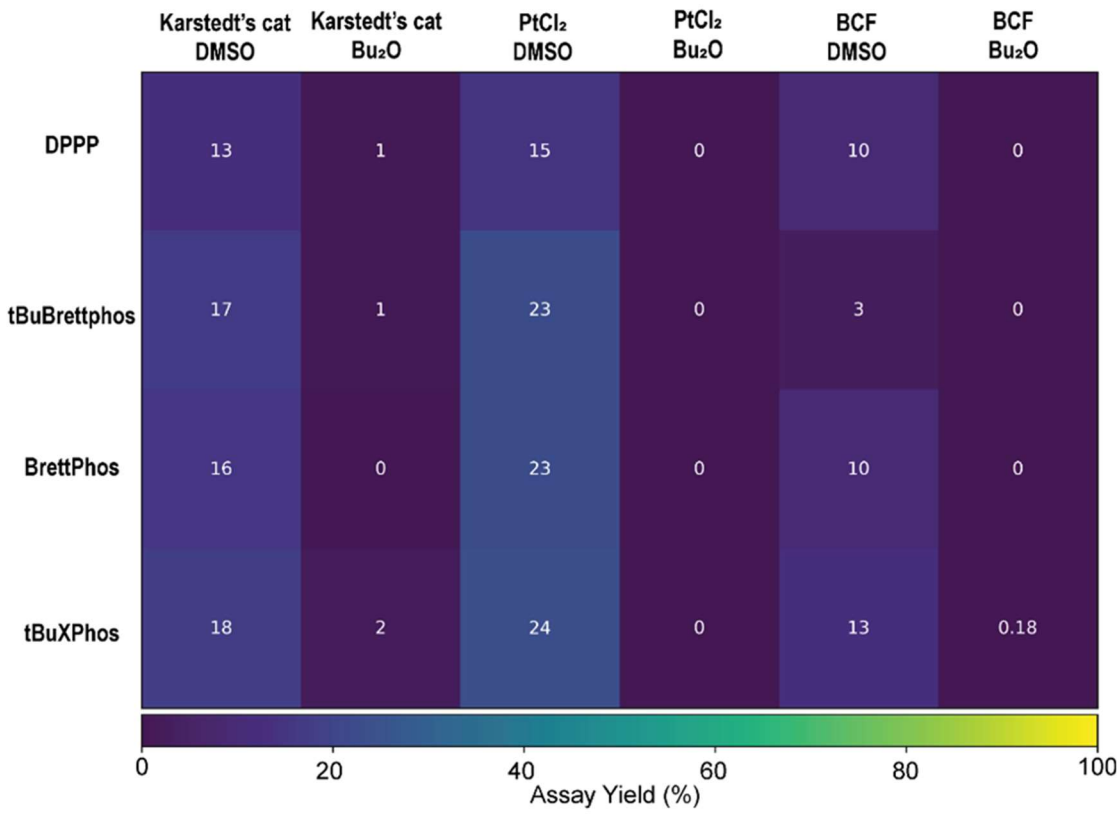

Figure 4.22 Results of amine optimization screen.

4.2.12 Primary scope screen (6 amines x 4 acids).

Initial scope determination screens were performed on all five reactions reported in chapter **4.1**. Due to the success of the amination rection, an additional scope screen was performed to evaluate its performance in other circumstances. Activation via acyl carbonate was found to only be effective for **4.**, so optimization screens were performed for the ketone screens to provide a more general method that worked on this library of compounds. An additional alkane scope screen looking at other carboxylic acids was also performed due to its failure to perform on other substrates in the initial screen.

Table 4.10 Table of substrates used to investigate scope. **4.2**, **4.11**, **4.12**, and **4.13** are partial PROTACs. **4.14** and **4.15** are representative linkers. **4.1** is a JQ1 derivative, **4.16** is indomethacin, **4.17** is an atorvastatin derivative, **4.18** is etodolac.

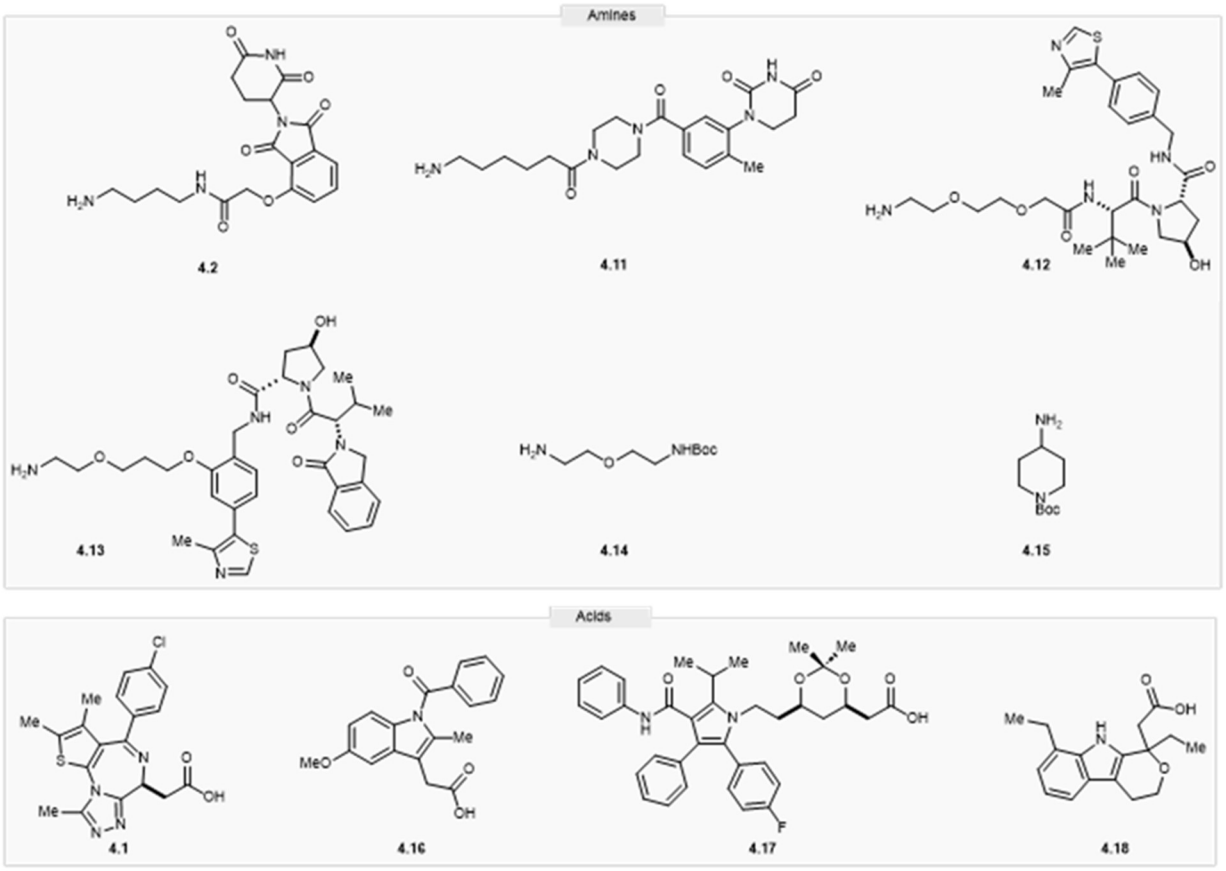

4.2.12.1 Primary amination scope screen

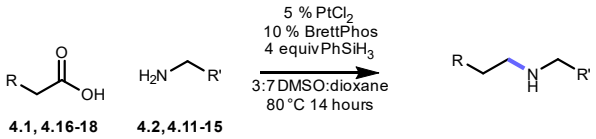

Table 4.11 Primary amine scope screen recipe. Reactions run at 0.1 M.

Reagents	Solvent	C_{stock} (M)	V_{dose} (µL)	Wells	Order Added
JQ1 Acid (**4.1**)	3:7 DMSO:dioxane	0.45	25	A, 1-6	1
Indomethacin (**4.16**)	3:7 DMSO:dioxane	0.45	25	B, 1-6	1
Atorvastatin Acetonide (**4.17**)	3:7 DMSO:dioxane	0.45	25	C, 1-6	1
Etodolac (**4.18**)	3:7 DMSO:dioxane	0.45	25	D, 1-6	1
Pom partial protac (**4.2**)	3:7 DMSO:dioxane	0.4	25	A,B,C,D, 1	2
Dihydrouracil amine (**4.11**)	3:7 DMSO:dioxane	0.4	25	A,B,C,D, 2	2
VHL amine 1 (**4.12**)	3:7 DMSO:dioxane	0.4	25	A,B,C,D, 3	2
VHL amine 2 (**4.13**)	3:7 DMSO:dioxane	0.4	25	A,B,C,D, 4	2
Primary Linker (**4.14**)	3:7 DMSO:dioxane	0.4	25	A,B,C,D, 5	2
Secondary Linker (**4.15**)	3:7 DMSO:dioxane	0.4	25	A,B,C,D, 6	2
PtCl2/BrettPhos/Phenylsilane mix	3:7 DMSO:dioxane	0.015/0.030/1.20	25	All	3

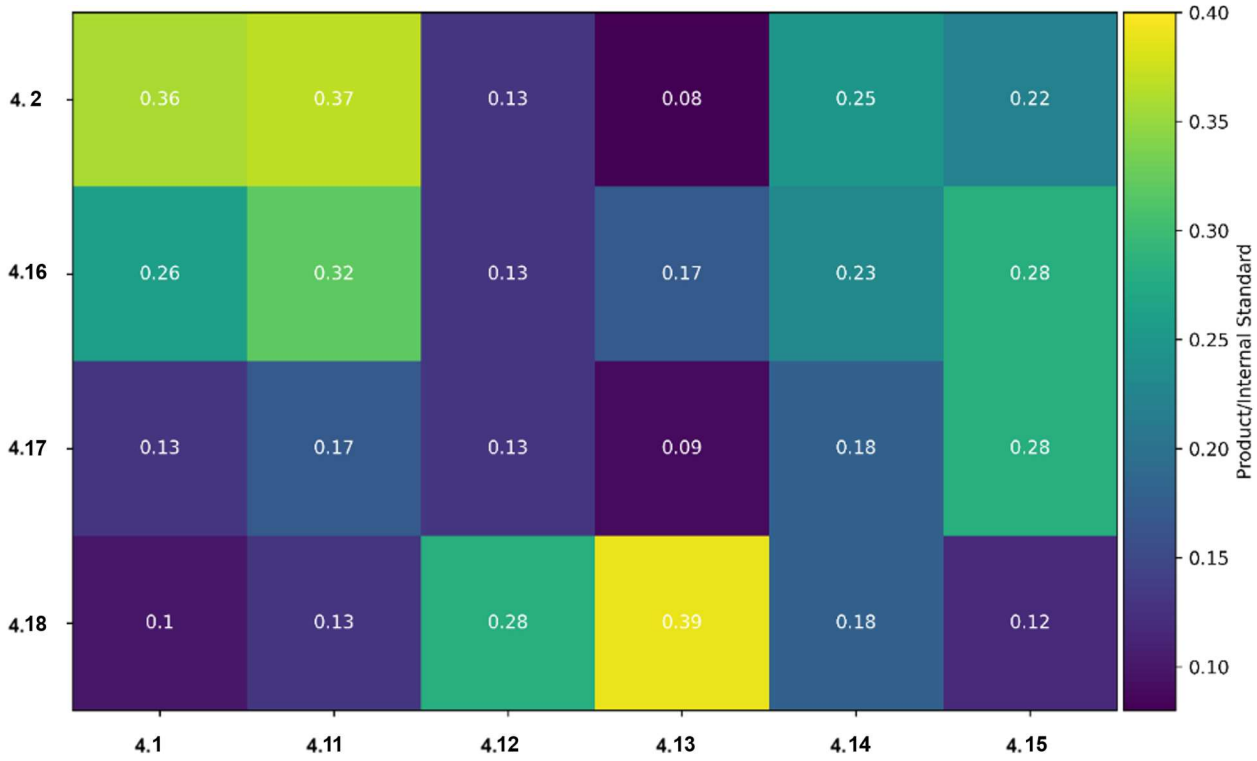

Figure 4.23 Primary amine scope screen results.

4.2.12.2 Secondary amination scope screen

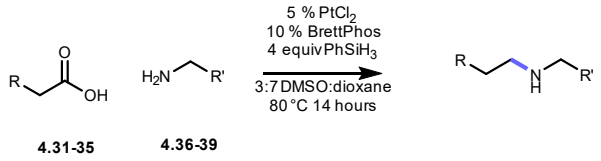

Table 4.12 Table of substrates used to investigate scope. **4.31** is guanosine, **4.34** is sulfadoxine, and **4.35** is an atorvastatin precursor. **4.37** is levofloxacin, **4.38** is isoxepac, **4.39** is probenecid.

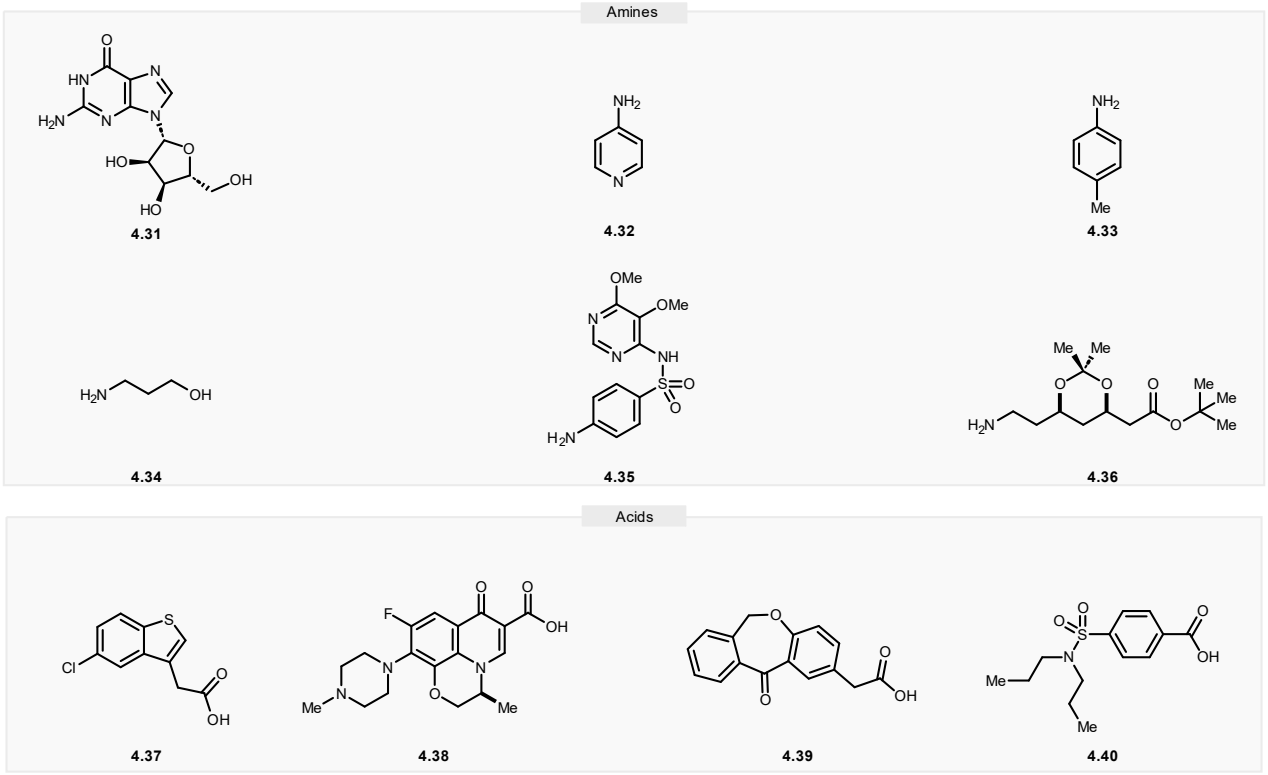

Table 4.13 secondary amination scope screen recipe. Reactions run at 0.1 M.

Reagents	Solvent	C_{stock} (M)	V_{dose} (µL)	Wells	Order Added
4.37	3:7 DMSO:dioxane	0.45	25	A, 1-6	1
levofloxacin (**4.38**)	3:7 DMSO:dioxane	0.45	25	B, 1-6	1
isoxepac(**4.39**)	3:7 DMSO:dioxane	0.45	25	C, 1-6	1
probenecid (**4.40**)	3:7 DMSO:dioxane	0.45	25	D, 1-6	1
guanosine (**4.31**)	3:7 DMSO:dioxane	0.4	25	A,B,C,D, 1	2
4.32	3:7 DMSO:dioxane	0.4	25	A,B,C,D, 2	2
4.33	3:7 DMSO:dioxane	0.4	25	A,B,C,D, 3	2
4.34	3:7 DMSO:dioxane	0.4	25	A,B,C,D, 4	2
sulfadoxin (**4.35**)	3:7 DMSO:dioxane	0.4	25	A,B,C,D, 5	2
atorvastatin intermediate (**4.36**)	3:7 DMSO:dioxane	0.4	25	A,B,C,D, 6	2
PtCl2/BrettPhos/Phenylsilane mix	3:7 DMSO:dioxane	0.015/0.030/1.20	25	All	3

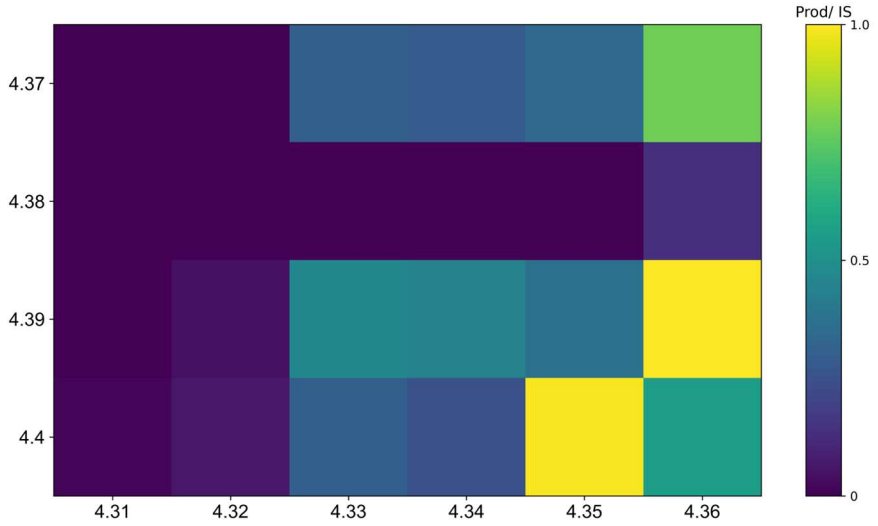

Figure 4.24 Result of secondary amination scope screen.

4.2.12.3 Primary amide scope screen.

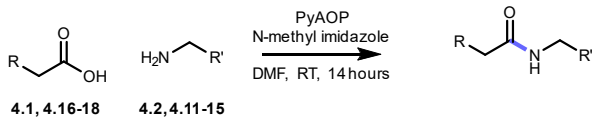

Table 4.14 Recipe for primary amide scope screen. Reactions run at 0.1 M.

Reagents	Solvent	C_{stock} (M)	V_{dose} (µL)	Wells	Order Added
JQ1 Acid (**4.1**)	DMF	0.4	25	A, 1-6	1
Indomethacin (**4.16**)	DMF	0.4	25	B, 1-6	1
Atorvastatin Acetonide (**4.17**)	DMF	0.4	25	C, 1-6	1
Etodolac (**4.18**)	DMF	0.4	25	D, 1-6	1
1-methylimidazole	DMF	0.4	25	All	2
PyAOP	DMF	0.4	25	All	3
Pom partial protac (**4.2**)	DMF	0.4	25	A,B,C,D, 1	4
Dihydrouracil amine (**4.11**)	DMF	0.4	25	A,B,C,D, 2	4
VHL amine 1 (**4.12**)	DMF	0.4	25	A,B,C,D, 3	4
VHL amine 2 (**4.13**)	DMF	0.4	25	A,B,C,D, 4	4
Primary Linker (**4.14**)	DMF	0.4	25	A,B,C,D, 5	4
Secondary Linker (**4.15**)	DMF	0.4	25	A,B,C,D, 6	4

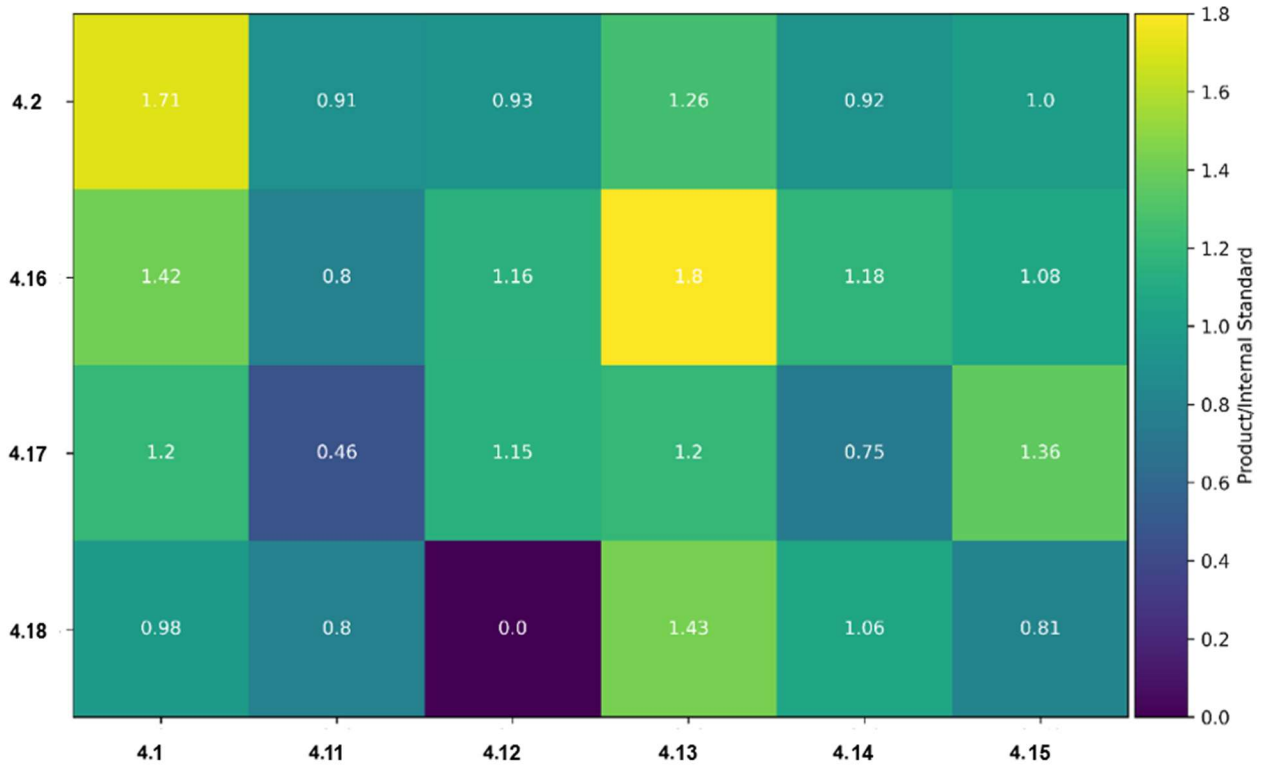

Figure 4.25 Results of primary amide scope screen

4.2.12.4 Primary esterification scope screen

To account for the insolubility of many of the reagents in dioxane at room temperature, potassium iodide and potassium *tert*-butoxide were suspended in diethyl ether and stirred at 1000 rpm until a suitable slurry was achieved. 5 mm of the end of a 300 µL pipette tip was cut off using scissors and 50 µL of each reagent was dispensed into every well. The solvent was evaporated by blowing a stream of nitrogen. The screen was then run according to general procedure B.

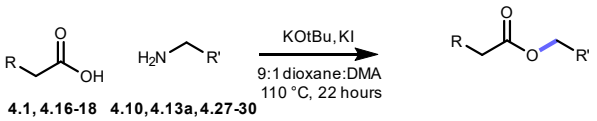

Table 4.15 Recipe for primary ester scope screen. Reactions run at 0.1 M. Negative signs in "Order Added" column indicate the reagents were pre-dosed and the solvent was evaporated.

Reagents	Solvent	Cstock (M)	Vdose (µL)	Wells	Order Added
Potassium Iodide	Diethyl Ether	0.4	50	All	–2
Potassium tert-butoxide	Diethyl Ether	0.2	50	All	–1
JQ1 Acid (**4.1**)	9:1 dioxane:DMA	0.2	50	A, 1-6	1
Indomethacin (**4.16**)	9:1 dioxane:DMA	0.2	50	B, 1-6	1
Atorvastatin Acetonide (**4.17**)	9:1 dioxane:DMA	0.2	50	C, 1-6	1
Etodolac (**4.18**)	9:1 dioxane:DMA	0.2	50	D, 1-6	1
Pom partial protac Kat Salt (**4.10**)	9:1 dioxane:DMA	0.2	50	A,B,C,D, 1	2
Dihydrouracil Kat Salt (**4.27**)	9:1 dioxane:DMA	0.2	50	A,B,C,D, 2	2
VHL Kat Salt 1 (**4.28**)	9:1 dioxane:DMA	0.2	50	A,B,C,D, 3	2
VHL Kat Salt 2 (**4.13a**)	9:1 dioxane:DMA	0.2	50	A,B,C,D, 4	2
Primary Linker Kat salt (**4.29**)	9:1 dioxane:DMA	0.2	50	A,B,C,D, 5	2
Secondary Linker (**4.30**)	9:1 dioxane:DMA	0.2	50	A,B,C,D, 6	2

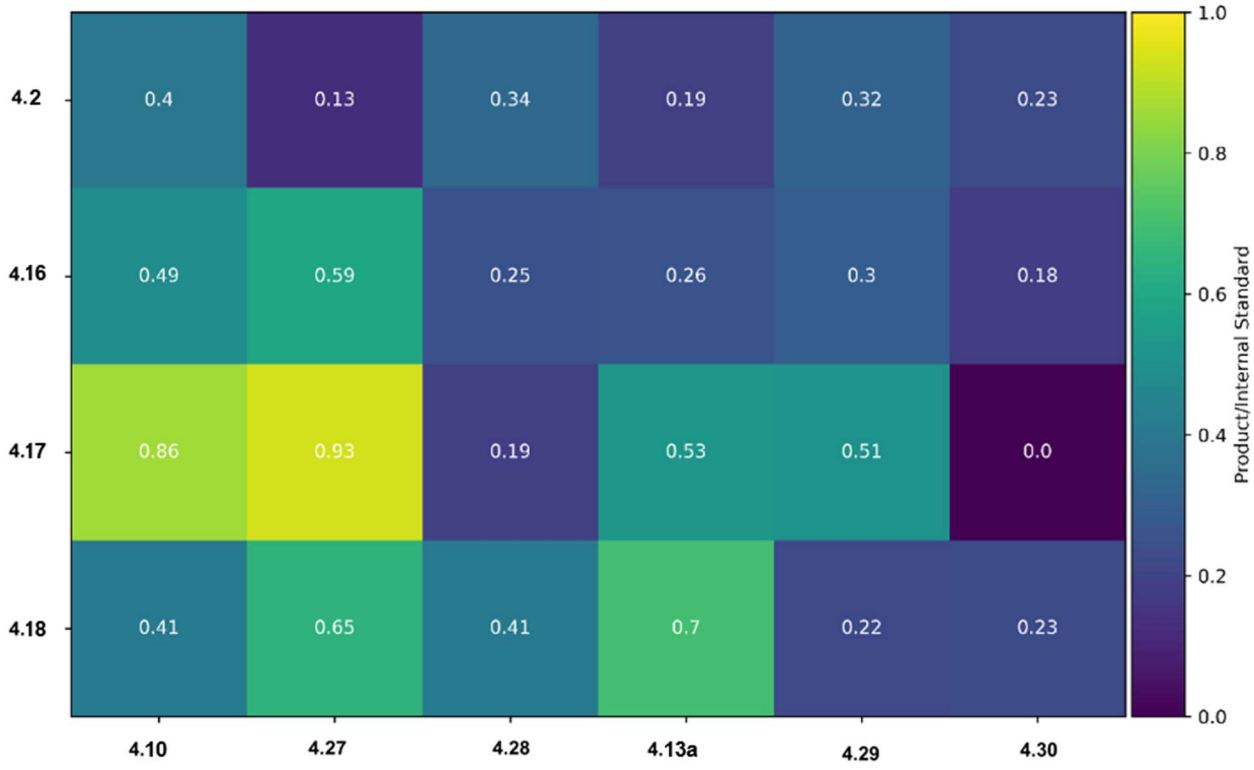

Figure 4.26 Results of primary esterification scope.

4.2.12.5 Ketone scope expansion optimization screen.

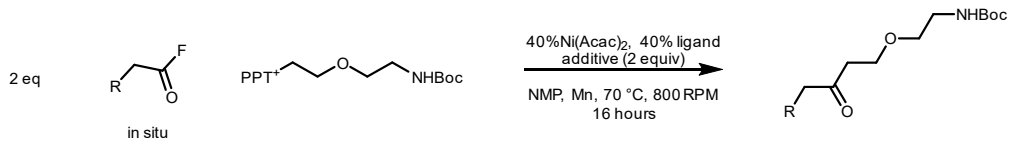

Table 4.16 Recipe for screen to determine conditions for ketone screen.

Reagents	Solvent	Cstock (M)	Vdose (µL)	Wells	Order Added
Nickel(II) Acetylacetonate	NMP	0.06	17	All	1
1,10-Phenanthroline-5,6-Dione	NMP	0.06	17	A,B,C,D, 1-3	2
Bathophenanthroline	NMP	0.06	17	A,B,C,D, 4-6	2
Indomethacin (**4.16**)	NMP	0.3	17	A,B,C,D 1,4	3
Etodolac (**4.18**)	NMP	0.3	17	A,B,C,D 2,5	3
Atorvastatin Acetonide (**4.17**)	NMP	0.3	17	A,B,C,D 3,6	3
Primary Linker Katritzky Salt (**4.29**)/Manganese	NMP	0.15/0.60	17	All	4
Lithium Chloride	NMP	0.6	17	A, 1-6	5
Zinc Chloride	NMP	0.3	17	B, 1-6	5
Magnesium Bromide	NMP	0.3	17	C, 1-6	5
Ruthenium (III) Chloride	NMP	0.3	17	D, 1-6	5

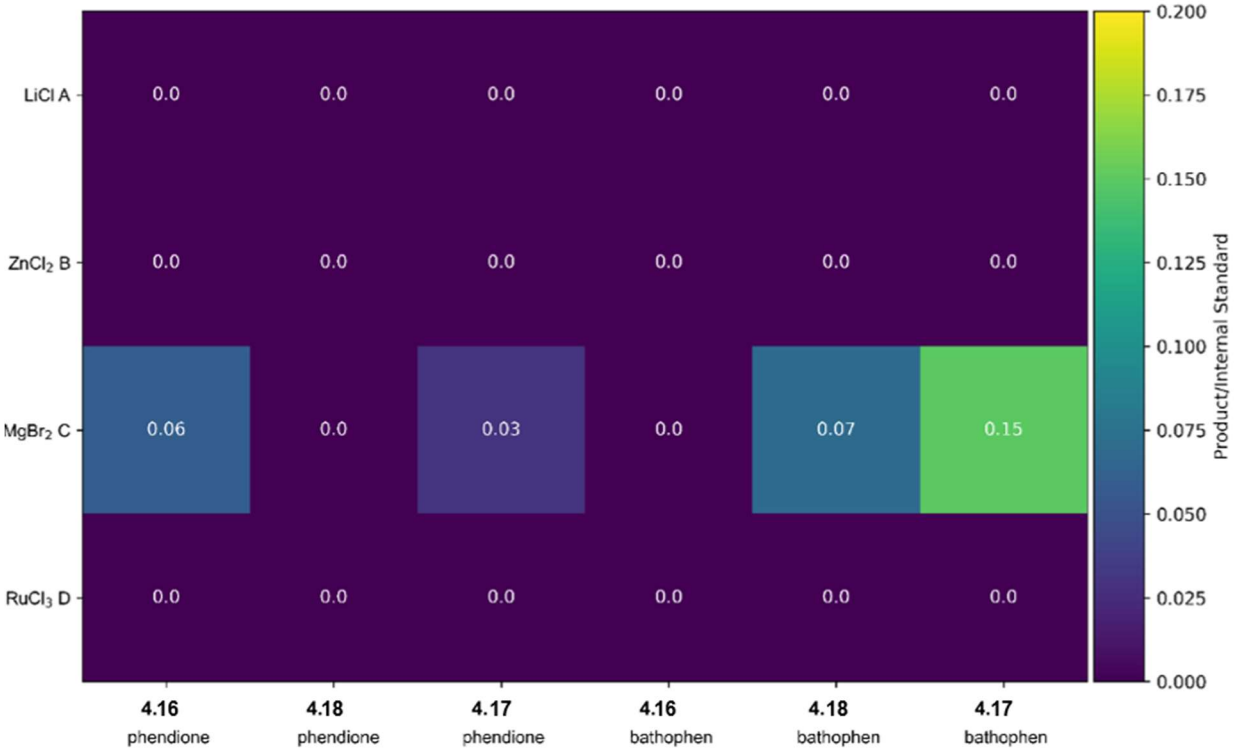

Figure 4.27 Results of ketone generality optimization screen.

4.2.12.6 Primary Ketonylation scope screen

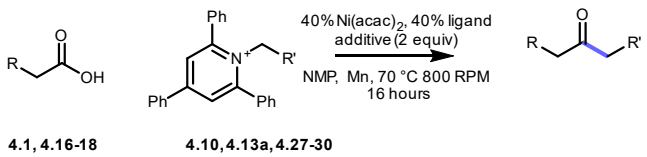

Table 4.17 Recipe for primary ketone scope screen. JQ1 required different conditions than all other acids as reflected by a unique catalyst/ligand/additive system. Ligand 1 = N-Z-Cyanopicolinimidamide.

Reagents	Solvent	Cstock (M)	Vdose (µL	Wells	Order Added
Manganese	NMP	0.5	20	All	1
Pom partial protac Kat Salt (**4.10**)	NMP	0.125	20	A,B,C,D 1	2
Dihydrouracil Kat Salt (**4.27**)	NMP	0.125	20	A,B,C,D 2	2
VHL Kat Salt 1 (**4.28**)	NMP	0.125	20	A,B,C,D 3	2
VHL Kat Salt 2 (**4.13a**)	NMP	0.125	20	A,B,C,D 4	2
Primary Linker Kat salt(**4.29**)	NMP	0.125	20	A,B,C,D 5	2
Secondary Linker (**4.30**)	NMP	0.125	20	A,B,C,D 6	2
JQ1 Acyl carbonate (**4.9**)	NMP	0.25	20	A, 1-6	3/4
Indomethacin acyl fluoride (**4.16**)	NMP	0.25	20	B, 1-6	3/4
Atorvastatin Acetonide acyl fluoride (**4.17**)	NMP	0.25	20	C, 1-6	3/4
Etodolac acyl fluoride (**4.18**)	NMP	0.25	20	D, 1-6	3/4
Triethylamine hydrochloride	NMP	0.25	20	A, 1-6	3/4
Magnesium Bromide	NMP	0.25	20	B,C,D 1-6	3/4
Nickel(II) Acetylacetonate/ligand 1	NMP	0.05/0.05	20	A, 1-6	5
Nickel(II) Acetylacetonate/bathophenanthroline	NMP	0.05/0.05	20	B,C,D 1-6	5

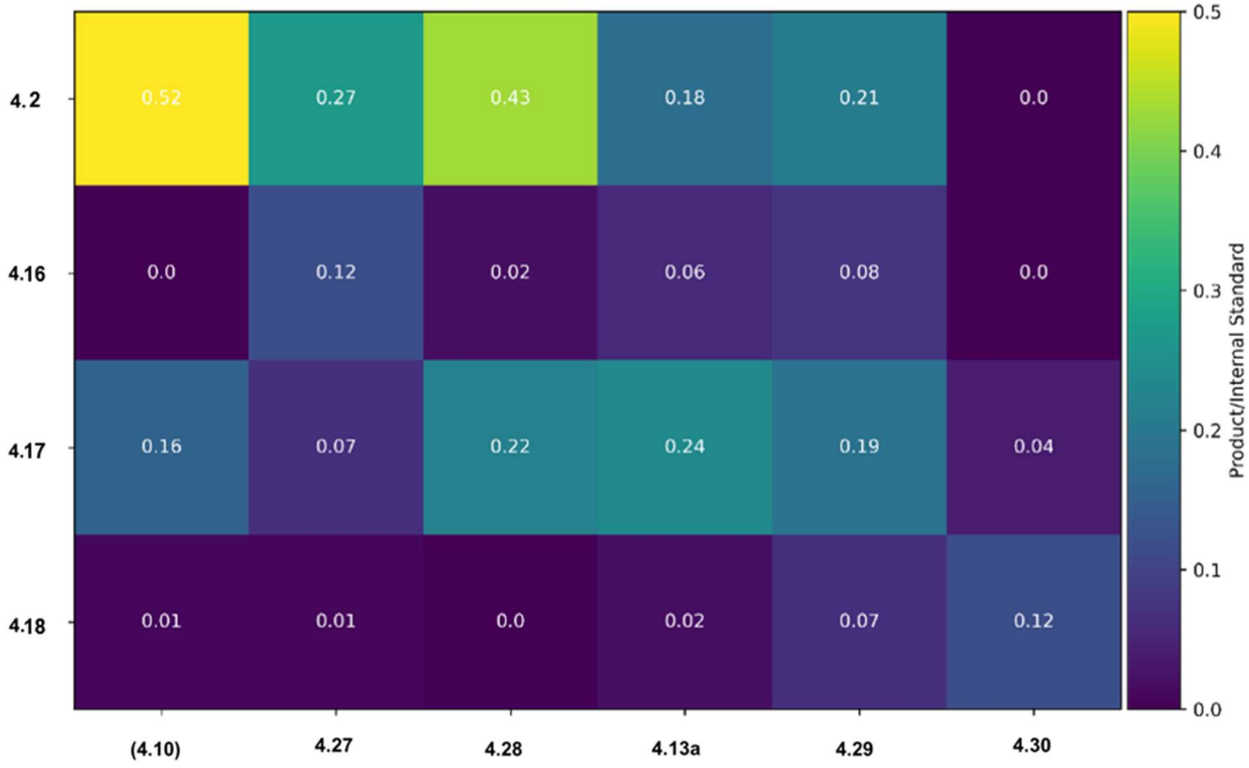

Figure 4.28 Primary Ketonylation scope results.

4.2.12.7 Primary alkylation scope screen

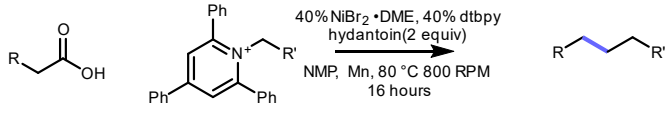

Table 4.18 Recipe for primary alkylation scope screen.

Reagents	Solvent	Cstock (M)	Vdose (µL	Wells	Order Added
Manganese	NMP	0.5	20	All	1
Pom partial protac Kat Salt (**4.10**)	NMP	0.125	20	A,B,C,D 1	2
Dihydrouracil Kat Salt (**4.27**)	NMP	0.125	20	A,B,C,D 2	2
VHL Kat Salt 1 (**4.28**)	NMP	0.125	20	A,B,C,D 3	2
VHL Kat Salt 2 (**4.13a**)	NMP	0.125	20	A,B,C,D 4	2
Primary Linker Kat salt(**4.29**)	NMP	0.125	20	A,B,C,D 5	2
Secondary Linker (**4.30**)	NMP	0.125	20	A,B,C,D 6	2
JQ1 Acyl carbonate (**4.9**)	NMP	0.25	20	A, 1-6	3/4
Indomethacin acyl fluoride (**4.16**)	NMP	0.25	20	B, 1-6	3/4
Atorvastatin Acetonide acyl fluoride (**4.17**)	NMP	0.25	20	C, 1-6	3/4
Etodolac acyl fluoride (**4.18**)	NMP	0.25	20	D, 1-6	3/4
hydantoin	NMP	0.25	20	All	3/4
Nickel(II)bromide dimethoxyethane/dtbpy	NMP	0.05/0.05	20	B,C,D 1-6	5

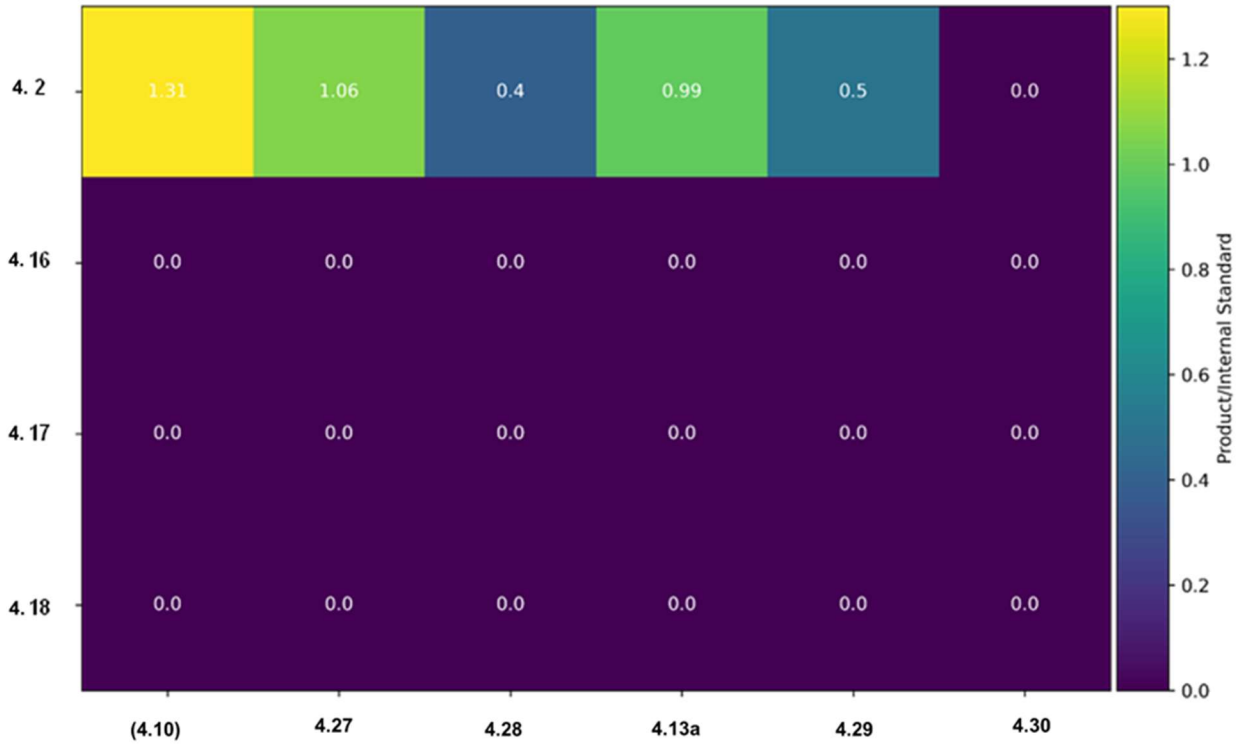

Figure 4.29 Results of alkane scope screen. Because only **4.2** had any reactivity, a follow up screen was performed to see if this reactivity could be seen in other classes of acid.

4.2.12.8 Secondary alkylation scope screen

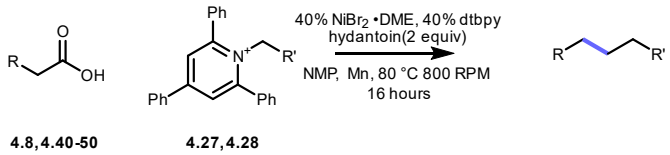

4.8,4.40-50 **4.27,4.28**

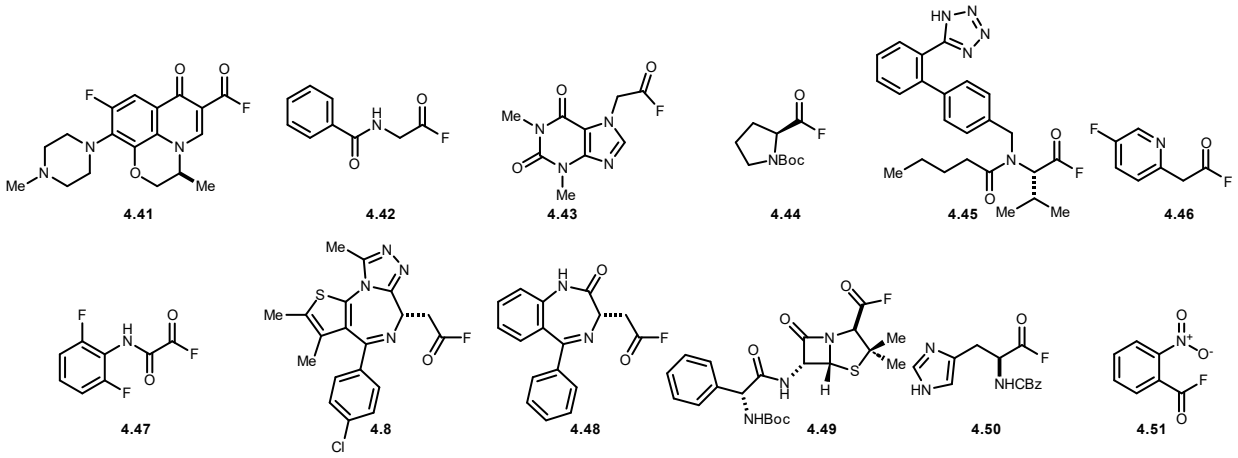

Figure 4.30 Collection of *in-situ* generated acyl fluorides for secondary alkylation scope screen.

Table 4.19 Recipe for secondary alkylation scope screen

Reagents	Solvent	Cstock (M)	Vdose (µL)	Wells	Order Added
Manganese	NMP	0.5	20	All	1
Dihydrouracil Kat Salt (**4.27**)	NMP	0.125	20	A,B, 1-6	2
VHL Kat Salt 1 (**4.28**)	NMP	0.125	20	C,D 1-6	2
Levofloxacin acyl fluoride(**4.41**)	NMP	0.25	20	A,C 1	3
Hippuric acyl fluoride (**4.42**)	NMP	0.25	20	A,C 2	3
Theophylline Acetic acyl fluoride (**4.43**)	NMP	0.25	20	A,C 3	3
boc-Proline acyl fluoride (**4.44**)	NMP	0.25	20	A,C 4	3
Valsartan acyl fluoride (**4.45**)	NMP	0.25	20	A,C 5	3
pyridine acetic acyl fluoride (**4.46**)	NMP	0.25	20	A,C 6	3
floro-oxanilic acyl fluoride (**4.47**)	NMP	0.25	20	B,D 1	3
JQ1 Acyl fluoride (**4.8**)	NMP	0.25	20	B,D 2	3
JQ1-like acyl fluoride (**4.48**)	NMP	0.25	20	B,D 3	3
boc ampicillin acyl fluoride (**4.49**)	NMP	0.25	20	B,D 4	3
CBz Histidine acyl fluoride (**4.50**)	NMP	0.25	20	B,D 5	3
Nitrobenzoic acyl fluoride (**4.51**)	NMP	0.25	20	B,D 6	3
Nickel(II) bromide DME/bathophenanthroline	NMP	0.05/0.05	20	A,B,C,D 1-6	4

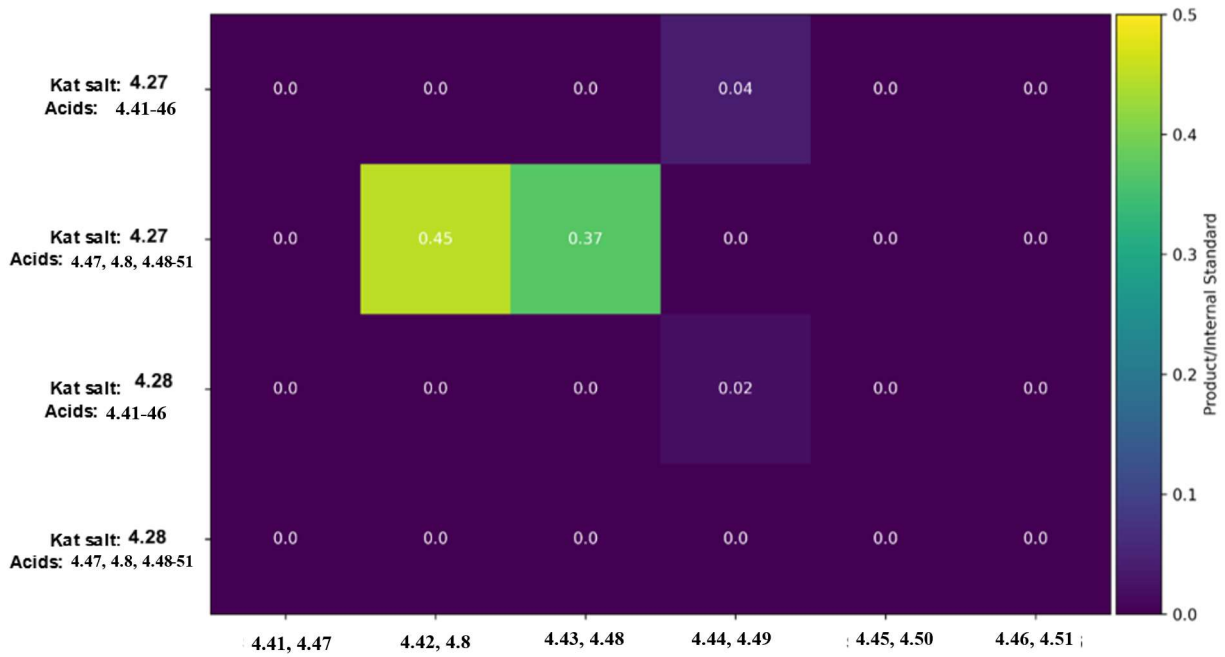

Figure 4.31 Results of alkane secondary scope screen.

4.2.13 Extended alkylation/ketonylation optimization data

Table 4.20 Optimization examining activation groups, ligands, and additives. a) THF instead of NMP, b) 0.05 M instead of 0.025 M.

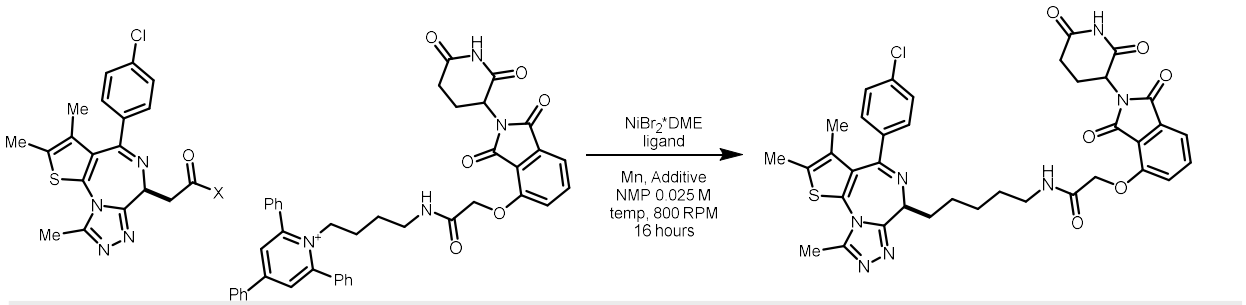

Entry	eq **1**	X	Ligand	Ni loading	Additive	Temp	Alkane Assay %	Ketone Assay %
1	3	NHPI	1,10 phenanthroline	60%	None	80 °C	ND	ND
2	3	Boc	1,10 phenanthroline	60%	None	80 °C	ND	ND
3	3	succinimide	1,10 phenanthroline	60%	$MgCl_2$	80 °C	ND	ND
4	3	Cl	bpy	60%	None	80 °C	ND	ND
5[a]	3	O-pyridyl	bathophenanthroline	60%	None	30 °C	ND	ND
6	3	F	1,10 phenanthroline	60%	None	80 °C	10	ND
7	3	F	PyBcamCN	40%	None	80 °C	10	Trace
8	3	F	PyBcamCN	40%	NH_4Cl	80 °C	13	3
9	2	F	PyBCamCN	40 %	None	70 °C	10	Trace
10	2	OCO_2Me	PyBcamCN	40 %	None	70 °C	15	5
11	2	OCO_2Me	PyBcamCN	40 %	NH4Cl	70 °C	23	12
12[b]	3	OCO_2Me	PyBcamCN	40 %	NH4Cl	70 °C	22	12
13	2	OCO_2Me	dtbpy	40 %	None	70 °C	27	ND
14	2	F	bathophenanthroline	40 %	None	70 °C	36	ND

4.2.14 Extended amination optimization data.

Table 4.21 Optimization examining reductant, temperature, solvent, and reductant/acid premix time. DMF = Dimethylformamide, DMAc = dimethylacetamide, MeCN = acetonitrile

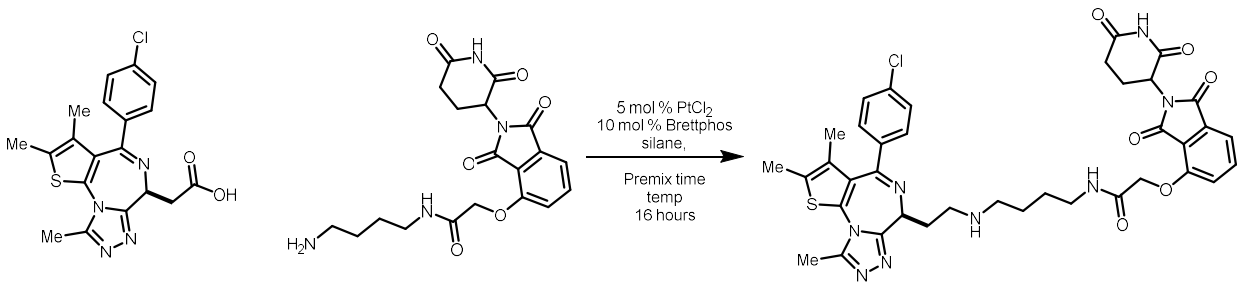

Entry	Silane	Temperature	Solvent	Premix time	Assay Yield %
1	$PhSiH_3$	80 °C	dioxane	15 min	5
2	Ph_3SiH	80 °C	dioxane	15 min	ND
3	Et_3SiH	80 °C	dioxane	15 min	ND
4	$PhMe_2SiH$	80 °C	dioxane	15 min	1
5	$PhSiH_3$	100 °C	dioxane	15 min	4
6	$PhSiH_3$	80 °C	dioxane + 1 equiv DMAc	15 min	trace
7	$PhSiH_3$	80 °C	80:20 dioxane:DMF	15 min	ND
8	$PhSiH_3$	80 °C	sulfolane	15 min	ND
9	$PhSiH_3$	80 °C	90:10 dioxane:MeCN	15 min	13
10	$PhSiH_3$	80 °C	MeCN	15 min	13
11	$PhSiH_3$	80 °C	95:5 dioxane:DMSO	15 min	10
12	$PhSiH_3$	80 °C	90:10 dioxane:DMSO	15 min	17
13	$PhSiH_3$	80 °C	70:30 dioxane:DMSO	15 min	26
14	$PhSiH_3$	80 °C	DMSO	15 min	26
15	$PhSiH_3$	80 °C	90:10 dioxane:DMSO	45 min	17
16	$PhSiH_3$	80 °C	90:10 dioxane:DMSO	5 min	18
17	$PhSiH_3$	80 °C	DMSO	0 min	27
18	$PhSiH_3$	80 °C	tetrahydropthiophene S-oxide	0 min	15

Table 4.22 Optimization of amination starting from amine salt. **a)** the trifluoroethylated product was obtained instead of the desired product[55]. **b)** Exclusively amide product was obtained. **c)** 7 equiv of $PhSiH_3$ were used instead of 5. **d)** The amine and KOtBu were prestirred in dioxane, followed by removal of solvent

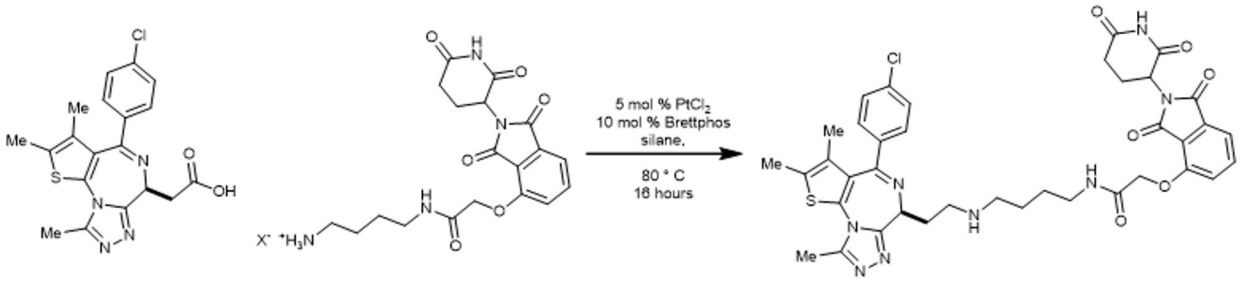

Entry	X⁻	Base	Solvent	LC/MS Product/ IS
1	Trifluoroacetate	None	90:10 DMSO:dioxane	ND [a]
2	Cl	DIPEA	90:10 DMSO:dioxane	ND
3	Cl	KO^{t}Bu	90:10 DMSO:dioxane	ND [b]
4	Cl	None	90:10 DMSO:dioxane	25[c]
5	Cl	None	10:90 DMSO:dioxane	3
6	Cl	KO^{t}Bu	10:90 DMSO:dioxane	20[d]

4.2.15 Mechanistic evidence for an aldehyde intermediate in the reductive amination

In a nitrogen filled glovebox, an oven dried one-dram vial, equipped with a Teflon-coated stir bar, was charged with Platinum (II) chloride (1.3 mg, 0.005 mmol, 0.05 equiv) and Brettphos (5.3 mg, 0.01 mmol, 0.01 equiv). 100 µL of DMSO-d6 was added and the solution stirred for 20 minutes at 30 °C and 300 rpm. An additional oven dried one-dram vial, was charged with **1** (20.0 mg, 0.05 mmol, 1.0 equiv). 500 µL of solvent was added. The catalyst solution had phenylsilane (30 µL, 0.25 mmol, 2.5 equiv) was added, and transferred to the vial containing **1**. This was transferred to an NMR tube and removed from the glovebox and an NMR taken after 5 minutes. After this, the NMR tube was subjected to heating via a heat gun for 30 seconds and left to stand. NMRs were taken at 45 min, 3 hours, and 24 hours. Signals grow at 9.90 corresponding to an aldehyde, and 5.0-5.5 indicative of various silyl acetal species[56]. These species are known to undergo reductive amination[55].

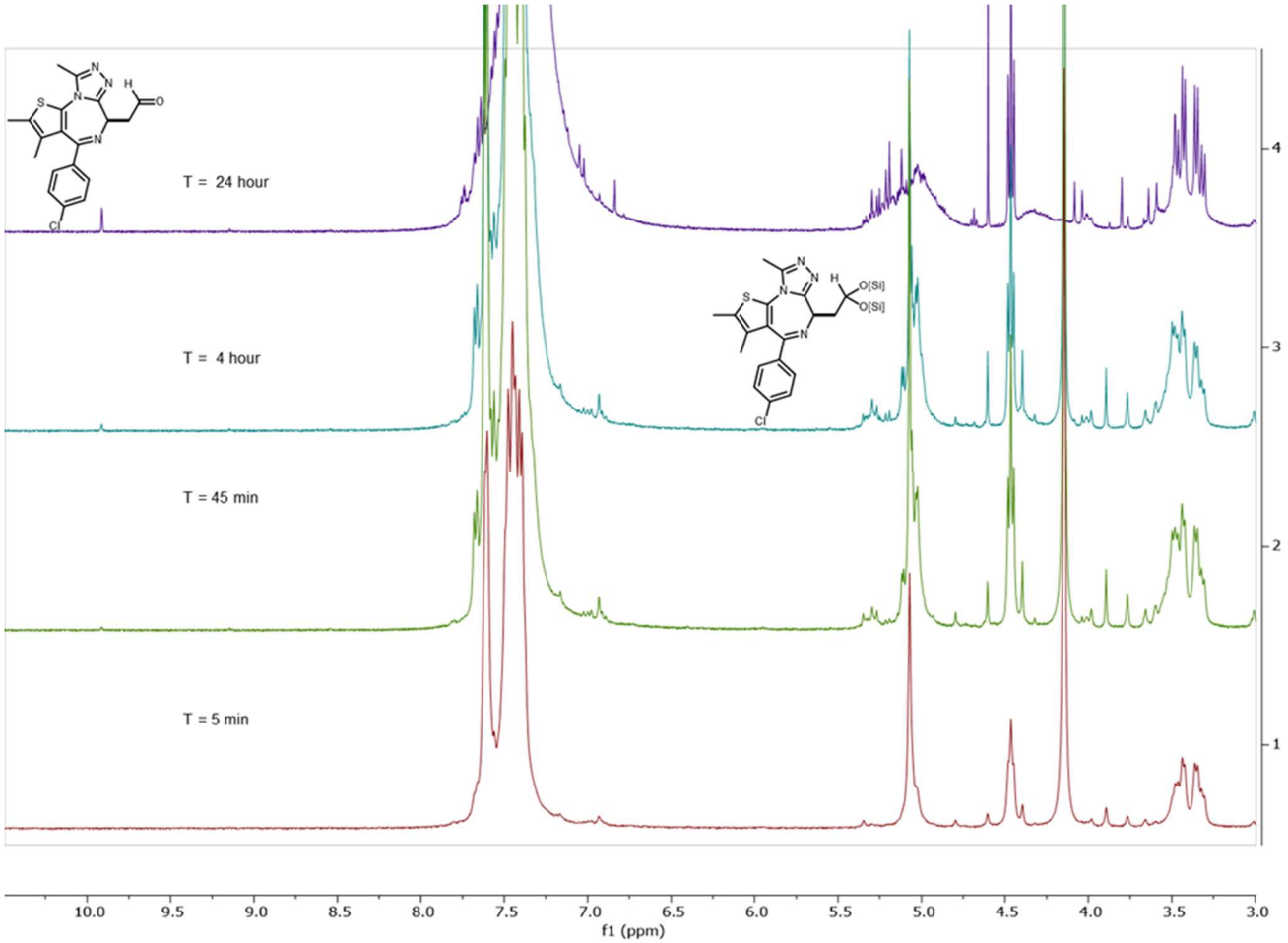

Figure 4.32 Stacked NMR spectra of 1 subjected to amination conditions at t = 5 min, 45 min, 4 hour, 24 hour.

4.2.16 Labeled Kernel Density Estimate plots.

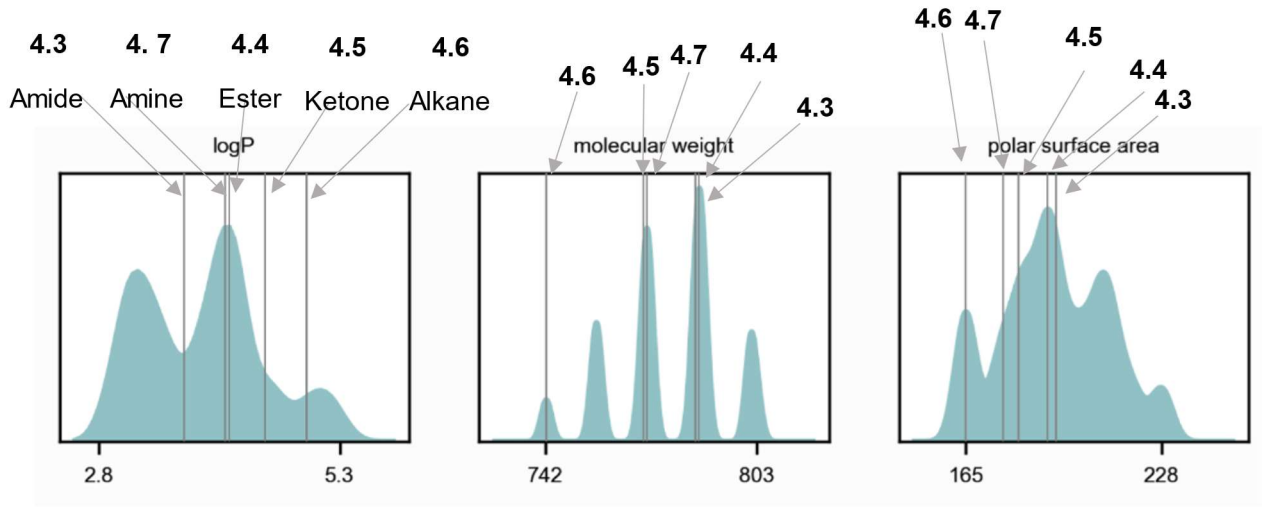

Figure 4.33 CRBN series calculated properties (Fig 4.5b). Note structures had properties calculated in their uncharged states.

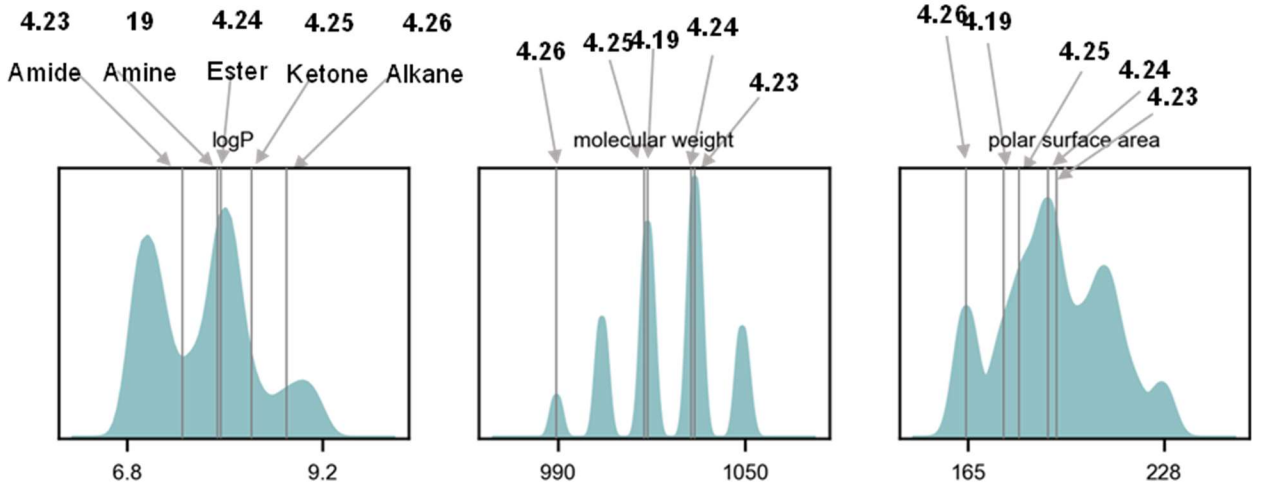

Figure 4.34 VHL series calculated properties (Fig 5d). Note structures had properties calculated in their uncharged states.

4.2.17 Characterization of products

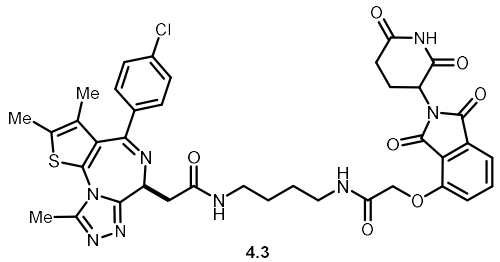

4.3

2-((*S*)-4-(4-chlorophenyl)-2,3,9-trimethyl-6H-thieno[3,2-f][1,2,4]triazolo[4,3-a][1,4]diazepin-6-yl)-N-(4-(2-((2-(2,6-dioxopiperidin-3-yl)-1,3-dioxoisoindolin-4-yl)oxy)acetamido)butyl)acetamide (dBet1) (4.3)

dBet1 (compound **4.3**) was prepared from **4.1** and **4.2** on a 0.1 mmol scale via general procedure 4.6. Upon completion of the reaction, it was quenched by the addition of 20 mL saturated aqueous Na2SO4 solution. The phases were then separated, and the aqueous phase was extracted with EtOAc (3 ´ 20 mL). The combined organic fractions were then washed with brine then dried over MgSO4, filtered, and concentrated in vacuo. The resulting residue was redissolved in MeCN: H2O (3:1 mL, HPLC grade) and purified via preparative HPLC to give 57.5 mg (73%) of desired amide as a white solid.

UPLC Retention time 2 min method: 0.97 min

^{1}H NMR (500 MHz, CD_3OD) δ 7.90 (s, 1H), 7.80 (t, *J* = 7.9 Hz, 1H), 7.52 (d, *J* = 7.3 Hz, 1H), 7.44 (td, *J* = 4.6, 2.2 Hz, 4H), 7.39 (dd, *J* = 8.7, 2.8 Hz, 2H), 5.10 (ddd, *J* = 12.2, 5.5, 3.1 Hz, 1H), 4.76 (s, 2H), 4.62 (dd, *J* = 8.9, 5.3 Hz, 1H), 3.45 – 3.31 (m, 9H), 3.31 – 3.24 (m, 2H), 2.87 – 2.75 (m, 1H), 2.75 – 2.62 (m, 6H), 2.43 (s, 3H), 2.10 (tp, *J* = 7.8, 3.8, 3.2 Hz, 1H), 1.75 – 1.55 (m, 7H).

^{13}C NMR (126 MHz, CD_3OD) δ 173.1, 171.3, 169.9, 169.9, 168.5, 166.9, 166.4, 164.9, 164.8, 155.6, 154.9, 150.8, 136.8, 136.7, 136.6, 133.5, 132.1, 131.8, 130.7, 130.6, 130.6, 129.9, 128.4, 120.5, 120.5, 118.0, 116.6, 78.1, 68.2, 53.8, 38.7, 38.7, 38.4, 37.5, 30.7, 30.7, 26.4, 26.2, 22.2, 13.0, 11.5, 10.2.

HRMS (ESI) Calculated $C_{38}H_{37}ClN_8O_7S^+$ $[M+H]^+$: 785.2267, Found 785.2268.

The spectra match those in literature.[24]

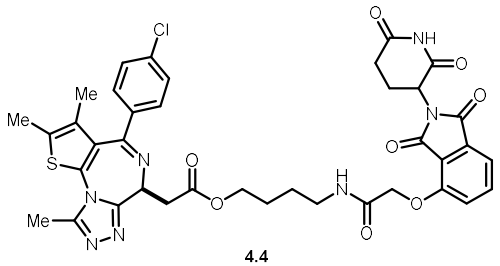

4.4

4-(2-((2-(2,6-dioxopiperidin-3-yl)-1,3-dioxoisoindolin-4-yl)oxy)acetamido)butyl 2-((*S*)-4-(4-chlorophenyl)-2,3,9-trimethyl-6H-thieno[3,2-f][1,2,4]triazolo[4,3-a][1,4]diazepin-6-yl)acetate (4.4)

Compound **4.4** was prepared from **4.1** and **4.10** on a 0.1 mmol scale via general procedure 4.7. Filtrate was reconstituted in acetonitrile and purified via preparative HPLC to give 42.5 mg (54%) of desired ester as an off white solid.

Compound **4.4** was also prepared via general procedure 4.8 in a one pot fashion to give 21.8 mg (28%) of desired ester.

UPLC Retention time 2 min method: 1.06 min

R_f 93:7 DCM:MeOH:

^{1}H NMR (600 MHz, DMSO) δ 10.90 (s, 1H), 7.80 (dd, *J* = 8.5, 7.2 Hz, 2H), 7.51 – 7.41 (m, 6H), 5.08 (dd, *J* = 12.5, 5.5 Hz, 1H), 4.75 (s, 2H), 4.50 (dd, *J* = 8.0, 6.3 Hz, 1H), 4.12 (qt, *J* = 10.9, 6.4 Hz, 2H), 3.48 (dd, *J* = 16.4, 6.3 Hz, 1H), 3.42 (dd, *J* = 16.4, 8.0 Hz, 1H), 2.88 (ddd, *J* = 16.8, 13.5, 5.7 Hz, 1H), 2.65 – 2.54 (m, 2H), 2.60 (s, 3H), 2.41 (s, 3H), 2.06 (tq, *J* = 7.9, 2.9 Hz, 1H), 1.67 – 1.59 (m, 2H),1.64 (s, 3H), 1.52 (p, *J* = 6.9 Hz, 2H).

^{13}C NMR (151 MHz, DMSO) δ 172.1, 170.1, 169.2, 166.4, 166.3, 165.2, 163.0, 154.9, 154.4, 149.5, 136.5, 136.4, 135.1, 132.8, 132.0, 130.5, 129.8, 129.6, 129.3, 128.2, 120.6, 116.9, 115.9, 67.9, 63.5, 53.3, 48.7, 37.7, 36.3, 30.7, 25.3, 25.2, 21.8, 13.5, 12.3, 10.8.

HRMS (ESI) Calculated $C_{38}H_{37}ClN_7O_8S^+$ $[M+H]^+$: 786.2107, Found 786.2098.

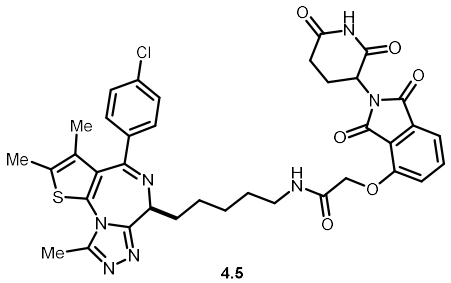

4.5

N-(5-((S)-4-(4-chlorophenyl)-2,3,9-trimethyl-6H-thieno[3,2-f][1,2,4]triazolo[4,3-a][1,4]diazepin-6-yl)pentyl)-2-((2-(2,6-dioxopiperidin-3-yl)-1,3-dioxoisoindolin-4-yl)oxy)acetamide (4.5)

Compound **4.5** was prepared from **4.1** and **4.10** on a 0.10 mmol scale via general procedure 4.10. The crude residue was passed through a plug of silica gel to remove the triphenylpyridine. The plug was initially washed with 50 mL of DCM followed by 50 mL of 7% methanol in DCM. The methanol/DCM fraction was evaporated, reconstituted in acetonitrile, and purified via preparative HPLC to give 24.5 mg (33%) of desired alkane product as a white solid.

UPLC Retention time 4 min method: 1.77 min

R_f 93:7 DCM:MeOH: 0.48

^{1}H NMR (500 MHz, $CDCl_3$) δ 7.70 (m, 1H), 7.66 (dt, J = 8.1, 4.1 Hz, 1H), 7.47 (dd, J = 7.3, 1.8 Hz, 1H), 7.37 (dd, J = 8.6, 2.6 Hz, 2H), 7.26 (dd, J = 10.0, 8.5 Hz, 2H), 7.11 (dd, J = 8.4, 6.0 Hz, 1H), 4.86 (dt, J = 12.6, 4.6 Hz, 1H), 4.61 (dd, J = 13.9, 2.0 Hz, 1H), 4.53 (dd, J = 13.9, 11.3 Hz, 1H), 3.86 (td, J = 10.2, 4.4 Hz, 1H), 3.72–3.56 (m, 1H), 3.17 (q, J = 7.9, 7.0 Hz, 1H), 2.83 – 2.55 (m, 4H), 2.61 (d, J = 6.7 Hz, 3H), 2.46 (qt, J = 12.4, 4.5 Hz, 1H), 2.34 (d, J = 3.8 Hz, 3H), 2.05 (dtd, J = 10.4, 5.2, 2.8 Hz, 1H), 1.90 – 1.70 (m, 1H), 1.70–1.50 (m, 5H), 1.62 (s, 3H), 1.49 – 1.34 (m, 1H).

^{13}C NMR (126 MHz, $CDCl_3$) δ 171.8, 171.7, 168.6, 168.4, 166.9, 166.7, 166.6, 166.2, 163.8, 156.3, 154.6, 154.6, 149.9, 137.0, 137.0, 136.8, 133.8, 132.2, 130.9, 130.7, 130.0, 129.9, 128.9,

128.8, 119.7, 119.6, 118.5, 117.5, 68.3, 68.2, 57.5, 57.3, 49.6, 49.5, 39.2, 39.0, 31.6, 31.4, 29.6, 29.4, 27.3, 27.2, 27.0, 26.9, 23.0, 14.6, 14.6, 13.3, 12.0.

HRMS (ESI) Calculated $C_{37}H_{37}ClN_7O_6S^+$ $[M+H]^+$: 742.2209, Found 742.2207.

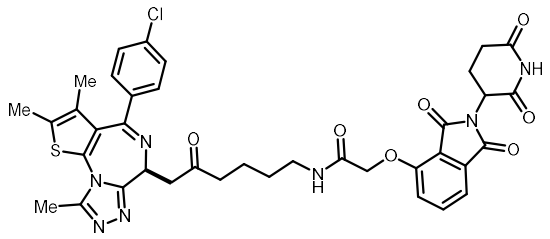

4.6

N-(6-((*S*)-4-(4-chlorophenyl)-2,3,9-trimethyl-6H-thieno[3,2-f][1,2,4]triazolo[4,3-a][1,4]diazepin-6-yl)-5-oxohexyl)-2-((2-(2,6-dioxopiperidin-3-yl)-1,3-dioxoisoindolin-4-yl)oxy)acetamide (4.6)

Compound **4.6** was prepared from **4.1** and **4.10** on a 0.10 mmol scale following general procedure 4.11. The crude residue was passed through a plug of silica gel to remove the triphenylpyridine. The plug was initially washed with 50 mL of DCM followed by 50 mL of 7% methanol in DCM. The methanol/DCM fraction was evaporated, reconstituted in acetonitrile, and purified via preparative HPLC to give 21.3 mg (28%) of desired ketone as a white solid.

UPLC Retention time 4 min method: 1.71 min

R_f 93:7 DCM:MeOH: 0.42

^{1}H NMR (499 MHz, $CDCl_3$) δ 7.74 (ddd, *J* = 8.9, 7.4, 2.0 Hz, 1H), 7.60 (q, *J* = 5.8 Hz, 1H), 7.54 (dd, *J* = 7.4, 2.2 Hz, 1H), 7.38 (dd, *J* = 8.4, 3.1 Hz, 2H), 7.32 (d, *J* = 8.3 Hz, 2H), 7.21 (dd, *J* = 8.4, 3.8 Hz, 1H), 4.97 (dd, *J* = 12.4, 5.4 Hz, 1H), 4.69 (dt, *J* = 6.7, 3.3 Hz, 1H), 4.66 (d, *J* = 4.8 Hz, 2H), 3.84 (ddd, *J* = 17.3, 6.4, 4.9 Hz, 1H), 3.68 (ddd, *J* = 17.4, 7.3, 4.5 Hz, 1H), 3.47 (dp, *J* = 12.4, 6.2 Hz, 1H), 3.38 (h, *J* = 6.9 Hz, 1H), 2.87 – 2.81 (m, 1H), 2.79 (dd, *J* = 9.2, 3.1 Hz, 1H),

2.78 – 2.72 (m, 1H), 2.72 – 2.68 (m, 1H), 2.66 (d, *J* = 2.1 Hz, 3H), 2.41 (s, 3H), 2.14 (ddd, *J* = 16.5, 12.2, 8.4 Hz, 1H), 1.84 – 1.72 (m, 3H), 1.72 – 1.64 (m, 5H).

^{13}C NMR (126 MHz, $CDCl_3$) δ 208.7, 208.6, 171.1, 171.0, 168.2, 168.1, 166.8, 166.7, 166.2, 166.1, 164.1, 163.9, 155.5, 154.6, 154.6, 149.9, 149.9, 137.0, 136.7, 133.6, 132.3, 132.2, 130.9, 130.8, 130.7, 130.4, 129.8, 128.7, 119.8, 118.4, 117.4, 68.3, 53.0, 49.4, 44.4, 44.3, 43.4, 43.4, 31.4, 28.7, 28.6, 22.7, 22.6, 21.0, 20.9, 14.4, 13.1, 11.8.

HRMS (ESI) Calculated $C_{38}H_{37}ClN_7O_7S^+$ $[M+H]^+$: 770.2158, Found 770.2147.

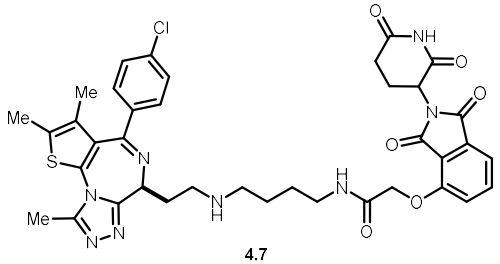

4.7

N-(4-((2-((S)-4-(4-chlorophenyl)-2,3,9-trimethyl-6H-thieno[3,2-f][1,2,4]triazolo[4,3-a][1,4]diazepin-6-yl)ethyl)amino)butyl)-2-((2-(2,6-dioxopiperidin-3-yl)-1,3-dioxoisoindolin-4-yl)oxy)acetamide (4.7)

Compound **4.7** was prepared from **4.1** and **4.2** on a 0.1 mmol scale relative to **4.2** via general procedure 4.9 where solvent = DMSO. Upon completion the reaction was quenched with 1 mL of methanol, filtered through a syringe filter, and purified via preparative HPLC to give 18.1 mg (23%) of desired amine as a white solid.

UPLC Retention time 2 min method: 0.82 min

^{1}H NMR (500 MHz, DMSO) δ 11.12 (s, 1H), 8.55 (s, 2H), 8.05 (t, J = 5.7 Hz, 1H), 7.82 (dd, J = 8.5, 7.3 Hz, 1H), 7.50 (d, J = 5.3 Hz, 5H), 7.40 (dd, J = 8.7, 3.4 Hz, 1H), 5.15 – 5.07 (m, 1H), 4.79 (s, 2H), 4.32 (dd, J = 7.6, 6.0 Hz, 1H), 3.42 – 3.33 (m, 1H), 3.31 – 3.23 (m, 1H), 3.20 (q, J = 6.6 Hz, 2H), 3.03 (dt, J = 14.0, 7.1 Hz, 2H), 2.90 (ddd, J = 16.3, 14.0, 5.4 Hz, 2H), 2.77 – 2.63

(m, 3H), 2.61 (s, 3H), 2.46 – 2.35 (m, 3H), 2.08 – 1.99 (m, 1H), 1.71 – 1.58 (m, 5H), 1.53 (dq, J = 14.1, 6.9 Hz, 2H).

^{13}C NMR (126 MHz, DMSO) δ 172.8, 169.9, 166.9, 166.7, 165.5, 163.7, 158.2, 158.0, 155.1, 155.0, 149.9, 137.0, 136.8, 135.3, 133.1, 132.4, 130.6, 130.3, 130.0, 129.6, 128.5, 120.5, 117.5, 116.8, 116.1, 67.7, 53.9, 48.8, 46.6, 44.2, 37.8, 30.9, 28.1, 26.2, 23.1, 22.0, 14.1, 12.6, 11.3.

HRMS (ESI) Calculated $C_{38}H_{40}ClN_8O_7S^+$ $[M+H]^+$: 771.2475, Found 771.2469.

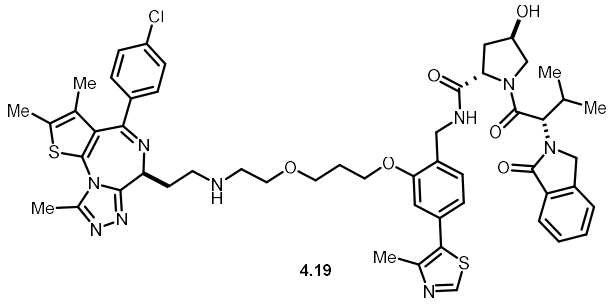

4.19

(2*S*,4*R*)-N-(2-(3-(2-((2-((*S*)-4-(4-chlorophenyl)-2,3,9-trimethyl-6H-thieno[3,2-f][1,2,4]triazolo[4,3-a][1,4]diazepin-6-yl)ethyl)amino)ethoxy)propoxy)-4-(4-methylthiazol-5-yl)benzyl)-4-hydroxy-1-((*S*)-3-methyl-2-(1-oxoisoindolin-2-yl)butanoyl)pyrrolidine-2-carboxamide (4.19)

Compound **4.19** was prepared from **4.1** and **4.13** on a 0.10 mmol scale relative to **4.13** via general procedure 4.9 where solvent = 95:5 dioxane:DMSO. Upon completion, the reaction mixture was concentrated *in vacuo* and redissolved in acetonitrile (3 mL, HPLC grade) then purified via preparative HPLC to 23 mg (22%) of desired amine.

UPLC Retention time 2 min method: 0.93 min

^{1}H NMR (400 MHz, DMSO) δ 8.27 (s, 1H), 8.07 (t, *J* = 5.6 Hz, 1H), 7.72 (d, *J* = 7.5 Hz, 1H), 7.64 – 7.58 (m, 1H), 7.50 (dt, *J* = 7.9, 4.0 Hz, 1H), 7.46 (s, 3H), 7.35 (d, *J* = 7.6 Hz, 1H), 7.00 (d, *J* = 8.3 Hz, 1H), 4.75 (d, *J* = 10.6 Hz, 1H), 4.57 (d, *J* = 18.0 Hz, 1H), 4.46 (q, *J* = 9.7, 8.4 Hz, 2H), 4.36 (d, *J* = 4.5 Hz, 1H), 4.31 (dd, *J* = 11.8, 5.8 Hz, 2H), 4.13 (ddt, *J* = 20.2, 13.7, 6.6 Hz,

3H), 3.79 (dd, *J* = 10.5, 4.8 Hz, 1H), 3.68 (d, *J* = 10.3 Hz, 1H), 3.59 (t, *J* = 6.3 Hz, 1H), 3.56 – 3.44 (m, 2H), 2.75 (t, *J* = 6.1 Hz, 1H), 2.59 (s, 3H), 2.56 – 2.42 (m, 9H), 2.41 – 2.32 (m, 3H), 2.24 (s, 1H), 2.08 – 1.91 (m, 4H), 1.64 (s, 3H), 0.97 (d, *J* = 6.5 Hz, 3H), 0.77 (d, *J* = 6.7 Hz, 3H).

^{13}C NMR (151 MHz, DMSO) δ 171.6, 168.1, 167.5, 163.2, 155.9, 155.4, 151.5, 149.7, 147.9, 142.2, 136.9, 135.2, 134.1, 132.3, 131.6, 131.4, 131.3, 131.0, 130.5, 130.2, 129.9, 129.6, 128.5, 127.9, 127.8, 127.2, 127.0, 123.6, 123.0, 120.9, 111.7, 79.2, 68.6, 66.9, 64.8, 58.7, 57.8, 55.4, 54.3, 48.0, 46.8, 45.3, 42.7, 38.1, 37.1, 29.0, 28.4, 18.9, 18.6, 16.0, 14.1, 14.0, 12.7, 11.3.

HRMS (ESI) Calculated $C_{53}H_{61}ClN_9O_6S_2^+$ $[M+H]^+$: 1018.3869, Found 1018.3862.

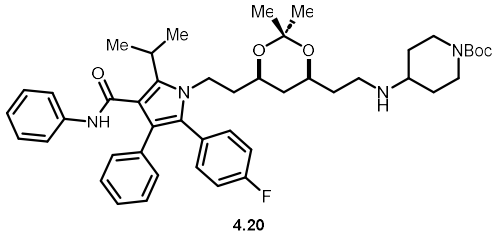

4.20

tert-butyl 4-((2-((4*S*,6*R*)-6-(2-(2-(4-fluorophenyl)-5-isopropyl-3-phenyl-4-(phenylcarbamoyl)-1*H*-pyrrol-1-yl)ethyl)-2,2-dimethyl-1,3-dioxan-4-yl)ethyl)amino)piperidine-1-carboxylate (Amine Well C6, 4.20)

Compound **4.20** was prepared from **4.17** and **4.15** on a 0.100 mmol scale relative to **4.15** via general via general procedure 4.9 on where solvent = 3:7 DMSO:dioxane. When the reaction was complete after 5 hours, it was cooled to room temperature and diluted with 30 mL of saturated sodium bicarbonate solution. This was extracted with DCM (3 × 25 mL). The organic layers were combined, washed with 30 mL of saturated sodium sulfate, dried over sodium sulfate, and concentrated. The residue was reconstituted in acetonitrile and purified via prep HPLC to give 28.4 mg (37%) of the desired amine as a white solid.

UPLC Retention time 2 min method: 1.12 min

^{1}H NMR (499 MHz, $CDCl_3$) δ 7.16 (dt, *J* = 12.3, 7.4 Hz, 9H), 7.06 (d, *J* = 8.0 Hz, 2H), 6.98 (td, *J* = 8.1, 7.5, 4.7 Hz, 3H), 6.85 (s, 1H), 4.08 (m, 4H), 3.89 – 3.76 (m, 3H), 3.65 (dd, *J* = 7.8, 4.6 Hz, 1H), 3.56 (p, *J* = 7.1 Hz, 1H), 2.84 (dq, *J* = 6.8, 4.1, 2.9 Hz, 2H), 2.81 – 2.66 (m, 3H), 1.91 (d, *J* = 12.7 Hz, 2H), 1.68 (q, *J* = 6.8 Hz, 3H), 1.52 (d, *J* = 7.1 Hz, 6H), 1.44 (s, 9H), 1.39 (d, *J* = 11.8 Hz, 2H), 1.33 (s, 3H), 1.29 (s, 3H), 1.22 (dt, *J* = 12.9, 2.5 Hz, 1H), 1.06 (q, *J* = 11.9 Hz, 1H).

^{13}C NMR (126 MHz, $CDCl_3$) δ 164.9, 162.4(d, *J* = 247.8 Hz), 154.8, 141.6, 138.5, 134.8, 133.3 (d, *J* = 8.0 Hz), 130.6, 128.9 (d, *J* = 10.4 Hz), 128.5, 126.7, 123.7, 119.7, 115.5 (d, *J* = 21.5 Hz), 98.7, 79.9, 66.6, 55.0, 42.3, 41.0, 38.2, 36.4, 30.2, 28.6, 28.6, 28.5, 26.2, 21.9, 21.8, 20.0.

^{19}F NMR (470 MHz, $CDCl_3$) δ -113.73.

HRMS (ESI) Calculated $C_{46}H_{60}FN_4O_5^+$ $[M+H]^+$: 767.4542, Found 767.4539

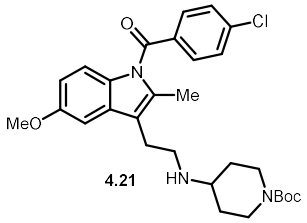

4.21

tert-butyl 4-((2-(1-(4-chlorobenzoyl)-5-methoxy-2-methyl-1*H*-indol-3-yl)ethyl)amino)piperidine-1-carboxylate (Amine Well B6, 21)

Compound **4.21** was prepared from **4.16** (indomethacin) and **4.15** via general procedure 4.9 on a 0.20 mmol scale where solvent = 3:7 DMSO:dioxane. When the reaction was complete after 3 hours, it was cooled to room temperature and diluted with 30 mL of saturated sodium bicarbonate solution. This was extracted with DCM (3 × 25 mL). The organic layers were combined, washed with 30 mL of saturated sodium sulfate, dried over sodium sulfate, and concentrated. The resulting residue was purified by column chromatography using

DCM/acetone/MeOH to give 35.0 mg (33%) of the desired amine as a yellow oil. The purified material had 20 μL of trifluoroacetic acid added to the NMR sample.

UPLC Retention time 2 min method: 0.98 min

^{1}H NMR (499 MHz, CD_3CN) δ 7.68 – 7.64 (m, 2H), 7.58 – 7.55 (m, 2H), 7.10 (d, *J* = 2.5 Hz, 1H), 6.99 (d, *J* = 9.0 Hz, 1H), 6.71 (dd, *J* = 9.0, 2.5 Hz, 1H), 4.12 (d, *J* = 13.7 Hz, 2H), 3.84 (s, 3H), 3.38 – 3.29 (m, 1H), 3.28 – 3.19 (m, 2H), 3.11 – 3.04 (m, 2H), 2.73 (d, *J* = 11.2 Hz, 2H), 2.29 (s, 3H), 2.03 (d, J = 11.9 Hz, 2H), 1.51 (qd, *J* = 12.3, 4.5 Hz, 2H), 1.43 (s, 9H).

^{13}C NMR (126 MHz, CD_3CN) δ 169.4, 158.7, 158.3, 157.2, 155.4, 139.7, 137.0, 135.3, 132.2, 132.1, 130.1, 117.0, 116.1, 114.7, 112.4, 102.2, 80.7, 57.5, 56.4, 45.5, 29.1, 28.5, 21.8, 13.7.

^{19}F NMR (470 MHz, CD_3CN) δ -76.86.

HRMS (ESI) Calculated $C_{29}H_{37}ClN_3O_4^+$ $[M+H]^+$: 526.2467, Found 526.2469.

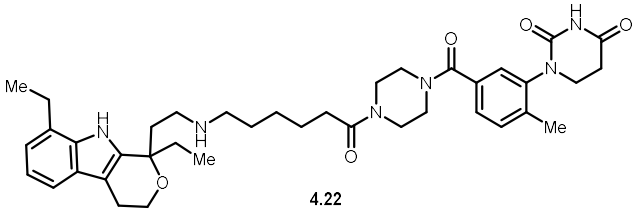

4.22

1-(5-(4-(6-((2-(1,8-diethyl-1,3,4,9-tetrahydropyrano[3,4-*b*]indol-1-yl)ethyl)amino)hexanoyl)piperazine-1-carbonyl)-2-methylphenyl)dihydropyrimidine-2,4(1*H*,3*H*)-dione (Amine Well D2, 4.22)

Compound **4.22** was prepared from **4.18** (etodolac) and **4.11** on a 0.100 mmol scale relative to **4.11** via general via general procedure 4.9 on where solvent = 3:7 DMSO:dioxane. When the reaction was complete after 5 hours, it was cooled to room temperature and diluted with 30 mL of saturated sodium bicarbonate solution. This was extracted with DCM (3 × 25mL). The organic layers were combined, washed with 30 mL of saturated sodium sulfate, dried over sodium

sulfate, and concentrated. The residue was reconstituted in acetonitrile and purified via prep HPLC to give 15.3 mg (23%) of the desired amine as a white solid.

UPLC Retention time 2 min method: 0.85 min

^{1}H NMR (499 MHz, $CDCl_3$) δ 10.75 (s, 1H), 8.61 (s, 1H), 7.36 (d, J = 7.9 Hz, 1H), 7.31 (d, J = 8.9 Hz, 3H), 7.04 (t, J = 7.4 Hz, 1H), 6.99 (d, J = 7.1 Hz, 1H), 4.09 – 4.02 (m, 1H), 3.96 (td, J = 11.0, 3.8 Hz, 1H), 3.85 – 3.78 (m, 1H), 3.78 – 3.29 (m, 9H), 2.95 (td, J = 15.8, 15.2, 7.8 Hz, 2H), 2.85 (ddt, J = 15.6, 12.4, 7.9 Hz, 6H), 2.76 – 2.66 (m, 2H), 2.53 (dd, J = 12.7, 6.5 Hz, 1H), 2.31 (s, 3H), 2.27 – 2.21 (m, 1H), 2.17 (s, 1H), 2.13 (d, J = 7.3 Hz, 1H), 2.03 (dt, J = 14.9, 7.5 Hz, 1H), 1.90 (dq, J = 14.8, 7.4 Hz, 1H), 1.39 (p, J = 7.3 Hz, 3H), 1.32 (d, J = 7.6 Hz, 3H), 0.97 (t, J = 7.4 Hz, 4H).

^{13}C NMR (126 MHz, $CDCl_3$) δ 171.6, 169.7, 168.7, 139.9, 138.4, 136.6, 135.3, 133.5, 131.4, 128.2, 127.1, 126.6, 126.5, 121.8, 120.7, 119.4, 115.7, 108.5, 75.8, 60.5, 47.6, 45.21, 44.71, 33.5, 32.5, 31.6, 31.5, 25.7, 25.6, 24.2, 23.7, 22.5, 18.1, 14.4, 8.0.

HRMS (ESI) Calculated $C_{39}H_{53}N_6O_5^+$ $[M+H]^+$: 685.4072, Found 685.4067.

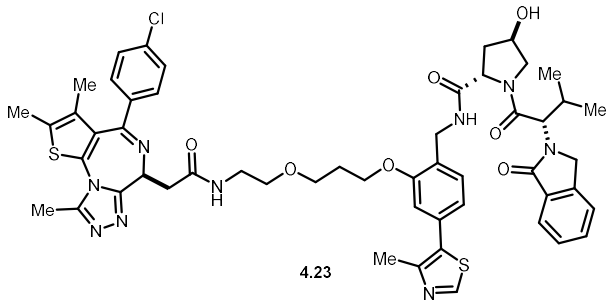

4.23

(2*S*,4*R*)-N-(2-(3-(2-(2-((*S*)-4-(4-chlorophenyl)-2,3,9-trimethyl-6H-thieno[3,2-f][1,2,4]triazolo[4,3-a][1,4]diazepin-6-yl)acetamido)ethoxy)propoxy)-4-(4-methylthiazol-5-yl)benzyl)-4-hydroxy-1-((*S*)-3-methyl-2-(1-oxoisoindolin-2-yl)butanoyl)pyrrolidine-2-carboxamide (4.23)

Compound **4.23** was prepared from **4.1** and **4.13** on a 0.10 mmol scale following general procedure 4.6. Upon completion the reaction was quenched by the addition of 20 mL saturated aqueous $NaHCO_3$ solution. The phases were then separated, and the aqueous phase was extracted with EtOAc (3 × 20 mL). The combined organic fractions were then washed with brine then dried over $MgSO_4$, filtered, and concentrated in vacuo. The resulting residue was redissolved in MeCN (3 mL, HPLC grade) and purified via preparative HPLC to give 48.5 mg (47%) of desired amide as a white solid.

Rf = 0.37 (10 % MeOH/DCM)

UPLC Retention time 2 min method: 1.13 min

^{1}H NMR (500 MHz, $CDCl_3$) δ 8.66 (s, 1H), 7.78 (s, 1H), 7.49 (t, *J* = 7.5 Hz, 1H), 7.41 – 7.33 (m, 5H), 7.30 (d, *J* = 7.9 Hz, 3H), 7.02 (m, 1H), 6.96 (d, *J* = 7.6 Hz, 1H), 6.92 (s, 1H), 4.79 (d, *J* = 10.8 Hz, 1H), 4.72 – 4.65 (m, 2H), 4.62 – 4.51 (m, 2H), 4.46 (dd, *J* = 14.7, 5.5 Hz, 1H), 4.37 (d, *J* = 17.5 Hz, 1H), 4.28 (d, *J* = 11.2 Hz, 1H), 4.14 (td, *J* = 11.7, 6.7 Hz, 2H), 3.72 (dh, *J* = 21.3, 6.1 Hz, 3H), 3.58 (d, *J* = 5.7 Hz, 2H), 3.47 (q, *J* = 5.5 Hz, 3H), 3.28 (dd, *J* = 14.6, 6.3 Hz, 1H), 2.56 (s, 4H), 2.52 – 2.43 (m, 8H), 2.39 (s, 4H), 2.14 (s, 1H), 1.65 (s, 3H), 1.30 – 1.22 (m, 1H), 0.92 (d, *J* = 6.5 Hz, 3H), 0.85 (d, *J* = 6.6 Hz, 3H).

^{13}C NMR (126 MHz, $CDCl_3$) δ 170.7, 170.2, 163.9, 156.9, 142.2, 136.9, 136.7, 131.8, 131.7, 131.0, 130.6, 129.9, 129.7, 128.8, 128.0, 126.5, 123.9, 122.9, 121.8, 112.4, 69.9, 69.5, 67.7, 65.2, 58.8, 58.7, 55.9, 47.4, 39.6, 39.2, 39.1, 36.4, 29.8, 29.5, 29.0, 19.2, 19.0, 16.3, 14.5, 13.2, 11.8.

HRMS (ESI) Calculated $C_{53}H_{59}ClN_9O_7S_2^+$ $[M+H]^+$: 1032.3662, Found 1032.3660.

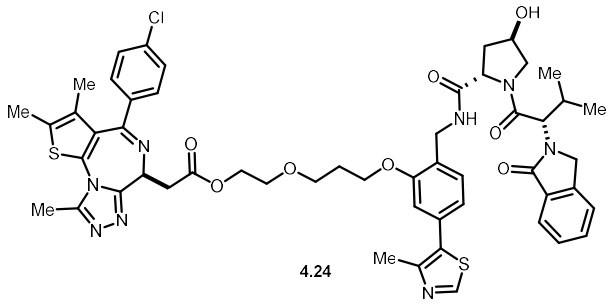

2-(3-(2-(((2*S*,4*R*)-4-hydroxy-1-((*S*)-3-methyl-2-(1-oxoisoindolin-2-yl)butanoyl)pyrrolidine-2-carboxamido)methyl)-5-(4-methylthiazol-5-yl)phenoxy)propoxy)ethyl 2-((*S*)-4-(4-chlorophenyl)-2,3,9-trimethyl-6H-thieno[3,2-f][1,2,4]triazolo[4,3-a][1,4]diazepin-6-yl)acetate (4.24)

Compound **4.24** was prepared from **4.1** and **4.13a** on a 0.10 mmol scale via general procedure 4.7. Filtrate was purified by flash chromatography on silica gel using DCM/Acetone (50 %) to MeOH/DCM (10 %) as eluent to 34.0 mg (36%) of desired ester as a white solid.

Compound **4.24** was also prepared from **4.1** and **4.13** on a 0.10 mmol scale via general procedure 4.8 to give 25.8 mg (25%).

Rf = 0.50 (10 % MeOH/DCM)

UPLC Retention time 2 min method: 1.21 min

^{1}H NMR (500 MHz, $CDCl_3$) δ 8.68 (s, 1H), 7.75 – 7.71 (m, 1H), 7.48 (td, *J* = 7.4, 1.1 Hz, 1H), 7.42 – 7.34 (m, 5H), 7.29 (dd, *J* = 8.3, 1.9 Hz, 3H), 6.93 (dd, *J* = 7.6, 1.6 Hz, 1H), 6.89 (d, *J* = 1.7 Hz, 1H), 4.76 (d, *J* = 10.9 Hz, 1H), 4.73 – 4.66 (m, 2H), 4.58 – 4.49 (m, 3H), 4.46 (dd, *J* = 15.0, 5.8 Hz, 1H), 4.40 – 4.32 (m, 3H), 4.26 (ddd, *J* = 11.8, 6.0, 3.7 Hz, 1H), 4.14 (t, *J* = 6.0 Hz, 2H), 3.78 – 3.68 (m, 5H), 3.62 – 3.51 (m, 2H), 2.61 (s, 3H), 2.51 (s, 3H), 2.46 (m, 1H), 2.39 (s, 3H), 2.18 – 2.09 (m, 3H), 1.66 (s, 3H), 0.93 (d, *J* = 6.5 Hz, 3H), 0.85 (d, *J* = 6.5 Hz, 3H).

^{13}C NMR (126 MHz, $CDCl_3$) δ 170.7, 170.2, 163.9, 156.9, 142.2, 136.9, 136.7, 131.8, 131.7, 131.0, 130.6, 129.9, 129.7, 128.8, 128.0, 126.5, 123.9, 122.9, 121.8, 112.4, 69.9, 69.5, 67.7, 65.2, 58.8, 58.7, 55.9, 47.4, 39.6, 39.2, 39.1, 36.4, 29.8, 29.5, 29.0, 19.2, 19.0, 16.3, 14.5, 13.2, 11.8.

HRMS (ESI) Calculated $C_{53}H_{58}ClN_8O_8S_2^+$ $[M+H]^+$: 1033.3502, Found 1033.3502.

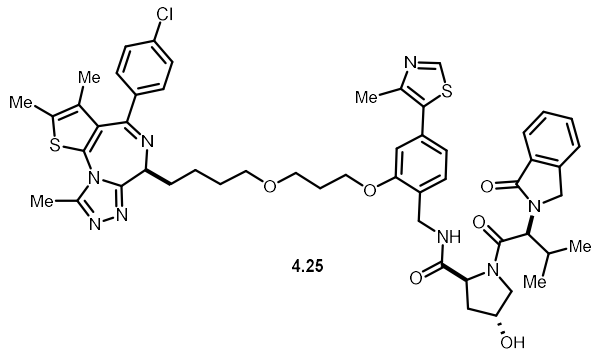

4.25

(2*S*,4*R*)-N-(2-(3-(4-((*S*)-4-(4-chlorophenyl)-2,3,9-trimethyl-6H-thieno[3,2-f][1,2,4]triazolo[4,3-a][1,4]diazepin-6-yl)butoxy)propoxy)-4-(4-methylthiazol-5-yl)benzyl)-4-hydroxy-1-((S)-3-methyl-2-(1-oxoisoindolin-2-yl)butanoyl)pyrrolidine-2-carboxamide (4.25)

Compound **4.25** was prepared from **4.1** and **4.13a** on a 0.10 mmol scale following general procedure 4.10. The product was purified via preparative HPLC to 21 mg (20%) of desired alkane product as a white solid.

UPLC Retention time 8 min method: 4.19 min

^{1}H NMR (400 MHz, CD_3CN) δ 8.71 (s, 1H), 7.70 (d, *J* = 7.5 Hz, 1H), 7.61 – 7.40 (m, 6H), 7.38 – 7.33 (m, 2H), 7.31 (d, *J* = 8.0 Hz, 1H), 7.25 (t, *J* = 6.1 Hz, 1H), 6.98 (d, *J* = 1.9 Hz, 1H), 4.74 (d, *J* = 10.9 Hz, 1H), 4.57 (d, *J* = 17.8 Hz, 1H), 4.48 – 4.41 (m, 2H), 4.39 – 4.34 (m, 4H), 4.11 (t, *J* = 6.1 Hz, 2H), 3.97 (dd, *J* = 8.4, 5.9 Hz, 1H), 3.86 (d, *J* = 10.9 Hz, 1H), 3.75 (dd, *J* = 10.9, 4.3 Hz, 1H), 3.64 (t, *J* = 6.1 Hz, 2H), 3.58 (td, *J* = 6.4, 3.2 Hz, 2H), 3.37 (d, *J* = 4.1 Hz, 1H), 2.54 (s,

2H), 2.45 (s, 3H), 2.40 (td, J = 7.8, 2.5 Hz, 1H), 2.35 (s, 3H), 2.15 (s, 3H), 2.06 (td, J = 12.6, 5.5 Hz, 4H), 1.86 – 1.73 (m, 1H), 1.62 (s, 3H), 0.92 (d, J = 6.5 Hz, 3H), 0.76 (d, J = 6.7 Hz, 3H).

^{13}C NMR (126 MHz, CD_3CN) δ 172.3, 170.2, 169.1, 164.4, 157.7, 157.0, 151.6, 150.8, 149.4, 143.5, 138.4, 136.7, 133.7, 132.9, 132.8, 132.5, 131.5, 131.4, 131.1, 129.7, 129.3, 128.8, 127.9, 124.3, 124.0, 122.0, 113.1, 79.2, 71.6, 70.5, 67.9, 66.3, 60.0, 59.3, 57.7, 56.4, 48.0, 39.0, 38.4, 30.4, 29.7, 27.3, 21.1, 19.4, 19.0, 16.5, 14.6, 13.1

HRMS (ESI) Calculated $C_{52}H_{58}ClN_8O_6S_2^+$ $[M+H]^+$: 989.3604, Found 989.3594.

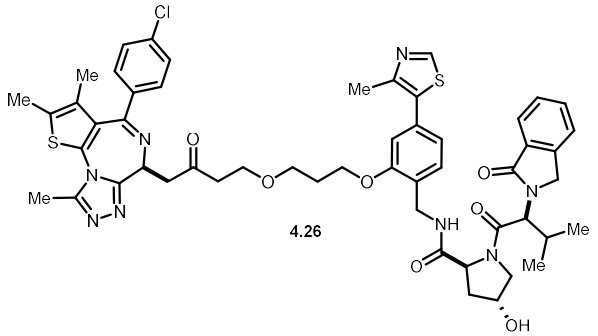

(2*S*,4*R*)-*N*-(2-(3-(4-((*S*)-4-(4-chlorophenyl)-2,3,9-trimethyl-*6H*-thieno[3,2-*f*][1,2,4]triazolo[4,3-a][1,4]diazepin-6-yl)-3-oxobutoxy)propoxy)-4-(4-methylthiazol-5-yl)benzyl)-4-hydroxy-1-((*S*)-3-methyl-2-(1-oxoisoindolin-2-yl)butanoyl)pyrrolidine-2-carboxamide (4.26)

Compound **4.26** was prepared from **4.1** and **4.13a** on a 0.95 mmol scale following a modified general procedure 4.11 where saturated sodium sulfate was replaced with saturated sodium bicarbonate to remove residual **4.1**. The crude residue was passed through a plug of silica gel to remove the triphenylpyridine. The plug was initially washed with 50 mL of DCM followed by 50 mL of 10% methanol in DCM. The methanol/DCM fraction was evaporated, reconstituted in acetonitrile, and purified via preparative HPLC to give 18.6 mg (19%) of desired ketone as a white solid.

UPLC Retention time 2 min method: 4.01 min

^{1}H NMR (499 MHz, $CDCl_3$) δ 8.66 (s, 1H), 7.77 (d, *J* = 7.2 Hz, 1H), 7.50 (td, *J* = 7.3, 1.1 Hz, 1H), 7.42 (d, *J* = 8.0 Hz, 2H), 7.41 – 7.25 (m, 8H), 6.92 (dd, *J* = 7.6, 1.6 Hz, 1H), 6.84 (d, *J* = 1.6 Hz, 1H), 4.76 (d, *J* = 10.9 Hz, 1H), 4.72 – 4.63 (m, 2H), 4.56 (t, *J* = 7.5 Hz, 1H), 4.55 – 4.49 (m, 1H), 4.48 (dd, *J* = 5.9, 4.0 Hz, 2H), 4.40 – 4.34 (m, 2H), 4.10 (t, *J* = 6.1 Hz, 2H), 3.84 (t, *J* = 6.4 Hz, 1H), 3.79 – 3.58 (m, 5H), 3.48 (s, 1H), 2.99 (dt, *J* = 16.5, 6.2 Hz, 1H), 2.88 (dt, *J* = 16.5, 6.5 Hz, 1H), 2.69 – 2.65 (m, 1H), 2.57 (s, 3H), 2.54 – 2.45 (m, 1H), 2.49 (s, 3H), 2.41 (td, *J* = 7.9, 7.1, 3.7 Hz, 2H), 2.38 (s, 3H), 2.17 – 2.05 (m, 3H), 1.72 – 1.65 (m, 1H), 1.64 (s, 3H), 0.91 (d, *J* = 6.5 Hz, 3H), 0.86 (d, *J* = 6.6 Hz, 3H).

^{13}C NMR (126 MHz, $CDCl_3$) δ 207.2, 170.8, 170.2, 169.4, 164.0, 156.9, 155.5, 150.3, 148.5, 142.3, 136.9, 136.8, 131.9, 131.8, 131.0, 130.9, 130.5, 129.9, 129.6, 128.8, 128.0, 126.5, 123.9, 123.0, 121.6, 112.1, 76.9, 70.2, 67.6, 65.8, 65.0, 58.7, 56.0, 52.8, 47.5, 44.8, 44.1, 39.1, 36.3, 29.7, 28.9, 19.2, 19.1, 16.2, 14.5, 13.2, 11.8.

HRMS (ESI) Calculated $C_{53}H_{58}ClN_8O_7S_2^+$ $[M+H]^+$: 1017.3553, Found 1017.3559

4.2.17.1 Characterization of screen scale ups

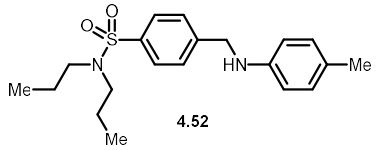

4.52

N,N-dipropyl-4-((*p*-tolylamino)methyl)benzenesulfonamide (Amine primary screen, Well D3, 4.52)

Compound **4.52** was prepared from **4.40** and **4.33** on a 0.20 mmol via general via general procedure 4.9 on where solvent = DMSO. When the reaction was complete after 5 hours, it was cooled to room temperature and diluted with 30 mL of saturated sodium bicarbonate solution. This was extracted with DCM (3 × 25mL). The organic layers were combined, washed with 30

mL of saturated sodium sulfate, dried over sodium sulfate, and concentrated. The residue was reconstituted with ethyl acetate and hexanes to give 47.3 mg (~66%) of impure desired amine as a clear oil.

^{1}H NMR (499 MHz, $CDCl_3$) δ 7.77 (d, *J* = 7.8 Hz, 2H), 7.50 (d, *J* = 8.0 Hz, 2H), 7.00 (d, *J* = 8.1 Hz, 2H), 6.54 (d, *J* = 8.4 Hz, 2H), 4.41 (s, 2H), 3.09 (t, *J* = 8.1 Hz, 4H), 2.25 (s, 3H), 1.56 (h, *J* = 6.9 Hz, 4H), 0.89 (t, *J* = 7.4 Hz, 6H).

^{13}C NMR (126 MHz, $CDCl_3$) δ 145.4, 144.7, 129.8, 127.61, 127.4, 127.2, 113.1, 50.1, 48.1, 22.07, 20.4, 11.2.

LRMS (UPLC) Calculated $C_{20}H_{29}N_2O_2S^+$ $[M+H]^+$: 361, Found 361

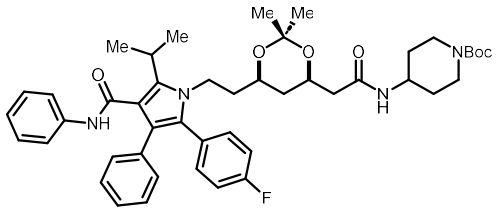

4.53

tert-butyl 4-(2-((4*R*,6*R*)-6-(2-(2-(4-fluorophenyl)-5-isopropyl-3-phenyl-4-(phenylcarbamoyl)-1*H*-pyrrol-1-yl)ethyl)-2,2-dimethyl-1,3-dioxan-4-yl)acetamido)piperidine-1-carboxylate (Amide primary screen, Well C5, 4.53)

Compound **4.53** was prepared from **4.17** and **4.15** on a 0.10 mmol scale according to procedure 4.6. Upon completion the reaction was quenched by the addition of 20 mL saturated aqueous $NaHCO_3$ solution. The phases were then separated, and the aqueous phase was extracted with EtOAc (3 × 20 mL). The combined organic fractions were then washed with brine then dried over $MgSO_4$, filtered, and concentrated in vacuo. The crude product was purified by chromatography on silica gel using 70 % EtOAc in hexanes to give 60.0 mg (77%) of desired amide as a white solid.

UPLC Retention time 2 min method: 1.45 min

^{1}H NMR (400 MHz, CD_3CN) δ 7.78 (s, 1H), 7.25 (m, 6H), 7.16 – 7.05 (m, 7H), 7.01 (t, *J* = 6.8 Hz, 1H), 6.38 (d, *J* = 7.8 Hz, 1H), 4.12 (dd, *J* = 11.4, 7.2 Hz, 1fH), 3.99 (ddd, *J* = 15.2, 10.4, 5.2 Hz, 1H), 3.87 (m, 3H), 3.80 – 3.67 (m, 2H), 3.37 (p, *J* = 7.1 Hz, 1H), 2.84 (m, 2H), 2.22 – 2.07 (m, 4H), 1.77 – 1.70 (m, 2H), 1.59 (m, 2H), 1.48 – 1.37 (m, 15H), 1.33 (s, 3H), 1.21 (s, 3H), 0.94 (q, *J* = 12.0 Hz, 1H).

^{13}C NMR (126 MHz, CD_3CN) δ 170.0, 166.7, 163.3 (d, *J* = 245.5 Hz), 155.4, 140.0, 139.6, 136.2, 134.7 (d, *J* = 8.3 Hz), 131.1, 129.8 (d, *J* = 3.7 Hz), 129.2, 127.1, 124.5, 122.6, 120.5, 116.1 (d, *J* = 21.6 Hz), 99.4, 79.8, 67.3, 67.1, 47.1, 43.8, 41.4, 38.8, 36.6, 32.5, 30.4, 28.6, 27.0, 22.4, 22.3, 20.2.

^{19}F NMR (470 MHz, CD_3CN) δ -72.21, -115.60.

HRMS (ESI) Calculated $C_{46}H_{57}FN_4O_6^+$ $[M+H]^+$: 781.4335, Found 781.4308.

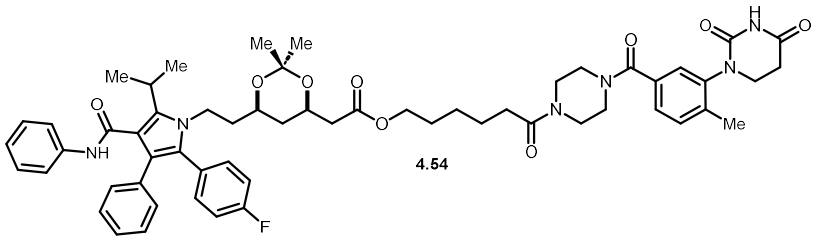

4.54

6-(4-(3-(2,4-dioxotetrahydropyrimidin-1(2*H*)-yl)-4-methylbenzoyl)piperazin-1-yl)-6-oxohexyl 2-((4*R*,6*R*)-6-(2-(2-(4-fluorophenyl)-5-isopropyl-3-phenyl-4-(phenylcarbamoyl)-1*H*-pyrrol-1-yl)ethyl)-2,2-dimethyl-1,3-dioxan-4-yl)acetate (Ester primary screen, Well C2, 4.54)

Compound **4.54** was prepared on a 0.10 mmol scale from **4.17** and **4.27** following general procedure 4.7. Purification was achieved via column chromatography using chloroform/acetone/methanol to give 88.2 mg (88%) of desired ester as a yellow solid.

Rf 48:48:4 chloroform:acetone:methanol: 0.40

UPLC Retention time 2 min method: 1.32 min

^{1}H NMR (499 MHz, $CDCl_3$) δ 8.13 (s, 1H), 7.50 – 7.35 (m, 4H), 7.29 (dd, *J* = 10.0, 6.1 Hz, 8H), 7.19 (d, *J* = 8.0 Hz, 2H), 7.11 (t, *J* = 7.8 Hz, 3H), 7.01 (s, 1H), 4.32 (dt, *J* = 13.3, 7.1 Hz, 1H), 4.19 (t, *J* = 6.8 Hz, 3H), 3.94 (ddd, *J* = 15.7, 10.6, 6.4 Hz, 2H), 3.87 – 3.54 (m, 10H), 2.95 (q, *J* = 6.2 Hz, 2H), 2.60 (dd, *J* = 15.6, 7.0 Hz, 1H), 2.46 (d, *J* = 8.0 Hz, 2H), 2.43 (s, 3H), 1.78 (q, *J* = 7.6 Hz, 6H), 1.65 (d, *J* = 7.0 Hz, 6H), 1.56 – 1.45 (m, 3H), 1.48 (s, 3H), 1.41 (s, 3H), 1.38 (d, *J* = 4.3 Hz, 1H), 1.15 (dt, *J* = 25.7, 12.6 Hz, 1H).

^{13}C NMR (126 MHz, $CDCl_3$) δ 171.5, 171.0, 169.5, 164.9, 162.4 (d, *J* = 247.8 Hz), 141.6, 140.1, 138.5, 138.1, 134.7, 134.2, 133.3 (d, *J* = 8.1 Hz), 131.6, 131.2, 130.6, 128.9, 128.8, 128.4 (d, *J* = 5.7 Hz), 127.0, 126.7, 126.6, 123.6, 121.9, 119.7, 119.2, 115.5 (d, *J* = 21.4 Hz), 115.5, 98.8, 66.5, 65.7, 64.4, 45.2, 41.3, 40.9, 38.1, 36.1, 33.1, 31.6, 30.0, 29.4, 28.6, 26.2, 25.8, 24.8, 21.9, 21.7, 19.8, 19.7, 18.1.

^{19}F NMR (470 MHz, $CDCl_3$) δ -113.74.

HRMS (ESI) Calculated $C_{58}H_{67}FN_6NaO_9^+$ $[M+Na]^+$: 1033.4851, Found 1033.4834.

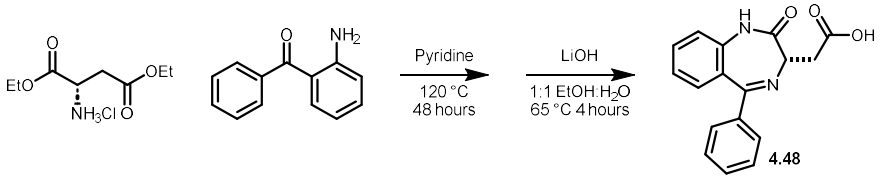

Scheme 4.6 Synthesis of 4.48[57]

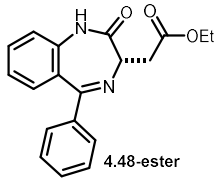

ethyl (*S*)-2-(2-oxo-5-phenyl-2,3-dihydro-1*H*-benzo[*e*][1,4]diazepin-3-yl)acetate (4.48-ester)

Following a reported procedure[57], to an oven dried 100 mL round bottom flask charged with a Teflon coated stir bar was added 2-amino benzophenone (**SI-17**) (1200 mg, 6.1 mmol, 1.0 equiv) and L-aspartic acid diethyl ester hydrochloride salt (2060 mg, 9.1 mmol, 1.5 equiv). A reflux

condenser and rubber septum were fitted, and the flask evacuated and refilled under a nitrogen atmosphere 3x. To the flask was added 40.0 mL of pyridine and the solution was stirred for 48 hours at 120 °C and 300 rpm. After cooling to room temperature, the reaction was concentrated *in vacuo* and poured over 50 mL of ice water. This was extracted with DCM (3 ´ 75 mL). The organic layers were combined and washed with 50 mL of 0.1 M HCl followed by drying with sodium sulfate and concentration *in vacuo*. The residue was purified by column chromatography 0à50% Ethyl acetate in hexanes to give 500 mg (26%) of **4.48-ester** as a tan solid.

R_f 50:50 Ethyl acetate: hexanes: 0.50

^{1}H NMR (499 MHz, $CDCl_3$) δ 9.23 (s, 1H), 7.54 – 7.47 (m, 3H), 7.43 (t, *J* = 7.4 Hz, 1H), 7.41 (s, 0H), 7.36 (t, *J* = 7.5 Hz, 2H), 7.32 (dd, *J* = 7.9, 1.5 Hz, 1H), 7.16 (dd, *J* = 16.6, 8.7 Hz, 2H), 4.24 – 4.14 (m, 3H), 3.43 (dd, *J* = 16.7, 7.4 Hz, 1H), 3.22 (dd, *J* = 16.7, 6.7 Hz, 1H), 1.29 (dd, *J* = 14.3, 1.2 Hz, 3H).

^{13}C NMR (126 MHz, $CDCl_3$) δ 172.1, 171.6, 169.9, 149.9, 139.3, 138.4, 131.9, 131.4, 130.5, 129.9, 128.3, 127.7, 123.6, 121.4, 60.6, 60.4, 36.8, 14.4.

HRMS (ESI) Calculated $C_{19}H_{19}N_2O_3^+$ $[M+H]^+$: 323.1390, Found 323.1391

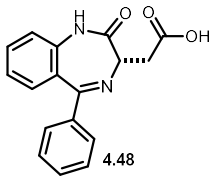

4.48

(*S*)-2-(2-oxo-5-phenyl-2,3-dihydro-1*H*-benzo[*e*][1,4]diazepin-3-yl)acetic acid (4.48)

to a two-dram vial charged with a Teflon coated stir bar was added **4.48-ester** (200 mg, 0.62 mmol, 1.0 equiv). This was dissolved in 2.0 mL of ethanol followed by addition of 2.0 mL of 1M aqueous LiOH. The vial was capped and stirred for 4 hours at 60 °C and 800 RPM. After cooling to room temperature, the ethanol was removed *in vacuo* and the remaining water cooled in an ice bath. The pH was adjusted to ~4 using 1M HCl and the solid precipitate was filtered and washed

with water. This precipitate was dissolved in ethyl acetate, dried over sodium sulfate, filtered, and concentrated *in vacuo* to give 100 mg (55%) of **4.48** as a white solid.

^{1}H NMR (400 MHz, CD_3CN) δ 8.80 (s, 1H), 7.65 – 7.56 (m, 1H), 7.54 – 7.48 (m, 2H), 7.48 – 7.39 (m, 2H), 7.35 – 7.18 (m, 3H), 4.01 (dd, *J* = 7.0, 5.3 Hz, 1H), 3.13 (dd, *J* = 16.6, 7.0 Hz, 1H), 2.99 (dd, *J* = 16.6, 5.3 Hz, 1H).

^{13}C NMR (101 MHz, CD_3CN) δ 173.08, 171.30, 139.71, 133.22, 132.09, 131.68, 130.65, 129.28, 127.89, 124.43, 122.21, 61.03, 36.22.

HRMS (ESI) Calculated $C_{17}H_{15}N_2O_3^+$ $[M+H]^+$: 295.1077, Found 295.1070

4.2.18 Cell titer glow assay data.

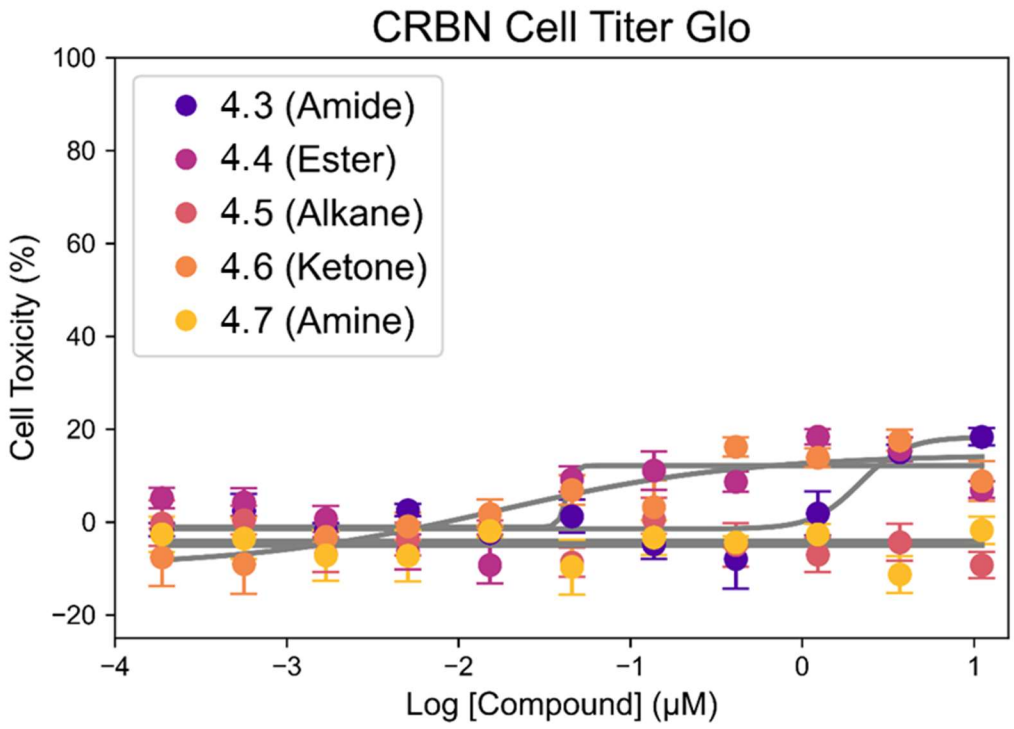

Figure 4.35 Results of Cell Titer Glo assay for compounds **4.3-7**. Data are from N=4 replicates

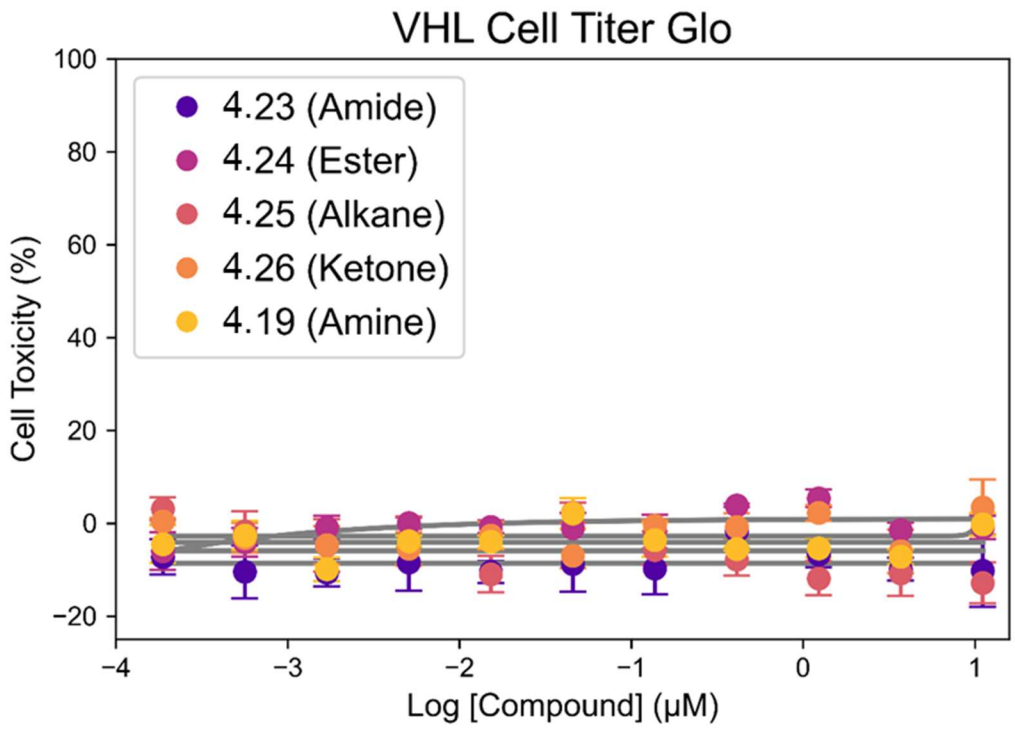

Figure 4.36 Results of Cell Titer Glo assay for compounds **4.19**, **4.23**-**26**. Data are from N=4 replicates.

4.2.19 BRD4-BD1 binding data

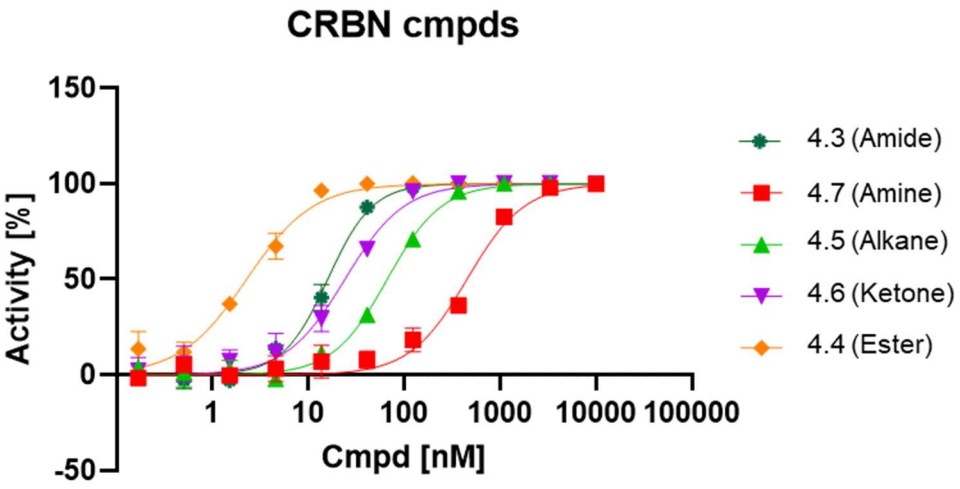

Figure 4.37 Results of BRD4-BD1 binding assay for compounds **4.3**-**7**. Data are from N=3 replicates.

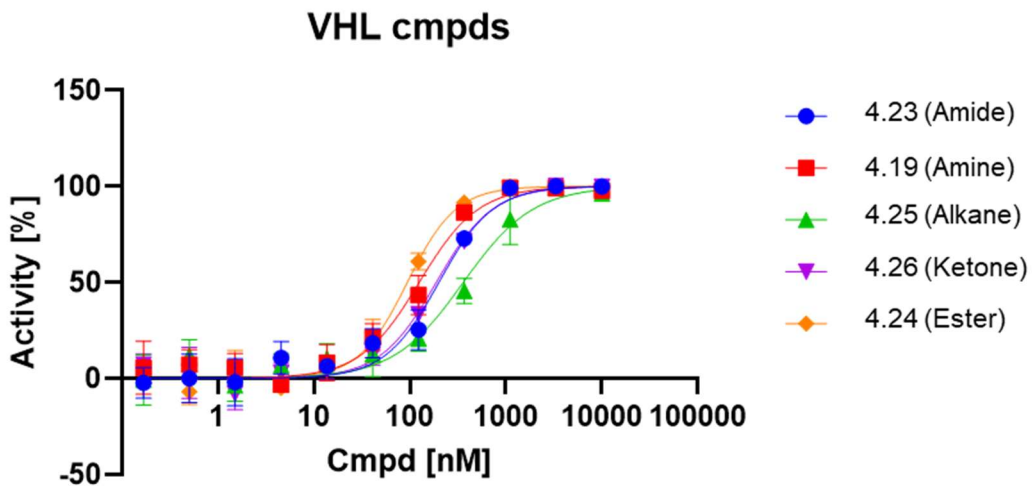

Figure 4.38 Results of BRD4-BD1 binding assay for compounds **4.19, 4.23-6**. Data are from N=3 replicates.

4.2.20 Extended VHL permeability data

Table 4.23 Results of nanoBRET assay in permeabilized and live cells for compounds **4.19**, **4.23-26** as well as calculated RBA values. Data are from N=5 replicates.

Linker Type (#)	nanoBRET Live (nM)	nanoBRET Permeabilized (nM)	nBREt RBA
amide (**23**)	2195 ± 55	927 ± 54	2.4
ester (**24**)	5989 ± 145	2345 ± 84	2.6
alkane (**25**)	3918 ± 186	1870 ± 59	2.1
ketone (**26**)	15731 ± 520	2884 ± 107	2.7
amine (**19**)	2498 ± 46	618 ± 56	4.0

4.2.21 Interaction Diagrams of Compounds in BRD4-BD1 Binding Pocket.

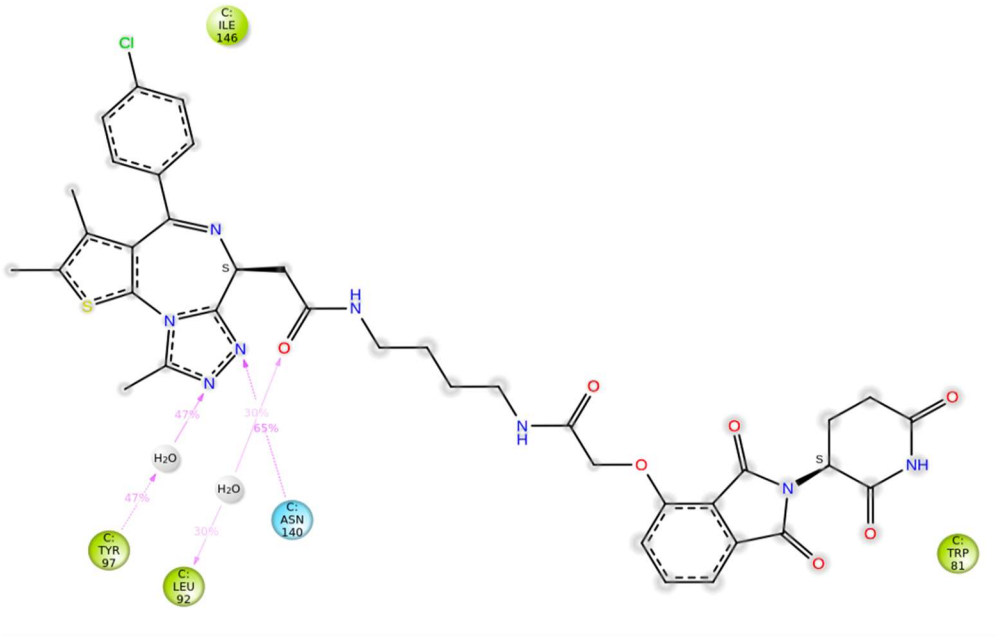

Figure 4.39 Diagram of interactions of **4.3** in binding pocket of BRD4-BD1.

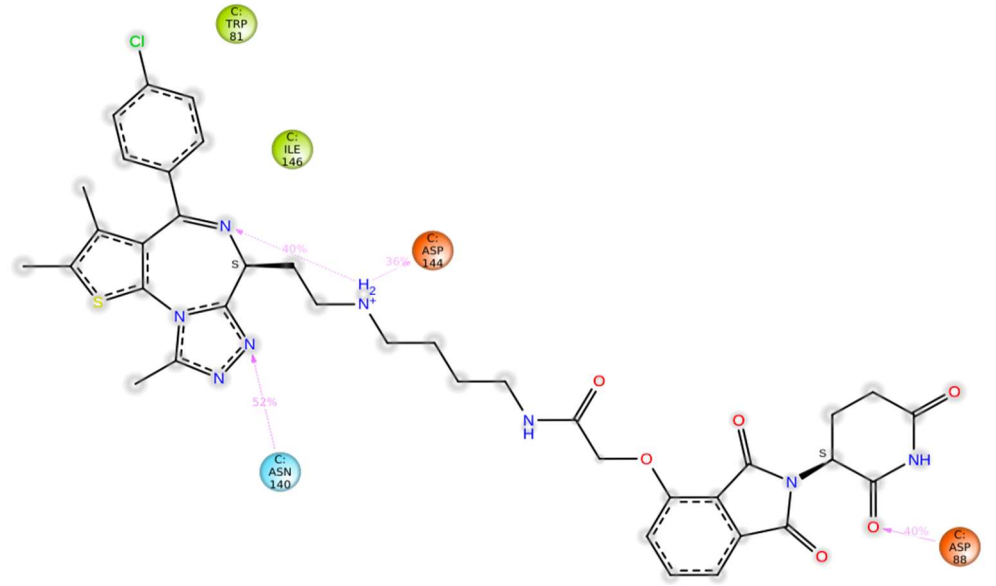

Figure 4.40 Diagram of interactions of **4.7** in binding pocket of BRD4-BD1. Note hydrogen bond between amine and imine as well as amine and ASP 144.

4.3 The influence of amine–acid couplings on cellular distribution.[10]

4.3.1 Introduction

The ability for a drug molecule to exert its desired effect is dependent upon its ability to bind to a target protein. In the context of a biochemical assay, this is a straightforward task. However, in the context of a cell or organism, this can be much more complicated. The molecule must traverse several membranes to reach the desired tissue without excessive trapping by plasma proteins.[58,59] For intracellular targets, an additional layer of complexity is added, particularly if the target is localized within a specific organelle. This results in only a small fraction of the dosed drug reaching its site of action.[60] This has important implications in the context of toxicity and efficacy, particularly with cytotoxic agents.[61] It has been demonstrated that beyond tissue and cell type, where a small molecule localizes within a cell also has important implications on both toxicity and mechanism of action.[62–64] Current strategies to target small molecules to specific organelles include conjugation to other small molecules,[65,66] peptides[67], or nanoparticle encapsulation.[68] Each of these methods have proven effective, but the conjugation of another molecule may alter the efficacy or oral availability of the drug. As such it would be ideal to incorporate organelle targeting properties into the structure of the drug itself. It has been demonstrated that the properties of a small molecule can influence its subcellular distribution profile.[59,63,69]

We have demonstrated amine acid couplings have a pronounced effect on the properties of a molecule.[16] Based upon this we would be able to influence the subcellular distribution of an amine and carboxylic acid coupling pair by varying the reaction conditions used to unite them.

[10] Compounds **4.59** and **4.60** were synthesized by Dr. Sam Zhang. Dr. Chris Audu assisted with developing imaging protocols.

By taking advantage of a naturally fluorescent carboxylic acid, fluorescein (**4.55**), we were able to circumvent many of the challenges associated with determining the localization of the molecules we synthesized. [59,70,71]

4.3.2 Synthesis of fluorescent dyes from an amine–acid pair.

To begin our studies, we selected **4.55** and **4.33** as coupling partners. We selected four reactions as a starting point for our chemistry: amidation, esterification, reductive amination, and α-arylation. Amidation was accomplished using diisopropylcarbodiimide (DIC) and dimethylamino pyridine (DMAP) in DMF at 80 °C. Initial attempts to use chemistry developed in our lab to synthesize the ester from the diazonium salt of **4.33** produced complex mixtures that were low yielding in the desired ester, and as such the ester was prepared from the acid chloride of **4.55** and p-cresol. We encountered as similar issue for the α-arylation chemistry[72] and instead used chemistry developed by the Weix group using aryl iodide **4.56** (Figure **4.39**, A). A 24 well array examining two catalysts, six ligands, and two solvents was performed to optimize the reductive amination reaction for fluorescein (see experimental section). The highest yielding hit from the screen was scaled up to synthesize **4.58** (Figure 4.39, B).

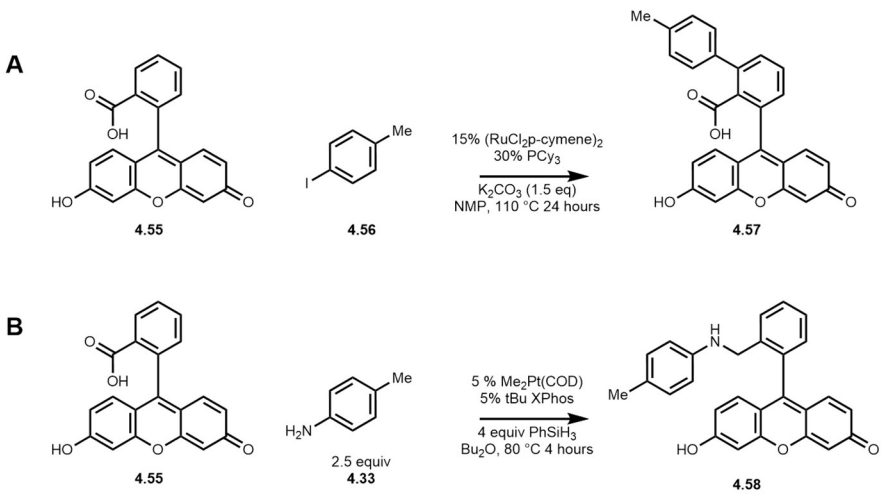

Figure 4.41 Synthesis of fluorescein derivatives. A) Synthesis of alpha arylated product **4.57**. B) Synthesis of aminated product **4.58**.

4.3.3 Visualization of dye derivatives in cells.

With our dye derivatives in hand, we began exploring their distribution in NIH-3T3 cells. To accomplish this, we incubated live cells with known organelle tracking dyes as well as our derivatives and observed them with live cell imaging. While not absolute, we did observe bias in the distribution of each derivative using Pearson's correlation.[73] We found amide **4.60**, made using, a carbodiimide catalyst, was only slightly permeable to the cell membrane and did not selectively localize whereas ester **4.59**, which can be made using a copper catalyst, was found more in the lysosome then other organelles. Arylated product **4.57** made with a ruthenium catalyst, generally localized to the mitochondria, and alkyl amine product **4.58**, made with a platinum catalyst, was preferentially found in the golgi.

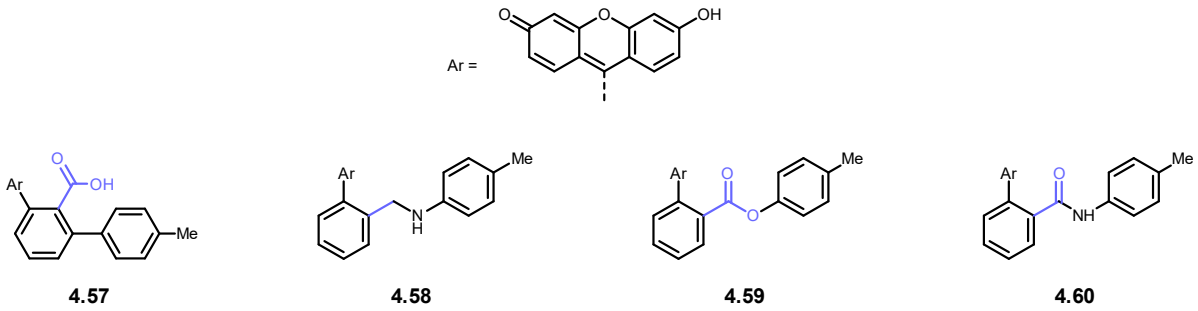

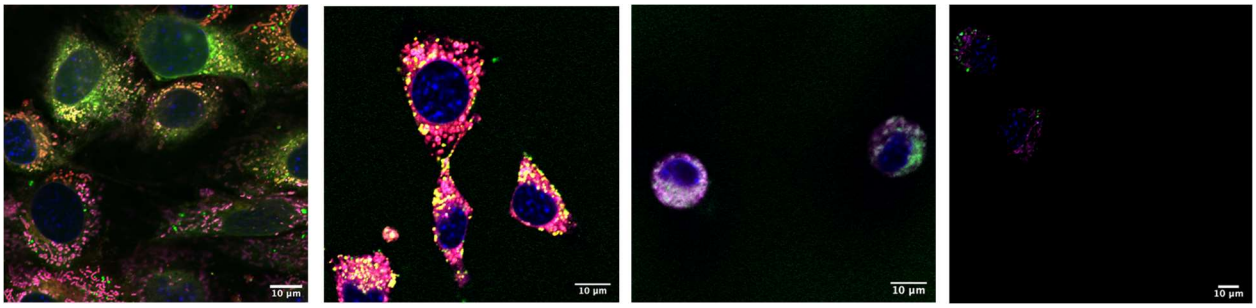

Figure 4.42 Overlayed images of fluorescein derivatives with localization dyes. Red is lysosome, blue is nucleus, magenta is mitochondria, green is fluorescein derivative. Yellow indicates overlap between lysosome and fluorescein.

4.3.4 Visualization of PROTAC derivatives in cells

By taking advantage of the natural green fluorescence of pomalidomide[74] we were able to image the degraders synthesized in chapter **4.1** as well. In contrast to the fluorescein derivatives, we observed that **4.4**, **4.5**, and **4.7** all localized in the lysosome. This is possibly attributed to the much larger molecular weight (cf. 800 vs 400) or the dense functionalization present in these derivatives causing trafficking to the lysosome.

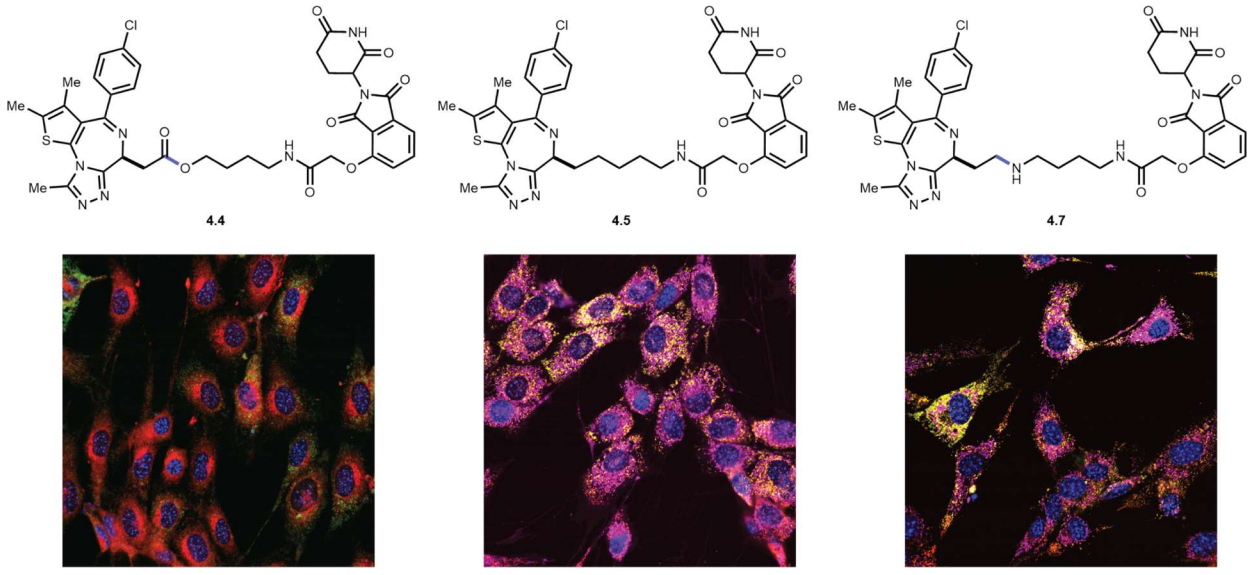

Figure 4.43 Overlayed images of PROTACs with localization dyes. Red is lysosome, blue is nucleus, magenta is mitochondria, green is PROTAC derivative. Yellow indicates overlap between lysosome and PROTAC.

4.3.5 Conclusions

We have demonstrated that in small molecule fluorescent dyes, the choice of catalyst used to couple two building blocks together can have a dramatic impact on where the molecule localizes within mouse fibroblasts. This is likely due to the difference in properties imparted by the change. Further studies into this effect are ongoing in our lab, and we will observe the impact of other transformations on localization in the near future. We see as the molecules become larger, single atom changes have a more nuanced effect on the overall properties of the molecule. This may in part explain the differences observed between the fluorescein and dbet1 derivatives. These proof-of-concept studies serve to demonstrate that there is a direct connection between the functional outcome of a molecule and the materials used to make it.

4.4 Experimental section for the influence of amine–acid couplings on cellular distribution.

Please see section 4.2.1 for general methods.

4.4.1 Cell growth for microscopy.

Immortalized murine embryonic fibroblast cells (NIH3T3) cells were grown in Complete Media (10% Fetal Bovine serum + 100 ug/mL streptomycin + 100 U/mL Penicillin all dissolved in Dulbelcco's Modified Eagle's medium - DMEM) and incubated at 37 °C with 5% CO_2. After 36 - 48hrs, cells were trypsin digested, and aliquoted into microscopy chamber slides at approximately $1x10^4$ cells/mL and incubated until near confluence.

4.4.2 Organelle staining and microscopy.

Into 1 mL aliquots of warm Complete Media was added 1 μL nuclear DAPI solution (Biotium, Cat # 40011) along with standard stains for each organelle (Lysosome – Biotium LysoView 640

#70085-T; Mitochondria – Biotium MitoViewTM 720 #70068-T; Golgi – Invitrogen BODIPY TR Ceramide #D7540) according to manufacturer protocol. Each fluorescent compound **4.4**, **4.5**, **4.7**, **4.57-60** was diluted to 1 mg/mL in DMSO. The compound was added to obtain a final concentration of approximately 10 mM (and < 10% DMSO) in the complete media. Cells were then incubated with this complete media containing the stains at 37 °C, 5% CO_2 for 15 min. The cells were then washed with unstained Complete Media and incubated with 1mL of Live Cell Imaging solution (Invitrogen; Cat #: A14291DJ).

Live cell images were then obtained on a confocal microscope (Nikon A1 Standard Sensitivity Confocal). Cellular organelle co-localization was estimated using Pearson correlation coefficients of each respective standard organelle dye colour with the fluorescent compound. This was computed with FIJI (NIH ImageJ software).

4.4.3 Pearson's R table.

	4.57	4.58	4.59	4.60
Golgi	0.26	0.74	0.14	0.31
Mitochondria	0.78	0.56	0.63	0.29
Lysosome	0.15	0.33	0.75	0.11
Nucleus	-0.16	-0.27	0.02	-0.05

4.4.4 Synthesis of fluorescent dyes

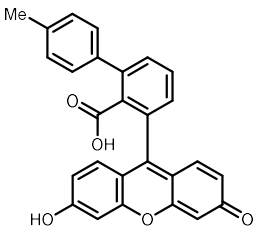

4.57

3-(6-hydroxy-3-oxo-3*H*-xanthen-9-yl)-4'-methyl-[1,1'-biphenyl]-2-carboxylic acid (4.57)

According to a modified literature procedure[75] in a nitrogen filled glovebox, an oven dried two-dram vial charged with a stir bar was loaded with fluorescein (167 mg, 0.5 mmol, 1.0 equiv), potassium carbonate (104 mg, 0.75 mmol, 1.5 equiv), Dichloro(*p*-cymene)ruthenium(II) dimer (45 mg, 0.075 mmol, 0.15 equiv), tricyclohexylphosphine (42.0 mg, 0.15 mmol, 0.3 equiv), and **4.56** (163 mg, 0.75 mmol, 1.5 equiv). 2.0 mL of NMP were added, the vial capped, removed from the glovebox, and subsequently stirred at 1200 rpm and 110 °C for 24 hours. Upon completion, the reaction was diluted with 50 mL of ethyl acetate and washed 3x with 25 mL of 1M HCl in water. The organic layer was dried, evaporated and the crude residue purified with hexane, DCM, and acetone to give 126 mg (60%) of a yellow solid.

R_f = 0.3 in 1:1:1 DCM: acetone: hexanes

1H NMR (499 MHz, CD_3OD) δ 7.72 (t, J = 7.6 Hz, 1H), 7.56 – 7.50 (m, 3H), 7.29 (d, J = 7.8 Hz, 2H), 7.08 (dd, J = 7.7, 0.9 Hz, 1H), 6.69 – 6.68 (m, 3H), 6.66 (s, 1H), 6.55 (dd, J = 8.7, 2.4 Hz, 2H), 2.42 (s, 3H).

13C NMR (126 MHz, CD_3OD) δ 169.2, 159.5, 152.5, 142.0, 138.0, 134.9, 133.7, 131.0, 129.31, 128.8, 128.3, 122.6, 122.1, 112.0, 110.2, 102.1, 19.9.

LRMS (UPLC) Calculated $C_{27}H_{19}O_5^+$ $[M+H]^+$: 423, Found 423

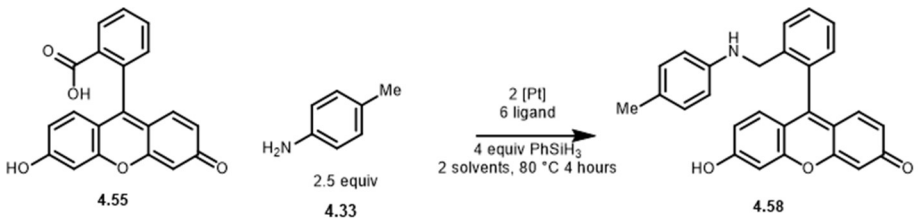

Table 4.24 Recipe for fluorescein reductive amination optimization screen.

Reagents	Solvent	C_{stock} (M)	V_{dose} (µL)	Wells	Order Added
Platinum (II) Chloride	Bu2O	0.5	20	A, 1-6	1
dimethyl cyclooctadiene platinum (0)	Bu2O	0.5	20	B, 1-6	1
BrettPhos	Bu2O	0.5	20	A,B, 1	2
tBuXPhos	Bu2O	0.5	20	A,B, 2	2
diphenylphosphinoethane	Bu2O	0.5	20	A,B, 3	2
triphenylphosphine	Bu2O	0.5	20	A,B, 4	2
Terpyridine	Bu2O	0.5	20	A,B, 5	2
di-tert-butylbipyridine	Bu2O	0.5	20	A,B, 6	2
Fluorescein	Bu2O	0.5	20	A,B, 1-6	3
p-toluidine	Bu2O	0.75	20	A,B, 1-6	4
Phenylsilane	Bu2O	2	20	A,B, 1-6	5
Platinum (II) Chloride	DMSO	0.5	25	C, 1-6	1
dimethyl cyclooctadiene platinum (0)	DMSO	0.5	25	D, 1-6	1
BrettPhos	DMSO	0.5	25	C,D 1	2
tBuXPhos	DMSO	0.5	25	C,D 2	2
diphenylphosphinoethane	DMSO	0.5	25	C,D 3	2
triphenylphosphine	DMSO	0.5	25	C,D 4	2
Terpyridine	DMSO	0.5	25	C,D 5	2
di-tert-butylbipyridine	DMSO	0.5	25	C,D 6	2
Fluorescein	DMSO	0.5	25	C,D 1-6	3
p-toluidine	DMSO	0.75	20	C,D 1-6	4
Phenylsilane	DMSO	2	25	C,D 1-6	5

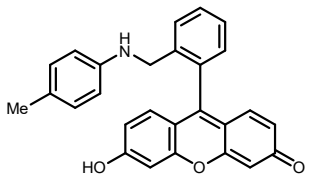

4.58

6-hydroxy-9-(2-((p-tolylamino)methyl)phenyl)-3H-xanthen-3-one (4.58)

In a nitrogen filled glovebox, an oven dried two-dram vial, equipped with a Teflon-coated stir bar, was charged with dimethyl cyclooctadiene platinum (0) (3.3 mg, 0.01 mmol, 0.05 equiv) and tBuXphos (4.2 mg, 0.01 mmol, 0.01 equiv). 200 µL of Bu_2O was added and the solution stirred for 20 minutes at 30 °C and 300 rpm. Outside of the glovebox, an additional oven dried two-dram vial, equipped with a Teflon-coated stir bar, was charged with **4.33** (0.30 mmol, 1.5 equiv) and **4.55** (0.10 mmol, 1.0 equiv). 900 µL of solvent was added. The catalyst solution was removed from the glovebox, cooled to room temperature, and phenylsilane (97 µL, 0.8 mmol, 4.0 equiv) added via syringe. **Note the solution will bubble vigorously and generate hydrogen**

gas. The yellow solution was transferred via syringe to the amine/acid vial which was subsequently heated at 80°C for 4 hours and a stir rate of 500 rpm. Upon completion, the reaction was diluted with 25 mL ethyl acetate and washed with 25 mL of saturated sodium sulfate. The organic layer was dried over sodium sulfate and purified by preparative LC to give 38.2 mg (47 %) of a yellow solid.

^{1}H NMR (499 MHz, dmso) δ 9.63 (s, 2H), 7.45 (dt, *J* = 7.6, 1.0 Hz, 1H), 7.22 (td, *J* = 7.5, 1.1 Hz, 1H), 7.12 (dd, *J* = 7.6, 1.2 Hz, 1H), 6.78 – 6.73 (m, 2H), 6.65 (dt, *J* = 7.7, 0.9 Hz, 1H), 6.61 (d, *J* = 8.5 Hz, 2H), 6.56 (d, *J* = 2.4 Hz, 2H), 6.40 – 6.35 (m, 2H), 6.31 (dd, *J* = 8.6, 2.4 Hz, 2H), 2.03 (s, 3H).

^{13}C NMR not performed.

LRMS (UPLC) Calculated $C_{27}H_{22}NO_3^+$ $[M+H]^+$: 408, Found 408

4.5 NMR spectra

4.5.1 NMRs from chapter 4.1

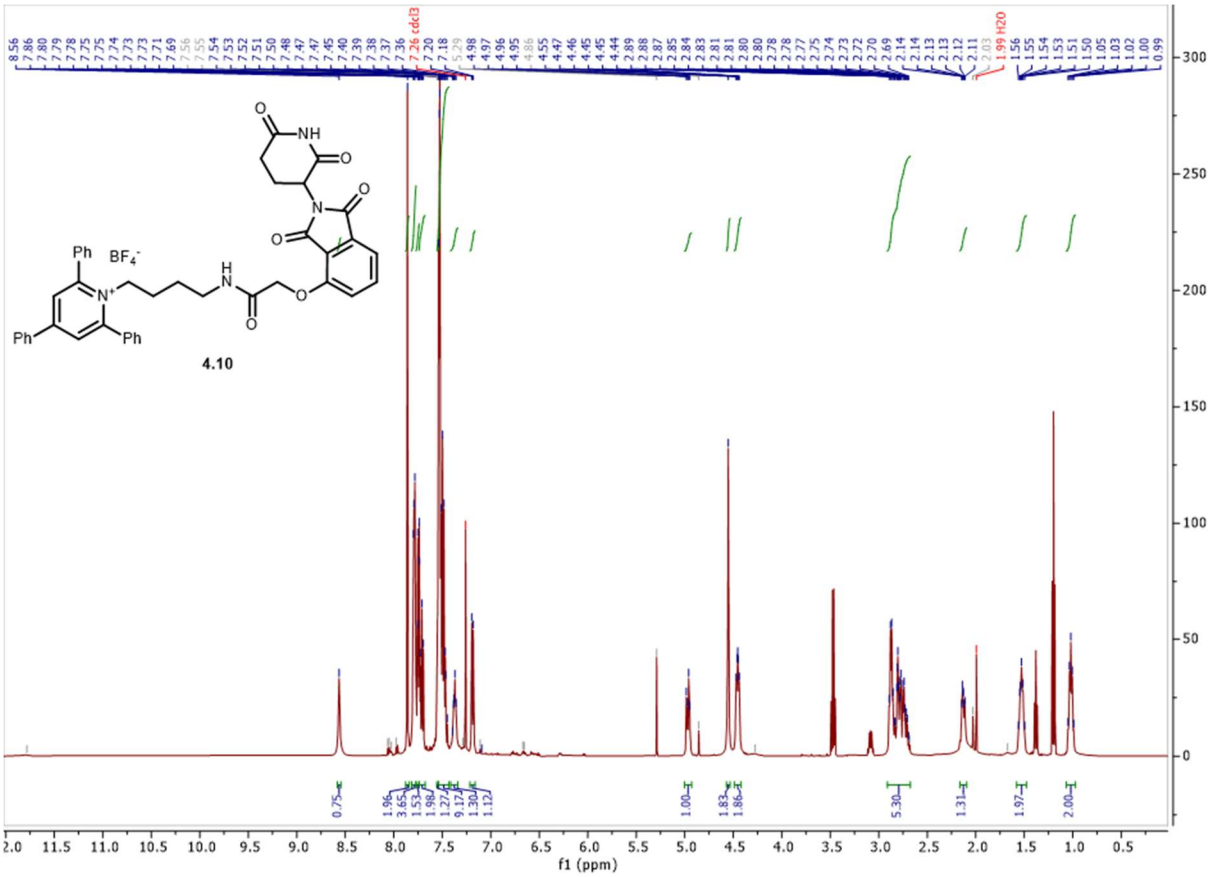

Spectrum 4.1 ^{1}H NMR of **4.10**.

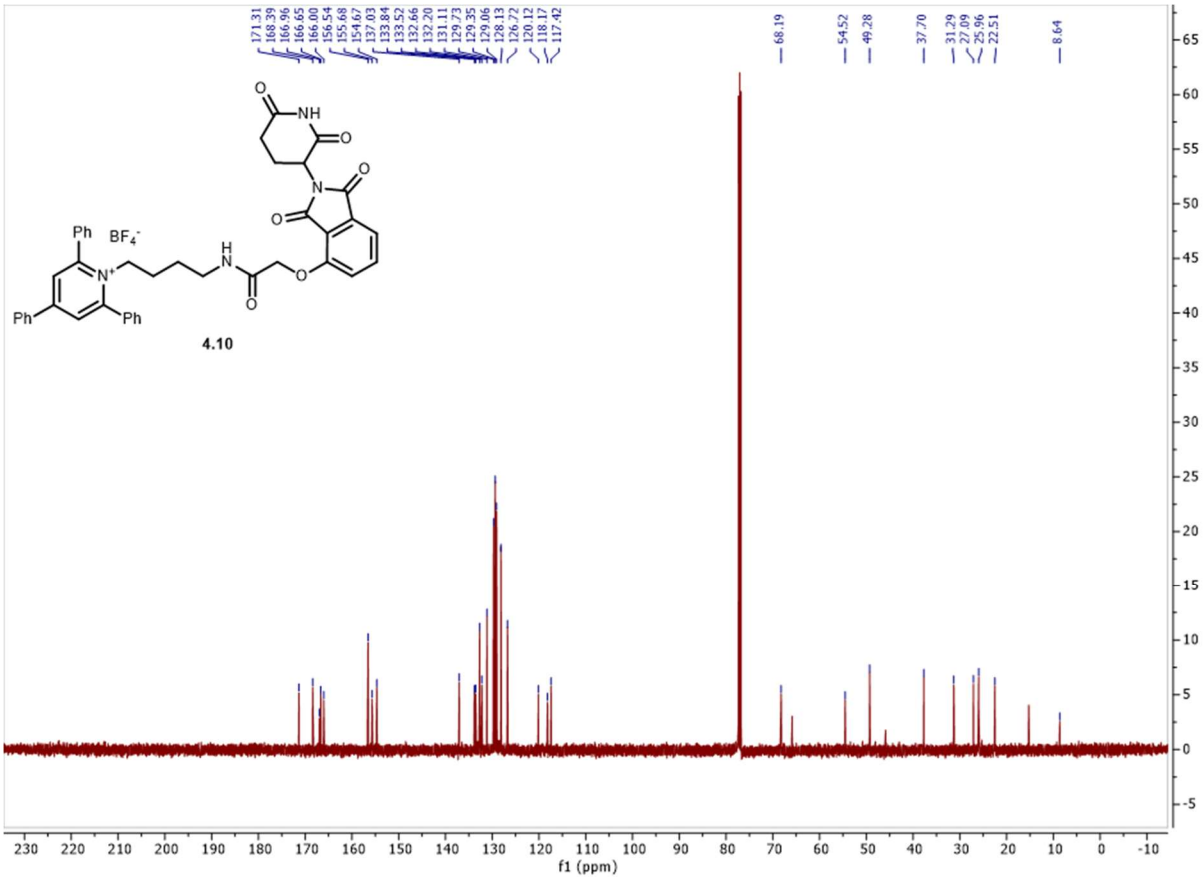

Spectrum 4.2 ^{13}C NMR of **4.10**.

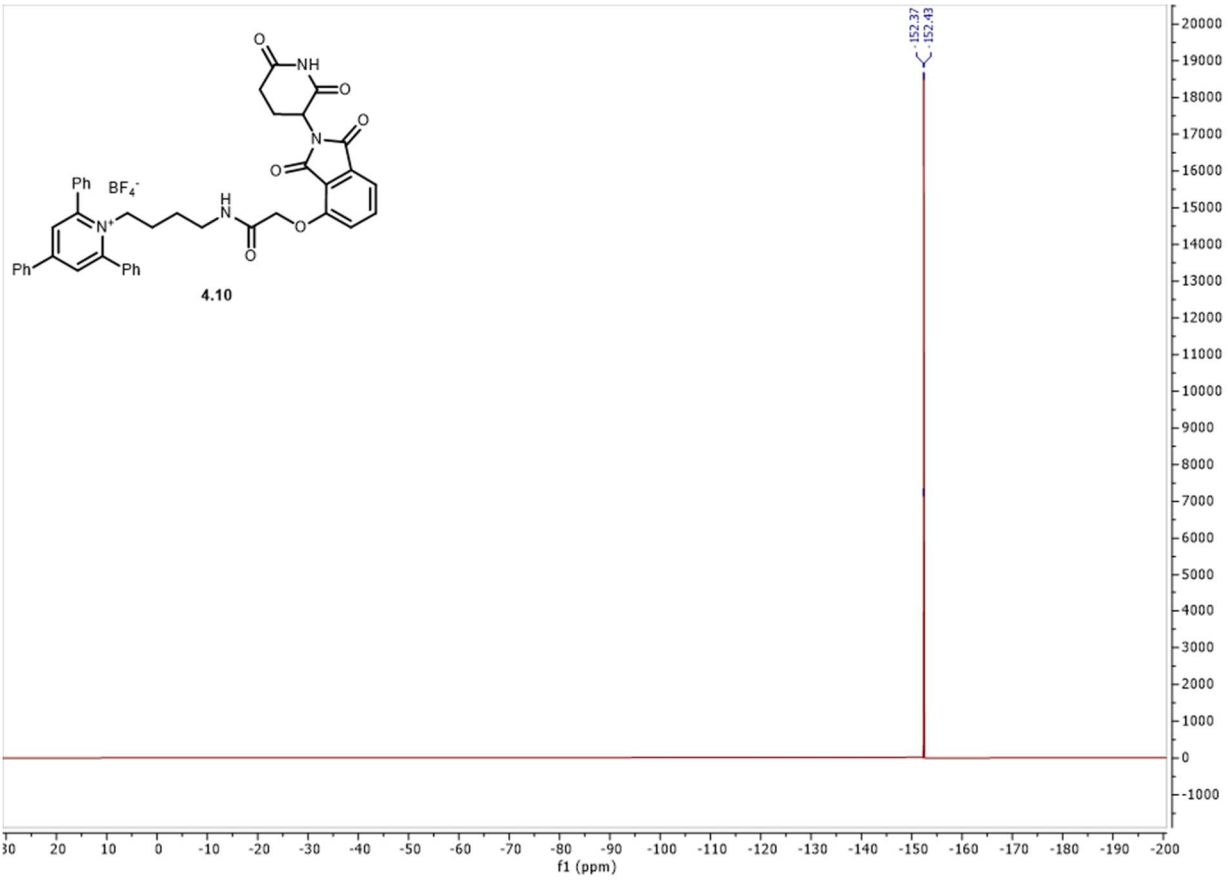

Spectrum 4.3 ^{19}F NMR of **4.10**

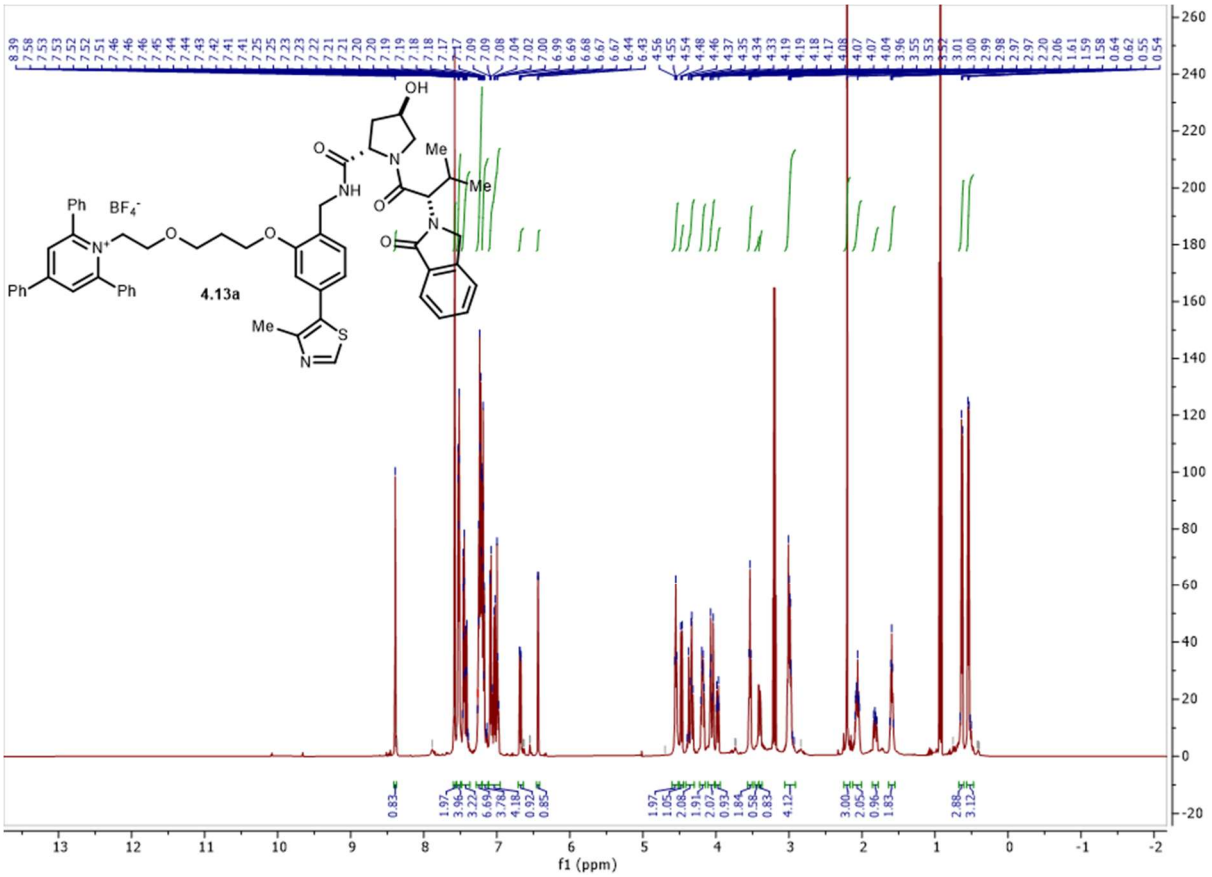

Spectrum 4.4 ^{1}H NMR of **4.13a**.

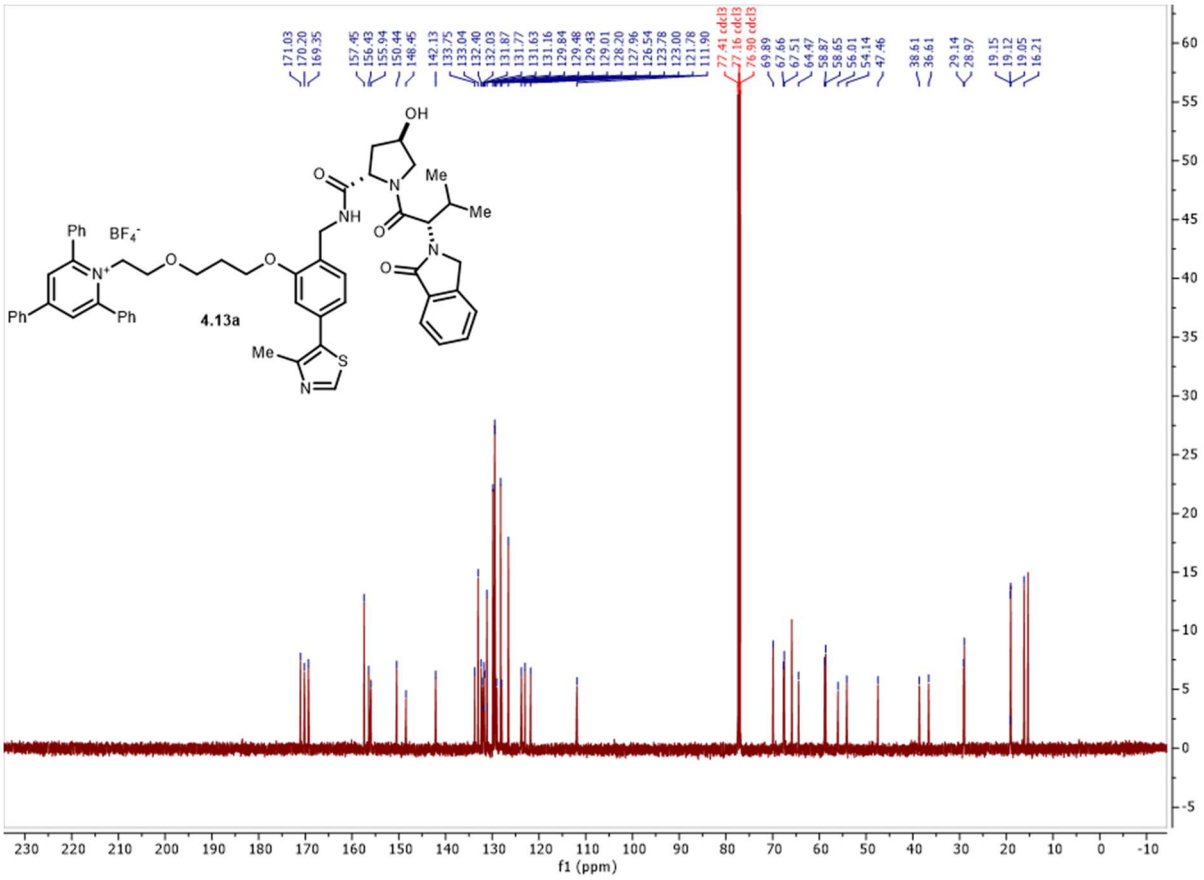

Spectrum 4.5 ^{13}C NMR of **4.13a**.

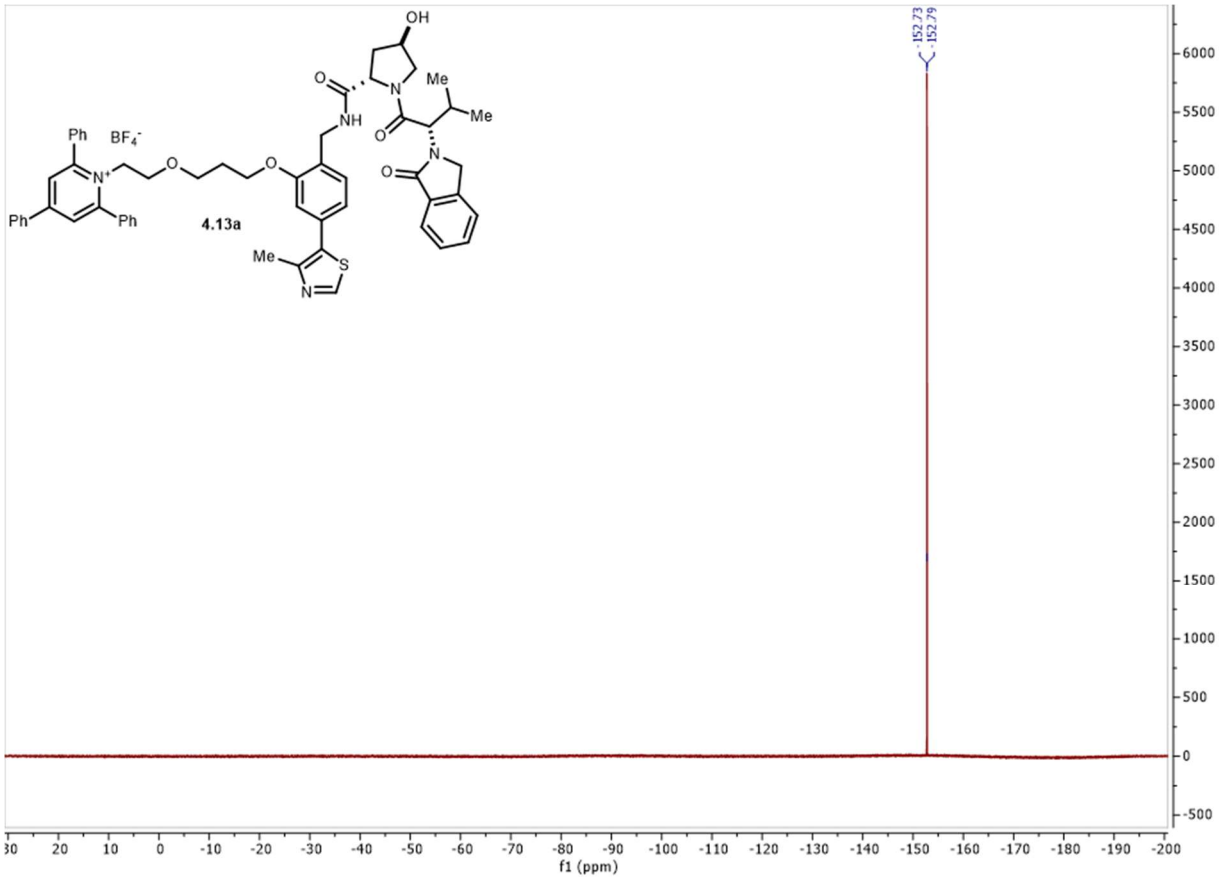

Spectrum 4.6 ^{19}F NMR of **4.13a**.

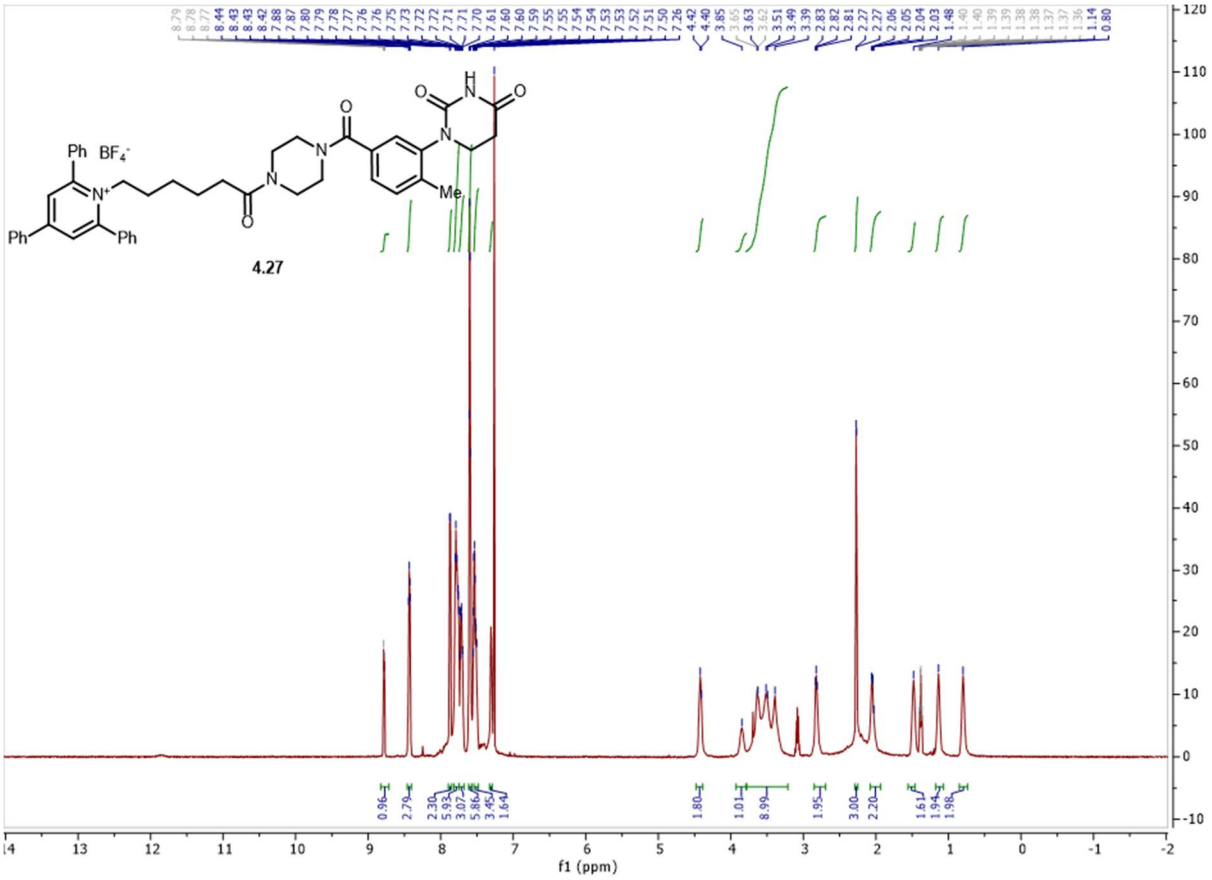

Spectrum 4.7 ^{1}H NMR of **4.27**.

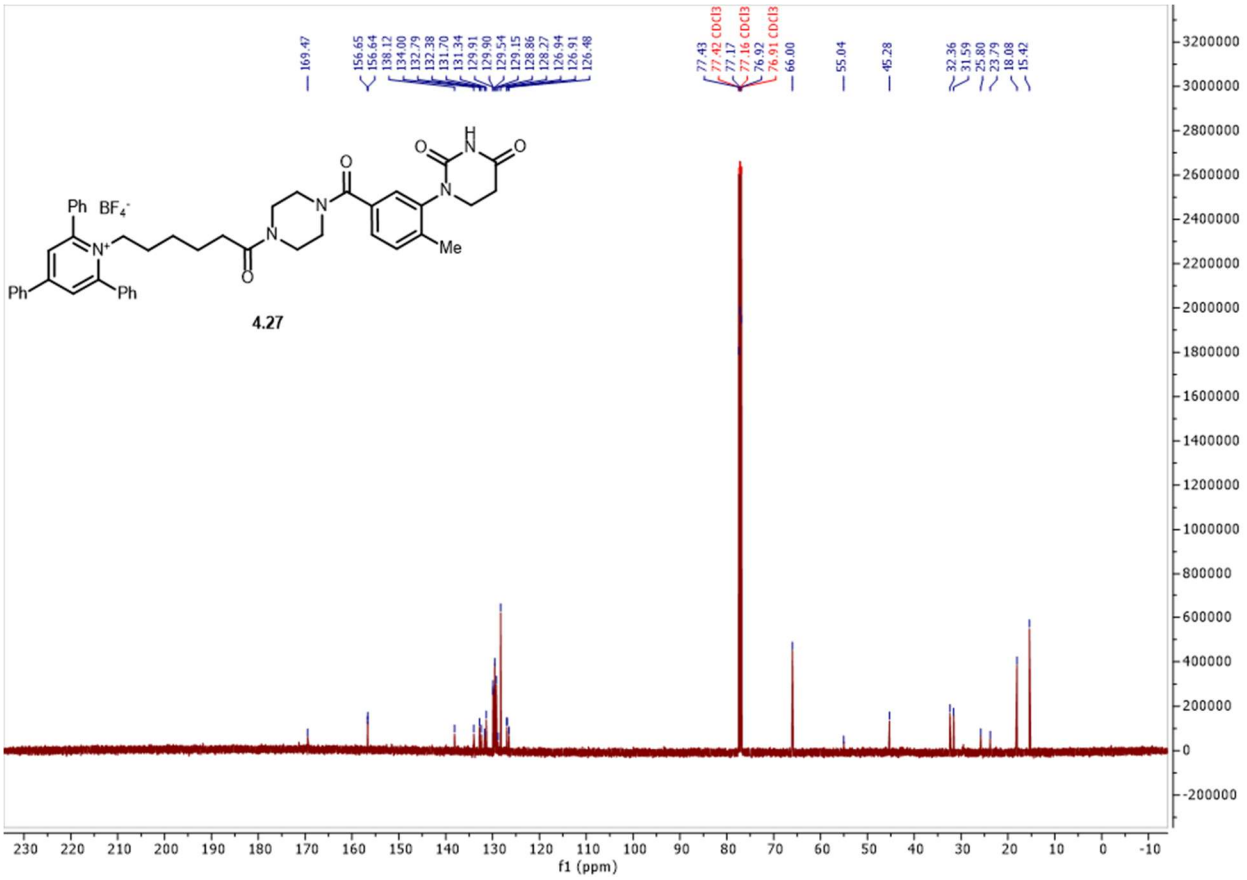

Spectrum 4.8 ^{13}C NMR of **4.27.**

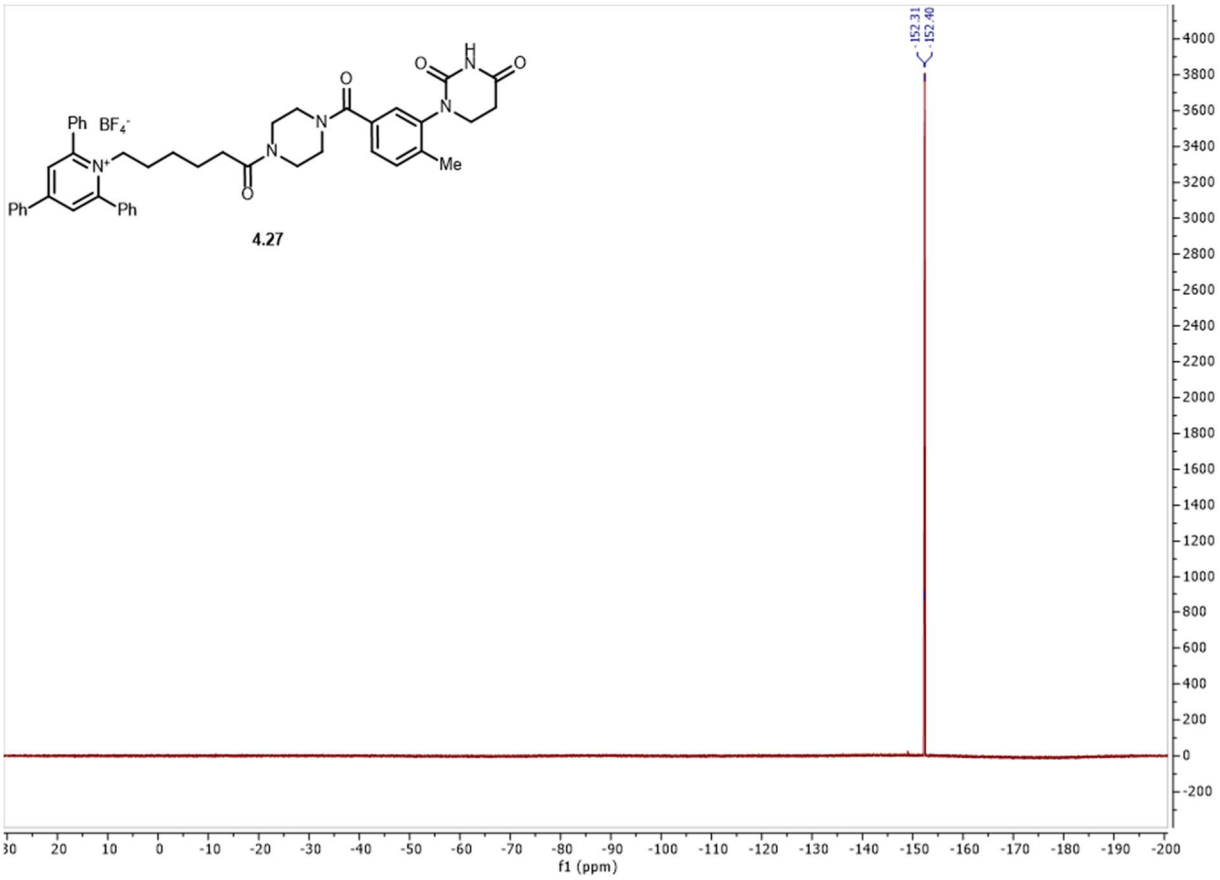

Spectrum 4.9 ^{19}F NMR of **4.27**.

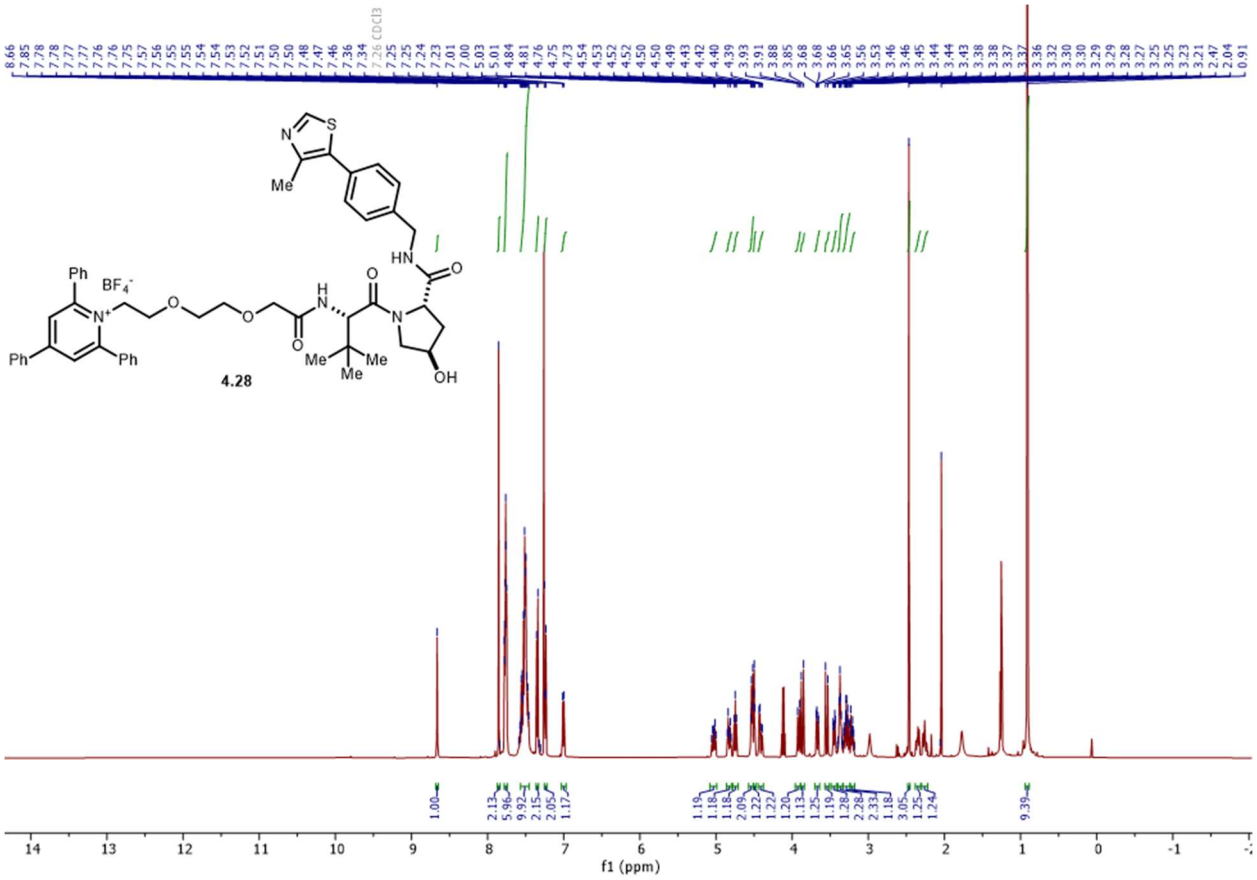

Spectrum 4.10 ^{1}H NMR of **4.28**.

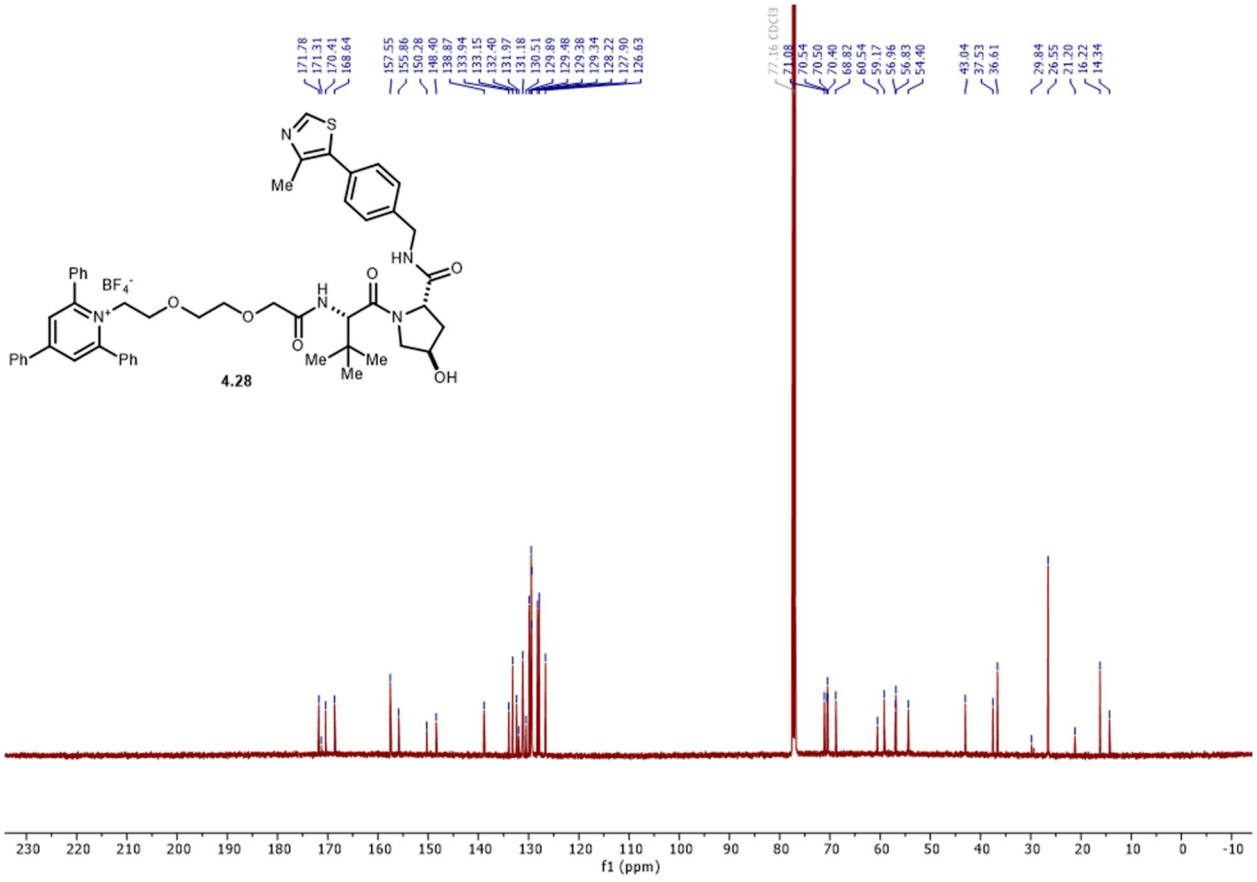

Spectrum 4.11 ^{13}C NMR of **4.28**.

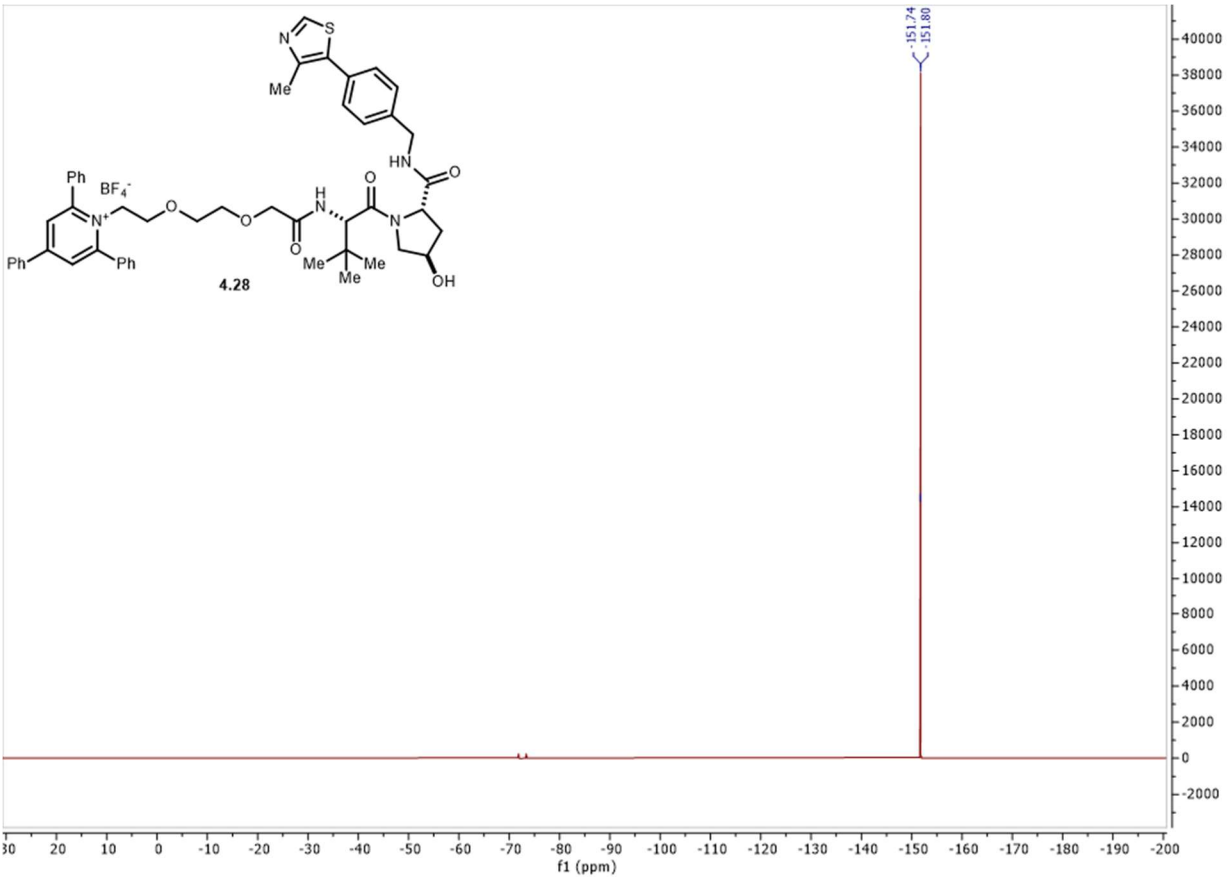

Spectrum 4.12 ^{19}F NMR of **4.28**

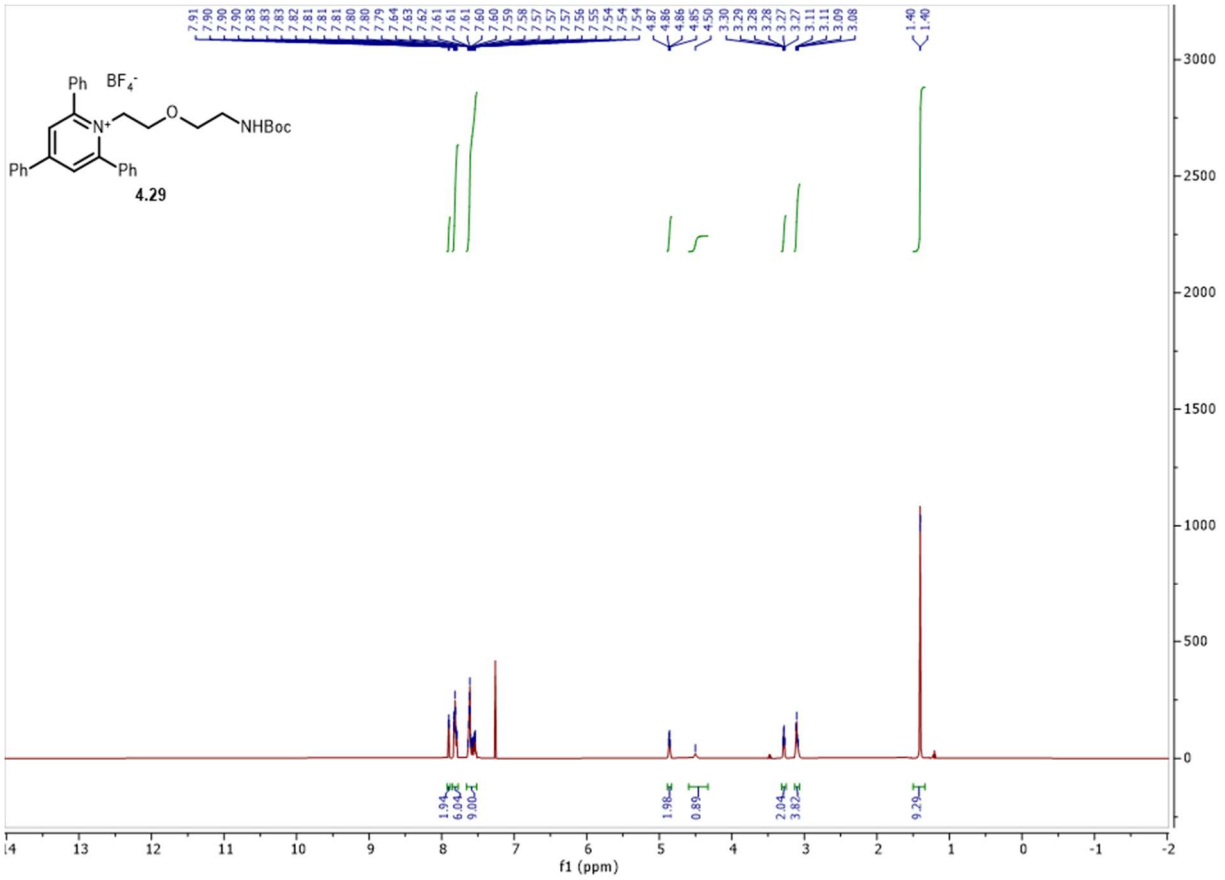

Spectrum 4.13 ^{1}H NMR of **4.29.**

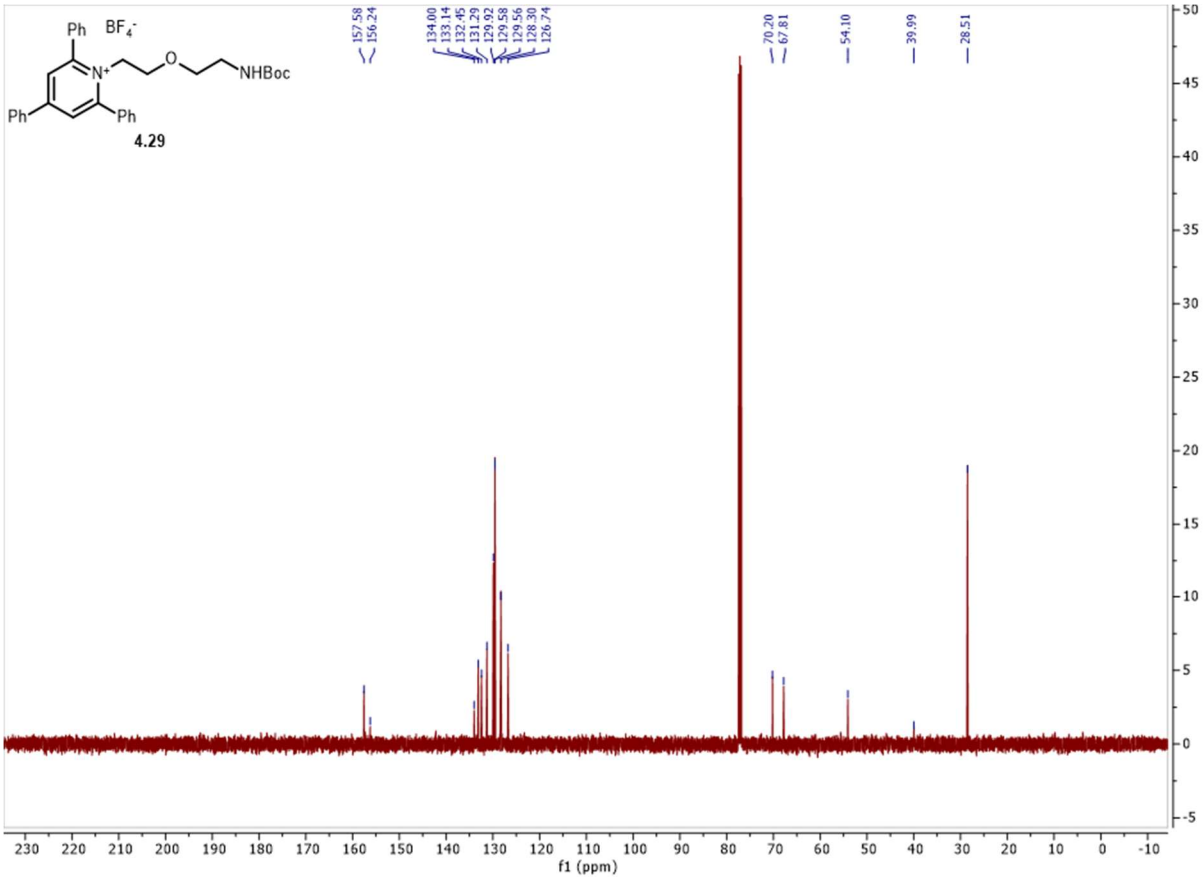

Spectrum 4.14 ^{13}C NMR of **4.29**.

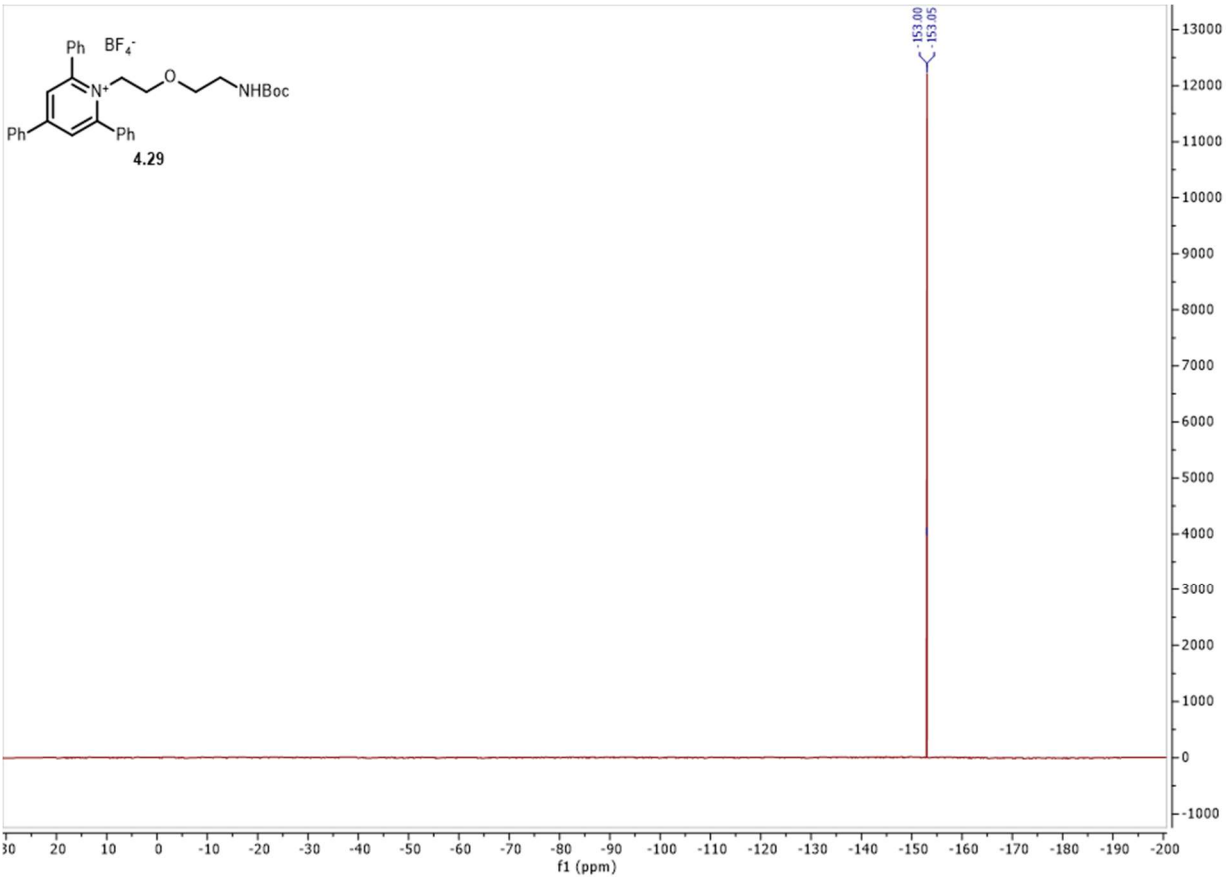

Spectrum 4.15 ^{19}F NMR of **4.29**.

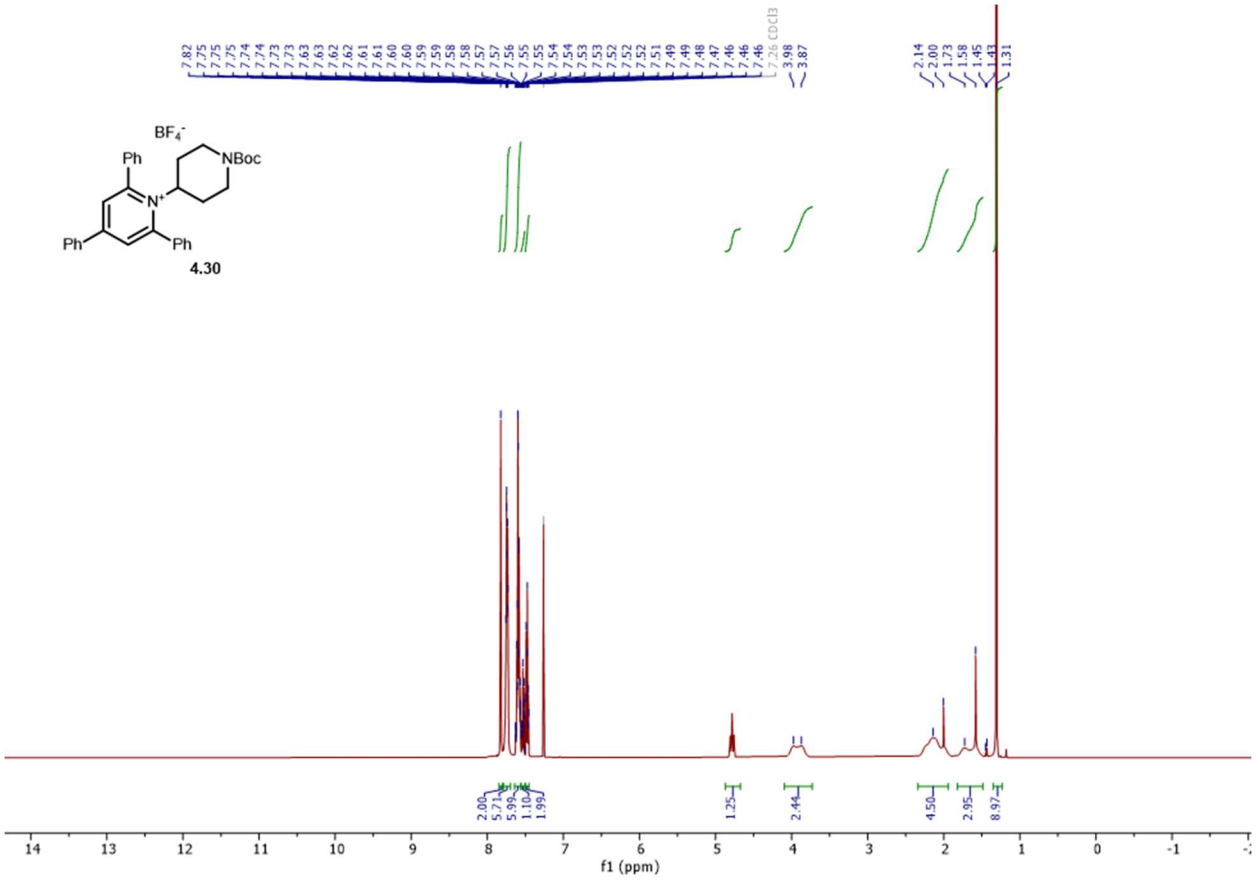

Spectrum 4.16 ^{1}H NMR of **4.30**.

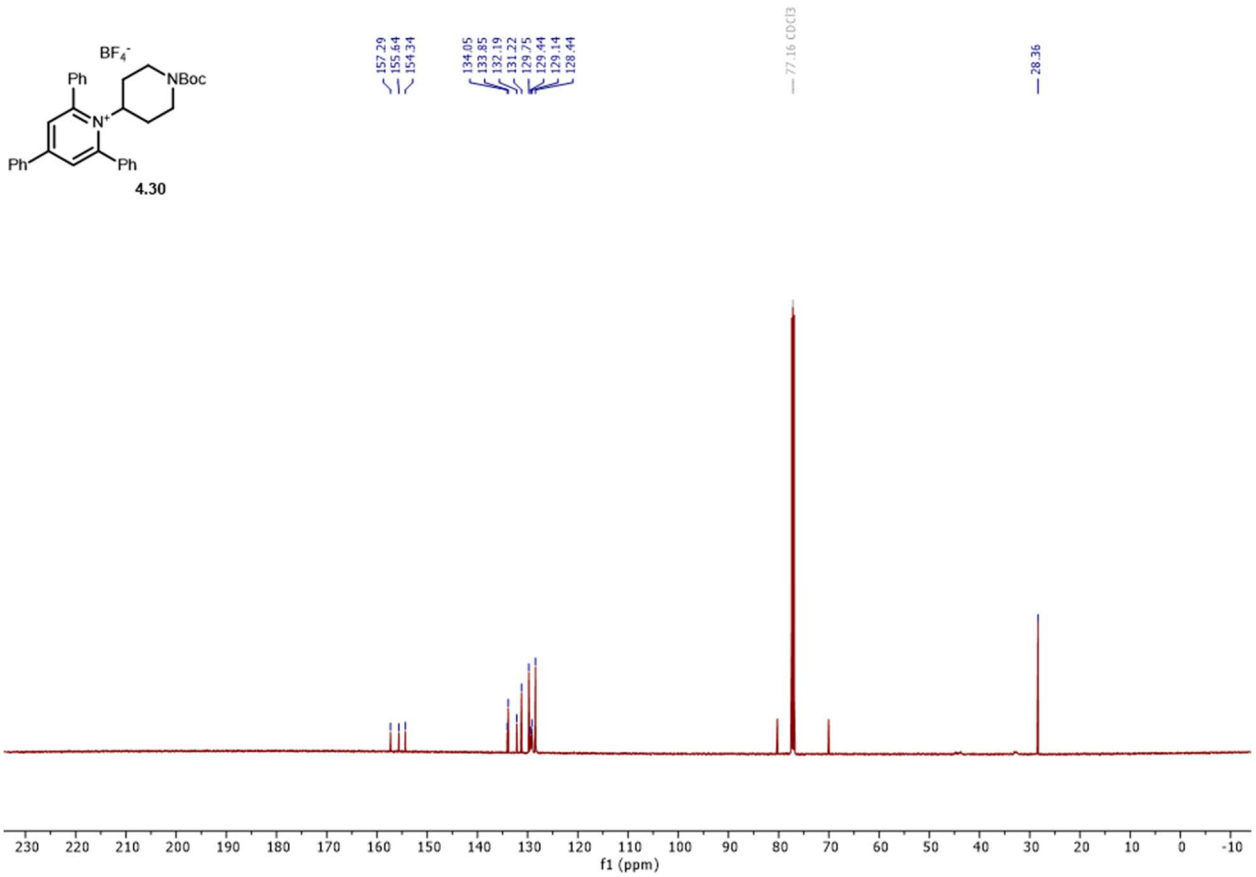

Spectrum 4.17 ^{13}C NMR of **4.30**.

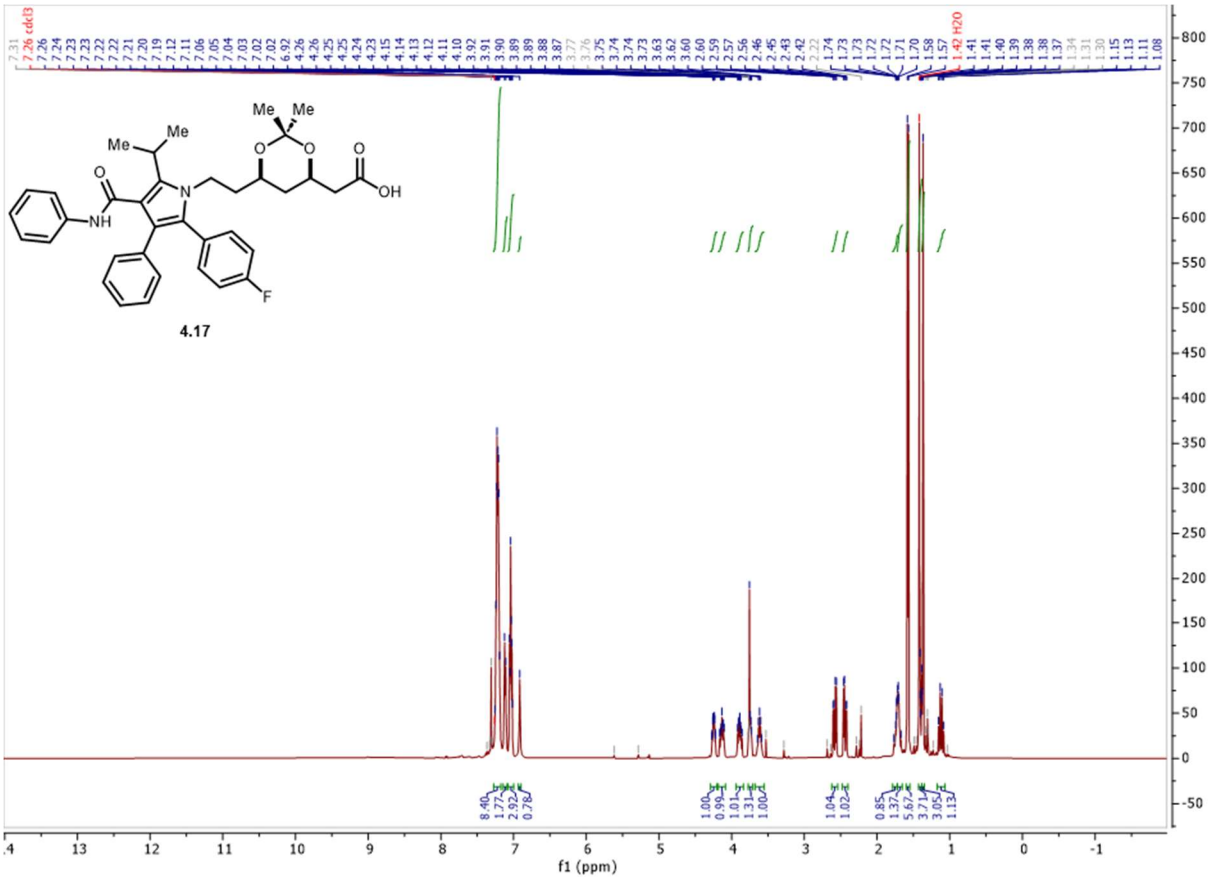

Spectrum 4.18 ^{1}H NMR of **4.17**.

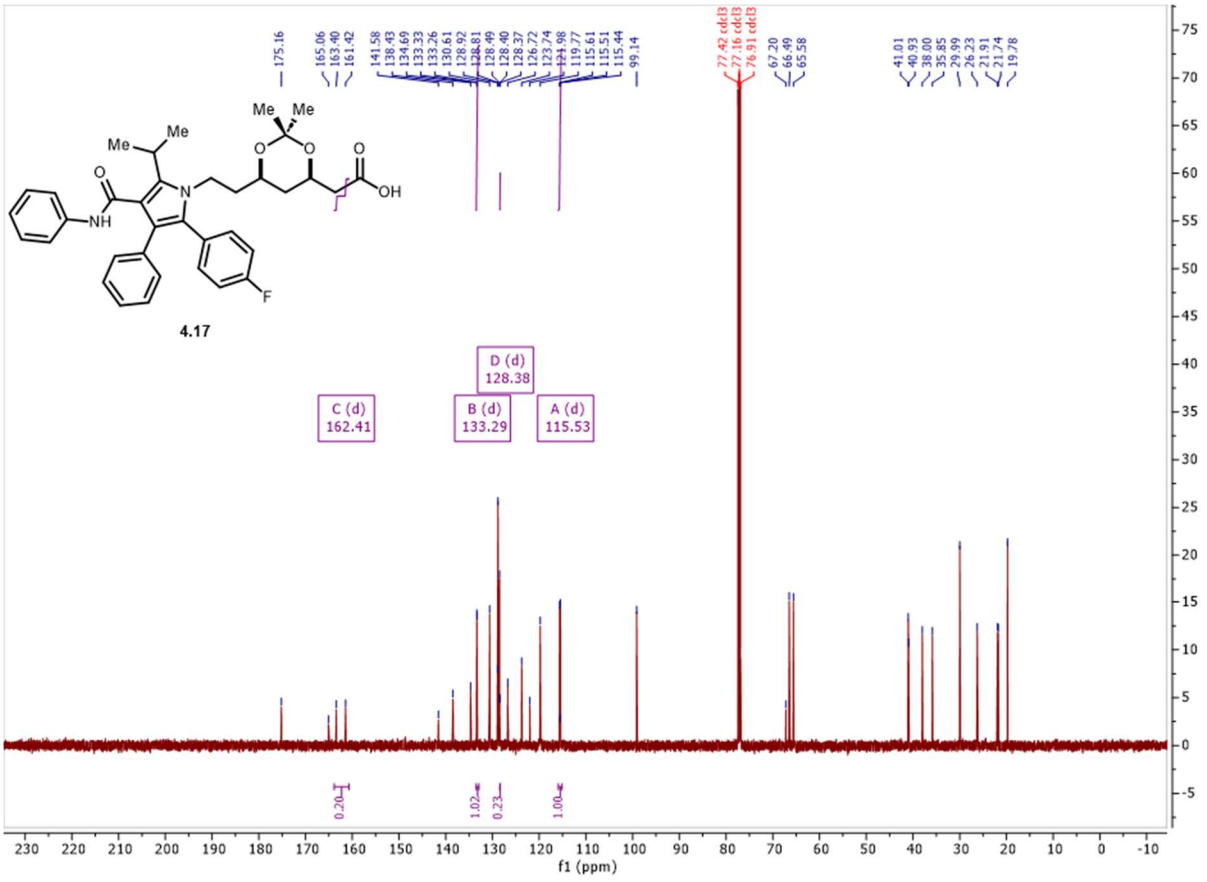

Spectrum 4.19 ^{13}C NMR of **4.17**.

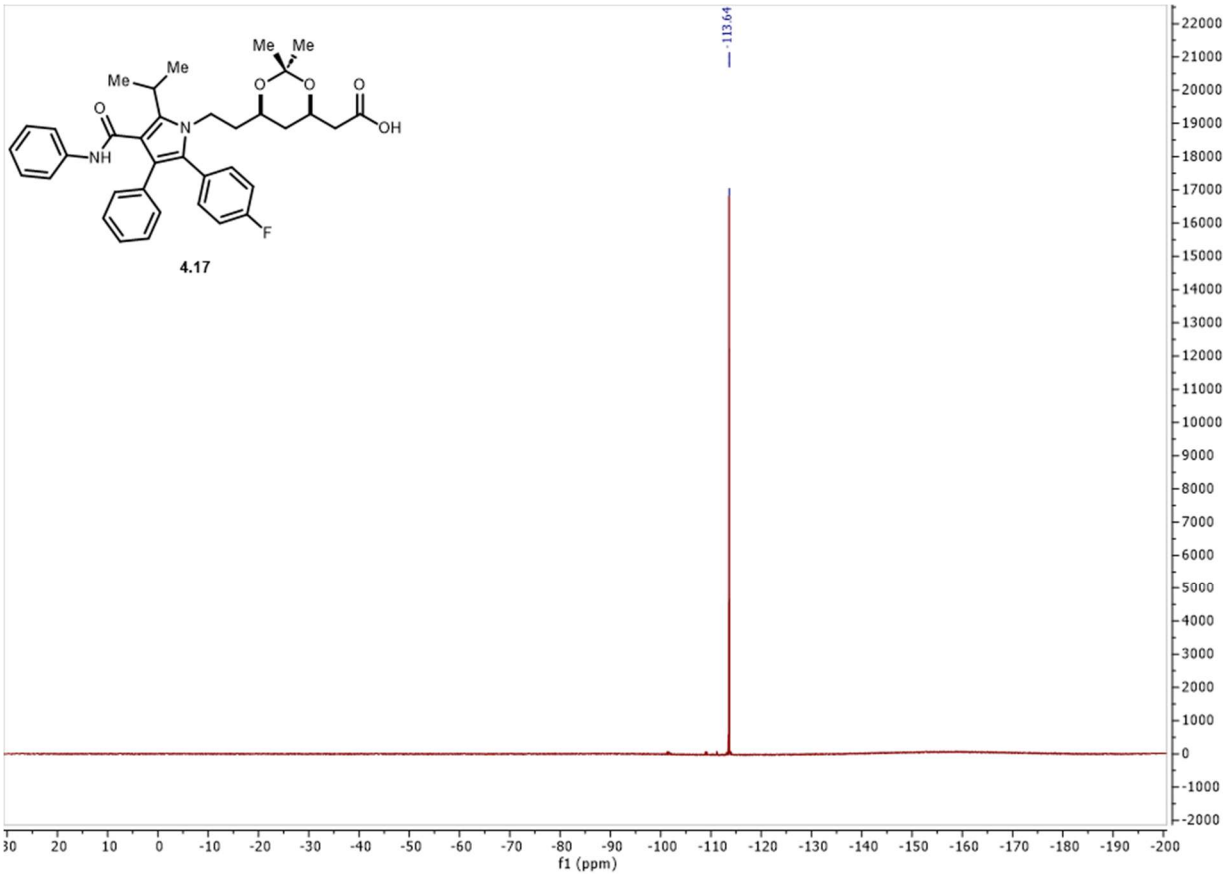

Spectrum 4.20 ^{19}F NMR of **4.17**.

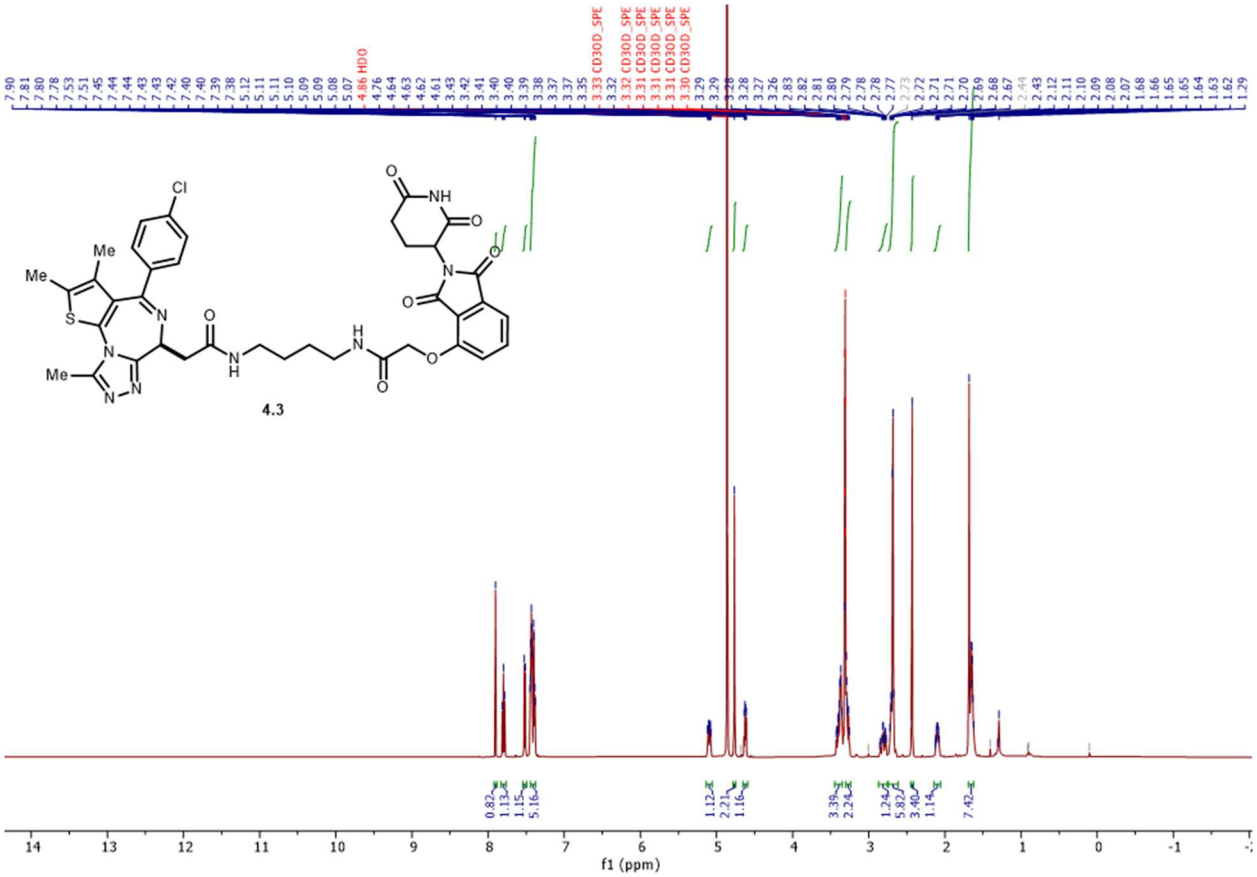

Spectrum 4.21 ^{1}H NMR of **4.3**.

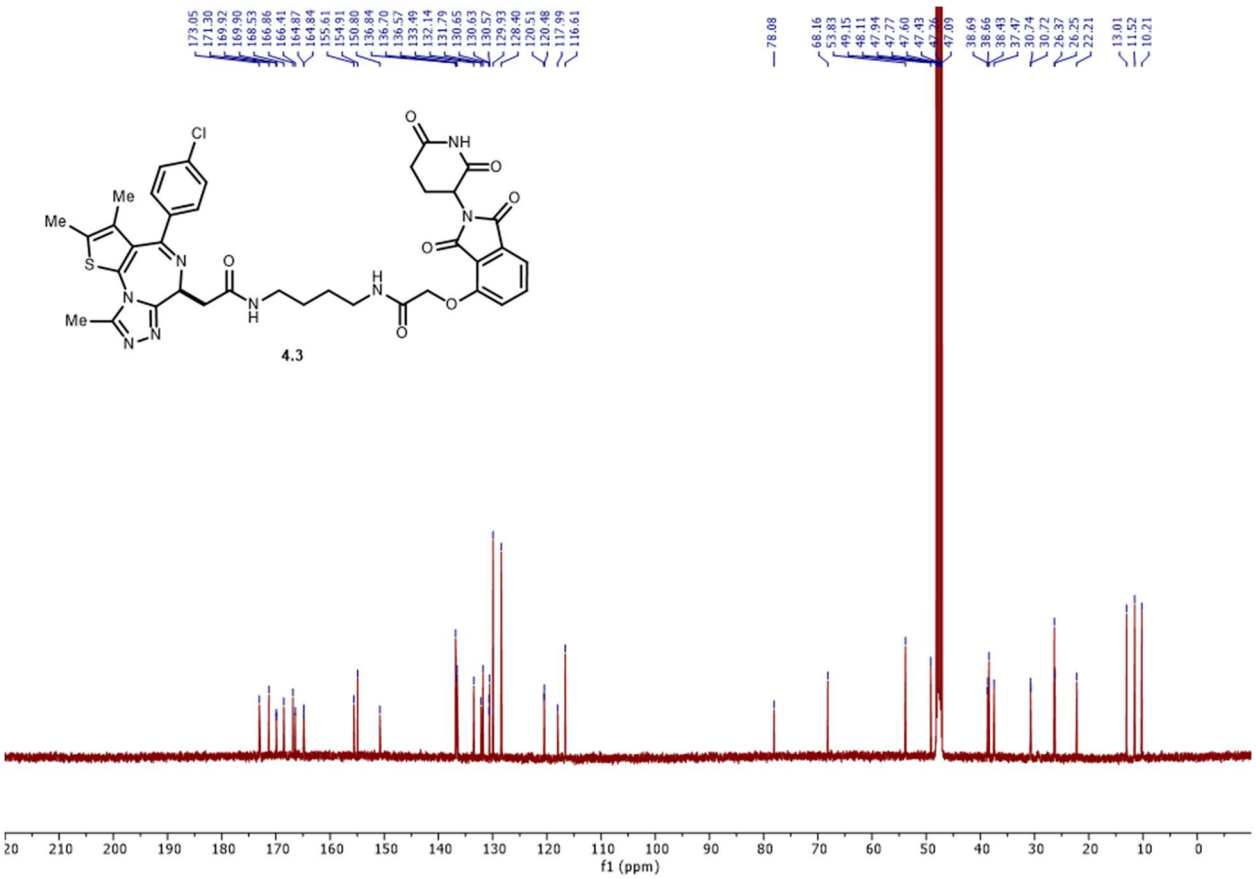

Spectrum 4.22 ^{13}C NMR of **4.3**.

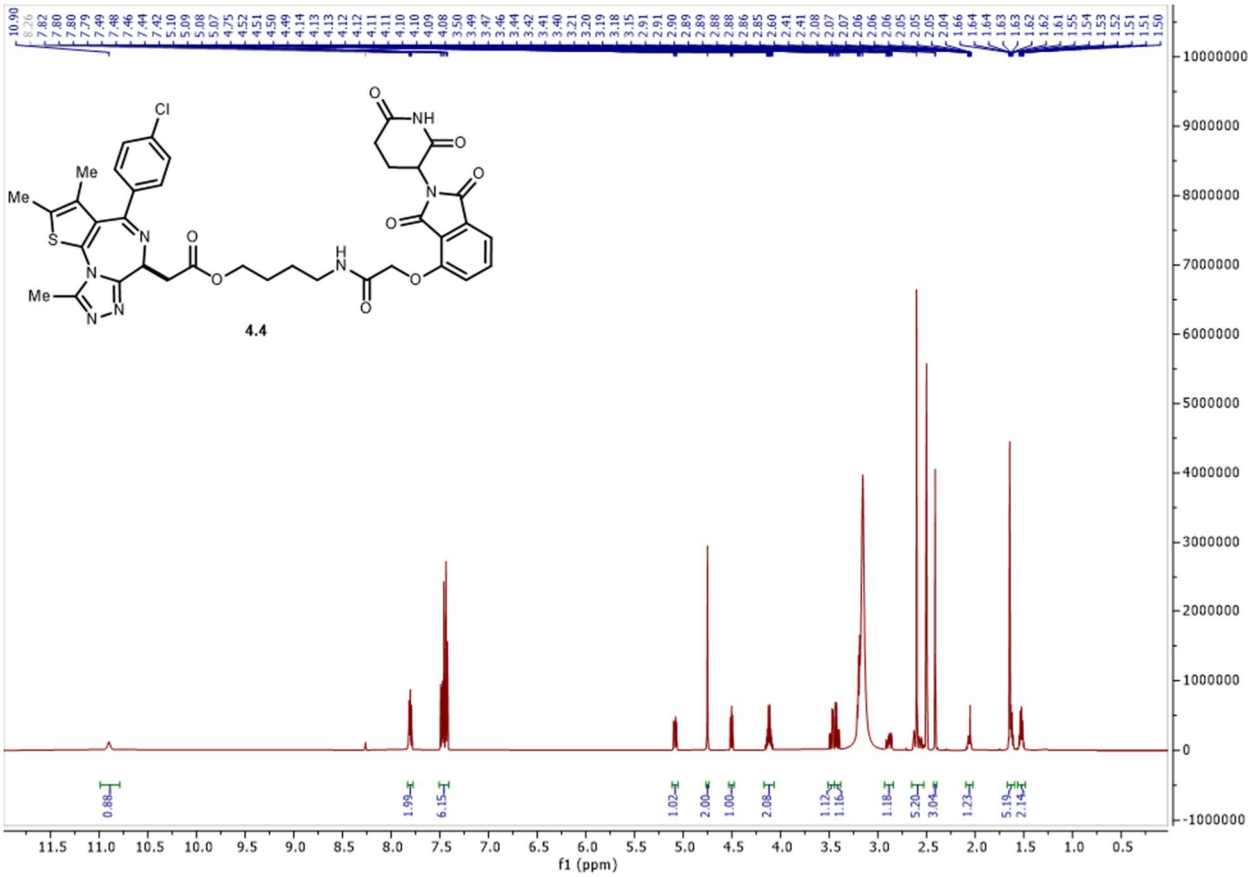

Spectrum 4.23 ^{1}H NMR of **4.4**.

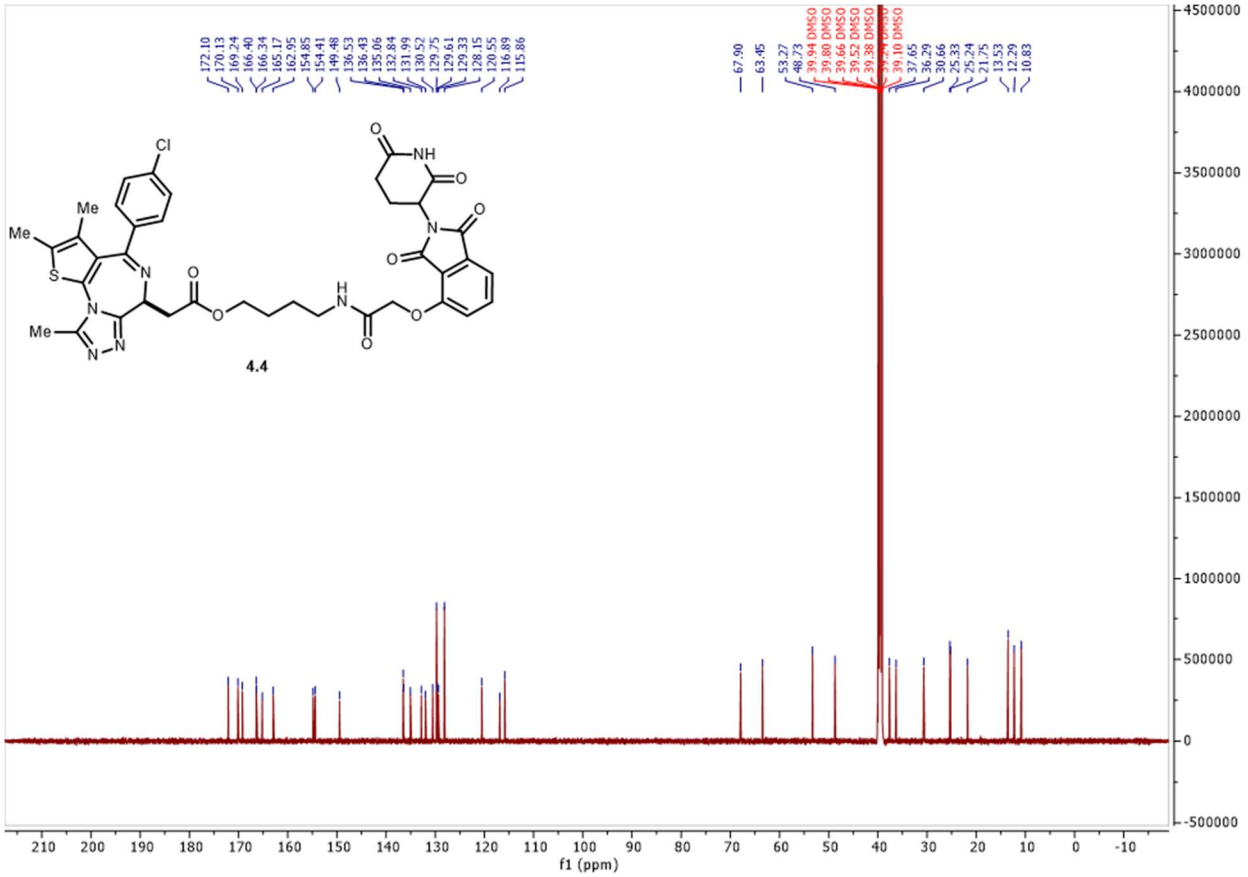

Spectrum 4.24 ^{13}C NMR of **4.24**.

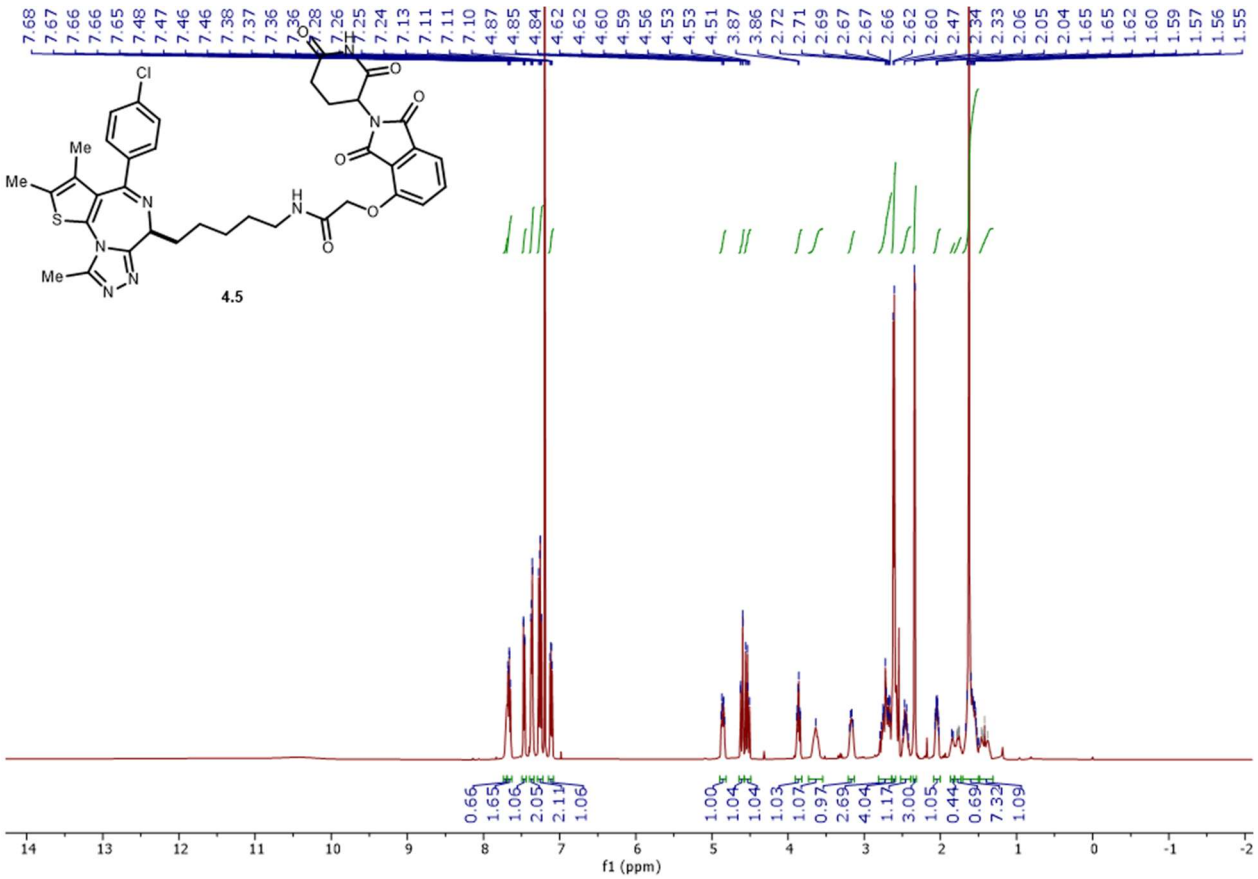

Spectrum 4.25 ^{1}H NMR of **4.5.**

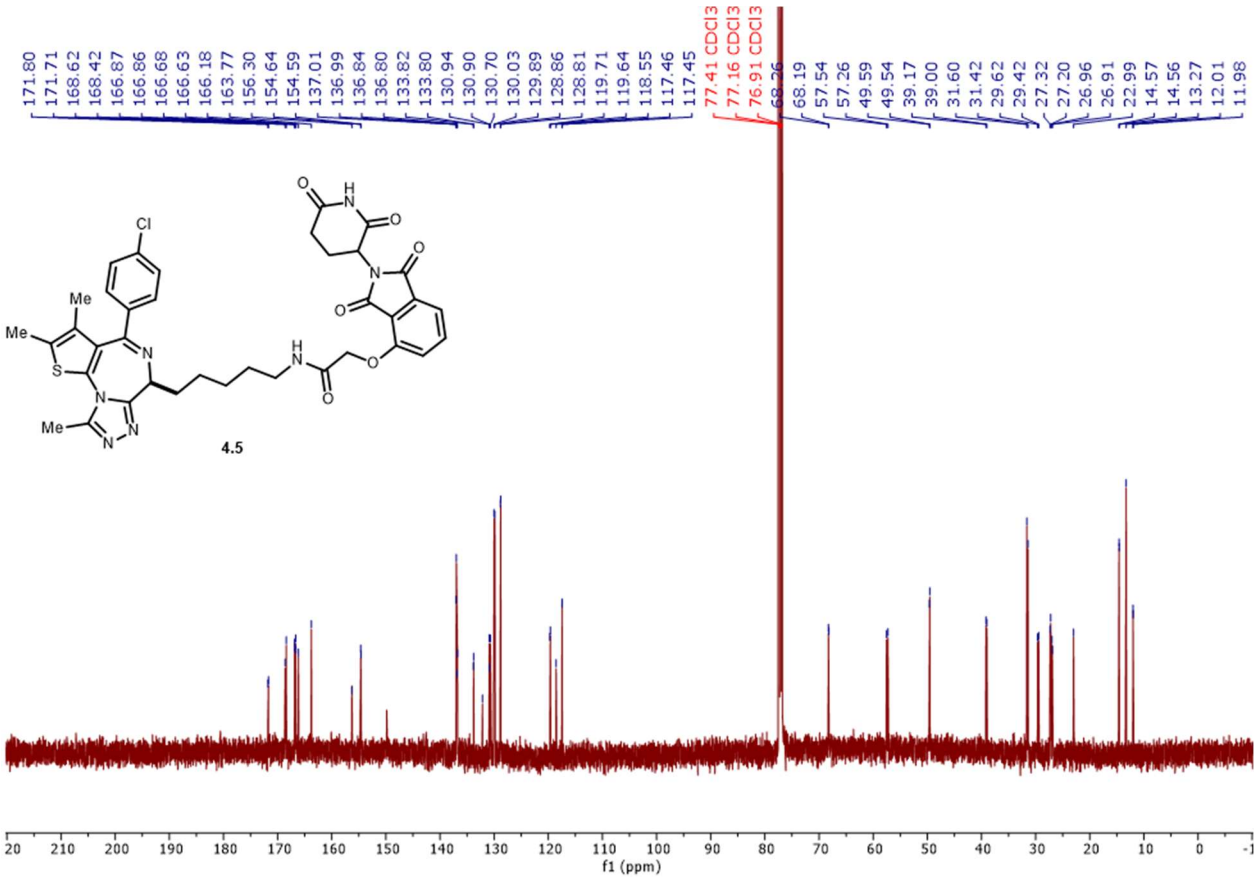

Spectrum 4.26 ^{13}C NMR of **4.5**.

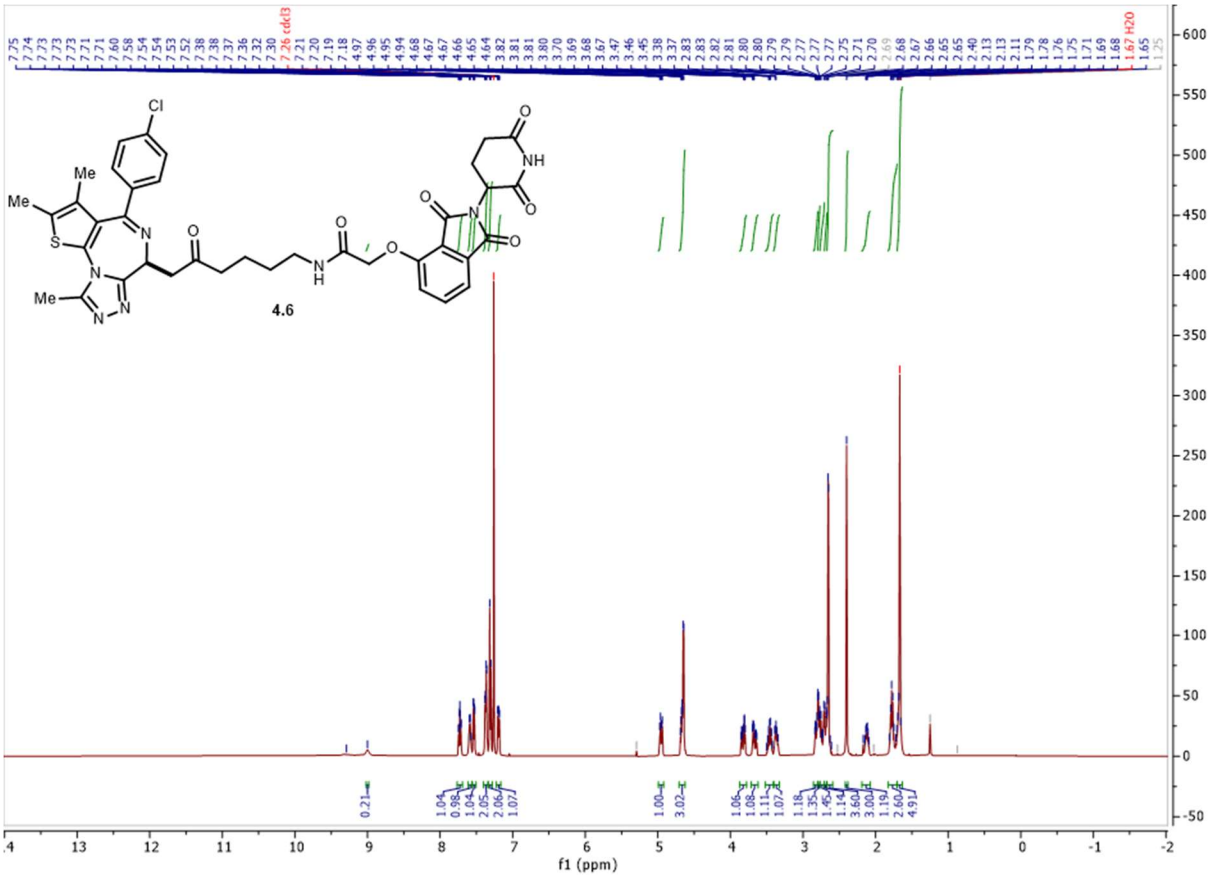

Spectrum 4.27 ^{1}H NMR of **4.6**.

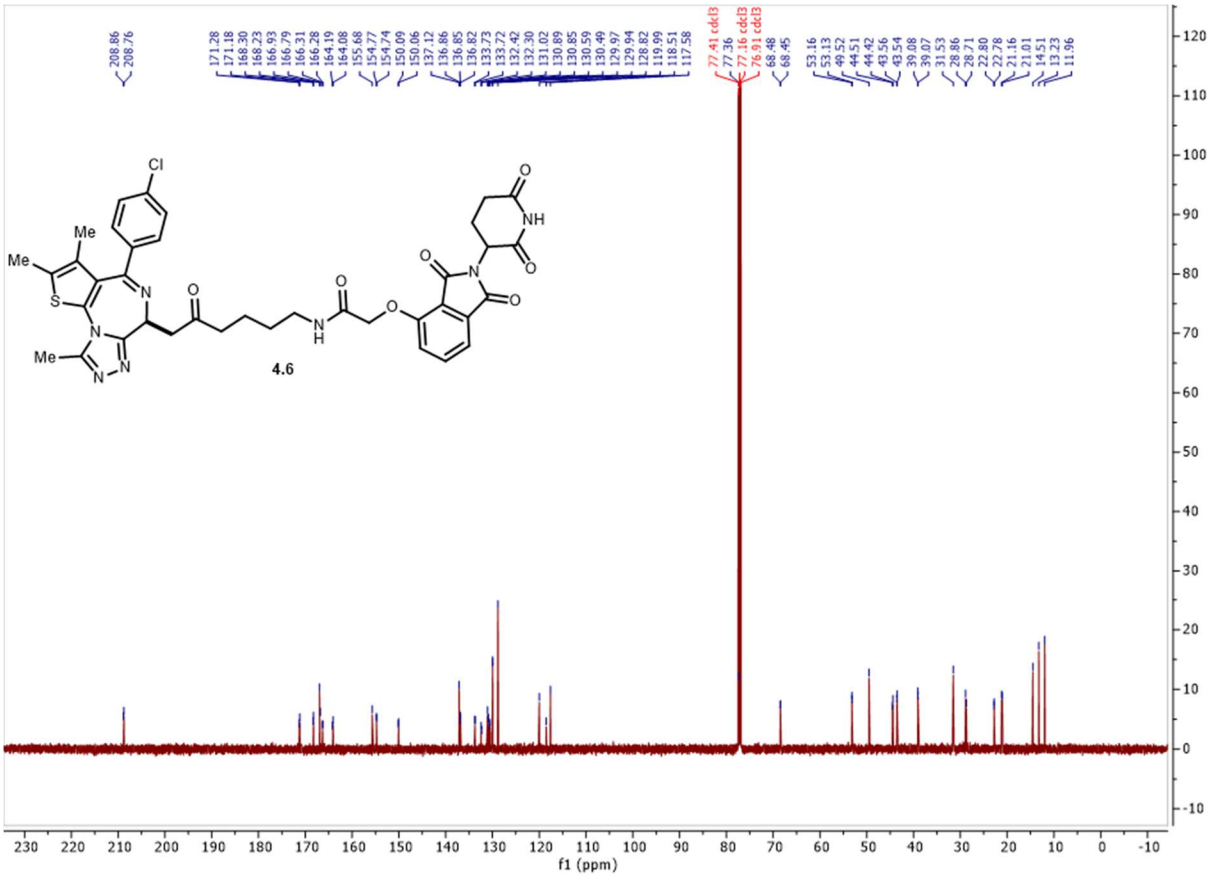

Spectrum 4.28 ^{13}C NMR of **4.6**.

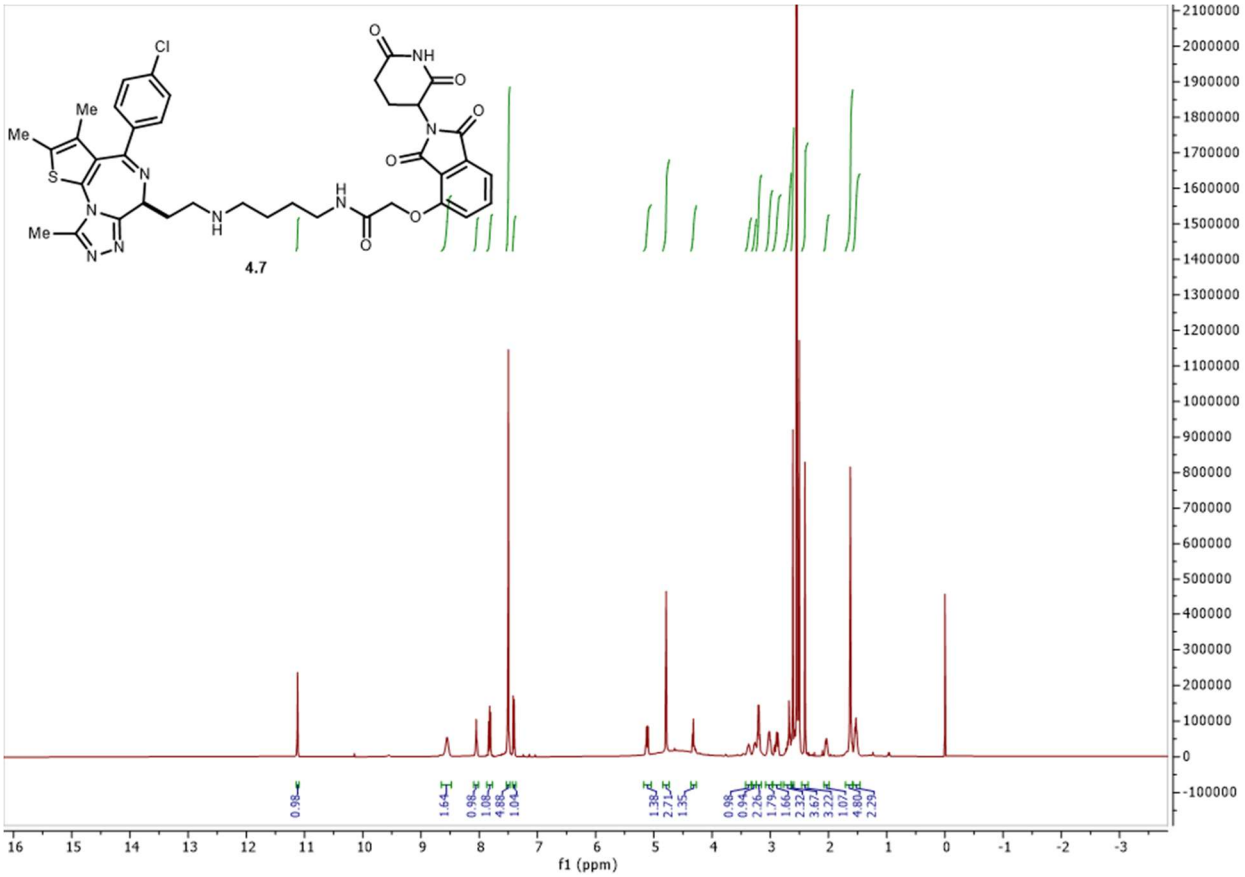

Spectrum 4.29 ^{1}H NMR of **4.7**.

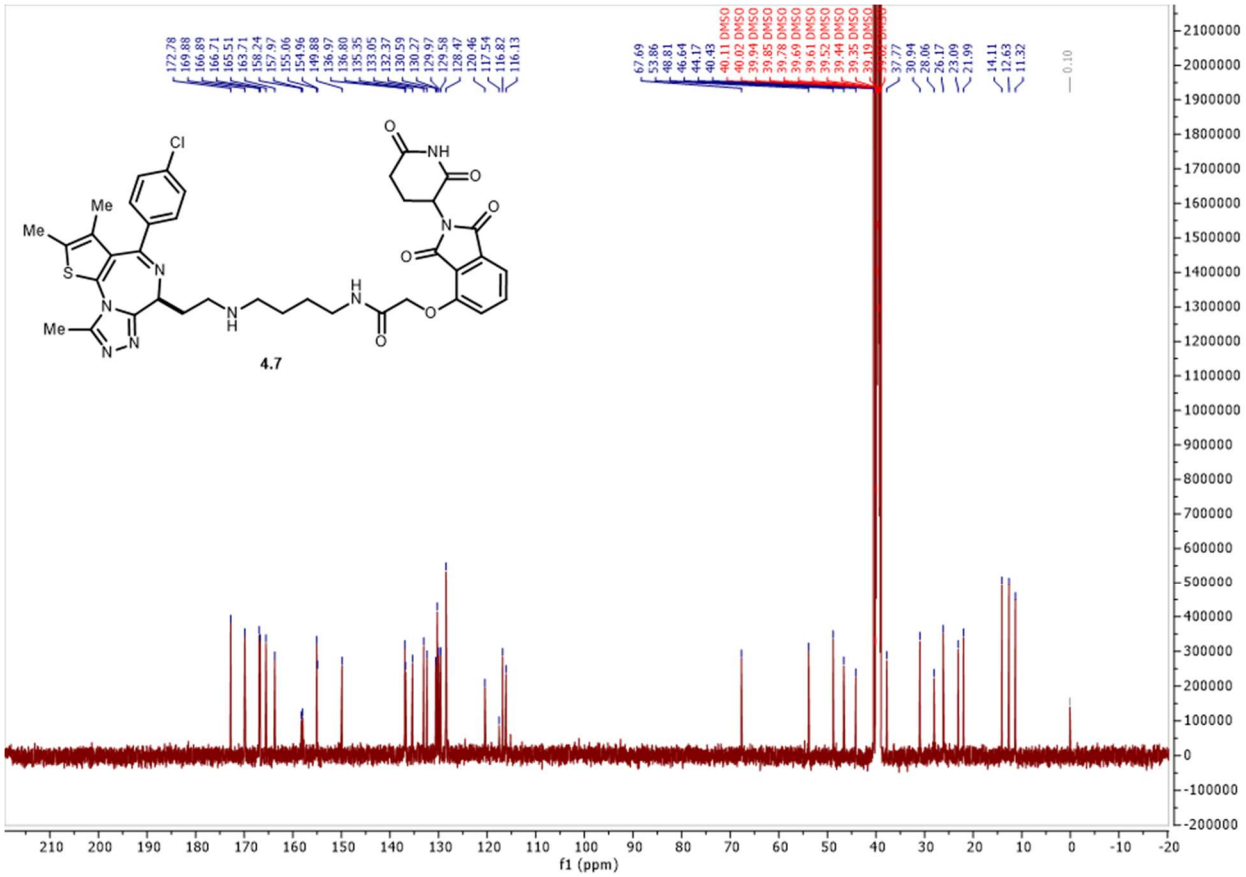

Spectrum 4.30 ^{13}C NMR of **4.7**.

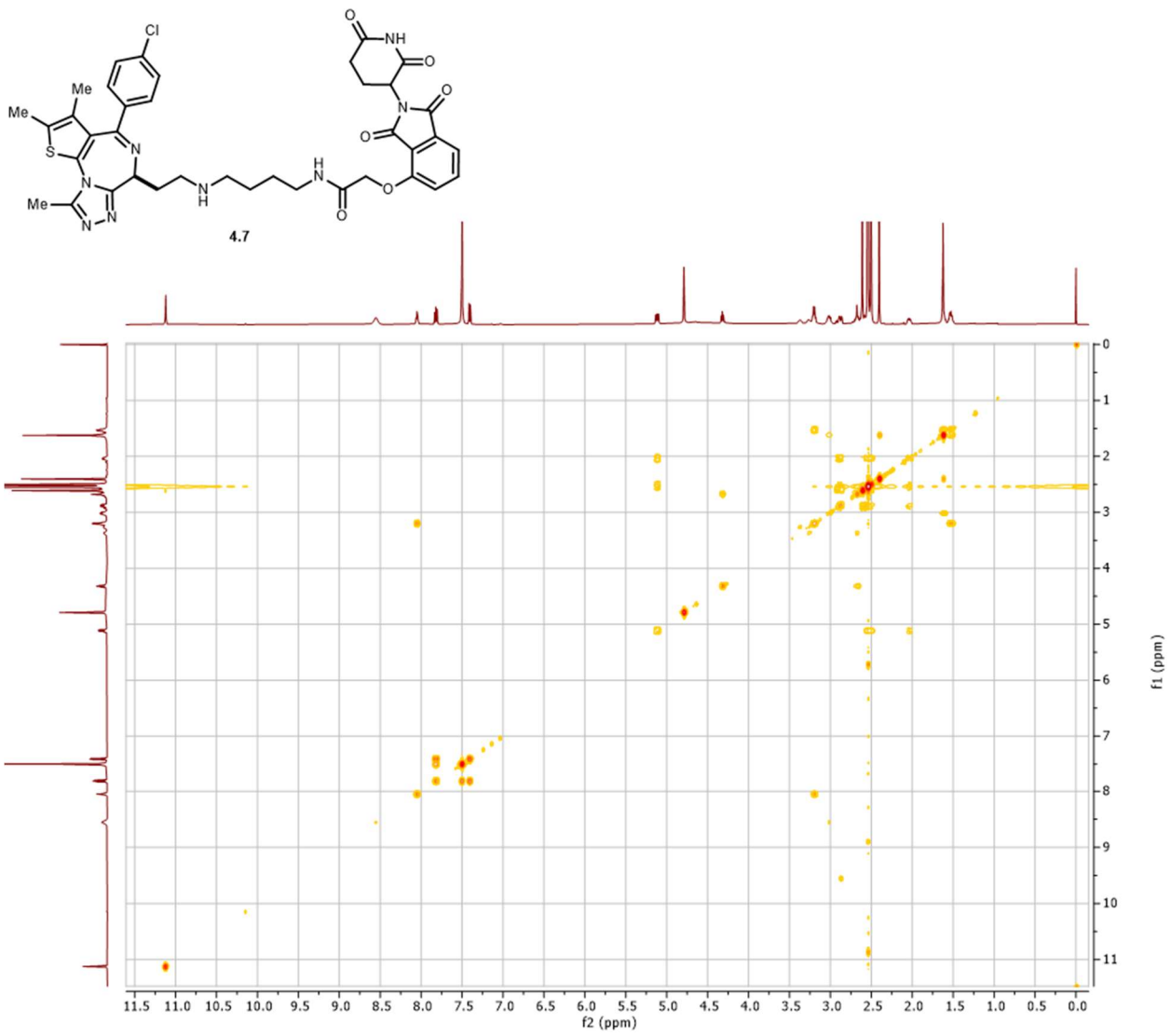

Spectrum 4.31 COSY of **4.7**.

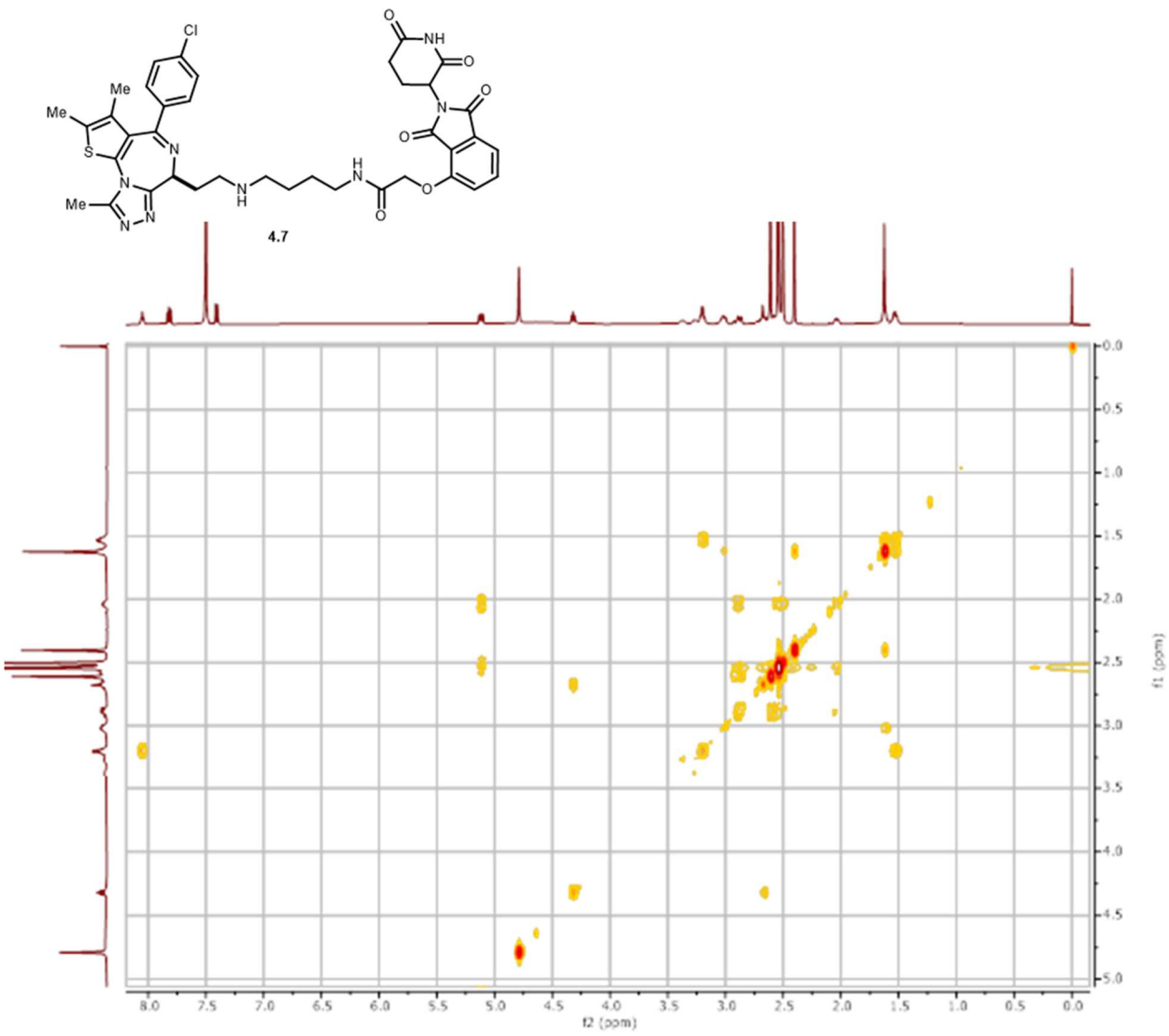

Spectrum 4.32 Zoomed in COSY of **4.7.**

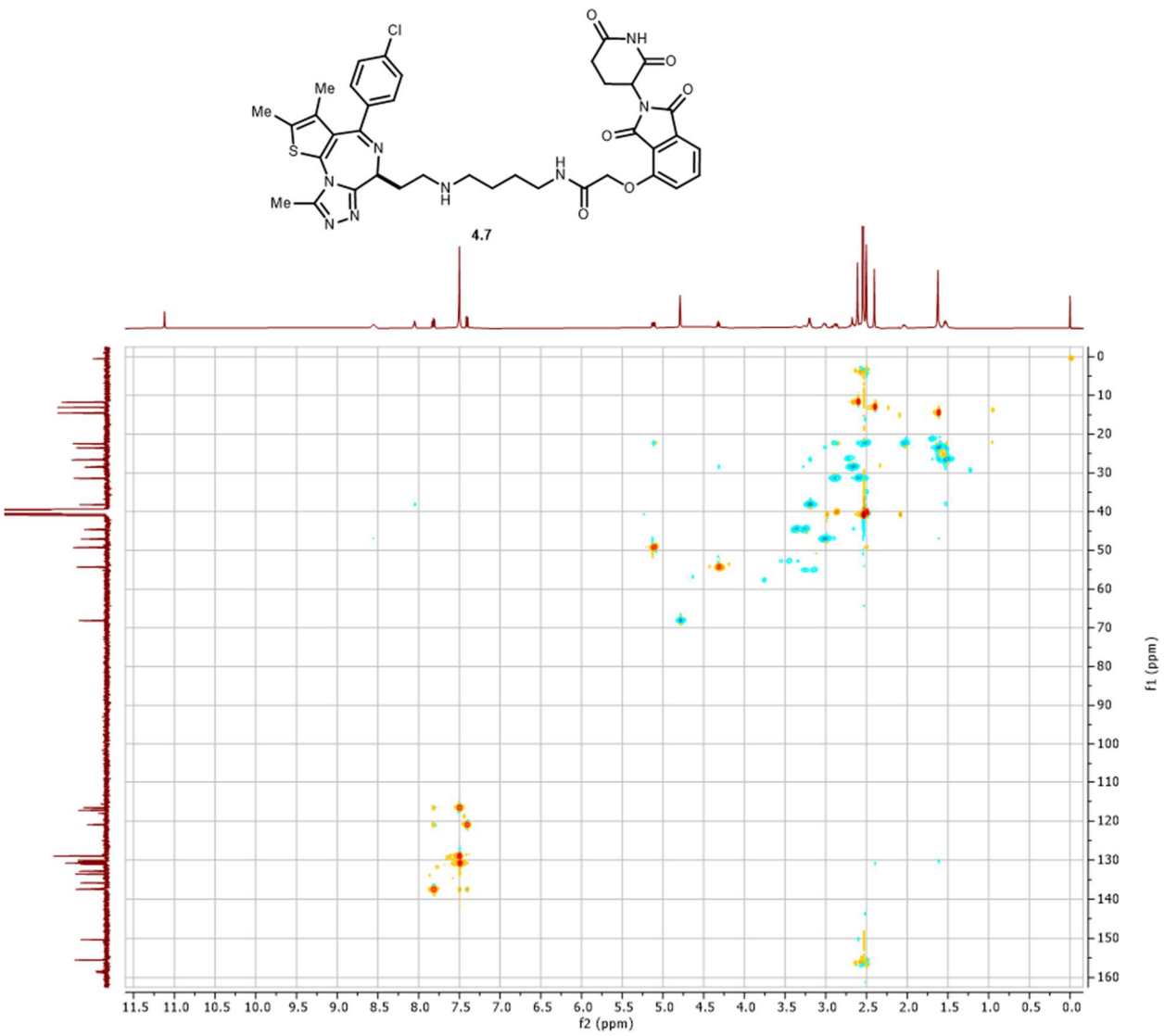

Spectrum 4.33 HSQC of **4.7**.

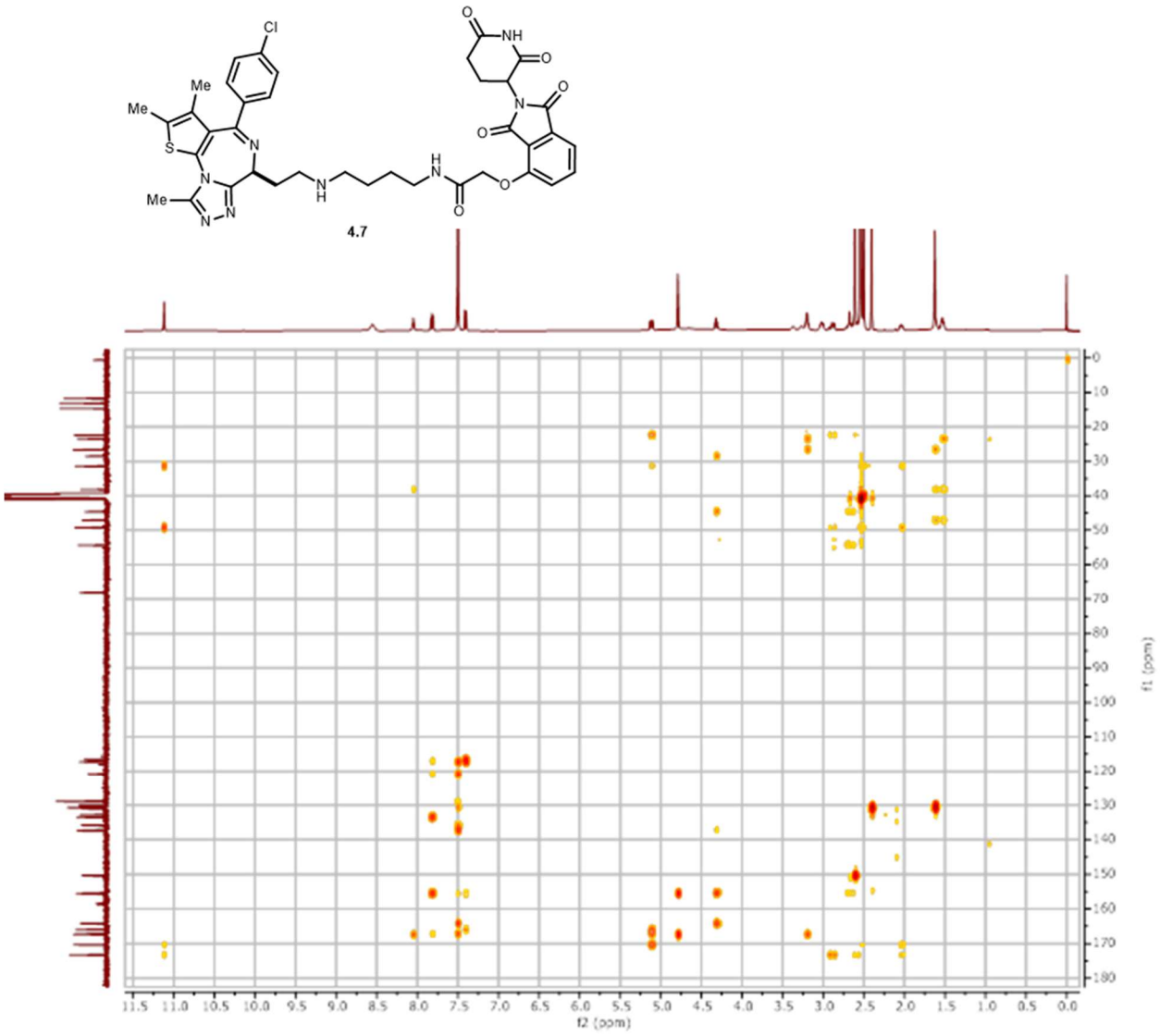

Spectrum 4.34 HMBC of **4.7**.

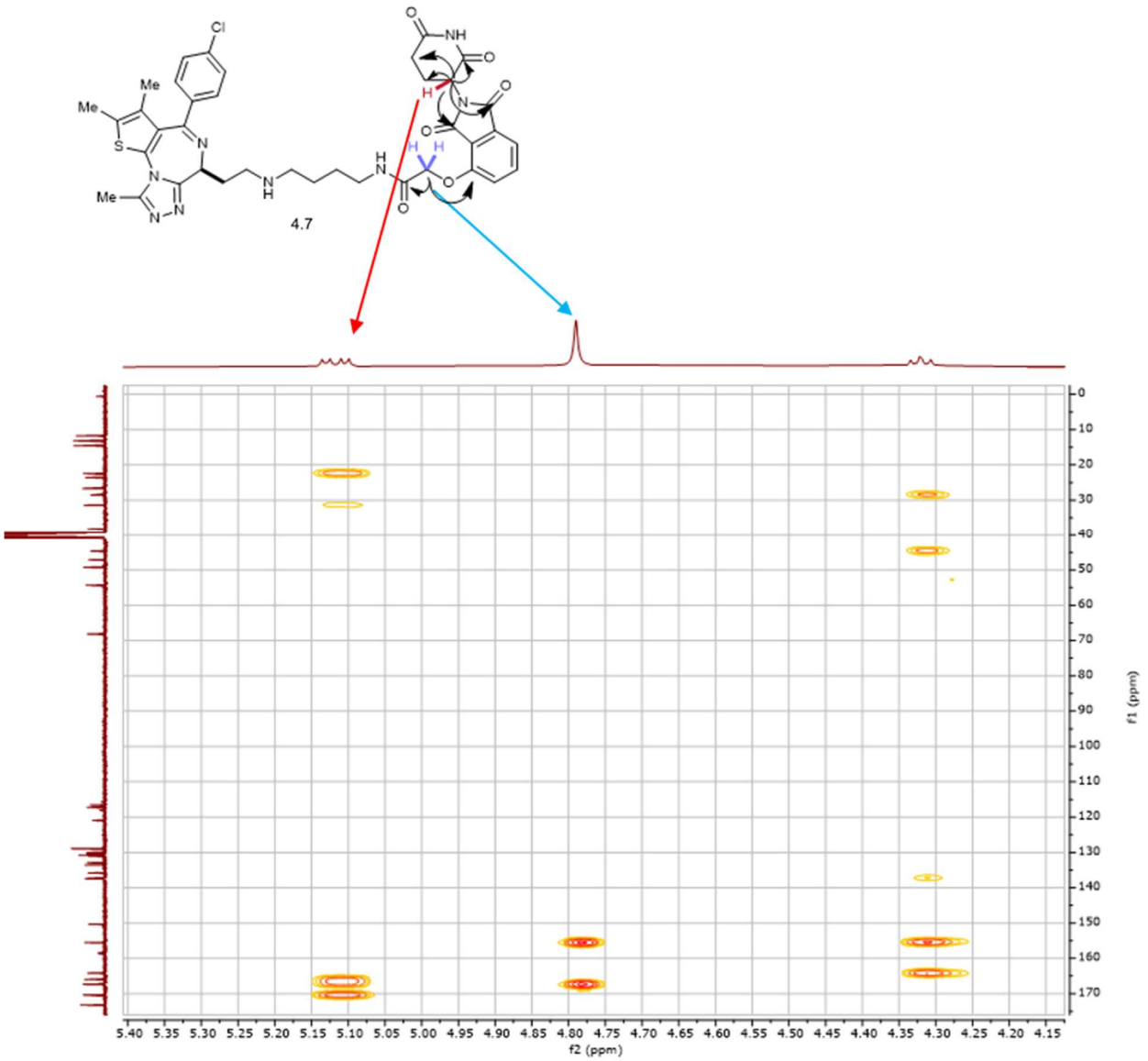

Spectrum 4.35 Zoomed in HMBC of **4.7** for indicated hydrogens.

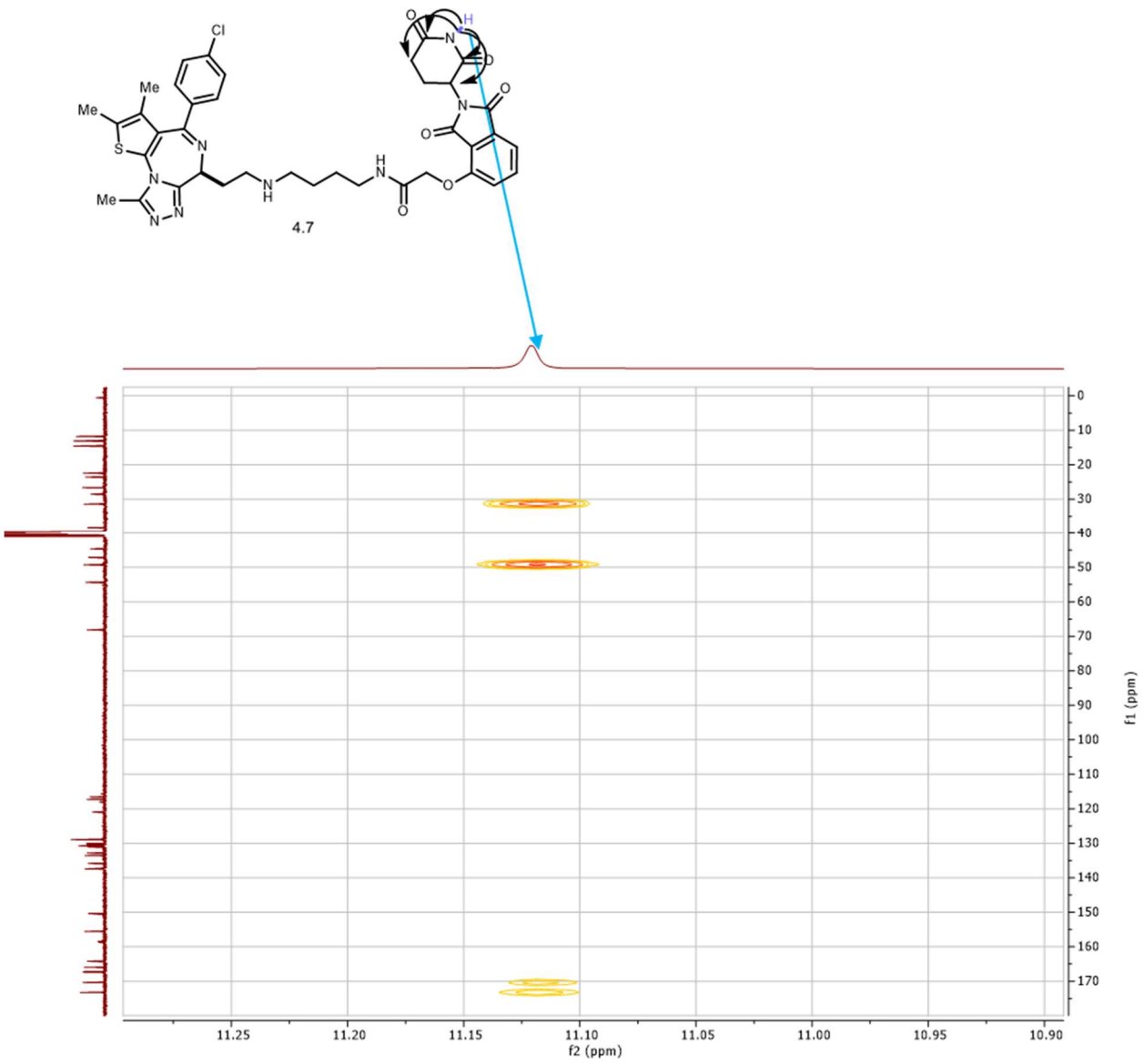

Spectrum 4.36 Zoomed in HMBC of **4.7** for indicated hydrogen.

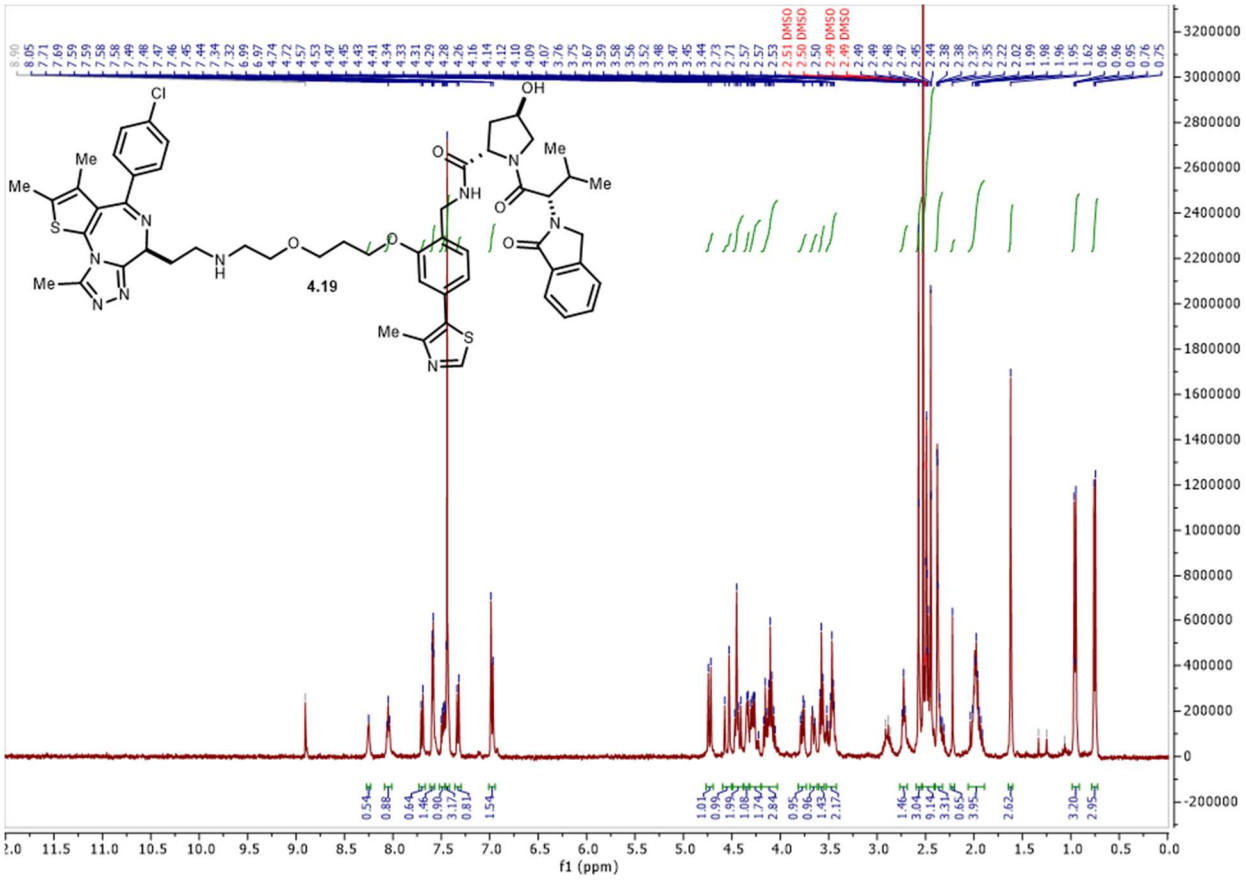

Spectrum 4.37 ^{1}H NMR of **4.19**.

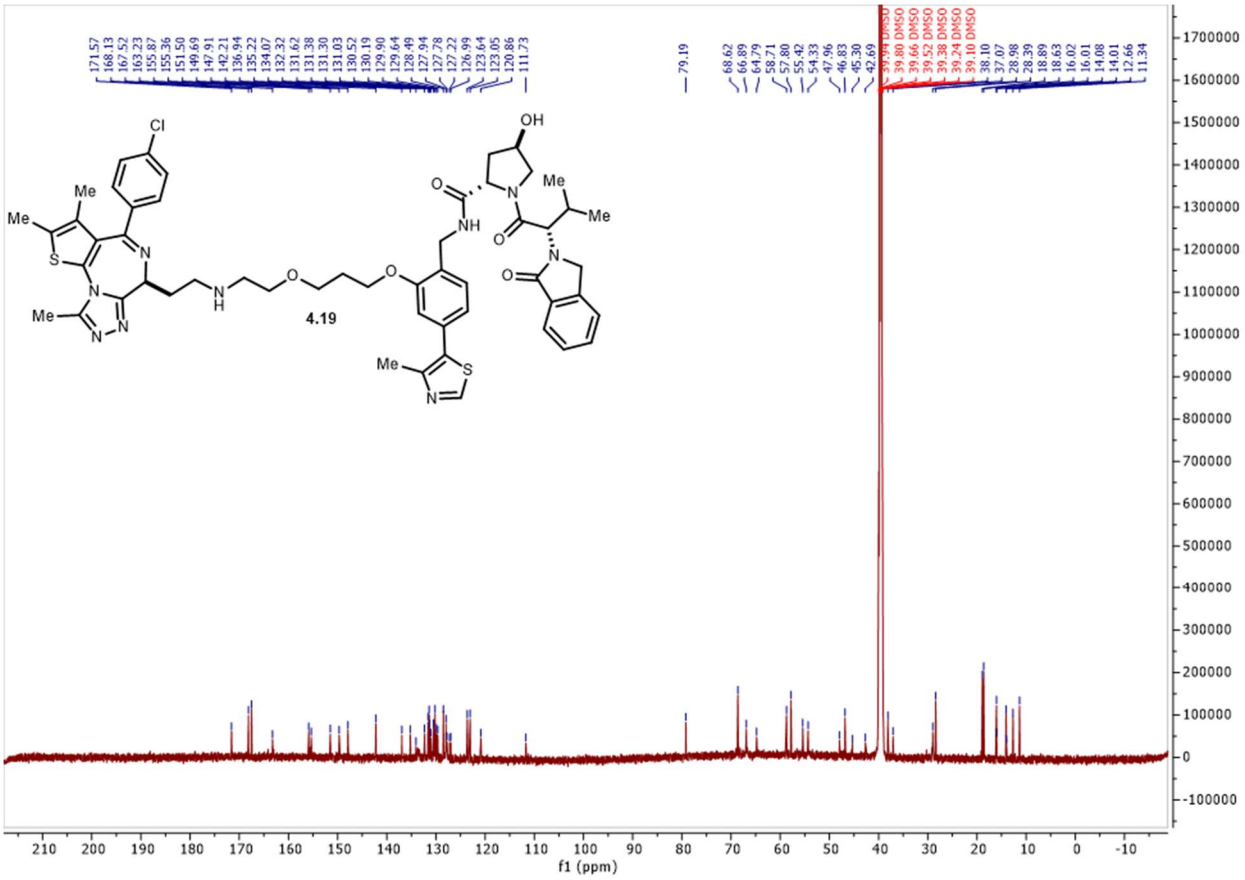

Spectrum 4.38 ^{13}C NMR of **4.19**.

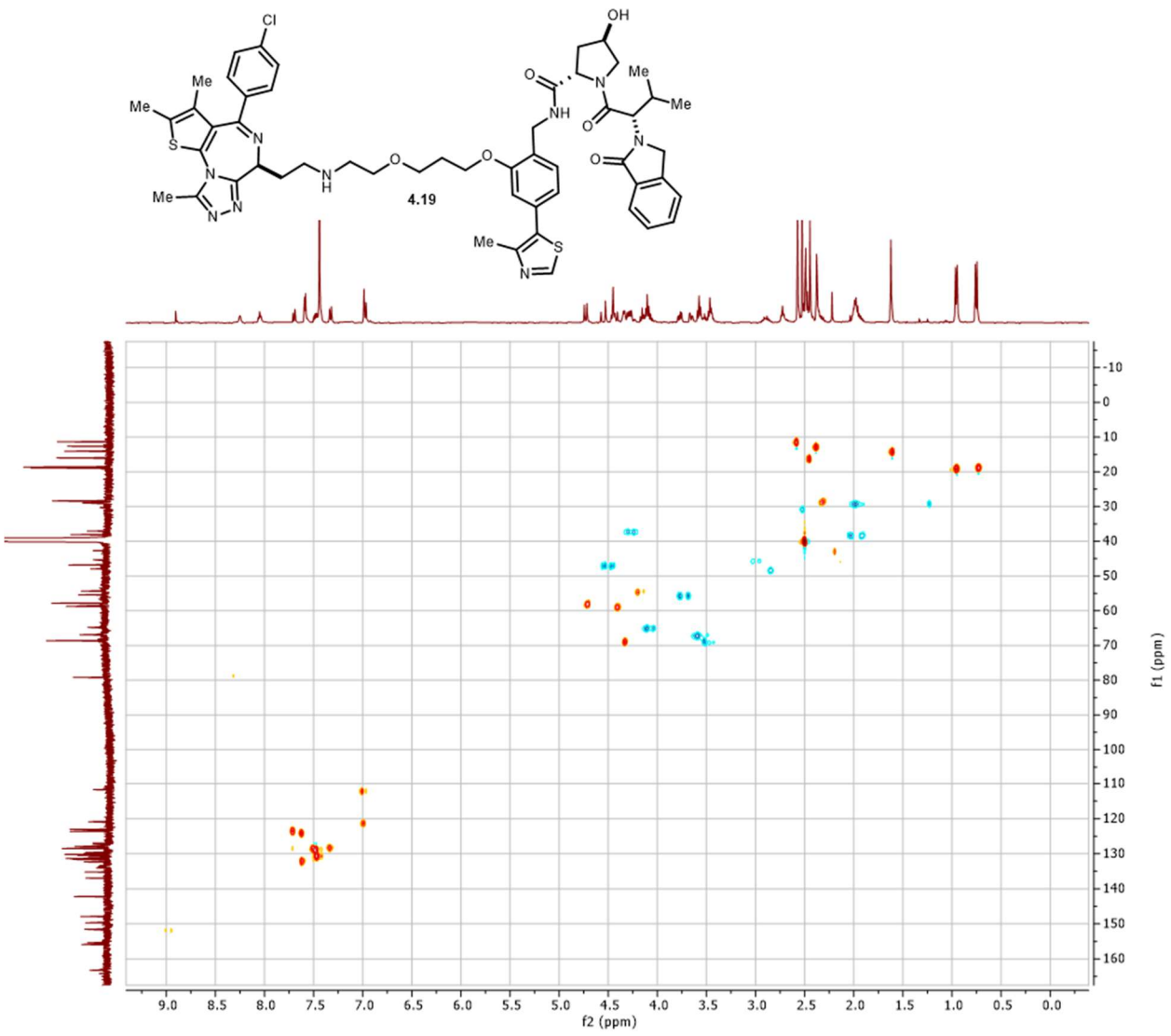

Spectrum 4.39 HSQC of **4.19**

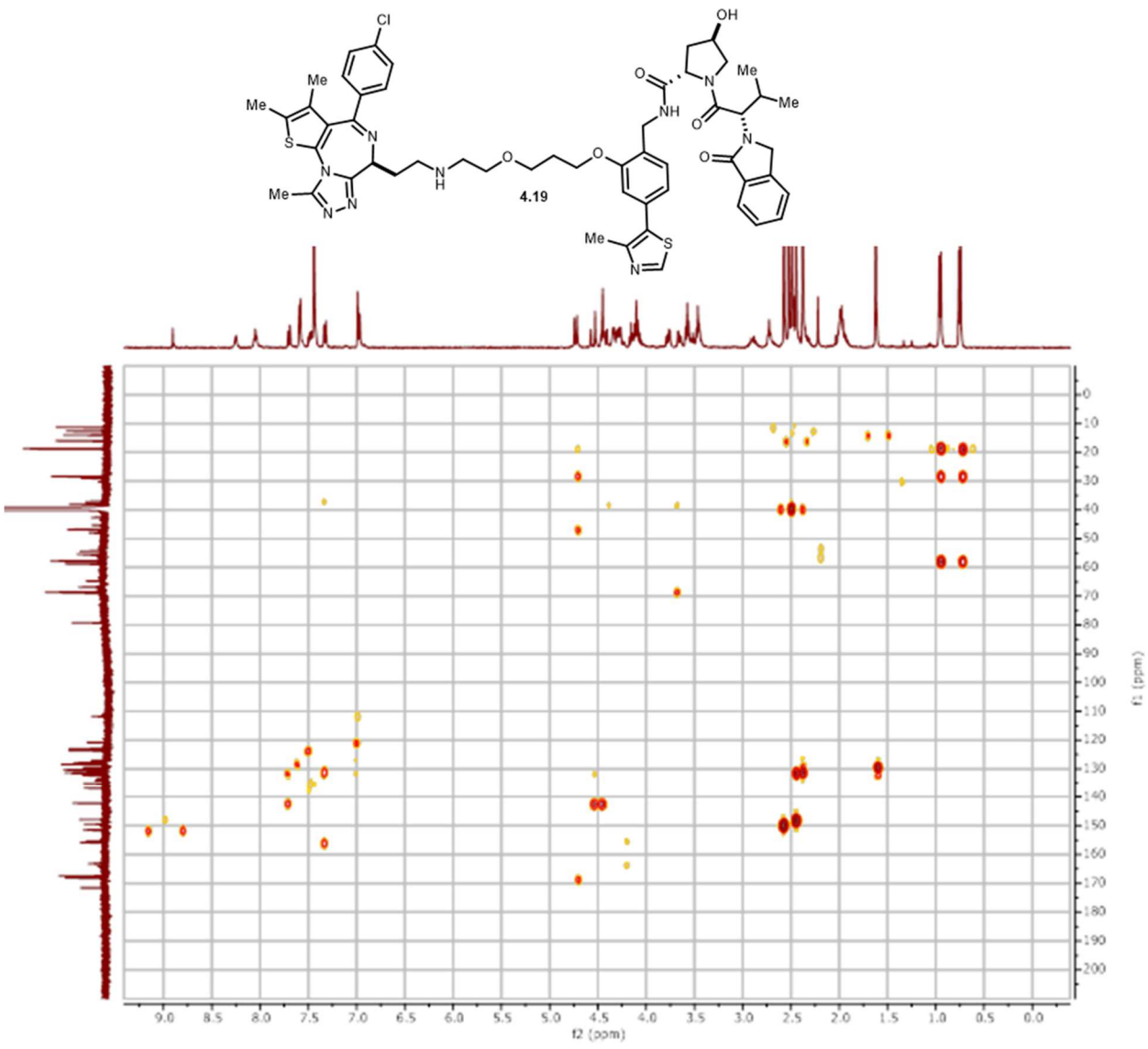

Spectrum 4.40 HMBC of **4.19**

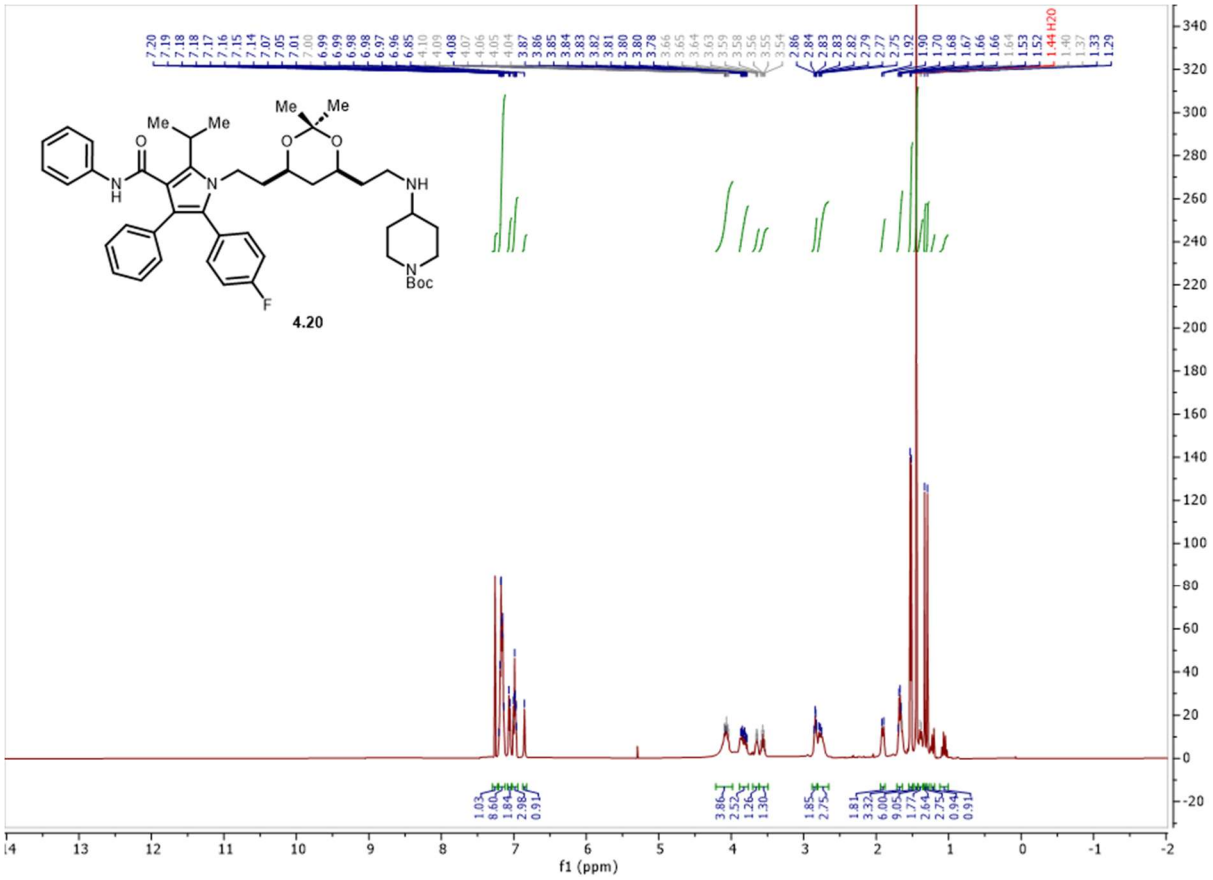

Spectrum 4.41 ^{1}H NMR of **4.20**.

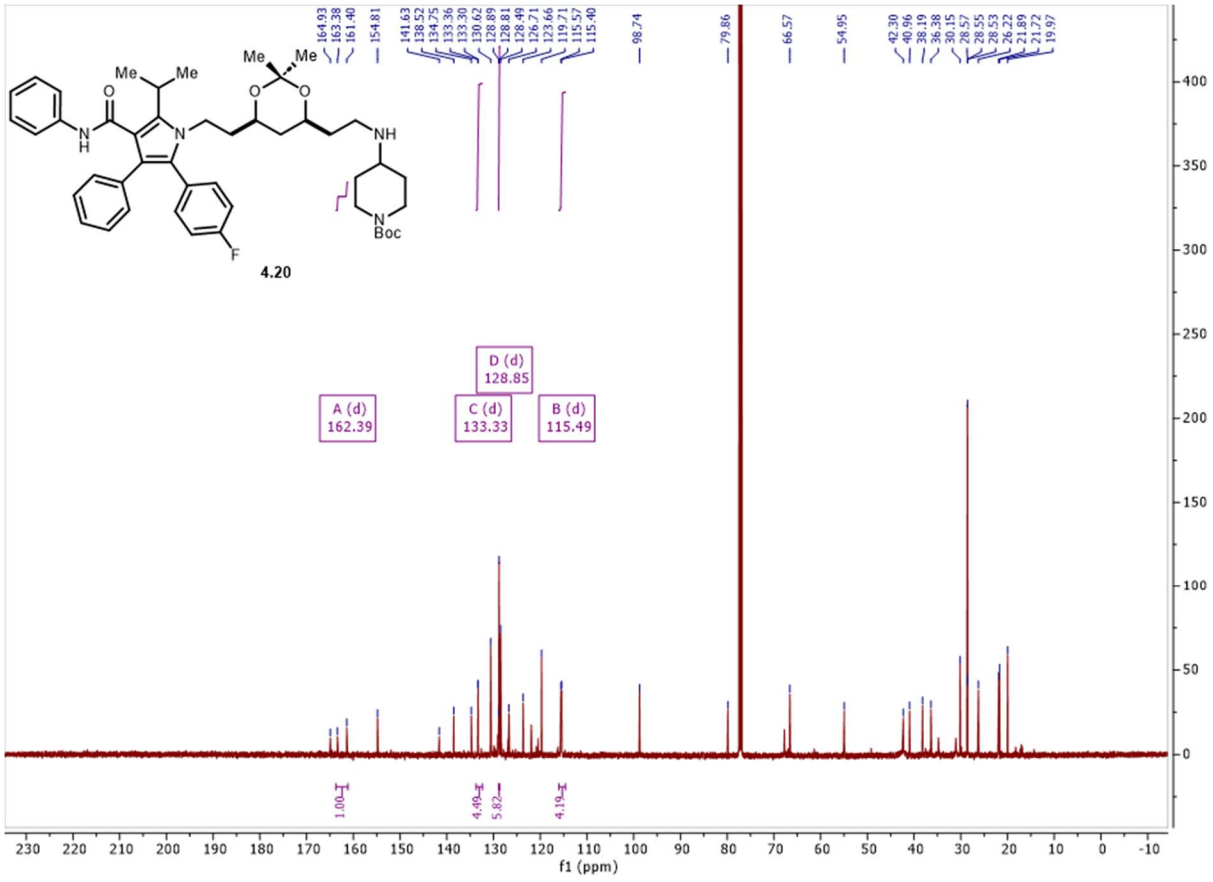

Spectrum 4.42 ^{13}C NMR of **4.20**.

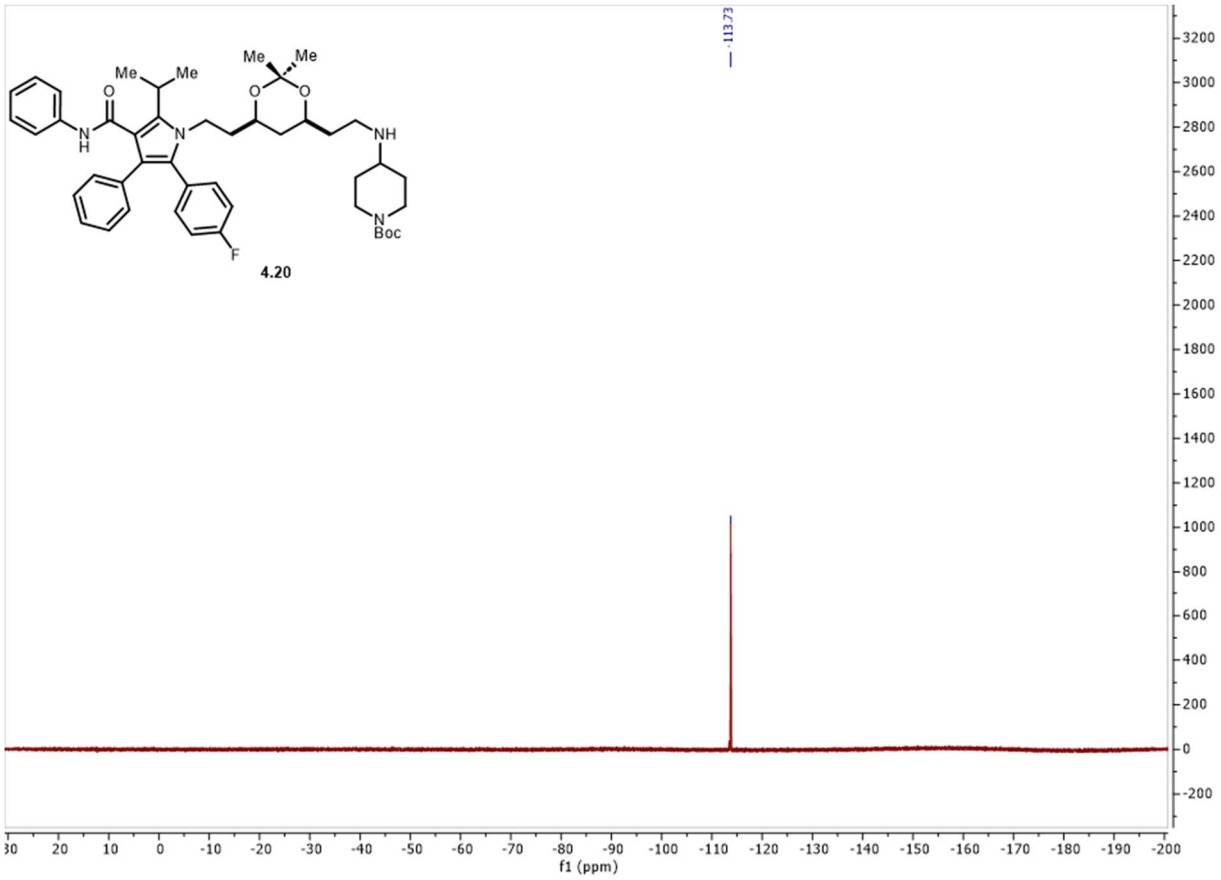

Spectrum 4.43 ^{19}F NMR of **4.20**.

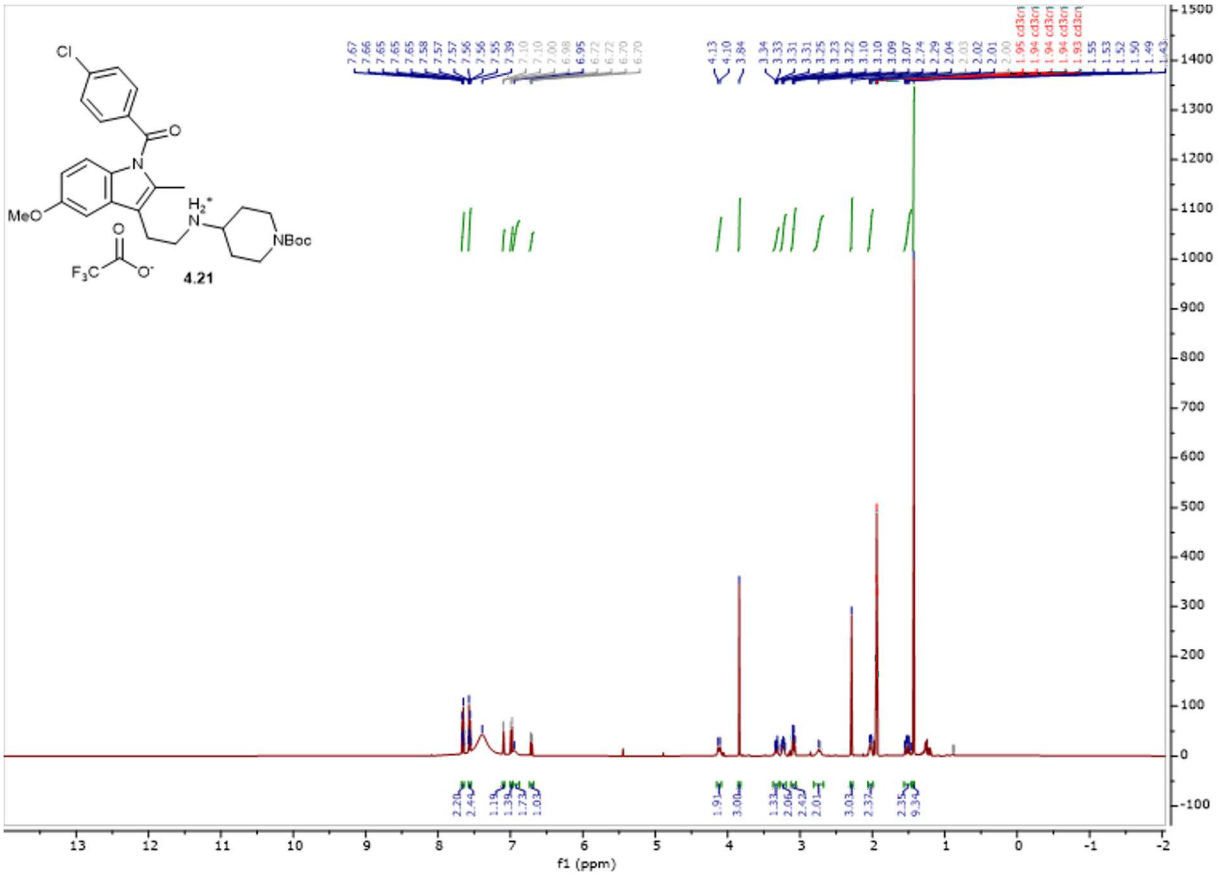

Spectrum 4.44 ^{1}H NMR of **4.21**.

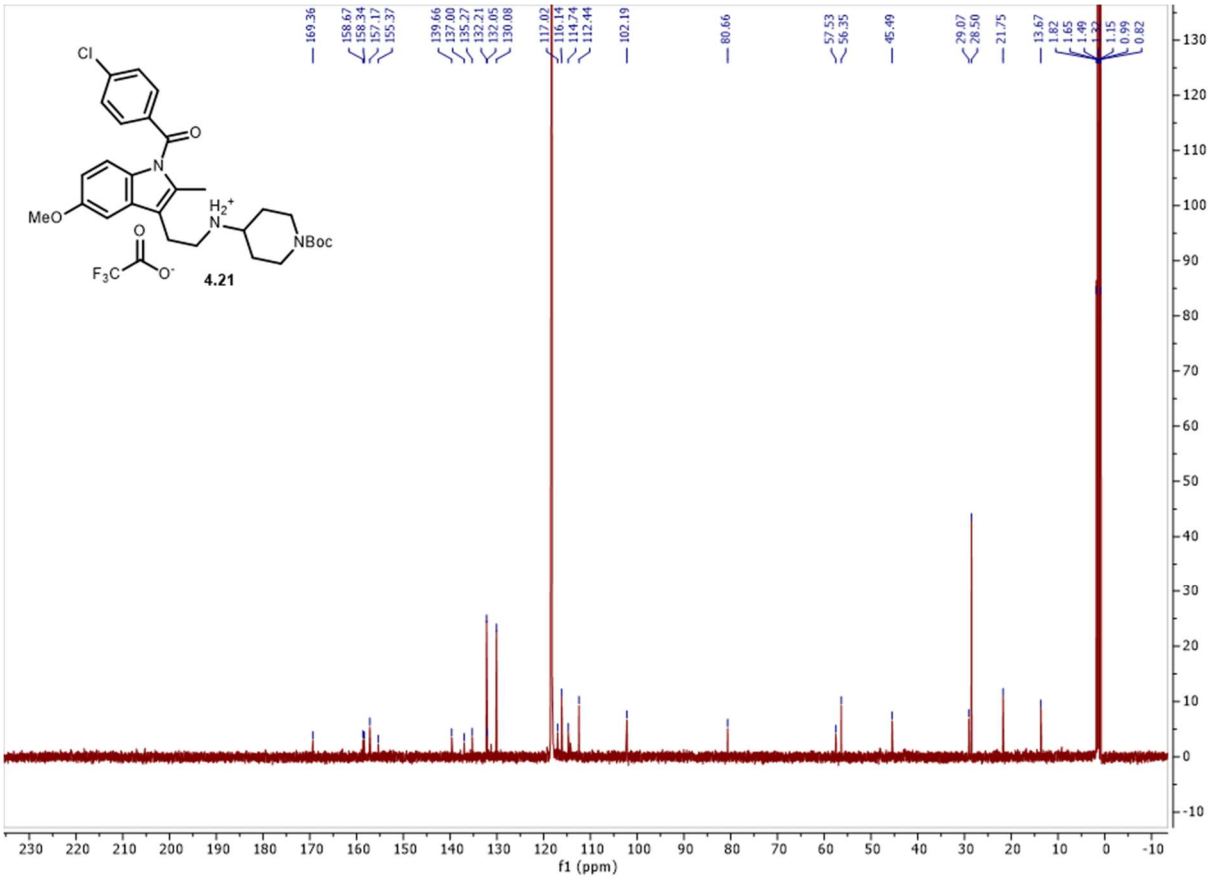

Spectrum 4.45 ^{13}C NMR of **4.21**.

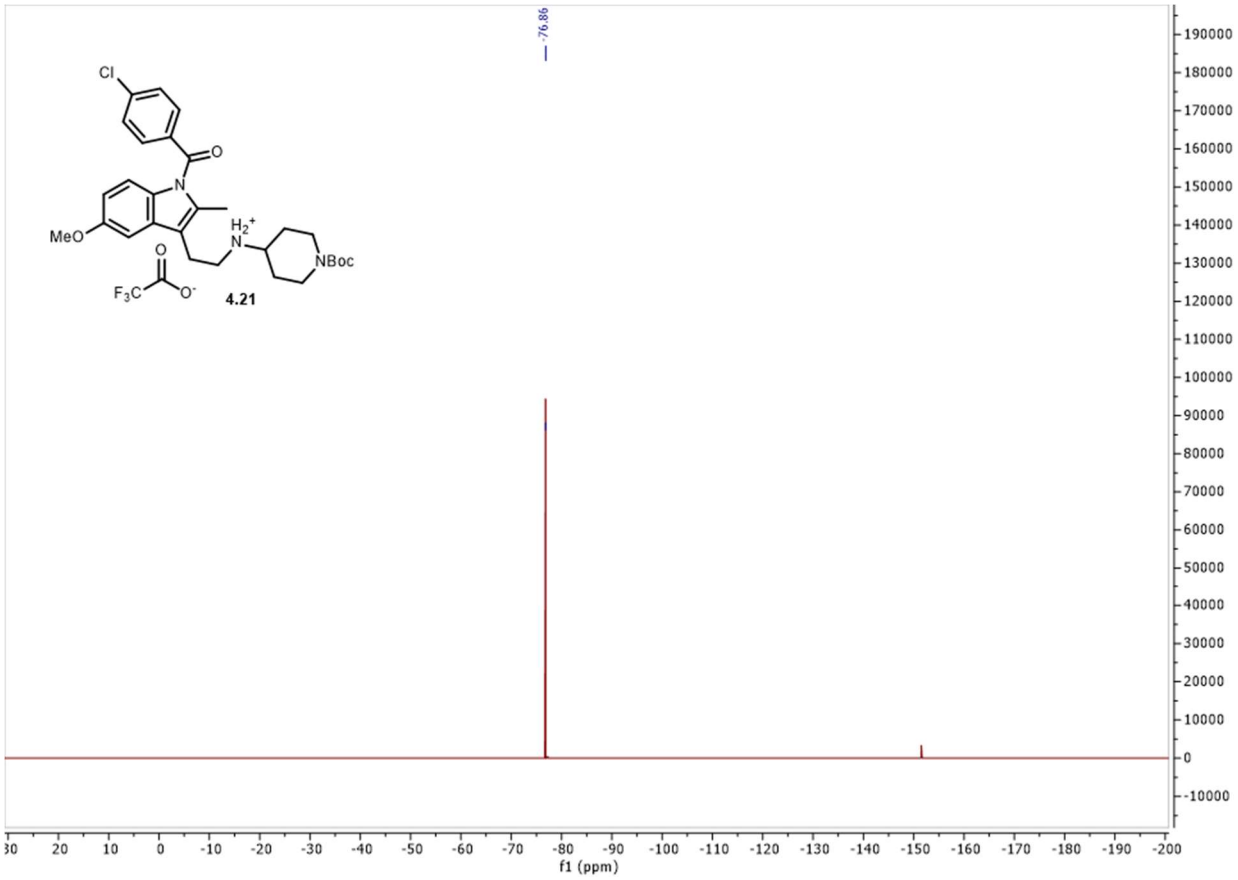

Spectrum 4.46 ^{19}F NMR of **4.21**.

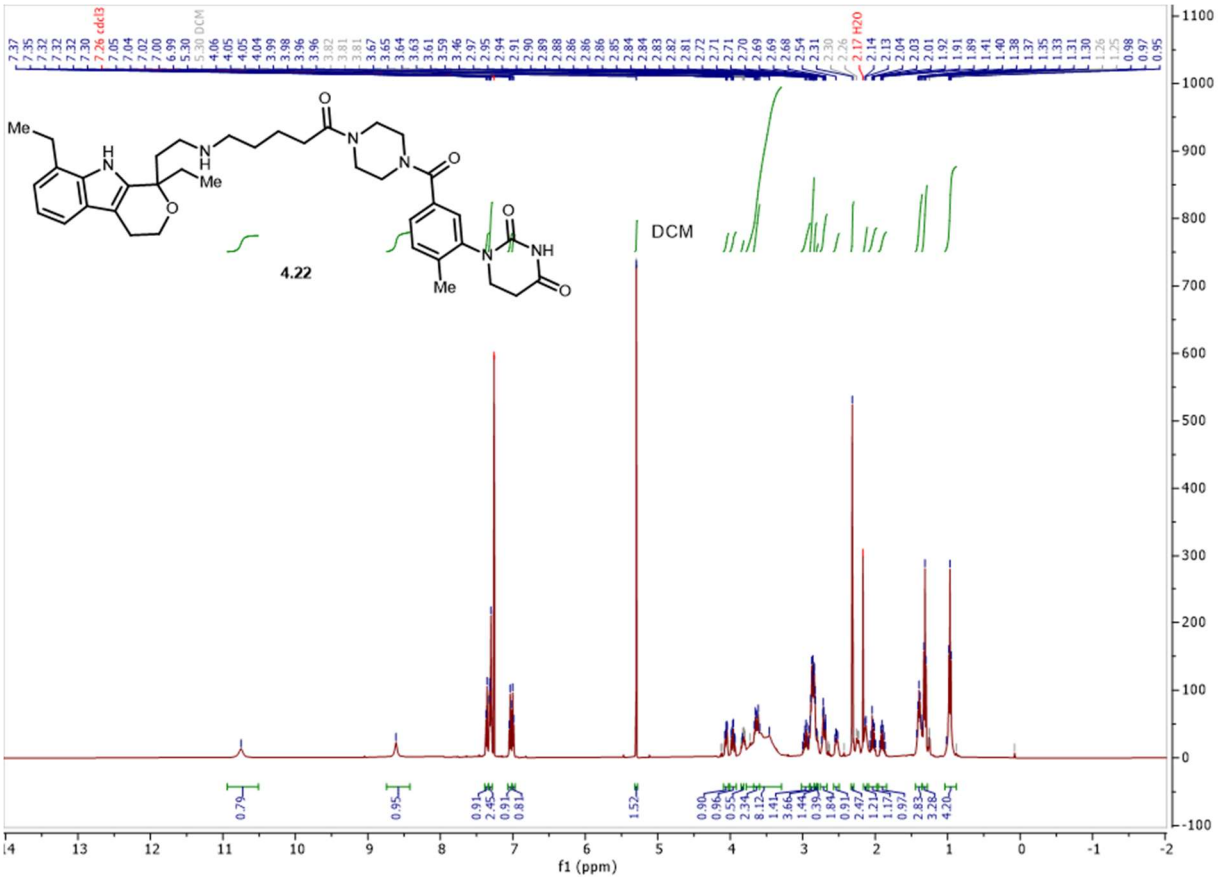

Spectrum 4.47 ^{1}H NMR of **4.22**.

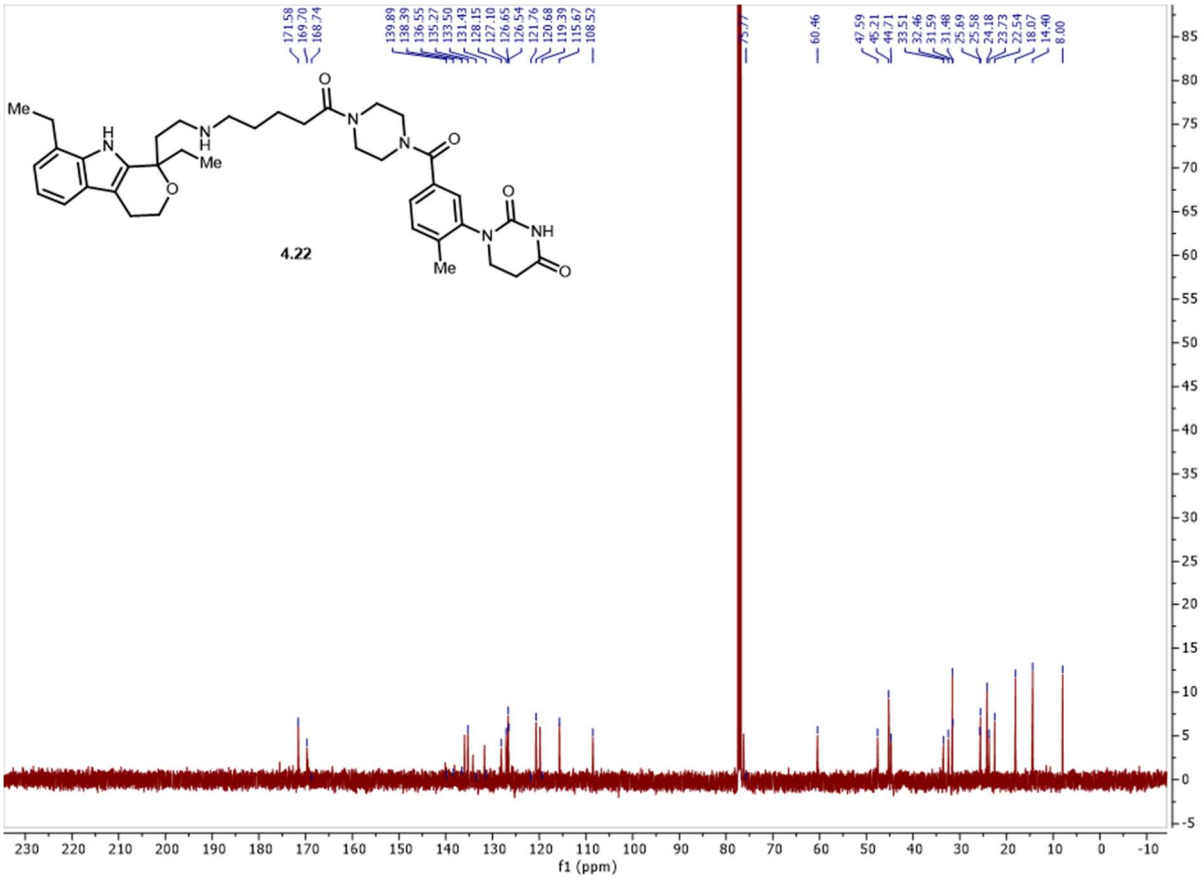

Spectrum 4.48 ^{13}C NMR of **4.22**.

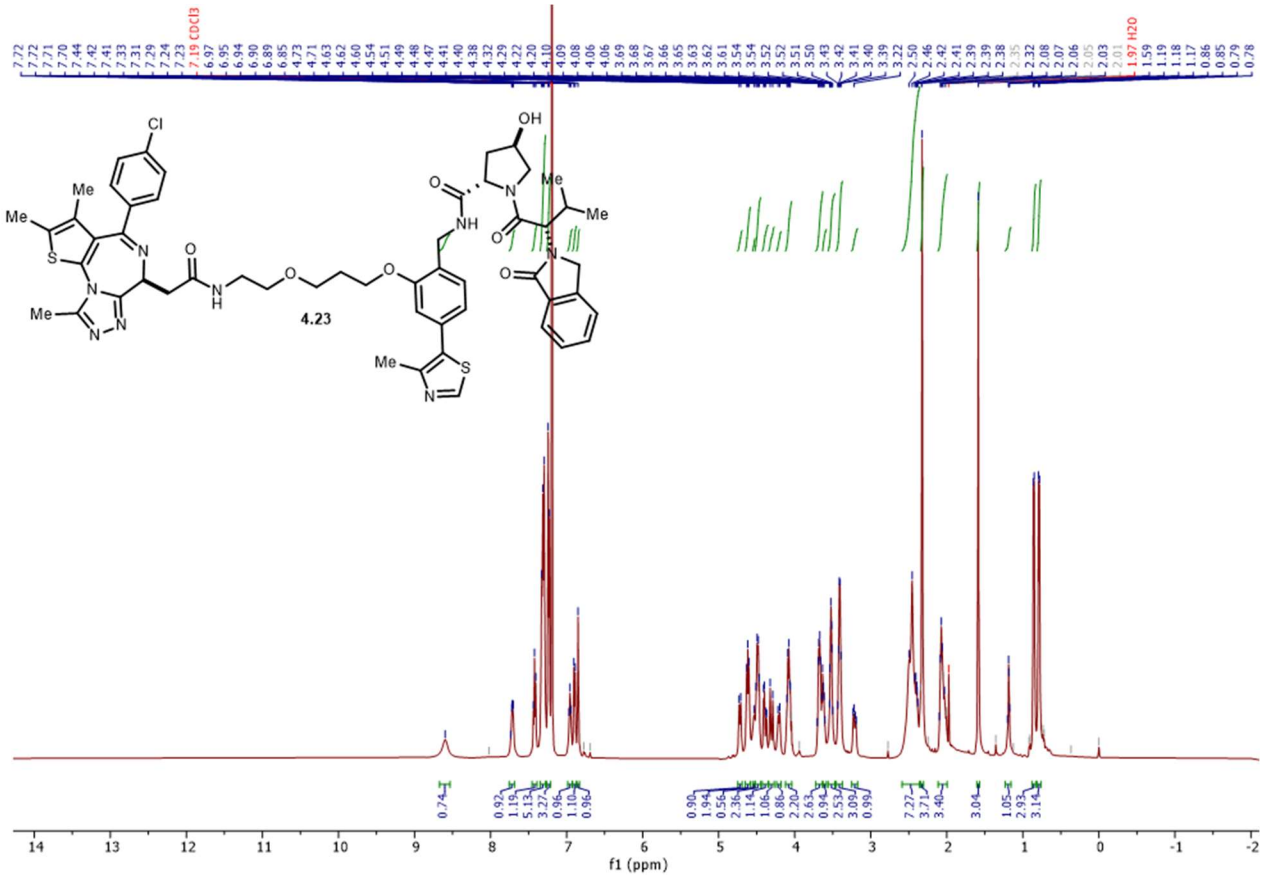

Spectrum 4.49 ^{1}H NMR of **4.23**.

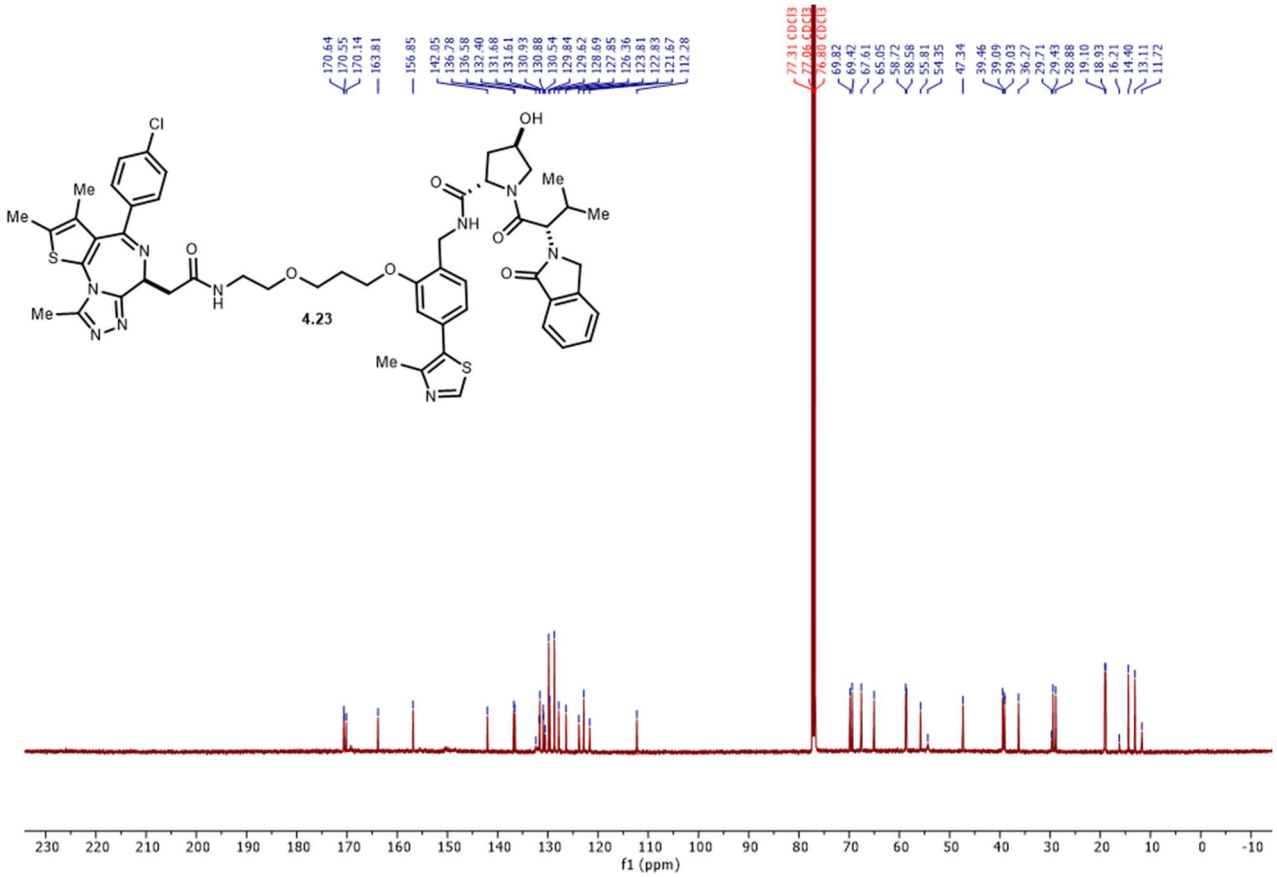

Spectrum 4.50 ^{13}C NMR of **4.23**.

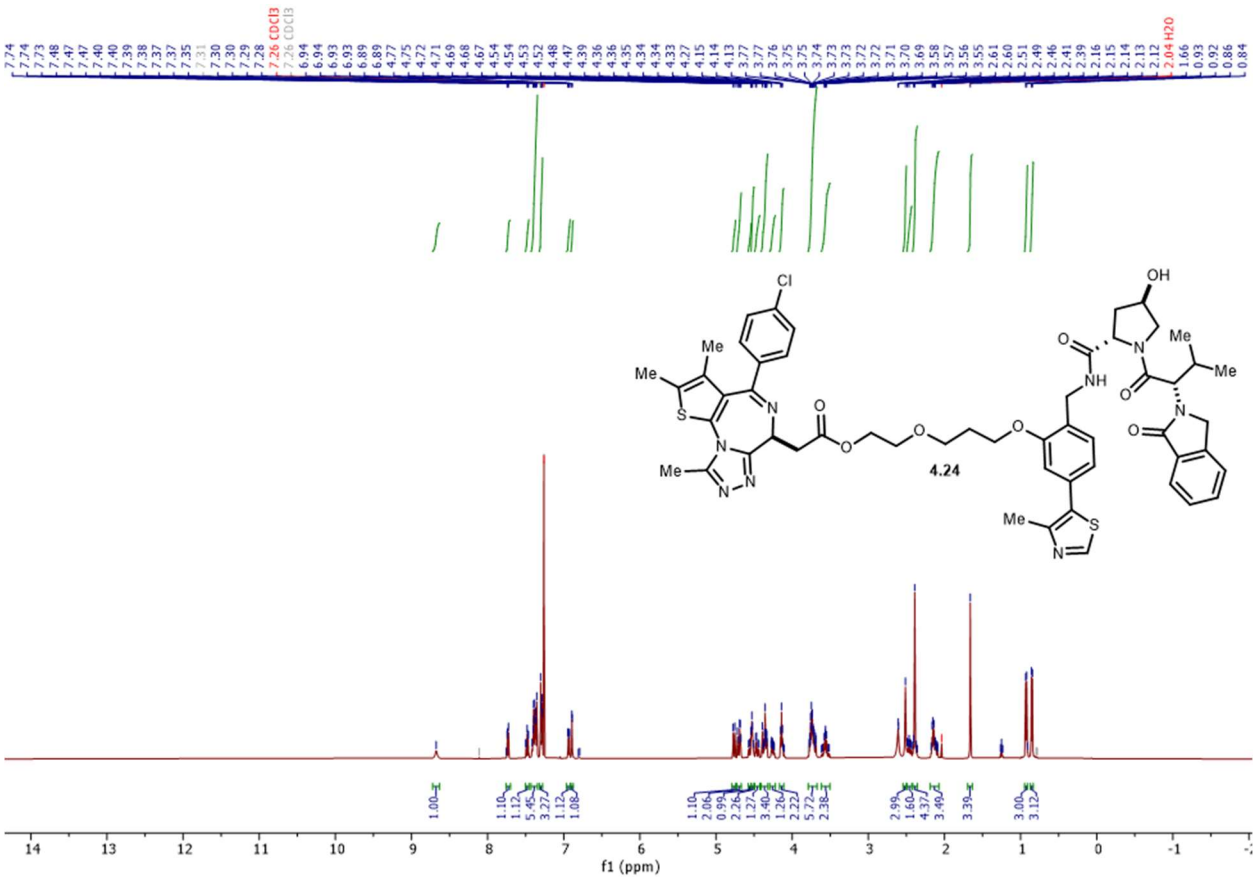

Spectrum 4.51 ^{1}H NMR of **4.24**.

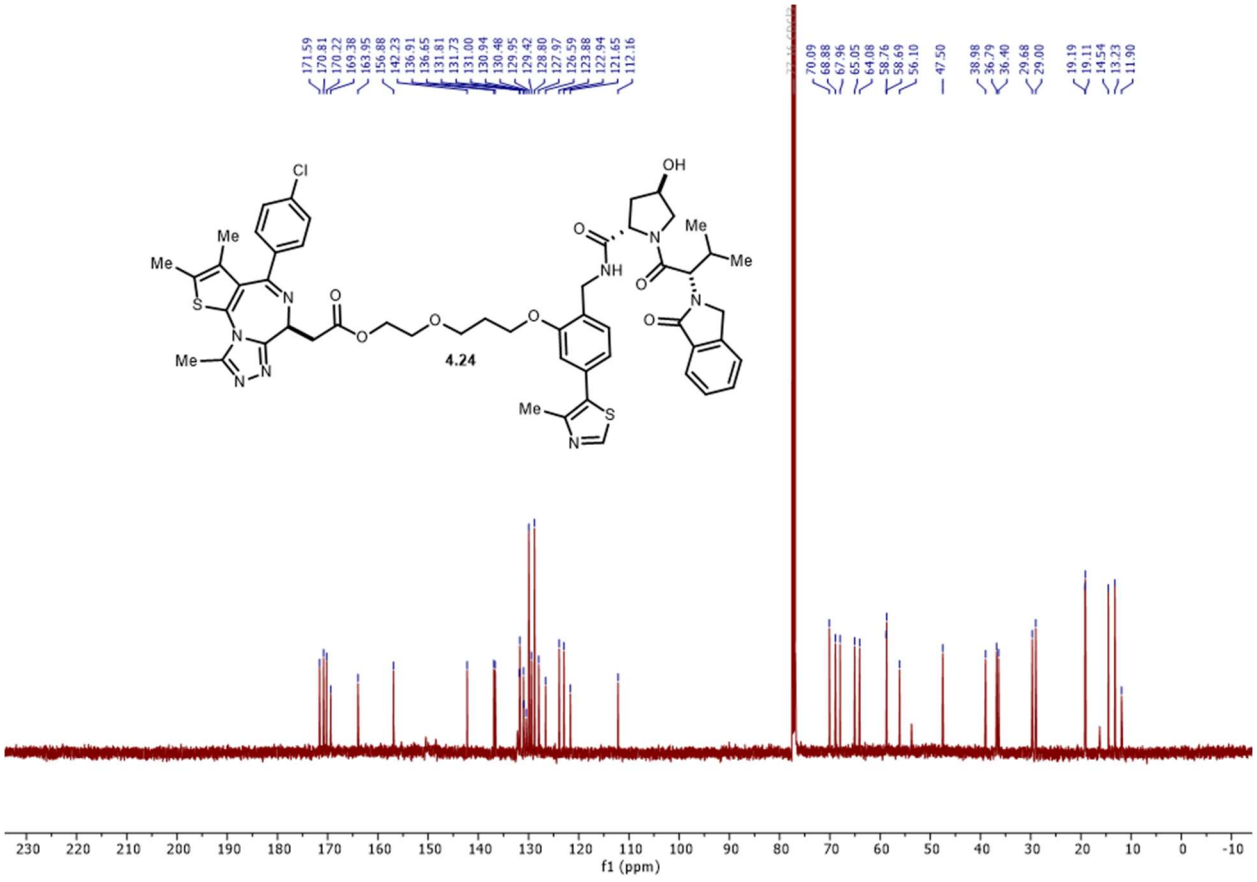

Spectrum 4.52 ^{13}CNMR of **4.24**.

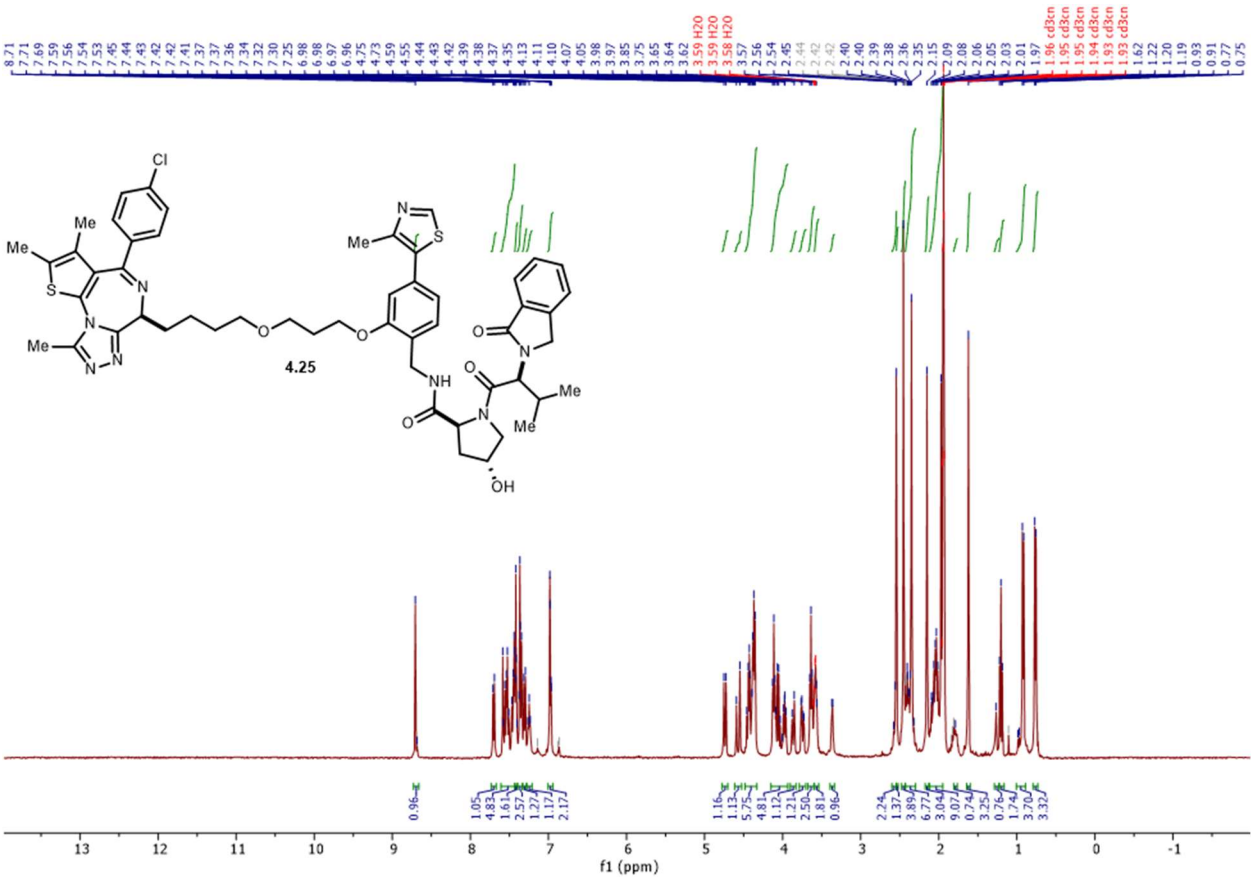

Spectrum 4.53 ^{1}H NMR of **4.25**.

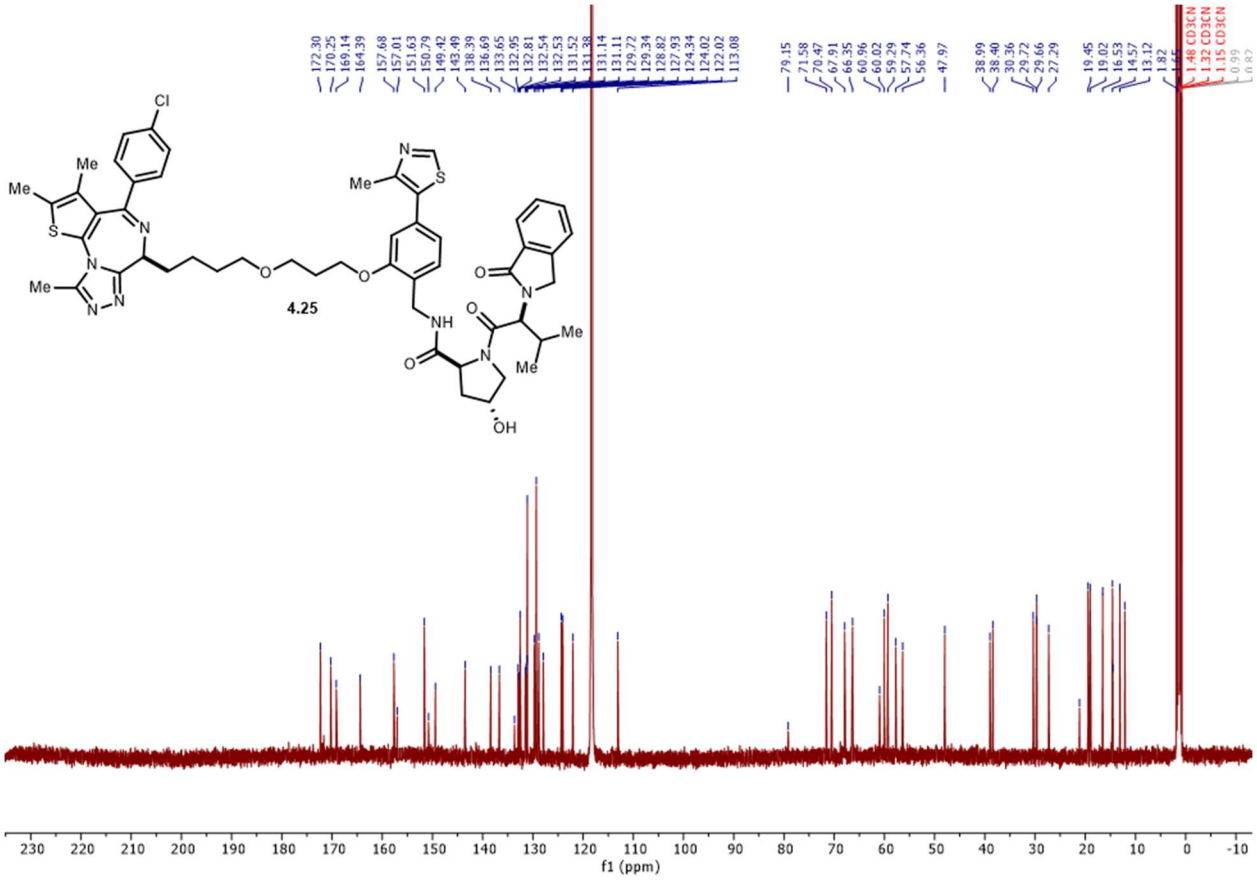

Spectrum 4.54 ^{13}C NMR of **4.25**.

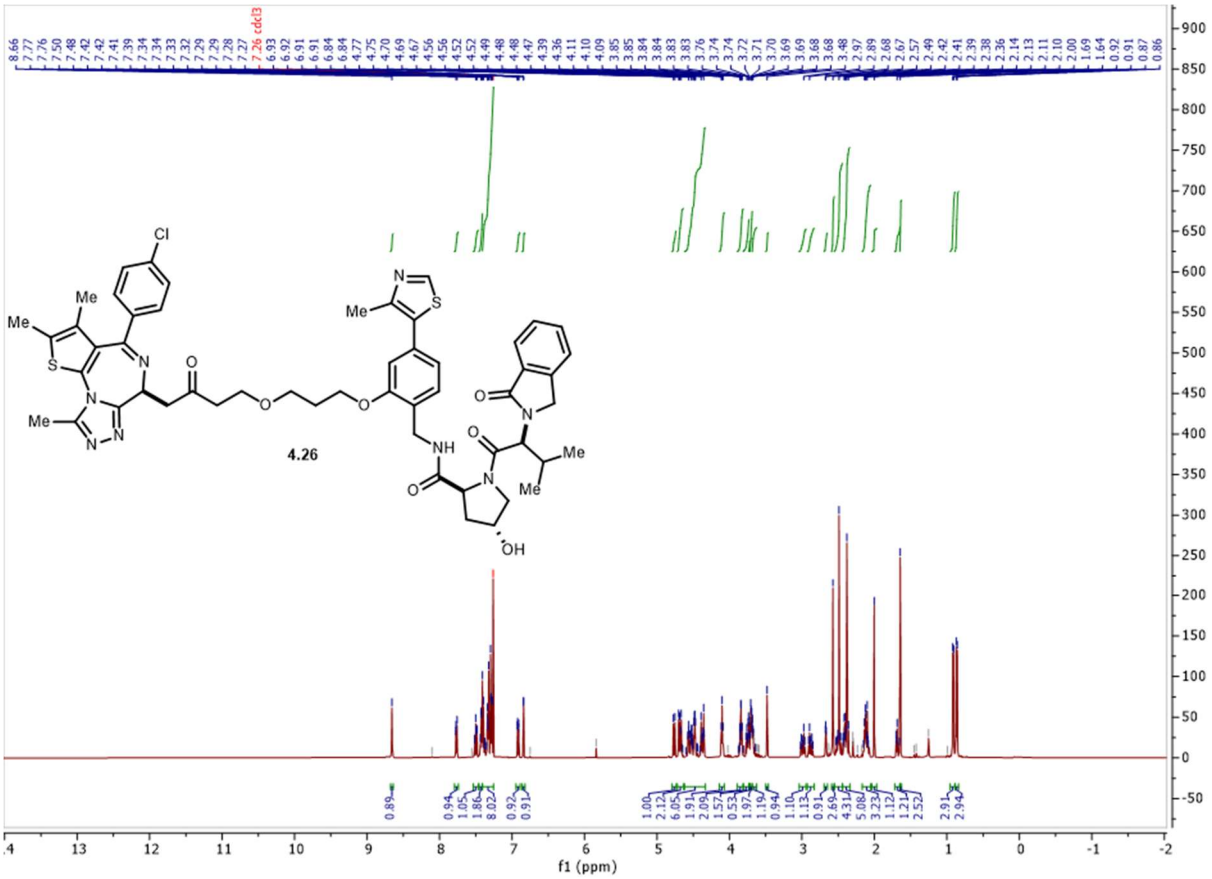

Spectrum 4.55 ^{1}HNMR of **4.26**.

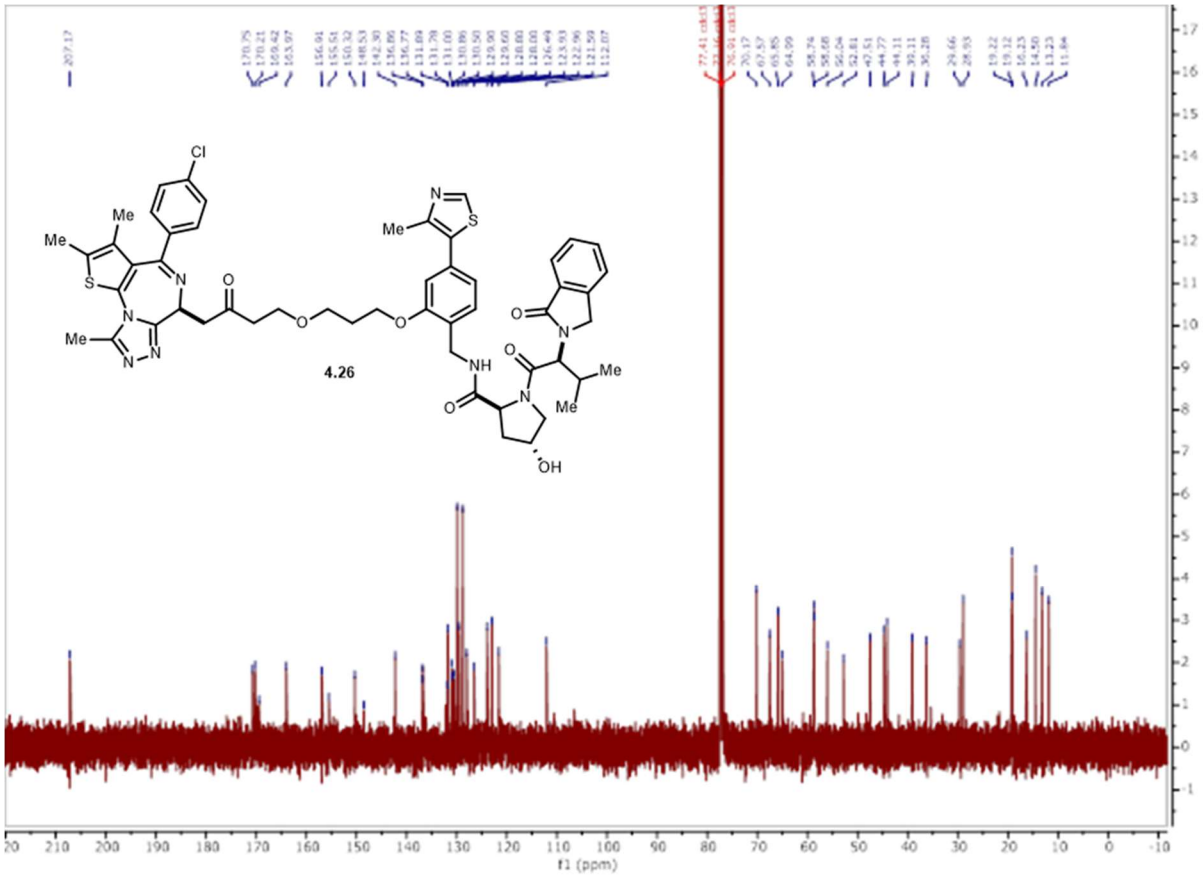

Spectrum 4.56 ^{13}C NMR of **4.26**

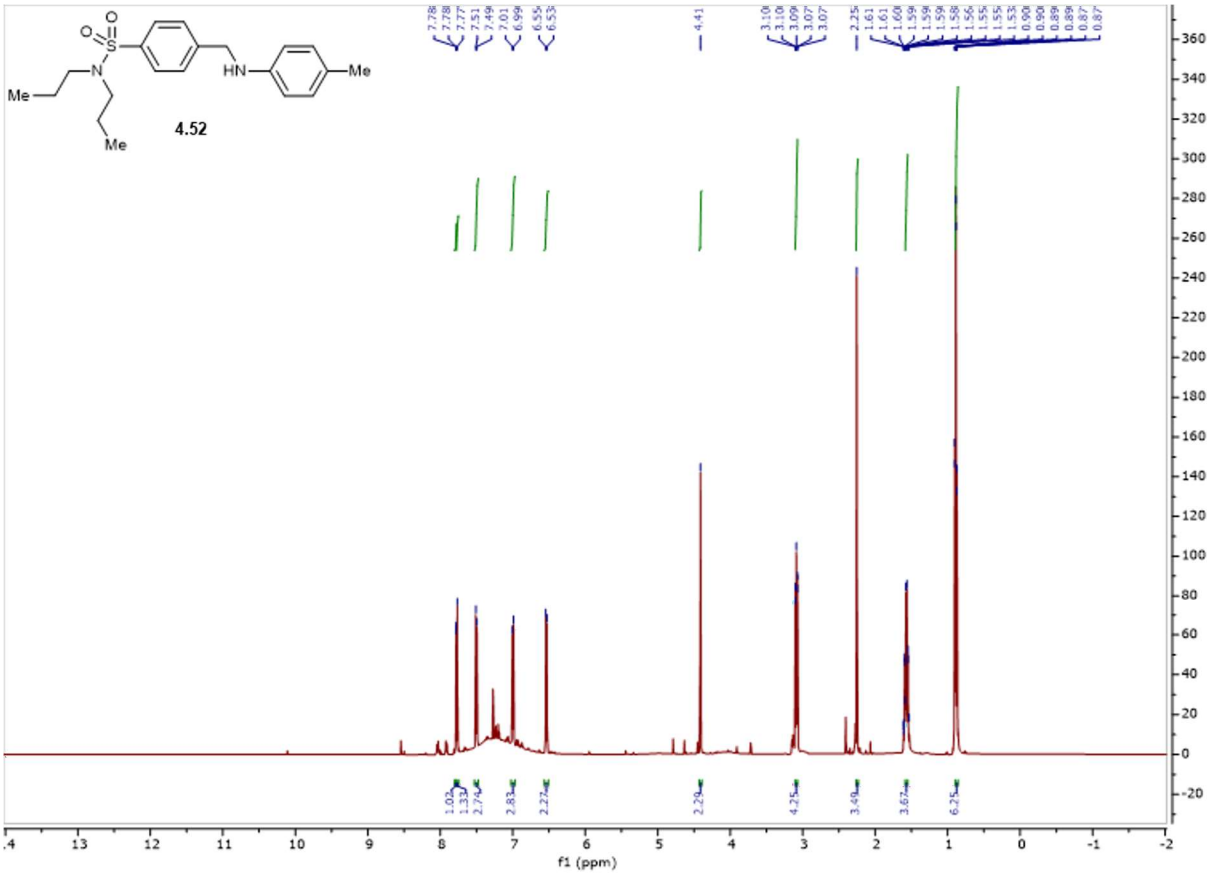

Spectrum 4.57 ^{1}H NMR of **4.52.**

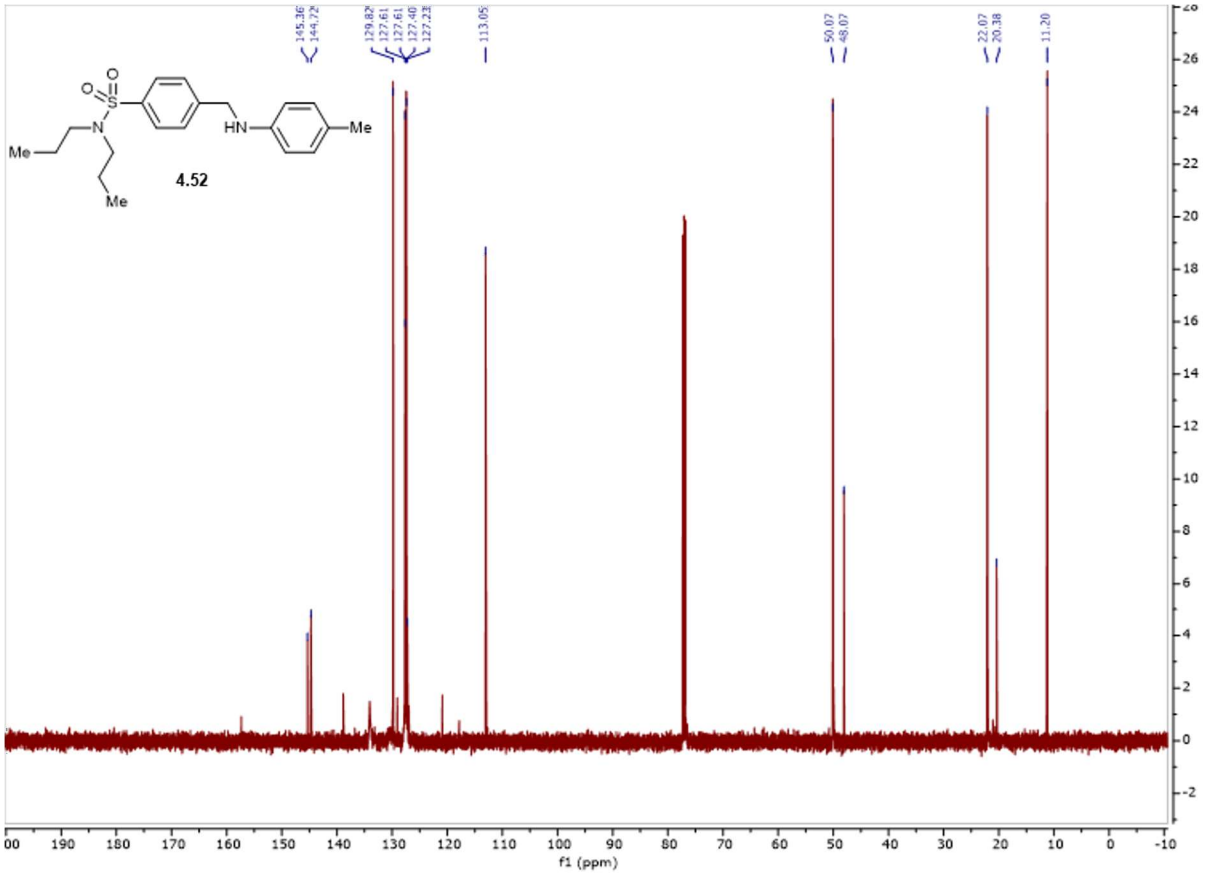

Spectrum 4.58 ^{13}C NMR of **4.52**.

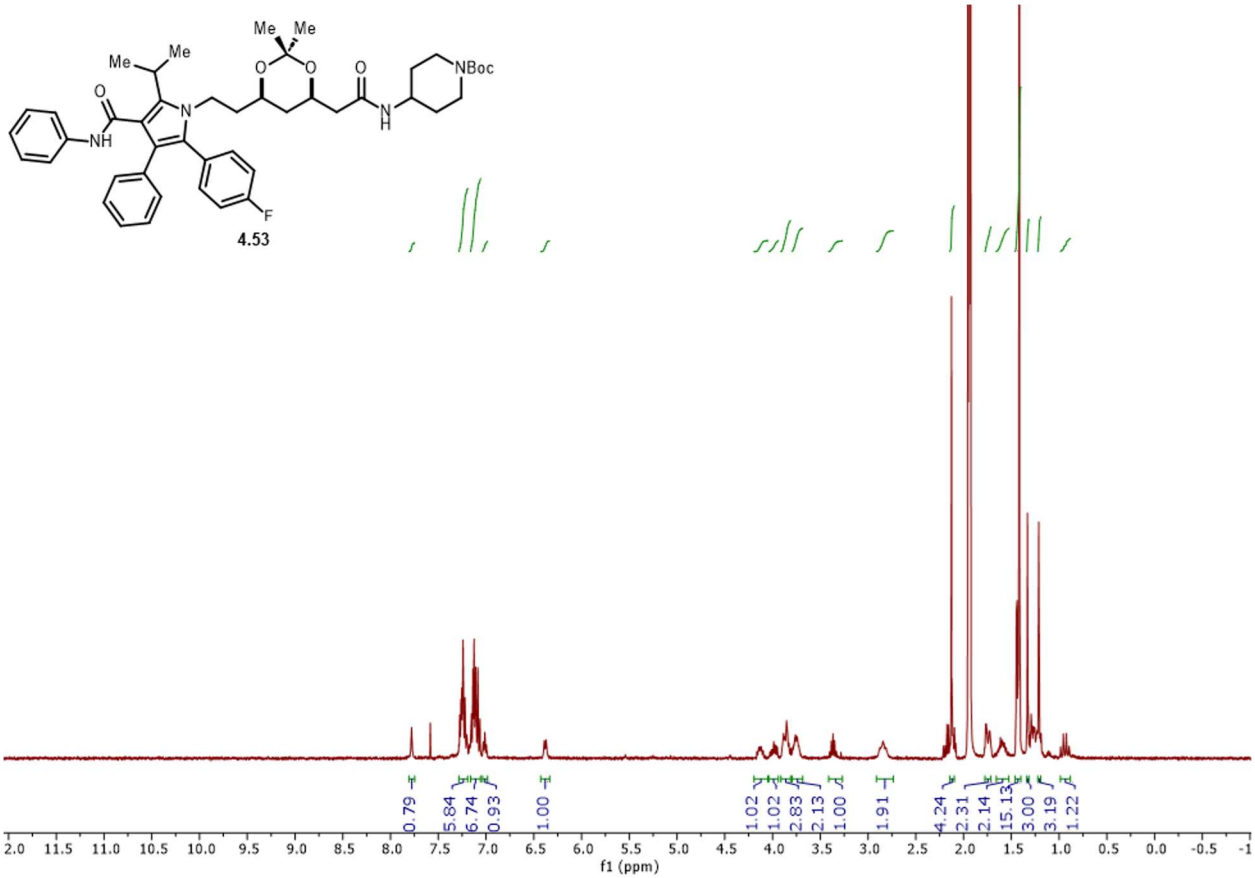

Spectrum 4.59 ^{1}H NMR of **4.53**.

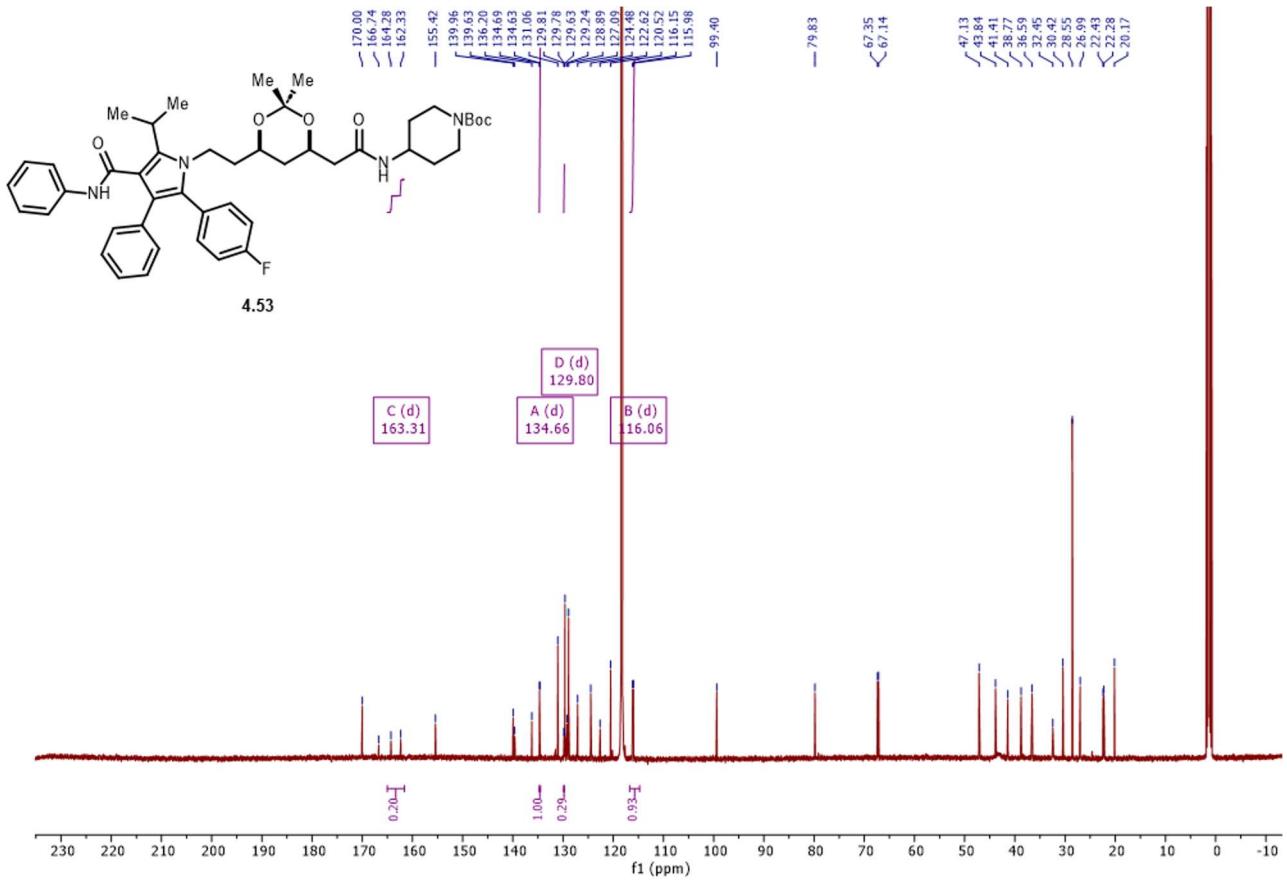

Spectrum 4.60 ^{13}C NMR of **4.53**.

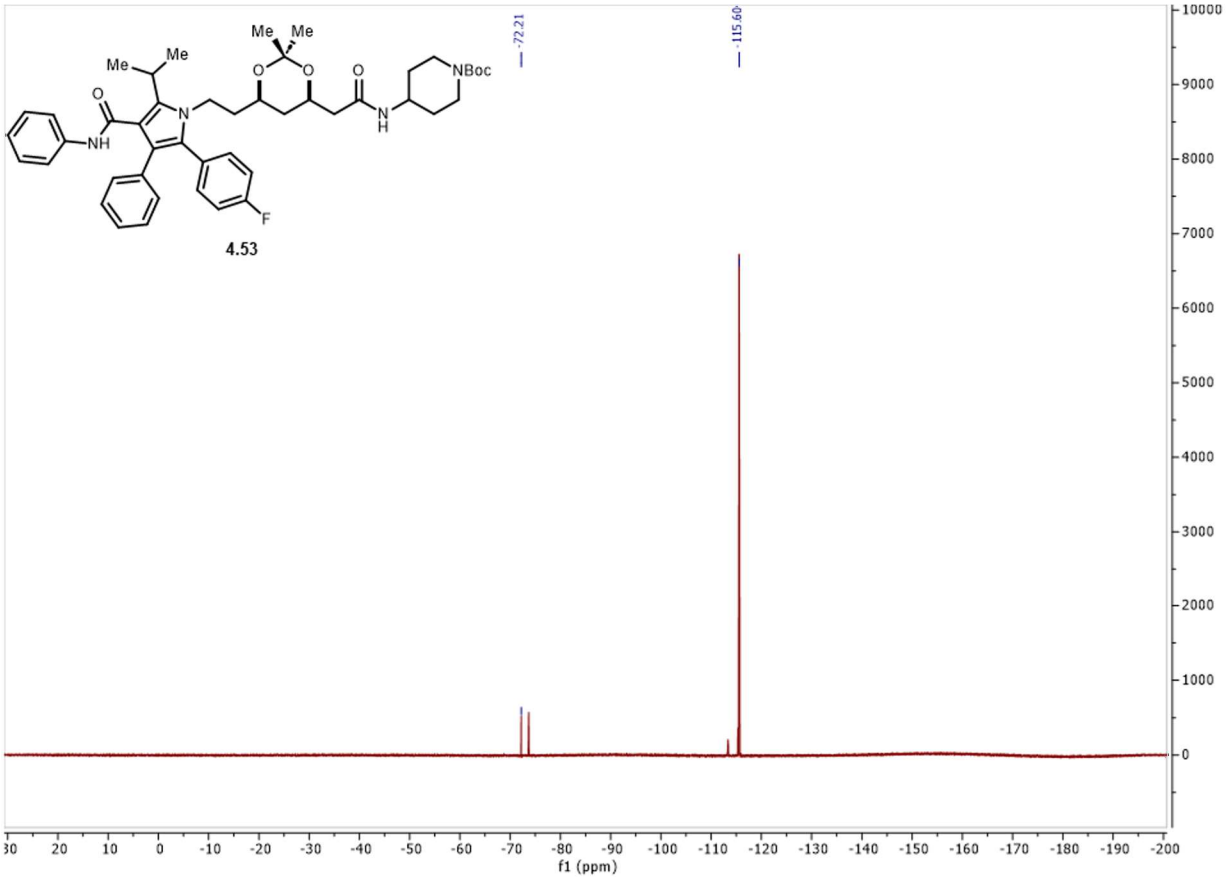

Spectrum 4.61 ^{19}F NMR of **4.53**.

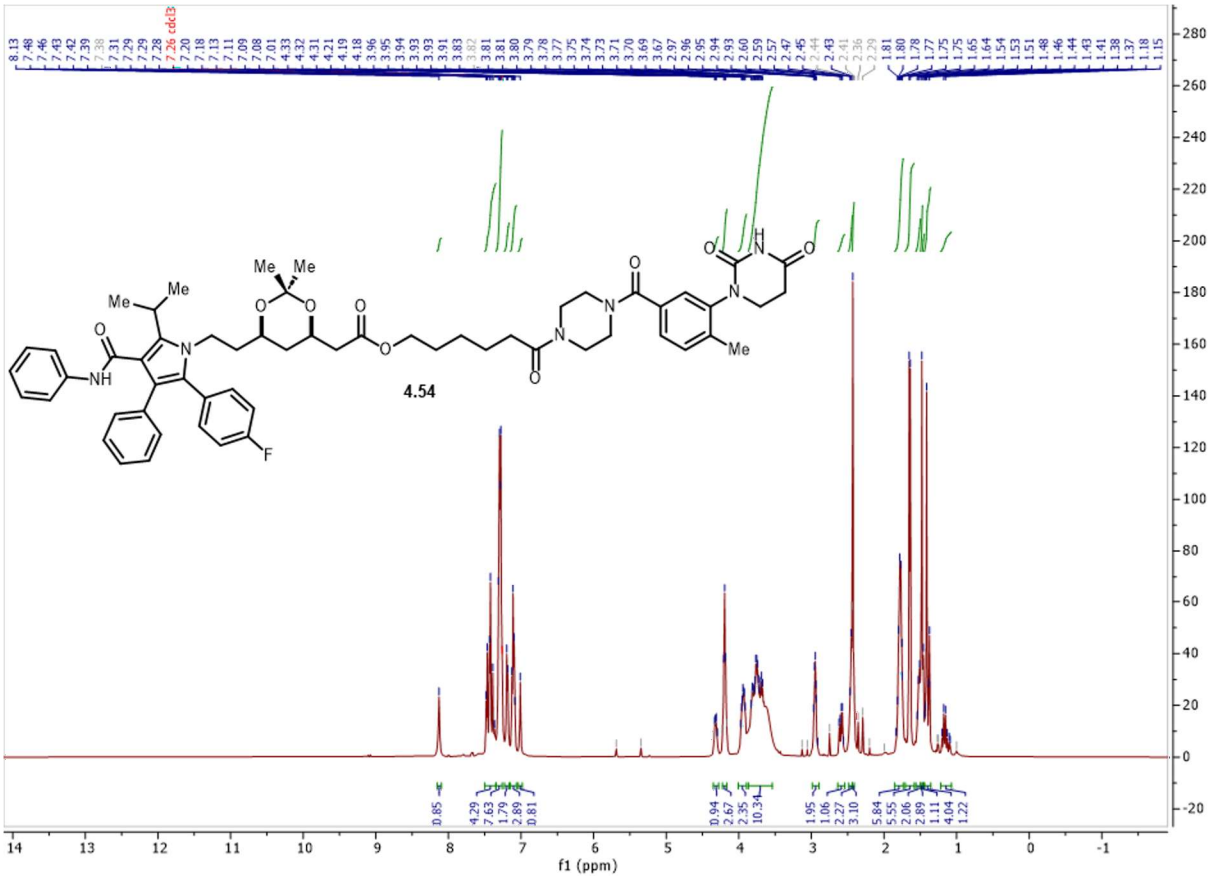

Spectrum 4.62 ^{1}H NMR of **4.54**.

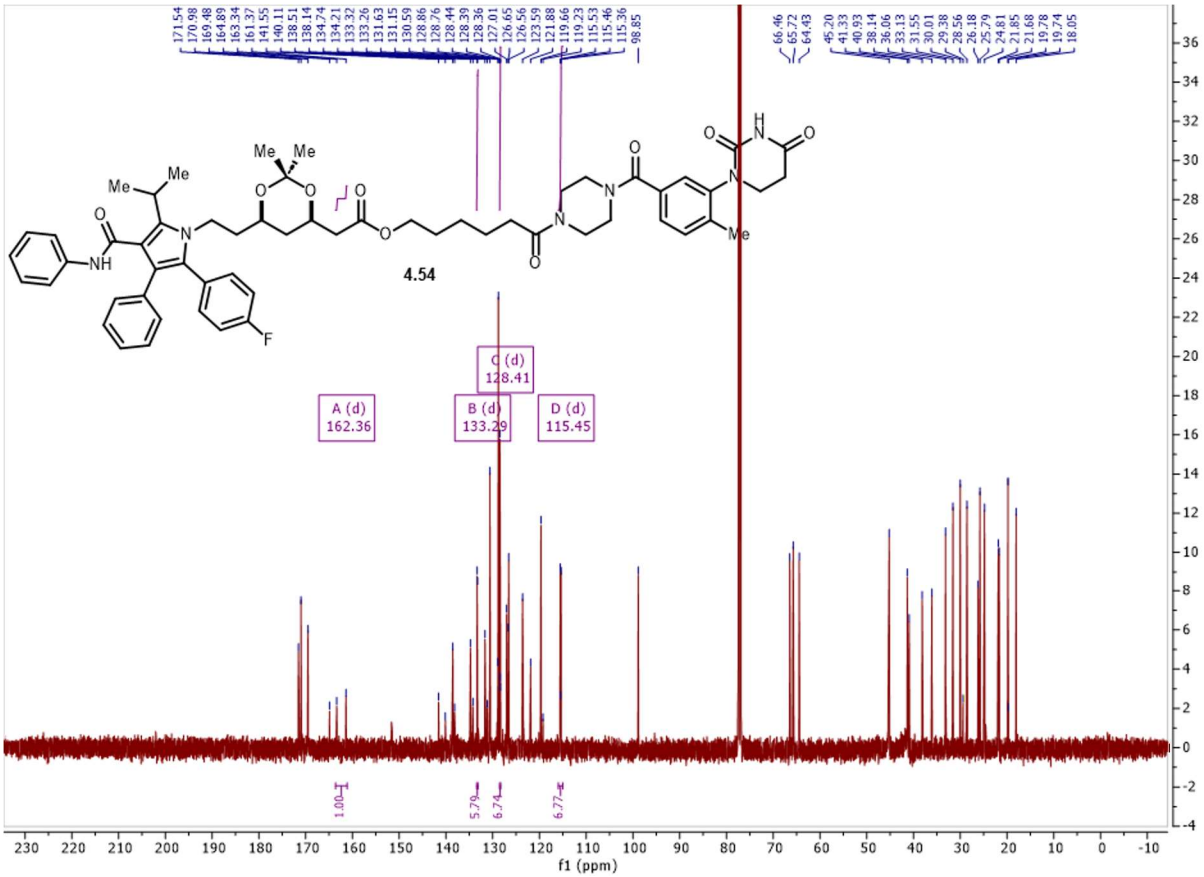

Spectrum 4.63 ^{13}C NMR of **4.54**.

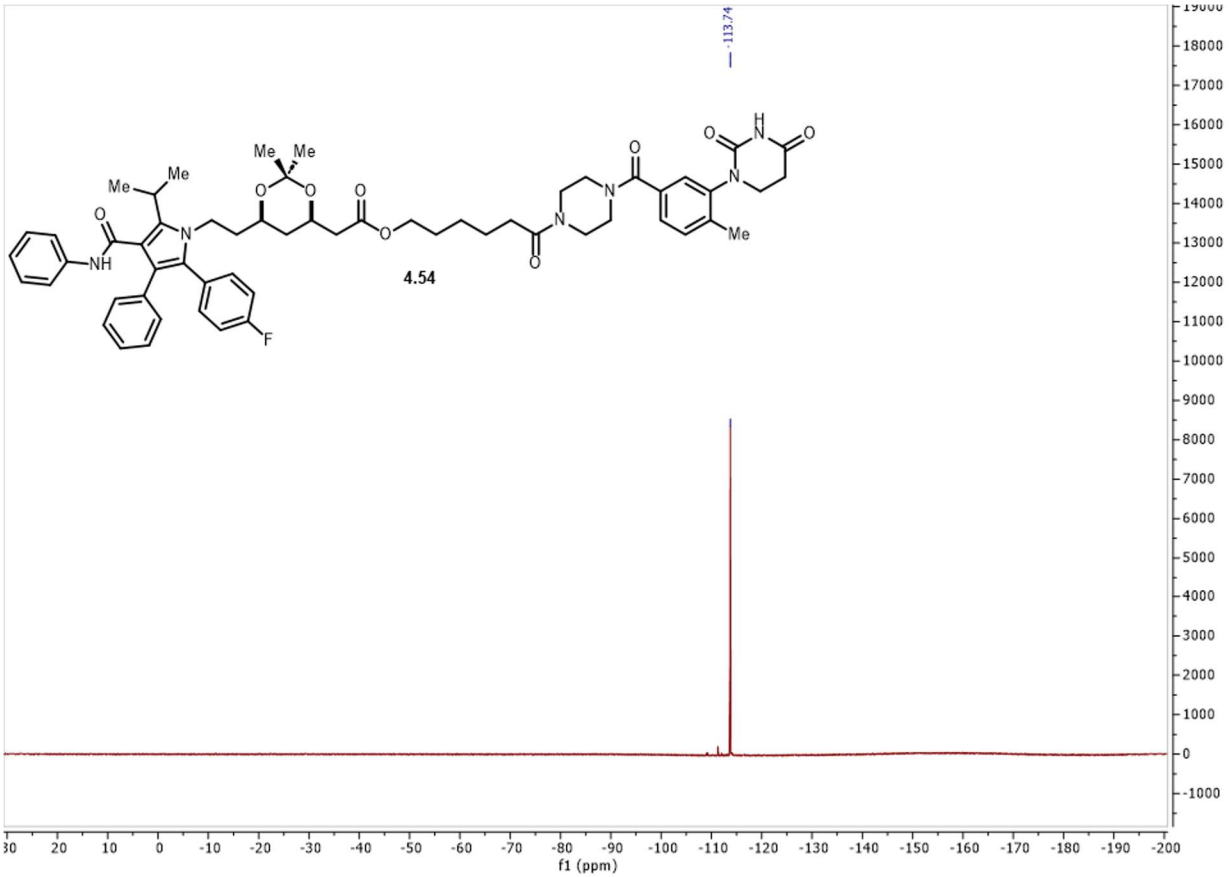

Spectrum 4.64 ^{19}F NMR of **4.54**.

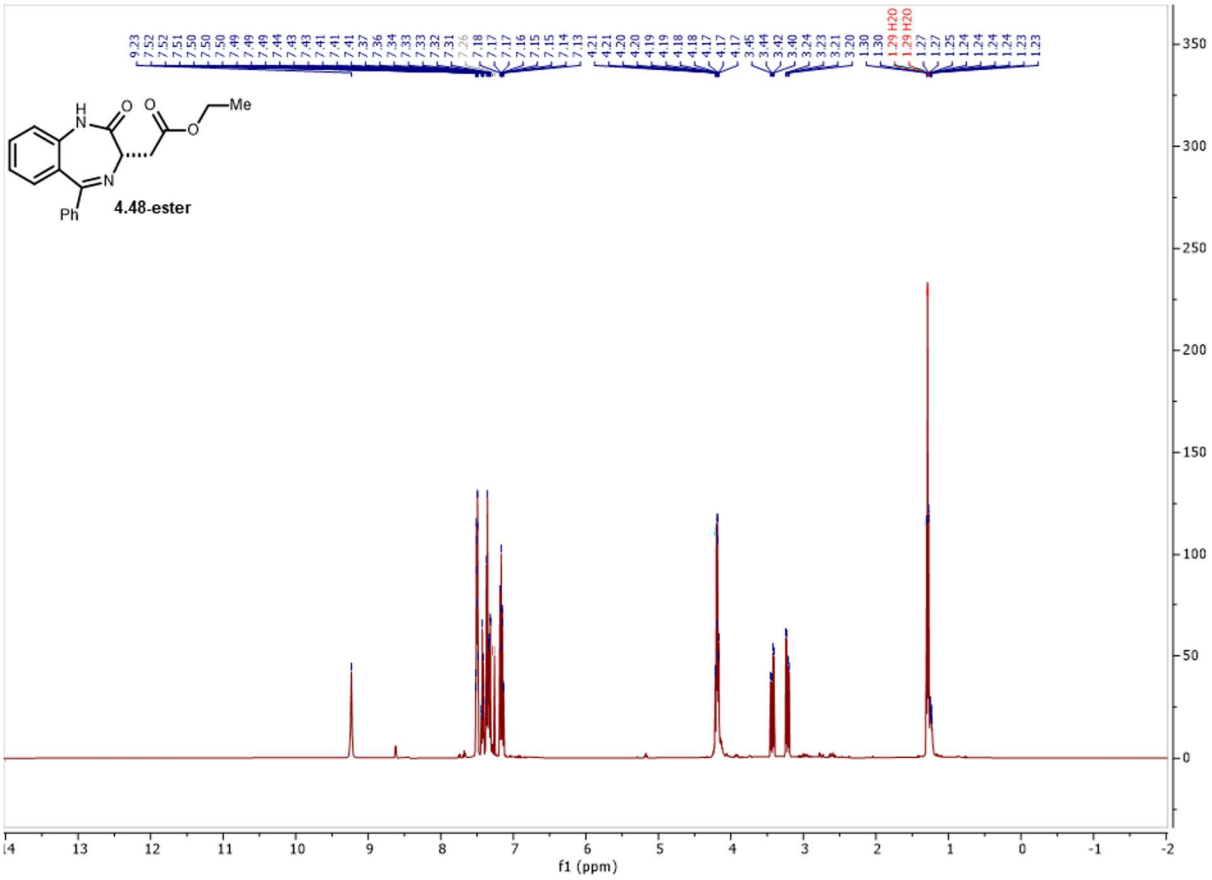

Spectrum 4.65 ^{1}H NMR of **4.48-ester**.

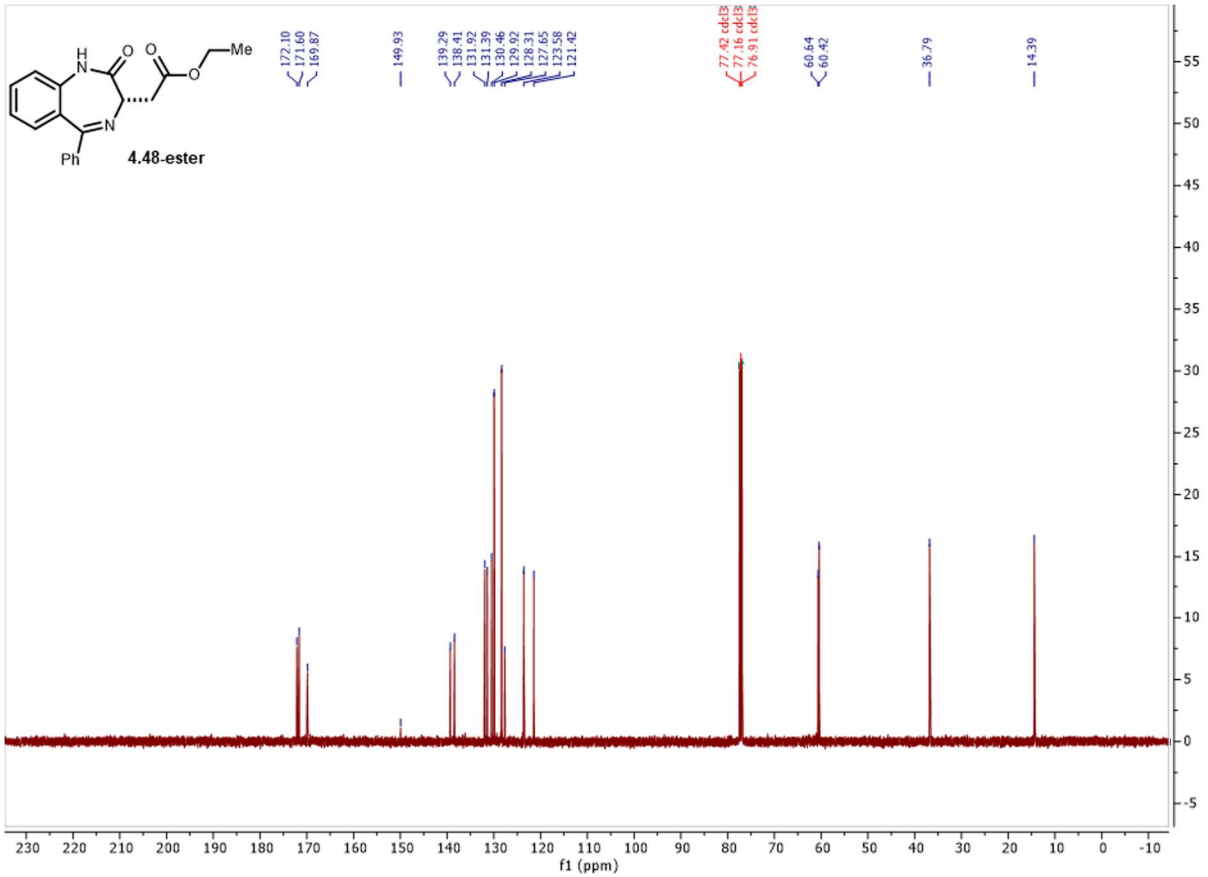

Spectrum 4.66 ^{13}C NMR of **4.48-ester**.

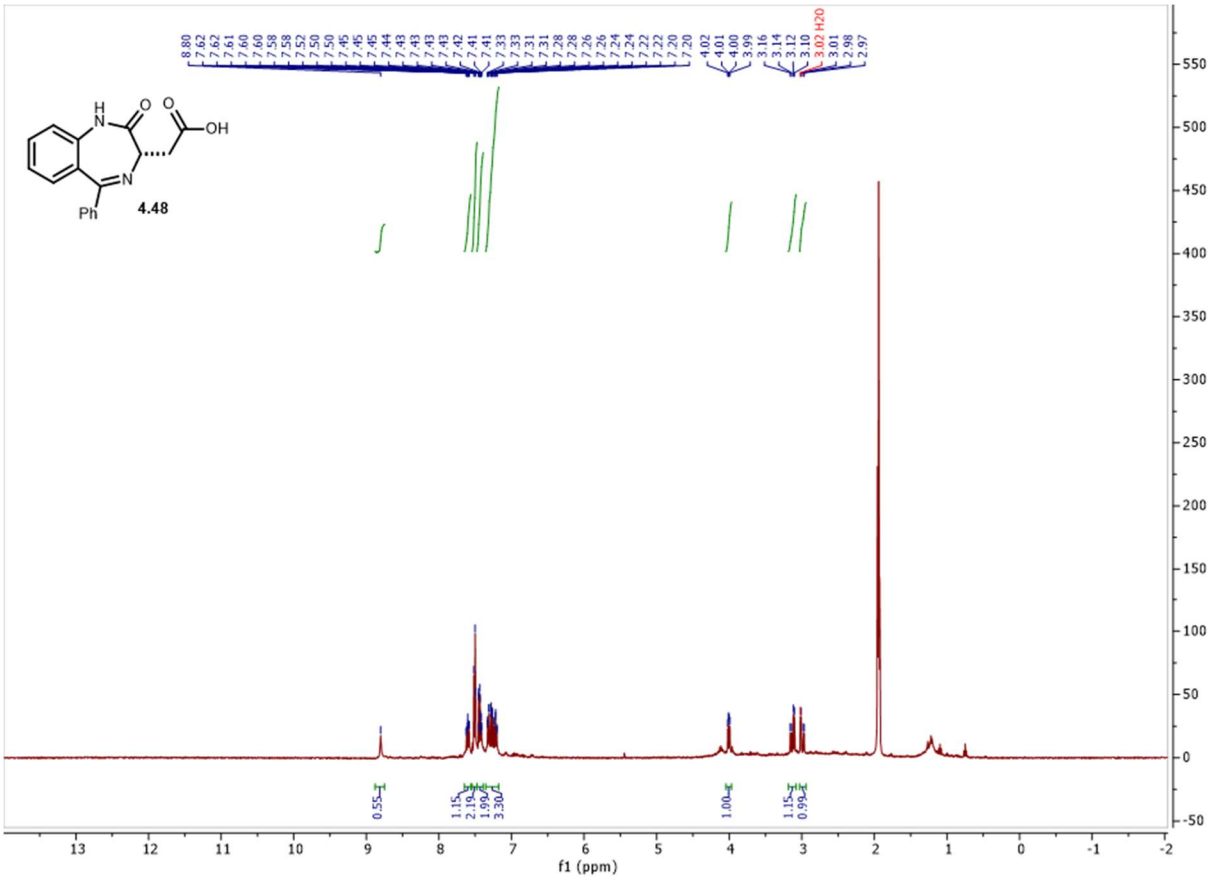

Spectrum 4.67 ^{1}H NM$ of **4.48**.

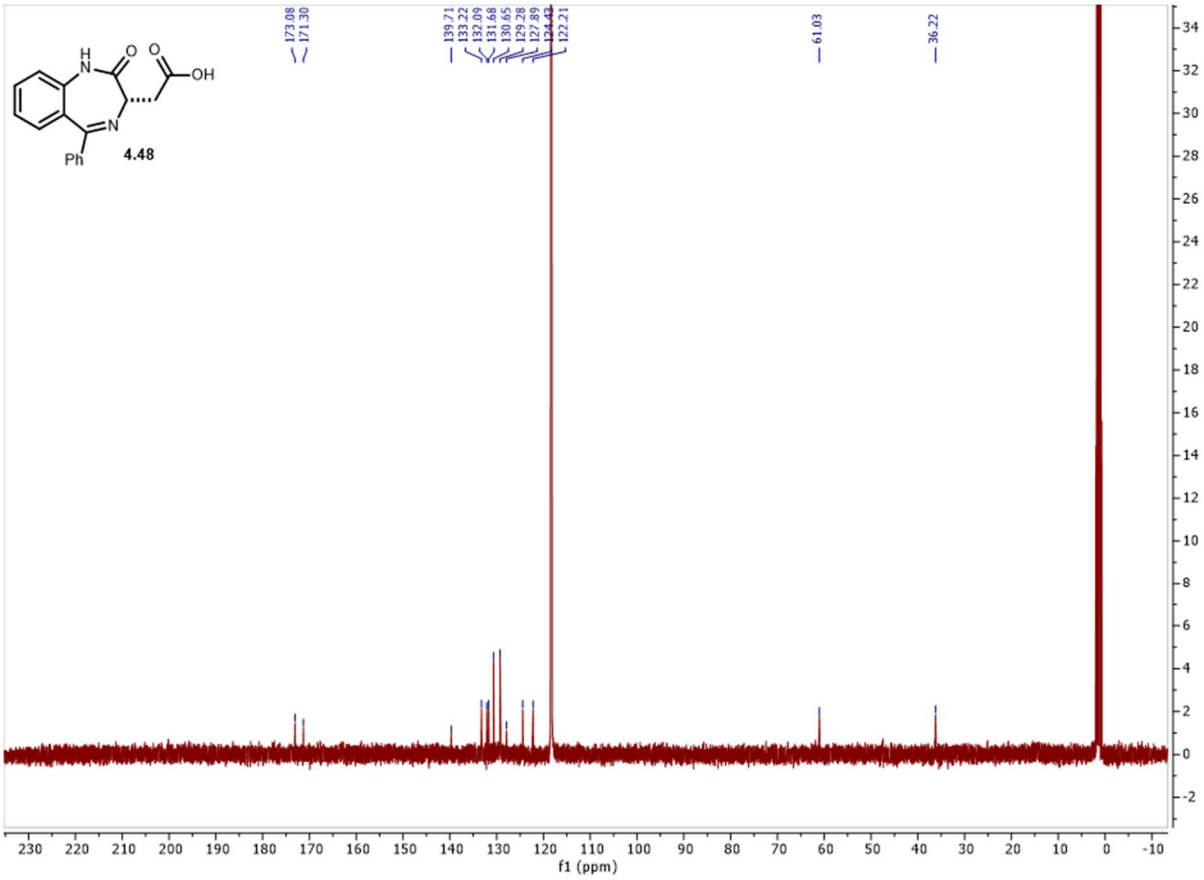

Spectrum 4.68 ^{13}C NMR of **4.48**.

4.5.2 NMR spectra from 4.3

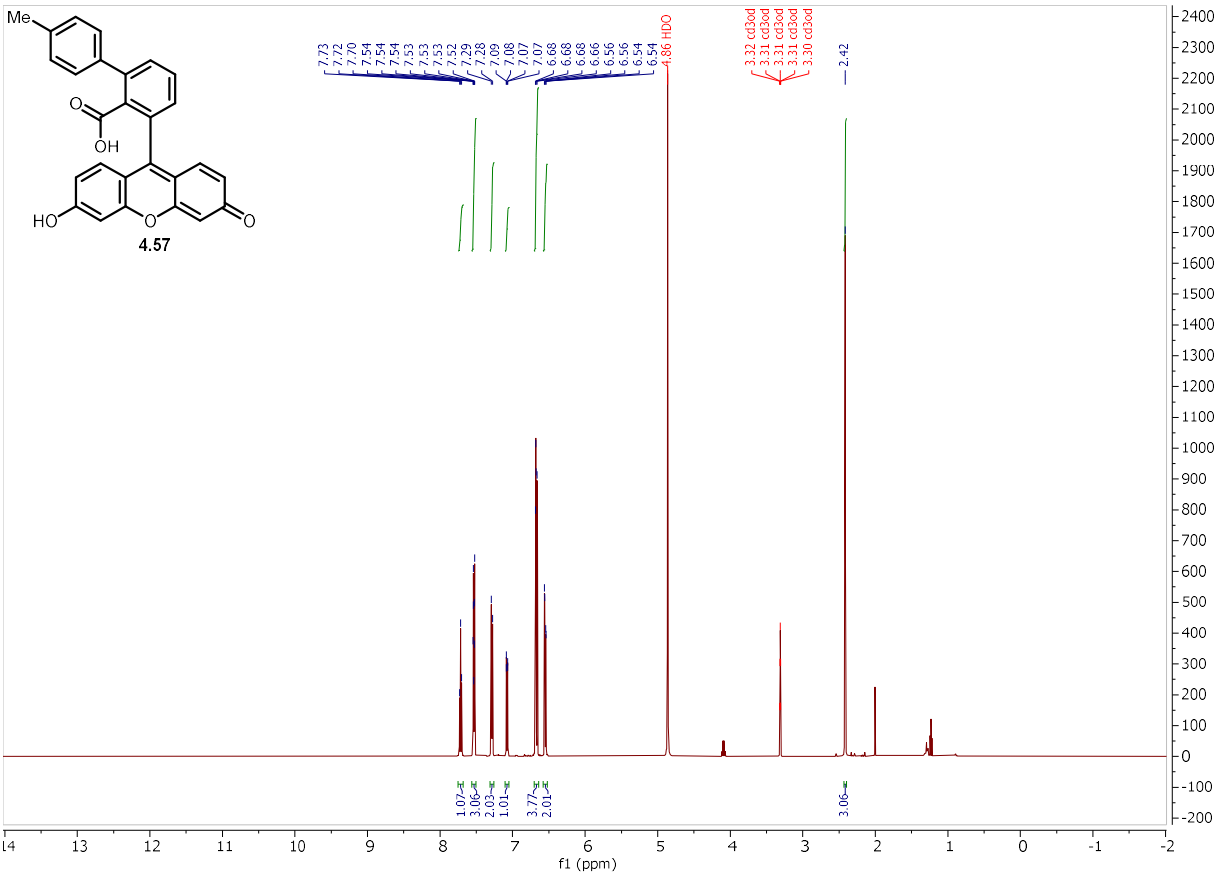

Figure 4.44 ^{1}H NMR of **4.57**.

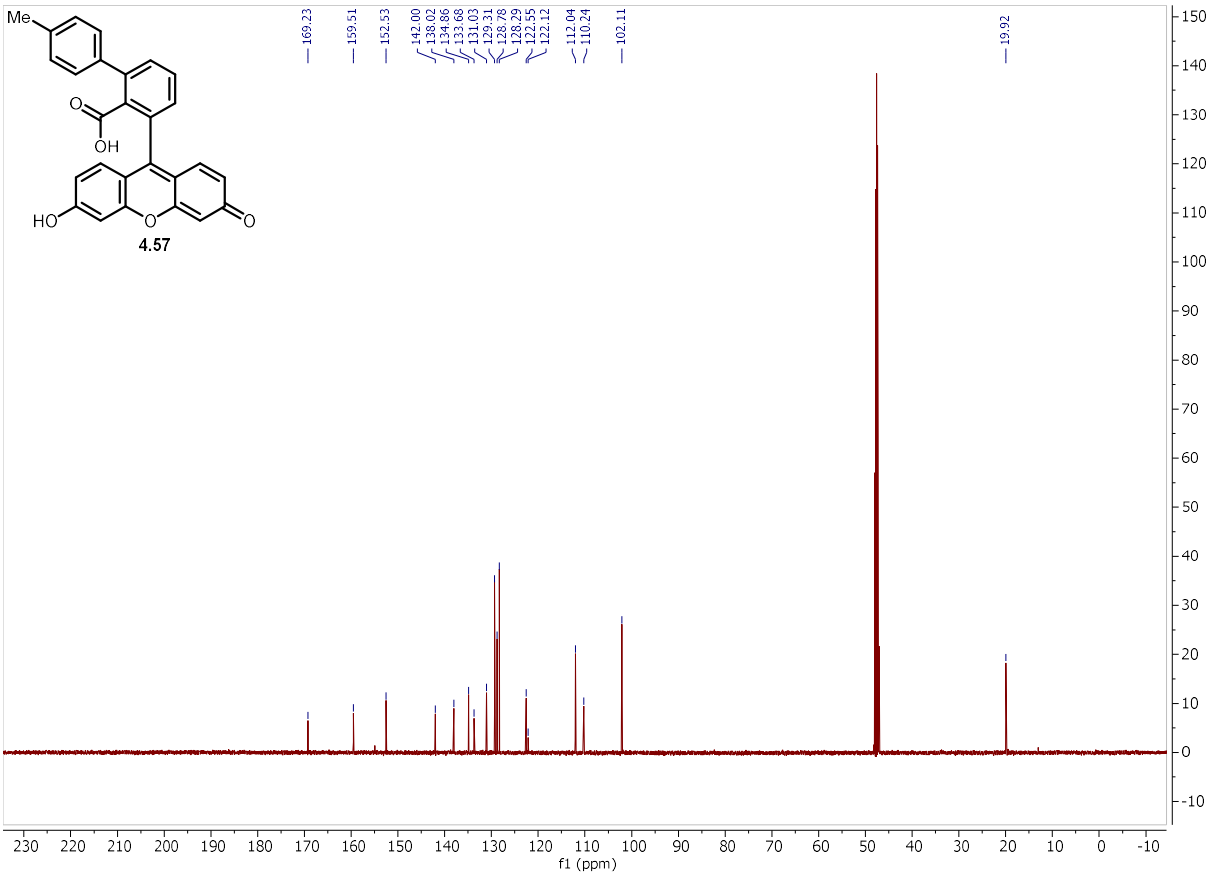

Figure 4.45 ^{13}C NMR of **4.57**.

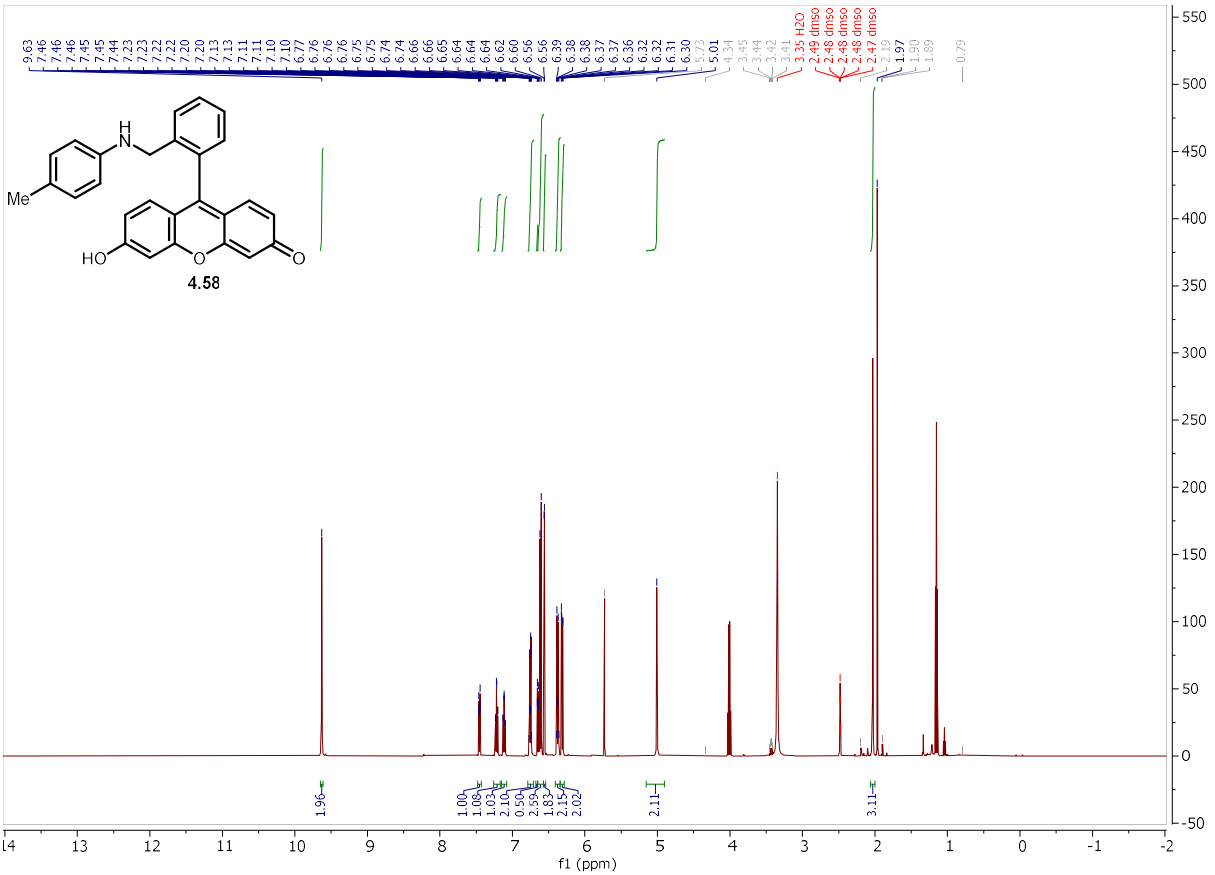

Figure 4.46 ^{1}H NMR of **4.58**.

4.6 References

(1) Cyrus, K.; Wehenkel, M.; Choi, E.-Y.; Han, H.-J.; Lee, H.; Swanson, H.; Kim, K.-B. Impact of Linker Length on the Activity of PROTACs. *Mol. BioSyst.* **2011**, *7* (2), 359–364. https://doi.org/10.1039/C0MB00074D.

(2) Bashore, F. M.; Foley, C. A.; Ong, H. W.; Rectenwald, J. M.; Hanley, R. P.; Norris-Drouin, J. L.; Cholensky, S. H.; Mills, C. A.; Pearce, K. H.; Herring, L. E.; Kireev, D.; Frye, S. V.; James, L. I. PROTAC Linkerology Leads to an Optimized Bivalent Chemical Degrader of Polycomb Repressive Complex 2 (PRC2) Components. *ACS Chem. Biol.* **2023**, *18* (3), 494–507. https://doi.org/10.1021/acschembio.2c00804.

(3) Zoppi, V.; Hughes, S. J.; Maniaci, C.; Testa, A.; Gmaschitz, T.; Wieshofer, C.; Koegl, M.; Riching, K. M.; Daniels, D. L.; Spallarossa, A.; Ciulli, A. Iterative Design and Optimization of Initially Inactive Proteolysis Targeting Chimeras (PROTACs) Identify VZ185 as a Potent, Fast, and Selective von Hippel–Lindau (VHL) Based Dual Degrader Probe of BRD9 and BRD7. *J. Med. Chem.* **2019**, *62* (2), 699–726. https://doi.org/10.1021/acs.jmedchem.8b01413.

(4) Hu, J.; Hu, B.; Wang, M.; Xu, F.; Miao, B.; Yang, C.-Y.; Wang, M.; Liu, Z.; Hayes, D. F.; Chinnaswamy, K.; Delproposto, J.; Stuckey, J.; Wang, S. Discovery of ERD-308 as a Highly Potent Proteolysis Targeting Chimera (PROTAC) Degrader of Estrogen Receptor (ER). *J. Med. Chem.* **2019**, *62* (3), 1420–1442. https://doi.org/10.1021/acs.jmedchem.8b01572.

(5) Li, M.; Zhi, Y.; Liu, B.; Yao, Q. Advancing Strategies for Proteolysis-Targeting Chimera Design. *J. Med. Chem.* **2023**, *66* (4), 2308–2329. https://doi.org/10.1021/acs.jmedchem.2c01555.

(6) Maple, H. J.; Clayden, N.; Baron, A.; Stacey, C.; Felix, R. Developing Degraders: Principles and Perspectives on Design and Chemical Space. *Med. Chem. Commun.* **2019**, *10* (10), 1755–1764. https://doi.org/10.1039/C9MD00272C.

(7) Békés, M.; Langley, D. R.; Crews, C. M. PROTAC Targeted Protein Degraders: The Past Is Prologue. *Nature Reviews Drug Discovery* **2022**, *21* (3), 181–200. https://doi.org/10.1038/s41573-021-00371-6.

(8) Papatzimas, J. W. ; G., Evgueni; Brownsey, Duncan K. ;. Maity, Ranjan; Bahlis, Nizar J. ;. Derksen, Darren J. A General Strategy for the Preparation of Thalidomide-Conjugate Linkers. *Synlett* **2017**, *28* (20), 2881–2885. https://doi.org/10.1055/s-0036-1588539.

(9) Bhela, I. P.; Ranza, A.; Balestrero, F. C.; Serafini, M.; Aprile, S.; Di Martino, R. M. C.; Condorelli, F.; Pirali, T. A Versatile and Sustainable Multicomponent Platform for the Synthesis of Protein Degraders: Proof-of-Concept Application to BRD4-Degrading PROTACs. *J. Med. Chem.* **2022**, *65* (22), 15282–15299. https://doi.org/10.1021/acs.jmedchem.2c01218.

(10) Klein, V. G.; Bond, A. G.; Craigon, C.; Lokey, R. S.; Ciulli, A. Amide-to-Ester Substitution as a Strategy for Optimizing PROTAC Permeability and Cellular Activity. *J. Med. Chem.* **2021**, *64* (24), 18082–18101. https://doi.org/10.1021/acs.jmedchem.1c01496.

(11) Wurz, R. P.; Dellamaggiore, K.; Dou, H.; Javier, N.; Lo, M.-C.; McCarter, J. D.; Mohl, D.; Sastri, C.; Lipford, J. R.; Cee, V. J. A "Click Chemistry Platform" for the Rapid Synthesis of Bispecific Molecules for Inducing Protein Degradation. *J. Med. Chem.* **2018**, *61* (2), 453–461. https://doi.org/10.1021/acs.jmedchem.6b01781.

(12) Brownsey, D. K.; Rowley, B. C.; Gorobets, E.; Gelfand, B. S.; Derksen, D. J. Rapid Synthesis of Pomalidomide-Conjugates for the Development of Protein Degrader Libraries. *Chem. Sci.* **2021**, *12* (12), 4519–4525. https://doi.org/10.1039/D0SC05442A.

(13) Hayhow, T. G.; Borrows, R. E. A.; Diène, C. R.; Fairley, G.; Fallan, C.; Fillery, S. M.; Scott, J. S.; Watson, D. W. A Buchwald–Hartwig Protocol to Enable Rapid Linker Exploration of Cereblon E3-Ligase PROTACs**. *Chemistry – A European Journal* **2020**, *26* (70), 16818–16823. https://doi.org/10.1002/chem.202003137.

(14) Guo, L.; Zhou, Y.; Nie, X.; Zhang, Z.; Zhang, Z.; Li, C.; Wang, T.; Tang, W. A Platform for the Rapid Synthesis of Proteolysis Targeting Chimeras (Rapid-TAC) under Miniaturized

Conditions. *European Journal of Medicinal Chemistry* **2022**, *236*, 114317. https://doi.org/10.1016/j.ejmech.2022.114317.

(15) Qiu, X.; Sun, N.; Kong, Y.; Li, Y.; Yang, X.; Jiang, B. Chemoselective Synthesis of Lenalidomide-Based PROTAC Library Using Alkylation Reaction. *Org. Lett.* **2019**, *21* (10), 3838–3841. https://doi.org/10.1021/acs.orglett.9b01326.

(16) Mahjour, B.; Shen, Y.; Liu, W.; Cernak, T. A Map of the Amine–Car boxylic Acid Coupling System. *Nature* **2020**, *580* (7801), 71–75. https://doi.org/10.1038/s41586-020-2142-y.

(17) Zhang, R.; Mahjour, B.; Cernak, T. Exploring the Combinatorial Explosion of Amine–Acid Reaction Space via Graph Editing. *ChemRxiv* **2022**. https://doi.org/10.26434/chemrxiv-2022-917k5.

(18) Shen, Y.; Mahjour, B.; Cernak, T. Development of Copper-Catalyzed Deaminative Esterification Using High-Throughput Experimentation. *Communications Chemistry* **2022**, *5* (1), 83. https://doi.org/10.1038/s42004-022-00698-0.

(19) McGrath, A.; Zhang, R.; Shafiq, K.; Cernak, T. Repurposing Amine and Carboxylic Acid Building Blocks with an Automatable Esterification Reaction. *Chem. Commun.* **2023**, *59* (8), 1026–1029. https://doi.org/10.1039/D2CC05670D.

(20) Zhang, Z.; Cernak, T. The Formal Cross-Coupling of Amines and Carboxylic Acids to Form Sp3–Sp3 Carbon–Carbon Bonds. *Angewandte Chemie International Edition* **2021**, *60* (52), 27293–27298. https://doi.org/10.1002/anie.202112454.

(21) Douthwaite, J. L.; Zhao, R.; Shim, E.; Mahjour, B.; Zimmerman, P. M.; Cernak, T. Formal Cross-Coupling of Amines and Carboxylic Acids to Form Sp3–Sp2 Carbon–Carbon Bonds. *J. Am. Chem. Soc.* **2023**, *145* (20), 10930–10937. https://doi.org/10.1021/jacs.2c11563.

(22) Hendrick, C. E.; Jorgensen, J. R.; Chaudhry, C.; Strambeanu, I. I.; Brazeau, J.-F.; Schiffer, J.; Shi, Z.; Venable, J. D.; Wolkenberg, S. E. Direct-to-Biology Accelerates PROTAC Synthesis and the Evaluation of Linker Effects on Permeability and Degradation. *ACS Med. Chem. Lett.* **2022**, *13* (7), 1182–1190. https://doi.org/10.1021/acsmedchemlett.2c00124.

(23) Boström, J.; Brown, D. G.; Young, R. J.; Keserü, G. M. Expanding the Medicinal Chemistry Synthetic Toolbox. *Nature Reviews Drug Discovery* **2018**, *17* (10), 709–727. https://doi.org/10.1038/nrd.2018.116.

(24) Winter, G. E.; Buckley, D. L.; Paulk, J.; Roberts, J. M.; Souza, A.; Dhe-Paganon, S.; Bradner, J. E. Phthalimide Conjugation as a Strategy for in Vivo Target Protein Degradation. *Science* **2015**, *348* (6241), 1376–1381. https://doi.org/10.1126/science.aab1433.

(25) Mahjour, B.; Shen, Y.; Cernak, T. Ultrahigh-Throughput Experimentation for Information-Rich Chemical Synthesis. *Acc. Chem. Res.* **2021**, *54* (10), 2337–2346. https://doi.org/10.1021/acs.accounts.1c00119.

(26) Shen, Y.; Borowski, J. E.; Hardy, M. A.; Sarpong, R.; Doyle, A. G.; Cernak, T. Automation and Computer-Assisted Planning for Chemical Synthesis. *Nature Reviews Methods Primers* **2021**, *1* (1), 23. https://doi.org/10.1038/s43586-021-00022-5.

(27) Mahjour, B.; Zhang, R.; Shen, Y.; McGrath, A.; Zhao, R.; Mohamed, O. G.; Lin, Y.; Zhang, Z.; Douthwaite, J. L.; Tripathi, A.; Cernak, T. Rapid Planning and Analysis of High-Throughput Experiment Arrays for Reaction Discovery. *Nature Communications* **2023**, *14* (1), 3924. https://doi.org/10.1038/s41467-023-39531-0.

(28) Mahjour, B.; Hoffstadt, J.; Cernak, T. Designing Chemical Reaction Arrays Using Phactor and ChatGPT. *Org. Process Res. Dev.* **2023**, *27* (8), 1510–1516. https://doi.org/10.1021/acs.oprd.3c00186.

(29) Wong, H.; Cernak, T. Reaction Miniaturization in Eco-Friendly Solvents. *Current Opinion in Green and Sustainable Chemistry* **2018**, *11*, 91–98. https://doi.org/10.1016/j.cogsc.2018.06.001.

(30) Gruntz, U.; Katritzky, A. R.; Kenny, D. H.; Rezende, M. C.; Sheikh, H. Pyridines as Leaving Groups in Synthetic Transformations: Conversion of Amines into Esters. *J. Chem. Soc., Chem. Commun.* **1977**, No. 20, 701–701. https://doi.org/10.1039/C39770000701.

(31) Ni, S.; Li, C.-X.; Mao, Y.; Han, J.; Wang, Y.; Yan, H.; Pan, Y. Ni-Catalyzed Deaminative Cross-Electrophile Coupling of Katritzky Salts with Halides via C─N Bond Activation. *Sci Adv* **2019**, *5* (6), eaaw9516–eaaw9516. https://doi.org/10.1126/sciadv.aaw9516.

(32) Yi, J.; Badir, S. O.; Kammer, L. M.; Ribagorda, M.; Molander, G. A. Deaminative Reductive Arylation Enabled by Nickel/Photoredox Dual Catalysis. *Org. Lett.* **2019**, *21* (9), 3346–3351. https://doi.org/10.1021/acs.orglett.9b01097.

(33) Yue, H.; Zhu, C.; Shen, L.; Geng, Q.; Hock, K. J.; Yuan, T.; Cavallo, L.; Rueping, M. Nickel-Catalyzed C–N Bond Activation: Activated Primary Amines as Alkylating Reagents in Reductive Cross-Coupling. *Chem. Sci.* **2019**, *10* (16), 4430–4435. https://doi.org/10.1039/C9SC00783K.

(34) Liao, J.; Basch, C. H.; Hoerrner, M. E.; Talley, M. R.; Boscoe, B. P.; Tucker, J. W.; Garnsey, M. R.; Watson, M. P. Deaminative Reductive Cross-Electrophile Couplings of Alkylpyridinium Salts and Aryl Bromides. *Org. Lett.* **2019**, *21* (8), 2941–2946. https://doi.org/10.1021/acs.orglett.9b01014.

(35) Martin-Montero, R.; Yatham, V. R.; Yin, H.; Davies, J.; Martin, R. Ni-Catalyzed Reductive Deaminative Arylation at Sp3 Carbon Centers. *Org. Lett.* **2019**, *21* (8), 2947–2951. https://doi.org/10.1021/acs.orglett.9b01016.

(36) Wang, J.; Hoerrner, M. E.; Watson, M. P.; Weix, D. J. Nickel-Catalyzed Synthesis of Dialkyl Ketones from the Coupling of N-Alkyl Pyridinium Salts with Activated Carboxylic Acids. *Angewandte Chemie International Edition* **2020**, *59*, 13484. https://doi.org/10.1002/anie.202002271.

(37) Wang, J.; Ehehalt, L. E.; Huang, Z.; Beleh, O. M.; Guzei, I. A.; Weix, D. J. Formation of C(Sp2)–C(Sp3) Bonds Instead of Amide C–N Bonds from Carboxylic Acid and Amine Substrate Pools by Decarbonylative Cross-Electrophile Coupling. *J. Am. Chem. Soc.* **2023**. https://doi.org/10.1021/jacs.2c11552.

(38) Amani, J.; Molander, G. A. Direct Conversion of Carboxylic Acids to Alkyl Ketones. *Org. Lett.* **2017**, *19* (13), 3612–3615. https://doi.org/10.1021/acs.orglett.7b01588.

(39) Cornella, J.; Edwards, J. T.; Qin, T.; Kawamura, S.; Wang, J.; Pan, C.-M.; Gianatassio, R.; Schmidt, M.; Eastgate, M. D.; Baran, P. S. Practical Ni-Catalyzed Aryl–Alkyl Cross-Coupling of Secondary Redox-Active Esters. *J. Am. Chem. Soc.* **2016**, *138* (7), 2174–2177. https://doi.org/10.1021/jacs.6b00250.

(40) Prieto Kullmer, C. N.; Kautzky, J. A.; Krska, S. W.; Nowak, T.; Dreher, S. D.; MacMillan, D. W. C. Accelerating Reaction Generality and Mechanistic Insight through Additive Mapping. *Science* **2022**, *376* (6592), 532–539. https://doi.org/10.1126/science.abn1885.

(41) Malapit, C. A.; Bour, J. R.; Brigham, C. E.; Sanford, M. S. Base-Free Nickel-Catalysed Decarbonylative Suzuki–Miyaura Coupling of Acid Fluorides. *Nature* **2018**, *563* (7729), 100–104. https://doi.org/10.1038/s41586-018-0628-7.

(42) Fehér, P. P.; Stirling, A. Theoretical Study on the Formation of Ni(PR3)(Aryl)F Complexes Observed in Ni-Catalyzed Decarbonylative C–C Coupling of Acyl Fluorides. *Organometallics* **2020**, *39* (14), 2774–2783. https://doi.org/10.1021/acs.organomet.0c00387.

(43) Fu, M.-C.; Shang, R.; Cheng, W.-M.; Fu, Y. Boron-Catalyzed N-Alkylation of Amines Using Carboxylic Acids. *Angewandte Chemie International Edition* **2015**, *54* (31), 9042–9046. https://doi.org/10.1002/anie.201503879.

(44) Sorribes, I.; Junge, K.; Beller, M. Direct Catalytic N-Alkylation of Amines with Carboxylic Acids. *J. Am. Chem. Soc.* **2014**, *136* (40), 14314–14319. https://doi.org/10.1021/ja5093612.

(45) Stoll, E. L.; Tongue, T.; Andrews, K. G.; Valette, D.; Hirst, D. J.; Denton, R. M. A Practical Catalytic Reductive Amination of Carboxylic Acids. *Chem. Sci.* **2020**, *11* (35), 9494–9500. https://doi.org/10.1039/D0SC02271C.

(46) Zhang, Q.; Fu, M.-C.; Yu, H.-Z.; Fu, Y. Mechanism of Boron-Catalyzed N-Alkylation of Amines with Carboxylic Acids. *J. Org. Chem.* **2016**, *81* (15), 6235–6243. https://doi.org/10.1021/acs.joc.6b00778.

(47) Zengerle, M.; Chan, K.-H.; Ciulli, A. Selective Small Molecule Induced Degradation of the BET Bromodomain Protein BRD4. *ACS Chem. Biol.* **2015**, *10* (8), 1770–1777. https://doi.org/10.1021/acschembio.5b00216.

(48) Jarusiewicz, J. A.; Yoshimura, S.; Mayasundari, A.; Actis, M.; Aggarwal, A.; McGowan, K.; Yang, L.; Li, Y.; Fu, X.; Mishra, V.; Heath, R.; Narina, S.; Pruett-Miller, S. M.; Nishiguchi, G.; Yang, J. J.; Rankovic, Z. Phenyl Dihydrouracil: An Alternative Cereblon Binder for PROTAC Design. *ACS Med. Chem. Lett.* **2023**, *14* (2), 141–145. https://doi.org/10.1021/acsmedchemlett.2c00436.

(49) Min, J.; Mayasundari, A.; Keramatnia, F.; Jonchere, B.; Yang, S. W.; Jarusiewicz, J.; Actis, M.; Das, S.; Young, B.; Slavish, J.; Yang, L.; Li, Y.; Fu, X.; Garrett, S. H.; Yun, M.-K.; Li, Z.; Nithianantham, S.; Chai, S.; Chen, T.; Shelat, A.; Lee, R. E.; Nishiguchi, G.; White, S. W.; Roussel, M. F.; Potts, P. R.; Fischer, M.; Rankovic, Z. Phenyl-Glutarimides: Alternative Cereblon Binders for the Design of PROTACs. *Angewandte Chemie International Edition* **2021**, *60* (51), 26663–26670. https://doi.org/10.1002/anie.202108848.

(50) Riching, K. M.; Mahan, S.; Corona, C. R.; McDougall, M.; Vasta, J. D.; Robers, M. B.; Urh, M.; Daniels, D. L. Quantitative Live-Cell Kinetic Degradation and Mechanistic Profiling of PROTAC Mode of Action. *ACS Chem. Biol.* **2018**, *13* (9), 2758–2770. https://doi.org/10.1021/acschembio.8b00692.

(51) Vasta, J. D.; Corona, C. R.; Robers, M. B. A High-Throughput Method to Prioritize PROTAC Intracellular Target Engagement and Cell permeability Using NanoBRET. In *Targeted Protein Degradation: Methods and Protocols*; Cacace, A. M., Hickey, C. M., Békés, M., Eds.; Springer US: New York, NY, 2021; pp 265–282. https://doi.org/10.1007/978-1-0716-1665-9_14.

(52) RBA Is Defined as the Ratio of a Compound's Affinity in Live versus Permeabilized Cells. A Larger Right Shift in Measured Affinity in the Live-Cell Mode Leads to Larger RBA Values and Is an Indication of Lower Permeability.

(53) Basch, C. H.; Liao, J.; Xu, J.; Piane, J. J.; Watson, M. P. Harnessing Alkyl Amines as Electrophiles for Nickel-Catalyzed Cross Couplings via C–N Bond Activation. *J. Am. Chem. Soc.* **2017**, *139* (15), 5313–5316. https://doi.org/10.1021/jacs.7b02389.

(54) Wu, Y.; Liu, M.-J.; Huang, H.-Q.; Huang, G.-X.; Xiong, F.-J.; Chen, F.-E. Asymmetric Synthesis of Atorvastatin Calcium through Intramolecular Oxidative Oxygen-Nucleophilic Bromocyclization. *European Journal of Organic Chemistry* **2017**, *2017* (25), 3681–3688. https://doi.org/10.1002/ejoc.201700387.

(55) Andrews, K. G.; Faizova, R.; Denton, R. M. A Practical and Catalyst-Free Trifluoroethylation Reaction of Amines Using Trifluoroacetic Acid. *Nature Communications* **2017**, *8* (1), 15913. https://doi.org/10.1038/ncomms15913.

(56) Zheng, J.; Chevance, S.; Darcel, C.; Sortais, J.-B. Selective Reduction of Carboxylic Acids to Aldehydes through Manganese Catalysed Hydrosilylation. *Chem. Commun.* **2013**, *49* (85), 10010–10012. https://doi.org/10.1039/C3CC45349A.

(57) Anzini, M.; Valenti, S.; Braile, C.; Cappelli, A.; Vomero, S.; Alcaro, S.; Ortuso, F.; Marinelli, L.; Limongelli, V.; Novellino, E.; Betti, L.; Giannaccini, G.; Lucacchini, A.; Daniele, S.; Martini, C.; Ghelardini, C.; Di Cesare Mannelli, L.; Giorgi, G.; Mascia, M. P.; Biggio, G. New Insight into the Central Benzodiazepine Receptor–Ligand Interactions: Design, Synthesis, Biological Evaluation, and Molecular Modeling of 3-Substituted 6-Phenyl-4H-Imidazo[1,5-a][1,4]Benzodiazepines and Related Compounds. *J. Med. Chem.* **2011**, *54* (16), 5694–5711. https://doi.org/10.1021/jm2001597.

(58) Smith, D. A.; Di, L.; Kerns, E. H. The Effect of Plasma Protein Binding on in Vivo Efficacy: Misconceptions in Drug Discovery. *Nature Reviews Drug Discovery* **2010**, *9* (12), 929–939. https://doi.org/10.1038/nrd3287.

(59) Zheng, N.; Tsai, H. N.; Zhang, X.; Shedden, K.; Rosania, G. R. The Subcellular Distribution of Small Molecules: A Meta-Analysis. *Mol. Pharmaceutics* **2011**, *8* (5), 1611–1618. https://doi.org/10.1021/mp200093z.

(60) Chen, C.; Zhou, H.; Guan, C.; Zhang, H.; Li, Y.; Jiang, X.; Dong, Z.; Tao, Y.; Du, J.; Wang, S.; Zhang, T.; Du, N.; Guo, J.; Wu, Y.; Song, Z.; Luan, H.; Wang, Y.; Du, H.; Zhang, S.; Li, C.; Chang, H.; Wang, T. Applicability of Free Drug Hypothesis to Drugs with Good Membrane Permeability That Are Not Efflux Transporter Substrates: A Microdialysis Study in Rats. *Pharmacology Research & Perspectives* **2020**, *8* (2), e00575. https://doi.org/10.1002/prp2.575.

(61) Veselov, V. V.; Nosyrev, A. E.; Jicsinszky, L.; Alyautdin, R. N.; Cravotto, G. Targeted Delivery Methods for Anticancer Drugs. *Cancers* **2022**, *14* (3). https://doi.org/10.3390/cancers14030622.

(62) Ellegaard, A.-M.; Groth-Pedersen, L.; Oorschot, V.; Klumperman, J.; Kirkegaard, T.; Nylandsted, J.; Jäättelä, M. Sunitinib and SU11652 Inhibit Acid Sphingomyelinase, Destabilize Lysosomes, and Inhibit Multidrug Resistance. *Molecular Cancer Therapeutics* **2013**, *12* (10), 2018–2030. https://doi.org/10.1158/1535-7163.MCT-13-0084.

(63) Li, Q.; Zhou, T.; Wu, F.; Li, N.; Wang, R.; Zhao, Q.; Ma, Y.-M.; Zhang, J.-Q.; Ma, B.-L. Subcellular Drug Distribution: Mechanisms and Roles in Drug Efficacy, Toxicity, Resistance, and Targeted Delivery. *Drug Metabolism Reviews* **2018**, *50* (4), 430–447. https://doi.org/10.1080/03602532.2018.1512614.

(64) Louzoun-Zada, S.; Jaber, Q. Z.; Fridman, M. Guiding Drugs to Target-Harboring Organelles: Stretching Drug-Delivery to a Higher Level of Resolution. *Angewandte Chemie International Edition* **2019**, *58* (44), 15584–15594. https://doi.org/10.1002/anie.201906284.

(65) Chen, X.; Zhang, X.; Wang, H.-Y.; Chen, Z.; Wu, F.-G. Subcellular Fate of a Fluorescent Cholesterol-Poly(Ethylene Glycol) Conjugate: An Excellent Plasma Membrane Imaging Reagent. *Langmuir* **2016**, *32* (39), 10126–10135. https://doi.org/10.1021/acs.langmuir.6b02288.

(66) Chamberlain, G. R.; Tulumello, D. V.; Kelley, S. O. Targeted Delivery of Doxorubicin to Mitochondria. *ACS Chem. Biol.* **2013**, *8* (7), 1389–1395. https://doi.org/10.1021/cb400095v.

(67) Fagerlund, R.; Melén, K.; Kinnunen, L.; Julkunen, I. Arginine/Lysine-Rich Nuclear Localization Signals Mediate Interactions between Dimeric STATs and Importin A5*. *Journal of Biological Chemistry* **2002**, *277* (33), 30072–30078. https://doi.org/10.1074/jbc.M202943200.

(68) Parodi, A.; Corbo, C.; Cevenini, A.; Molinaro, R.; Palomba, R.; Pandolfi, L.; Agostini, M.; Salvatore, F.; Tasciotti, E. Enabling Cytoplasmic Delivery and Organelle Targeting by Surface Modification of Nanocarriers. *Nanomedicine* **2015**, *10* (12), 1923–1940. https://doi.org/10.2217/nnm.15.39.

(69) Zheng, N.; Tsai, H. N.; Zhang, X.; Rosania, G. R. The Subcellular Distribution of Small Molecules: From Pharmacokinetics to Synthetic Biology. *Mol. Pharmaceutics* **2011**, *8* (5), 1619–1628. https://doi.org/10.1021/mp200092v.

(70) Rovira-Clavé, X.; Jiang, S.; Bai, Y.; Zhu, B.; Barlow, G.; Bhate, S.; Coskun, A. F.; Han, G.; Ho, C.-M. K.; Hitzman, C.; Chen, S.-Y.; Bava, F.-A.; Nolan, G. P. Subcellular Localization of Biomolecules and Drug Distribution by High-Definition Ion Beam Imaging. *Nature Communications* **2021**, *12* (1), 4628. https://doi.org/10.1038/s41467-021-24822-1.

(71) Rutkowska, A.; Thomson, D. W.; Vappiani, J.; Werner, T.; Mueller, K. M.; Dittus, L.; Krause, J.; Muelbaier, M.; Bergamini, G.; Bantscheff, M. A Modular Probe Strategy for Drug Localization, Target Identification and Target Occupancy Measurement on Single Cell Level. *ACS Chem. Biol.* **2016**, *11* (9), 2541–2550. https://doi.org/10.1021/acschembio.6b00346.

(72) Huang, L.; Hackenberger, D.; Gooßen, L. J. Iridium-Catalyzed Ortho-Arylation of Benzoic Acids with Arenediazonium Salts. *Angewandte Chemie International Edition* **2015**, *54* (43), 12607–12611. https://doi.org/10.1002/anie.201505769.

(73) Dunn, K. W.; Kamocka, M. M.; McDonald, J. H. A Practical Guide to Evaluating Colocalization in Biological Microscopy. *American Journal of Physiology-Cell Physiology* **2011**, *300* (4), C723–C742. https://doi.org/10.1152/ajpcell.00462.2010.

(74) Brownsey, D. K.; Gafuik, C. J.; Kim, D.-S.; O'Sullivan, L.; Gorobets, E.; Krukowski, S.; Turk, M.; Jenne, C. N.; Mahoney, D. J.; Derksen, D. J. Utilising the Intrinsic Fluorescence of Pomalidomide for Imaging Applications. *Chem. Commun.* **2023**, *59* (98), 14532–14535. https://doi.org/10.1039/D3CC04314B.

(75) Huang, L.; Weix, D. J. Ruthenium-Catalyzed C–H Arylation of Diverse Aryl Carboxylic Acids with Aryl and Heteroaryl Halides. *Org. Lett.* **2016**, *18* (20), 5432–5435. https://doi.org/10.1021/acs.orglett.6b02862.

Chapter 5 Summaries and Future Directions

In chapter one, we provided an overview of systems chemistry, and discussed how molecular function is directly related to structure which is a function of the building blocks used to construct a molecule as well as the transformations used to unite them. We can use this knowledge coupled with machine learning to further our understanding of chemistry. We examined alternatives to the amide coupling from amines and carboxylic acids as well as overviewing methodologies to activate them. We further discussed applications of these methods in drug discovery and finally examined High throughput experimentation methods and how they can be used to train the next generation of scientists.

In chapter two, we focused on education incorporating new technologies that are becoming ever more prevalent in drug discovery. In the first part, we discussed a lab section that can be used to introduce undergraduates without a computer science background to python and chemoinformatics. The first section lays the foundation for using python to generate graphics as well as some of the language used in programming. The second section takes a more focused approach and dives into the use of informatics to manage large datasets. Students manipulated real world data from COVID molecules and used it to validate GSK's solubility forecast index as well as cluster molecules based on their properties using principal component analysis. These results have been published in the *Journal of Chemical Education* (https://doi.org/10.1021/acs.jchemed.3c00357). In the second part of chapter two, another lab section was introduced where undergraduates performed a Parallel Artificial Membrane

Permeability Assay using two colored drug molecules. In doing so they learned how the structure of a molecule relates to its permeability. Furthermore, they were able to expand on their Python knowledge by using an Opentrons robot to make a plate for calibration curves. These results are being prepared for submission. In the final part of chapter two we developed a children's toy that was introduced to first graders and met with excitement.

In chapter three we developed new amine–acid couplings. In the first part we developed a deaminative amine–acid esterification reaction via activation of the amine as its triphenyl pyridinium salt. This reaction is mediated by either a bromomalonate catalyst or potassium iodide. This strategy was used to prepare a library of esters including amide to ester substitutions of moclobemide (**3.32**) and metoclopramide (**3.33**). We also used this methodology to develop an automated platform for library synthesis. In doing so we made 96 derivatives of amlodipine. With this platform we demonstrated the reaction can be applied to nucleophiles beyond carboxylates as demonstrated by synthesis of thioether **3.42**. These results are published in *Chemical Communications* (https://doi.org/10.1039/D2CC05670D)**.** This lead us to discover an iodide intermediate in the reaction that could be prepared in a single pot from the free amine which we explored further in the second part of chapter three. We exploited this strategy to make chlorides, bromides, and iodides, of five drugs or drug intermediates. We further expanded the one pot methodology to incorporate phenols as a nucleophile and used it to make a unique bond between tyrosine and lysine (**3.92**) as well as a PROTAC of estradiol (**3.93**), though it would likely be inactive. Finally, we expanded our deaminative esterification into a deaminative etherification via an *in-situ* reduction of the intermediate ester. This is accomplished via a combination of gallium, boron (**3.68**), and silicon (**3.72**). This reduction appears to be selective for esters over amides. Preliminary mechanistic studies indicate gallium activates **3.72** to

generate a potent electrophile that binds to the ester. **3.68** then activates diphenylsilane and delivers a hydride to reduce the ester which collapses to an oxocarbenium and is reduced again. These results are being prepared for submission.

In chapter four, we investigated the biological (functional) effects of alternative amine–acid couplings. In the first part, we applied an esterification, amination, alkylation, and ketonylation reaction to an amine and acid pair to synthesize matched molecular pair analogues of the PROTAC dbet1. Each of these chemistries required development to work in the context of these complex substrates, and HTE was used to solve this. The amination reaction was found to be exquisitely selective over other carbonyls examined and was used to prepare a small library of reductive amination products (**4.19-23,4.52**). All these reactions were also applied to a VHL targeting partial PROTAC with similar efficiency. Each of these analogues had a unique set of physicochemical properties that affected their function. The ester, alkane, and ketone were all much more permeable than the amide while maintaining binding to the target, and had lower DC_{50} values, suggesting that the increase in permeability may increase potency. In addition to being far less permeable, the amine products lost all degradation efficiency. Computational studies investigating this effect revealed an important intramolecular hydrogen bond forming as well as the basicity of the amine being responsible for loss of binding to BRD4. These results have been posted to a preprint server (10.26434/chemrxiv-2023-bh0d1), and have been submitted for publication. In the second part of chapter four, we explored the effects of amine–acid couplings on cellular distribution. By synthesizing several different derivatives of fluorescein and imaging them in cells we were able to see that that transformation had an impact with the amide being impermeable, the ester localizing into the lysosome, the amine into the

golgi, and the alpha arylated acid tracking to the mitochondria. These studies remain an ongoing project in our lab.

The labs in chapter two could be expanded depending on the students taking the course. The python lab could be extended or modified to be more research based. For example, after introducing the techniques in lab, students could be given a dataset of toxic compounds and asked to determine which properties correlate most with toxicity. The PAMPA lab could be expanded to include a synthesis component, where students are given a set of building blocks to choose from and they are asked to make the most permeable molecule possible. This could be confirmed via PAMPA. The other opportunity would be to have the students write their own Opentrons script to run the entire lab without using manual pipetting.

In chapter one we reported examples from other labs of amide to ester substitution as a viable strategy to improve permeability while maintaining stability if the ester is sterically hindered. Given this data, the esterification reaction may be worth exploring in this context, though it would be ideal to explore other amine activation strategies that are more atom economical. An obvious limitation of the halogenation reaction is that it does not currently include fluorides, so expanding into this space would greatly increase the attractiveness of the reaction. Other nucleophiles beyond thiophenols and phenols could be explored as well. The incorporation of deuterium in the etherification may mitigate metabolic hotspots in some molecules, and this effect would be worth investigating. Further, if the intermediate of the reduction is indeed an oxocarbenium ion, it may be possible to trap it with a mild nucleophile such as allyl-TMS to perform a three-component coupling.

There are opportunities to develop the PROTACs work further in several directions. Firstly, mechanistic studies to understand what is unique about **4.1** that it readily decarbonylates

under reductive nickel conditions could have important implications for decarboxylative couplings in general. If it is an electronic effect of the substrate, substrate design could improve the scope of the reactivity. However, if it is a different effect, perhaps an additional additive could help facilitate the decarbonylation for a general solution. For the amination reaction, since it is known that trifluoroacetic acid (TFA) will react spontaneously with phenylsilane and alkyl amines to form trifluoroethylated amines, it may be possible that working the reaction up with TFA generates a new, more lipophilic product. It would be interesting to see these analogues of **4.7** and **4.19** especially as it may rescue their activity by removing the intramolecular hydrogen-bond and attenuating the basicity. Finally, there is room to investigate the effects these transformations have on non-BRD4 based PROTACs. The cell imaging project could be expanded to incorporate a direct to biology platform. This would greatly increase the throughput of the study and would allow for a comparison of distribution effects mediated by building blocks as well as transformations. This would generate a large data set that is ripe for machine learning to examine the interplay between building block, transformation, and distribution and could greatly speed up the understanding of these effects.